

# HOT CORROSION STUDIES ON PLASMA SPRAY COATINGS OVER SOME Ni- AND Fe- BASED SUPERALLOYS

## A THESIS

*Submitted in partial fulfilment of the  
requirements for the award of the degree  
of*

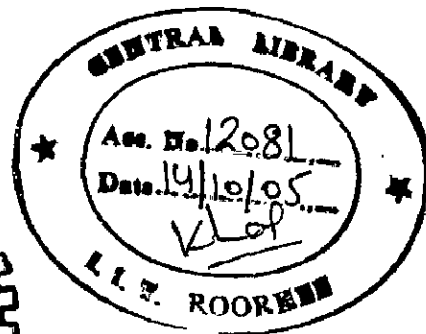
DOCTOR OF PHILOSOPHY

*in*

METALLURGICAL AND MATERIALS ENGINEERING

*By*

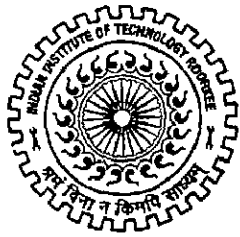
**HARPREET SINGH**



DEPARTMENT OF METALLURGICAL AND MATERIALS ENGINEERING  
INDIAN INSTITUTE OF TECHNOLOGY ROORKEE  
ROORKEE-247 667 (INDIA)

APRIL, 2005

© INDIAN INSTITUTE OF TECHNOLOGY, ROORKEE, 2005  
ALL RIGHTS RESERVED



INDIAN INSTITUTE OF TECHNOLOGY ROORKEE  
ROORKEE

CANDIDATE'S DECLARATION

I hereby certify that the work which is being presented in the thesis, entitled "**HOT CORROSION STUDIES ON PLASMA SPRAY COATINGS OVER SOME Ni- AND Fe-BASED SUPERALLOYS**" in partial fulfilment of the requirements for the award of the Degree of Doctor of Philosophy and submitted in the Department of Metallurgical and Materials Engineering of the Institute is an authentic record of my own work carried out during a period from July, 2002 to April, 2005 under the supervision of **Dr. Satya Prakash** and **Dr. Devendra Puri**.

The matter presented in this thesis has not been submitted by me for the award of any other degree of this or any other University/Institute.


  
(HARPREET SINGH)

Signature of the Candidate

This is to certify that the above statement made by the candidate is correct to the best of our knowledge.

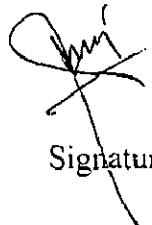
Date: 28.04.05

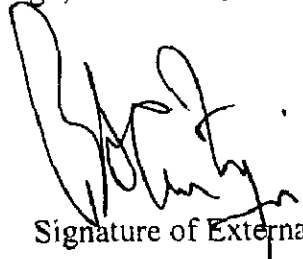
  
(Dr. DEVENDRA PURI)  
Assistant Professor

  
(Dr. SATYA PRAKASH)  
Professor

Department of Metallurgical and Materials Engineering  
Indian Institute of Technology Roorkee  
Roorkee – 247 667, India

The Ph.D. Viva-Voice examination of Harpreet Singh, Research Scholar, has been held on 17.09.05

  
Signature of Supervisor(s)

  
Signature of External Examiner

# ABSTRACT

---

Hot corrosion is an accelerated oxidation of materials at elevated temperatures induced by a thin film of fused salt deposits, which is mostly observed in boilers, gas turbines, internal combustion engines, fluidized bed combustion, industrial waste incinerators, diesel engines and chemical plants. The hot corrosion of an alloy usually occurs in the environments where molten salts such as sulphates ( $\text{Na}_2\text{SO}_4$ ), chlorides ( $\text{NaCl}$ ) or oxides ( $\text{V}_2\text{O}_5$ ) are deposited onto the surfaces. Sodium vanadyl vanadate ( $\text{Na}_2\text{O} \cdot \text{V}_2\text{O}_4 \cdot 5\text{V}_2\text{O}_5$ ), which melts at a relatively low temperature  $550^\circ\text{C}$  is found to be the most common salt deposit on boiler superheaters.

Superalloys are well known candidates for the above mentioned high temperature applications. Although the superalloys have adequate mechanical strength at elevated temperatures, yet often lack resistance to oxidizing/corroding environments during long time exposures. One possible way to combat this problem of hot corrosion and oxidation constitutes the use of protective coatings. Among the various techniques used for deposition of coatings, plasma spraying is a versatile technology that has been successful as a reliable cost-effective solution for many industrial problems.

In the present study, oxidation behaviour of some superalloys designated as Superni 75, Superni 600, Superni 601, Superni 718 and Superfer 800H as per the manufacturer's catalogue, has been investigated with and without the application of plasma sprayed coatings in air as well as  $\text{Na}_2\text{SO}_4$ -60% $\text{V}_2\text{O}_5$  environment. These superalloys are being developed by Mishra Dhatu Nigam Limited, Hyderabad (India) for the high temperature applications such as boilers and gas turbine parts, heat exchangers and piping in chemical industries, jet engines, pump bodies, high temperature furnace parts and heat treatment jigs.

Argon shrouded plasma spray process was utilised to develop four types of coatings viz. Ni-22Cr-10Al-1Y (NiCrAlY), Ni-20Cr,  $\text{Ni}_3\text{Al}$  and Stellite-6 on the given superalloys.  $\text{Ni}_3\text{Al}$  alloy powder was prepared by mixing nickel and aluminium powders in the stoichiometric ratios. The NiCrAlY was also used as bond coat of approximately  $150\ \mu\text{m}$  thickness before the final coating in all cases. As-sprayed coatings were characterised by metaflography, SEM, EDAX and EPMA before conducting oxidation studies.



In as-sprayed condition, the formation of Ni<sub>3</sub>Al as main phase was confirmed by XRD analysis in case of Ni<sub>3</sub>Al coatings. In almost all the coating formulations, a slight increase in microhardness values for the substrate superalloys was observed near the bond coat/substrate interface, which might be due to the high speed impact of the coating particles during plasma spray deposition. Interdiffusion of various elements between the substrate and plasma spray coats was observed to be marginal and it was relatively high between the bond coat and top coat.

Oxidation studies in air and Na<sub>2</sub>SO<sub>4</sub>-60%V<sub>2</sub>O<sub>5</sub> environments were performed in the laboratory furnace for 50 cycles; each cycle consisted of 1 hour heating at 900<sup>0</sup>C followed by 20 minutes cooling. At the end of each cycle the specimens were critically examined regarding the colour, luster, tendency to spall and adherence of scale and then subjected to weight change measurements. In case of studies in the molten salt, a uniform layer of the mixture of Na<sub>2</sub>SO<sub>4</sub>-60%V<sub>2</sub>O<sub>5</sub> was applied on the preheated specimens (200<sup>0</sup>C) with the help of camel hair brush in such a manner that the weight of the applied salt does not exceed 3-5 mg/cm<sup>2</sup>. XRD and SEM/EDAX techniques were used to identify the phases obtained and the elemental analysis of the surface scale. These oxidised samples were then cut across the cross-sections and mounted to study the cross-sectional details by EPMA and SEM/EDAX.

Among the bare superalloys, Superni 600 showed the best resistance to air oxidation, whereas Superni 75 exhibited maximum oxidation rate. Based on the thermogravimetric data for 50 cycles the oxidation rates for the uncoated superalloys could be arranged in following order:

Superni 75 > Superni 718 > Superni 601 > Superfer 800H > Superni 600

Thermogravimetric data showed that the overall weight gains after 50 cycles of air oxidation were lower for the uncoated superalloys than their coated counterparts in all the cases. Among the various coatings, NiCrAlY coatings showed minimum oxidation rates in all the cases, the sequence for observed oxidation rates based on weight gain values for the NiCrAlY coated superalloys after 50 cycles of oxidation was as follows:

Superni 75 >Superni 601>Superni 600> Superfer 800H > Superni 718

However, the performance of other coatings could not be sequenced in general, as it was observed to vary with the change in substrate superalloy. Comparing the oxidation resistance of Ni-20Cr, Ni<sub>3</sub>Al and Stellite-6 coatings in the air, sequences observed for the various coated alloys were as follows:

Ni <sub>3</sub> Al > Stellite-6 > Ni-20Cr	for	Superni 75 and Superni 601
Stellite-6 > Ni <sub>3</sub> Al > Ni-20Cr	for	Superni 600
Ni-20Cr > Ni <sub>3</sub> Al > Stellite-6	for	Superni 718
Ni <sub>3</sub> Al > Ni-20Cr > Stellite-6	for	Superfer 800H

In case of Na<sub>2</sub>SO<sub>4</sub>-60%V<sub>2</sub>O<sub>5</sub> induced hot corrosion, the bare superalloys have indicated higher rates of corrosion as compared to those shown in air oxidation. The Fe-base superalloy Superfer 800H has shown least resistance to the hot corrosion amongst the Superalloys Superni 75, 600, 601 and Superfer 800H. The weight gain values for the fifth superalloy Superni 718 could not be measured upto 50 cycles due to intensive spalling and sputtering of the scale. This might be due the Mo content present in the superalloy, which might have led to acidic fluxing of the protective scales. On the basis of thermogravimetric data for 50 cycles of hot corrosion, corrosion rate of the superalloys under study could be arranged in the following order:

Superfer 800H > Superni 601 > Superni 600 > Superni 75

The NiCrAlY coating was found to be successful in reducing the oxidation rate in the given molten salt environment for all the superalloys, while Ni-20Cr also slowed down the oxidation rates for all the superalloys with an exception of Superni 75, where Ni-20Cr coated sample showed somewhat higher weight gain as compared to uncoated case. Ni<sub>3</sub>Al coating reduced overall weight gain in case of Superni 601, 718 and Superfer 800H. Stellite-6 coating was found to be effective in case of Superni 718 and Superfer 800H. The overall performance of the coatings in the Na<sub>2</sub>SO<sub>4</sub>-60%V<sub>2</sub>O<sub>5</sub> environment has indicated the following trend:

NiCrAlY > Ni-20Cr > Ni<sub>3</sub>Al > Stellite-6

In both the environments, the coatings maintained their integrity with the substrate superalloys and internal oxidation of the superalloys was not indicated, in general. The oxidation kinetics could be approximated by parabolic rate in all the cases. Rate of oxidation was observed to be high in the early cycles of the study for all the coated specimens, which might partly be attributed to availability of diffusion paths in coatings along the splat boundaries. During transient period of oxidation, the

oxidizing species might have penetrated into the coatings along the interconnected network of pores and splat boundaries to cause rapid oxidation. However, once all these possible diffusion paths were blocked by the formation of oxides, the oxidation might have become limited mainly to the surface of the coatings, thereby entered into a steady state.

All the coated specimens exposed to air or molten salt oxidation indicated the presence of mainly oxides in their scales as has been revealed by XRD and EDAX analysis. The oxides identified were those of chromium and/or aluminium, and spinels containing mixed oxides of nickel-chromium or nickel-aluminium or cobalt-chromium. These oxides are reported to be protective in nature against oxidation/hot corrosion due to their low growth rate, strongly bounded compositions and ability to act as effective barriers against ionic migration. The spinel phases may further enhance the oxidation resistance as these are suggested to have much smaller diffusion coefficients of the cations and anions than those in their parent oxides. Moreover, in some cases, chromium was seen forming thin continuous streaks at the bond coat/base alloy interface, which might further have improved the oxidation resistance towards both the given environments.

The NiCrAlY coated Superfer 800H superalloy showed the highest oxidation resistance to both the air and molten salt environments. The best protection indicated by NiCrAlY coating, in general, might also be ascribed to the simultaneous formation of an additional protective oxide  $\alpha$ -Al<sub>2</sub>O<sub>3</sub> alongwith Cr<sub>2</sub>O<sub>3</sub> and NiCr<sub>2</sub>O<sub>4</sub> in its oxide scale, which grows very slowly and is thermodynamically stable. Moreover, the presence of yttrium in the coating might also have reduced the scale growth rates and hence the overall weight gains.

The splat structure could be clearly seen after air as well as molten salt oxidation for the NiCrAlY coated specimens, where the splats (Ni-rich) were in un-oxidised state. The ingress of corrosive species in the initial stages along the splat boundaries resulted in formation of oxides of mainly aluminium, alongwith those of yttrium and chromium. Bond coat was found to have retained its identity in case of Ni-20Cr, Ni<sub>3</sub>Al and Stellite-6 coated samples in both the environments of the current investigation. The Ni-rich splats present in the bond coats were found to be, by and large, in un-oxidised state, whereas oxides of aluminium, yttrium and chromium were observed to be formed along the pores and splat boundaries. In case of Stellite-6 coating, chromium and oxygen were found to co-exist along the splat boundaries in both the environments of study, whereas cobalt rich splats, by and large, remained un-oxidised.

Sulphur got penetrated through the scale to/under the substrate-scale interface in most of the cases during molten salt induced oxidation, while vanadium was mainly restricted to the top scales. Titanium indicated significant diffusion into the scales in case of NiCrAlY, Ni-20Cr and Ni<sub>3</sub>Al coated Superni 75, 718 and Superfer 800H during molten salt as well as air oxidation. Diffusion of iron into the scales of NiCrAlY, Ni-20Cr and Ni<sub>3</sub>Al coatings was also noticed in most of the cases after exposure to oxidation/hot corrosion, which was relatively high in case of molten salt induced corrosion. Minor diffusion of some other basic elements of the superalloy substrates such as Mn, Mo, Ta and Si into the scales was also noticed in most of the cases. However, this diffusion has been reported to be a life-limiting factor if coatings are operated at temperatures greater than 1000<sup>0</sup>C for prolonged periods of time.

Slight spalling of the scales in powder form was observed in most of the coated cases, when subjected to molten salt corrosion. Minor spallation of the coatings was also noticed during oxidation in both the given environments in most of the cases, which perhaps, got initiated from the microcracks and, was confined to the edges of the coated specimens. It may be attributed to the thermal coefficient mismatch between the oxide scale and the remaining coating.

The coatings under study have been found to be successful in protecting the given substrate superalloys at an elevated temperature of 900<sup>0</sup>C in the very aggressive simulated conditions of boilers (and gas turbines), from which it can be inferred that these coatings can also perform well in the actual boiler and gas turbine environments. The temperature, at which these coated superalloys have been tested and found successful in reducing the corrosion, can enhance the thermal efficiency by a significant fraction particularly in case of boilers. In context with the Indian boilers, the hot corrosion problem are relatively more severe as the Indian coal contains high ash content and therefore, the coatings can bring still more revenues. Further, these coatings will also be beneficial to arrest oil ash corrosion.

# ACKNOWLEDGEMENTS

---

The author has great privilege and pride to express his immense sense of gratitude to **Dr. Satya Prakash**, Professor, Department of Metallurgical and Materials Engineering (MMED), Indian Institute of Technology, Roorkee for his valuable and intellectual guidance throughout the tenure of this work. He has been a motivating and driving force where targets appeared to be arduous during the course of work. Without his timely help, constructive criticism, positive attitude and painstaking efforts, it would have been impossible to complete this thesis in the present form. The author is highly grateful to **Dr. Devendra Puri**, for his continuous encouragement and support as a co-supervisor.

Deep sense of gratitude is acknowledged to (Late) Jathedar Gurcharan Singh Tohra, President, Managing Committee and Dr. D.S. Hira, Principal, BBSB Engineering College, Fatehgarh Sahib, who were kind enough to sponsor the author to pursue Ph.D under QIP Scheme of Govt. of India by putting their best efforts. Thanks are due to Dr. S. Ray, Ex-Head, MMED and Dr. S. C Handa, Ex-Coordinator, QIP Centre, Indian Institute of Technology Roorkee for giving the author an opportunity to carry out the present work in the department.

Author is highly indebted to Dr. V. K. Tiwari, Head, MMED for his co-operation in extending the necessary facilities and supports during the concluding phase of this work. Author is grateful to Dr. P. S. Misra and Dr. Surendra Singh for their valuable suggestions and timely help during the course of this work. Author wishes to record his deep sense of gratitude to Head, Institute Instrumentation Centre (IIC), Indian Institute of Technology Roorkee for extending necessary facilities during the experimental and analysis work.

Author is highly obliged and wishes to owe his sincere thanks to the technical and administrative staff of the MMED, especially to Mr. Rajinder S. Sharma, Mr. Shamsheer Singh, Mr. N. K. Seth, Mr. Vidya Prakash, Mr. T. K. Sharma, Mr. R. K. Sharma, Mr. H. K. Ahuja, Mr. Shakti Gupta, Mr. Dhan Prakash, Mr. M. Pandey, Mr. B. Sharma, Mr. Jasbir Singh, Mr. V. P. Verma and Mr. M. Aslam, who helped him in all possible ways during the experimental work.

Author would like to express his sincere thanks to Mr. S. K. Saini and Ms. Solan, Mrs. Rekha Sharma, and Mr. T. K. Ghosh of IIC, IIT, Roorkee for carrying out XRD, SEM and EPMA work respectively. Thanks are also acknowledged to Mr. Puran Sharma for preparing high quality micrographs and Mr. N. K. Varshney for tracing of the drawings. Sincere thanks are acknowledged to Mr. Narendra Kumar and Mr. Subodh Saini for typesetting of thesis manuscript.

Author is highly obliged to Dr. Ajay Gupta, Director IUC DAE, Indore, Dr. M. Srinivas, Scientist 'F', Defense Metallurgical Research Laboratory (DMRL), Hyderabad, Dr. M. Chakraborty, Professor, Metallurgical and Materials Engineering Department, IIT, Kharagpur, Dr. G. B. Kale, Scientist Officer, Material Science Division (MMD), BARC, Mumbai, and Dr. R. K. Sidhu, Ex-Head, Thapar Centre for Industrial Research and Development, Patiala for extending their support and facilities to perform the analysis work. Special thanks are due to Mr. R. K. Tandon, Managing Director, Anod Plasma Spray Ltd., Kanpur for kindly providing plasma spray facility.

Author owes his sincere thanks to Dr. D. M Phase and Mr. Vinay Ahire of IUC DAE, Indore and Mr. Dr. Rabindranath Maiti of CRF IIT Khargpur for performing EDAX analysis. Thanks are due to Mr. V.V. Rama Rao of DMRL, Hyderabad and Mr. A. Laik of BARC, Mumbai for conducting EPMA.

Author would like to record his sense of gratitude for the library staff of IIT Roorkee, IIT Mumbai, IIT Kharagpur, IIT Madras, DMRL, Hyderabad and BARC Mumbai for their kind co-operation to carry out the literature survey. Thanks are also due to Mr. Sunil Sharma, Librarian of MMED for providing all the necessary help.

Author feels highly indebted to faculty and staff of BBSB Engineering College, Fatehgarh Sahib, who have to put extra efforts during his deputation to IITR for pursuing the current work. The financial support rendered by All India Council of Technical Education (AICTE) New Delhi under Quality Improvement Programme (QIP) is highly acknowledged.

Author wishes to thank his friends and colleagues for their moral support and camaraderie help to keep things in perspective. Thanks are due to Mrs. & Mr. Ranjit Singh, Mrs. Seema Chopra and Mr. Suresh Papneja, Mrs. Daljit Kaur, Dr. Gitanjali, Dr. Buta Singh, Mr. S. B. Misra, Mr. T. S. Sidhu, Mr. B. S. Sidhu, Mr. Sandeep Bansal, Mr. Sanjay Panwar, Mr. Laljee Prasad, Mr. Satbir Singh, Mr. Ravinder Kumar, Mr. M. R. Ramesh, Mr. Jasbir Singh, Mr. H. S. Bhatti, Mr. Tajinder Singh, Mr.

Arivazaghan and Mr. Anupam Singhal. Special thanks to Mr. Happy Khera, Mr. Rakesh Kumar, Mr. Bakhshinder Singh and Mr. Hari Om Gupta for their everlasting support.

Author would like to express his reverence and great admiration for his parents, who have always been the guiding and encouraging force for him. He would like to humbly dedicate this thesis to his mother-in-law, symbol of motherly love and care, who gave her best to his family during the tenure of this work by sacrificing her comforts. Author sincerely acknowledges the help extended by his father-in-law in this regard with immense gratitude. Author is highly grateful to his sisters Amarjeet Kaur and Pushpinder Kaur, and brother-in-law Mr. Baltej Singh for their continual co-operation during the course of this work. A sense of forgiveness is recorded for his brother Gurpreet Singh, who probably missed the help and enthusiasm expected from the author during his wedding days. Author would like to thank his sister-in-law Satnam Kaur for her best wishes extended from time to time.

A sense of apology is due to author's sweet daughter Agamnoor Kaur and loving son Harsimran Singh, who probably missed many precious moments of fatherly love and care. The wife of author, Gurmeet Kaur deserves special thanks and grand appreciation for her persistent moral support and capability to rejuvenate the author during the leaning phases of the work. Author is falling short of words to express gratitude to her for the determination shown to bear extra household responsibilities during the tenure of this work.

Above all, author is highly indebted to almighty God who blessed him with spiritual support and fortitude at each and every stage of this work.

**(HARPREET SINGH)**

# PREFACE

---

The entire work carried out for this investigation has been presented into eight chapters.

Chapter-1 contains the introductory remarks about hot corrosion phenomenon and its impact on the various engineering equipments and components. The ways to counteract this problem are also briefly presented.

Chapter-2 begins with exhaustive survey of literature regarding various aspects and mechanisms of high temperature oxidation and hot corrosion. The different preventive measures have been summarised and the plasma spray process detailed. After reviewing the available literature the problem has been formulated.

Chapter-3 introduces the experimental techniques and procedures employed for applying the coatings and their characterisation, the oxidation studies and analysis of the corrosion products. Further, specifications of the equipments and other instruments used for the present investigation are mentioned.

Chapter-4 includes the findings and discussions of the investigation regarding the characterisation of as-sprayed coatings.

Chapter-5 contains the data regarding the cyclic oxidation studies performed on uncoated and coated superalloys in air at 900<sup>0</sup>C. It also includes the *critical discussion* of results in view of the existing literature.

Chapter-6 describes the findings regarding the behaviour of coated and uncoated superalloys subjected to cyclic hot corrosion in molten salt ( $\text{Na}_2\text{SO}_4\text{-60\%V}_2\text{O}_5$ ) at 900<sup>0</sup>C along with discussion on the results, with an effort to suggest modes of corrosion attack.

Chapter-7 presents the comprehensive discussion on the results with an attempt to explain the comparative performance of the different coatings in both the environments of the study.

Chapter-8 compiles the salient conclusions of the present study regarding the characterisation, oxidation and hot corrosion behaviour of uncoated and coated superalloys.



# CONTENTS

---

	Page No.
<i>Candidate's Declaration</i>	i
<i>Abstract</i>	ii
<i>Acknowledgements</i>	vii
<i>Preface</i>	x
<i>List of Figures</i>	xix
<i>List of Tables</i>	xl
<i>Research Papers Presented/Published</i>	xli
<i>Abbreviations</i>	xlii
<b>CHAPTER 1                    INTRODUCTION</b>	<b>1</b>
<b>CHAPTER 2                    LITERATURE REVIEW</b>	<b>7</b>
<b>2.1    HIGH TEMPERATURE OXIDATION</b>	<b>7</b>
2.1.1    Oxidation of Superalloys	10
2.1.2    Oxidation Studies on Iron-Based Alloys	12
2.1.3    Oxidation Studies on Nickel and Nickel-Based Alloys	13
<b>2.2    HOT CORROSION</b>	<b>16</b>
2.2.1    High Temperature (Type I) Hot Corrosion (HTHC)	16
2.2.2    Low Temperature (Type II) Hot Corrosion (LTHC)	16
2.2.3    Hot Corrosion of Superalloys	17
2.2.4    Mechanisms of Hot Corrosion	19
2.2.5    Salt Chemistry	22
2.2.5.1    Chemistry and Phase Stability of Na <sub>2</sub> SO <sub>4</sub> Salt	22
2.2.5.2    Vanadate Solution Chemistry	22

2.2.5.3	<i>Chemistry of Salts in Combustion of Coal/Fuel Oils</i>	23
2.2.5.4	<i>Solubilities of Al<sub>2</sub>O<sub>3</sub> and Cr<sub>2</sub>O<sub>3</sub></i>	23
<b>2.3</b>	<b>STUDIES ON Na<sub>2</sub>SO<sub>4</sub>-V<sub>2</sub>O<sub>5</sub> INDUCED HOT CORROSION</b>	
	<b>CORROSION</b>	26
2.3.1	<b>Iron and Iron-Based Alloys</b>	26
2.3.2	<b>Nickel and Nickel-Based Alloys</b>	29
<b>2.4</b>	<b>COUNTERMEASURES AGAINST HOT CORROSION</b>	35
<b>2.5</b>	<b>USE OF PROTECTIVE COATINGS</b>	37
2.5.1	<b>Desirable Features of Effective Coating System</b>	38
2.5.2	<b>Coating Processes</b>	39
2.5.2.1	<i>Thermal Spray Coating Processes</i>	40
<b>2.6</b>	<b>PLASMA SPRAYING</b>	43
2.6.1	<b>Plasma Spraying-The Process</b>	44
2.6.1.1	<i>Plasma Jets</i>	44
2.6.1.2	<i>Coating Formulation</i>	45
2.6.1.3	<i>Adhesion of the Plasma Sprayed Coatings</i>	48
2.6.1.4	<i>Plasma Spray Process Variables</i>	49
2.6.2	<b>Process Variants of Plasma Spraying</b>	49
2.6.2.1	<i>Atmospheric Plasma Spraying (APS)</i>	51
2.6.2.2	<i>Vacuum (VPS) or Low Pressure Plasma Spraying (LPPS)</i>	51
2.6.2.3	<i>Shrouded Plasma Spraying (SPS)</i>	51
2.6.2.4	<i>Controlled Atmosphere Plasma Spraying (CAPS)</i>	52
<b>2.7</b>	<b>ROLE OF METALLIC COATINGS</b>	52
2.7.1	<b>MCrAlY Coatings</b>	52
2.7.2	<b>Nickel-Chromium coatings</b>	58

2.7.3	Nickel Aluminide Coatings	62
2.7.4	Cobalt Based Coatings	66
<b>2.8</b>	<b>PROBLEM FORMULATION</b>	<b>69</b>
2.8.1	Scope	69
2.8.2	Aim	71
<b>CHAPTER 3</b>	<b>EXPERIMENTAL TECHNIQUES AND PROCEDURES</b>	<b>74</b>
3.1	SELECTION OF SUBSTRATE MATERIALS	74
3.2	DEVELOPMENT OF COATINGS	74
3.2.1	Preparation of Substrate Materials	74
3.2.2	Alloy Powders for Coatings	74
3.2.3	Formulation of Coatings	75
3.3	CHARACTERISATION OF COATINGS	75
3.3.1	Measurement of Coating Thickness	75
3.3.2	Measurement of Porosity	77
3.3.3	Metallographic Studies	77
3.3.4	Measurement of Microhardness	78
3.3.5	X-Ray Diffraction (XRD) Analysis	78
3.3.6	Scanning Electron Microscopy (SEM) and Energy Dispersive X-Ray (EDAX) Analysis	78
3.3.7	Electron Probe Micro Analyser (EPMA)	79
3.4	HIGH TEMPERATURE OXIDATION AND HOT CORROSION STUDIES	79
3.4.1	Experimental Setup	79

3.4.2	Oxidation Studies in Air	80
3.4.3	Hot Corrosion Studies in Molten Salt (Na <sub>2</sub> SO <sub>4</sub> -60%V <sub>2</sub> O <sub>5</sub> )	80
3.4.3.1	<i>Molten Salt Coating</i>	80
3.4.3.2	<i>Hot Corrosion Studies</i>	80
3.5	<b>ANALYSIS OF CORROSION PRODUCTS OF OXIDATION IN AIR AND MOLTEN SALT</b>	81
3.5.1	Visual Observation	81
3.5.2	Thermogravimetric Studies	81
3.5.3	Measurement of Scale Thickness	81
3.5.4	X-Ray Diffraction (XRD) Analysis	81
3.5.5	SEM/EDAX Analysis	82
3.5.5.1	<i>Surface Morphology</i>	82
3.5.5.2	<i>Cross-Sectional Morphology</i>	82
3.5.6	Electron Probe Micro Analyser (EPMA)	83
CHAPTER 4	<b>CHARACTERISATION OF SUPERALLOYS AND COATINGS</b>	84
4.1	<b>MICROSTRUCTURES OF THE SUBSTRATE SUPERALLOYS</b>	84
4.2	<b>VISUAL EXAMINATION OF THE COATINGS</b>	84
4.3	<b>MEASUREMENTS OF COATING THICKNESSES</b>	85
4.4	<b>POROSITY ANALYSIS</b>	85
4.5	<b>EVALUATION OF MICROHARDNESS</b>	89
4.6	<b>METALLOGRAPHIC STUDIES FOR THE COATINGS</b>	89

4.6.1	<b>Surface Structure</b>	89
4.6.1.1	<i>NiCrAlY Coating</i>	89
4.6.1.2	<i>Ni-20Cr Coating</i>	90
4.6.1.3	<i>Ni<sub>3</sub>Al Coating</i>	90
4.6.1.4	<i>Stellite-6 Coating</i>	90
4.6.2	<b>Cross-Sectional Structures</b>	90
4.7	<b>XRD ANALYSIS</b>	98
4.8	<b>SEM ANALYSIS</b>	98
4.9	<b>EDAX ANALYSIS</b>	99
4.10	<b>EPMA ANALYSIS</b>	99
4.11	<b>DISCUSSION</b>	112
<b>CHAPTER 5</b>	<b>OXIDATION STUDIES IN AIR</b>	119
5.1	<b>RESULTS</b>	119
5.1.1	<b>Uncoated Superalloys</b>	119
5.1.1.1	<i>Visual Examination</i>	119
5.1.1.2	<i>Thermogravimetric Data</i>	120
5.1.1.3	<i>Scale Thickness Measurement</i>	120
5.1.1.4	<i>X-ray Diffraction Analysis</i>	124
5.1.1.5	<i>SEM/EDAX Analysis</i>	124
5.1.1.6	<i>EPMA Analysis</i>	125
5.1.2	<b>NiCrAlY Coating</b>	136
5.1.2.1	<i>Visual Examination</i>	136
5.1.2.2	<i>Thermogravimetric Data</i>	136
5.1.2.3	<i>Scale Thickness Measurement</i>	137
5.1.2.4	<i>X-ray Diffraction Analysis</i>	137
5.1.2.5	<i>SEM/EDAX Analysis</i>	143
5.1.2.6	<i>EPMA Analysis</i>	144

<b>5.1.3</b>	<b>Ni-20Cr Coating</b>	153
5.1.3.1	<i>Visual Examination</i>	153
5.1.3.2	<i>Thermogravimetric Data</i>	153
5.1.3.3	<i>Scale Thickness Measurement</i>	153
5.1.3.4	<i>X-ray Diffraction Analysis</i>	154
5.1.3.5	<i>SEM/EDAX Analysis</i>	154
5.1.3.6	<i>EPMA Analysis</i>	155
<b>5.1.4</b>	<b>Ni<sub>3</sub>Al Coating</b>	170
5.1.4.1	<i>Visual Examination</i>	170
5.1.4.2	<i>Thermogravimetric Data</i>	170
5.1.4.3	<i>Scale Thickness Measurement</i>	170
5.1.4.4	<i>X-ray Diffraction Analysis</i>	171
5.1.4.5	<i>SEM/EDAX Analysis</i>	171
5.1.4.6	<i>EPMA Analysis</i>	180
<b>5.1.5</b>	<b>Stellite-6 Coating</b>	181
5.1.5.1	<i>Visual Examination</i>	181
5.1.5.2	<i>Thermogravimetric Data</i>	182
5.1.5.3	<i>Scale Thickness Measurement</i>	182
5.1.5.4	<i>X-ray Diffraction Analysis</i>	182
5.1.5.5	<i>SEM/EDAX Analysis</i>	183
5.1.5.6	<i>EPMA Analysis</i>	197
<b>5.2</b>	<b>SUMMARY OF RESULTS</b>	205
<b>5.3</b>	<b>DISCUSSION</b>	207
5.3.1	<b>Uncoated Superalloys</b>	207
5.3.2	<b>NiCrAlY Coating</b>	210
5.3.3	<b>Ni-20Cr Coating</b>	215
5.3.4	<b>Ni<sub>3</sub>Al Coating</b>	216
5.3.5	<b>Stellite-6 Coating</b>	219

<b>CHAPTER 6</b>	<b>OXIDATION STUDIES IN MOLTEN SALT ENVIRONMENT</b>	223
<b>6.1</b>	<b>RESULTS</b>	223
6.1.1	<b>Uncoated Superalloys</b>	223
6.1.1.1	<i>Visual Examination</i>	223
6.1.1.2	<i>Thermogravimetric Data</i>	224
6.1.1.3	<i>Scale Thickness Measurement</i>	227
6.1.1.4	<i>X-ray Diffraction Analysis</i>	227
6.1.1.5	<i>SEM/EDAX Analysis</i>	227
6.1.1.6	<i>EPMA Analysis</i>	235
6.1.2	<b>NiCrAlY Coating</b>	236
6.1.2.1	<i>Visual Examination</i>	236
6.1.2.2	<i>Thermogravimetric Data</i>	243
6.1.2.3	<i>Scale Thickness Measurement</i>	243
6.1.2.4	<i>X-ray Diffraction Analysis</i>	244
6.1.2.5	<i>SEM/EDAX Analysis</i>	244
6.1.2.6	<i>EPMA Analysis</i>	251
6.1.3	<b>Ni-20Cr Coating</b>	258
6.1.3.1	<i>Visual Examination</i>	258
6.1.3.2	<i>Thermogravimetric Data</i>	259
6.1.3.3	<i>Scale Thickness Measurement</i>	265
6.1.3.4	<i>X-ray Diffraction Analysis</i>	265
6.1.3.5	<i>SEM/EDAX Analysis</i>	265
6.1.3.6	<i>EPMA Analysis</i>	267
6.1.4	<b>Ni<sub>3</sub>Al Coating</b>	279
6.1.4.1	<i>Visual Examination</i>	279
6.1.4.2	<i>Thermogravimetric Data</i>	280
6.1.4.3	<i>Scale Thickness Measurement</i>	286
6.1.4.4	<i>X-ray Diffraction Analysis</i>	286
6.1.4.5	<i>SEM/EDAX Analysis</i>	286
6.1.4.6	<i>EPMA Analysis</i>	288

6.1.5	<b>Stellite-6 Coating</b>	301
6.1.5.1	<i>Visual Examination</i>	301
6.1.5.2	<i>Thermogravimetric Data</i>	301
6.1.5.3	<i>Scale Thickness Measurement</i>	302
6.1.5.4	<i>X-ray Diffraction Analysis</i>	302
6.1.5.5	<i>SEM/EDAX Analysis</i>	302
6.1.5.6	<i>EPMA Analysis</i>	304
6.2	<b>SUMMARY OF RESULTS</b>	322
6.3	<b>DISCUSSION</b>	326
6.3.1	Uncoated Superalloys	326
6.3.2	NiCrAlY Coating	329
6.3.3	Ni-20Cr Coating	332
6.3.4	Ni <sub>3</sub> Al Coating	333
6.3.5	Stellite-6 Coating	335
CHAPTER 7	<b>COMPARATIVE DISCUSSION</b>	339
CHAPTER 8	<b>CONCLUSIONS</b>	344
	<b>SUGGESTIONS FOR FUTURE WORK</b>	350
	<b>APPENDIX</b>	351
	<b>REFERENCES</b>	364



# LIST OF FIGURES

Figure No.	Particulars	Page No.
Fig. 2.1	Schematic representation showing transient oxidation and subsequent development of a healing $\text{Cr}_2\text{O}_3$ -rich layer on Ni-20%Cr at high temperature (Stott, 1998).	9
Fig. 2.2	Schematic diagram illustrating the conditions that develop during the initiation and the propagation of hot corrosion attack and to identify the factors that determine the time at which the transition from the initiation to the propagation stage occurs (Pettit and Meier, 1985).	18
Fig. 2.3	Schematic representation of the reaction sequence during low-temperature hot corrosion of a Co-30%Cr alloy exposed to $\text{O}_2$ - $\text{SO}_2$ - $\text{SO}_3$ environment where $\text{Na}_2\text{SO}_4$ - $\text{CoSO}_4$ liquid and $\text{Co}_3\text{O}_4$ are stable. At higher concentration of $\text{SO}_3$ where $\text{Co}_3\text{O}_4$ is unstable at the gas-salt interface, the outward migrating cobalt will form $\text{CoSO}_4$ (s) or $\text{Co}_3\text{O}_4$ and $\text{CoSO}_4$ (s) (Luthra, 1983).	21
Fig. 2.4	Na-Cr-S-O phase stability diagram for 1200 K (Rapp, 1986).	24
Fig. 2.5	Phase stability diagram for Na-V-S-O system at 900 °C (Hwang and Rapp, 1989).	25
Fig. 2.6	Corrosion rate of Type 304 stainless steel in different mixtures of $\text{Na}_2\text{SO}_4$ - $\text{V}_2\text{O}_5$ (Natesan, 1976).	28
Fig. 2.7	Phase Diagram for $\text{Na}_2\text{SO}_4$ - $\text{V}_2\text{O}_5$ System (Otero et al, 1987).	33
Fig. 2.8	Schematic diagram showing probable hot corrosion mechanism in $\text{Na}_2\text{SO}_4$ -60% $\text{V}_2\text{O}_5$ after exposure for 50 cycles at 900°C for alloys (Gitanjaly, 2003) (a) Superni 75                      (b) Superni 601.	36
Fig. 2.9	Coating deposition technologies (Bhushan and Gupta, 1991).	41

<b>Fig. 2.10</b>	The plasma spraying process (Batchelor et al, 2003)	46
<b>Fig. 2.11</b>	Temperature distribution and geometry of plasma jet (Knotek, 2001).	47
<b>Fig. 2.12</b>	Plasma spray process variables (Bhusari, 2001).	50
<b>Fig. 2.13</b>	Types of high-temperature attack for metallic coatings (aluminide, chromide, MCrAlY, etc.) on nickel-base superalloys with approximate temperature regimes and severity of attack (National Materials Advisory Board, 1996).	53
<b>Fig. 2.14</b>	Morphological changes in a NiCrAlY coating during corrosion/oxidation (Hocking et al, 1993B).	56
<b>Fig. 2.15</b>	Schematic diagram showing probable hot corrosion mechanism for Ni-20Cr coated T11 steel exposed to Na <sub>2</sub> SO <sub>4</sub> -60%V <sub>2</sub> O <sub>5</sub> at 900 <sup>0</sup> C for 50 cycles (Singh (2003).	63
<b>Fig. 2.16</b>	Schematic diagram showing probable oxidation mechanism for Stellite-6 coated GrA1 steel exposed to air at 900 <sup>0</sup> C for 50 cycles (Singh, 2003).	68
<b>Fig. 4.1</b>	Optical micrographs of the substrate superalloys (a) Superni 75    (b) Superni 600    (c) Superni 601 (d) Superni 718    (e) Superfer 800H.	86
<b>Fig. 4.2</b>	Macrographs of as sprayed specimens with (a) NiCrAlY coating    (b) Ni-20Cr coating (c) Ni <sub>3</sub> Al coating    (d) Stellite-6 coating.	87
<b>Fig. 4.3</b>	BSEI micrographs showing cross-sectional morphology of different plasma sprayed coatings on Superfer 800H (a) NiCrAlY coating    (b) Ni-20Cr coating with bond coat (c) Ni <sub>3</sub> Al coating with bond coat    (d) Stellite-6 coating with bond coat.	88
<b>Fig. 4.4</b>	Microhardness profiles of plasma sprayed NiCrAlY coating for different substrate superalloys along the cross-section.	91
<b>Fig. 4.5</b>	Microhardness profiles of plasma sprayed Ni-20Cr coating with NiCrAlY bond coat for different substrate superalloys along the cross-section.	91

<b>Fig. 4.6</b>	Microhardness profiles of plasma sprayed Ni <sub>3</sub> Al coating with NiCrAlY bond coat for different substrate superalloys along the cross-section.	92
<b>Fig. 4.7</b>	Microhardness profiles of plasma sprayed Stellite-6 coating with NiCrAlY bond coat for different substrate superalloys along the cross-section.	92
<b>Fig. 4.8</b>	Optical micrographs showing surface morphology of plasma sprayed NiCrAlY coating on substrate superalloys (a) Superni 75 (b) Superni 600 (c) Superni 601 (d) Superni 718 (e) Superfer 800H.	93
<b>Fig. 4.9</b>	Optical micrographs showing surface morphology of plasma sprayed Ni-20Cr coating on substrate superalloys (a) Superni 75 (b) Superni 600 (c) Superni 601 (d) Superni 718 (e) Superfer 800H.	94
<b>Fig. 4.10</b>	Optical micrographs showing surface morphology of plasma sprayed Ni <sub>3</sub> Al coating on substrate superalloys (a) Superni 75 (b) Superni 600 (c) Superni 601 (d) Superni 718 (e) Superfer 800H.	95
<b>Fig. 4.11</b>	Optical micrographs showing surface morphology of plasma sprayed Stellite-6 coating on substrate superalloys (a) Superni 75 (b) Superni 600 (c) Superni 601 (d) Superni 718 (e) Superfer 800H.	96
<b>Fig. 4.12</b>	Optical micrographs along cross-section of different plasma sprayed coatings on superalloy Superfer 800H (a) NiCrAlY coating (b) Ni-20Cr coating with bond coat (c) Ni <sub>3</sub> Al coating with bond coat (d) Stellite-6 coating with bond coat.	97
<b>Fig. 4.13</b>	X-ray diffraction patterns for the plasma spray NiCrAlY coated superalloys.	100
<b>Fig. 4.14</b>	X-ray diffraction patterns for the plasma spray Ni-20Cr coated superalloys.	101
<b>Fig. 4.15</b>	X-ray diffraction patterns for the plasma sprayed Ni <sub>3</sub> Al coated superalloys.	102

<b>Fig. 4.16</b>	X-ray diffraction patterns for the plasma sprayed Stellite-6 coated superalloys.	103
<b>Fig. 4.17</b>	SEM micrographs showing surface morphology of plasma sprayed NiCrAlY coating on substrate superalloys (a) Superni 75            (b) Superni 600   (c) Superni 601 (d) Superni 718        (e) Superfer 800H.	104
<b>Fig. 4.18</b>	SEM micrographs showing surface morphology of plasma sprayed Ni-20Cr coating on substrate superalloys (a) Superni 75            (b) Superni 600   (c) Superni 601 (d) Superni 718        (e) Superfer 800H.	105
<b>Fig. 4.19</b>	SEM micrographs showing surface morphology of plasma sprayed Ni <sub>3</sub> Al coating on substrate superalloys (a) Superni 75            (b) Superni 600   (c) Superni 601 (d) Superni 718        (e) Superfer 800H.	106
<b>Fig. 4.20</b>	SEM micrographs showing surface morphology of plasma sprayed Stellite-6 coating on substrate superalloys (a) Superni 75            (b) Superni 600   (c) Superni 601 (d) Superni 718        (e) Superfer 800H.	107
<b>Fig. 4.21</b>	SEM/EDAX analysis of the plasma sprayed coatings showing elemental composition (%) at selected points (a) NiCrAlY coating   (b) Ni-20Cr coating.	108
<b>Fig. 4.22</b>	SEM/EDAX analysis of the plasma sprayed coatings showing elemental composition (%) at selected points (a) Ni <sub>3</sub> Al coating                    (b) Stellite-6 coating.	109
<b>Fig. 4.23</b>	BSEI and X-ray mappings of the cross-section of plasma spray NiCrAlY coating on the superalloy Superni 601.	110
<b>Fig. 4.24</b>	BSEI and X-ray mappings of the cross-section of plasma spray Ni-20Cr coating on the superalloy Superni 718.	111
<b>Fig. 4.25</b>	BSEI and X-ray mappings of the cross-section of plasma spray Ni <sub>3</sub> Al coating on the superalloy Superni 601.	114

<b>Fig. 4.26</b>	BSEI and X-ray mappings of the cross-section of plasma spray Stellite-6 coating on the superalloy Superni 718.	115
<b>Fig. 5.1</b>	Macrographs of the uncoated superalloys subjected to cyclic oxidation in air at 900 <sup>0</sup> C for 50 cycles (a) Superni 75      (b) Superni 600      (c) Superni 601 (d) Superni 718      (e) Superfer 800H.	121
<b>Fig. 5.2</b>	Weight gain vs. number of cycles plot for the uncoated superalloys subjected to cyclic oxidation for 50 cycles in air at 900 <sup>0</sup> C.	122
<b>Fig. 5.3</b>	(Weight gain/area) <sup>2</sup> vs. number of cycles plot for the uncoated superalloys subjected to cyclic oxidation for 50 cycles in air at 900 <sup>0</sup> C.	122
<b>Fig. 5.4</b>	SEM back scattered image for the uncoated superalloys after cyclic oxidation in air at 900 <sup>0</sup> C (a) Superni 75      (b) Superni 601      (c) Superni 718 (d) Superfer 800H.	123
<b>Fig. 5.5</b>	X-ray diffraction patterns for the uncoated superalloys subjected to cyclic oxidation in air at 900 <sup>0</sup> C after 50 cycles (a) Superni 75      (b) Superni 600      (c) Superni 601.	126
<b>Fig. 5.6</b>	X-ray diffraction patterns for the uncoated superalloys subjected to cyclic oxidation in air at 900 <sup>0</sup> C after 50 cycles (a) Superni 718      (b) Superfer 800H.	127
<b>Fig. 5.7</b>	Surface scale morphology and EDAX analysis for the uncoated superalloys subjected to cyclic oxidation in air at 900 <sup>0</sup> C for 50 cycles (a) Superni 75      (b) Superni 600      (c) Superni 601.	128
<b>Fig. 5.8</b>	Surface scale morphology and EDAX analysis for the uncoated superalloys subjected to cyclic oxidation in air at 900 <sup>0</sup> C for 50 cycles (a) Superni 718      (b) Superfer 800H.	129

<b>Fig. 5.9</b>	Oxide scale morphology and variation of elemental composition across the cross-section of superalloy Superni 600 subjected to cyclic oxidation in air at 900°C after 50 cycles.	130
<b>Fig. 5.10</b>	BSEI and X-ray mappings of the cross-section of Superni 75 subjected to cyclic oxidation at 900°C in air after 50 cycles.	131
<b>Fig. 5.11</b>	BSEI and X-ray mappings of the cross-section of Superni 600 subjected to cyclic oxidation at 900°C in air after 50 cycles.	132
<b>Fig. 5.12</b>	BSEI and X-ray mappings of the cross-section of Superni 601 subjected to cyclic oxidation at 900°C in air after 50 cycles.	133
<b>Fig. 5.13</b>	BSEI and X-ray mappings of the cross-section of Superni 718 subjected to cyclic oxidation at 900°C in air after 50 cycles.	134
<b>Fig. 5.14</b>	BSEI and X-ray mappings of the cross-section of Superfer 800H subjected to cyclic oxidation at 900°C in air after 50 cycles.	135
<b>Fig. 5.15</b>	Macrographs of the NiCrAlY coating with bond coat subjected to cyclic oxidation in air at 900°C for 50 cycles having substrate superalloys (a) Superni 75      (b) Superni 600      (c) Superni 601 (d) Superni 718      (e) Superfer 800H.	138
<b>Fig. 5.16</b>	Weight gain vs. number of cycles plots for uncoated and NiCrAlY coated superalloys subjected to cyclic oxidation for 50 cycles in air at 900°C.	139
<b>Fig. 5.17</b>	(Weight gain/area) <sup>2</sup> vs. number of cycles plots for the NiCrAlY coated superalloys subjected to cyclic oxidation for 50 cycles in air at 900°C.	140
<b>Fig. 5.18</b>	SEM back scattered images for the NiCrAlY coated superalloys after cyclic oxidation in air for 50 cycles at 900°C (a) Superni 600   (b) Superni 718   (c) Superfer 800H.	141

<b>Fig. 5.19</b>	X-ray diffraction patterns for the NiCrAlY coated superalloys subjected to cyclic oxidation in air at 900°C after 50 cycles.	142
<b>Fig. 5.20</b>	Surface scale morphology and EDAX analysis for the plasma sprayed NiCrAlY coated superalloys subjected to cyclic oxidation in air at 900°C for 50 cycles (a) Superni 75 (b) Superni 600 (c) Superni 601.	145
<b>Fig. 5.21</b>	Surface scale morphology and EDAX analysis for the plasma sprayed NiCrAlY coated superalloys subjected to cyclic oxidation in air at 900°C for 50 cycles (a) Superni 718 (b) Superfer 800H.	146
<b>Fig. 5.22</b>	Oxide scale morphology and variation of elemental composition across the cross-section of NiCrAlY coated superalloys subjected to cyclic oxidation in air at 900°C after 50 cycles (a) Superni 75 (b) Superni 601.	147
<b>Fig. 5.23</b>	BSEI and X-ray mappings of the cross-section of NiCrAlY coated superalloy Superni 75 subjected to cyclic oxidation at 900°C in air after 50 cycles.	148
<b>Fig. 5.24</b>	BSEI and X-ray mappings of the cross-section of NiCrAlY coated superalloy Superni 600 subjected to cyclic oxidation at 900°C in air after 50 cycles.	149
<b>Fig. 5.25</b>	BSEI and X-ray mappings of the cross-section of NiCrAlY coated superalloy Superni 601 subjected to cyclic oxidation at 900°C in air after 50 cycles.	150
<b>Fig. 5.26</b>	BSEI and X-ray mappings of the cross-section of NiCrAlY coated superalloy Superni 718 subjected to cyclic oxidation at 900°C in air after 50 cycles.	151
<b>Fig. 5.27</b>	BSEI and X-ray mappings of the cross-section of NiCrAlY coated superalloy Superfer 800H subjected to cyclic oxidation at 900°C in air after 50 cycles.	152
<b>Fig. 5.28</b>	Macrographs of the Ni-20Cr coating with bond coat subjected to cyclic oxidation in air at 900°C for 50 cycles having substrate superalloys (a) Superni 75 (b) Superni 600 (c) Superni 601 (d) Superni 718 (e) Superfer 800H.	157

<b>Fig. 5.29</b>	Weight gain vs. number of cycles plots for uncoated and Ni-20Cr coated superalloys subjected to cyclic oxidation for 50 cycles in air at 900°C.	158
<b>Fig. 5.30</b>	(Weight gain/area) <sup>2</sup> vs. number of cycles plots for the Ni-20Cr coated superalloys subjected to cyclic oxidation for 50 cycles in air at 900°C.	159
<b>Fig. 5.31</b>	SEM back scattered images for the Ni-20Cr coated superalloy Superni 718 after cyclic oxidation in air for 50 cycles at 900°C.	159
<b>Fig. 5.32</b>	X-ray diffraction patterns for the Ni-20Cr coated superalloys subjected to cyclic oxidation in air at 900°C after 50 cycles.	160
<b>Fig. 5.33</b>	Surface scale morphology and EDAX analysis for the plasma sprayed Ni-20Cr coated superalloys subjected to cyclic oxidation in air at 900°C for 50 cycles (a) Superni 75 (b) Superni 600 (c) Superni 601.	161
<b>Fig. 5.34</b>	Surface scale morphology and EDAX analysis for the plasma sprayed Ni-20Cr coated superalloys subjected to cyclic oxidation in air at 900°C for 50 cycles (a) Superni 718 (b) Superfer 800H.	162
<b>Fig. 5.35</b>	Oxide scale morphology and variation of elemental composition across the cross-section of Ni-20Cr coated superalloys subjected to cyclic oxidation in air at 900°C after 50 cycles (a) Superni 75 (b) Superni 600.	163
<b>Fig. 5.36</b>	Oxide scale morphology and variation of elemental composition across the cross-section of Ni-20Cr coated superalloys subjected to cyclic oxidation in air at 900°C after 50 cycles (a) Superni 601 (b) Superfer 800H.	164
<b>Fig. 5.37</b>	BSEI and X-ray mappings of the cross-section of Ni-20Cr coated superalloy Superni 75 subjected to cyclic oxidation at 900°C in air after 50 cycles.	165



<b>Fig. 5.38</b>	BSEI and X-ray mappings of the cross-section of Ni-20Cr coated superalloy Superni 600 subjected to cyclic oxidation at 900°C in air after 50 cycles.	166
<b>Fig. 5.39</b>	BSEI and X-ray mappings of the cross-section of Ni-20Cr coated superalloy Superni 601 subjected to cyclic oxidation at 900°C in air after 50 cycles.	167
<b>Fig. 5.40</b>	BSEI and X-ray mappings of the cross-section of Ni-20Cr coated superalloy Superni 718 subjected to cyclic oxidation at 900°C in air after 50 cycles.	168
<b>Fig. 5.41</b>	BSEI and X-ray mappings of the cross-section of Ni-20Cr coated superalloy Superfer 800H subjected to cyclic oxidation at 900°C in air after 50 cycles.	169
<b>Fig. 5.42</b>	Macrographs of the Ni <sub>3</sub> Al coating with bond coat subjected to cyclic oxidation in air at 900°C for 50 cycles having substrate superalloys (a) Superni 75      (b) Superni 600      (c) Superni 601 (d) Superni 718      (e) Superfer 800H.	172
<b>Fig. 5.43</b>	Weight gain vs. number of cycles plots for uncoated and Ni <sub>3</sub> Al coated superalloys subjected to cyclic oxidation for 50 cycles in air at 900°C.	173
<b>Fig. 5.44</b>	(Weight gain/area) <sup>2</sup> vs. number of cycles plots for the Ni <sub>3</sub> Al coated superalloys subjected to cyclic oxidation for 50 cycles in air at 900°C.	174
<b>Fig. 5.45</b>	SEM back scattered images for the Ni <sub>3</sub> Al coated superalloys after cyclic oxidation in air for 50 cycles at 900°C (a) Superni 600    (b) Superni 601    (c) Superni 718.	175
<b>Fig. 5.46</b>	X-ray diffraction patterns for the Ni <sub>3</sub> Al coated superalloys subjected to cyclic oxidation in air at 900°C after 50 cycles.	176
<b>Fig. 5.47</b>	Surface scale morphology and EDAX analysis for the plasma sprayed Ni <sub>3</sub> Al coated superalloys subjected to cyclic oxidation in air at 900°C for 50 cycles (a) Superni 75 (b) Superni 600 (c) Superni 601.	177

<b>Fig. 5.48</b>	Surface scale morphology and EDAX analysis for the plasma sprayed Ni <sub>3</sub> Al coated superalloys subjected to cyclic oxidation in air at 900°C for 50 cycles (a) Superni 718 (b) Superfer 800H.	178
<b>Fig. 5.49</b>	Oxide scale morphology and variation of elemental composition across the cross-section of Ni <sub>3</sub> Al coated superalloys subjected to cyclic oxidation in air at 900°C after 50 cycles (a) Superni 75 (b) Superfer 800H.	179
<b>Fig. 5.50</b>	BSEI and X-ray mappings of the cross-section of Ni <sub>3</sub> Al coated superalloy Superni 75 subjected to cyclic oxidation at 900°C in air after 50 cycles.	184
<b>Fig. 5.51</b>	BSEI and X-ray mappings of the cross-section of Ni <sub>3</sub> Al coated superalloy Superni 600 subjected to cyclic oxidation at 900°C in air after 50 cycles.	185
<b>Fig. 5.52</b>	BSEI and X-ray mappings of the cross-section of Ni <sub>3</sub> Al coated superalloy Superni 601 subjected to cyclic oxidation at 900°C in air after 50 cycles.	186
<b>Fig. 5.53</b>	BSEI and X-ray mappings of the cross-section of Ni <sub>3</sub> Al coated superalloy Superni 718 subjected to cyclic oxidation at 900°C in air after 50 cycles.	187
<b>Fig. 5.54</b>	BSEI and X-ray mappings of the cross-section of Ni <sub>3</sub> Al coated superalloy Superfer 800H subjected to cyclic oxidation at 900°C in air after 50 cycles.	188
<b>Fig. 5.55</b>	Macrographs of the Stellite-6 coating with bond coat subjected to cyclic oxidation in air at 900°C for 50 cycles having substrate superalloys (a) Superni 75 (b) Superni 600 (c) Superni 601 (d) Superni 718 (e) Superfer 800H.	189
<b>Fig. 5.56</b>	Weight gain vs. number of cycles plots for uncoated and Stellite-6 coated superalloys subjected to cyclic oxidation for 50 cycles in air at 900°C.	190
<b>Fig. 5.57</b>	(Weight gain/area) <sup>2</sup> vs. number of cycles plots for the Stellite-6 coated superalloys subjected to cyclic oxidation for 50 cycles in air at 900°C.	191

<b>Fig. 5.58</b>	SEM back scattered images for the Stellite-6 coated superalloys after cyclic oxidation in air for 50 cycles at 900°C (a) Superni 600 (b) Superfer 800H.	192
<b>Fig. 5.59</b>	X-ray diffraction patterns for the Stellite-6 coated superalloys subjected to cyclic oxidation in air at 900°C after 50 cycles.	193
<b>Fig. 5.60</b>	Surface scale morphology and EDAX analysis for the plasma sprayed Stellite-6 coated superalloys subjected to cyclic oxidation in air at 900°C for 50 cycles (a) Superni 75 (b) Superni 600 (c) Superni 601.	194
<b>Fig. 5.61</b>	Surface scale morphology and EDAX analysis for the plasma sprayed Stellite-6 coated superalloys subjected to cyclic oxidation in air at 900°C for 50 cycles (a) Superni 718 (b) Superfer 800H.	195
<b>Fig. 5.62</b>	Oxide scale morphology and variation of elemental composition across the cross-section of Stellite-6 coated superalloys subjected to cyclic oxidation in air at 900°C after 50 cycles (a) Superni 75 (b) Superni 601.	196
<b>Fig. 5.63</b>	Oxide scale morphology and variation of elemental composition across the cross-section of Stellite-6 coated superalloy Superni 718 subjected to cyclic oxidation in air at 900°C after 50 cycles.	199
<b>Fig. 5.64</b>	BSEI and X-ray mappings of the cross-section of Stellite-6 coated superalloy Superni 75 subjected to cyclic oxidation at 900°C in air after 50 cycles.	200
<b>Fig. 5.65</b>	BSEI and X-ray mappings of the cross-section of Stellite-6 coated superalloy Superni 600 subjected to cyclic oxidation at 900°C in air after 50 cycles.	201
<b>Fig. 5.66</b>	BSEI and X-ray mappings of the cross-section of Stellite-6 coated superalloy Superni 601 subjected to cyclic oxidation at 900°C in air after 50 cycles.	202

<b>Fig. 5.67</b>	BSEI and X-ray mappings of the cross-section of Stellite-6 coated superalloy Superni 718 subjected to cyclic oxidation at 900°C in air after 50 cycles.	203
<b>Fig. 5.68</b>	BSEI and X-ray mappings of the cross-section of Stellite-6 coated superalloy Superfer 800H subjected to cyclic oxidation at 900°C in air after 50 cycles.	204
<b>Fig. 5.69</b>	Schematic diagram showing probable oxidation mechanism for the uncoated superalloy Superni 600 exposed to air at 900°C for 50 cycles.	211
<b>Fig. 5.70</b>	Schematic diagram showing probable oxidation mode for the NiCrAlY coated Superni 75 exposed to air at 900°C for 50 cycles.	214
<b>Fig. 5.71</b>	Schematic diagram showing probable oxidation mode for the Ni-20Cr coated Superni 718 exposed to air at 900°C for 50 cycles.	217
<b>Fig. 5.72</b>	Schematic diagram showing probable oxidation mode for the Ni <sub>3</sub> Al coated Superni 601 exposed to air at 900°C for 50 cycles.	220
<b>Fig. 5.73</b>	Schematic diagram showing probable oxidation mode for the Stellite-6 coated Superfer 800H exposed to air at 900°C for 50 cycles.	222
<b>Fig. 6.1</b>	Macrographs of the uncoated superalloys subjected to cyclic oxidation in Na <sub>2</sub> SO <sub>4</sub> -60%V <sub>2</sub> O <sub>5</sub> at 900°C for 50 cycles (a) Superni 75            (b) Superni 600    (c) Superni 601 (d) Superni 718        (e) Superfer 800H.	225
<b>Fig. 6.2</b>	Weight gain vs. number of cycles plot for the uncoated superalloys subjected to cyclic oxidation for 50 cycles in Na <sub>2</sub> SO <sub>4</sub> -60%V <sub>2</sub> O <sub>5</sub> at 900°C.	226
<b>Fig. 6.3</b>	(Weight gain/area) <sup>2</sup> vs. number of cycles plot for the uncoated superalloys subjected to cyclic oxidation for 50 cycles in Na <sub>2</sub> SO <sub>4</sub> -60%V <sub>2</sub> O <sub>5</sub> at 900°C.	226

<b>Fig. 6.4</b>	SEM back scattered image for the uncoated superalloys after cyclic oxidation in $\text{Na}_2\text{SO}_4$ -60% $\text{V}_2\text{O}_5$ for 50 cycles at 900°C (a) Superni 75      (b) Superni 600      (c) Superni 601 (d) Superni 718      (e) Superfer 800H.	229
<b>Fig. 6.5</b>	X-ray diffraction patterns for the uncoated superalloys subjected to cyclic oxidation in $\text{Na}_2\text{SO}_4$ -60% $\text{V}_2\text{O}_5$ at 900°C after 50 cycles.	230
<b>Fig. 6.6</b>	X-ray diffraction patterns for the uncoated superalloys subjected to cyclic oxidation in $\text{Na}_2\text{SO}_4$ -60% $\text{V}_2\text{O}_5$ at 900°C after 50 cycles (a) Superni 718      (b) Superfer 800H.	231
<b>Fig. 6.7</b>	Surface scale morphology and EDAX analysis for the uncoated superalloys subjected to cyclic oxidation in $\text{Na}_2\text{SO}_4$ -60% $\text{V}_2\text{O}_5$ at 900°C for 50 cycles (a) Superni 75      (b) Superni 600      (c) Superni 601.	232
<b>Fig. 6.8</b>	Surface scale morphology and EDAX analysis for the uncoated superalloys subjected to cyclic oxidation in $\text{Na}_2\text{SO}_4$ -60% $\text{V}_2\text{O}_5$ at 900°C for 50 cycles (a) Superni 718      (b) Superfer 800H.	233
<b>Fig. 6.9</b>	Oxide scale morphology and variation of elemental composition across the cross-section of uncoated superalloy Superni 718 subjected to cyclic oxidation in $\text{Na}_2\text{SO}_4$ -60% $\text{V}_2\text{O}_5$ at 900°C after 50 cycles.	234
<b>Fig. 6.10</b>	BSEI and X-ray mappings of the cross-section of Superni 75 subjected to cyclic oxidation in $\text{Na}_2\text{SO}_4$ -60% $\text{V}_2\text{O}_5$ at 900°C after 50 cycles.	237
<b>Fig. 6.11</b>	BSEI and X-ray mappings of the cross-section of Superni 600 subjected to cyclic oxidation in $\text{Na}_2\text{SO}_4$ -60% $\text{V}_2\text{O}_5$ at 900°C after 50 cycles.	238
<b>Fig. 6.12</b>	BSEI and X-ray mappings of the cross-section of Superni 601 subjected to cyclic oxidation in $\text{Na}_2\text{SO}_4$ -60% $\text{V}_2\text{O}_5$ at 900°C after 50 cycles.	239

<b>Fig. 6.13</b>	BSEI and X-ray mappings of the cross-section of Superni 718 subjected to cyclic oxidation in Na <sub>2</sub> SO <sub>4</sub> -60%V <sub>2</sub> O <sub>5</sub> at 900°C after 50 cycles.	240
<b>Fig. 6.14</b>	BSEI and X-ray mappings of the cross-section of Superni 800H subjected to cyclic oxidation in Na <sub>2</sub> SO <sub>4</sub> -60%V <sub>2</sub> O <sub>5</sub> at 900°C after 50 cycles.	241
<b>Fig. 6.15</b>	Macrographs of the NiCrAlY coating with bond coat subjected to cyclic oxidation in Na <sub>2</sub> SO <sub>4</sub> -60%V <sub>2</sub> O <sub>5</sub> at 900°C for 50 cycles having substrate superalloys (a) Superni 75      (b) Superni 600      (c) Superni 601 (d) Superni 718      (e) Superfer 800H.	242
<b>Fig. 6.16</b>	Weight gain vs. number of cycles plot for uncoated and NiCrAlY coated superalloys subjected to cyclic oxidation for 50 cycles in Na <sub>2</sub> SO <sub>4</sub> -60%V <sub>2</sub> O <sub>5</sub> at 900°C.	245
<b>Fig. 6.17</b>	(Weight gain/area) <sup>2</sup> vs. number of cycles plot for the NiCrAlY coated superalloys subjected to cyclic oxidation for 50 cycles in Na <sub>2</sub> SO <sub>4</sub> -60%V <sub>2</sub> O <sub>5</sub> at 900°C.	246
<b>Fig. 6.18</b>	SEM back scattered images for the NiCrAlY coated superalloys after cyclic oxidation in Na <sub>2</sub> SO <sub>4</sub> -60%V <sub>2</sub> O <sub>5</sub> for 50 cycles at 900°C: (a) Superni 75      (b) Superni 601      (c) Superni 718.	247
<b>Fig. 6.19</b>	X-ray diffraction patterns for the NiCrAlY coated superalloys subjected to cyclic oxidation in Na <sub>2</sub> SO <sub>4</sub> -60%V <sub>2</sub> O <sub>5</sub> at 900°C after 50 cycles.	248
<b>Fig. 6.20</b>	Surface scale morphology and EDAX analysis for the plasma spray NiCrAlY coated superalloys subjected to cyclic oxidation in Na <sub>2</sub> SO <sub>4</sub> -60%V <sub>2</sub> O <sub>5</sub> at 900°C for 50 cycles (a) Superni 75      (b) Superni 600      (c) Superni 601.	249
<b>Fig. 6.21</b>	Surface scale morphology and EDAX analysis for the plasma spray NiCrAlY coated superalloys subjected to cyclic oxidation in Na <sub>2</sub> SO <sub>4</sub> -60%V <sub>2</sub> O <sub>5</sub> at 900°C for 50 cycles (a) Superni 718      (b) Superfer 800H.	250

<b>Fig. 6.22</b>	Oxide scale morphology and variation of elemental composition across the cross-section of NiCrAlY coated superalloys subjected to cyclic oxidation in Na <sub>2</sub> SO <sub>4</sub> -60%V <sub>2</sub> O <sub>5</sub> at 900°C after 50 cycles (a) Superni 600      (b) Superfer 800H.	253
<b>Fig. 6.23</b>	BSEI and X-ray mappings of the cross-section of NiCrAlY coated superalloy Superni 75 subjected to cyclic oxidation in Na <sub>2</sub> SO <sub>4</sub> -60%V <sub>2</sub> O <sub>5</sub> at 900°C after 50 cycles.	254
<b>Fig. 6.24</b>	BSEI and X-ray mappings of the cross-section of NiCrAlY coated superalloy Superni 75 subjected to cyclic oxidation in Na <sub>2</sub> SO <sub>4</sub> -60%V <sub>2</sub> O <sub>5</sub> at 900°C after 50 cycles showing oxygen distribution also.	255
<b>Fig. 6.25</b>	BSEI and X-ray mappings of the cross-section of NiCrAlY coated superalloy Superni 600 subjected to cyclic oxidation in Na <sub>2</sub> SO <sub>4</sub> -60%V <sub>2</sub> O <sub>5</sub> at 900°C after 50 cycles.	256
<b>Fig. 6.26</b>	BSEI and X-ray mappings of the cross-section of NiCrAlY coated superalloy Superni 601 subjected to cyclic hot corrosion at 900°C in Na <sub>2</sub> SO <sub>4</sub> -60%V <sub>2</sub> O <sub>5</sub> after 50 cycles.	257
<b>Fig. 6.27</b>	BSEI and X-ray mappings of the cross-section of NiCrAlY coated superalloy Superni 718 subjected to cyclic hot corrosion at 900°C in Na <sub>2</sub> SO <sub>4</sub> -60%V <sub>2</sub> O <sub>5</sub> after 50 cycles.	260
<b>Fig. 6.28</b>	BSEI and X-ray mappings of the cross-section of NiCrAlY coated superalloy Superfer 800H subjected to cyclic hot corrosion at 900°C in Na <sub>2</sub> SO <sub>4</sub> -60%V <sub>2</sub> O <sub>5</sub> after 50 cycles.	261
<b>Fig. 6.29</b>	Macrographs of the Ni-20Cr coating with bond coat subjected to cyclic oxidation in Na <sub>2</sub> SO <sub>4</sub> -60%V <sub>2</sub> O <sub>5</sub> at 900°C for 50 cycles having substrate superalloys (a) Superni 75      (b) Superni 600      (c) Superni 601 (d) Superni 718      (e) Superfer 800H.	262

<b>Fig. 6.30</b>	Weight gain vs. number of cycles plot for uncoated and Ni-20Cr coated superalloys subjected to cyclic oxidation for 50 cycles in Na <sub>2</sub> SO <sub>4</sub> -60%V <sub>2</sub> O <sub>5</sub> at 900°C.	263
<b>Fig. 6.31</b>	(Weight gain/area) <sup>2</sup> vs. number of cycles plot for the Ni-20Cr coated superalloys subjected to cyclic oxidation for 50 cycles in Na <sub>2</sub> SO <sub>4</sub> -60%V <sub>2</sub> O <sub>5</sub> at 900°C.	264
<b>Fig. 6.32</b>	X-ray diffraction patterns for the Ni-20Cr coated superalloys subjected to cyclic oxidation in Na <sub>2</sub> SO <sub>4</sub> -60%V <sub>2</sub> O <sub>5</sub> at 900°C after 50 cycles.	269
<b>Fig. 6.33</b>	Surface scale morphology and EDAX analysis for the plasma spray Ni-20Cr coated superalloys subjected to cyclic oxidation in Na <sub>2</sub> SO <sub>4</sub> -60%V <sub>2</sub> O <sub>5</sub> at 900°C for 50 cycles (a) Superni 75      (b) Superni 600      (c) Superni 601.	270
<b>Fig. 6.34</b>	Surface scale morphology and EDAX analysis for the plasma spray Ni-20Cr coated superalloys subjected to cyclic oxidation in Na <sub>2</sub> SO <sub>4</sub> -60%V <sub>2</sub> O <sub>5</sub> at 900°C for 50 cycles (a) Superni 718      (b) Superfer 800H.	271
<b>Fig. 6.35</b>	Oxide scale morphology and variation of elemental composition across the cross-section of Ni-20Cr coated superalloys subjected to cyclic oxidation in Na <sub>2</sub> SO <sub>4</sub> -60%V <sub>2</sub> O <sub>5</sub> at 900°C after 50 cycles (a) Superni 75      (b) Superni 600.	272
<b>Fig. 6.36</b>	Oxide scale morphology and variation of elemental composition across the cross-section of Ni-20Cr coated superalloys subjected to cyclic oxidation in Na <sub>2</sub> SO <sub>4</sub> -60%V <sub>2</sub> O <sub>5</sub> at 900°C after 50 cycles (a) Superni 601      (b) Superni 718.	273
<b>Fig. 6.37</b>	Oxide scale morphology and variation of elemental composition across the cross-section of Ni-20Cr coated superalloy Superfer 800H subjected to cyclic oxidation in Na <sub>2</sub> SO <sub>4</sub> -60%V <sub>2</sub> O <sub>5</sub> at 900°C after 50 cycles.	274



Fig. 6.38	BSEI and X-ray mappings of the cross-section of Ni-20Cr coated superalloy Superni 75 subjected to cyclic oxidation in Na <sub>2</sub> SO <sub>4</sub> -60%V <sub>2</sub> O <sub>5</sub> at 900°C after 50 cycles.	275
Fig. 6.39	BSEI and X-ray mappings of the cross-section of Ni-20Cr coated superalloy Superni 600 subjected to cyclic oxidation in Na <sub>2</sub> SO <sub>4</sub> -60%V <sub>2</sub> O <sub>5</sub> at 900°C after 50 cycles.	276
Fig. 6.40	BSEI and X-ray mappings of the cross-section of Ni-20Cr coated superalloy Superni 600 subjected to cyclic oxidation in Na <sub>2</sub> SO <sub>4</sub> -60%V <sub>2</sub> O <sub>5</sub> at 900°C after 50 cycles showing oxygen distribution also.	277
Fig. 6.41	BSEI and X-ray mappings of the cross-section of Ni-20Cr coated superalloy Superni 601 subjected to cyclic oxidation in Na <sub>2</sub> SO <sub>4</sub> -60%V <sub>2</sub> O <sub>5</sub> at 900°C after 50 cycles.	278
Fig. 6.42	BSEI and X-ray mappings of the cross-section of Ni-20Cr coated superalloy Superni 718 subjected to cyclic oxidation in Na <sub>2</sub> SO <sub>4</sub> -60%V <sub>2</sub> O <sub>5</sub> at 900°C after 50 cycles.	281
Fig. 6.43	BSEI and X-ray mappings of the cross-section of Ni-20Cr coated superalloy Superfer 800H subjected to cyclic oxidation in Na <sub>2</sub> SO <sub>4</sub> -60%V <sub>2</sub> O <sub>5</sub> at 900°C after 50 cycles.	282
Fig. 6.44	Macrographs of the Ni <sub>3</sub> Al coating with bond coat subjected to cyclic oxidation in Na <sub>2</sub> SO <sub>4</sub> -60%V <sub>2</sub> O <sub>5</sub> at 900°C for 50 cycles having substrate superalloys (a) Superni 75            (b) Superni 600    (c) Superni 601 (d) Superni 718        (e) Superfer 800H.	283
Fig. 6.45	Weight gain vs. number of cycles plot for uncoated and Ni <sub>3</sub> Al coated superalloys subjected to cyclic oxidation for 50 cycles in Na <sub>2</sub> SO <sub>4</sub> -60%V <sub>2</sub> O <sub>5</sub> at 900°C.	284
Fig. 6.46	(Weight gain/area) <sup>2</sup> vs. number of cycles plot for the Ni <sub>3</sub> Al coated superalloys subjected to cyclic oxidation for 50 cycles in Na <sub>2</sub> SO <sub>4</sub> -60%V <sub>2</sub> O <sub>5</sub> at 900°C.	285

<b>Fig. 6.47</b>	SEM back scattered images for the Ni <sub>3</sub> Al coated superalloys after cyclic oxidation in Na <sub>2</sub> SO <sub>4</sub> -60%V <sub>2</sub> O <sub>5</sub> for 50 cycles at 900 <sup>0</sup> C (a) Superni 75                      (b) Superni 601.	290
<b>Fig. 6.48</b>	X-ray diffraction patterns for the Ni <sub>3</sub> Al coated superalloys subjected to cyclic oxidation in Na <sub>2</sub> SO <sub>4</sub> -60%V <sub>2</sub> O <sub>5</sub> at 900 <sup>0</sup> C after 50 cycles.	291
<b>Fig. 6.49</b>	Surface scale morphology and EDAX analysis for the plasma spray Ni <sub>3</sub> Al coated superalloys subjected to cyclic oxidation in Na <sub>2</sub> SO <sub>4</sub> -60%V <sub>2</sub> O <sub>5</sub> at 900 <sup>0</sup> C for 50 cycles (a) Superni 75      (b) Superni 600      (c) Superni 601.	292
<b>Fig. 6.50</b>	Surface scale morphology and EDAX analysis for the plasma spray Ni <sub>3</sub> Al coated superalloys subjected to cyclic oxidation in Na <sub>2</sub> SO <sub>4</sub> -60%V <sub>2</sub> O <sub>5</sub> at 900 <sup>0</sup> C for 50 cycles (a) Superni 718      (b) Superfer 800H.	293
<b>Fig. 6.51</b>	Oxide scale morphology and variation of elemental composition across the cross-section of Ni <sub>3</sub> Al coated superalloys subjected to cyclic oxidation in Na <sub>2</sub> SO <sub>4</sub> -60%V <sub>2</sub> O <sub>5</sub> at 900 <sup>0</sup> C after 50 cycles (a) Superni 75      (b) Superni 600.	294
<b>Fig. 6.52</b>	Oxide scale morphology and variation of elemental composition across the cross-section of Ni <sub>3</sub> Al coated superalloys subjected to cyclic oxidation in Na <sub>2</sub> SO <sub>4</sub> -60%V <sub>2</sub> O <sub>5</sub> at 900 <sup>0</sup> C after 50 cycles (a) Superni 718      (b) Superfer 800H.	295
<b>Fig. 6.53</b>	BSEI and X-ray mappings of the cross-section of Ni <sub>3</sub> Al coated superalloy Superni 75 subjected to cyclic oxidation in Na <sub>2</sub> SO <sub>4</sub> -60%V <sub>2</sub> O <sub>5</sub> at 900 <sup>0</sup> C after 50 cycles.	296
<b>Fig. 6.54</b>	BSEI and X-ray mappings of the cross-section of Ni <sub>3</sub> Al coated superalloy Superni 600 subjected to cyclic oxidation in Na <sub>2</sub> SO <sub>4</sub> -60%V <sub>2</sub> O <sub>5</sub> at 900 <sup>0</sup> C after 50 cycles.	297

<b>Fig. 6.55</b>	BSEI and X-ray mappings of the cross-section of Ni <sub>3</sub> Al coated superalloy Superni 601 subjected to cyclic oxidation in Na <sub>2</sub> SO <sub>4</sub> -60%V <sub>2</sub> O <sub>5</sub> at 900°C after 50 cycles.	298
<b>Fig. 6.56</b>	BSEI and X-ray mappings of the cross-section of Ni <sub>3</sub> Al coated superalloy Superni 718 subjected to cyclic oxidation in Na <sub>2</sub> SO <sub>4</sub> -60%V <sub>2</sub> O <sub>5</sub> at 900°C after 50 cycles.	299
<b>Fig. 6.57</b>	BSEI and X-ray mappings of the cross-section of Ni <sub>3</sub> Al coated superalloy Superfer 800H subjected to cyclic oxidation in Na <sub>2</sub> SO <sub>4</sub> -60%V <sub>2</sub> O <sub>5</sub> at 900°C after 50 cycles.	300
<b>Fig. 6.58</b>	Macrographs of the Stellite-6 coating with bond coat subjected to cyclic oxidation in Na <sub>2</sub> SO <sub>4</sub> -60%V <sub>2</sub> O <sub>5</sub> at 900°C for 50 cycles having substrate superalloys (a) Superni 75      (b) Superni 600      (c) Superni 601 (d) Superni 718      (e) Superfer 800H.	305
<b>Fig. 6.59</b>	Weight gain vs. number of cycles plot for uncoated and Stellite-6 coated superalloys subjected to cyclic oxidation for 50 cycles in Na <sub>2</sub> SO <sub>4</sub> -60%V <sub>2</sub> O <sub>5</sub> at 900°C.	306
<b>Fig. 6.60</b>	(Weight gain/area) <sup>2</sup> vs. number of cycles plot for the Stellite-6 coated superalloys subjected to cyclic oxidation for 50 cycles in Na <sub>2</sub> SO <sub>4</sub> -60%V <sub>2</sub> O <sub>5</sub> at 900°C.	307
<b>Fig. 6.61</b>	X-ray diffraction patterns for the Stellite-6 coated superalloys subjected to cyclic oxidation in Na <sub>2</sub> SO <sub>4</sub> -60%V <sub>2</sub> O <sub>5</sub> at 900°C after 50 cycles.	308
<b>Fig. 6.62</b>	Surface scale morphology and EDAX analysis for the plasma spray Stellite-6 coated superalloys subjected to cyclic oxidation in Na <sub>2</sub> SO <sub>4</sub> -60%V <sub>2</sub> O <sub>5</sub> at 900°C for 50 cycles (a) Superni 75      (b) Superni 600      (c) Superni 601.	309
<b>Fig. 6.63</b>	Surface scale morphology and EDAX analysis for the plasma spray Stellite-6 coated superalloys subjected to cyclic oxidation in Na <sub>2</sub> SO <sub>4</sub> -60%V <sub>2</sub> O <sub>5</sub> at 900°C for 50 cycles (a) Superni 718      (b) Superfer 800H.	310

<b>Fig. 6.64</b>	Oxide scale morphology and variation of elemental composition across the cross-section of Stellite-6 coated superalloys subjected to cyclic oxidation in Na <sub>2</sub> SO <sub>4</sub> -60%V <sub>2</sub> O <sub>5</sub> at 900°C after 50 cycles (a) Superni 75      (b) Superni 600.	311
<b>Fig. 6.65</b>	Oxide scale morphology and variation of elemental composition across the cross-section of Stellite-6 coated superalloys subjected to cyclic oxidation in Na <sub>2</sub> SO <sub>4</sub> -60%V <sub>2</sub> O <sub>5</sub> at 900°C after 50 cycles (a) Superni 601      (b) Superni 718.	312
<b>Fig. 6.66</b>	Oxide scale morphology and variation of elemental composition across the cross-section of Stellite-6 coated superalloy Superfer 800H subjected to cyclic oxidation in Na <sub>2</sub> SO <sub>4</sub> -60%V <sub>2</sub> O <sub>5</sub> at 900°C after 50 cycles.	313
<b>Fig. 6.67</b>	BSEI and X-ray mappings of the cross-section of Stellite-6 coated superalloy Superni 75 subjected to cyclic oxidation in Na <sub>2</sub> SO <sub>4</sub> -60%V <sub>2</sub> O <sub>5</sub> at 900°C after 50 cycles.	314
<b>Fig. 6.68</b>	BSEI and X-ray mappings of the cross-section of Stellite-6 coated superalloy Superni 600 subjected to cyclic oxidation in Na <sub>2</sub> SO <sub>4</sub> -60%V <sub>2</sub> O <sub>5</sub> at 900°C after 50 cycles.	317
<b>Fig. 6.69</b>	BSEI and X-ray mappings of the cross-section of Stellite-6 coated superalloy Superni 600 subjected to cyclic oxidation in Na <sub>2</sub> SO <sub>4</sub> -60%V <sub>2</sub> O <sub>5</sub> at 900°C after 50 cycles showing oxygen distribution also.	318
<b>Fig. 6.70</b>	BSEI and X-ray mappings of the cross-section of Stellite-6 coated superalloy Superni 601 subjected to cyclic oxidation in Na <sub>2</sub> SO <sub>4</sub> -60%V <sub>2</sub> O <sub>5</sub> at 900°C after 50 cycles.	319
<b>Fig. 6.71</b>	BSEI and X-ray mappings of the cross-section of Stellite-6 coated superalloy Superni 718 subjected to cyclic oxidation in Na <sub>2</sub> SO <sub>4</sub> -60%V <sub>2</sub> O <sub>5</sub> at 900°C after 50 cycles.	320

Fig. 6.72	BSEI and X-ray mappings of the cross-section of Stellite-6 coated superalloy Superfer 800H subjected to cyclic oxidation in $\text{Na}_2\text{SO}_4$ -60% $\text{V}_2\text{O}_5$ at 900°C after 50 cycles.	321
Fig. 6.73	Schematic diagram showing probable hot corrosion mechanism for the uncoated superalloy Superni 718 exposed to $\text{Na}_2\text{SO}_4$ -60% $\text{V}_2\text{O}_5$ at 900°C for 50 cycles.	328
Fig. 6.74	Schematic diagram showing probable hot corrosion mode for the NiCrAlY coated Superni 75 exposed to $\text{Na}_2\text{SO}_4$ -60% $\text{V}_2\text{O}_5$ at 900°C for 50 cycles.	331
Fig. 6.75	Schematic diagram showing probable hot corrosion mode for the Ni-20Cr coated Superni 600 exposed to $\text{Na}_2\text{SO}_4$ -60% $\text{V}_2\text{O}_5$ at 900°C for 50 cycles.	334
Fig. 6.76	Schematic diagram showing probable hot corrosion mode for the $\text{Ni}_3\text{Al}$ coated Superni 718 exposed to $\text{Na}_2\text{SO}_4$ -60% $\text{V}_2\text{O}_5$ at 900°C for 50 cycles.	337
Fig. 6.77	Schematic diagram showing probable hot corrosion mode for the Stellite-6 coated Superni 600 exposed to $\text{Na}_2\text{SO}_4$ -60% $\text{V}_2\text{O}_5$ at 900°C for 50 cycles.	338
Fig. 7.1	Bar charts showing cumulative weight gain ( $\text{mg}/\text{cm}^2$ ) for the coated and uncoated superalloys subjected to cyclic oxidation in air at 900°C for 50 cycles.	341
Fig. 7.2	Bar charts showing cumulative weight gain ( $\text{mg}/\text{cm}^2$ ) for the coated and uncoated superalloys subjected to cyclic oxidation in $\text{Na}_2\text{SO}_4$ -60% $\text{V}_2\text{O}_5$ environment at 900°C for 50 cycles.	341

## LIST OF TABLES

---

<b>Table No.</b>	<b>Particulars</b>	<b>Page No.</b>
<b>Table 2.1</b>	Desirable features for effective coating system (Nicholls, 2000)	39
<b>Table 3.1</b>	Nominal composition and industrial applications of the superalloys used	76
<b>Table 3.2</b>	Parameters of the argon shrouded plasma spray process	77
<b>Table 4.1</b>	Composition, particle size and designation of the coating powders	85
<b>Table 4.2</b>	Average coating thickness and porosity of the plasma sprayed coatings	89
<b>Table 5.1</b>	Summary of the results for coated and uncoated superalloys oxidised in air at 900 <sup>0</sup> C for 50 cycles	205
<b>Table 6.1</b>	Summary of the results for coated and uncoated superalloys oxidised in molten salt (Na <sub>2</sub> SO <sub>4</sub> -60%V <sub>2</sub> O <sub>5</sub> ) at 900 <sup>0</sup> C for 50 cycles	322
<b>Table A.1</b>	Summary of oxidation of Fe-, Ni- & Co- base alloys in air, Na <sub>2</sub> SO <sub>4</sub> and V <sub>2</sub> O <sub>5</sub> environments	351
<b>Table A.2</b>	Thermal expansion coefficients of substrate superalloys, coatings and oxides	362
<b>Table A.3</b>	Chemical composition (Wt%) of the Ni- and Fe-based superalloys and coatings powders, and environmental conditions employed	363

## RESEARCH PAPERS PRESENTED/PUBLISHED

---

1. **Singh, H., Puri, D. and Prakash, S.,** (2005), "Some Studies on Hot Corrosion Performance of Plasma Sprayed Coatings on a Fe-Based Superalloy," *Surf. Coat. Technol.*, Vol. 192, No. 1, pp. 27-38.
2. **Singh, H., Puri, D. and Prakash, S.,** (2005), "Corrosion Behaviour of Plasma Sprayed Coatings on a Ni-base Superalloy in  $\text{Na}_2\text{SO}_4$ -60% $\text{V}_2\text{O}_5$  Environment at  $900^\circ\text{C}$ ," *Metall. Mater. Trans. A*, Vol. 36, No 4, pp. 1007-1015.
3. **Singh, H., Puri, D. and Prakash, S.,** (2005), "Studies of Plasma Spray Coatings on a Fe-base Superalloy, their Structure and High Temperature Oxidation Behaviour," *Anti Corros. Method M.*, Vol. 52, No. 2, pp. 84-95.
4. **Prakash, S., Puri, D. and Singh, H.,** (2005), "Hot Corrosion Behaviour of Plasma Sprayed Coatings on a Ni-Based Superalloy in  $\text{Na}_2\text{SO}_4$  -60% $\text{V}_2\text{O}_5$  environment," *ISIJ Int.*, to be published in Vol.45, No.6.
5. **Singh, H., Puri, D. and Prakash, S.,** (2004), "High Temperature Oxidation Behaviour of Plasma Sprayed NiCrAlY Coatings on Ni-Based Superalloys in Air," *Inter. Sympos. of Research Scholars on 'Mater. Sci. & Eng.'*, Dec., 20-22, IITM, Chennai, INDIA and to be published *Trans. Indian I. Metals*.
6. **Singh, H., Puri, D. and Prakash, S.,** (2004), "An Overview of High Temperature Oxidation of Metals and Alloys," *Indo-Japan Conf. on 'Damage Tolerant Design and Materials'*, Dec., 16-18, IITM, Chennai, Pub. Assoc. Machines and Mechanisms, India, pp.157-162.
7. **Singh, H., Puri, D. and Prakash, S.,** (2004), "Hot Corrosion of Some Superalloys and Role of Plasma Spray Coatings- A Review," 7<sup>th</sup> Punjab Sci. Congress, Feb.7-9, GNDU, Amritsar, INDIA.
8. **Prakash, S., Puri, D. and Singh, H.,** "Cyclic Oxidation Behaviour of Plasma Sprayed Stellite-6 Coated Ni-Base Superalloys in Air and in  $\text{Na}_2\text{SO}_4$  -60% $\text{V}_2\text{O}_5$  Environment," accepted for presentation at 'Materials Degradation: Innovation, Inspection, Control and Rehabilitation Symposium, COM 2005,' to be held on August 21-24, 2005, in Calgary, Alberta Canada.

# ABBREVIATIONS

---

APS	Air Plasma Spray
Bal	Balance
BSEI	Back Scattered Electron Image
EDAX	Energy Dispersive X-ray Analysis
EPMA	Electron Probe Micro Analyser
hr	Hour
HVOF	High Velocity Oxy-Fuel
Kcps	Kilocycles per Second
$K_p$	Parabolic Rate Constant
LPPS	Low Pressure Plasma Spray
m.p.	Melting Point
min	Minute
Ni-20Cr	Ni-20 Wt% Cr
NiCrAlY	Ni-22Cr-10Al-1Y
SEM	Scanning Electron Microscopy
VPS	Vacuum Plasma Spray
Wt%	Weight Percentage
Wt. Gain	Weight Gain.
XRD	X-ray Diffraction



# CHAPTER 1

## INTRODUCTION

---

Corrosion is a natural occurrence commonly defined as the deterioration of a substance (usually metal) or its properties as a consequence of its reaction with the environment. According to a recent study, the total annual estimated direct cost of metallic corrosion in the U.S. is a staggering \$276 billion—approximately 3.1% of the Nation's Gross Domestic Product (GDP). This cost is more than the annual cost of weather related disasters, which is just averaging \$17 billion annually. However, unlike weather related disasters, corrosion can be controlled, but at a cost. The report further revealed that the 25% to 30% of annual corrosion costs in the U.S. could be saved if proper corrosion management practices were employed (Koch et al, 2002). An estimated 40% of total US steel production goes to replacement of corroded parts and products. So far as India is concerned, the corrosion costs may touch Rs. 24000 crore (Rs. 240000 million). This cost is for the materials corrosion in building structures, bridges, chemical plants, offshore platforms, power plants, ships, pipe lines for transportation of hydrocarbon, electrical and electronics components (Gupta, 2003).

Metals and alloys get oxidised when they are heated to elevated temperatures in air or highly oxidising environments, such as a combustion gas with excess of air or oxygen. They often rely on the oxidation reaction to develop a protective oxide scale to resist corrosion attack, such as sulphidation, carburisation, ash/salt deposit corrosion etc. That is why oxidation is considered to be the most important high-temperature corrosion reaction. Further the rate of oxidation for metals and alloys increases with increasing temperature (Lai, 1990).

Hot corrosion is the degradation of materials caused by the presence of a deposit of salt or ash in a general sense. In a more restricted sense, hot corrosion is the degradation of metals and alloys owing to oxidation process, which are affected by a liquid salt deposit. In hot corrosion, metals and alloys are subject to degradation at much higher rates than in gaseous oxidation, with a porous, non-protective oxide scale formed at their surface, and sulphides in the substrate.

Hot corrosion was first recognized as a serious problem in 1940s in connection with the degradation of fireside boiler tubes in coal-fired steam generating plants. Since then the problem has been observed in boilers, internal combustion engines, gas turbines, fluidized bed combustion and industrial waste incinerators. Turbine manufacturers and users became aware of the hot corrosion in the late 1960's when serious corrosive attacks occurred for helicopters and rescue planes in service over and near sea water during Vietnam conflict (Rapp, 1986 and Rapp, 2002).

An excellent review by Stringer covered the work done in the field of hot corrosion up to about 1976 (1977). Most of the work was aimed at developing improved alloys and understanding the hot corrosion processes. Much of the mechanisms proposed during that period were focused on thermochemistry. Bornstein and DeCrescente (1969 and 1971) and Bornstein et al (1973) proposed a hot corrosion mechanism based on the basic dissolution of the protective oxide scale by a reaction involving  $\text{Na}_2\text{O}$ , the basic minority component of the fused salt. Goebel and Pettit (1970A) also interpreted the hot corrosion of pure nickel in terms of basic dissolution and re-precipitation of  $\text{NiO}$  in the fused salt film. Goebel et al (1973) extended this mechanism to include acidic fluxing and oxide reprecipitation to account for the catastrophic oxidation caused by pure  $\text{Na}_2\text{SO}_4$  for alloys containing strong acid components such as vanadium or molybdenum. The next important contribution in the fluxing model was made by Rapp and Goto (1981), who proposed that if the gradient in solubility of the protective oxide with distance into the salt layer becomes negative at the oxide/salt interface, accelerated attack could be sustained. Sodium vanadyl vanadate ( $\text{Na}_2\text{O} \cdot \text{V}_2\text{O}_4 \cdot 5\text{V}_2\text{O}_5$ ), which melts at a relatively low temperature  $550^\circ\text{C}$  is found to be the most common salt deposit on boiler superheaters. Addition of  $\text{Na}_2\text{O}$  to liquid  $\text{V}_2\text{O}_5$  causes an increase in the basicity of the melt with a corresponding increase in corrosivity with respect to the acidic oxides. Moreover,  $\text{Na}_2\text{O}$  has also been reported to decrease the viscosity. Therefore the protective oxides become porous and non-adherent. The formation of binary and tertiary low melting eutectics increase the surface attack thereby reducing the useful life of the component.

Corrosion problems caused by low-quality fuels are often tackled by decreasing the steam temperature in super heaters. For instance, in case of boilers burning low-chlorine fuels, such as coal, the steam temperature is usually limited to  $570^\circ\text{C}$  (Natesan, 1993), whereas boilers combusting high-chlorine fuels, like waste (Kawahara, 1997) or black liquor (Tran et al, 1988) operate with steam temperatures below  $500^\circ\text{C}$ . Unacceptable corrosion rates have occurred when biofuel fired boiler has been operated

with steam temperature of 530°C. These lower steam temperatures drastically decrease the efficiency of electricity production. Furthermore, the high-temperature corrosion caused by such combustion environments is usually an accelerated oxidation or sulphidation process.

Due to depletion of high-grade fuels and for economic reason use of residual fuel oil in these energy generation systems is well known. Residual fuel oil contains sodium, vanadium and sulphur as impurities. Sodium and sulphur form  $\text{Na}_2\text{SO}_4$  (melting point 884°C) by reactions in the combustion system. Whereas during combustion of the fuel, vanadium reacts with oxygen to form an oxide  $\text{V}_2\text{O}_5$  (melting point 670°C). Thus  $\text{V}_2\text{O}_5$  is a liquid at gas turbine operating temperature. These compounds (known as ash) deposit on the surface of the materials and induce accelerated oxidation (hot corrosion) in energy generation systems. When considering coal-gasification processes, hot corrosion is expected to be a problem because the gas environment generally has large sulphur activities and low oxygen activities and also contains substantial amount of salts (Natesan, 1976).

The operating temperatures in case of gas turbines are usually very high, which are expected to increase further with the advances in materials development and cooling schemes for the new-generation gas turbine engines. The combination of such high temperatures with an aircraft environment that contains contaminants such as sodium, sulphur, vanadium and various halides requires special attention to the phenomena of hot corrosion (Eliaz et al, 2002). Moreover, Goward (1998) has suggested that the corrosion in boilers and turbines had much in common.

According to a recent study conducted in U.S. it has been recommended that the U.S. must find more and better ways to encourage, support, and implement optimal corrosion control practices in spite of the fact that corrosion management has improved over the past several decades. Moreover, corrosion prevention and control is critical to protecting public safety and the environment (Koch et al, 2002). A number of countermeasures are currently in use or under investigation to combat different types of corrosion. While selecting a particular corrosion control strategy it is always emphasised that the protection system must be practical, reliable and economically viable. So far as the hot corrosion problem of metals and alloys is concerned, it may be tackled by designing a suitable industrial alloy, controlling the process parameters, use of inhibitors, protective coatings and superficially applied oxides as per requirements in the given environment.

Controlling the various process parameters (air/fuel ratio, temperature, pressure etc.) of the boiler and gas turbine is useful to some extent to combat corrosion, but these parameters can be controlled only within certain limits. There are numerous inhibitors commercially available that are intended to reduce the severity of oil ash corrosion, particularly Mg and Mn-based inhibitors, which have proven to be effective (Paul and Seeley, 1991). Investigations in the area of inhibitors like MgO, CeO<sub>2</sub>, CaO, MnO<sub>2</sub>, etc. have already been done in the department and the decrease in the extent of hot corrosion in the most aggressive environment of Na<sub>2</sub>SO<sub>4</sub>-60%V<sub>2</sub>O<sub>5</sub> at 900<sup>0</sup>C has been achieved. But the major problem being faced is how to inject these inhibitors along with the fuel in the combustion chamber in actual industrial environment (Tiwari and Prakash, 1998 and Gitanjaly et al, 2002).

Abrasion and corrosion resistance of components can be greatly increased by protective coatings and this is a growing industry of considerable economic importance. Coatings are used in both aqueous and high temperature applications. The purpose of these coatings is to form long-lived corrosion protective scales. Coal gasification electric power generation and waste incineration involves severe conditions and thick coatings have proved effective (Hocking, 1993A). This is the preferred approach, even when relatively hot corrosion-resistant base alloys are used. The numerous variants of high temperature coatings that are in use today, may be categorized into three generic types: diffusion, overlay, and thermal barrier coatings (Eliaz et al, 2002). In the service environment, the coating forms an oxide surface layer which ideally inhibits corrosion. To a degree, the oxide surface layer can be selected according to the environment, and the coating is designed to serve as a reservoir for the element forming the surface oxide. The oxide required here are Al<sub>2</sub>O<sub>3</sub>, Cr<sub>2</sub>O<sub>3</sub> and SiO<sub>2</sub> and the coating compositions are selected accordingly to allow these oxides to form in service (Nicoll and Wahl, 1983 and Stroosnijder et al, 1994).

Among the various coating methods plasma spraying fosters progress in both development of materials and modern coating technology because of advances in powder and wire productions. The advanced plasma technique has many advantages such as high productivity for thick coating films of more than 100µm and good applicability for a wide range of coating materials including ceramic powder, further the process does not cause degradation of the mechanical properties of the alloy substrate (Gill and Tucker, 1986 and Nicoll et al, 1986). Plasma spraying is a well established means of forming thick coatings (~300µm) used, for instance, for their resistance to corrosion, oxidation,

and wear; friction, electric, magnetic, and ionic conduction properties; thermal protection; coefficient of thermal expansion tailored to service conditions; and strength with free-standing spray-formed components (Fauchais et al, 2001). They are used in many industrial applications; mechanics, aeronautics, aerospace, chemistry and oil, electric, military, automotive, medical, marine, and mining, and their development has continuously increased over the last decade (Fauchais et al, 2004A). However, due to the intrinsic properties of thermal spraying technique, it must be emphasized that more work is needed in order to get a reliable corrosion resistant coating in many environments (Hodgkiess and Neville, 1998).

Iron- and nickel- base superalloys are the commercial alloys commonly used for the high temperature applications e.g. manufacture of components used in aggressive environments of gas turbines, steam boilers etc. The superior mechanical performance and good corrosion resistance of the superalloys, especially the nickel-base superalloys at high temperature make them favourites as base materials for hot components (such as blades or vanes) in industrial gas turbines and other energy conversion systems. However, the presence of combustion gases constitutes an extreme environment and hot corrosion is inevitable when alloys are used at high temperatures for long periods of time (Goebel et al, 1973). To improve the oxidation and corrosion resistance of superalloys and to increase the service life of superalloy components at high temperatures, two approaches have been employed, adding fair amounts of Al, Cr, and Ti, and small amounts of Y, Zr and Hf to the alloy, which help to improve oxidation and corrosion resistance (Wang et al, 1989). Another method is coating the alloy with a protective layer using various surface treatment techniques. Many coating techniques have been proposed such as pack cementation, plasma spraying and chemical vapour deposition (Bai et al, 2004). Although considerable efforts have been made to study behaviour of these coated materials under various corrosive environments, still it has been realized that the understanding of the degradation and failure mechanisms of high-temperature coatings in the field need to be improved, particularly with respect to the effects of engine operation and environment on the coating performance (e.g., thermal cycling) (National Materials Advisory Board, 1996).

With no promising turbine materials beyond coated nickel-base superalloys apparent in the foreseeable future, continued progress will likely be made by further refinement of control of thermally grown oxide adherence, and by more cost effective manufacturing processes for contemporary types of coatings. Manufacture of overlay

coatings by EBPVD dominated through the 1970s. Low-pressure (LPPS) and then the Union Carbide (Praxair) shrouded plasma torch are being favored for more complex formulations towards the end of 20<sup>th</sup> century (Goward, 1998). According to Goward (1998) a complete understanding of oxide adherence is still elusive and is one of the most important areas of research, for both coatings and superalloys, to provide further advances in engine efficiency and service life. Research and development on coating processing for diffusion, overlay and thermal barrier systems deserves equally strong support. He further predicted that the future for coating science and technology is brightening than ever in the current millennium.

# CHAPTER 2

## LITERATURE REVIEW

---

This chapter contains a comprehensive review of the literature with a special reference to oxidation and hot corrosion of metals and alloys, and protective coatings. Plasma spray process has been described in detail. The problem has been formulated after critical analysis of the literature towards the end of this chapter.

### 2.1 HIGH TEMPERATURE OXIDATION

Metal and alloys get oxidised when they are heated to elevated temperatures in air or highly oxidising environments, such as a combustion gas with excess of air or oxygen. Considering the total chemical equation for the reaction between a metal and oxygen gas to form the metal oxide,



oxidation of metals may seem to be among the simplest chemical reactions. However, according to Kofstad (1966), the reaction path and oxidation behaviour of a metal may depend on a variety of factors, and reaction mechanisms as a result may prove to be complex. The initial step in the metal-oxygen reaction involves the adsorption of gas on the metal surface. As the reaction proceeds, oxygen may dissolve in the metal, resulting in the formation of oxide on the surface either as a film or as separate oxide nuclei. Both the adsorption and the initial oxide formation are functions of surface orientation, crystal defects at the surface, surface preparation and impurities in both the metal and the gas. Thermodynamically, an oxide is likely to form on a metal surface when the oxygen potential in the environment is greater than the oxygen partial pressure in the equilibrium with the oxide (Kofstad, 1966).

The surface oxide then separates the metal and the gas. When a compact film covers the surface, the reaction may proceed only through a solid-state diffusion of the reactants through the film. For thin films the driving force for this transport of reactants may be due the electric fields in or across the film, whereas for thick film or scales it is determined by the chemical potential gradient across the scale. Metals may also form porous oxide scales which as such do not serve as a solid-state diffusion barrier between the reactants. In such cases the reaction may be limited by processes occurring at phase boundaries. Further, at high temperatures, the oxide may also be liquid or volatile (Kofstad, 1966).

Stott (1998) has explained that the establishment of an oxide layer on an alloy takes place by a nucleation and growth process. According to him, when a clean component is exposed to an oxygen rich gas, small impinging nuclei of all the thermodynamically stable oxides develop on the surface. These initial nuclei of oxide coalesce rapidly to give a complete layer. During the initial or transient stage, the rate of oxidation is rapid, all the elements in the alloy oxidise and the amounts of various oxides in the layer are approximately proportional to the concentration of the elements in the alloy.

Once the transient oxide layer has been established, it continues to grow following diffusion of metal ions to the scale/gas interface or oxygen to the scale/alloy interface. The rate of thickening of the scale is determined by the temperature, the oxygen pressure and the spatial distribution, the amount, the composition and the structure of the initial oxide phases (Chattopadhyay and Wood, 1970).

Stott (1998) has described the phenomena for Ni-20Cr alloy oxidation, according to which approximately 80% of the surface gets covered with NiO phase and 20% by the Cr<sub>2</sub>O<sub>3</sub> phase during initial stage of oxidation (neglecting the possible formation of NiCr<sub>2</sub>O<sub>4</sub>). The fast growing NiO phase overgrows the Cr<sub>2</sub>O<sub>3</sub> phase and a transient oxide scale layer of essential NiO develops, incorporating the other transient oxide phases. At the same time, he opined that the thermodynamically favoured oxide (Cr<sub>2</sub>O<sub>3</sub>) attempts to establish as a complete layer at the base of the transient oxide layer. This is achieved after a short period for this alloy at high temperatures (>600°C). Sufficient Cr<sub>2</sub>O<sub>3</sub> nuclei develop to coalesce and form a complete layer, the oxygen activity at the transient oxide scale layer/alloy interface being sufficiently high to oxidise selectively in the alloy. This has been shown schematically in Fig. 2.1. The rate of oxidation is then controlled by transport of reactants across this Cr<sub>2</sub>O<sub>3</sub>-rich layer, a much slower process than across the initially formed NiO-rich layer. He concluded that the oxide which forms the steady state scale depends, in general, on various factors such as alloy composition, oxygen, oxygen solubility and diffusivity in the alloy, alloy interdiffusion coefficients, growth rates of various oxides, microstructure and surface condition of the alloy, mechanical properties, particularly temperature and oxygen partial pressure.

Further, the requirement of a protective oxide scale is to have a slow growth rate. Oxidation reactions of protective oxide generally follow a parabolic rate equation given by:

$$x^2 = K_p t$$

where  $x$  is the scale thickness in dimensions of length,  $t$  is the time and  $K_p$  the parabolic-growth rate constant in dimensions of length<sup>2</sup>/time. However minor deviations from the parabolic behaviour are often observed (Doychak, 1995).



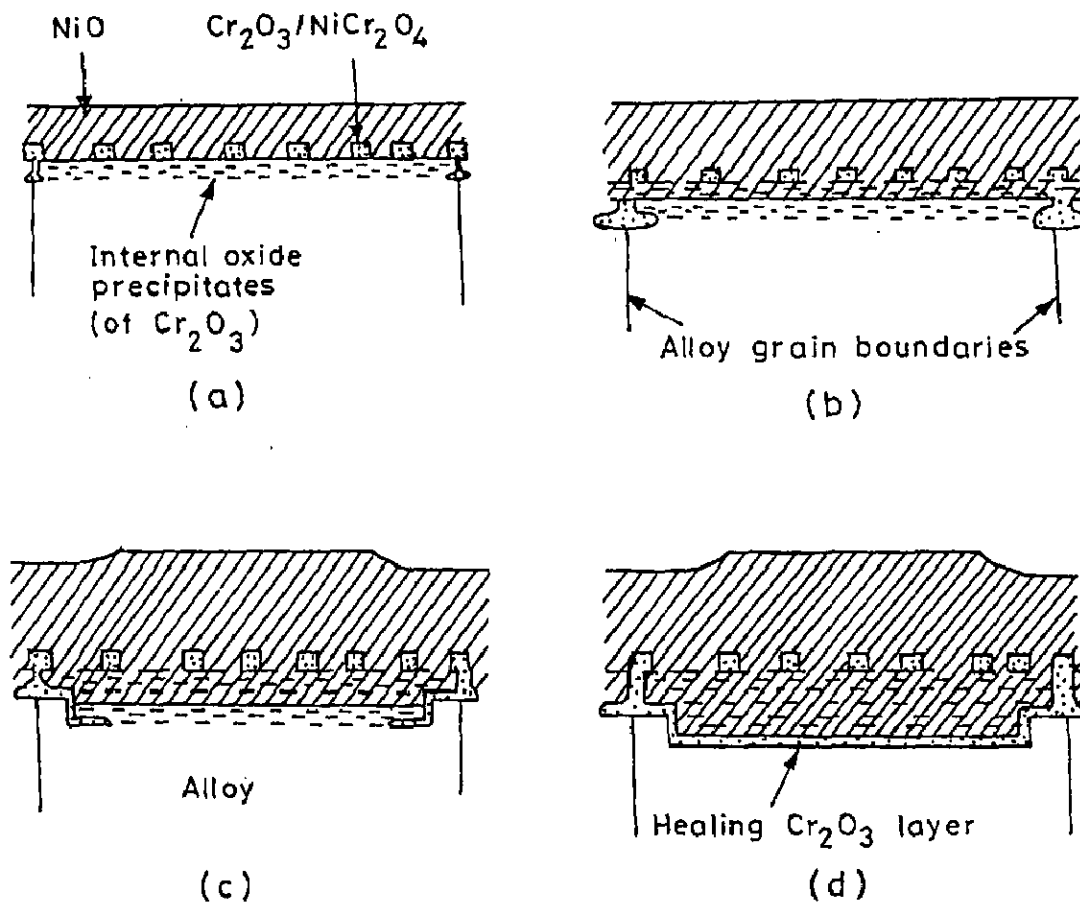


**Fig. 2.1** Schematic representation showing transient oxidation and subsequent development of a healing  $\text{Cr}_2\text{O}_3$ -rich layer on Ni-20%Cr at high temperature (Stott, 1998).

Li et al (2003A) have opined that although considerable insight has been accumulated on mechanisms of high temperature oxidation, from both engineering and more fundamental studies, reaction mechanisms are often not fully understood. They further stated that the degradation by oxidation is one of the main failure modes of hot-section components in the gas turbines, so an understanding of the oxidation phenomenon is very necessary, particularly for the superalloys (Li et al, 2003A). Plenty of literature is available on the high temperature oxidation of metals and alloys, which is difficult to review in a sensible manner in such a short space. As an alternative it is proposed to overview the high temperature phenomenon in context with some current studies conducted by various researchers in the field, which may form basis for the formulation the problem.

### **2.1.1 Oxidation of Superalloys**

The superalloys have been developed to achieve oxidation resistance by utilising the concept of selective oxidation. The selective oxidation approach to obtain oxidation resistance in superalloys consists of oxidising essentially only one element in the superalloy and relying upon this element's oxide for protection. For effective protection, it is anticipated that the oxide should cover the whole surface of the alloy and it must be an oxide through which the diffusion of the reactants takes place at comparatively slow rate. Nickel-, cobalt- and iron-base superalloys make use of the selective oxidation of the aluminium or chromium to develop oxidation resistance (Pettit and Meier, 1985). Further, Pettit and Meier (1985) have reported that the selective oxidation processes are affected by a number of factors such as alloy composition, alloy surface conditions, gas environment and cracking of the oxide scale. Cyclic oxidation conditions whereby the oxide scales crack and spall, as well as certain phases present in the superalloys, both affect the capability to selectively oxidise aluminium or chromium in the superalloys.

Pettit and Meier (1985) opined that during isothermal oxidation of Ni-base superalloys  $\text{Cr}_2\text{O}_3$  and  $\text{Al}_2\text{O}_3$  scales are expected to be formed. Whereas under cyclic conditions depletion of chromium and aluminium results eventually in formation of NiO scale. Some alloys move toward the NiO scale formation much more rapidly than others. They further concluded that the application of aluminide coatings to two nickel based

superalloys B-1900 and Mar M200 makes them remain in alumina scale formation range for even longer times than obtained for the uncoated. The time over which nickel base superalloys can maintain protective, external scales of alumina or chromia is affected by temperature, the gas environment and alloy composition. Generally the superalloys remain alumina or chromia formers for longer times as the aluminium or chromium concentrations are increased. Other elements such as yttrium or cerium can extend this time as these elements improve the oxide scale adherence. Further the alloys which are in alumina formers generally have better oxidation resistance than the chromia formers since diffusion through the alumina scales is generally slower than through chromia.

So far as the Co- and Fe-based superalloys are concerned, they usually cannot be made to contain enough aluminium to permit them to be alumina formers as it will have detrimental effect on their mechanical properties. That is why the Co- and Fe-base superalloys have to rely on the chromia scales for oxidation resistance. Consequently the oxidation resistance of Co- and Fe-base superalloys is inferior to that of Ni-base superalloys. Furthermore, even when considering the Ni-base superalloys that are chromia formers, as degradation begins i.e. the chromia scales are damaged, the less protective oxides formed on the Ni-base alloys contain significant amount of nickel oxide as compared to cobalt and iron oxides on the cobalt and iron-base superalloys respectively. Since nickel oxides are more protective than cobalt and iron oxides, the oxidation resistance drop-off is more abrupt in the case of the Co- and Fe-base superalloys. Further the oxidation resistance of the Co- and Fe-base superalloys usually increases with the chromium concentrations and the oxidation resistance of the alloys with less than about 20% chromium is comparatively poor (Pettit and Meier, 1985).

Further, according to Chatterjee et al (2001), the mixed oxides of the general composition  $AB_2O_4$  (A and B represent two metallic components) have often been identified as oxidation products of Fe-, Ni- and Co- based alloys. The most important properties of these compounds with respect to oxidation resistance are the diffusion coefficients of the cations and anions, which are usually much smaller than in their parent oxides.

## 2.1.2 Oxidation Studies on Iron-Based Alloys

Sadique et al (2000) showed that aluminium additions have marked effects on the oxidation characteristics of Fe-10Cr at all temperatures. They observed reduction in rate of oxidation in terms of specific weight gain with increasing aluminium content. The amount of spallation of the oxide scale was also found to decreasing with increasing Al content. Al content was shown to help in enhancing the adhesion of  $\text{Cr}_2\text{O}_3$ . Failure of the protective scale was inhibited either through the immediate reformation of an external protective scale or through the internal oxidation and subsequent formation of a sub-scale layer. It was concluded that a minimum level of aluminium exists for the formation of a complete protective scale on the alloy surface depending upon the temperature.

Haugsrud (2001) reviewed some studies on the oxidation of binary alloys, A-B, such as those based on Fe, Co, Ni or Cu and containing 0-30% of a higher valent, less noble metal, B. He reported that the oxidation essentially follows parabolic kinetics and the rate constant reaches a maximum with additions of B around 5-10%. The oxygen pressure dependencies and temperature dependencies of the parabolic rate constants are stronger than for the unalloyed metal, A. He further suggested that the oxide scale morphology for the binary alloys is considerably more complex than for unalloyed A and the oxide usually comprises an outer region consisting of AO and an inner two-phase region containing dispersed BO-particles and pores in a matrix of AO.

Comparison of the oxidation kinetics of four commercial heat-resisting alloys namely Hastelloy C-4, SS 304L, Incoloy 800H and Incoloy 825 in air from 600 to 1200<sup>0</sup>C has been presented by Hussain et al (1994). Hastelloy C-4 was found to be the most resistant to oxidation for temperatures upto 1000<sup>0</sup>C following a cubic-rate law. SS 304L was reported to be oxidised in the form of stratified nodules of two distinct layers, which grow in opposite directions at the metal-oxide interface irrespective of time and temperature of oxidation. Incoloy 800H and Incoloy 825 showed similar kinetics, following parabolic-rate law at 1000<sup>0</sup>C and 1200<sup>0</sup>C. They also observed the deleterious effect of Mo on the oxidation resistance of Incoloy 825.

Khalid et al (1999) conducted similar studies for comparison of high temperature oxidation behaviour of Incoloy 800H and Incoloy 825 at 1000 and 1200<sup>0</sup>C. Incoloy 800H exhibited compact, dense and adherent oxide layer, whereas the Incoloy 825 decomposed completely into the oxide. They attributed the comparatively less oxidation resistance of the Incoloy 825 to the presence of coarse Ti-rich inclusions, which shows the less dissolution of Ti in the alloy.

Singh (2003) carried out high temperature oxidation studies on the GrA1, T11 and T22 boiler steels in air at 900<sup>0</sup>C. He observed that the Mo containing T22 steel showed least oxidation resistance. He attributed this to the formation of a low melting point MoO<sub>3</sub> phase. This low melting point phase (795<sup>0</sup>C) was reported to cause the disruption and dissolution of the protective oxide scale, resulting in accelerated oxidation of the steel.

### 2.1.3 Oxidation Studies on Nickel and Nickel-Based Alloys

Haugsrud (2003) revisited the high-temperature oxidation of Ni with an extensive review and conducted experiments to study the oxidation behaviour of Ni in the range of 500-1300<sup>0</sup>C and oxygen pressure from 1X10<sup>-4</sup> to 1 atm. The oxidation behaved according to a parabolic rate law at 1100<sup>0</sup>C and the rate was found to be governed by outward lattice diffusion of Ni via either singly or doubly charged Ni vacancies. At lower temperatures the oxidation mechanism has been reported to be more complex and contradictions are found in the literature. Short circuit mechanisms of both Ni and oxygen are of importance, where the influence of oxygen transport increases with decreasing temperature. Further he concluded that the mechanism of oxygen ingress is not fully clear, but since the oxygen diffusivity in NiO is too slow to account for the inward growth, oxygen is assumed to penetrate the scale as gaseous species.

Ul-Hamid (2002) investigated the oxidation behaviour of alloy grain boundaries in Ni-10Cr and Ni-20Cr alloys in air for 50 hours at 1000<sup>0</sup>C. He pointed out that the grain boundaries intersecting the alloy surface in Ni-10Cr exhibited no oxidation, whereas the alloy formed a thick ( $\approx 60\mu\text{m}$ ) oxide layer inwardly. Further it was observed by him that the Ni-20Cr cross-section revealed preferential oxidation at a depth of 65 $\mu\text{m}$  at the alloy grain boundaries intersecting its surface, while the oxide at the surface was a few micrometers thick. He noted that the extent to which the grain-boundary oxidation differs from the alloy surface oxidation depends on the Cr content of the alloy. Further during the isothermal oxidation of Ni-20Cr binary alloy at 750 and 1000<sup>0</sup>C in air, he observed formation of  $\alpha\text{-Cr}_2\text{O}_3$ , NiCr<sub>2</sub>O<sub>4</sub> and NiO phases (Ul-Hamid, 2003). He further conducted the microstructural study of the alloy perpendicular to the plane of oxidation and revealed co-lateral formation of diverse scale configuration at its surface. He opined that the protection imparted was found to be mainly due to the presence of  $\alpha\text{-Cr}_2\text{O}_3$ , however various regions of the oxidised alloy surface constituted predominantly of NiCr<sub>2</sub>O<sub>4</sub>.

Studies of the protective alumina scales which formed on NiCrAlY-alloys after isothermal oxidation in the temperature range of 950-1100°C with Si addition showed that the Si additions upto 2 mass% have only a minor effect on the scale growth of Ni-20Cr-10Al-Y (Nickel et al, 2002). Similarly they concluded that the small additions of Ti (around 0.4 mass-%) can improve the scale adherence.

Levy et al (1989) reported studies on the cyclic oxidation resistance of three single-crystal nickel base superalloys and DS Mar M 200 at 1093°C using a tube furnace and burner rig. The same ranking of the alloys was reported in both tests with the single-crystal superalloys having better oxidation resistance than the directionally solidified alloy DS Mar M 200. They further opined that tube furnace tests can be used in place of burner-rig tests to rank alloys. Oxidation tests at 900°C using the tube furnace produced a ranking of the alloys consistent with the 1093°C results.

Delaunay et al (2000) studied the isothermal oxidation of Inconel 718 in air at 900°C. The oxidation led to the formation of a layer of a rhombohedral phase  $\text{Cr}_{2-x}\text{M}_x\text{O}_3$  high in Cr. They observed that rapid Mn and Ti diffusion across this scale contributed to the formation of a spinel phase and  $\text{TiO}_2$  crystals on the surface of the scale. Nb was observed to be rapidly diffusing along the grain boundaries of the alloy in the very first stages of the oxidation. This formed an oxide on the surface of the alloy which was suggested to be  $\text{CrNbO}_4$ . For longer oxidation times, the rapid formation of a chromia scale led to the development of a Cr depleted zone in the substrate. This zone was observed to be affected by an intergranular oxidation of Ti near the interface and of Al deep in the alloy. Further the rate of the oxide scale growth, the depth of the intergranular oxide penetration and the depth of Cr and Ti depletion were all lower than those obtained under the same conditions on Inconel X and Incoloy 800.

Whereas from the mass-gain measurements, Greene and Finfrock (2000) identified three regimes of oxidation for Inconel 718, a low-temperature regime in which the alloy behaved as if passivated after an initial period of transient oxidation, an intermediate-temperature regime in which the rate of oxidation was limited by diffusion and exhibited a constant parabolic rate dependence, and a high-temperature regime in which material deformation and damage accompanied an accelerated oxidation rate above the parabolic regime.

The oxidation behaviour of a single-crystal Ni-base superalloy has been studied using discontinuous thermogravimetric analysis and prolonged exposure in air at 800 and 900°C by Li et al (2003A), and over the temperature range from 1000–1150°C by Li et al

(2003B). They observed that the mass gain at 900<sup>0</sup>C was lower than that at 800<sup>0</sup>C due to the formation of a protective inner  $\alpha$ -Al<sub>2</sub>O<sub>3</sub> layer at 900<sup>0</sup>C. The scale formed at 900<sup>0</sup>C was found to be more uniform than that formed at 800<sup>0</sup>C, which consisted of several layers: an NiO outer layer, spinel-rich sublayer, a CrTaO<sub>4</sub>-rich layer and an  $\alpha$ -Al<sub>2</sub>O<sub>3</sub> inner layer. Whereas in the temperature range of 1000–1150<sup>0</sup>C, the outer NiO layer was observed to be replaced by an outer layer of spinel, a sublayer of mainly  $\alpha$ -Al<sub>2</sub>O<sub>3</sub>, with unchanged composition of inner layers of the scale. Further, no internal oxides or nitrides were observed below the inner  $\alpha$ -Al<sub>2</sub>O<sub>3</sub> layer after 1000 hr at 1000<sup>0</sup>C, and after 200 hr at 1100 and 1150<sup>0</sup>C.

Li, Y. et al (2003) studied the oxidation kinetics and oxidation layer of a cast Ni-base superalloy K35 at 800<sup>0</sup>C by still TGA method. The results showed that oxidation kinetics of the superalloy obeyed the parabolic law. They further observed that oxidation rate of the superalloy was dependent on the growth dynamics of Cr<sub>2</sub>O<sub>3</sub>. Moreover, the oxide layer was found to be thin and, consisted of Cr<sub>2</sub>O<sub>3</sub> mainly with a bit of NiCr<sub>2</sub>O<sub>4</sub> and TiO.TiO<sub>2</sub>. Internal oxidation of the alloy was also observed.

Zhao et al (2005) investigated the oxidation behaviour of a new nickel-based superalloy in air at 950<sup>0</sup>C and 1000<sup>0</sup>C for 140 hours and reported that the alloy obeyed the parabolic rate law at 950<sup>0</sup>C, whereas small deviations were observed at 1000<sup>0</sup>C. No oxide spallation was observed at 950<sup>0</sup>C, while minor spallation was seen at 1000<sup>0</sup>C. The oxide scale was found to be consisted of Cr<sub>2</sub>O<sub>3</sub>, (Ni, Co)Cr<sub>2</sub>O<sub>4</sub>, TiO<sub>2</sub>, SiO<sub>2</sub>, TiO<sub>2</sub> and Al<sub>2</sub>O<sub>3</sub>. Internal oxidation of the superalloy was also indicated at both the temperatures of the investigation.

The effects of thin surface applied Y<sub>2</sub>O<sub>3</sub>, Al<sub>2</sub>O<sub>3</sub> and Cr<sub>2</sub>O<sub>3</sub> coatings or films on the selective oxidation of chromium for Ni-15Cr and Ni-10Cr alloys in air at 1000<sup>0</sup>C have been studied by Yedong and Stott (1994). The oxide films were deposited by an electrochemical method. They observed the establishment of chromia scale which was promoted effectively by the presence of an Y<sub>2</sub>O<sub>3</sub> film on Ni-15Cr and at least locally on Ni-10Cr. In comparison with the cases of surface deposited Al<sub>2</sub>O<sub>3</sub> and Cr<sub>2</sub>O<sub>3</sub> oxide films, the additional beneficial effect of the Y<sub>2</sub>O<sub>3</sub> film in maintaining the selective oxidation of chromium reportedly attributed to its ability to improve the mechanical integrity and adhesion of the chromium scale.

Some other oxidation studies which may be relevant to the present work are summarised in Appendix A.1.

## 2.2 HOT CORROSION

According to Rapp and Zhang (1994), metals and alloys sometimes experience accelerated oxidation when their surfaces are covered with a thin film of fused salt in an oxidizing gas atmosphere at elevated temperatures. This is known as hot corrosion where a porous non-protective oxide scale is formed at the surfaces and sulphides in the substrate.

If concentration of the sulphate exceeds the saturation vapour pressure at the operating metal temperature for turbine blades, vanes and energy generation components (700-1100<sup>0</sup>C), then Na<sub>2</sub>SO<sub>4</sub> will deposit on the surface of these components. At higher temperatures these deposits of Na<sub>2</sub>SO<sub>4</sub> are molten (m.p.884<sup>0</sup>C) and can cause accelerated attack of Ni- and Co-base superalloys. Further the accelerated corrosion can also be caused by other salts, such as vanadates or sulphates-vanadate mixtures and in the presence of solid or gaseous salts such as chlorides.

### 2.2.1 High Temperature (Type I) Hot Corrosion (HTHC)

High temperature (Type I) hot corrosion (HTHC) is nominally observed in the temperature range of about 825-950<sup>0</sup>C when the condensed salt film is clearly liquid. The typical microstructure for HTHC shows the formation of sulphides and a corresponding depletion of the reactive component in the alloy substrate. The external corrosion products frequently comprise oxide precipitates dispersed in the salt film (Rapp and Zhang, 1994). The dominant salt in HTHC is Na<sub>2</sub>SO<sub>4</sub> due to its high thermodynamic stability. The macroscopic appearance of HTHC is characterised in many cases by severe peeling of the metal and by significant colour changes (greenish tone, resulting from the formation of NiO) in the area of the accelerated attack (Eliaz et al, 2002).

### 2.2.2 Low Temperature (Type II) Hot Corrosion (LTHC)

Low temperature (Type II) hot corrosion (LTHC) occurs well below the melting point of pure Na<sub>2</sub>SO<sub>4</sub>. The reaction product morphology for this type of corrosion can be characterised by a non-uniform attack in the form of pits, with only little sulphide formation close to the alloy/scale interface and little depletion of Cr or Al in the alloy substrate (Rapp and Zhang, 1994). This form of corrosion is observed mainly within the temperature range 650-800<sup>0</sup>C (Nicholls, 2000). The formation of low melting point eutectics causes typical LTHC pitting for instance the formation of Na<sub>2</sub>SO<sub>4</sub>-NiSO<sub>4</sub> eutectics for nickel-based superalloys. Wright (1987) suggested that a high partial pressure of SO<sub>3</sub> in the gaseous phase is required in the LTHC reactions to occur, in contrary to HTHC.



### 2.2.3 Hot Corrosion of Superalloys

Hot corrosion degradation process of the superalloys usually consists of two stages, namely an initiation stage and a propagation stage (Pettit and Meier, 1985 and Pettit and Giggins, 1987). According to Pettit and Meier (1985), it is a fact that all corrosion resistant alloys degrade via these two stages and, it is the result of using selective oxidation to develop oxidation or corrosion resistance. They further elaborated that the conditions causing hot corrosion therefore do nothing more than shortening the time for which the superalloys can form protective alumina or chromia scales via selective oxidation.

During the initiation stage of hot corrosion superalloys are being degraded at rates similar to those that would have prevailed in the absence of the deposits. Elements in the alloy are oxidised and electrons are transferred from metallic atoms to the reducible substances in the deposit. Consequently, the reaction product barrier that forms beneath the deposit on the alloy surface usually exhibits primarily those features resulting from the gas-alloy reaction (Pettit and Giggins, 1987).

In some cases of hot corrosion an increasing amount of sulphide particles become evident in the alloy beneath the protective reaction product barrier. In other small holes become evident in the protective reaction product barrier where the molten deposit begins to penetrate it. Eventually the protective barrier formed via selective oxidation is rendered ineffective, and the hot corrosion process enters into the propagation stage. Obviously in attempting to develop resistance to hot corrosion one should strive to have the superalloys remain in the initiation stage as long as possible (Pettit and Meier, 1985).

Numerous factors affect the time at which the hot corrosion process moves from the initiation stage into the propagation stage as shown in Fig. 2.2. These factors also play the dominant role in determining the type of reaction product that is formed in the propagation stage. This fact is responsible for variety of hot corrosion processes that have been observed when superalloys are exposed to different environments (Pettit and Meier, 1985).

The propagation stage of the hot corrosion sequence is the stage for which the superalloy must be removed from service since this stage always has much larger corrosion rates than for the same superalloy in the initiation stage (Pettit and Meier, 1985 and Pettit and Giggins, 1987). The pertinent mechanism behind this mode of hot corrosion has been summarised in Section 2.4.4.

# HOT CORROSION CHRONOLOGY

## Initiation Stage

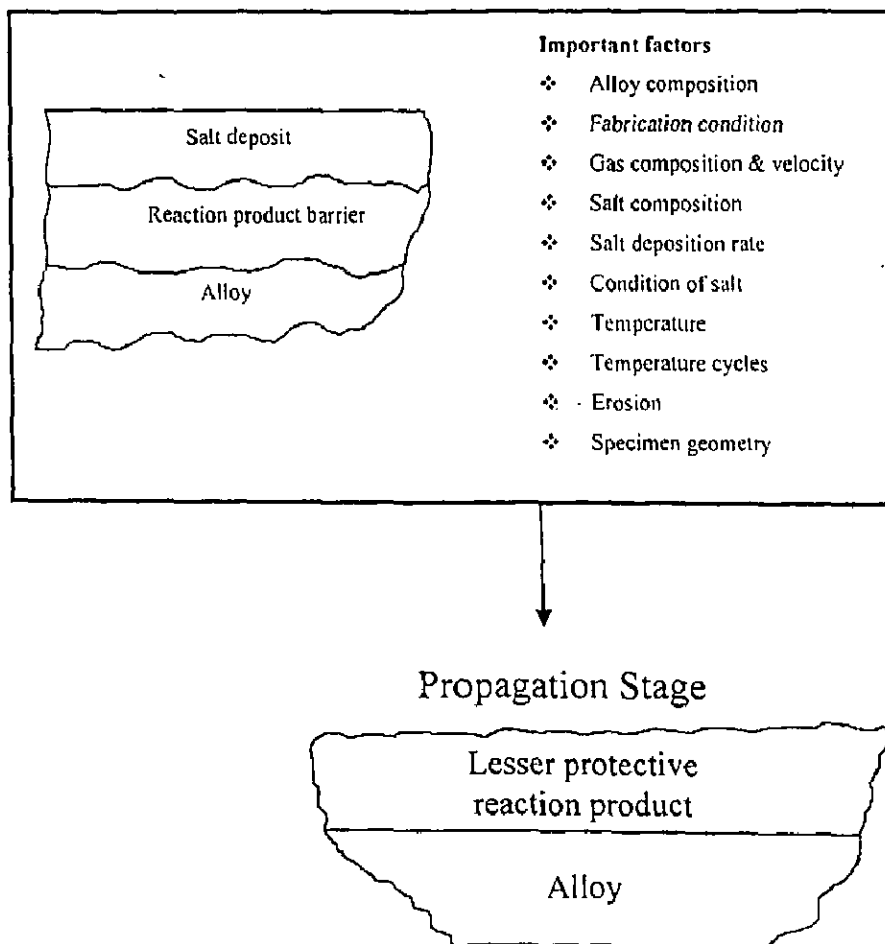


**Fig. 2.2** Schematic diagram illustrating the conditions that develop during the initiation and the propagation of hot corrosion attack and to identify the factors that determine the time at which the transition from the initiation to the propagation stage occurs (Pettit and Meier, 1985).

However, Pettit and Giggins (1987) opined that the hot corrosion degradation sequence is not always clearly evident, and the time for which protective reaction products are stable beneath the salt layer is influenced by a number of factors. The alloys must be depleted of certain elements before non-protective products can be formed, or the composition of the deposits must change to prevent the formation of protective scales. There are cases when the initiation stage does not exist at all and the degradation process directly enters into the propagation stage.

As per the views of Yoshida (1993), Ni-based superalloys are well known to be susceptible to hot corrosion associated with combined reaction processes such as sulphidation-oxidation and occasionally together with chlorination. In practice, it is a serious problem for such alloy systems when used for hot section components of various heat engines such as gas turbines subjected to corrosion-induced strength degradation.

#### **2.2.4 Mechanisms of Hot Corrosion**

Several mechanisms have been proposed to describe the phenomenon of hot corrosion (Goebel and Pettit, 1970A, Goebel and Pettit, 1970B, Beltran and Shores, 1972, Rapp and Goto, 1981, Rapp, 1986, Pettit and Giggins, 1987, Stringer, 1987, Otsuka and Rapp, 1990 and Zhang et al, 1993). Eliaz et al (2002) briefed in their review on failures of turbine materials that the initiation of high temperature hot corrosion (HTHC) is often attributed to failure of the protective oxide layer, which allows the molten salt to access directly the substrate metal. This failure may result from erosion, thermal stresses, erosion-corrosion, chemical reactions etc. The mechanisms proposed for the HTHC propagation stage are the sulphidation-oxidation mechanism and the salt fluxing mechanisms (Stringer, 1987). The salt fluxing mechanism was firstly proposed by Goebel and Petit (1970A and 1970B). According to this model, the protection efficiency of the surface oxide layer might be lost as a result of fluxing of this layer in the molten salt. This fluxing may be either due to combination of oxides with  $O^{2-}$  to form anions (basic fluxing) or by decomposition of the oxides into the corresponding cations and  $O^{2-}$  (acidic fluxing). As compared to basic fluxing, acidic fluxing causes more severe oxidation. The acidic fluxing takes place when the  $O^{2-}$  activity in the molten salt is markedly lowered. In contrast to basic fluxing the acidic fluxing can be self-sustaining

because the displacement of the salt from the stoichiometry does not become progressively more difficult as the reaction proceeds (Stringer, 1987). In general the hot corrosion of superalloys with high contents of aluminium and chromium is often reported to occur according to the basic fluxing mechanism. Whereas the hot corrosion of alloys with high contents of tungsten, molybdenum and vanadium has been reported to follow the acidic fluxing mechanism.

Rapp and Goto (1981) measured the oxide solubilities in molten  $\text{Na}_2\text{SO}_4$  as a function of the acidity of the salt. They suggested on the basis of these measurements that a negative gradient of the solubility of the protective oxide in the salt film at the oxide/salt interface should lead to oxide dissolution at this interface and to precipitation of a non-protective oxide away from the interface, where the solubility is lower. Fluxing arises in this case only because of the local variation of sodium oxide activity and/or oxygen partial pressure across the salt film, without any necessity of sulphide-forming reaction. This mechanism can explain a self-sustaining process of dissolution of the protective oxide to maintain an accelerated corrosion attack (Stringer, 1987).

The effect of vanadium on HTHC has also been studied by different researchers. Bornstein et al (1973) and Goebel et al (1973) opined that a self-sustained acidic dissolution of the protective  $\text{Cr}_2\text{O}_3$  or  $\text{Al}_2\text{O}_3$  scales could take place when the salt film contains vanadium, because  $\text{V}_2\text{O}_5$  is a strong acidic oxide. Further, Zhang and Rapp (1987) believed that every oxide should form an acidic solute with much higher solubility in the presence of vanadate, which should contribute to the more accelerated attack of oxides by mixed sulphate-vanadate melts than by a pure sulphate melt.

The phenomenon of LTHC was explained by Luthra (1983) with the help of a common model, according to which LTHC follows two stages. In the first stage liquid sodium-cobalt sulphate is formed on the surface, whereas in the second stage propagation of the attack takes place, refer Fig. 2.3. The propagation is suggested to occur via migration of  $\text{SO}_3$  and cobalt inward and outward, respectively, through the liquid salt.

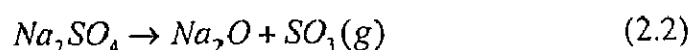
Some of hot corrosion studies conducted by various investigators in  $\text{Na}_2\text{SO}_4$  or  $\text{V}_2\text{O}_5$  environments are summarised in Appendix A.1.



## 2.2.5 Salt Chemistry

### 2.2.5.1 Chemistry and Phase Stability of $\text{Na}_2\text{SO}_4$ Salt

Oxyanion melts of alkali nitrates, carbonates, hydroxides and sulphates exhibit an acid base character whereby the acid components may be considered as  $\text{NO}_2(\text{g})$ ,  $\text{CO}_2(\text{g})$ ,  $\text{H}_2\text{O}(\text{g})$  or  $\text{SO}_3(\text{g})$  respectively. Although the use of the Lux-Flood selection of  $\text{NO}_3^-$ ,  $\text{CO}_3^{2-}$ ,  $\text{OH}^-$  and  $\text{SO}_4^{2-}$  as the basic components is common for such fused salts, the oxide ion can be alternatively chosen as the Lewis base in common for all of these salts (Rapp, 1986 and 2002). For a melt of pure  $\text{Na}_2\text{SO}_4$  (m.p.  $884^\circ\text{C}$ ), there exists the equilibrium as given below:

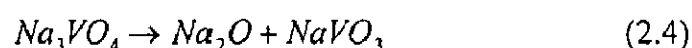
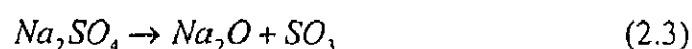


According to Rapp (1986), in examining the expected stability of the protective oxide  $\text{Cr}_2\text{O}_3$ , with respect to dissolution either as acidic solutes such as  $\text{Cr}_2(\text{SO}_4)_3$  or as basic solutes such as  $\text{Na}_2\text{CrO}_4$  or  $\text{NaCrO}_2$ , the phase stability diagram for the Cr-S-O system can be superimposed on that for Na-S-O, as shown in Fig. 2.4. The two abscissa scales at the bottom and top of figure provide alternate parameters for melt basicity (or acidity). Under no conditions is the metal chromium stable in contact with  $\text{Na}_2\text{SO}_4$  at 1200 K ( $927^\circ\text{C}$ ) (Rapp, 1986).

### 2.2.5.2 Vanadate Solution Chemistry

Among the transition metals vanadium is unique, in that it forms a low-melting oxide  $\text{V}_2\text{O}_5$ . This low melting temperature ( $670^\circ\text{C}$  under 1 atm of oxygen) results from the peculiar crystal structure of the compound in which vanadium is 5-coordinated with oxygen and in which there occur four different vanadium-oxygen bond lengths (Suito and Gaskell, 1971).

The phase stability diagram for the Na-V-S-O system at  $900^\circ\text{C}$  reported by Hwang and Rapp (1989) has been shown in Fig. 2.5. The dashed lines present the isoactivity lines for the vanadate species in the salt solution. They determined the dependence of the equilibrium concentrations of various vanadate solutes in the sodium sulphate-vanadate solutions on the melt basicity by considering following equilibrium reactions:

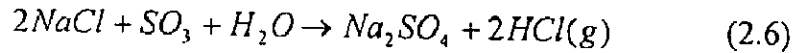


The equilibrium concentration of each vanadium compound varies continuously with melt basicity.  $\text{Na}_3\text{VO}_4$  is the dominant component in the melt at basicity less than

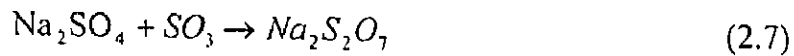
8.2 and  $V_2O_5$  is dominant at basicity greater than 16.3. For basicities between 8.2 and 16.3,  $NaVO_3$  is the most important vanadium solute (Hwang and Rapp, 1989).

### 2.2.5.3 Chemistry of Salts in Combustion of Coal/Fuel Oils

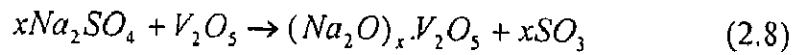
As suggested by Khanna and Jha (1998), the sulphur present in coal and fuel oils yields  $SO_2$  on combustion which is partially oxidised to  $SO_3$ . The  $NaCl$  (either as impurities in the fuel or in the air) reacts with  $SO_3$  and water vapours at combustion temperatures to yield  $Na_2SO_4$  as below:



At lower temperatures  $Na_2SO_4$  can further react with  $SO_3$  to form sodium pyrosulphate,  $Na_2S_2O_7$  with melting point (m. p.) of  $401^\circ C$ :



Small amounts of vanadium may be present in fuel oils, which on combustion forms  $V_2O_5$ . This may further react with  $Na_2SO_4$  to form low melting sodium vanadates, which are highly corrosive.

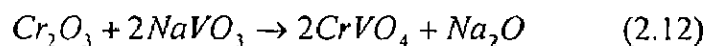
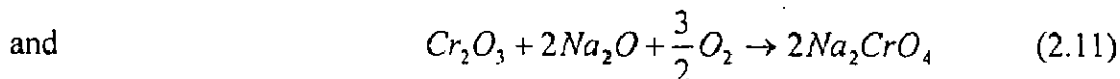
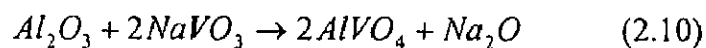
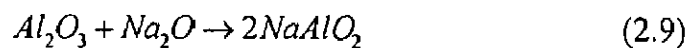


Thus metals and alloys in combustion gases are exposed to various corrosives such as  $O_2$ ,  $SO_2/SO_3$ , molten salts, e.g.  $Na_2SO_4$  or sulphate mixtures, sodium vanadates,  $NaCl$  etc. (Khanna and Jha, 1998).

### 2.2.5.4 Solubilities of $Al_2O_3$ and $Cr_2O_3$

Rapp and Zhang (1994) opined that upon contacting a fused salt, metals and alloy components are oxidised to form thin scales whose protectiveness depends upon the stability of the oxide in the salt.

Hwang and Rapp (1989) have reported the solubilities of  $Al_2O_3$  and  $Cr_2O_3$  in a fused  $Na_2SO_4$ -30 mole %  $NaVO_3$  salt solution as follows:



They reported that the vanadate ions greatly increase the acidic solubilities of  $Al_2O_3$  and  $Cr_2O_3$  over a wide range of melt basicity.

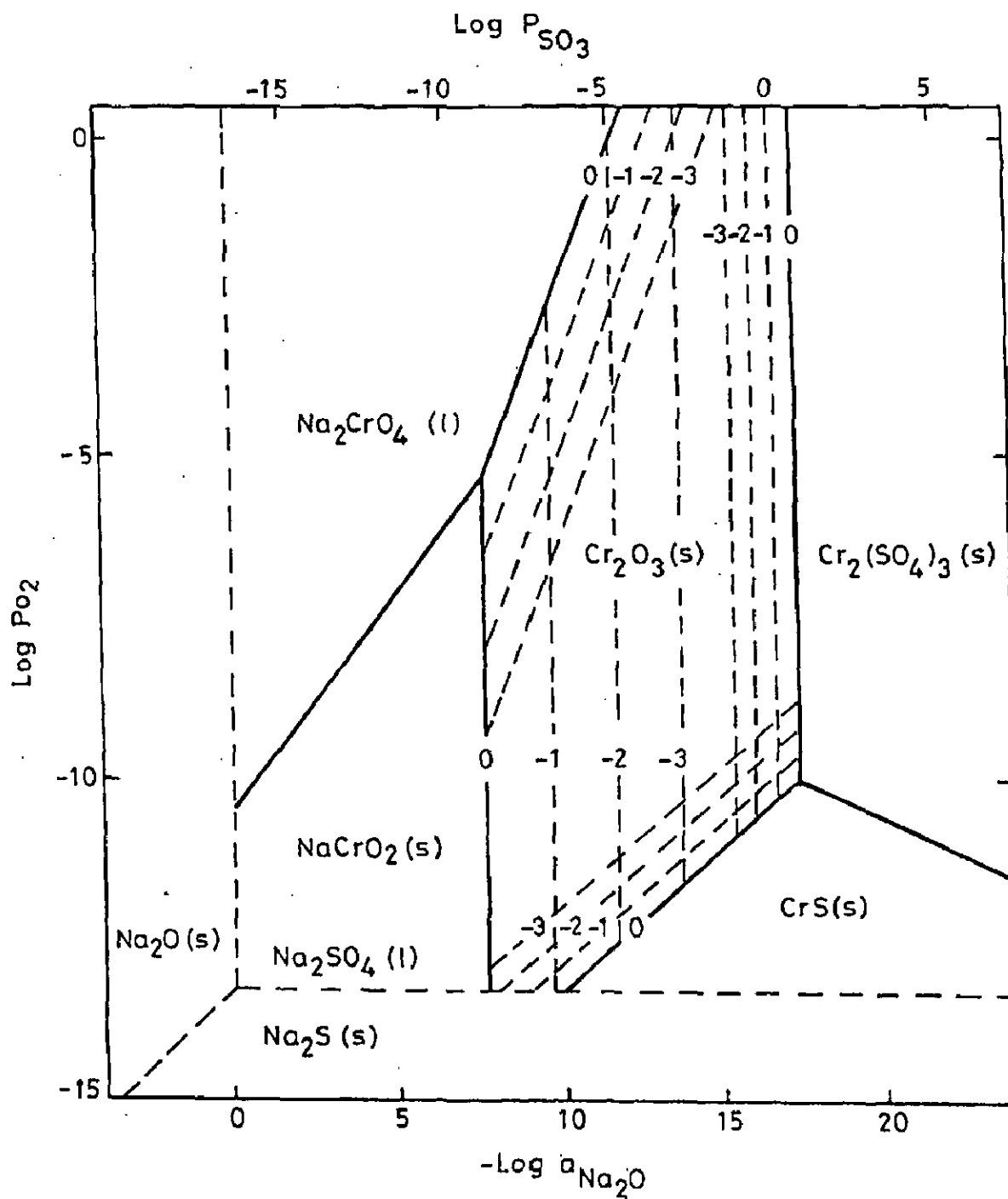


Fig. 2.4 Na-Cr-S-O phase stability diagram for 1200 K (Rapp, 1986).



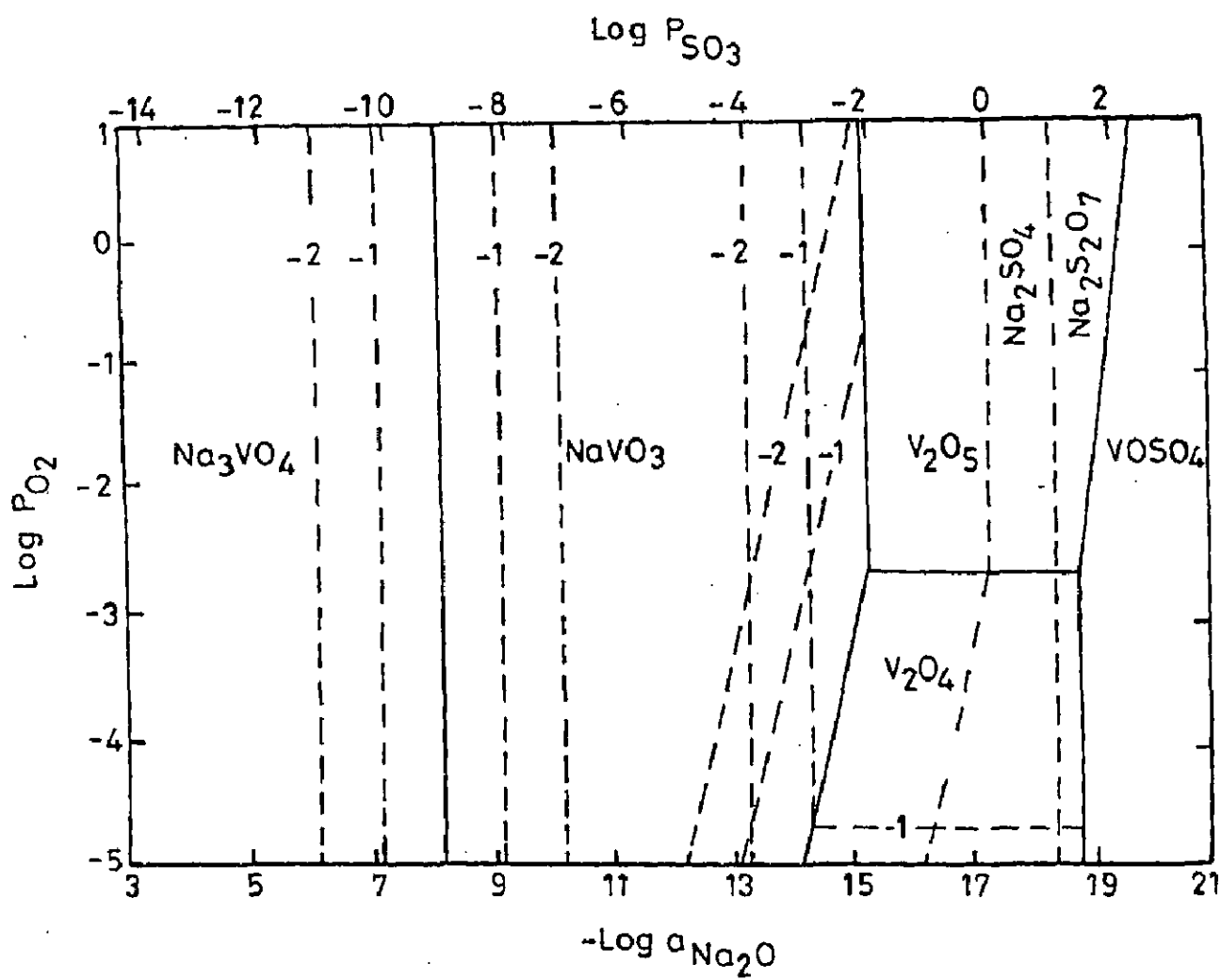


Fig. 2.5 Phase stability diagram for Na-V-S-O system at 900 °C (Hwang and Rapp, 1989).

## 2.3 STUDIES ON $\text{Na}_2\text{SO}_4\text{-V}_2\text{O}_5$ INDUCED HOT CORROSION

The kinetics of the reactions between  $\text{Na}_2\text{SO}_4$  (X) and  $\text{V}_2\text{O}_5$  (Y) as studied by Kolta et al (1972) revealed that the rate of reaction depended both on the temperature (600-1300°C) and the molar ratios of X: Y. They further found that with increase in the reaction period (>30 min.), there was decrease in reaction rate which finally reached to zero order. This decrease in the reaction rate has been attributed to the formation of vanadosulphate complexes such as  $(\text{NaV}_3\text{O}_8)_2\cdot\text{Na}_2\text{SO}_4$  and  $(\text{NaVO}_3)_2\cdot\text{Na}_2\text{SO}_4$  which get decomposed at higher temperatures giving the meta- and pyro-vanadates respectively.

Kofstad (1988) proposed that during combustion, the vanadium contaminants are oxidized to the higher valence vanadium oxides ( $\text{V}_2\text{O}_4$  and  $\text{V}_2\text{O}_5$ ) and sodium vanadates are formed by the reaction of vanadium oxides and sodium salts, e.g.  $\text{Na}_2\text{SO}_4$ . Accordingly the composition of the vanadates may be presented in a simplified form as  $(\text{Na}_2\text{O})_x\text{V}_2\text{O}_5$ , but the detailed compositions of the individual vanadates may be more complex as part of the vanadium may be in the +IV state. The solid compounds comprise  $(\text{Na}_2\text{O})_x\text{V}_2\text{O}_4(\text{V}_2\text{O}_5)_{12-x}$  (often termed  $\beta$  bronze),  $(\text{Na}_2\text{O})_5(\text{V}_2\text{O}_4)_x(\text{V}_2\text{O}_5)_{12-x}$  (K bronze),  $\text{NaVO}_3$  (sodium metavanadate),  $\text{Na}_4\text{V}_2\text{O}_7$  (sodium pyrovanadate) and  $\text{Na}_3\text{VO}_4$  (sodium orthovanadate). A notable feature of the vanadates is that they have relatively low melting points, which extend from 535°C upwards. Furthermore, metal oxides dissolved in the vanadates may suppress the melting points and eutectic temperatures even further. He further reported that the slags developed on valves in diesel engines consist predominantly of sodium sulphate and sodium vanadates and have a melting points as low as 400°C.

Molten vanadates flux oxide ceramics. The solubilities of metal oxides may be high and are dependent on the Na:V ratio. The solubilities of  $\text{Cr}_2\text{O}_3$  and  $\text{Fe}_2\text{O}_3$  are highest at Na : V ratios close to 5 : 12 and amount to about 50 mol.%. For NiO the solubility is about 60 mol.% for Na : V = 3 : 2 and decreases to about 55 mol.% for Na : V = 5 : 12. As  $\text{V}_2\text{O}_5$  is acidic, it will in general react with more basic oxides to form the corresponding vanadates.

### 2.3.1 Iron and Iron-Based Alloys

Natesan (1976) reported that the fuels containing only 50 ppm vanadium can cause severe attack on stainless steels. Fig. 2.6 shows the corrosion rate of Type 304 stainless steel in different  $\text{V}_2\text{O}_5\text{-Na}_2\text{SO}_4$  mixtures at temperatures between 790 and 900

<sup>0</sup>C, as has been presented by him. At temperatures below the melting point of ash, the rate of attack of stainless steel is low and follows the normal oxidation rate. It was concluded that all stainless steels and other common engineering alloys are severely attacked by fuel ash that contains vanadium with or without sulphates.

Fairman (1962) studied some metal specimens in an ash mixture ( $V_2O_5 + 10\% Na_2SO_4$ ) environment in air. The corrosion was found to be severe at the ash/air or ash/atmosphere interface. The intensity of attack, however, was still higher at the locations where the concentration of oxygen and vanadium pentoxide was greatest, suggesting the transfer of oxygen atoms or ions by the pentoxide to the metal surface:  $2V_2O_5 \rightarrow 2V_2O_4 + 2O \downarrow$ . He opined that the mechanism of accelerated attack could be most satisfactorily explained by the catalytic action of  $V_2O_5$  operating with an increase in the defect concentration of the scale.

Valdes et al (1973), in study of AISI 446 stainless steel under  $V_2O_5$  and  $Na_2O \cdot 6V_2O_5$  environment in the temperature range 700-900<sup>0</sup>C in air found that the oxide scale was mainly  $Cr_2O_3$  with some vanadium oxide which acted as a moderate barrier to corrosion. Above 850<sup>0</sup>C in  $V_2O_5$ , a breakaway corrosion reaction occurred. No  $Cr_2O_3$  oxide barrier was present but there was a continuous oxide that comprised of  $Cr_2O_3$ ,  $Fe_2O_3$  and  $V_2O_5$  at the metal/oxide interface where the crystals grew. They suggested that the addition of  $Na_2O$  to  $V_2O_5$  increased the oxide ion ( $O^{2-}$ ) content of the melt and made it more aggressive to acidic oxides such as  $Cr_2O_3$ .

Tiwari and Prakash (1996 and 1997) and Tiwari (1997) have reported hot corrosion studies on some industrial superalloys in temperature range 700-900<sup>0</sup>C in the environments comprising of pure  $Na_2SO_4$ ,  $Na_2SO_4-15\%V_2O_5$  and  $Na_2SO_4-60\%V_2O_5$ . Corrosion rates were observed to very high in the environment having  $Na_2SO_4-60\%V_2O_5$  composition. The extremely corrosive nature of this composition was attributed to its low melting point i.e. 500<sup>0</sup>C. Tiwari et al (1997) further revealed that in  $Na_2SO_4-60\%V_2O_5$  melt, the degradation was due to the cracking of the protective scale under the influence of the fluxing action of the melt for both Fe-base alloy Superfer 800H and Co- base alloy Supercor 605. The enhanced degradation was reported to be due to the presence of tungsten in form of  $Na_2WO_4-WO_3$  compound. No oxidation and sulphidation into the substrate was observed by them in Co-base alloy. Tewari (1997) concluded that the Co-base alloy has inferior corrosion resistance than the Ni-base alloy in  $Na_2SO_4-60\%V_2O_5$  environment at 900<sup>0</sup>C.

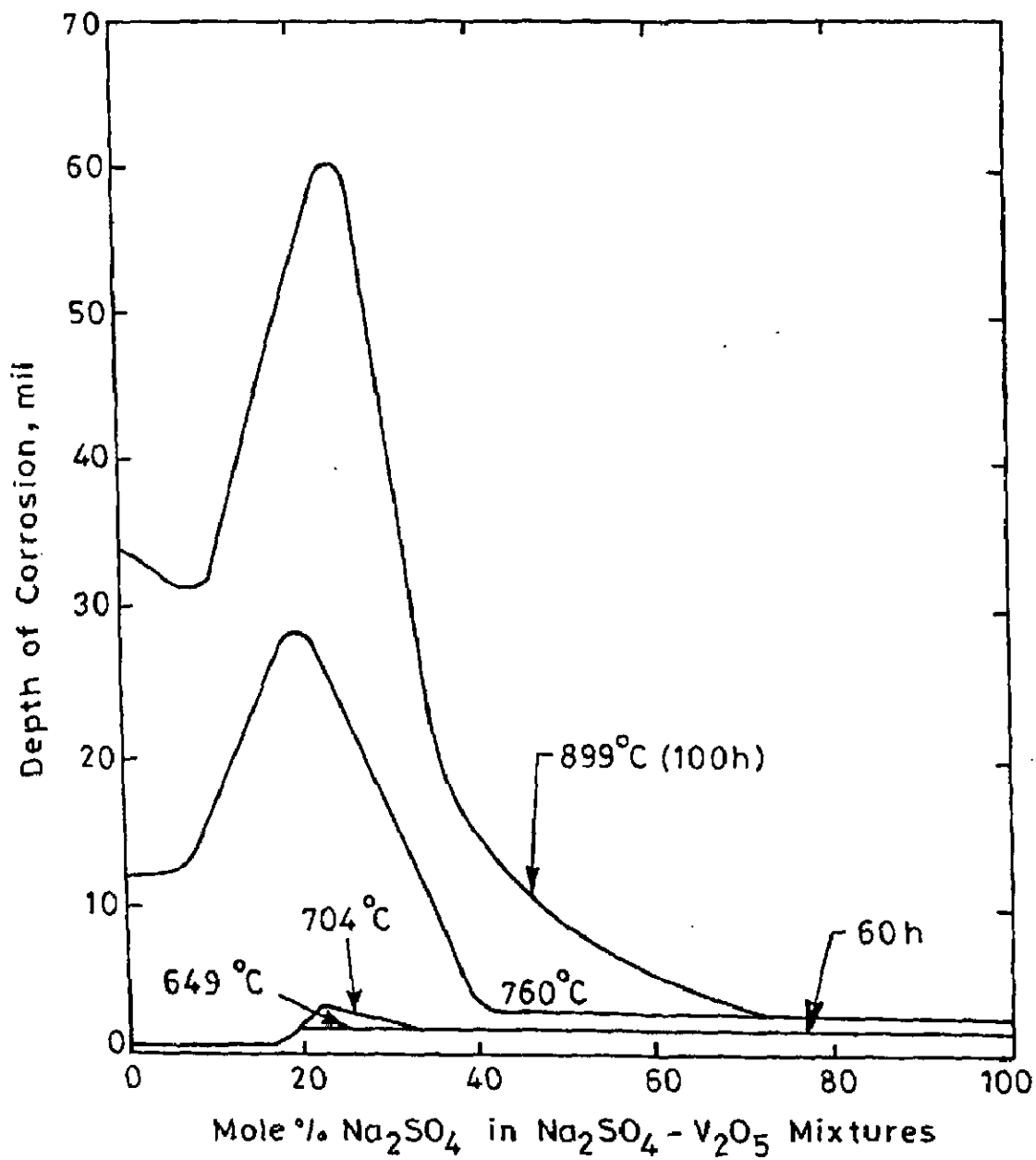


Fig. 2.6 Corrosion rate of Type 304 stainless steel in different mixtures of Na<sub>2</sub>SO<sub>4</sub>-V<sub>2</sub>O<sub>5</sub> (Natesan, 1976).

Almeraya et al (1998A) carried out electrochemical studies of hot corrosion of steel AISI-SA-213-TP-347H in 80 wt%  $V_2O_5$  + 20 wt%  $Na_2SO_4$  at 540<sup>0</sup>C–680<sup>0</sup>C and reported the corrosion rate values of around 0.58-7.14 mm/year. They observed an increase in corrosion rate with time. However the corrosion potential was observed to be decreasing with increase in temperature from 540 to 680<sup>0</sup>C. Almeraya et al (1998 B) further conducted similar studies on type 347H stainless steel under same environment and temperature range, and revealed the fact that with change in temperature from 540 to 680<sup>0</sup>C the corrosion potential decreased.

Cuevas-Arteaga et al (2001) used both LPR (Linear Polarisation Resistance) and weight loss techniques, in their hot corrosion study on alloy 800 in  $Na_2SO_4$ -20% $V_2O_5$ , and reported slightly higher corrosion rate at 900<sup>0</sup>C than at 700<sup>0</sup>C. They further reported that in both the techniques, corrosion rates increased in the beginning of the experiment but decreased later on until steady values reached.

Singh (2003), during his studies on the hot corrosion of GrA1, T11 and T22 boiler steels in an environment of  $Na_2SO_4$ -60% $V_2O_5$  at 900<sup>0</sup>C, observed that the Mo containing T22 steel showed least resistance to the hot corrosion attack. This was attributed to the formation of a low melting point  $MoO_3$  phase, which reacted with molten salt resulting in formation of  $Na_2MoO_4$ . This low melting point oxide was suggested to cause the acidic fluxing of the protective scale.

### 2.3.2 Nickel and Nickel-Based Alloys

Thilakan et al (1967) studied hot corrosion of nickel free austenitic stainless steel, Cr-Ni stainless steel and Inconel in oxygen atmosphere at different temperatures with vanadium-sodium slags of varying composition. They justified the use of saturated solution of  $Na_2SO_4$  as the liquid medium because of its low gas solubility, vapour pressure and viscosity. Threshold temperature was found to lie between 700 and 800<sup>0</sup>C. Above the threshold temperature the extent of attack initially increased but with increasing temperature either it became constant (as observed for Inconel) or decreased (for other alloys). Increase in amount of  $Na_2SO_4$  in sodium sulphate-vanadium pentaoxide mixtures first increased and then decreased the rate of oxidation at the temperature of 820 and 870<sup>0</sup>C. At 950<sup>0</sup>C, all  $Na_2SO_4$  additions to  $V_2O_5$  decreased its corrosive effect. The fluidity of slag was observed to be important in allowing diffusion of oxygen. According to an interesting observation of their study, nickel free stainless steel was found to have a high resistance to attack against  $V_2O_5$ - $Na_2SO_4$  mixture, and under the experimental conditions showed a resistance superior to that of even Inconel at temperatures above 850<sup>0</sup>C especially in 70%  $V_2O_5$ -30%  $Na_2SO_4$  environment.

Bornstein et al (1973) investigated the relationship between vanadium oxide and  $\text{Na}_2\text{SO}_4$  accelerated oxidation for nickel-base superalloy B-1900 and seven binary nickel-base alloys. It was established that the corrosion attack commenced by dissolution of the normally protective oxide scale into the fused salt. The dissolution was suggested to occur by a reaction between oxide ions present in melt and the oxide scale. They further opined that the sulphidation attack can be inhibited by decreasing the oxide ion content of the fused salt. In another study, Bornstein et al (1975) reported the effect of vanadium and sodium on the accelerated oxidation of nickel base alloys. The initial rapid rate of oxidation between  $\text{V}_2\text{O}_5$  and metal substrate was attributed to the reduction of  $\text{V}_2\text{O}_5$  by the substrate. According to them, intermetallics  $\text{Ni}_3\text{Al}$  and  $\text{NiAl}$  were particularly susceptible to  $\text{V}_2\text{O}_5$  corrosion. They further concluded that the sulphidation attack can be attenuated if the initial oxide ion content of the melt is prevented from increasing. Oxides such as  $\text{Cr}_2\text{O}_3$  have been reported to react preferentially with oxide ions.

A 50Cr-50Ni commercial alloy was corroded in pure  $\text{V}_2\text{O}_5$  and in vanadate melts containing sodium sulphate and chloride in the temperature range 750 to 950<sup>0</sup>C in a rotating disc apparatus by Dooley et al (1975). The study reported the formation of chromium rich oxide scale in pure  $\text{V}_2\text{O}_5$  which dissolved only slowly into the liquid melt and thus observed to act as a barrier layer. In  $\text{Na}_2\text{O}.6\text{V}_2\text{O}_5$ , this barrier layer was not observed. Marked internal oxidation of the Cr-rich  $\alpha$ -phase was noticed in chloride containing melts throughout the temperature range 750-950<sup>0</sup>C.

Thermogravimetric studies which delineate the conditions for simultaneous sulphate and vanadate induced corrosion at 650 to 800<sup>0</sup>C have been carried out by Seiersten and Kofstad (1987). They found that the corrosion caused by sodium sulphate/sodium vanadate mixtures have a complex mechanism. Samples coated with sodium vanadate were exposed to  $\text{O}_2 + 4\% \text{SO}_2$  and the initial reaction was observed to be same as that observed in pure oxygen. After an incubation period the duration was found to decrease with increasing temperature and sufficient  $\text{SO}_3$  got dissolved in the molten vanadate which resulted in formation of a mixture of  $\text{NiSO}_4$  and  $\text{Na}_2\text{SO}_4$  near the metal. When a molten  $\text{NiSO}_4$ - $\text{Na}_2\text{SO}_4$  solution containing small amounts of vanadate was formed as an intermediate layer the reaction reportedly proceeded as sulphate-induced hot corrosion. The corrosion mechanism was observed to change from initial vanadate-induced to essentially sulphate induced hot corrosion when the sulphur trioxide pressure was high enough to form sodium sulphate.

Sidky and Hocking (1987) investigated the mechanisms of hot corrosion by molten sulphate-vanadate deposits for Ni-10Cr, Ni-30Cr, Ni-20Cr-3Al, Ni-21Cr-0.3Si, Ni-20Cr-5V alloys and IN738 superalloy. The effect of adding Cr to Ni was found to be beneficial in the  $\text{Na}_2\text{SO}_4$  melt, however, on increasing the  $\text{VO}_3^-$  concentration in the melt, this effect diminished, becoming harmful in pure  $\text{NaVO}_3$  due to the formation of the non protective  $\text{CrVO}_4$ . According to them alloying element Al was found to be harmful in  $\text{Na}_2\text{SO}_4$ - $\text{NaVO}_3$  melts. Cr depletion was observed in rich  $\text{VO}_3^-$  melts but internal corrosion was more obvious in the  $\text{SO}_4^{2-}$  rich melts. Corrosion in rich  $\text{VO}_3^-$  melts was aggressive due to the fluxing action of the salt, which takes place along internally sulphidised areas. According to their study, IN738 suffered tremendous internal attack due to its  $\gamma$  precipitates which became sulphidation prone areas, and were fluxed by the  $\text{VO}_3^-$  melt.

The presence of sulphur and its oxidised compounds favour the formation of isolated lobes with radial morphology (Otero et al, 1987) during the hot corrosion of IN657 at 908K in molten salt environment. These lobes had great permeability which facilitated the access of oxygen; therefore the protection character of the scale was reduced. They further reported that the presence of vanadium and its oxidised products generate compounds with aciculate morphology, which is not very much covering and contribute to reduce the protective character of the scale. The equilibrium diagram for varying composition of  $\text{Na}_2\text{SO}_4$  is shown in Fig. 2.7 and the mixture of  $\text{Na}_2\text{SO}_4$ -60% $\text{V}_2\text{O}_5$  is seen to be the lowest eutectic temperature.

The effects of chromate and vanadate anions on the hot corrosion of Ni by a thin fused  $\text{Na}_2\text{SO}_4$  film in an  $\text{SO}_2$ - $\text{O}_2$  gas atmosphere at  $900^\circ\text{C}$  were investigated by Otsuka and Rapp (1990). Their results showed that the inhibition of sulphidation may result from the precipitation of solid  $\text{Cr}_2\text{O}_3$  from the melt and thereby partially sealing/plugging the crack defects and grain boundaries of the original protective oxide layer. They proposed that vanadate anions enhanced the onset of the hot corrosion and sulphidation probably via rapid dissolution of the protective oxide scale at cracks/defects or grain boundaries.

Lambert et al (1991) studied the oxidation and hot corrosion of Ni-17Cr-6Al-0.5Y and Ni-16Cr-5.7Al-0.47Y-5Si alloys at  $700^\circ\text{C}$  in  $\text{Na}_2\text{SO}_4$ -60% $\text{V}_2\text{O}_5$  to ascertain the effect of addition of Si. They observed an outer layer of NiO developed on the surface of the Ni-17Cr-6Al-0.5Y alloy whereas a thin  $\text{Al}_2\text{O}_3$  oxide scale formed on the Si-enriched alloy. They further opined that the condensed vanadates of sodium are highly corrosive and can markedly increase the rate of oxidation of nickel base superalloys.

In the same aggressive environment ( $\text{Na}_2\text{SO}_4$ -60% $\text{V}_2\text{O}_5$ ) the hot corrosion behaviour of Superalloy IN-657 at 1000 K has been investigated by Otero et al (1990, 1992). They reported that corrosion rate of the alloy in contact with molten salt mixtures was approximately reduced by one order of magnitude over exposure times of 210 hr when the amount of molten salt was kept constant. During the initial stages of the exposures the corrosion rate increased with the temperature up to 1000 K and decreased for still higher temperature. After 100 hr of exposure, it was observed that the temperature scarcely influenced the corrosion kinetics.

Swaminathan and Raghvan (1992) reported that cracking and fluxing of the protective scales together with easier crack nucleation and growth at grain boundaries in the presence of liquid deposits of sodium metavanadate and sodium metavanadate plus 15wt% sodium sulphate at 650-750<sup>0</sup>C accounted for the enhanced creep rates and reduced rupture life for Superni-600. During similar study on Superni-C 276 in the same temperature range, they have reported that eutectic  $\text{NaVO}_3$  + 15wt%  $\text{Na}_2\text{SO}_4$  mixture was more severe in degrading the creep properties (Swaminathan and Raghavan, 1994). The corrosives were found to reduce the rupture life through enhanced creep deformation. They further opined that the degradation of the alloy in case of  $\text{NaVO}_3$  melt was due to the cracking of the protective scales under the influence of the applied stress and the fluxing action of the melt. The addition of sodium sulphate to sodium metavanadate increased the corrosivity of the deposit by lowering the melting point and by formation of molten Ni-Ni<sub>3</sub>S<sub>2</sub> eutectic which initiates a self-sustaining hot corrosion. It was suggested that the additional presence of molybdenum compounds  $\text{Na}_2\text{MoO}_4$ - $\text{MoO}_3$  caused enhanced degradation.

Oxidation and hot corrosion in sulphate, chloride and vanadate environment of a cast nickel base superalloy have been reported by Deb et al (1996). Weight gain studies were carried out in air for the uncoated samples and coated with 100%  $\text{Na}_2\text{SO}_4$ , 75%  $\text{Na}_2\text{SO}_4$  + 25%  $\text{NaCl}$  and 60%  $\text{Na}_2\text{SO}_4$  + 30%  $\text{NaVO}_3$  + 10%  $\text{NaCl}$ . The presence of sulphur in the form of sulphates has been reported to cause internal sulphidation of the alloy beneath the external oxide layer. They observed the formation of volatile species by chlorides which further led to formation of voids and pits at grain boundaries. These voids and pits were suggested to provide easy path for flow of corrodents. It was proposed that the presence of vanadate in conjunction with sulphate and chloride provided additional fluxing action, which destroyed the integrity of the alloy and weakened its mechanical properties.



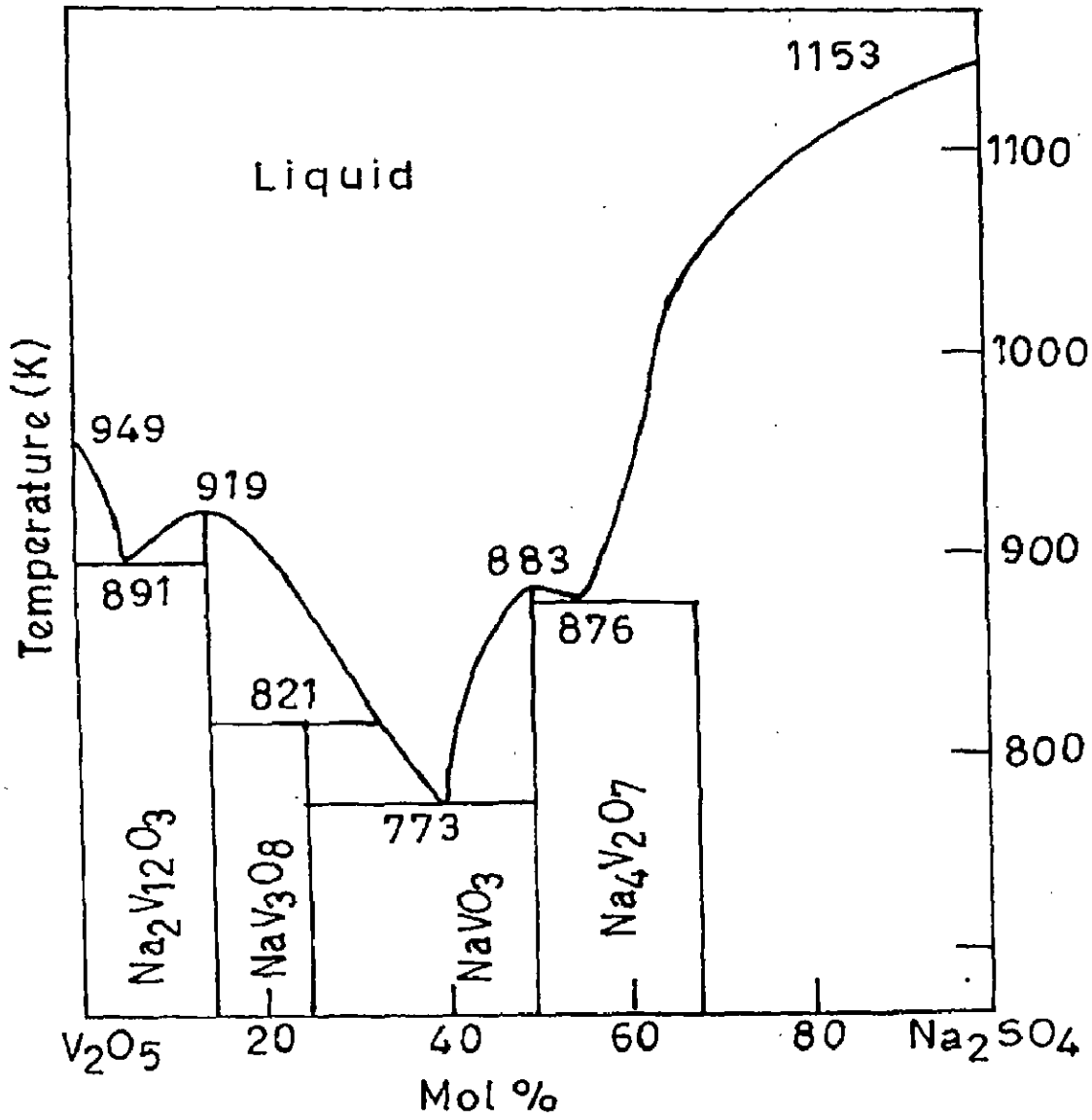


Fig. 2.7 Phase Diagram for  $\text{Na}_2\text{SO}_4$ - $\text{V}_2\text{O}_5$  System (Otero et al, 1987).

Gurrappa (1999) during hot corrosion studies on CM 247 LC Superalloy in  $\text{Na}_2\text{SO}_4$  and  $\text{Na}_2\text{SO}_4+\text{NaCl}$  mixtures at  $900^\circ\text{C}$  observed that the superalloy CM 247 LC got severely corroded in just 4 hr, while it was completely consumed in 70 hr when tested in  $90\%\text{Na}_2\text{SO}_4+10\%\text{NaCl}$  at  $900^\circ\text{C}$ . The life of the superalloy, however, further decreased to just 2 hours in  $90\%\text{Na}_2\text{SO}_4+5\%\text{NaCl}+5\%\text{V}_2\text{O}_5$  at  $900^\circ\text{C}$ .

Lee and Lin (2002) carried out studies on the molten salt-induced oxidation/sulphidation on nickel aluminide intermetallic compound ( $\text{Ni}_3\text{Al}$ ) in the  $1\%\text{SO}_2/\text{air}$  gas mixtures. Their observations on hot-corroded specimen tested at different period of time showed the formation of only  $\text{NiO}$  at  $605^\circ\text{C}$ , and  $\text{NiO}$  and  $\text{NiAl}_2\text{O}_4$  at  $800$  and  $1000^\circ\text{C}$ . EDAX analysis revealed the presence of  $\text{AlS}_x$  and/or  $\text{NiS}_x$  beneath the oxide scale at all the temperatures. Based on the experimental studies, a hot corrosion mechanism was proposed by the investigators, according to which  $\text{NiO}$  oxide formation consumed the oxygen in the molten salt, which locally reduced the oxygen and increased the sulphur partial pressure in the molten salt. Stability diagram was used to represent this partial pressure change of sulphur. They suggested that as the increased partial pressure of the sulphur reaches to equilibrium partial pressure region of  $\text{NiS}_x$  and/or  $\text{AlS}_x$ ,  $\text{NiS}_x$  and/or  $\text{AlS}_x$  will form at the salt/alloy interface through sulphidation reaction. The consumption of sulphur will balance out the sulphur, and oxygen partial pressure increases in the molten salt. This will force  $\text{NiO}$  to form. This process confirmed the simultaneous formation of  $\text{NiO}$ ,  $\text{NiS}_x$  and/or  $\text{AlS}_x$ . They further opined that as the sulphides are thermodynamically unstable when the oxygen partial pressure increases, it is possible for sulphide to convert into oxides  $\text{NiO}$ ,  $\text{Al}_2\text{O}_3$  and  $\text{NiAl}_2\text{O}_4$  through necessary reactions. Two possibilities have been pointed out for the formation of spinel phase, either through the reaction of Al and Ni with oxygen in the molten salt or through the evolution of sulphides.

Gitanjaly (2003) has conducted hot corrosion studies on some Ni-, Fe- and Co-based superalloys in an environment of  $\text{Na}_2\text{SO}_4+60\%\text{V}_2\text{O}_5$  at  $900^\circ\text{C}$ . Whilst the observed corrosion rate was significant in all the superalloys, Ni-base superalloy Superni 75 showed lowest rate of corrosion and the Co-base superalloy Superco-605 the highest. Better corrosion resistance of Ni-base superalloys was attributed to the presence of refractory nickel vanadate  $\text{Ni}(\text{VO}_3)_2$  which acted as a diffusion barrier for the oxidising species. The proposed hot corrosion mechanisms of this study for the superalloys Superni 75 and Superni 601 have been schematically shown in Fig. 2.8.

Tzvetkoff & Gencheva (2003) presented a review on mechanism of formation of corrosion layers on nickel and nickel-based alloys in melts containing oxyanions. The molten sulphate mixtures are stated to be particularly aggressive towards Ni superalloys. In such environments, the formation of Cr-rich passive films such as spinel-type oxides could be protective to some extent. They further revealed that at metal/oxide interface, sulphides are detected which do not offer plausible protection except for a possible positive role of MoS<sub>2</sub> formed on Ni alloys containing significant amounts of Mo. Furthermore, acidic oxides such as those of V and Mo have been reported to induce rapid fluxing of the oxide scale and therefore catastrophic hot corrosion. Whereas, the chromates were stated to be beneficial for the repassivation of the surfaces following fluxing of the oxide scale by the molten salt.

## 2.4 COUNTERMEASURES AGAINST HOT CORROSION

Corresponding to the variety of corrosive environments is the number of countermeasures that have been developed to avoid excessive material damage. They can be grouped into following categories as suggested by Heath et al (1997):

1. Alloy selection: A large number of Fe, Ni- and Co-based alloys exist today especially designed for good resistance to oxidation, sulphidation or corrosion by ash/salt deposits.
2. Design aspect: Improve temperature distribution (avoid hot spots), avoid excessive deposition of ash and slags by use of soot blower, rapping, screens etc.
3. Chemical additives: Neutralisation of corrosive components in the flue gases by injecting additives such as limestone and dolomite.
4. Shielding: SiC tiles in waste incinerations, other type of refractory linings
5. Coatings: Different coating techniques are applied to protect the critical surface areas from corrosive gases, including co-extrusion, chromising, weld overlay and thermal spray coatings.

Various time-proven methods for preventing and controlling corrosion depend on the specific material to be protected, environmental concerns such as soil resistivity, humidity, and exposure to saltwater or industrial environments, the type of product to be processed or transported and many other factors (Koch et al, 2002).

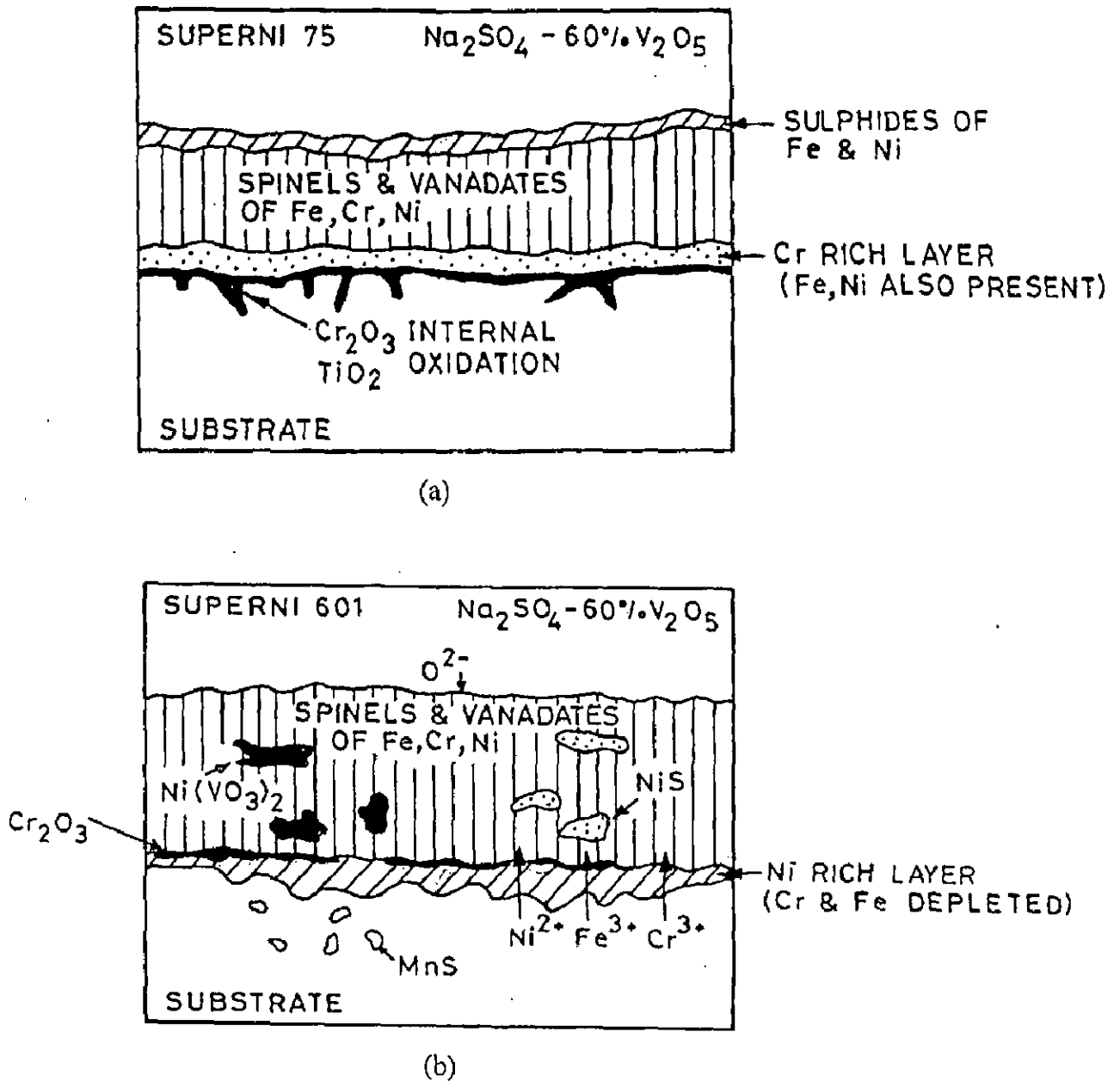


Fig. 2.8 Schematic diagram showing probable hot corrosion mechanism in  $\text{Na}_2\text{SO}_4-60\% \text{V}_2\text{O}_5$  after exposure for 50 cycles at  $900^\circ\text{C}$  for alloys (Gitanjaly, 2003)  
 (a) Superni 75 (b) Superni 601.

Depletion of high grade fuels and for economic reasons use of residual fuel oil in energy generation systems are well known. Fuels with sulphur and other impurities bring about hot corrosion which significantly reduces the life of components (Sharma, 1996). The option to use low grade fuel limits the improvement in hot corrosion environment.

Inhibitors and fuel additives have been used with varying success to prevent oil ash corrosion. There are a number of inhibitors commercially available that are intended to reduce the severity of oil ash corrosion. Because of its effectiveness and relatively low cost the most common fuel additives are based upon MgO (Paul and Seeley, 1991). The inhibition of hot corrosion by MgSO<sub>4</sub> has also been reported by Barbooti et al (1988) for Stainless Steel 304. Further the inhibitors like MgO, CaO, ZnSO<sub>4</sub>, MnO<sub>2</sub>, CeO<sub>2</sub>, Y<sub>2</sub>O<sub>3</sub>, ZrO<sub>2</sub> and SnO<sub>2</sub> are reported to be effective to decrease the extent of hot corrosion pertaining to molten salt environment (Na<sub>2</sub>SO<sub>4</sub>-60%V<sub>2</sub>O<sub>5</sub>) for iron-, nickel- and cobalt-based superalloys by Gitanjaly and Prakash (1999), Gitanjaly et al (2002) and Gitanjaly (2003). However, a major challenge still exist as to how to apply these inhibitors at the corrosion prone locations such as in the energy generation systems, gas turbine engines etc.

## 2.5 USE OF PROTECTIVE COATINGS

A coating can be defined as a layer of material, formed naturally or synthetically or deposited artificially on the surface of an object made of another material, with the aim of obtaining required technical or decorative properties (Burakowski and Wierzchon, 1999). There are three main kinds or compositions of barriers: Inert or essentially inert, inhibitive and sacrificial. Various combinations of these types are found in coating systems designed to use some or all of the several protective advantages provided. It must be remembered that there is no such thing as a "perfect" coating in a practical sense so none of these types or any combination can be expected to give perfect protections (Hamner, 1977).

Coatings provide a way of extending the limits of use of materials at the upper end of their performance capabilities, by allowing the mechanical properties of the substrate materials to be maintained while protecting them against wear or corrosion (Sidky and Hocking, 1999).

The demand for protective coatings has increased recently for almost all types of superalloys with improved strength, since high-temperature corrosion problem become much more significant for these alloys with increasing operating temperatures of modern heat engines (Yoshida, 1993). The desire for higher operating temperature, improved performance, extended component lives, and cleaner and more fuel-efficient power plant/processes places severe demands on the structural materials used to construct such a high-temperature plant. As a result, many components operating at high temperature within such plants are coated or surface treated (Nicholls, 2000).

In addition to the development of the conventional steam-raising plant, alternative energy supply systems, such as combined cycle plants, in which a gas turbine and a steam turbine are coupled, offer the prospect of even higher thermal efficiencies, as the gas turbine inlet temperatures are 1200<sup>o</sup>C and above (Nickel et al, 2002). According to them, such high temperatures result in increased oxidation rates, therefore protective coatings with higher temperature capabilities are required.

Further, Porcayo-Calderon et al (1998) have reported the use of protective coatings for the superheater/re-heater components of boiler where the material severely suffers on fireside corrosion. According to Taylor and Evans (2001), a few earlier attempts have been made on the thermal sprayed protective coatings for fossil power plants though the thermal spray process is extensively used for gas turbine applications. Sundararajan et al (2003A and B) advocate the need for applying thermal spray coatings on the boiler components.

### **2.5.1 Desirable Features of Effective Coating System**

Nicholls (2000) has summarised the desirable features for effective coating systems as in Table 2.1. These features form the framework around which the design requirements of a coating for good oxidation/corrosion resistance can be discussed. The coatings produced by various deposition methods do not have the same properties and this is related to microstructure variations. Further the process conditions can be varied for any given coating method and this will affect the microstructure. In view of these facts, Bull (1994) emphasized that considerable attention should be paid to microstructure of the coating if performance is to be understood.

**Table 2.1** Desirable features for effective coating system (Nicholls, 2000)

Coating Property	Requirement	Location of Requirement		
		Coating Surface	Bulk	Coating/ Substrate Interface
Oxidation/ Corrosion Resistance	Low rates of scale formation	X	-	-
	Uniform surface attack	X	-	-
	A thermodynamically stable surface oxide	X	-	-
	Ductile surface scales	X	-	-
	Adherent surface scales	X	-	-
	High concentration of scale forming elements within the coating to act as reserve for the scale repair	X	X	-
Interface Stability	Low rate of diffusion across interface at operating temperatures	-	-	X
	Limited compositional changes across interface	-	-	X
	Absence of embrittling phase formation during service	-	-	X
Good Adhesion	Matched coating and substrate properties to minimise coating mismatch and stress generation at coating/substrate interface	-	X	X
	Optimum surface condition before coating	-	-	X
	Growth stresses during formation should be minimised	-	X	X
Mechanical Strength	Coating must withstand all stress (creep, fatigue and impact loading) that is generated at component surface during service	-	X	-
	Well matched thermal expansion coefficients between coating and substrate to minimise thermal stressing and thermal fatigue	-	X	X

### 2.5.2 Coating Processes

The commonly employed methods of applying metallic coatings have been enlisted in Fig. 2.9 (Bhushan and Gupta, 1991). From a production point of view, three methods are in current use, these being chemical vapour deposition (CVD) from a pack, physical vapour deposition (PVD) and thermal spraying (metal spraying). A serious drawback of the pack process is the inclusion of pack particles in the coating which can lead to coating failure (Nicoll, 1984). Moreover, disadvantage of the CVD process is that, because it is a non-line-of-site technique, proper masking and tooling become design considerations and an expense (DeMasi-Marcin and Gupta, 1994). Moreover, according to DeMasi-Marcin and Gupta (1994), the PVD method is a complex process,

especially in case of deposition of M-Cr-Al-Y type coatings as the vaporisation pressures of each of the elements of interest must be considered for producing controlled alloy chemistry. Still vapour deposition and plasma spray (a thermal spray process) have been reported to be two major coating processing technologies used worldwide by them. Ilavsky et al (2000) have also reported that the thermally sprayed deposits have often superior properties with potentially lower application cost or less environmental issues as and when compared to other industrially used coatings such as CVD, PVD, hard chromium plating.

It is worth noting that as operating temperature is increased, it no longer becomes possible to achieve the desired service lives using diffusion coatings, so overlay coatings are the only possible development route (Nicholls and Stephenson, 1995). Further it has been learnt from the literature that for depositing overlay coatings, thermal spray technologies are often considered.

#### **2.5.2.1 Thermal Spray Coating Processes**

M.U. Schoop was the first scientist to explore the possibility that a stream of metallic particles formed from molten metal might be used to produce coatings in the early 1900s. But the thermal spraying technologies expanded in the 70s due to development of thermal plasmas, and the increasing demand of high temperature and wear resistant materials and coating systems (Knotek, 2001). In the 1990s thermal spraying was highly available and had become a standard tool for improving surfaces in most industries. Thermal spraying is the application of a material (the consumable) to a substrate by melting the material into droplets and impinging the softened or molten droplets on a substrate to form a continuous coating (Budinski, 1998). The spray processes that have been used to deposit coatings for protection against high temperature corrosion are enlisted below, as summarised by Heath et al (1997):

- Flame spraying with a powder or wire
- Electric arc wire spraying
- Plasma spraying
- High Velocity Oxy-fuel (HVOF) spraying
- Spray and fuse



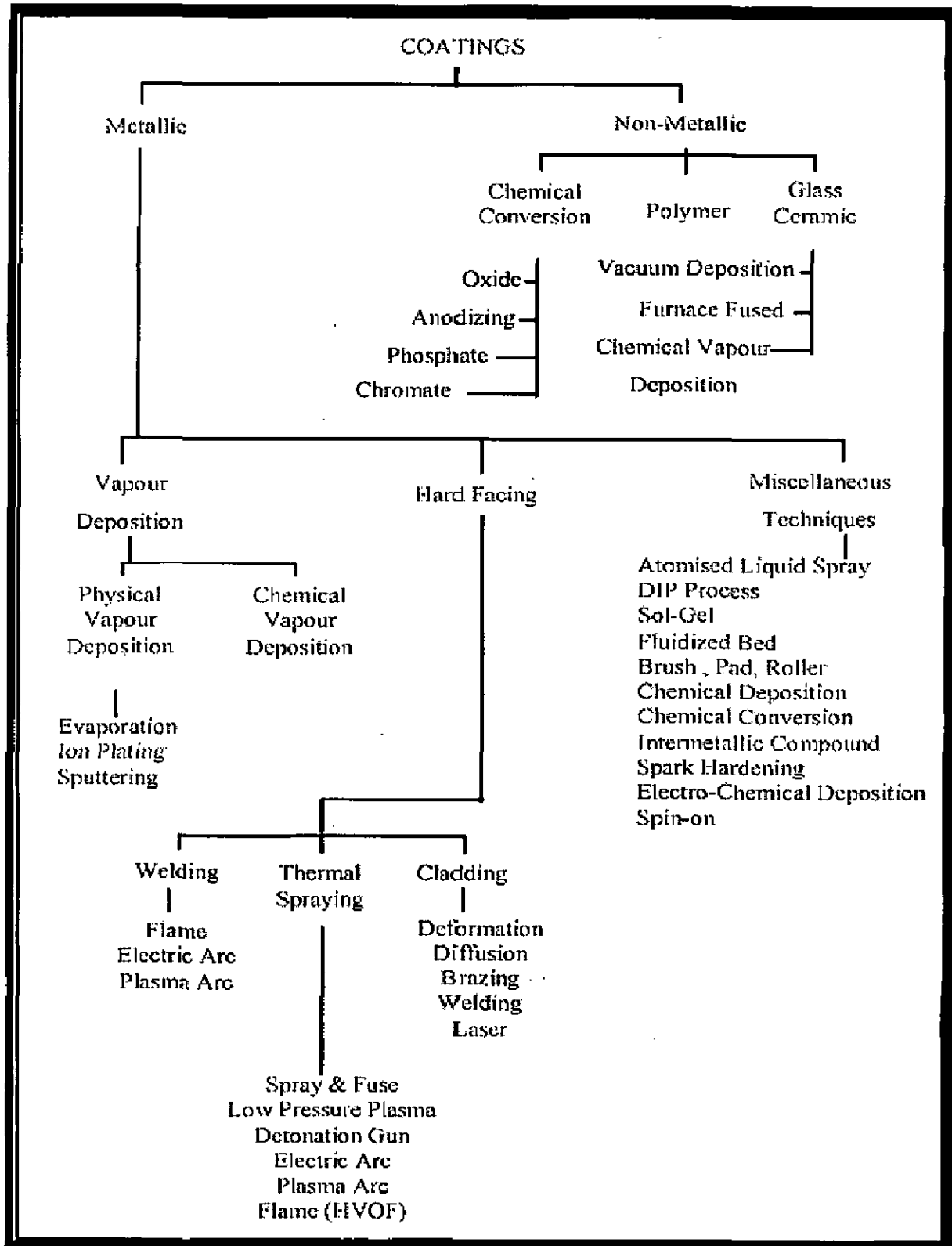


Fig. 2.9 Coating deposition technologies (Bhushan and Gupta, 1991).

These processes are basically differentiated from each other on the basis of particle speed, flame temperature and spray atmosphere. The typical properties which are influenced by the coating procedure are coating porosity, oxide content and bond strength. In spray processes the coating adhesion is very sensitive to surface preparation, as the coating adhesion usually depends upon the mechanical anchorage to the surface of the substrate (Heath et al, 1997). Therefore, a thorough substrate surface preparation is necessary. Contaminants such as rust, scale grease, moisture, etc. must be removed from the surface. After cleaning usually a roughening of the substrate surface follows to ensure coating adhesion. Common methods for surface roughening, which are often combined (Knotek, 2001), are:

- Dry abrasive grit blasting.
- Machining or macro roughening.
- Applying a bond coat.

The thermal spray coating process should start as soon as possible after the surface preparation is completed, since the prepared surface is very active and, oxidation, recontamination, etc. should be avoided. In general, the thermal spraying processes used for hard coatings may be divided into two basic processes: combustion spraying and plasma spraying (Knotek, 2001).

The main advantages of the thermal spray coatings have been presented by Heath et al (1997) as follows:

1. Very flexible concerning alloy selection and optimisation for specific resistance to corrosive environments and particle abrasion/erosion. Surface properties can be separated from required mechanical properties of the structural components.
2. Coating systems (multi-layer or functionally graded) can be used, combining for example good adhesion with optimised corrosion and erosion behaviour.
3. Unique alloys and microstructures can be obtained with thermal spraying which are not possible with a wrought material. These include continuously graded composites and corrosion resistant amorphous phases.
4. Cost of the coating solution are normally significantly lower than those of a highly alloyed bulk material, thermal spray coatings are specially interesting for their cost/performance ratio.
5. Thermal spray coatings additionally offer the possibilities of on-site application and repair of components, given a sufficient accessibility for the sprayer and his equipment. However, thermal spraying in the work shop is preferred, whenever possible, to achieve optimum results.

Among the thermal spray coating processes, plasma spraying is reported to be versatile technology that has been successful as a reliable cost-effective solution for many industrial problems by Fauchais et al (1997). Plasma spraying is the most flexible thermal spray process with respect to the sprayed materials. The high temperatures of plasma spray processes permit the deposition of coatings for applications in areas of liquid and high temperature corrosion and wear protection and also special applications for thermal, electrical and biomedical purposes (Knotek, 2001). Plasma-sprayed metallic coatings are used in high-temperature applications e.g. in diesel engines, air-craft engines and land-based gas turbines to protect the component from oxidation and corrosion (Niranatlumpong et al, 2000).

## 2.6 PLASMA SPRAYING

Plasma spraying is part of thermal spraying, a group of processes in which finely divided metallic and non-metallic materials are deposited in a molten or semi-molten state on a prepared substrate (Fauchais, 2001).

In the fifties, the plasma torches were developed to test materials at high enthalpies for simulated re-entry vehicles. Then in late fifties and early sixties, the first serious attempts were reported using plasma torches for spraying of primarily refractory materials. Almost any material can be used for plasma spraying on almost any type of substrate. This flexibility is probably one of the major reasons for the rapid expansion of this technology (Pfender, 1988). The high temperatures enable the use of coating materials with very high melting points such as ceramics, cermets and refractory alloys. Materials can be processed as long as there is a temperature difference of at least 300K between the melting temperature and decomposition or evaporation temperature (Fauchais et al, 1991).

Plasma techniques are capable of producing thick coatings films more than 100  $\mu\text{m}$  at high production rates with no degradation of the mechanical properties of the alloy substrate (Yoshida, 1993). But problems that may be encountered are porosity and poor adhesion, especially in case of adhesion of ceramics to metals. Further, adhesion can be improved by the use of bond coat interlayer and /or powder of small particle size.

Among other key features of plasma spraying are formation of microstructures with fine, noncolumnar and equiaxed grains, ability to produce homogeneous coatings that do not change in composition with thickness (length of deposition time), ability to process materials in virtually any environment (e.g., air, reduced-pressure inert gas, high pressure, under water) (National Materials Advisory Board, 1996).

Applications for plasma spraying include corrosion, temperature and abrasion resistant coatings and production of monolithic and near net shape shapes, which at the same time take advantage of the rapid solidification process. Powder of glassy metals can be plasma sprayed without changing their amorphous characteristics. High temperature superconductive materials have also been deposited by the plasma spray process (Pfender, 1988). The plasma spray also finds application in reclamation of worn or corroded components, production of aerospace and nuclear power components. A new application of plasma spraying is in producing hydroxyapatite coatings onto the stems of orthopaedic endoprostheses (Batchelor et al, 2003).

## 2.6.1 Plasma Spraying-The Process

### 2.6.1.1 Plasma Jets

A plasma torch or gun consists of a water cooled copper anode and a thoriated (2 wt%) tungsten cathode as shown in Fig. 2.10. Argon gas flows around the cathode and through the anode. The shape of the anode is made as a constricting nozzle. A gas, usually argon or nitrogen or a mixture of these with hydrogen or helium flows around the cathode and exits through the anode nozzle. The typical value of the flow rate of the gas as reported by Sidky and Hocking (1999) is  $3.5 \text{ L min}^{-1}$ . Further material used for the anode is usually high purity oxygen free copper (Fauchais, 2004B).

A dc arc is maintained between the electrodes and plasma of ions and atoms emerges at a temperature of  $6,000\text{-}12,000^{\circ}\text{C}$  at a distance of 1 cm from the nozzle, decreasing rapidly to  $3000^{\circ}\text{C}$  at a distance of 10 cm from the nozzle. The gas plasma generated by the arc consists of free electrons, ionised atoms and some neutral atoms and undissociated diatomic molecules if nitrogen or hydrogen is used as reported by Tucker (1994). The point of entry of the powder into the plasma jet is usually in the diverging portion of the nozzle or sometimes the powder is fed externally. In some applications RF (Radio frequency) discharges are used as heat sources instead of dc arc. Compared to dc arc torches the main difference is in the torch internal diameter, resulting in flow velocities below  $100 \text{ ms}^{-1}$  and the axial injection of particles (Fauchais, 2004B).

Plasma gas velocities with most conventional torches are subsonic, but supersonic velocities can be generated by using converging-diverging nozzles with critical exit angles. The most important parameters relative to the powder particles at impact on the surface are their temperature, velocity and extent of reaction with the gaseous environment (Tucker, 1994). Near the nozzle, the gas velocity is  $200\text{-}600 \text{ ms}^{-1}$  but the particle velocity is only  $20 \text{ ms}^{-1}$ . However the particle acceleration (due to gas

frictional forces) is 100 000 g so that 18  $\mu\text{m}$  particles reach a maximum velocity of 275  $\text{ms}^{-1}$  at a distance of 6 cm from the nozzle (Sidky and Hocking, 1999).

The very high temperature generated in plasma spray process melts even the most refractory particles. But at the same time low melting point materials such as plastics can also be sprayed. The temperature of the core of the plasma may exceed 30,000 $^{\circ}\text{C}$  (Tucker, 1994). A schematic of a typical distribution of temperature in the plasma has been shown in Fig.2.11 (Knotek, 2001). Further, Plasma spraying operates at high energy levels; the power consumption of a typical coating unit is approximately 50 kW with an electric current of several hundred amperes flowing in the plasma arc (Batchelor et al, 2003).

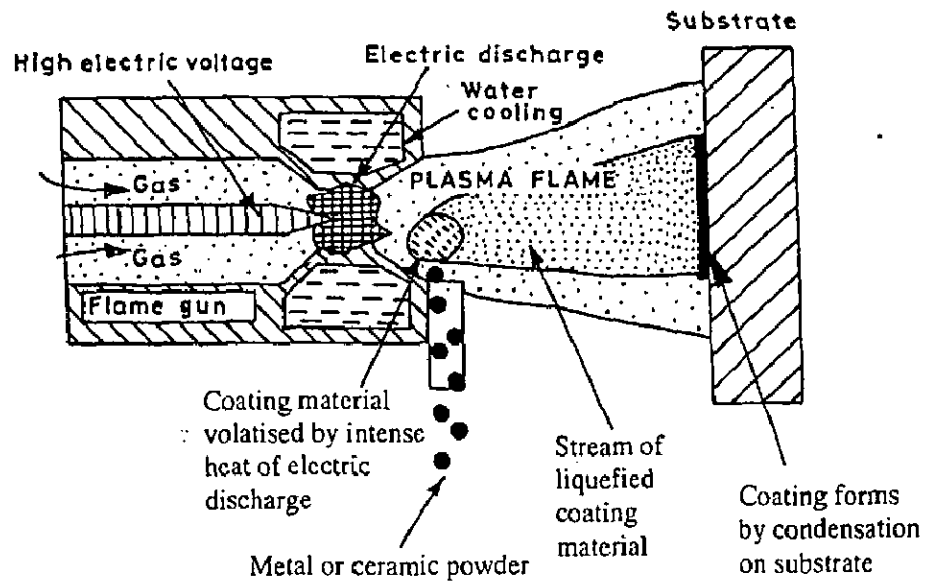
The plasma jet is typically 5 cm in length and distance from the substrate is of the order of 15 cm. Oxidation is minimal because of low dwell time and use of a reducing gas. The temperature of the substrate rarely exceeds 320 $^{\circ}\text{C}$  and is often below 150 $^{\circ}\text{C}$ . Plasma spraying process is a process which causes no distortion of the substrate (Sidky and Hocking, 1999).

#### **2.6.1.2 Coating Formulation**

For strong dense plasma sprayed coatings, most of the particles must be molten before impingement and must have sufficient velocity to splat into the irregularities of the previous splats. Many coatings contain readily oxidised elements (e.g. aluminium, molybdenum and titanium) for which plasma spraying at low pressure (20 mbar) or in argon is advantageous. Underwater plasma spraying offers much scope for deposition of wear and corrosion resistant coatings on submerged substrates such as offshore structures (Sidky and Hocking, 1999).

The high impingement speeds of the molten particles during spraying are intended to ensure that the molten droplets disintegrate on contact instead of remaining as discrete droplets, this process is known as splat formation. The structure of the plasma sprayed coatings can be envisaged as a series of interlocking splats (Batchelor et al, 2003). The splats have columnar or equi axed structures with grain sizes between 50 and 200 nm. However this fine structure is altered by grain size effect, large volume fraction of internal interfaces, voids, pores and so on (Fauchais, 2004B). Further a rapid quenching of the sprayed particles takes place due to the radial spreading and increase in surface area of rather small mass of the spray particles. The necessary time for solidification is between about  $10^{-8}$  and  $10^{-6}$  seconds (Knotek, 2001). The solidification is generally achieved before the next particle impacts at the same location (Fauchais, 2004B).

## PLASMA SPRAYING APPARATUS



## MECHANISM OF COATING DEPOSITION

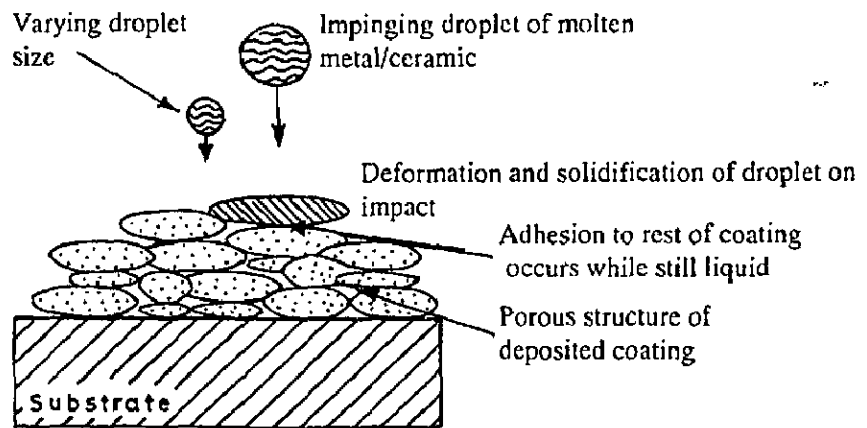
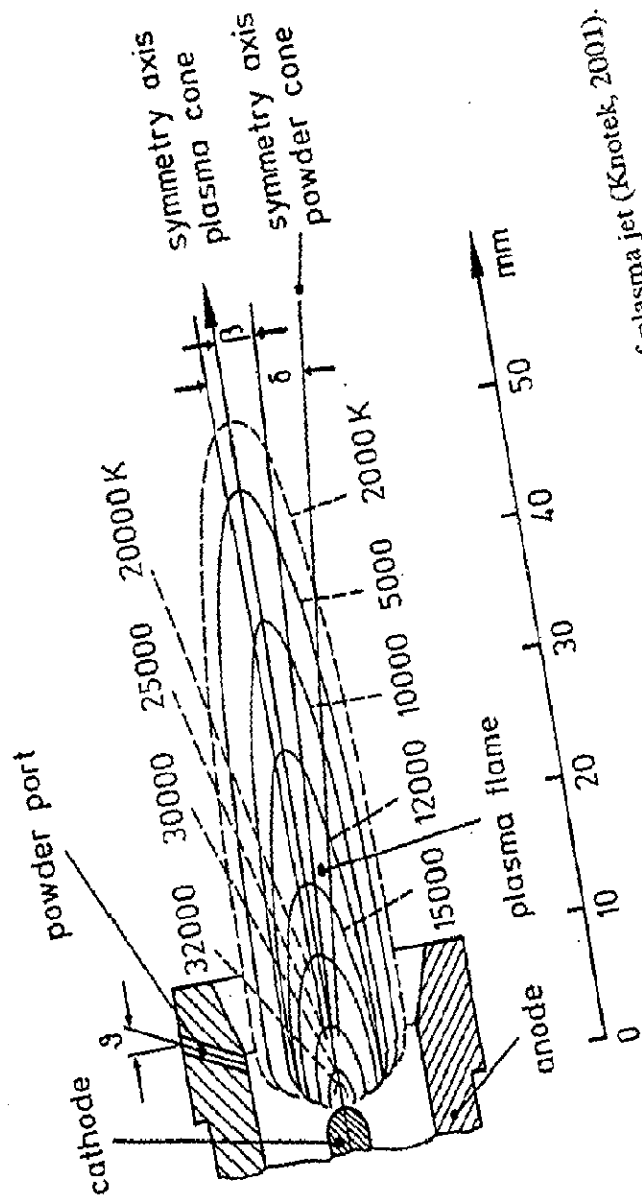


Fig. 2.10 The plasma spraying process (Batchelor et al, 2003)



Temperature distribution and geometry of plasma jet (Knotek, 2001).

Fig. 2.11

The distance between the plasma spraying gun and the substrate can be allowed to vary up to 10mm without significant effect on the coating quality. The coating deposition rates in plasma spraying are typically range from 1 to 10 kilograms of coating per hour. Plasma spraying offers a faster coating rate than most of the other coating techniques (Batchelor et al, 2003).

The extent of reaction of the powder with its gaseous environment during transit depends both on the composition of the plasma gas and the amount of intermixing of the plasma gas with the ambient gas between the nozzle and the substrate. It is generally assumed that argon and helium are inert and no degradation of the powder occurs in the torch when they are used as only plasma gases. The extent of reaction of the powder with oxygen or nitrogen from the air inspirated into the plasma stream after it exits from the nozzle is usually of greater concern than the reaction of powder with plasma gas (Tucker, 1994). The plasma spray is often done in closed chamber filled with inert gas, to prevent the escape of any polluting or toxic debris from the process and to suppress the oxidation of the metal powder during the plasma spraying. Oxide contamination can greatly weaken the sprayed coating as oxides act as brittle inclusions within the microstructure of the coatings (Batchelor et al, 2003). Further the use of inert gas atmospheres, argon shroud or low pressure chamber are reported to decrease the porosity of the coatings. In addition, the plasma jet becomes longer and therefore the nozzle-workpiece distance is increased substantially, which increases the dwell time in the plasma resulting in more uniform particle heating (Nicoll, 1984).

### **2.6.1.3 Adhesion of the Plasma Sprayed Coatings**

The strength of adhesion or bonding between the coating and substrate is critical to the performance of the coating. Usually the surface to be plasma sprayed is roughened by mechanical means such as abrasive blasting, grit blasting or rough turning, which also activate and clean the surfaces prior to coating. With plasma spraying the bonding is suggested to be obtained from the mechanical interlock and solid state adhesion between the atoms in the coatings and substrate. Mechanical interlocking is physical keying between an often deliberately roughened substrate and a coating that is in very close contact with the substrate (Batchelor et al, 2003). The quenching stresses within the spray particles increase the interlocking effects (Knotek, 2001).



Solid state adhesion involves either electron transfer between the outermost atoms of the coating and the substrate or the formation of a much thicker layer of a compound material. It is modelled that the molten droplets dissolve or sweep away any oxide and contaminants that cover a metal surface. The cleaned metal substrate then reacts with the molten droplets before they solidify (Batchelor et al, 2003).

Coating properties are also governed by the splat layering which further depends on the particle parameters at impact, the shape and topology of already deposited layers, the ability of the flattening particle to accommodate their pores, asperities etc, and finally, of their temperature at the moment of impact (Fauchais, 2004B).

The substrate and coating temperature also influence the coating properties. These temperatures control the inter-lamellar contacts, the residual stress distribution within the coating and the pass temperature. For instance, if the pass temperature is high, the sticking of the small particles resulting from the re-condensation of vaporised sprayed material will occur and create defects between passes (Fauchais, 2004B).

#### **2.6.1.4 Plasma Spray Process Variables**

Bhusari (2001) has summarised the plasma spray process variables as shown in Fig. 2.12. According to him, the thermal sprayer responsible for the application of the plasma sprayed coatings need not be a trained scientist, however should be at least aware of the issues detailed in the Fig. 2.12.

#### **2.6.2 Process Variants of Plasma Spraying**

The plasma spray process can take place in different atmospheres at different pressure levels and the various process variants as discussed by Knotek (2001) are:

1. Atmospheric Plasma Spraying (APS)
2. Vacuum (VPS) or Low Pressure Plasma Spraying (LPPS)
3. Shrouded Plasma Spraying (SPS)
4. Controlled Atmosphere Plasma Spraying (CAPS)

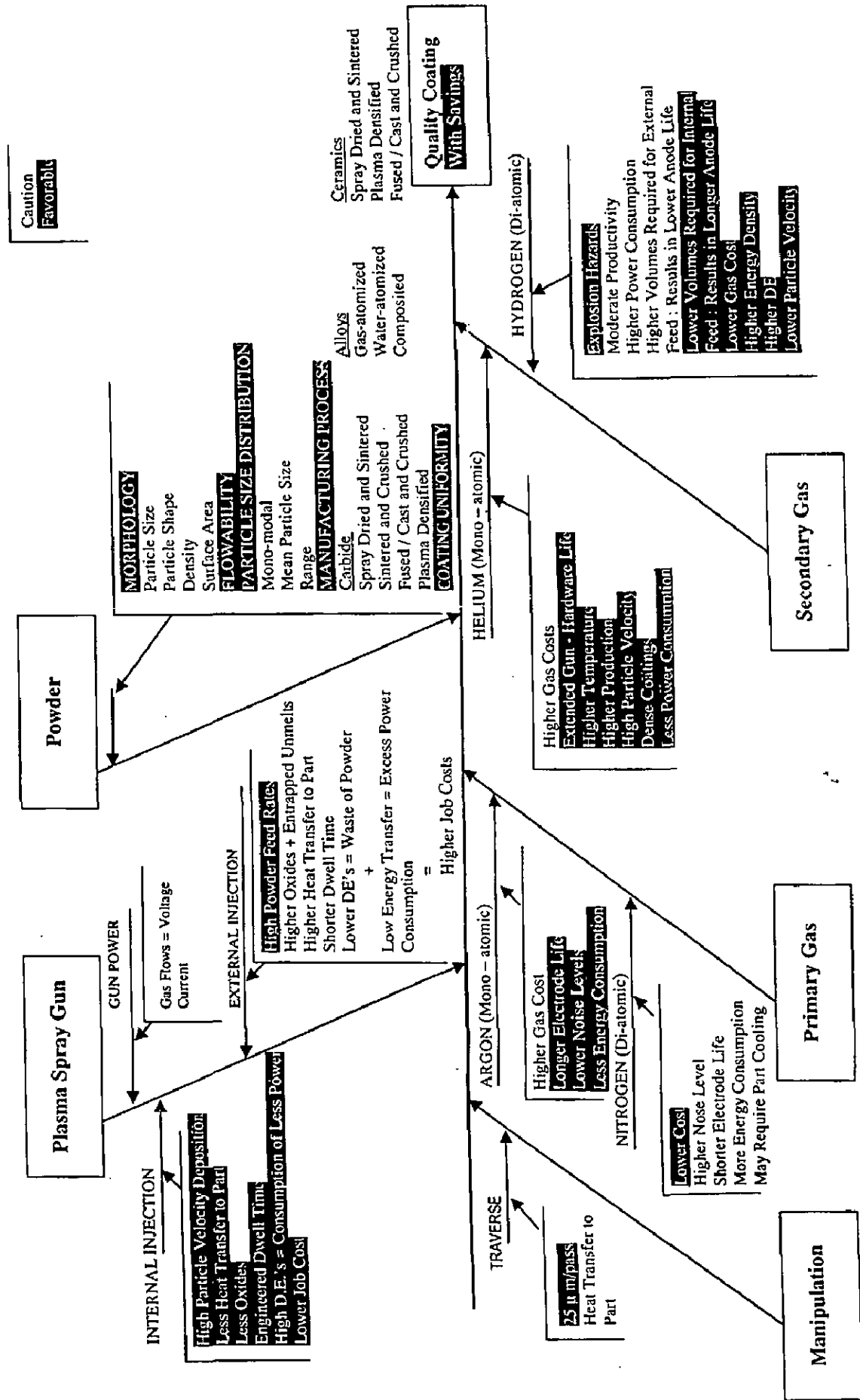


Fig. 2.12 Plasma spray process variables (Bhusari, 2001).

### **2.6.2.1 Atmospheric Plasma Spraying (APS)**

Atmospheric plasma spraying (APS) is the most economical process variant which is carried out in air. The powder particles can interact with the air atmosphere, which may limit the choice of the spray material, since the originating oxides are built into the coating. The major fields for APS-applications are coatings for wear and corrosion (liquid and gaseous) protection, often based on oxide ceramic materials. Other typical coating materials are metals and some alloys especially insensitive to oxidation. The porosity of APS-coatings is generally between 1 and 5%.

### **2.6.2.2 Vacuum (VPS) or Low Pressure Plasma Spraying (LPPS)**

The coating process of VPS takes place in a closed chamber with reduced pressure. The coating process, started after the chamber is evacuated to pressures  $< 10^{-1}$  mbar and refilled with an inert gas atmosphere, takes place at about 50 to 400 mbar. To be able to constantly follow the working chamber pressure, efficient pump systems have to be employed in order to remove the steadily injected plasma gases. These methods are used for the metals that are too reactive to be sprayed in air. The increase in particle velocity results in high quality pure coatings. The jet velocity is Mach 3, giving low porosity and strong adhesion (Sidky and Hocking, 1999). Another advantage of VPS technology is the option to clean the substrate surface especially from oxide layers and preheat the substrate, both giving better adhesion. The main drawback of the system is high technical effort/expense for achieving the vacuum conditions. For some application using low melting point material as substrates, there is insufficient convective heat transfer within the chamber.

### **2.6.2.3 Shrouded Plasma Spraying (SPS)**

Shrouded plasma spraying has been developed to reduce the effort for chamber and pumping system for less expensive applications. Similar to shrouded welding processes, envelope of an inert gas, which is not ionized, protects the plasma jet from the surrounding oxygen containing atmosphere and also improves substrate cooling. Both argon-shrouded and low pressure, inert-gas-chamber spray coating methods are used in the commercial production of the very reactive MCrAlY coatings on gas turbine components (Tucker, 1994).

#### **2.6.2.4 Controlled Atmosphere Plasma Spraying (CAPS)**

Combining vacuum plasma spraying and inert-gas plasma spraying in one system leads to controlled atmosphere plasma spraying (CAPS). For a pressure range from 50 to 400 mbar VPS-coatings are deposited, whereas at pressures around 1 bar inert gas plasma spray coatings are produced. Further with pressures up to 4 bar high pressure plasma spray coatings are deposited.

### **2.7 ROLE OF METALLIC COATINGS**

At high temperatures, coatings that protect against oxidation form a compact, adherent oxide scale that provides a barrier between the high-temperature gases and the underlying metal (National Materials Advisory Board, 1996). Bluni and Marder (1996) have suggested that the thermal spray coatings must possess following properties in order to protect the base alloy against high-temperature corrosion:

1. Have a composition that promotes the formation of protective oxides at splat boundaries.
2. Be dense enough that protective oxides can form within and fill voids.
3. Be thick enough to postpone the diffusion of corrosive species to the substrate material before protective oxide can form within the coating fast diffusion paths. Guilemany et al (2002) have also reported that in case of the metallic coatings thicker layer provides better resistance against corrosion.

Fig.2.13 shows the types of high-temperature attack for metallic coatings (aluminide, chromide, MCrAlY, etc.) on nickel-base superalloys with approximate temperature regimes and severity of attack (National Materials Advisory Board, 1996).

#### **2.7.1 MCrAlY Coatings**

The plasma sprayed MCrAlY coatings are commonly used as thick coatings on large industrial components, to lengthen service life under oxidising atmosphere (Wu, X. et al, 2001). Many MCrAlY coatings are secondary aluminium oxide formers, that is, they initially form a chromic oxide external scale when exposed to an oxidising environment at high temperature, then aluminium oxide forms under the chromic oxide layer (Warnes, 2003). Also the MCrAlY coatings used as bond coats in many applications provide a rough surface for mechanical bonding of the top coat, protect the underlying alloy substrate against high temperature oxidation corrosion and minimize the effect of coefficient of thermal expansion mismatch between the substrate and the top coat materials (Hocking, 1993A and Evans and Taylor, 2001).

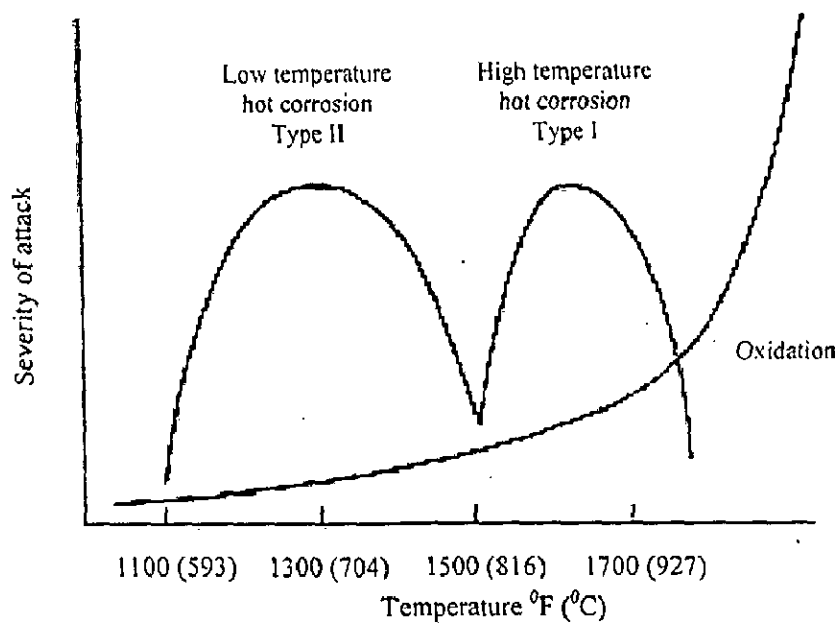


**Fig. 2.13** Types of high-temperature attack for metallic coatings (aluminide, chromide, MCrAlY, etc.) on nickel-base superalloys with approximate temperature regimes and severity of attack (National Materials Advisory Board, 1996).

NiCrAlY bond coats may also help in the formation of metallurgical bonds between the mating surfaces. MCrAlX-type bond coats can be deposited by a variety of methods, but plasma spraying is frequently used (Evans and Taylor, 2001). Fig. 2.14 depicts the morphological changes in a NiCrAlX coating during corrosion/oxidation as suggested by Hocking et al (1993B).

Seiersten and Kofstad (1986) conducted studies on the hot corrosion of MCrAlY coatings on Inconel by  $\text{NaVO}_3\text{-V}_2\text{O}_5$  mixtures in  $\text{O}_2$  at 650 to 800<sup>0</sup>C and found that the corrosion rates increased with increasing  $\text{V}_2\text{O}_5$  content. Later on they studied the hot corrosion behaviour of EB-PVD and air plasma sprayed NiCrAlY coatings on Inconel 600 with  $\kappa$ -sodium vanadyl vanadate deposits (Seiersten and Kofstad, 1987). The samples were exposed to oxygen environment containing 4% sulphur dioxide at 650 to 800<sup>0</sup>C. They observed that the initial reaction was essentially the same as for the reaction in pure oxygen, but after an incubation period, whose duration decreased with increasing temperature, sufficient  $\text{SO}_3$  was dissolved in the molten vanadate to allow a molten mixture of  $\text{NiSO}_4$  and  $\text{Na}_2\text{SO}_4$  to be formed near the metal. This molten mixture was found to be responsible for sulphate-induced hot corrosion.

During high temperature isothermal oxidation of MCrAlY coating on a Ni-base superalloy, Y could modify the oxidation behaviour of the coatings by various mechanisms (Tawancy et al, 1994). They observed Y-rich oxide “pegs” within the  $\alpha\text{-Al}_2\text{O}_3$  scale, which improved the adherence of scale with the coating. Secondly, it was suggested that the presence of small concentrations of Y within the scale in solid solution could have the effect of reducing the scale growth rate. Thirdly, segregation of Y to the grain boundaries of the scale was suggested to reduce its growth rate as well as improve its elevated temperature mechanical strength.

Toma et al (1999) conducted short-time oxidation experiments on vacuum plasma sprayed (VPS) and HVOF-sprayed MCrAlY coatings and observed that the formation of metastable alumina led to a fast oxidation rate in the transient stage in case on VPS sprayed coating. This effect also influenced the oxidation rate in steady-state stage. Whereas formation of  $\alpha\text{-Al}_2\text{O}_3$  as only phase in the oxide scale of the HVOF coating after a short oxidation time (~2.5 hours) determined the slow oxide growth. They suggested that the fine oxide dispersion formed in HVOF-sprayed MCrAlY coatings had a beneficial effect on the high-temperature oxidation behaviour of the coatings.

Isothermal and cyclic oxidation of freestanding HVOF sprayed Ni-20Cr-10Cr-1Y thick coatings was investigated by Serghini and Dallaire (2000) at 1200<sup>0</sup>C. The coatings were found to be dense and remained crack free after thermal treatments. They further observed that the protective oxide layer formed did not flake off upon cyclic oxidation and concluded that the coatings could be used as anti-oxidant barriers in both isothermal and cyclic oxidation. Interdiffusion between the coating and substrate with a slight increase in chromium concentration at the interface was also noticed. The element distribution within the oxide layer was found to follow the order: Al-(oxide)/Y-(oxide)/Cr-(oxide)/Ni-(oxide)/NiCrAlY from the outermost oxide layer to the bulk of the coating.

The oxidation behaviour of air-plasma sprayed (APS) overlay coatings of Ni-25Cr-6Al-Y was studied by Niranatlumpong et al (2000) at 1100 <sup>0</sup>C in air. A protective alumina scale developed after 5- to 10-hr exposure with, initially, parabolic growth kinetics. With protracted exposures (>100 hr), sub-parabolic behaviour developed, associated with aluminium depletion within the coating caused, principally, by internal oxidation of the low-density APS structure. This depletion caused intrinsic chemical failure, manifested by the formation of a layer of Cr, Al, Ni-rich oxide beneath the residual alumina layer. They further observed the formation of a layer of porous Ni, Cr-rich oxide above the alumina layer that was suggested to be associated with this process of chemical failure. Oxide spallation occurred by delamination within this layer during cooling. The spallation sites showed tendency to lie above protuberances in the underlying coating. They observed that initial spallation occurred at a critical temperature drop, which decreased rapidly with increasing exposure time.

Gurrappa (2001) conducted hot corrosion studies on air plasma spray coatings on CM 247 LC superalloy at 900<sup>0</sup>C in the corrosive environments of 95% Na<sub>2</sub>SO<sub>4</sub>+5%NaCl and 90% Na<sub>2</sub>SO<sub>4</sub>+5%NaCl+5%V<sub>2</sub>O<sub>5</sub> by using crucible immersion technique. The different coatings used were NiCoCrAlY, NiCoCrAlY+1% Hf, NiCoCrAlY+1% Si, NiCrAlY, CoCrAlY. The coating of composition 22Co-18Cr-12Al-0.5Y was found to exhibit maximum life among the investigated coatings in both sodium chloride and vanadium containing environments. The improvement in the durability of the coating was attributed to the formation of a thick, protective, thermodynamically and chemically stable alumina scale on the surface of the coating after exposure to the given environment.

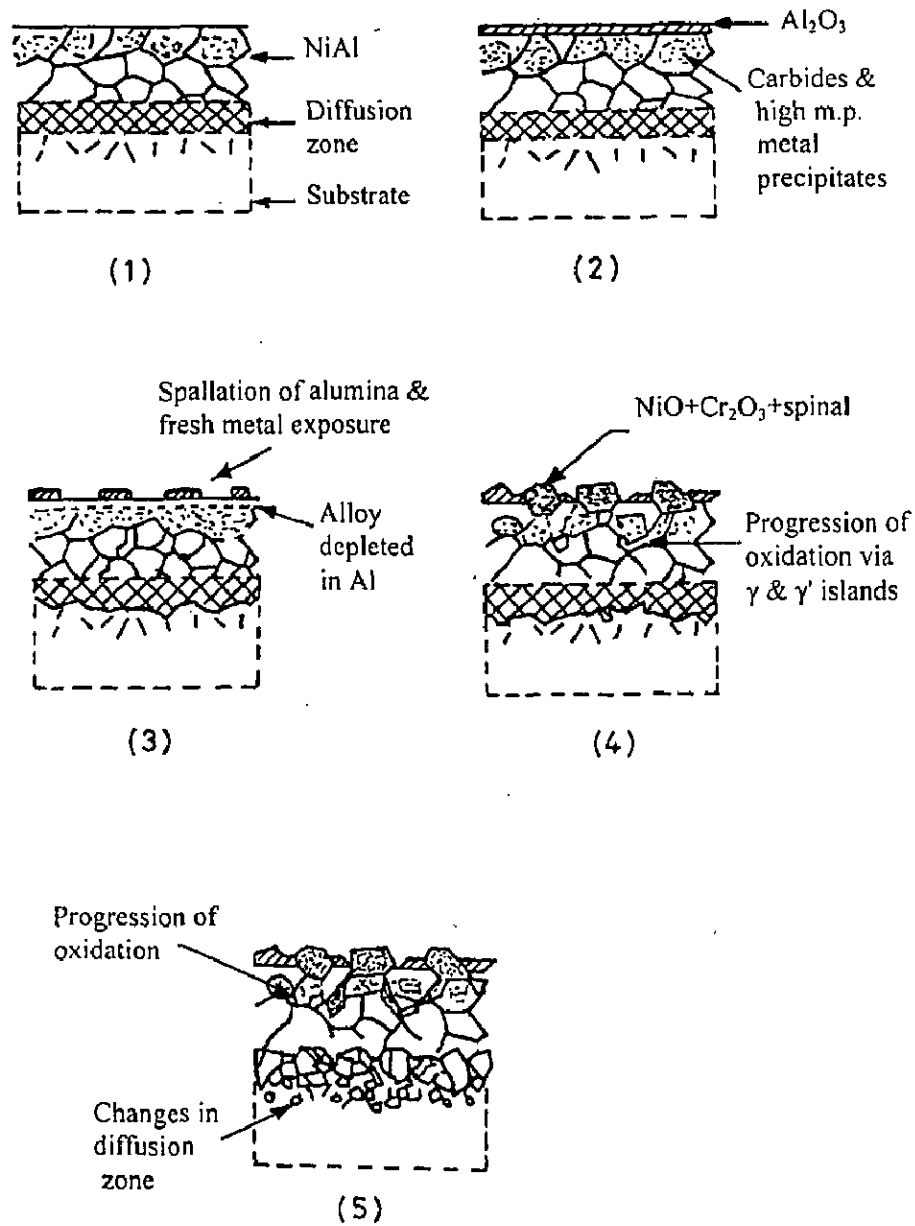


Fig. 2.14 Morphological changes in a NiCrAlY coating during corrosion/oxidation (Hocking et al, 1993B).



Rinaldi et al (2001) studied shrouded arc sprayed FeCrAl, NiCrAl and NiCrTi coatings for boiler applications and shrouded AMDRY 995 coatings for gas turbine blades. A sulphidising gaseous atmosphere was used to simulate boiler environment burning sulphur rich fuel as Orimulsion. The corrosion behaviour after 1000h at 450°C was observed to be as good as that of an HVOF sprayed similar coating, without any delamination during thermal cycling. Whereas the hot corrosion behaviour of the heat treated AMDRY 995 coatings on two Ni-base superalloys was studied by "Dean Tests" at 850°C, which ensured a continuous supply of Na<sub>2</sub>SO<sub>4</sub> vapours with a carrier gas mixture of 0.3%SO<sub>2</sub>, 10%O<sub>2</sub>, 8%CO<sub>2</sub> and N<sub>2</sub> balance. The hot corrosion behaviour of the coating in this simulated gas turbine environment was found to be similar to that of VPS AMDRY coatings. Applicability of the shrouded technique to the field of gas turbines was confirmed instead of the costly VPS technique.

Cyclic oxidation behaviour of NiCrAlY and CoNiCrAlY coatings was determined at a maximum temperature of 1273 K in air by Belzunce et al (2001). The authors reported that high frequency pulse detonation (HFPD) coatings were dense and exhibit interconnected porosity along droplet boundaries. Adherence of the coatings with the substrate was found to be good, which remained unaffected after the cyclic oxidation. The oxidant atmosphere penetrated into the coatings through the open porosity and internal oxidation occurred until all the accessible internal surfaces were oxidised. Subsequently, the oxidation took place only on the external surface, where a continuous and uniform layer of alumina protected the coating from further oxidation.

The isothermal oxidation behaviours of plasma-sprayed NiCrAlY bond coatings (Ni22Cr10Al1Y and Ni31Cr11Al0.6Y) have been evaluated by Choi et al (2002). They observed two unique microstructures; oxide stringers and improperly flattened zones, in the air plasma spray (APS) bond coatings. Improperly flattened zones had a high density of open pores. According to them, these features affected the oxidation behaviours in both the transient and the steady-state stages. In the transient oxidation stage, NiO, Cr<sub>2</sub>O<sub>3</sub> and  $\alpha$ -Al<sub>2</sub>O<sub>3</sub> were observed on the surface simultaneously. The oxide stringers and improperly flattened zones had an especially high density of NiO and Cr<sub>2</sub>O<sub>3</sub>, which implied that these regions had inherently lower contents of Al. During steady-state oxidation, a continuous  $\alpha$ -Al<sub>2</sub>O<sub>3</sub> layer reduced the diffusion rate of oxygen and thus the rate of isothermal oxidation became low. As the oxidation time was increased, depletions of Al, the formation of NiAl<sub>2</sub>O<sub>4</sub> layers and the formation of Cr<sub>2</sub>O<sub>3</sub> subsequently took place.

The oxidation behaviour of arc ion plated NiCrAlY coatings on cast Ni-based IN100 superalloy was investigated by Wang et al (2002) under cyclic as well as isothermal conditions at temperatures of 900 and 1000<sup>0</sup>C. They observed a marked improvement in the oxidation resistance of the superalloy in both the cyclic and isothermal conditions. The oxides formed at 900<sup>0</sup>C were reported as  $\alpha$ -Al<sub>2</sub>O<sub>3</sub> and Cr<sub>2</sub>O<sub>3</sub>, whereas at 1000<sup>0</sup>C, NiO,  $\alpha$ -Al<sub>2</sub>O<sub>3</sub> and Cr<sub>2</sub>O<sub>3</sub> phases formed in the initial stage of oxidation. With further oxidation at 1000<sup>0</sup>C, complex reactions were observed.

The oxidation studies of sputter-deposited NiCrAlY coating on a Ni-base single crystal superalloy showed phase transformation from  $\theta$ - Al<sub>2</sub>O<sub>3</sub> to  $\alpha$ - Al<sub>2</sub>O<sub>3</sub> (Li et al, 2003C). This transformation was observed to be faster at high temperatures. They further suggested that the diffusion of both Al and O might have contributed to scale growth during the steady stage of oxidation. The scale formed on the coating was found to be exclusively of alumina at 900-1100<sup>0</sup>C. They attributed this favourable oxidation behaviour to the high aluminium content, the third element Cr and the nanocrystallised microstructure of the coating. During the oxidation,  $\beta$ -NiAl was seen to be transformed to  $\gamma'$ -Ni<sub>3</sub>Al and  $\gamma$ -phase because of the diffusion and formation of Al<sub>2</sub>O<sub>3</sub>.

Arc ion plated NiCrAlY coatings deposited on the superalloy IC-6 (Ni<sub>3</sub>Al-base superalloy) had shown better oxidation resistance than NiCoCrAlY coating, when exposed at 1000<sup>0</sup>C (Wang et al, 2003). It was further noticed that the oxidation resistance was not influenced by the presence of Co in NiCrAlY at 900<sup>0</sup>C in static atmosphere. Both the coatings were shown to obey the parabolic law at 900 and 1000<sup>0</sup>C.

Plasma sprayed Ni-22Cr-10Al-1Y coatings were utilised by Singh (2003) to increase the hot corrosion and oxidation resistance of boiler steels and considerable improvement was observed. The coatings were subjected to air oxidation as well as molten salt corrosion at 900<sup>0</sup>C, and were also tested in the actual industrial boiler. The formation of phases like Cr<sub>2</sub>O<sub>3</sub> and NiCr<sub>2</sub>O<sub>4</sub> in the upper scale was believed to provide the resistance against the hot corrosion.

## 2.7.2 Nickel-Chromium Coatings

The high resistance of high-chromium, nickel-chromium alloys to high-temperature oxidation and corrosion makes them widely used as welded and thermally sprayed coatings in fossil fuel-fired boilers, waste incineration boilers, and electric furnaces (Kawahara, 1997). Modern thermal spray processes such as high velocity

oxyfuel (HVOF) and plasma spraying are often applied to deposit high-chromium, nickel coatings onto the outer surface of various parts of the boilers, e.g. tubes to prevent the penetration of hot gases, molten ashes, and liquids to the less noble carbon steel boilers tube (Tuominen et al, 2002).

High temperature oxidation of as-sprayed as well as gas flame sprayed NiCrAl, FeNiCrAl and NiCr coatings has been studied Longa and Takemoto (1992) in a mixed salt of 15%  $\text{Na}_2\text{SO}_4$ - $\text{V}_2\text{O}_5$  at  $900^\circ\text{C}$ . The results showed that the laser glazed NiCrAl and FeNiCrAl coatings offered excellent corrosion resistance compared to the as sprayed coatings. However, the NiCr coatings showed better corrosion resistance in as sprayed condition in comparison to that in laser glazed condition. Laser glazed NiCr coating showed exfoliation from its substrate after high temperature testing, which was ascribed to poor adhesion of the coating to the substrate.

Yamamoto and Hashimoto (1995) estimated the high-temperature oxidation and corrosion resistance of plasma transferred arc welded Ni-Cr alloy coatings and observed that the Ni-20Cr coatings showed good oxidation resistance, while the Ni-50Cr coating collapsed because of a large amount of oxide scales. In case of vanadium induced corrosion, they noticed that resistance of the coatings got better with an increase in Cr content. They found that addition of Al in the Ni-50Cr coating improved the oxidation resistance of the coating in air. They developed an alloy coating with composition Ni-50Cr-3Al, which exhibited good resistance against both oxidation and vanadium attack.

Longa-Nava et al (1996) studied the hot corrosion behaviour of LPPS 80Ni-20Cr and flame sprayed Ni-20Cr-4Al coatings on type 304 stainless steel, by thin films of  $\text{Na}_2\text{SO}_4$  and 0.7 mole fraction  $\text{Na}_2\text{SO}_4$ -0.3 mole fraction of  $\text{NaVO}_3$  at  $900^\circ\text{C}$  in a 1%  $\text{SO}_2$ - $\text{O}_2$  gas atmosphere. The Ni-20Cr coatings were tested in as-sprayed condition, whereas Ni-20Cr-4Al coatings were tested under as-sprayed and laser-glazed conditions and found these coatings successful in resisting hot corrosion. They observed the formation of Cr-rich oxide layer of approximately  $30\mu\text{m}$  after 16 hours exposure in case of LPPS 80Ni-20Cr coatings. It was observed that the formation of chromatic solute anions prevented sulphidation of the alloy.

Erosion wear and mechanical properties of nickel- and iron-based as well as chromium-nickel plasma sprayed coatings on carbon steel have been studied by Hidalgo et al (1997, 2000) in the simulated industrial service conditions in boilers. These types of coatings are used as heat transfer and structural elements in boilers. They have performed experiments in laboratory combustion unit which was simulated to boiler service

conditions at 400, 600 and 800<sup>0</sup>C. Coatings were reported to have a moderate to low oxidation indexes.

The oxidation behaviour of Ni-20Cr foils of 100- and 200- $\mu$ m thickness has been investigated by Calvarin et al (2000) in air between 500 and 900<sup>0</sup>C. They found that the scale formed at all the temperatures was complex with an outer NiO layer having columnar grains and an outer layer of equiaxed NiCr<sub>2</sub>O<sub>4</sub>+NiO+Cr<sub>2</sub>O<sub>3</sub> grains. It was further observed that at low temperatures (500-600<sup>0</sup>C), the chromium content was insufficient to form a continuous Cr<sub>2</sub>O<sub>3</sub> layer, while such a continuous layer formed at the inner interface at oxidation temperatures of 700 to 900<sup>0</sup>C. The formation of all these oxides layers was found to be in agreement with the Wagner Theory and was justified on the basis of effective diffusion coefficients.

Yamada et al (2002) carried out studies to evaluate the high-temperature corrosion resistance of Ni-20Cr, Ni-50Cr and Cr coated boiler tubes in actual refuse incineration plant as well as in laboratory tests. It was observed that detonation sprayed Ni-50Cr coating exhibited the highest corrosion resistance in laboratory test at 873K among the detonation gun sprayed, plasma sprayed and HVOF sprayed coatings. The detonation sprayed Ni-50Cr coated tubes performed very well for seven years of testing in the actual plant without any problems and were expected to have a longer life. They further concluded that the Incolloy 825 and Inconel 625, having high nickel content possessed higher corrosion resistance than stainless steels.

Uusitalo et al (2003) reported the use of HVOF sprayed Ni/Cr and Fe<sub>3</sub>Al coatings on ferritic and austenitic boiler steels and studied the high temperature corrosion of the coatings in oxidising atmosphere of 500 vppm HCl, 3%O<sub>2</sub>, 14%CO<sub>2</sub>, 20% H<sub>2</sub>O and Argon as balance. Ni-49Cr-2 Si coating performed well as no corrosion products were detected at the coating surface. No internal attack or attack on the substrate through this coating was observed. Whereas Ni-57CrMoSiB and Ni-21Cr-9MoFe coatings were proved to be poor in resisting the high temperature oxidation as the substrates were attacked by corrosive species through the voids and oxides. Fe<sub>3</sub>Al coatings also suffered corrosion degradation, which even started during the spraying and, the Al content was found to insufficient to form the intermetallic structure.

Uusitalo et al (2004) again investigated the high temperature behaviour of the same coatings in the presence of a salt environment of 40% Na<sub>2</sub>SO<sub>4</sub>-40% K<sub>2</sub>SO<sub>4</sub>-10NaCl-10KCl in two environments viz. oxidising environment of N<sub>2</sub>-20H<sub>2</sub>O-14CO<sub>2</sub>-

3O<sub>2</sub>-500 vppm HCl, reducing environment of N<sub>2</sub>-20H<sub>2</sub>O-5CO-0.06H<sub>2</sub>S-500 vppm HCl. They found that the corrosion was more severe in oxidising environments as compared to the corrosion in reducing environment. Active oxidation was responsible for the accelerated corrosion in oxidising environments. The coatings were prone to chlorine attack in both atmospheres through interconnected oxide network at splat boundaries. Ni-57CrMoSiB coating was the only material forming a protective oxide layer. Whereas in reducing conditions materials with high chromium content were found to be able to form a protective layer containing chromium, sulphur, and sodium. The corrosion resistance of this layer increased with increasing chromium content. Further it was concluded that the corrosion resistance of nickel-based, high chromium coating materials was satisfactory in the test conditions.

Singh (2003) developed Ni-20Cr coatings on boiler steels by plasma spray process and evaluated their oxidation and hot corrosion performance in laboratory tests at 900<sup>0</sup>C. The coatings were tested in the actual boiler environment also. He observed an increase in the resistance towards air oxidation as well as hot corrosion with the application of coatings. The formation of phases like Cr<sub>2</sub>O<sub>3</sub> and NiCr<sub>2</sub>O<sub>4</sub> in the protective scale of the coatings was suggested to induce the requisite resistance in the boiler steels. A schematic diagram as suggested by him showing the probable hot corrosion mechanism for Ni-20Cr coated T11 boiler steel is reported in Fig. 2.15.

Sundararanjan et al (2003A) evaluated the steam oxidation resistance of Ni-20Cr metallic coatings on 9Cr-1Mo type steel at four steam temperatures in the range of 600-750<sup>0</sup>C. They used high velocity oxy-fuel (HVOF) as well as air plasma spray to deposit the coatings. The formation of protective oxide scale of Cr<sub>2</sub>O<sub>3</sub> was observed on the coating surfaces. The diffusion of nickel from the coatings to the substrate and, the diffusion of iron from the substrate to the coatings for longer exposures to steam oxidation was also noticed. The rate of diffusion of Ni and Fe were found to be almost similar. The diffusion of iron caused formation of Fe<sub>2</sub>O<sub>3</sub> scale, which was suggested to be reason for non-protectiveness of coatings for longer exposure times. Additionally, in case of APS coating, the scale initiation was also observed at the interface between the coating and the substrate, which propagated with testing temperature and duration. Whereas in case of Ni-50Cr coatings, the formation of Fe<sub>2</sub>O<sub>3</sub> scale was noticed in case of APS coatings only (Sundararanjan et al, 2003B).

### 2.7.3 Nickel Aluminide Coatings

Intermetallic compounds containing aluminium, such as NiAl, offer possibilities for developing low-density, high-strength structural alloys which might be used at temperatures higher than those currently possible with conventional titanium- and nickel based alloys. The intermetallic alloys and their composites enable the design and production of higher performance, lighter (high trust-to-weight ratio) engines for future military aircraft and supersonic commercial transport vehicles. Strong bonding between aluminium and nickel, which persists at high temperatures can provide high strength at elevated temperatures (Darolia, 1991).

Unlike aluminide and chromo-aluminide coatings which have been used on steels, the nickel aluminide coatings are yet to be introduced in large scale for general industrial applications involving high temperature corrosive environments (Malik et al, 1992). The yield strength of Ni<sub>3</sub>Al was observed to increase rather than decrease with increase in temperature and the aluminide reported to have good oxidation resistance. In addition, it has a considerably lower density than commercial nickel-based super alloys (Nishimura and Liu, 1993). The proper processing of these aluminides into useful shapes has been reported to be important from an economic standpoint as well as the processing influence the final microstructure (Dey and Sekhar, 1998).

Ordered intermetallic aluminides have received much attention as potential structural materials because of their low density, high strength at elevated temperatures, oxidation resistance, and excellent creep properties (Kumar and Liu, 1993, and Saffarian et al, 1996). The oxidation/sulphidation behaviour of intermetallic compounds is in many ways similar to that of the metallic elements of the alloys from which they are prepared. The oxide is often the same as that on the metallic solid solutions containing the same constituents (Okafor and Reddy, 1999). So far very rare hot corrosion studies for the aluminide intermetallic compounds have been conducted (Kai et al, 2002).

Hot corrosion behaviour of pure and alloyed  $\gamma$ - Ni<sub>3</sub>Al (major strengthening phase in Ni-base superalloys) and  $\beta$ -NiAl (the primary constituent of aluminide coatings) phases at 1600F has been studied by McCarron et al (1976) using burner rig tests. They observed that pure  $\beta$ -NiAl was more corrosion resistant than  $\gamma$ - Ni<sub>3</sub>Al for exposure times greater than 100 hours, whereas for shorter times the kinetics were found to be comparable. They characterised the corrosion of  $\gamma$ - Ni<sub>3</sub>Al by an incubation period of the order of 100 hours. Velon and Olefjord (2001) have reported the formation of islands of Al<sub>2</sub>O<sub>3</sub> and NiO combined with NiAl<sub>2</sub>O<sub>4</sub> on the surface of oxidised Ni<sub>3</sub>Al at temperature of 300<sup>0</sup>C, whereas at 500<sup>0</sup>C, the Ni oxides were seen growing laterally and covering Al<sub>2</sub>O<sub>3</sub> islands.

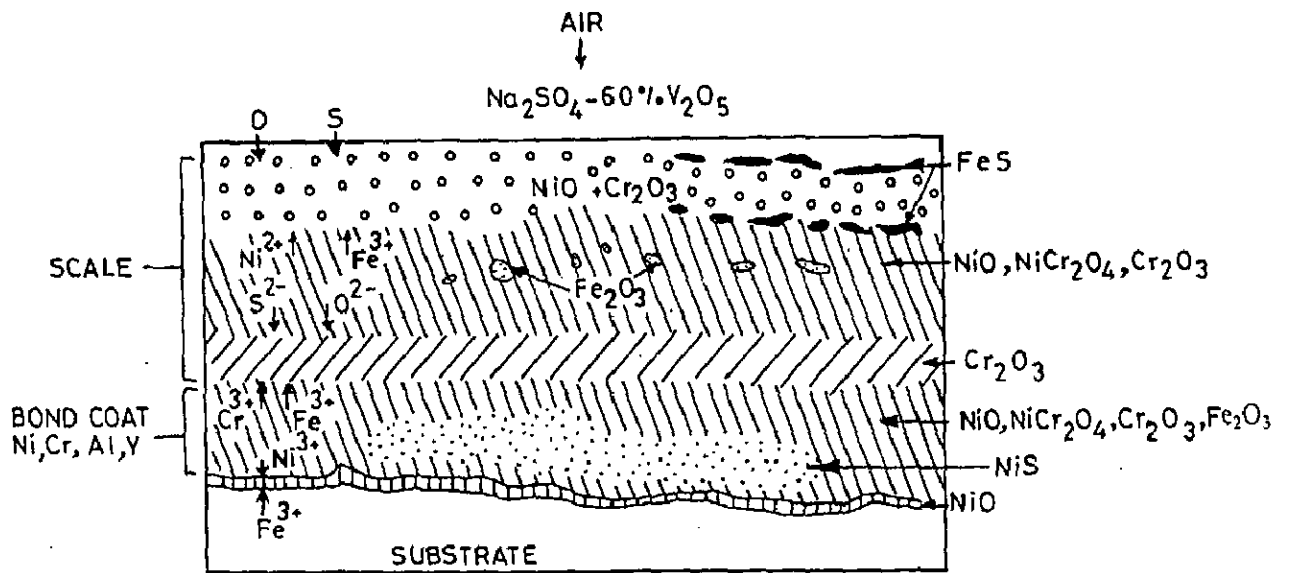


Fig. 2.15 Schematic diagram showing probable hot corrosion mechanism for Ni-20Cr coated T11 steel exposed to Na<sub>2</sub>SO<sub>4</sub>-60%V<sub>2</sub>O<sub>5</sub> at 900°C for 50 cycles (Singh, 2003).

Malik et al (1992) developed nickel aluminide coatings on mild steel by pack cementation process and studied the high temperature behaviour of the coatings at 750, 800 and 850<sup>0</sup>C in flowing air. From the parabolic nature of the weight gain vs time plots, the oxidation of the coatings was suggested to be a diffusion controlled process. At high temperatures, the oxidation rates of the nickel aluminide coatings were lowered down markedly irrespective of the rare earth oxide concentration.

Ni<sub>3</sub>Al coatings were fabricated by La et al (1999) on the carbon steel by the self-propagating high-temperature synthesis (SHS) casting route. The microstructure of the coatings was reported to be pure and dense. They observed that the coatings possessed resistance to oxidation at elevated temperature, as was noticed during the friction experiment, where the temperature reached to 873 K.

Matsuura et al (1999) formulated the nickel aluminide coating on the steel by using reactive sintering. The compact thickness was below 5 mm but the synthesis reaction has been reported to be incomplete because of heat loss due to absorption by the steel block and intermediate products such as Ni<sub>3</sub>Al and NiAl<sub>3</sub> remain in the compact. However in situ coating was completed by further heating to 1473 K (1200<sup>0</sup>C) followed by holding for 0.54 ks.

According to Schneibel and Becher (1999) and Velon and Olefjord (2001) nickel aluminide intermetallics are not only oxidation and corrosion resistant, but also thermodynamically compatible with a wide range of ceramics. Ni<sub>3</sub>Al has been reported to exhibit a very good high temperature strength and oxidation resistance. Moreover its mechanical properties, including good creep resistance make it attractive for several industrial applications.

As per the views of Liu and Gao (2001), the studies on the oxidation behaviour of the intermetallic compound Ni<sub>3</sub>Al can be dated back to 1974. The authors further concluded that research on this material has been conducted more intensively since the last decade or so because Ni<sub>3</sub>Al base alloys had been found to be promising structural materials for high temperature applications. They carried out studies on isothermal and cyclic oxidation of Ni<sub>3</sub>Al + 5% Cr and Ni<sub>3</sub>Al + 5% Cr + 0.3% Y microcrystalline coatings, produced by a close-field, unbalanced magnetron-sputter deposition technique.



## 2.7.4 Cobalt Based Coatings

Cermet (WC/Co) thermal spray coatings are widely used in wear situations because they combine several advantages such as resistance to abrasion, erosion, high temperature and corrosive atmospheres (Chuanxian et al, 1984, Liao et al, 2000). Zhao et al (2002) reported an experiment in which a clad coating of Stellite Ni60 was prepared on AISI 1020 steel using home-made non-transferred arc plasma cladding equipment. It was pointed out that the non-transferred arc plasma cladding is an economical and environmental friendly process for cladding processes based upon their results. The wear resistance in corrosion environments of cobalt base Tribaloy (registered trade name) has been reported to be outstanding by Schmidt and Ferriss (1975). There were no signs of corrosion on the test surfaces and weight loss was low or moderate.

Co-25 wt% Cr, Co-25 wt% Cr-1 wt% Y and yttrium-implanted Co-25 wt% Cr alloy specimens were oxidised at 1000<sup>0</sup>C by Hou and Stringer (1988). The unimplanted binary alloy was reported to be oxidised to duplex Co-rich scale, but the Y-containing ternary alloy formed a continuous Cr<sub>2</sub>O<sub>3</sub> layer. A temporarily stable Cr<sub>2</sub>O<sub>3</sub> scale was seen to be formed on the most heavily implanted specimens (1x10<sup>18</sup> Y<sup>+</sup>/cm<sup>2</sup>). This Cr<sub>2</sub>O<sub>3</sub> scale consisted of very fine grained oxide, which was permeable to the outward transport of Cr and Co. Internal oxidation during pre-treatment of the ion-implanted specimens was reported to convert the Y metal to its oxide prior to the oxidation experiment, which enhanced the development of an external Cr<sub>2</sub>O<sub>3</sub> scale that has also been reported to be unstable. Selective oxidation of chromium in an ordinarily non-Cr<sub>2</sub>O<sub>3</sub>-forming alloy was reported to be due to the reactive element oxides acting as preferential nucleation sites on the alloy surfaces.

Loss of WC was observed by Lovelock et al (1998) during thermal spraying and reported to occur primarily by a combination of decarburisation and dissolution in the binder metal during spraying whereas WC-Co transformed to phases such as W<sub>2</sub>C, Co<sub>3</sub>W<sub>3</sub>C ( $\eta$  phases), Co<sub>6</sub>W<sub>6</sub>C ( $\epsilon$  phase), WC<sub>1-x</sub>, WO<sub>3</sub> and W. According to them, the original cobalt binder phase of the powder was replaced in the coating by an amorphous or nanocrystalline binder phase. The cast and crushed powder deposited badly and produced a coating with very weak abrasion resistance.

Aoh and Chen (2001) investigated the high temperature wear characteristics of Stellite 6 alloy containing Cr<sub>3</sub>C<sub>2</sub> after thermal fatigue and oxidation treatment at 700<sup>0</sup>C. The alloy powders Stellite 6 and Stellite 6 with Cr<sub>3</sub>C<sub>2</sub> were used by them to form hard

facing layers on medium carbon steel by plasma transferred arc (PTA) process. Thermal fatigue cracks initiated from the surface of Stellite 6 with  $\text{Cr}_3\text{C}_2$  and propagated into the clad layer along the carbide boundaries, whereas no thermal fatigue crack was observed on the Stellite 6 clad layer. It was further noticed that the formation of the oxide layer was enhanced by  $\text{Cr}_3\text{C}_2$  content in the alloy and the surface oxidation was beneficial to the improvement of wear resistance.

Laser surface alloying using NiCoCrB alloy (Ni-17% Co-19.6% Cr-14.5% Fe-3.5% B-1% C-0.9% Si) on mild Steel AISI 1050 and austenitic stainless steel AISI 316L was reported by Kwok et al (2001). Both steels alloyed with NiCoCrB were found to contain austenite as the main phase and carbides as the minor phases. The maximum hardness of laser alloyed 1050 and 316L steels increased to 545 and 410 Hv respectively with the cobalt content ranging from 4.5 to 12 wt%. The cavitation erosion resistance of the laser alloyed specimens was reported to increase with increase in cobalt contents. This increase was reportedly attributed to decrease in the stacking fault energy and enhancement of strain induced martensitic transformation due to the presence of cobalt.

Cha and Wolpert (2003) conducted high-temperature erosion and corrosion of thermally spray coatings on 15Mo3 and 13CrMo44 base materials. The coatings were Ni-based materials like Colmonoy 62 (NiCrFeBSi) and NiCrBSi/WC and Co-based material T800 fabricated by thermal spray processes like HVOF, Flame sprayed and sintered (FS/sinter) and air plasma spray (APS). The corrosion studies in the environment containing HCl,  $\text{H}_2\text{O}$ ,  $\text{O}_2$  and  $\text{N}_2$  at a temperature of  $500^\circ\text{C}$  indicated that the Colmonoy 62 applied by HVOF or by APS show the same corrosion rates. HVOF sprayed T800 coating experienced the highest corrosion rate. NiCrBSi/WC coating formed by FS/sinter proved to be a fair combination of erosion and corrosion resistance.

Studies on oxidation and hot corrosion resistance of Stellite-6 coatings on boiler steels were conducted by Singh (2003) in simulated as well as in actual boiler conditions. Coatings were found to be effective in all the environments. He opined that the formation of  $\text{CoCr}_2\text{O}_4$  spinel in all the environments might have contributed to requisite resistance, which was believed to block the diffusion activities through the CoO by suppressing the further formation of CoO as per views of Luthra (1985). Fig. 2.16 shows probable oxidation mechanism for Stellite-6 coated GrA1 boiler steel exposed to air at  $900^\circ\text{C}$  for 50 cycles as proposed by Singh (2003).

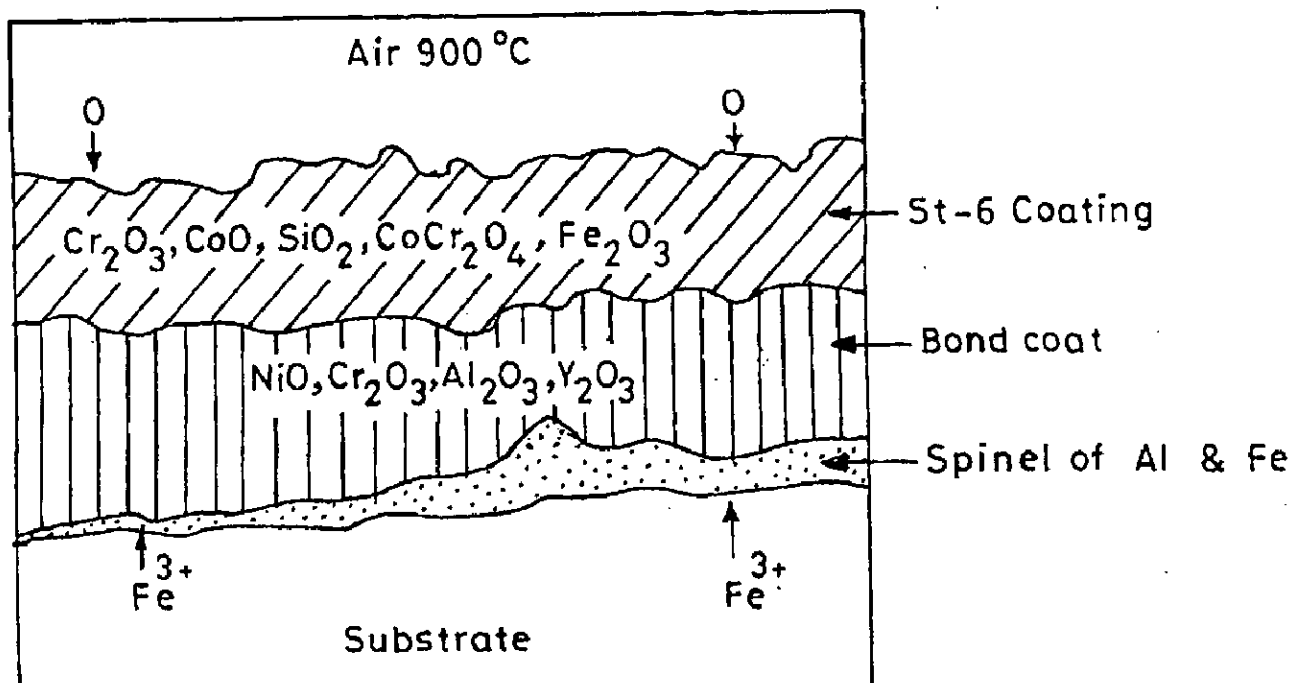


Fig. 2.16 Schematic diagram showing probable oxidation mechanism for Stellite-6 coated GrA1 steel exposed to air at 900°C for 50 cycles (Singh, 2003).

## 2.8 PROBLEM FORMULATION

### 2.8.1 Scope

Hot corrosion has been identified as a serious problem in high temperature applications such as in boilers, gas turbines, waste incinerations, diesel engines, coal gasification plants, chemical plants and other energy generation systems. It is basically induced by the impurities such as Na, V, S etc. present in the coal or in the fuel oil used for combustion in the mentioned applications. In some situations, these impurities may be inhaled from the working environment, for instance NaCl in marine atmospheres. There is a general agreement that condensed alkali metal salts notably,  $\text{Na}_2\text{SO}_4$ , are a prerequisite to hot corrosion (Beltran and Shores, 1972). Due to high cost of removing these impurities, the use of these low grade fuels is usually justified.

Although the natural gas has also been considered as an alternative to these traditional fuels for generation of electricity in combined cycle power plants, still there remains strong interest in the development of clean, high efficiency coal-base systems for power generation (Saunders et al, 1997). This might be due to anticipated saving of high grade energy such as natural gas. Similarly, in coal conversion processes, which are known to produce clean environmentally acceptable fuels, technical problem arises from the interaction of sulphur and ash in the coal with plant construction materials at high temperatures and pressures (Natesan, 1985).

For the reason that hot corrosion of the components in aforesaid high temperature environments is inevitable, the phenomenon has maintained its relevance from the last more than 60 years. Hot corrosion often increases the corrosion loss of heat resisting alloys by over hundred times, in comparison to that incurred by simple oxidation (Shinata et al, 1987).

Power plants are one of the major industries suffering from severe corrosion problems resulting in the substantial losses. For instance, steam temperature of boilers is limited by corrosion and creep resistance of boiler components, which affects the thermal efficiency of the boilers. Consequently, the thermal efficiency decreases and, hence the electricity production is reduced (Uusitalo et al, 2003). According to a survey (Metals Handbook, 1975) conducted over a period of 12 years, encompassing 413 investigations, overheating was listed as the cause of 201 failures or 48.7% of those investigated. Fatigue and corrosion fatigue were listed as the next most common causes

of failure accounting for a total of 89 failures or 21.5%. Corrosion, stress corrosion and hydrogen embrittlement caused a total of 68 failures or 16.5%. In another case study of a coal fired boiler of a power plant in north western region of India, Prakash et al (2001) have reported that out of 89 failures occurring in one year duration, 50 failures were found to be due to hot corrosion and erosion by ash. These facts emphasise the need to develop more and more corrosion resistant materials for such applications.

The use of Ni-, Fe- and Co- based superalloys in the high temperature applications such as gas turbines, boilers etc. is well known and many more applications are still to be explored, where these alloys may have tremendous potential. Although the superalloys have adequate mechanical strength for such high temperature applications, yet they are prone to degradation by high temperature oxidation/corrosion during long term exposures. Therefore, the superalloys need to be protected, but the protection system must be practical, reliable and economically viable. It has further been learnt from the literature that hot corrosion problem needs to be arrested through some other preventive means; prominent among them being controlling process parameters, use of inhibitors, application of protective coatings etc. as there lies little scope in improvement of the combustion environments. In Indian context, this is even more relevant as the Indian coal is found to have high ash content (Sharma, 1996).

Regarding the selection of a particular countermeasure against hot corrosion, it has been concluded from the literature that controlling the various process parameters (air/fuel ratio, temperature, pressure etc.) of the boiler and gas turbine to reduce corrosion has comparatively low significance as the parameters can be controlled only within certain limits. Further, the use of inhibitors is not easily viable due to practical implications in injecting these inhibitors along with the fuel in the combustion chamber in an actual industrial environment (Tiwari and Prakash, 1998 and Gitanjaly et al, 2002). In this regard, use of the protective coatings has been identified as a potential area for the present research.

Thermal spray has emerged as an important tool of increasingly sophisticated surface engineering technology. It is one of the many methods of applying overlay coatings for applications ranging from protection of materials in harsh environments, to dimensional restoration of worn machine elements (Yamada et al, 2002). Among the thermal spray coating processes, plasma spraying is reported to be versatile technology that has been successful as a reliable cost-effective solution for many industrial problems (Fauchais et al, 1997).

Recent reports emphasised that the understanding of the degradation and failure mechanisms of high-temperature coatings in the field need to be improved, particularly with respect to the effects of engine operation and environment on the coating performance (e.g., thermal cycling) (National Materials Advisory Board, 1996). In general, the reaction behaviour of protective coatings in environments of their use and their interactions with the substrate during high-temperature performance is not well understood (Chatterjee et al, 2001). Uusitalo et al (2003) has also suggested that there is a need to investigate the high temperature corrosion behaviour of thermal spray coated materials in different aggressive environments.

In an earlier work conducted by Singh (2003) in the department, laser remelting of the plasma sprayed coatings was attempted to eliminate the porosity of the coatings. However, he observed that these laser remelted coatings showed slightly inferior hot corrosion resistance in molten salt environment as compared to the as coated samples. This behaviour was attributed to the presence of vertical cracks in the laser remelted samples after exposure to hot corrosion, through which the oxidising environment could reach the substrate steels. Streiff (1987) have reported that the trapped oxygen in the coatings causes unfavourable oxide inclusions during the laser remelting process. These inclusions may develop into sites of oxidation attack. Longa and Takemoto (1992) observed that laser glazed NiCr coating showed exfoliation from the substrate after high temperature testing, due to poor adhesion to the substrate, and indicated less corrosion resistance to mixed salt (15% Na<sub>2</sub>SO<sub>4</sub>-V<sub>2</sub>O<sub>5</sub>) corrosion at 900<sup>0</sup>C in comparison to the coating in as-sprayed condition. Moreover, according to Zhao et al (2002) the efficiency of energy transfer of laser is rather low, and the expensive equipment and the dependence on the bulk material also limit its application.

## 2.8.2 Aim

The present study is an attempt to evaluate the high temperature oxidation behaviour of some plasma spray Ni-22Cr-10Al-1Y, Ni-20Cr, Stellite-6 and Ni<sub>3</sub>Al coated Ni- and Fe-based superalloys by the accelerated testing. The tests were planned to be carried out in air at an elevated temperature of 900<sup>0</sup>C with and without salt mixture of Na<sub>2</sub>SO<sub>4</sub>-60%V<sub>2</sub>O<sub>5</sub> under cyclic conditions. It was also decided to investigate the behaviour of bare superalloys under similar conditions of accelerated oxidation tests to predict the usefulness of the plasma sprayed coatings. Oxidation

time was selected to be 50 cycles (each cycle of 1 hour heating followed by 20 minutes cooling in air) in view of the fact that an oxidising time of 50 hours is considered adequate to allow for steady-state oxidation (Ul-Hamid, 2003). Experiments were proposed to be conducted in a silicon tube furnace because both furnaces as well as burner rig. tests are capable of reproducing the corrosion observed in service (Saunders and Nicholls, 1984). The temperature of study was deliberately kept high (900°C) as this will also take into consideration the overheating effects in case of boilers, which has been identified as the major cause of failure (Metals Handbook, 1975). Moreover, at 900°C, the rate of high temperature hot corrosion (HTHC) has been reported to be the severest, Fig. 2.13 (National Materials Advisory Board, 1996).

The hot corrosion environment selected for the study that is Na<sub>2</sub>SO<sub>4</sub>-60%V<sub>2</sub>O<sub>5</sub> constitutes an eutectics with a low melting point of 550°C and provides a very aggressive environment for accelerated testing under simulated laboratory conditions (Tiwari, 1997). Furthermore, sodium vanadyl vanadate (Na<sub>2</sub>O.V<sub>2</sub>O<sub>4</sub>.5V<sub>2</sub>O<sub>5</sub>), which melts at a relatively low temperature 550°C is found to be the most common salt deposit on boiler superheaters (Barbooti et al, 1988). This environment will also be pertinent to the gas turbines as the predominant species in the salt deposits forming on gas turbine surfaces are expected to Na<sub>2</sub>SO<sub>4</sub>, V<sub>2</sub>O<sub>5</sub> and Na<sub>2</sub>V<sub>2</sub>O<sub>6</sub> (Luthra & Spacil, 1982). According to Goward (1998) the corrosion in boilers and turbines had much in common. So far as the testing in air environment is concerned, the study could also provide useful information regarding the adhesion of the coatings and the spalling tendency of their oxide scales (Burman and Ericsson, 1983), apart from air oxidation behaviour of the coatings.

It was proposed to conduct the experiment under cyclic conditions as these conditions constitute more realistic approach towards solving the problem of metal corrosion in actual applications, where conditions are more or less cyclic, rather than isothermal (Sadique et al, 2000). Besides, Hancock and Hurst (1974) also emphasised that all potential commercial alloys should be subjected to thermal cyclic mode of testing to consider the effect of surface stresses developed due to disparity in coefficients of expansion of the base alloy, coating and oxide. Further, it could be seen from the literature survey that relatively fewer studies are reported on hot corrosion of the plasma sprayed coatings under cyclic conditions.

Several superalloys have been chosen for the study as it was intended to understand the effect of composition of the substrate alloy on the oxidation/hot corrosion behaviour of a particular coating, in the view of the fact that Smeggil and Bornstein

(1983) and Singh and Prakash (2003) have observed the effect of substrate alloying elements on the oxidation and hot corrosion resistance for diffusion aluminide and plasma sprayed Ni<sub>3</sub>Al coatings respectively. Besides, the study would be useful to rank the alloys under investigation with respect their oxidation and hot corrosion performance in the given environments of the study.

Ni- and Co-based metallic coatings are frequently considered for protection against oxidation, corrosion, wear and erosion etc. Therefore, it was planned to deposit the alloy powders namely NiCrAlY, Ni-20Cr, Ni<sub>3</sub>Al and Stellite-6 on all the chosen superalloys by shrouded plasma spray process with an aim to assess their behaviour in the energy conversion systems and other similar high temperature applications under simulated conditions.

Thermogravimetric studies were to be done under cyclic conditions in air and Na<sub>2</sub>SO<sub>4</sub>-60%V<sub>2</sub>O<sub>5</sub> environments to establish the kinetics of corrosion. The determination of corrosion resistance lies simply in how fast corrosion occurs (kinetic study) (Brasunas, 1977). Observations regarding the integration of the coating with the substrates after the completion of cyclic oxidation tests were decided to be accomplished with the help of cross-sectional SEM micrographs, in accordance with the studies carried out by Serghini and Dallaire (2000). Standard techniques such as X-ray Diffractometer (XRD), Scanning Electron Microscope (SEM), Energy Dispersive X-ray Analysis (EDAX) and Electron Micro Probe Analyser (EPMA) were chosen to be utilised to characterise the as sprayed coating and the oxidation/corrosion products, with an attempt to understand and propose mechanisms for the high temperature corrosion, wherever possible. The kinetics data and analysis of the results would be useful to assess the effectiveness of the chosen coatings in providing resistance to oxidation and hot corrosion for the superalloys and, to compare the performance of the different coatings under study. The analysis would further be beneficial to understand the effect of the substrate superalloys, if any, on the performance of the different coatings.



# CHAPTER 3

## EXPERIMENTAL TECHNIQUES AND PROCEDURES

---

---

This chapter presents the experimental techniques and procedures employed for applying the coatings and their characterisation, the oxidation studies and analysis of the corrosion products. Specifications of the equipments and other instruments used for the present investigation are also incorporated.

### 3.1 SELECTION OF SUBSTRATE MATERIALS

Selection of candidate material for the study has been made after consultation with Mishra Dhatu Nigham Ltd, Hyderabad (India). The alloys selected for the study are being developed by Mishra Dhatu Nigham Ltd, Hyderabad, which are basically Ni- and Fe-based superalloys having Midhani Grades Superni 75, Superni 600, Superni 601, Superni 718 and Superfer 800H. The alloys were procured in rolled sheet form with each alloy sheet having different thickness within a range of 4.20-5.80 mm. Nominal composition and industrial applications of these alloys are given in Table 3.1.

### 3.2 DEVELOPMENT OF COATINGS

#### 3.2.1 Preparation of Substrate Materials

Specimens with dimensions of approximately 20mmX15mmX5mm were cut from the alloy sheets. The specimens were polished with SiC papers down to 180 grit and subsequently grit blasted by alumina (Grit 60) before application of the coatings by *shrouded plasma spray process*.

#### 3.2.2 Alloy Powders for Coatings

Four types of coating powders namely Ni-20Cr (NI-105), Ni<sub>3</sub>Al, Stellite-6 (Eu Troloy) and Ni-22Cr-10Al-1Y (NI-343) were chosen for plasma spray deposition on the five types of superalloy substrates. In the first three cases of Ni-20Cr, Ni<sub>3</sub>Al and Stellite-

6 coatings, Ni-22Cr-10Al-1Y was also used as a bond coat, whereas entire coating of the Ni-22Cr-10Al-1Y powder was applied to constitute the fourth coating for the current investigation. All the coating powders were commercially available except the Ni<sub>3</sub>Al powder, which was prepared in the laboratory. Nickel powder with minimum assay 99.5% and size 200 mesh (Art. 4860) and aluminium fine powder with minimum assay 99.7% (Art. 880) supplied by Loba Chemical were mixed in stoichiometric ratio 3:1 in the laboratory ball mill for 8 hrs to form a uniform mixture of Ni<sub>3</sub>Al powder. Chemical composition and particle size of all the coating powders have been reported in Chapter 4 of the current study.

### **3.2.3 Formulation of Coatings**

The coating work was carried out by a commercial firm namely Anod Plasma Ltd. Kanpur (India). They used 40 kW Miller Thermal (USA) plasma spray apparatus to apply the coatings. Argon was used as powder carrying and shielding gas. All the process parameters were kept constant throughout the coating process while spraying distance was maintained in a narrow range of 90-110 mm. Ni-22Cr-10Al-1Y powder was deposited as a bond coat around 150 µm thick before applying the final coatings. The process parameters for the shrouded plasma spray process employed for applying the coatings are summarised in Table 3.2.

## **3.3 CHARACTERISATION OF COATINGS**

### **3.3.1 Measurement of Coating Thickness**

Thickness of the coatings was firstly monitored during the process of plasma spraying with Minitest-2000 made in Germany. Efforts were made to obtain coatings of uniform thickness. In order to verify the thickness of coatings some of as sprayed specimens were cut along the cross-section and mounted as explained in forthcoming Section 3.3.3. Scanning Electron Microscope (LEO 435VP) with attached Robinson Back Scattered Detector (RBSD) was used to obtain the BSE images. The average thickness of the coating was then measured from these BSE images and the same has been reported in Chapter 4 of the present study.

**Table 3.1** Nominal composition and industrial applications of the superalloys used

Sl. No.	Alloy Michani Grade (Similar grade)	Chemical Composition (wt.%)											Recommended Application (Manufacturer's Catalogue)		
		Fe	Ni	Cr	Ti	Al	Mo	Mn	Si	Cu	Ta	C			
1.	Superni 75 (Nimonic 75)	3.0	Bal	19.5	0.3	-	-	-	-	-	-	-	-	0.100	Gas Turbine, boiler parts
2.	Superni 600 (Inconel 600)	10.0 max	Bal	15.5	-	-	-	0.50	-	-	-	-	-	0.200	Furnace parts, heat treatment jigs
3.	Superni 601 (Inconel 601)	Bal	62	23.0	-	1.48	-	0.80	0.37	0.10	-	-	-	0.025	High temperature heat resistant alloy
4.	Superni 718 (Inconel 718)	18.5	Bal	19.0	0.9	0.50	3.05	0.18	0.18	0.15	5.13	-	0.040	Jet engines, pump bodies and parts	
5.	Superfer 800H (Incoloy 800H)	Bal	32	21.0	0.3	0.30	-	1.50 max	1.00 max	-	-	-	0.100 max	Steam boilers, furnace equipment, heat exchangers and piping in chemical industry, reformer, baffle plates/tubes in fertilizer plants	

**Table 3.2:** Parameters of the argon shrouded plasma spray process

Arc current (A)	700
Arc voltage (V)	35
Powder flow rate (rev./min)	3.2
Spraying distance (mm)	90-110
Plasma arc gas (Argon) (psi)	59
Carrier gas (psi)	40
Spray gun nozzle diameter (mm)	6

### 3.3.2 Measurement of Porosity

Porosity measurements for the plasma sprayed coatings have been made after polishing the specimens. Image Analyser having software Dewinter Material Plus 1.01 based on ASTM B276 was utilized to determine the porosity values. Images of the surface of the specimens were obtained through an attached PMP3 Inverted Metallurgical Microscope made in Japan. Ten values of porosity have been measured for each coating and are reported in Chapter 4.

### 3.3.3 Metallographic Studies

For metallographic studies the plasma spray coated specimens were cut along their cross-sections with diamond cutter (Buehler's Precision Diamond Saw, Model ISOMET 1000, USA make). Thereafter, the cut sections were hot mounted in Buehler's transoptic powder (20-3400-080) so as to show their cross-sectional details. This was followed by polishing of the mounted specimens by a belt sanding machine having emery belt (180 grit). The specimens were then polished manually down to 1000 grit using SiC emery papers. Final polishing was carried out using cloth polishing wheel machine with 1  $\mu\text{m}$  lavigated alumina powder suspension. Specimens were then washed and dried before being examined under Zeiss Axiovert 200 MAT Inverted Optical Microscope interfaced with imaging software Zeiss AxioVision Release 4.1, Germany. The same microscope was used to obtain surface microstructures of the coatings. Cross-sectional as well as surface microstructures of the specimens are presented in Chapter 4 of the ongoing study.

### 3.3.4 Measurement of Microhardness

Microhardness of the coatings was measured by Shimadzu Micro Hardness Tester HMV-2 Series, Made in Japan. 2.942N load was applied on the indenter for penetration and the hardness values were based on the relation  $Hv = 0.1891 \times \frac{F}{d^2}$  (Where F is load in N and d is the mean of the indentation diagonal length in mm). Each reported value of the microhardness is a mean of three observations. These microhardness values are plotted as a function of distance from the coating/substrate interface in Chapter 4. This analysis was carried out at Mechanical Engineering Department, SHSL Central Institute of Engineering and Technology, Longowal (India).

### 3.3.5 X-Ray Diffraction (XRD) Analysis

The plasma sprayed specimens were subjected to XRD analysis to identify various phases formed on their surfaces. Diffraction patterns were obtained by Bruker AXS D-8 Advance Diffractometer (Germany) with  $CuK_{\alpha}$  radiation and nickel filter at 20 mA under a voltage of 35 kV. The specimens were scanned with a scanning speed of 1 Kcps in  $2\theta$  range of  $10^{\circ}$  to  $110^{\circ}$  and the intensities were recorded at a chart speed of 1 cm/min with  $1^{\circ}$ /min as Goniometer speed. Assuming height of the most prominent peak as 100%, the relative intensities were calculated for all the peaks. The diffractometer being interfaced with Bruker DIFFRAC<sup>plus</sup> X-Ray diffraction software provides 'd' values directly on the diffraction pattern. These 'd' values were then used for identification of various phases with the help of inorganic ASTM X-Ray diffraction data cards.

### 3.3.6 Scanning Electron Microscopy (SEM) and Energy Dispersive X-Ray (EDAX) Analysis

Surface morphology of the as-sprayed coatings was also studied with the help of Scanning Electron Microscope (LEO 435VP) with an aim to understand the structure of the coatings and identify oxide inclusions, unmelted particles, pores etc. Whereas surface SEM/EDAX analysis was performed at Central Research Facilities (CRF), Indian Institute of Technology, Kharagpur (India) on JEOL (JSM-5800) Scanning Electron Microscope fitted with EDAX attachment of Oxford (Model-6841) made in England for some of the as sprayed specimens. The equipment could directly indicate the elements or

phases (oxides) present at a point alongwith their compositions (weight %) based on built-in EDAX software, which is a patented product of Oxford ISIS300. Although the compositions correspond to selected points on the as-sprayed surfaces, still the data could be useful to understand the formation of desired compositions in the coatings. SEM morphologies and the elemental analysis for the as sprayed coatings have been reported in Chapter 4 of this thesis.

### **3.3.7 Electron Probe Micro Analyser (EPMA)**

For detailed cross-sectional analysis the specimens were cut along the cross-section, mounted and polished in accordance with the procedure already discussed in section 3.3.3 and subjected to EPMA analysis. The mounted specimens were applied with carbon coating before performing the EPMA analysis. The EPMA analysis consisted of recording BSE Image and elemental X-ray mappings for representative area of each specimen. The selected area could have the three regions i.e. base specimen, coating and some epoxy region adjacent to the scale. X-ray mappings were obtained for all the elements of the substrate and the coatings, but only those mappings which indicate the presence of some element are reported in Chapter 4. EPMA analysis was done at Institute Instrumentation Centre (IIC), Indian Institute of Technology Roorkee, Roorkee (India) on JXA-8600M microprobe.

## **3.4 HIGH TEMPERATURE OXIDATION AND HOT CORROSION STUDIES**

### **3.4.1 Experimental Setup**

Oxidation and hot corrosion studies were conducted at 900<sup>0</sup>C in a laboratory silicon carbide tube furnace, Digitech, India make. The furnace was calibrated to an accuracy of  $\pm 5^0$ C using Platinum/Platinum-13% Rhodium thermocouple fitted with a temperature indicator of Electromek (Model-1551 P), India. The uncoated as well as the coated specimens were polished down to 1 $\mu$ m alumina wheel cloth polishing to obtain similar condition of reaction before being subjected to corrosion run. Physical dimensions of the specimens were then recorded carefully with vernier caliper to evaluate their surface areas. Subsequently the specimens were washed properly with acetone and dried in hot air to remove any moisture. During experimentation the prepared specimen was kept in an alumina boat and the weight of boat and specimen was measured. The alumina boats used for the studies were pre heated at a constant

temperature of 1200<sup>0</sup>C for 6 h and it was assumed that their weight would remain constant during the course of high temperature cyclic oxidation/corrosion study. Then the boat containing the specimen was inserted into hot zone of the furnace set at a temperature of 900<sup>0</sup>C. Holding time in the furnace was one hour in still air after which the boat with specimen was taken out and cooled at the ambient temperature for 20 minutes. Following this weight of the boat along with specimen was measured and this constituted one cycle of the oxidation study. Any spalled scale in the boat was also taken into consideration for the weight change measurements. Electronic Balance Model CB-120 (Contech, Mumbai, India) with a sensitivity of 10<sup>-3</sup> g was used to conduct the thermogravimetric studies. Visual observations were made after the end of each cycle with respect to colour, luster or any other physical aspect of the oxide scales being formed. All oxidation and hot corrosion studies were cyclic in this work and were carried out for 50 cycles. The reproducibility in the experiments was established by repeating hot corrosion experiments for five cases, where two specimens of the same description were subjected to similar hot corrosion test.

### **3.4.2 Oxidation Studies in Air**

The oxidation tests at 900<sup>0</sup>C were performed on all the five base superalloys as well as plasma spray coated superalloys in laboratory furnace up to 50 cycles as discussed in section 3.4.1.

### **3.4.3 Hot Corrosion Studies in Molten Salt (Na<sub>2</sub>SO<sub>4</sub>-60%V<sub>2</sub>O<sub>5</sub>)**

#### **3.4.3.1 Molten Salt Coating**

The plasma spray coated as well as uncoated specimens were prepared for studies as discussed in section 3.4.1. The specimens were then heated in an oven upto 250<sup>0</sup>C and a salt mixture of Na<sub>2</sub>SO<sub>4</sub>-60%V<sub>2</sub>O<sub>5</sub> dissolved in distilled water was coated on the warm polished specimens with the help of a camel hair brush. Amount of the salt coating was kept in the range of 3.0 -5.0 mg/cm<sup>2</sup>. The salt coated specimens as well as the alumina boats were then dried in the oven for 3-4 hours at 100<sup>0</sup>C and weighed before being exposed to hot corrosion tests.

#### **3.4.3.2 Hot Corrosion Studies**

The uncoated as well as plasma spray coated specimens after application of salt coating were subjected to hot corrosion in the laboratory furnace at 900<sup>0</sup>C for 50 cycles as discussed in section 3.4.1

## **3.5 ANALYSIS OF CORROSION PRODUCTS OF OXIDATION IN AIR AND MOLTEN SALT**

All the specimens subjected to oxidation as well as hot corrosion were analysed for the characterisation of corrosion products. The analysis was performed for surface and cross-section of the corroded specimens. Corroded specimens were subjected to XRD, SEM, EDAX, measurement of scale thickness and EPMA analysis.

### **3.5.1 Visual Observation**

Visual examination was made after each cycle and changes in colour, luster, adherence-spalling tendency, and growth of cracks in the coatings/oxide scales were recorded. After the completion of 50 cycles (each cycle of 1 hr heating and 20 minutes cooling) specimens were finally carefully examined and their macrographs were taken.

### **3.5.2 Thermogravimetric Studies**

The weight change values were measured at the end of each cycle with the aim to approximate the kinetics of corrosion. The weight change data was plotted with respect to number of cycles for each specimen and the plots have been given in the subsequent chapters.

### **3.5.3 Measurement of Scale Thickness**

The oxidized/corroded specimens after 50 cycles were cut across the cross-section and polished as discussed in section 3.3.3. In some cases, Scanning Electron Microscope (LEO 435VP) with attached Robinson Back Scattered Detector (RBSD) was used to obtain the BSE images at the areas where the scale thickness was observed to be the least. Average thickness of the scales was then measured from the respective BSE images and the data has been presented in Chapter 5 and 6. For the remaining specimens, the BSE images were taken with the Scanning Electron Microscope described in Section 3.5.6.2.

### **3.5.4 X-Ray Diffraction (XRD) Analysis**

For identification of different phases formed in the oxides scales of oxidized/hot corroded specimens after 50 cycles, X-ray diffraction analysis of most of the specimens was conducted on the diffractometer described in section 3.3.5. While some of the specimens were analysed by Philips X-ray diffractometer, model PW 1140/90 using Cu



target and nickel filter at 20 mA under a voltage of 35 kV. The specimens were scanned in the range  $(2\theta)$ , 10 to  $120^\circ$  and recorded at a chart speed of 1 cm/min and the Goniometer speed  $1^\circ/\text{min}$ . Assuming height of the most prominent peak as 100%, the relative intensities were calculated for all the peaks. For the intensity peaks and corresponding values of  $2\theta$ , the interplanar spacing 'd', has been calculated using Bragg's law.

$$2d \sin \theta = n\lambda$$

Where,  $\lambda$  is the wave length of Cu  $K_\alpha$  radiation used for the diffraction and is taken as 1.54 Å for estimating the 'd' values which were finally used for identification of various phases with the help of inorganic ASTM X-ray diffraction data cards.

### **3.5.5 SEM/EDAX Analysis**

#### **3.5.5.1 Surface Morphology**

SEM/EDAX analysis of the oxidized/hot corroded specimen surfaces after 50 cycles was conducted at CRF, Indian Institute of Technology, Kharagpur (India), and the details regarding the equipment have already been provided in section 3.3.6. The specimens were scanned under the microscope and the critical areas of interests were photographed with an aim to identify the inclusions, micro cracks and morphology of the surface scale. Point analysis by EDAX was carried out on various locations on these identified areas of interest with an aim to understand composition (weight %) of various phases in the oxide scales. Although these compositions correspond to selected points on the surfaces, still the data could be useful to support the formation of various phases in the oxide scales.

#### **3.5.5.2 Cross-Sectional Morphology**

SEM/EDAX analysis for some of the selected specimens was carried out along their cross-sections at Inter University Consortium (IUC) for Department of Atomic Energy (DAE) Facilities, Indore (India). The equipment consisted of a Scanning Electron Microscope of JEOL with EDAX attachment of Oxford model Flex Scan 520 England make. Cross-sectional BSE images were taken and some points of interest were identified on these images including scale/coating and substrate. EDAX analysis was then conducted to ascertain elemental composition (weight %) for these points. Although these compositions correspond to selected points along the cross-sections, still the data could be useful to approximate the distribution of various elements across the thickness of the scales. In some cases, the oxide scale thickness was also measured from these BSE images.

### **3.5.6 Electron Probe Micro Analyser (EPMA)**

For detailed cross-sectional analysis the specimens were cut along the cross-section, mounted and polished in accordance with the procedure already discussed in section 3.3.3 and subjected to EPMA analysis. The details regarding the EPMA equipment and preparation of the specimens have already been mentioned in Section 3.3.7 of this chapter. Besides, some specimens were analysed at Material Science Division, Bhabha Atomic Research Centre, Trombay, Mumbai (India), and Defense Metallurgical Research Laboratory, Hyderabad (India) using Cameca SX100, 3 Wavelength Dispersive Spectrometer, made in France.

During EPMA analysis, BSEI and elemental X-ray mappings were obtained for some critical area of interest on each specimen. The selected area could have the three regions i.e. base specimen, coating/oxide scale and some epoxy region at the top of the scale. X-ray mappings were obtained for all the elements present in the substrate, the coatings and the environment of study, but only those maps in which an element was identified in substantial concentrations have been reported in respective chapters.

# CHAPTER 4

## CHARACTERISATION OF SUPERALLOYS AND COATINGS

---

The chapter deals with critical examination of the substrate superalloys and the various coatings applied on them. The results of metallographic examination of substrate superalloys as well as the plasma spray coatings have been discussed. The physical properties like porosity and microhardness of as sprayed coatings have been reported and discussed with respect to the existing literature. The results of XRD, SEM/EDAX and EPMA analysis have been incorporated.

### 4.1 MICROSTRUCTURES OF THE SUBSTRATE SUPERALLOYS

Optical microstructures of the substrate steels are shown in Fig. 4.1, which are explained with reference to atlas of microstructures for industrial alloys (Metals Handbook, 1972 and ASM Handbook, 1995). The microstructures of Superni 75 and Superni 718, Fig. 4.1 (a) and (d) respectively can be characterised by a nickel-rich  $\gamma$ -solid solution matrix. In case of Superni 75, fine carbide particles are dispersed in the gamma matrix mainly along the grain boundaries. In  $\gamma$  matrix of the Superni 718, carbide segregation in the form of stringers is revealed. The microstructures of Superni 600 and Superni 601 show Ni-Cr-Fe solid solution containing fine as well as coarse carbides in the grains and along the grain boundaries, refer Fig. 4.1 (b) and (c). Twin boundaries are also visible in the structure of Superni 600. In case of Superni 601, thick black boundary envelope might have resulted from the precipitation of  $M_{23}C_6$  carbides as continuous streaks (ASM Handbook, 1995). Whereas the microstructure of the Superfer 800H consists of a solid solution matrix in which some of the grains are delineated by particles of precipitated carbides at the grain boundaries and by twinning lines (Metals Handbook, 1972).

### 4.2 VISUAL EXAMINATION OF THE COATINGS

Four types of coating powders were sprayed by argon shrouded plasma spray process on five superalloy substrates. The composition and designations used for the various coatings are given below in Table 4.1.

**Table 4.1** Composition, particle size and designation of the coating powders

Coating powder	Composition (wt %)	Particle size	Designation
Ni-22Cr-10Al-1Y (Praxair NI-343) <i>(also sprayed as a bond coat for each coating)</i>	Cr (22), Al (10), Y (1), Ni (bal.)	-45 $\mu\text{m}$ +10 $\mu\text{m}$	NiCrAlY
Ni-20Cr (Praxair NI-105)	Ni (80), Cr (20)	-45 $\mu\text{m}$ +5 $\mu\text{m}$	Ni-20Cr
Nickel and Aluminium	Stoichiometric ratio 3:1 (Ni:Al) <i>Ni (min. assay 99.5%) and Al (min. assay 99.7%) mixed in laboratory ball mill for 8 hrs</i>	Ni- 74 $\mu\text{m}$ Al- fine powder	Ni <sub>3</sub> Al
Stellite-6 (Eu Troloy)	Cr (19), C (0.7), Si (2.3), Fe (3), Ni (13.5), B (1.7), W (7.5), Mn (1 max.), Co (bal.)	-180 $\mu\text{m}$ +53 $\mu\text{m}$	Stellite-6

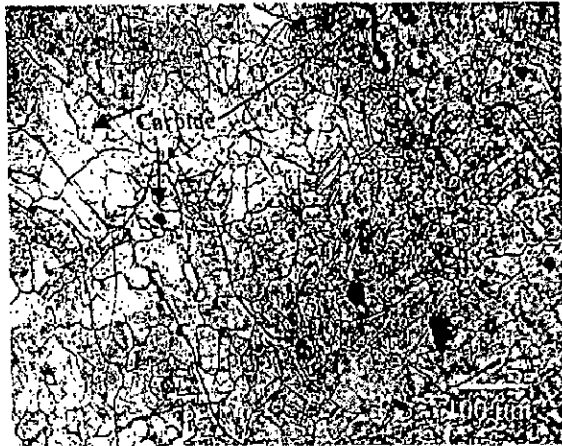
Macrographs for the as coated samples are shown in Fig. 4.2. NiCrAlY and Ni-20Cr coatings have the smooth surfaces with dull green appearance, whereas St-6 and Ni<sub>3</sub>Al coatings have shining grey colour with comparatively rough surfaces. Further these coatings are found to be free from surface cracks.

### 4.3 MEASUREMENTS OF COATING THICKNESSES

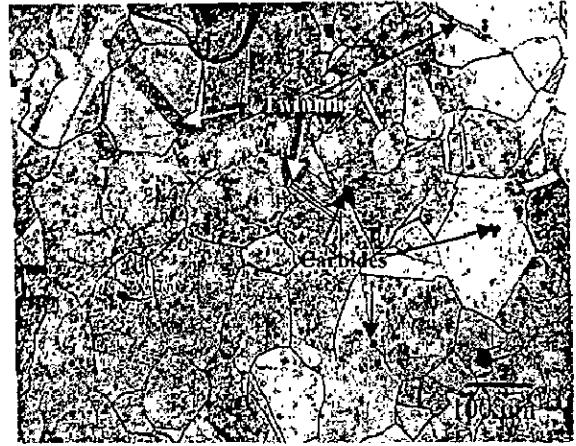
SEM micrographs were taken along cross-sections of the plasma sprayed coated specimens. Back Scattered Electron Images (BSEI) for these samples are shown in Fig. 4.3. In each of the micrographs shown in Fig. 4.3 (b)-(d), inner layer represents the bond coat i.e. NiCrAlY whereas outer layer the particular type of coating. While in case of Fig 4.3 (a), only single layer of NiCrAlY coating is visible. Thickness of the coatings has been measured from BSEI micrographs (Fig. 4.3) and has been reported in Table 4.2. In each case, thickness of the bond coat and the outer coat has been measured separately.

### 4.4 POROSITY ANALYSIS

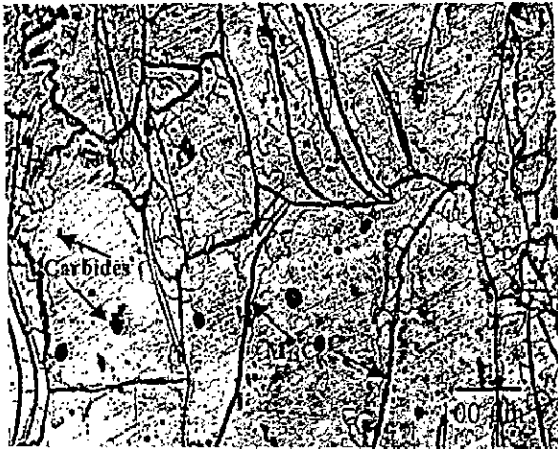
Porosity of the coatings has a significant role to play as far as the oxidation or hot corrosion resistance of plasma sprayed coatings is concerned. Dense coatings usually provide better corrosion resistance than the porous coatings. Porosity measurements were made for the plasma sprayed coatings, which are found to be in a range of 2.00-4.50% (Table 4.2).



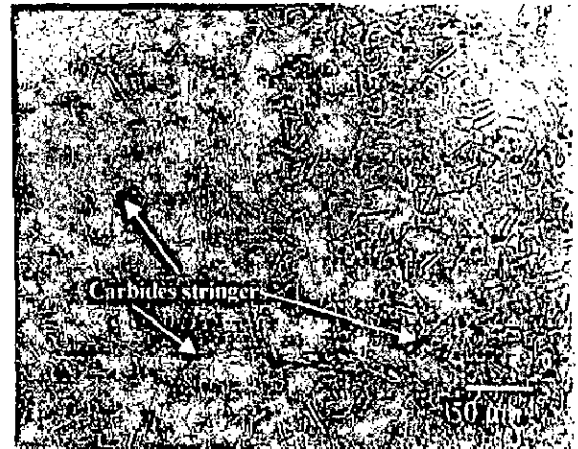
(a)



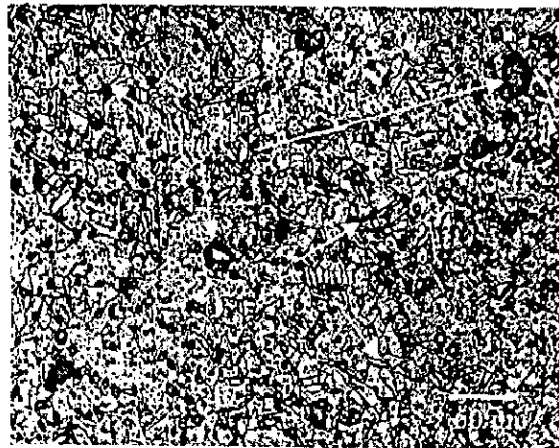
(b)



(c)



(d)



(e)

**Fig. 4.1** Optical micrographs of the substrate superalloys  
(a) Superni 75                      (b) Superni 600                      (c) Superni 601  
(d) Superni 718                      (e) Superfer 800H.

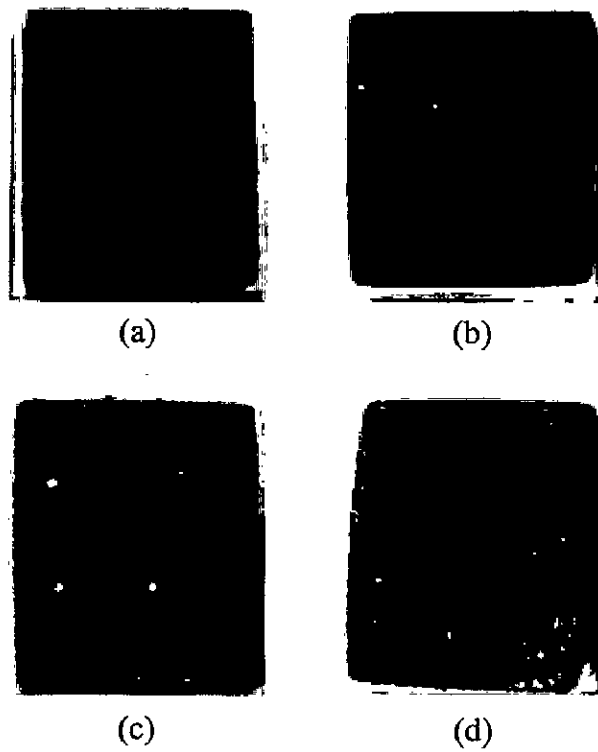


**Fig. 4.2** Macrographs of as sprayed specimens with  
(a) NiCrAlY coating      (b) Ni-20Cr coating  
(c) Ni<sub>3</sub>Al coating      (d) Stellite-6 coating.

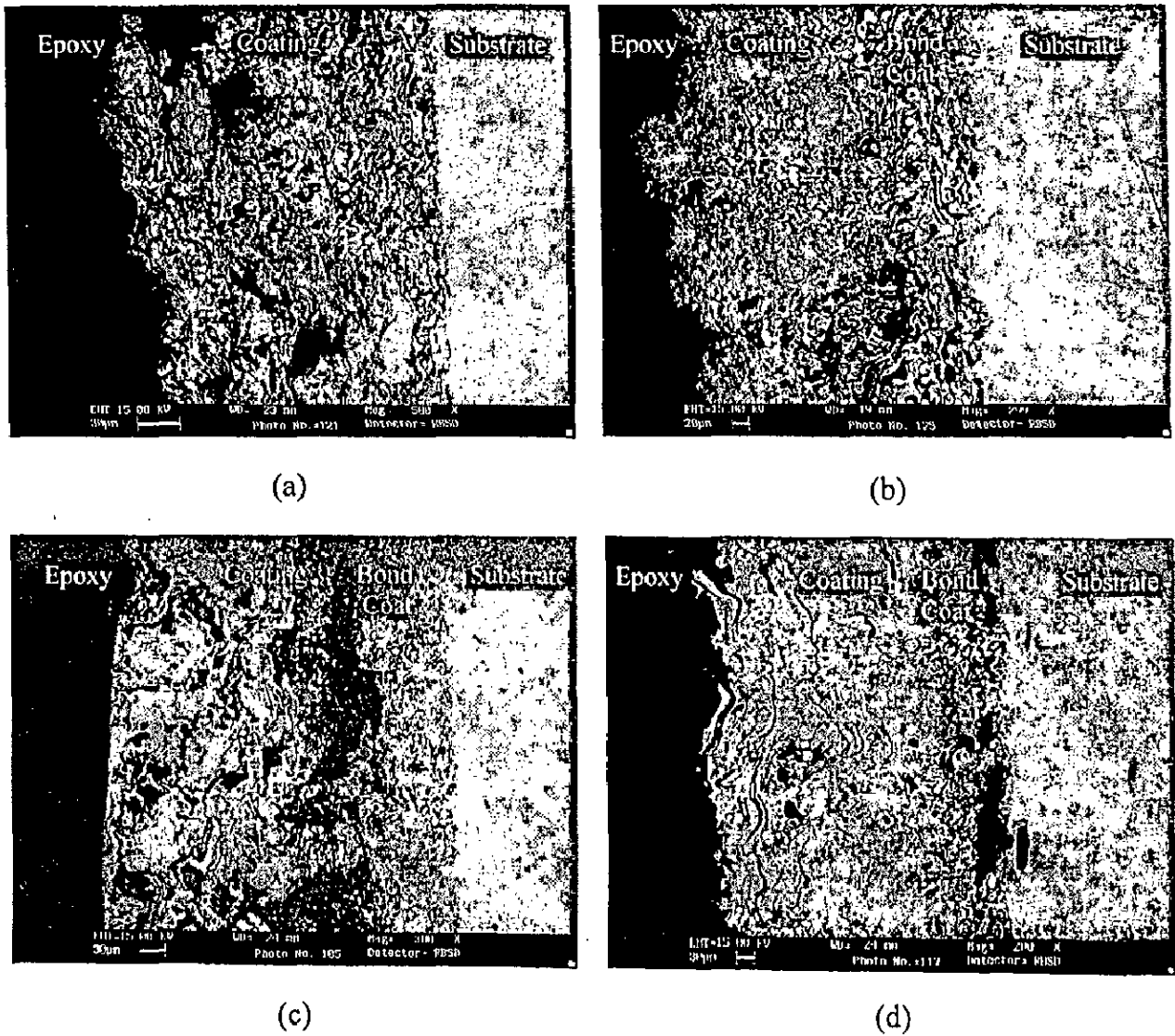


**Fig. 4.3** BSEI micrographs showing cross-sectional morphology of different plasma sprayed coatings on Superfer 800H  
 (a) NiCrAlY coating (b) Ni-20Cr coating with bond coat  
 (c) Ni<sub>3</sub>Al coating with bond coat (d) Stellite-6 coating with bond coat.

**Table 4.2** Average coating thickness and porosity of the plasma sprayed coatings

Coating	Coating thickness ( $\mu\text{m}$ )			Porosity (%)
	Bond coat (NiCrAlY)	Outer coat	Total	
NiCrAlY	228	--	228	2.88-4.42
Ni-20Cr	155	211	366	2.22-4.45
Ni <sub>3</sub> Al	166	247	413	2.37-4.01
Stellite-6	162	365	527	2.07-3.74

## 4.5 EVALUATION OF MICROHARDNESS

Microhardness of the coatings on different substrate superalloys has been measured along the cross-section. Profiles for microhardness versus distance from the coating-substrate interface are depicted in Fig. 4.4 to 4.7. The microhardness values for Superni 75, Superni 600, Superni 601 and Superfer 800H superalloys are observed to be in the range 230 to 365 Hv, whereas for Superni 718 these are in the range 320 to 415Hv. Microhardness of the NiCrAlY coating has been found to be in a range of 106 to 373Hv. From the microhardness profiles it is obvious that the Stellite-6 coating sprayed on Superfer 800H substrate has shown a maximum microhardness of the order of 490 Hv (Fig. 4.7), followed by Ni-20Cr (Fig. 4.5) and NiCrAlY (Fig. 4.4) coatings. Whereas the Ni<sub>3</sub>Al coating has indicated the least microhardness with a maximum value of the order of 223 Hv (Fig. 4.6), which is just 45% of that for the Stellite-6 coating.

## 4.6 METALLOGRAPHIC STUDIES FOR THE COATINGS

### 4.6.1 Surface Structure

Optical micrographs showing surface microstructures of the various plasma sprayed coatings (Fig. 4.8 to Fig. 4.11) reveal some voids and oxide inclusions in general with multiphase matrices. The existence of pores has also been indicated.

#### 4.6.1.1 NiCrAlY Coating

Figure 4.8 shows optical micrographs for the plasma sprayed NiCrAlY coating on the different superalloys. The microstructure can be characterised by irregularly shaped grains with black phase distributed at intergranular sites. The matrix grains are finest amongst the coatings under study.



#### **4.6.1.2 Ni-20Cr Coating**

Microstructure of the Ni-20Cr coated superalloys consists mainly of melted splats providing matrix dispersed with dark coloured phase where unmelted oxide particles and voids are also seen. There is certain directionality indicated by the matrix phase. The melted splats can be recognized as white and nearly columnar grains in the micrographs. Fig. 4.9 depicts the microstructures of the Ni-20Cr coated superalloys which are typical for a shrouded plasma spray process.

#### **4.6.1.3 Ni<sub>3</sub>Al Coating**

Optical micrographs of the Ni<sub>3</sub>Al coatings on different superalloy substrates are shown in Fig. 4.10. It can be seen that the deposited coating is having massive structure indicating large size splats which form the matrix with voids and unmelted oxides. The massiveness of the matrix phase, extent of voids and second dispersed phase, which may be unmelted oxides vary as the substrate is changed. Some pores are also seen in the structures.

#### **4.6.1.4 Stellite-6 Coating**

Structure of the as sprayed St-6 coating in all the cases consists primarily of M<sub>x</sub>C<sub>y</sub> particles in an alpha (fcc) matrix (Metals Handbook, 1972) as shown in Fig. 4.11. These M<sub>x</sub>C<sub>y</sub> carbides have shown their presence at the locations near grain boundaries in the eutectic mixture. There is some perceptible change in amount of carbides with change in the substrate superalloy. Voids are also indicated in the coatings.

### **4.6.2 Cross-Sectional Structures**

All the coatings were deposited on the stationary substrates by moving the plasma gun and the required thicknesses of the coatings have been obtained by varying number of passes. This might have led to the generation of lamellar structure of the coatings, as is obvious from the micrographs in Fig. 4.12. Oxide inclusions, in general can be seen in all the cases. The structure for the NiCrAlY and Ni-20Cr coatings consists of fine grains which are elongated in longitudinal direction, whereas that of the Ni<sub>3</sub>Al coating is found to be massive. The splat size is larger in the case of Ni<sub>3</sub>Al coating as compared to that in the NiCrAlY and Ni-20Cr coatings. Layers of the bond coat and upper coat can easily be identified in the micrographs for the as sprayed Ni<sub>3</sub>Al and Stellite-6 coatings, Fig. 4.12 (c) and (d)

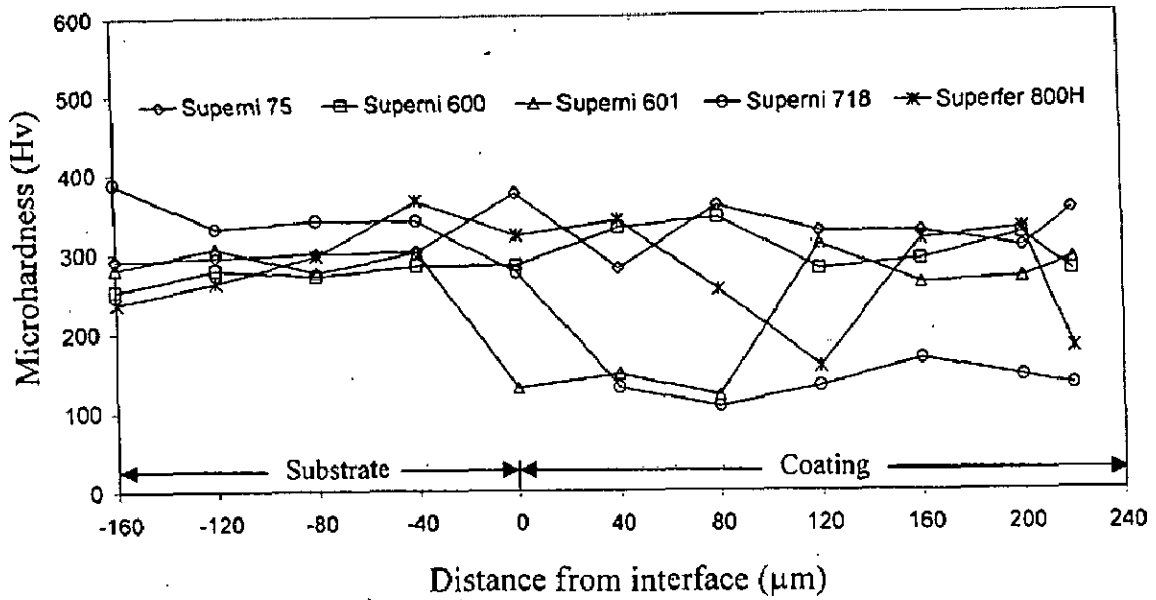


**Fig. 4.4** Microhardness profiles of plasma sprayed NiCrAlY coating for different substrate superalloys along the cross-section.

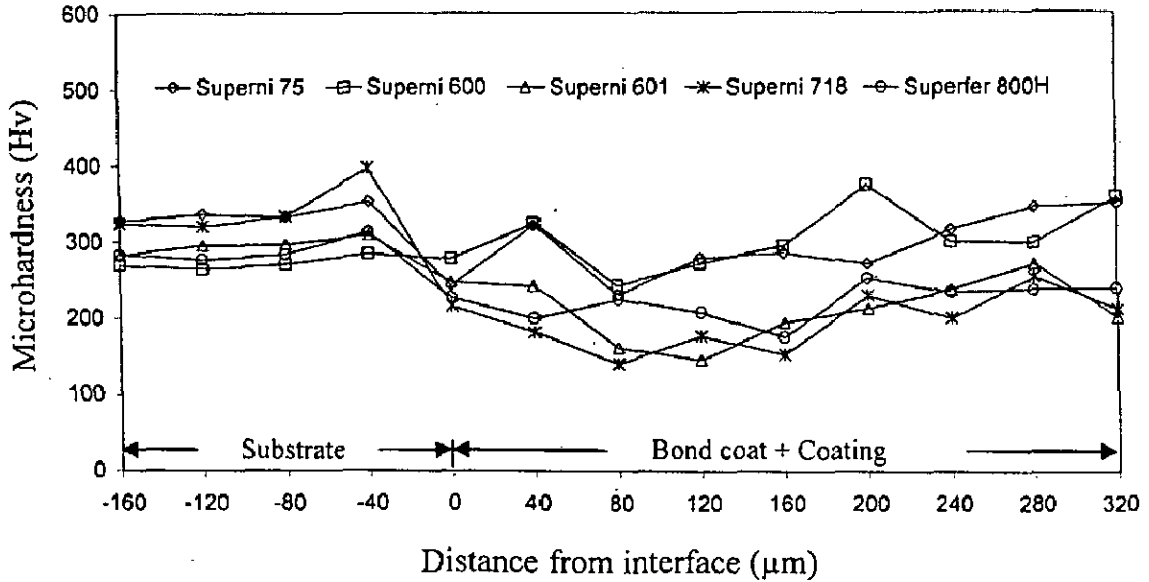


**Fig. 4.5** Microhardness profiles of plasma sprayed Ni-20Cr coating with NiCrAlY bond coat for different substrate superalloys along the cross-section.

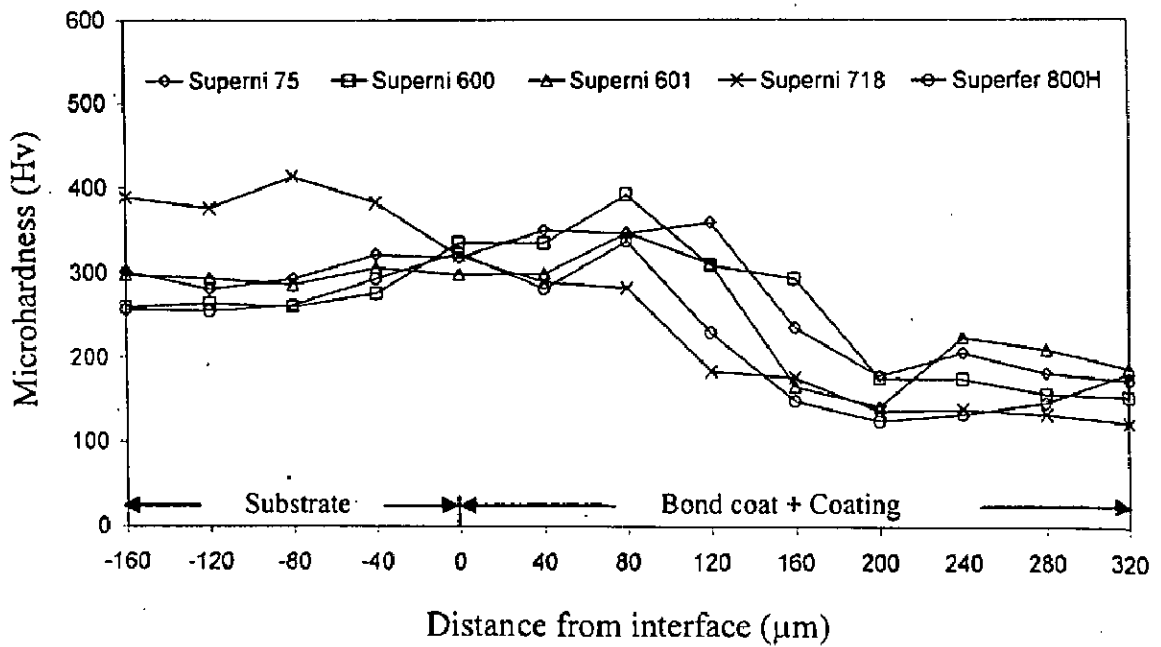


Fig. 4.6 Microhardness profiles of plasma sprayed  $Ni_3Al$  coating with NiCrAlY bond coat for different substrate superalloys along the cross-section.

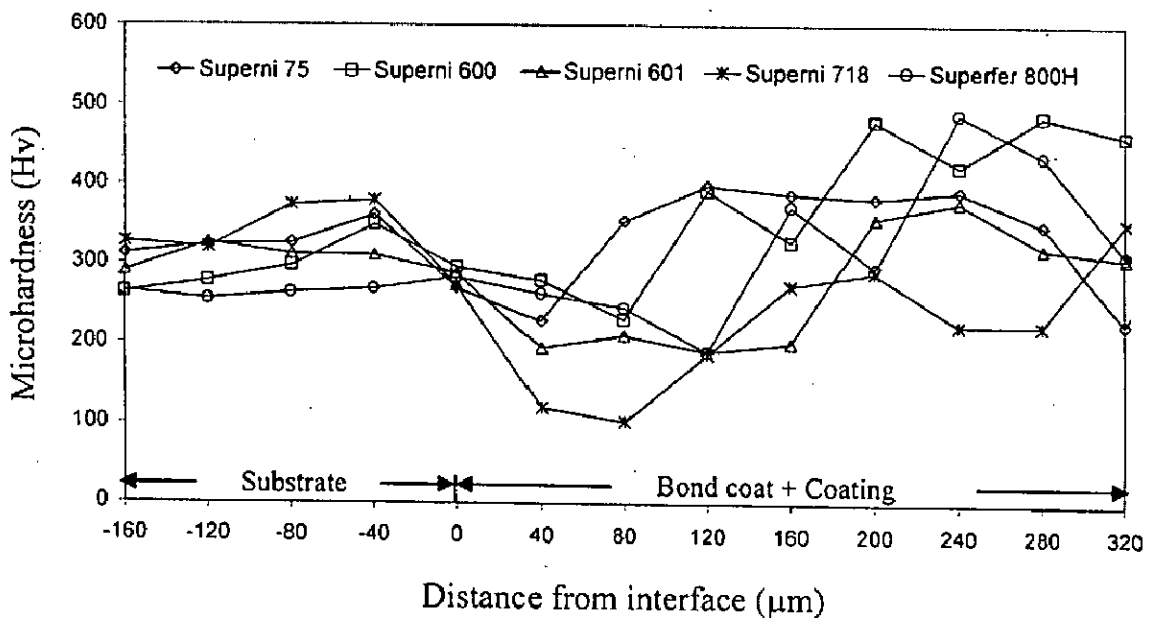
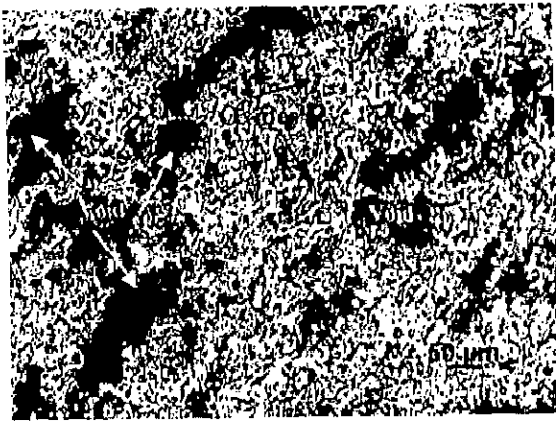
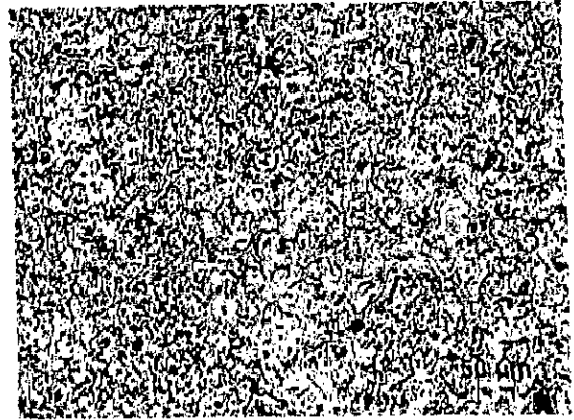


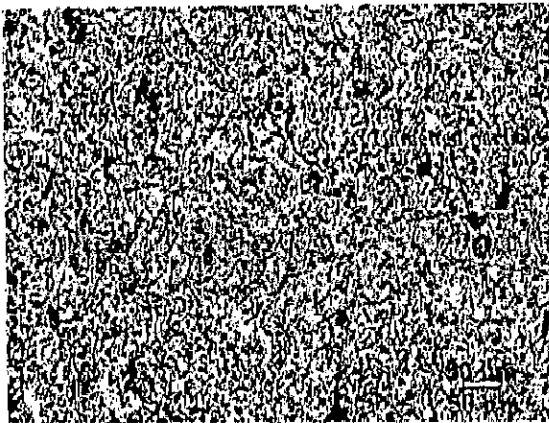
Fig. 4.7 Microhardness profiles of plasma sprayed Stellite-6 coating with NiCrAlY bond coat for different substrate superalloys along the cross-section.



(a)



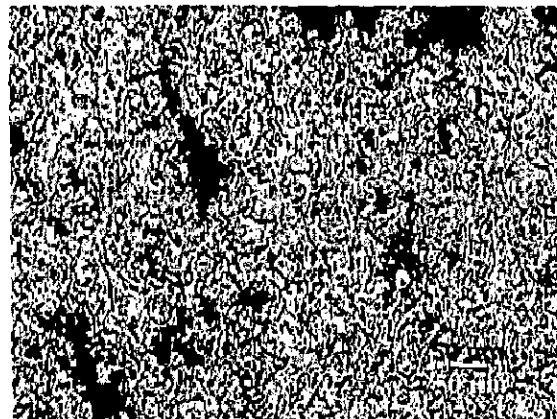
(b)



(c)

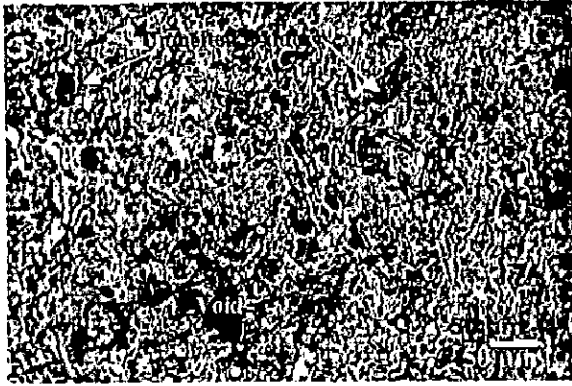


(d)

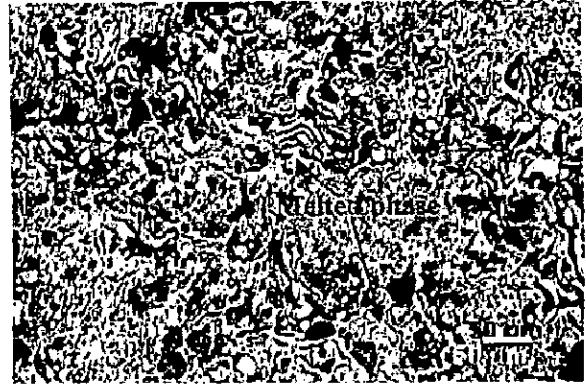


(e)

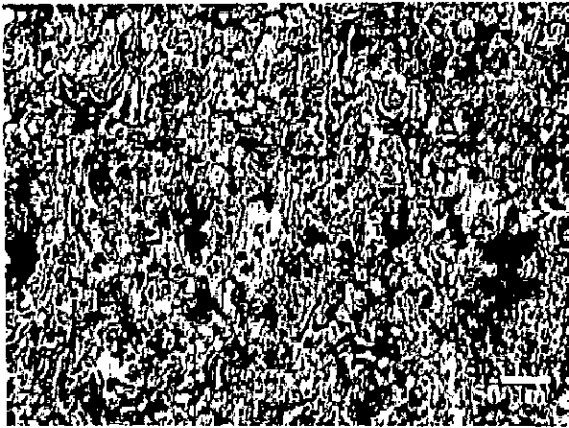
**Fig. 4.8** Optical micrographs showing surface morphology of plasma sprayed NiCrAlY coating on substrate superalloys  
(a) Superni 75                      (b) Superni 600                      (c) Superni 601  
(d) Superni 718                      (e) Superfer 800H.



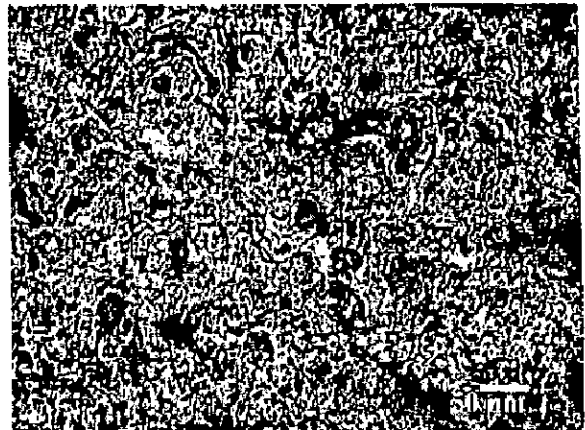
(a)



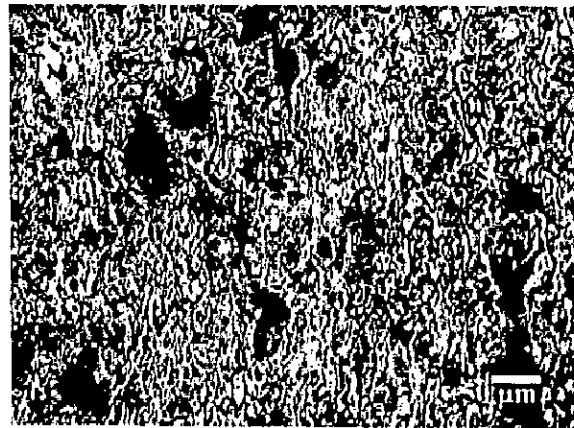
(b)



(c)



(d)



(e)

**Fig. 4.9** Optical micrographs showing surface morphology of plasma sprayed Ni-20Cr coating on substrate superalloys  
(a) Superni 75                      (b) Superni 600                      (c) Superni 601  
(d) Superni 718                      (e) Superfer 800H.

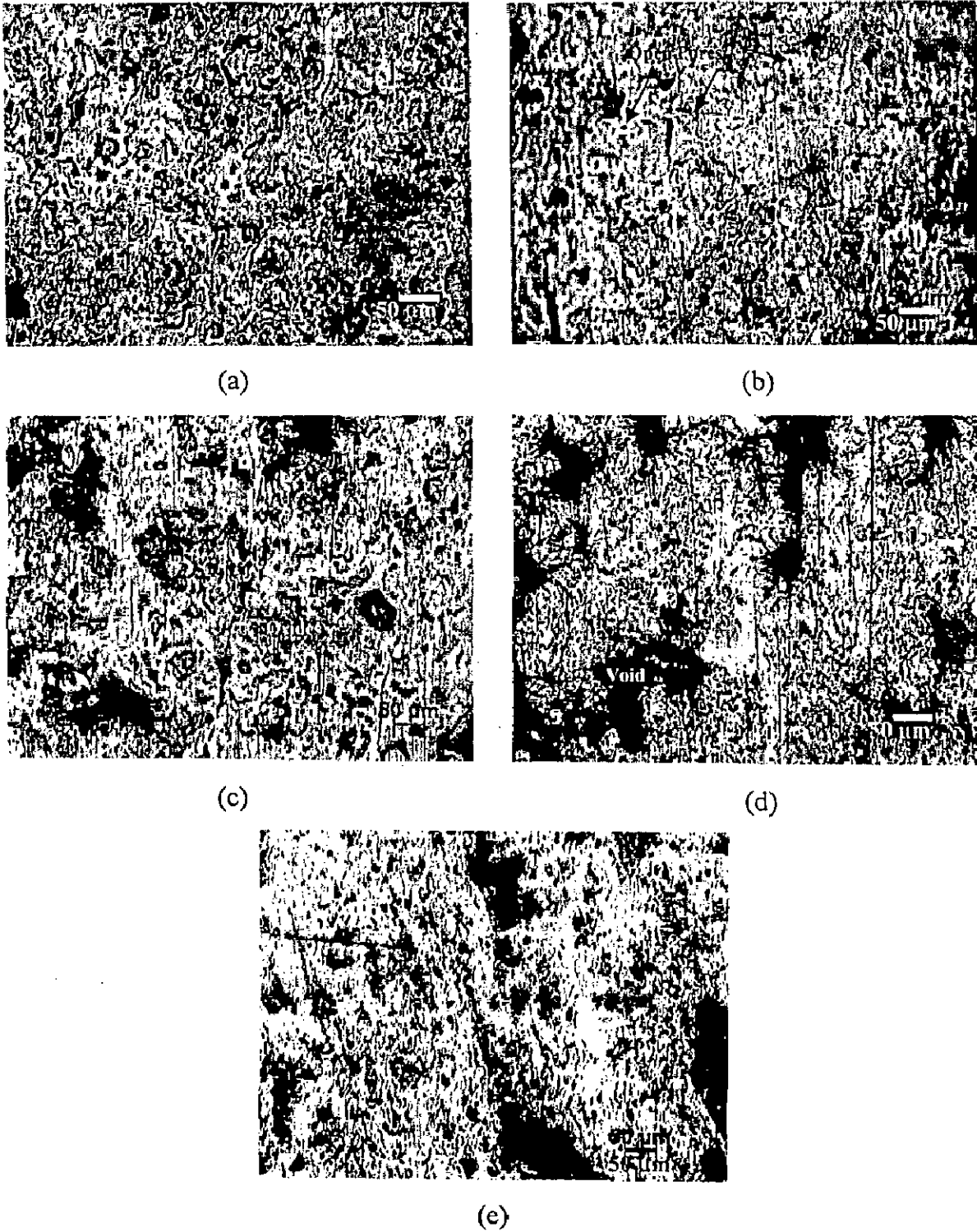
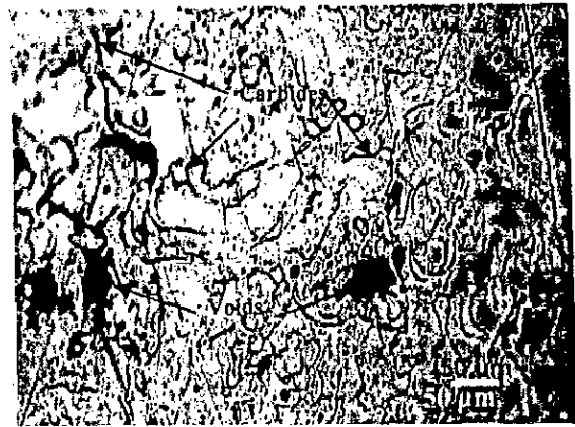


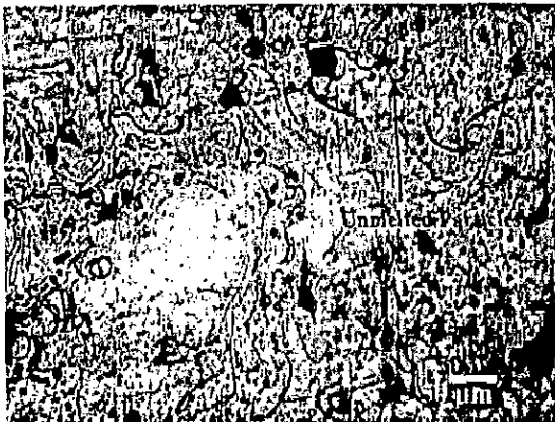
**Fig. 4.10** Optical micrographs showing surface morphology of plasma sprayed  $\text{Ni}_3\text{Al}$  coating on substrate superalloys;  
 (a) Superni 75 (b) Superni 600 (c) Superni 601  
 (d) Superni 718 (e) Superfer 800H.



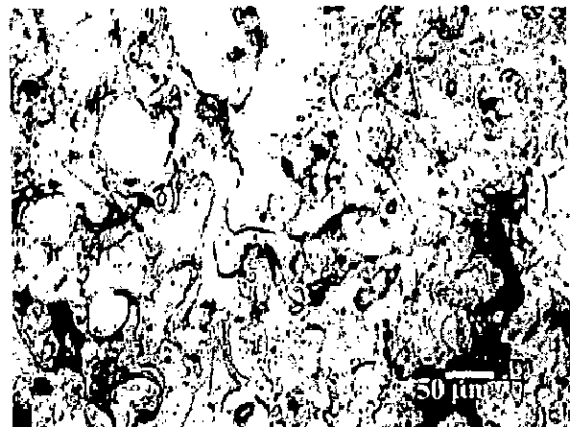
(a)



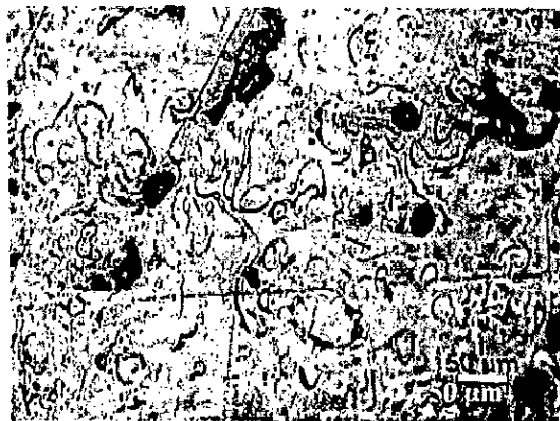
(b)



(c)



(d)



(e)

**Fig. 4.11** Optical micrographs showing surface morphology of plasma sprayed Stellite-6 coating on substrate superalloys

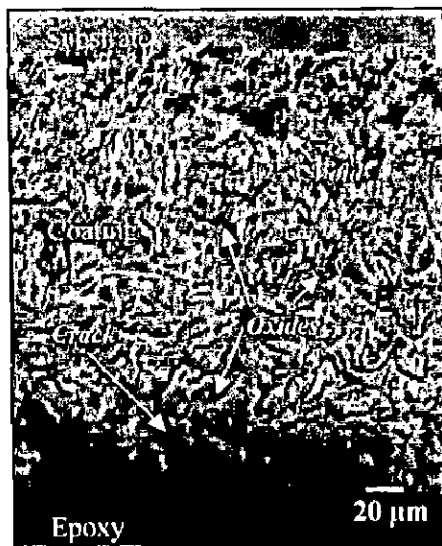
(a) Superni 75

(b) Superni 600

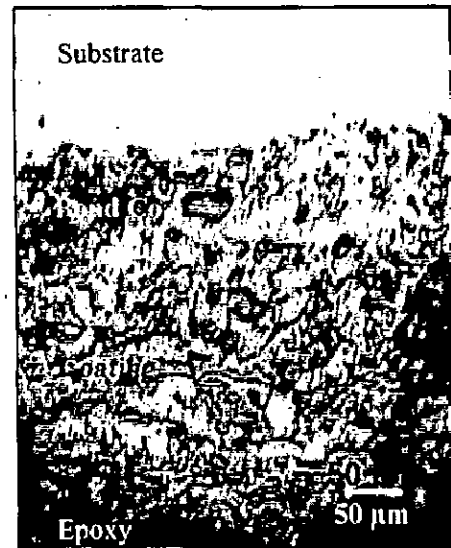
(c) Superni 601

(d) Superni 718

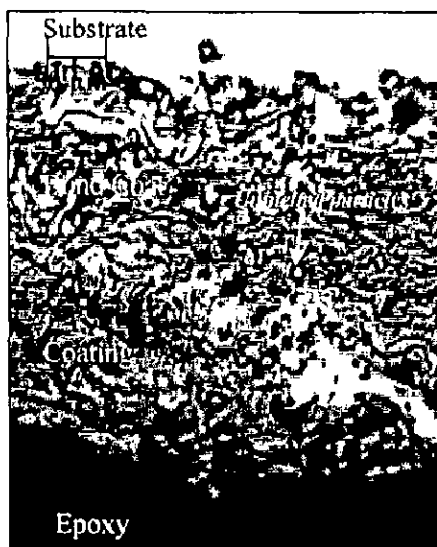
(e) Superfer 800H.



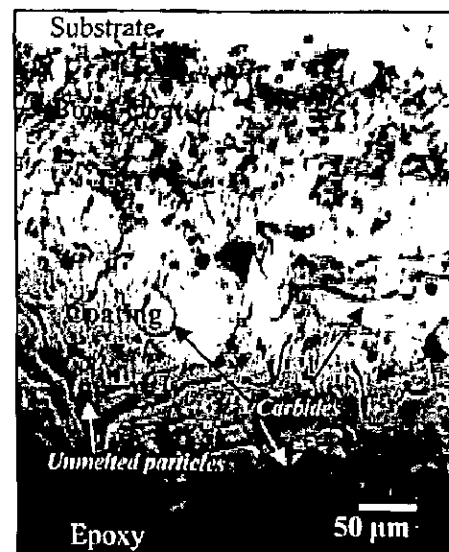
(a)



(b)



(c)



(d)

**Fig. 4.12** Optical micrographs along cross-section of different plasma sprayed coatings on superalloy Superfer 800H  
 (a) NiCrAlY coating (b) Ni-20Cr coating with bond coat  
 (c) Ni<sub>3</sub>Al coating with bond coat (d) Stellite-6 coating with bond coat.



respectively, alongwith the presence of some unmelted particles. The structure for the Stellite-6 coating has  $M_xC_y$  in an alpha (fcc) matrix (Metals Handbook, 1972). The alpha matrix is mainly Co-solid solution and is represented by large splats in the Stellite-6 coating. The carbides can be recognized as black streaks/spots dispersed in the matrix. The presence of few comparatively large blackish patches as evidenced in the micrographs might be indicating voids in the coatings.

#### 4.7 XRD ANALYSIS

XRD patterns for the surfaces of the plasma sprayed NiCrAlY, Ni-20Cr, Ni<sub>3</sub>Al and Stellite-6 coatings have been shown in the Fig.4.13 through Fig. 4.16 respectively on reduced scales. The NiCrAlY coated specimens has shown the presence of  $\gamma$ -Ni and  $\gamma'$ -Ni<sub>3</sub>Al as main phases, Fig. 4.13, whereas XRD of the Ni-20Cr coating has revealed  $\gamma$ -Ni as the main phase without formation of any intermetallic phase (Fig. 4.14). In case of Ni<sub>3</sub>Al coating, formation of the Ni<sub>3</sub>Al as a main phase has been confirmed by XRD as can be seen in Fig.4.15. Further  $\gamma$ -Co (fcc) and  $M_{23}C_6$  ( $Cr_{23}C_6$ ) have been detected as the main phases in case of St-6 coating, refer Fig. 4.16.

#### 4.8 SEM ANALYSIS

SEM morphologies for the plasma sprayed NiCrAlY, Ni-20Cr, Ni<sub>3</sub>Al and Stellite-6 coatings on the different superalloy substrates are shown in Fig. 4.17 to 4.20. Microstructures revealed are typical for a plasma spray process consisting of splats which are irregular shaped with distinct boundaries. Most of the splats are well formed without any sign of disintegration. Indications of globules near splat boundaries can be observed in most of the micrographs, which most likely are unmelted particles. These unmelted particle stick to surface due to high impact during plasma spray process and subsequently they cool and precipitate near splat boundaries as can be seen in the respective figures. Presence of some oxide stringers as well as open pores has also been noticed in general in all the coatings. Further some localized areas having higher densities of open pores and unmelted particles are also seen in most of the micrographs. The NiCrAlY and Ni-20Cr coatings have shown fine size splats in their structures, Fig. 4.17 and Fig. 4.18 respectively, whereas the splats are very coarse for the Stellite-6 coatings, refer Fig. 4.20. Medium sized splats are formed in the Ni<sub>3</sub>Al coatings as indicated in Fig. 4.19.

## 4.9 EDAX ANALYSIS

SEM micrographs, Fig. 4.21 and Fig. 4.22 indicate typical splat morphologies for the all the coatings in general with some indications of unmelted particles. EDAX analysis for NiCrAlY coating confirms the formation of required composition. Ni-20 Cr coating has shown two phases, the white one nearly corresponds to 20% Cr, thereby indicating probable formation of  $\gamma'$  phase, whereas the black phase has higher amount of Cr i.e. 45% which may be due to formation  $\gamma$  phase as per Ni-Cr phase diagram. Fig. 4.22 (a) indicates the formation of  $Ni_3Al$  crystalline phase. The structure of the St-6 coatings shows white dendritic regions and black interdendritic areas (Osma et al, 1996). The dendritic areas are rich in Cr and Si, while the interdendritic regions are having more Co and depleted of Si, Fig. 4.22 (b).

## 4.10 EPMA ANALYSIS

Cross-sectional BSEI of the as-sprayed NiCrAlY coating shows distinct layers of the coating and the substrate, Fig. 4.23 and a typical lamellar structure of the coating has been revealed. The elemental mappings for the coating show that the basic elements of the alloy powder viz. Ni, Cr, Al and Y have indicated uniformly distribution within the coating region. Nickel and chromium co-exist in the coating and at the places where these two are absent; Al and Y are found. Further minor diffusion of iron, manganese and silicon has been indicated from the substrate into the coating

Corresponding BSEI for the Ni-20Cr coating shows two distinct zones in the coating, where the top zone represents the Ni-20Cr top coat and the inner zone the bond coat. The top coating seems to be dense as compared to the bond coating. The elements of substrate, coating and bond coat are mainly confined to their original places except aluminum and to some extent titanium, tantalum, iron and manganese, Fig. 4.24. Aluminum have shown significant diffusion to the Ni-20Cr coating region especially at the places where Ni and Cr are absent. Some yttrium has also migrated to these places. Ti, Ta, Fe and Mn have also been noticed in very small but almost uniformly distributed concentration in the top coat as well as in the bond coat. This indicates probable diffusion of these elements from the substrate superalloy. In the top layers of Ni-20 Cr coat, at some places, where Ni and Cr are absent, Fe co-exists with aluminium in the form of clusters.

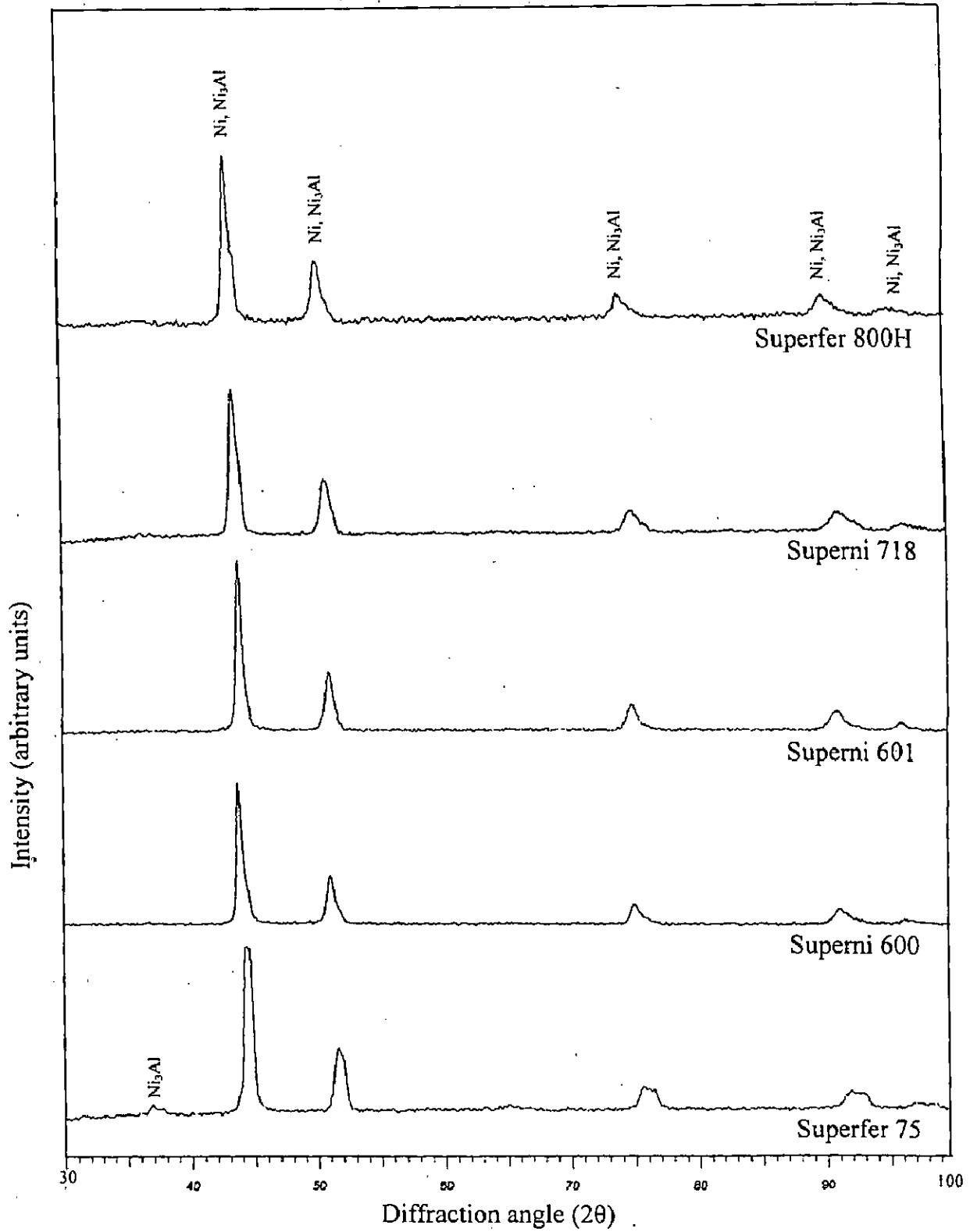


Fig. 4.13 X-ray diffraction patterns for the plasma spray NiCrAlY coated superalloys.

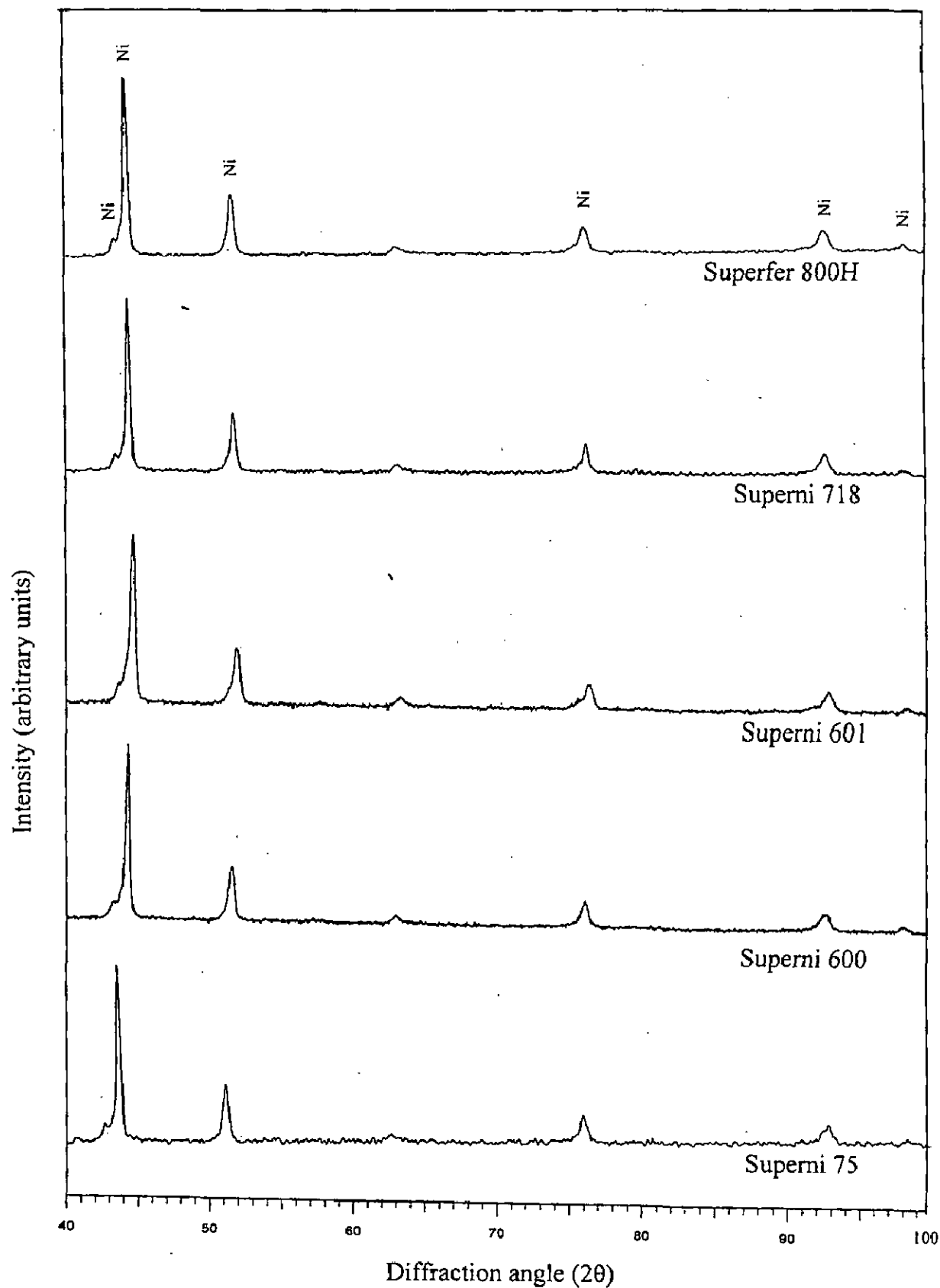


Fig. 4.14 X-ray diffraction patterns for the plasma spray Ni-20Cr coated superalloys.

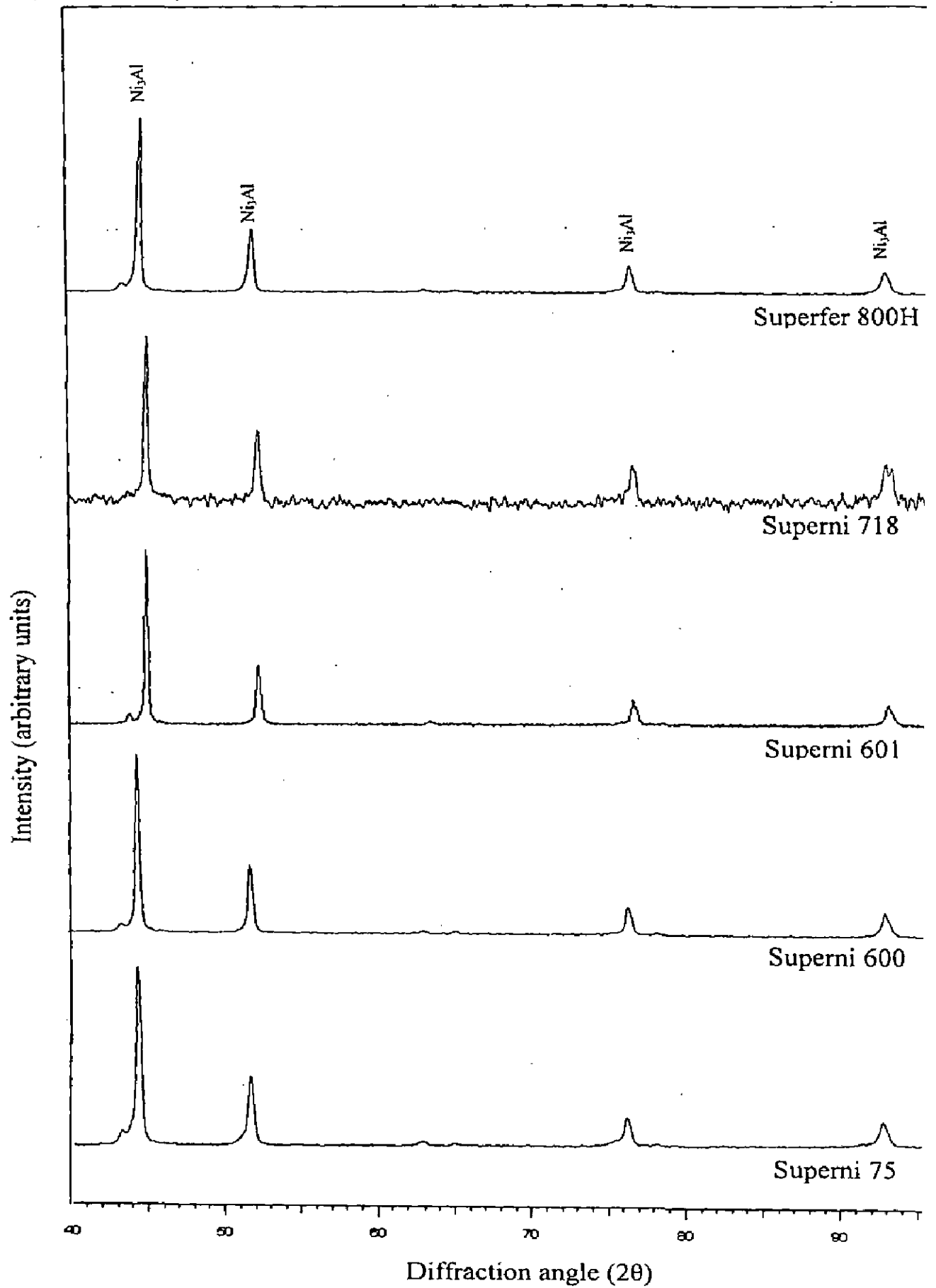


Fig. 4.15 X-ray diffraction patterns for the plasma sprayed  $\text{Ni}_3\text{Al}$  coated super

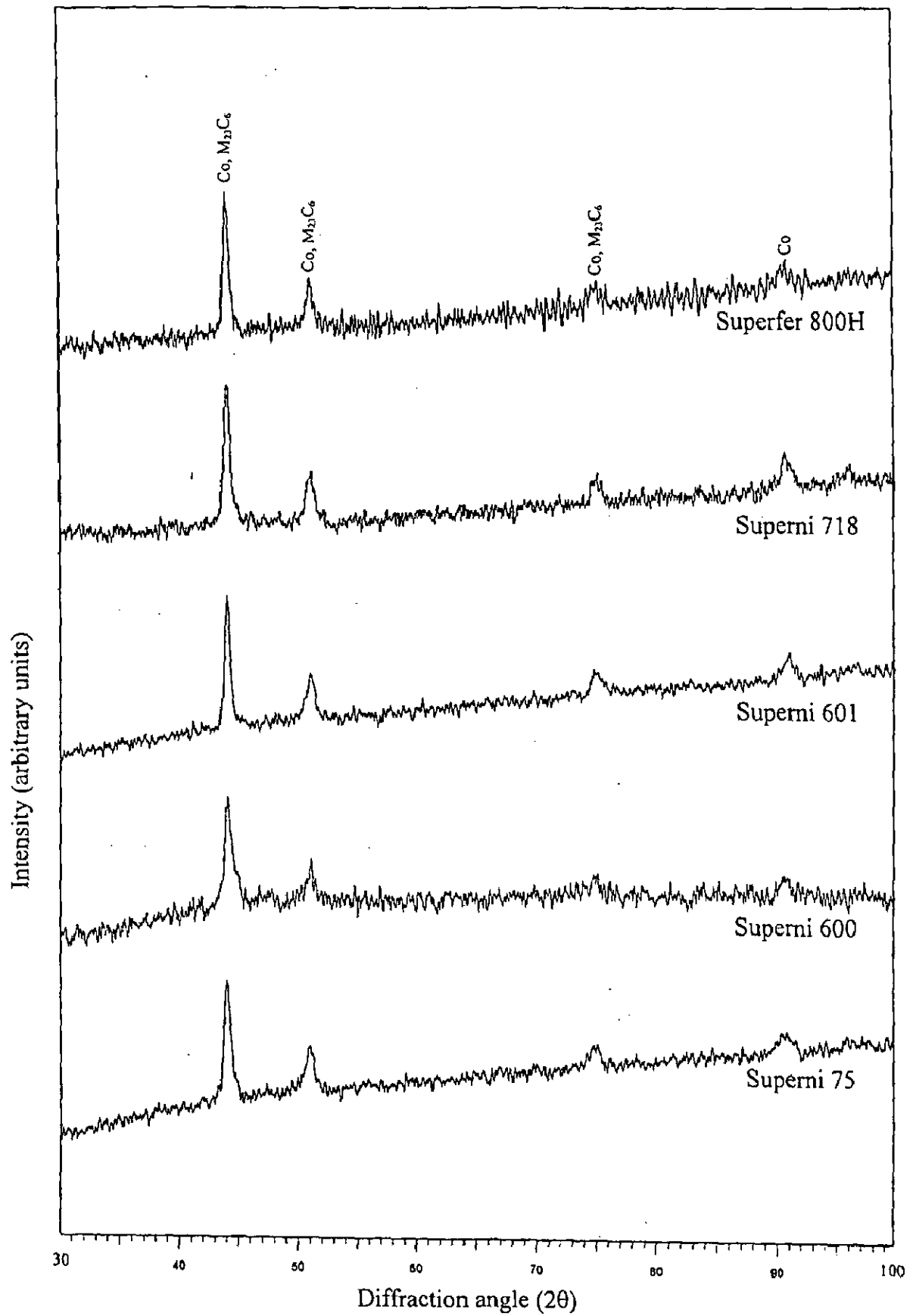
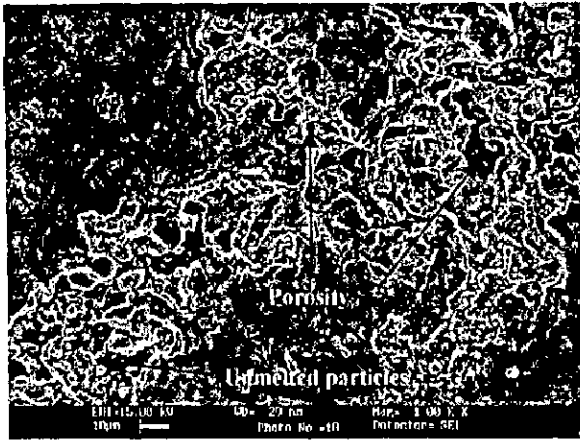
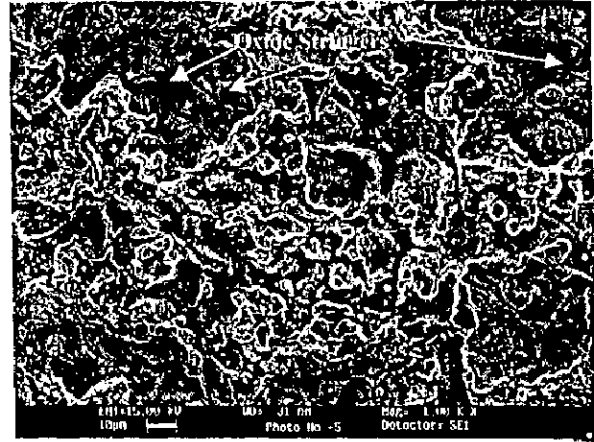


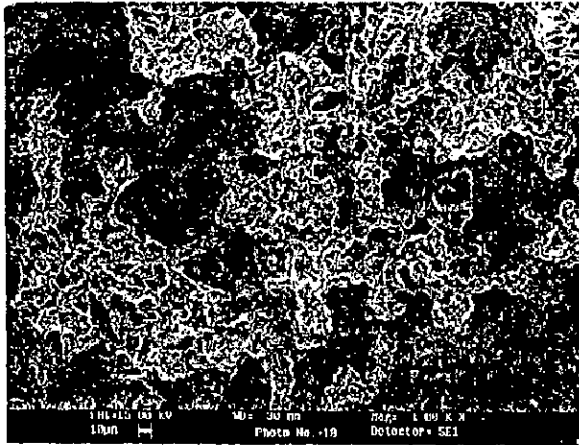
Fig. 4.16 X-ray diffraction patterns for the plasma sprayed Stellite-6 coated superalloys.



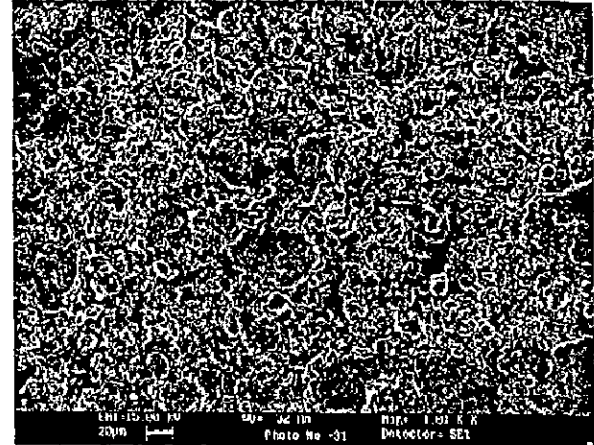
(a)



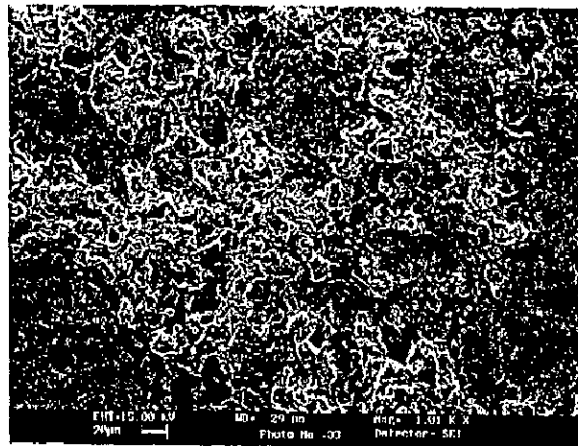
(b)



(c)

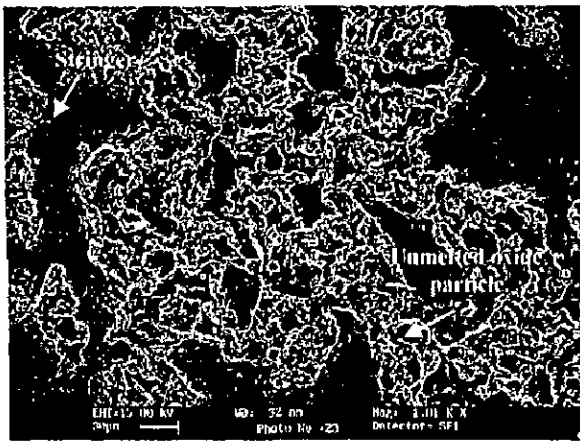


(d)

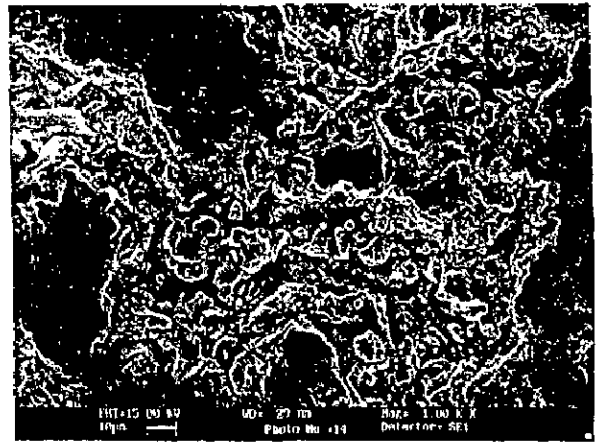


(e)

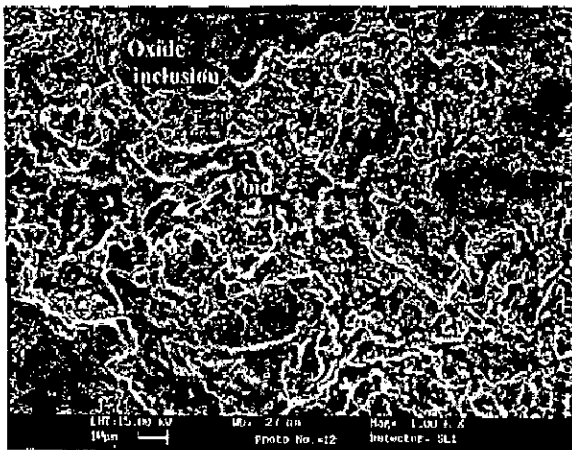
**Fig. 4.17** SEM micrographs showing surface morphology of plasma sprayed NiCrAlY coating on substrate superalloys  
 (a) Superni 75 (b) Superni 600 (c) Superni 601  
 (d) Superni 718 (e) Superfer 800H.



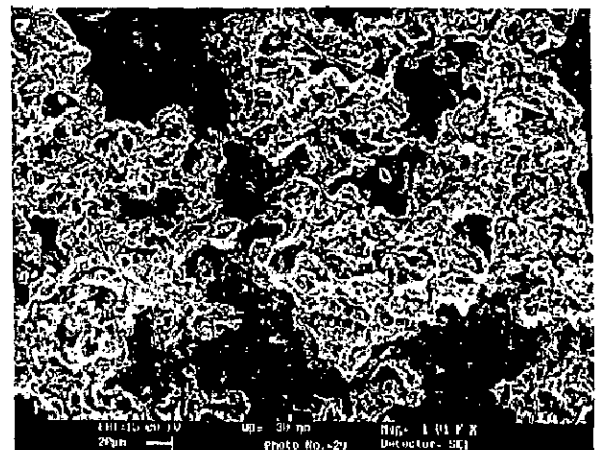
(a)



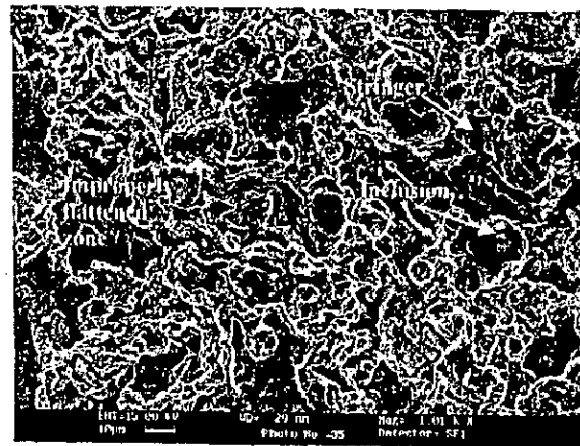
(b)



(c)



(d)



(e)

**Fig. 4.18** SEM micrographs showing surface morphology of plasma sprayed Ni-20Cr coating on substrate superalloys  
 (a) Superni 75                      (b) Superni 600                      (c) Superni 601  
 (d) Superni 718                      (e) Superfer 800H.



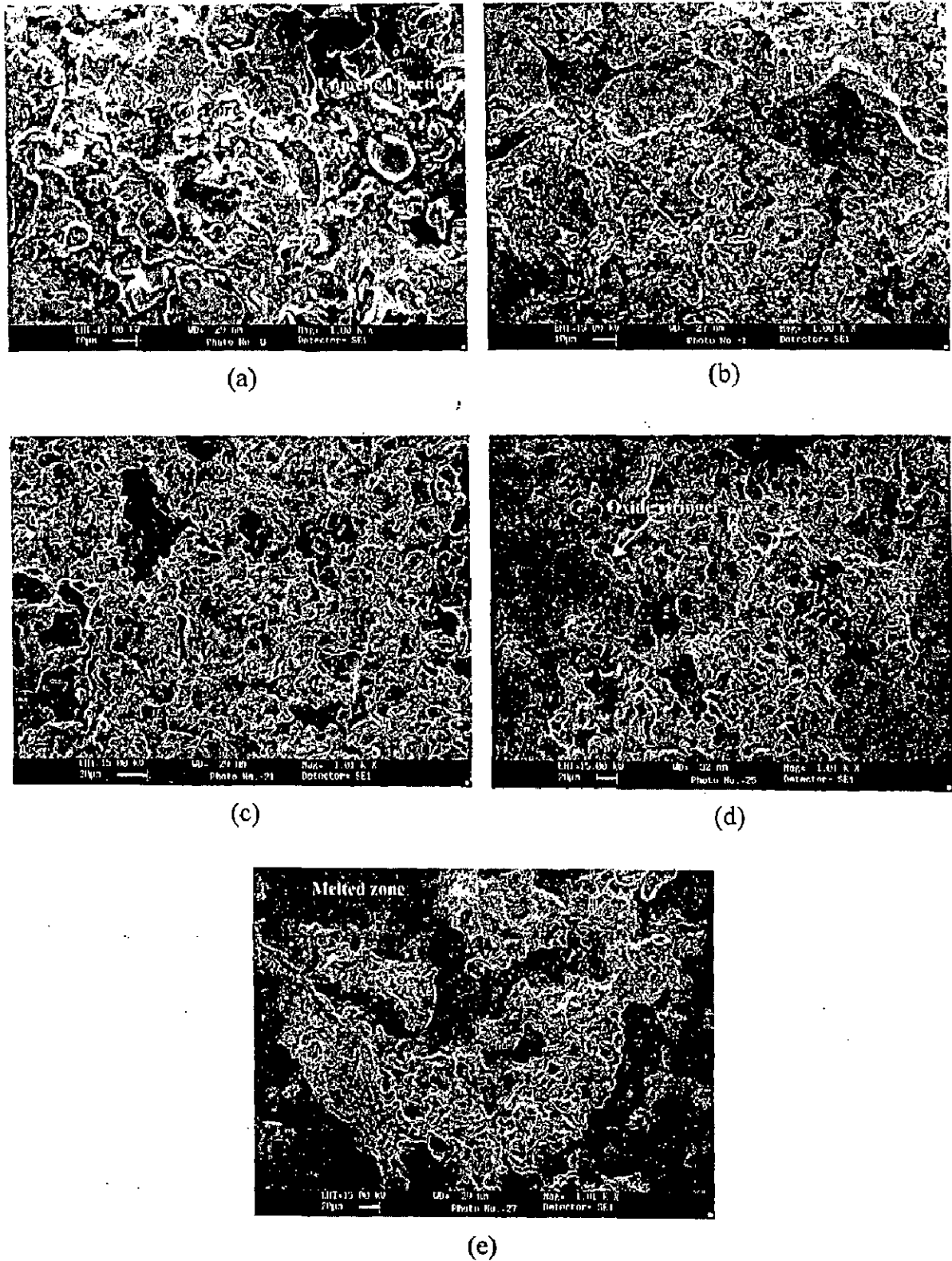
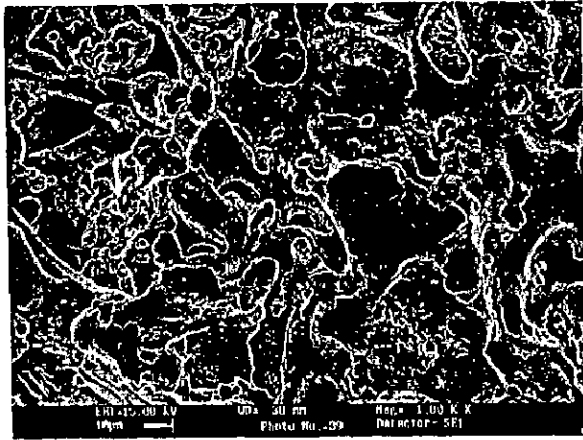
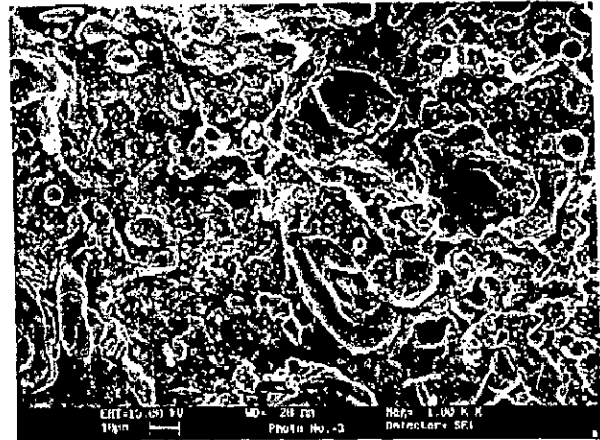


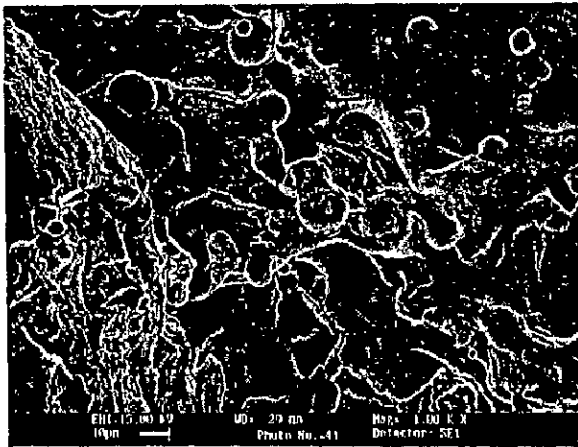
**Fig. 4.19** SEM micrographs showing surface morphology of plasma sprayed Ni<sub>3</sub>Al coating on substrate superalloys  
 (a) Superni 75                      (b) Superni 600                      (c) Superni 601  
 (d) Superni 718                      (e) Superfer 800H.



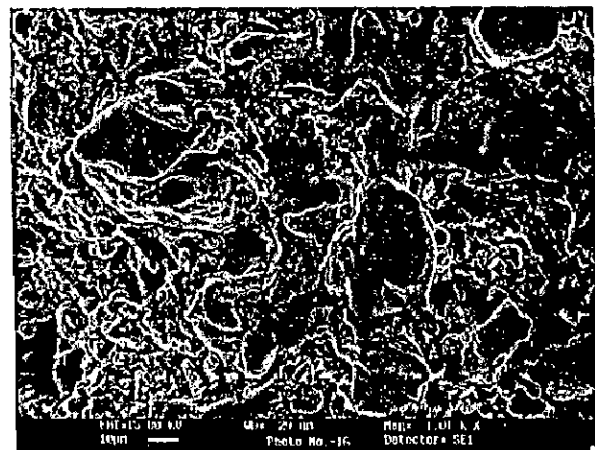
(a)



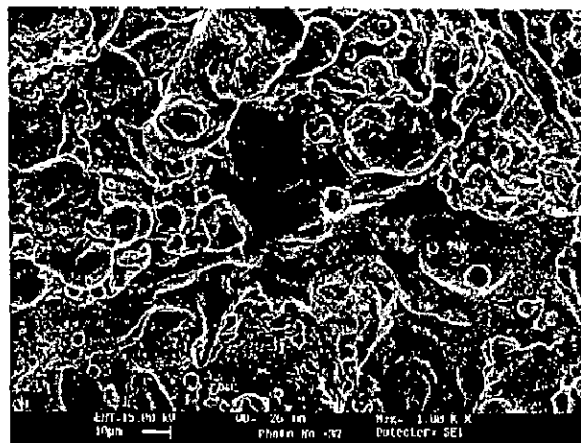
(b)



(c)



(d)



(e)

**Fig. 4.20** SEM micrographs showing surface morphology of plasma sprayed Stellite-6 coating on substrate superalloys

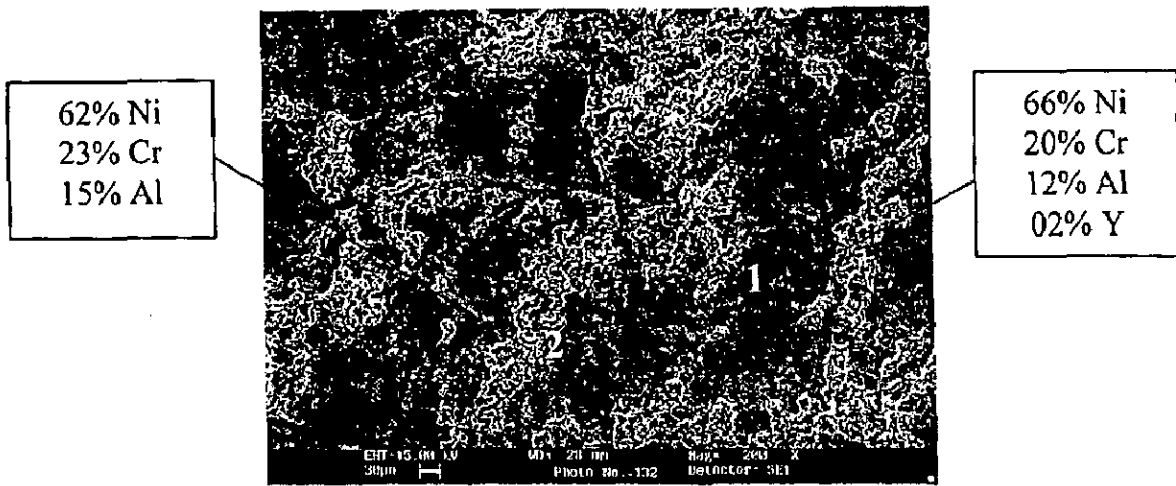
(a) Superni 75

(b) Superni 600

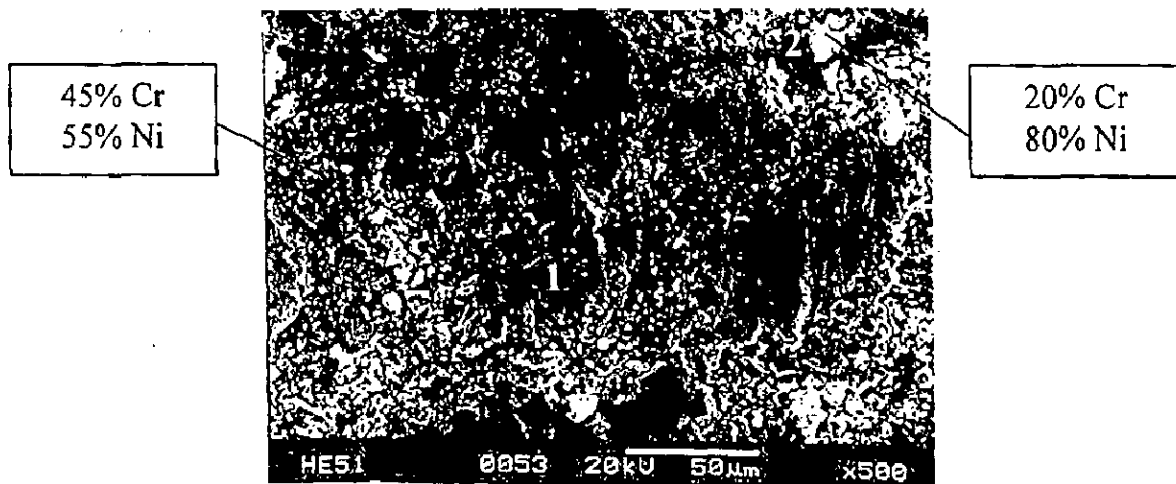
(c) Superni 601

(d) Superni 718

(e) Superfer 800H.

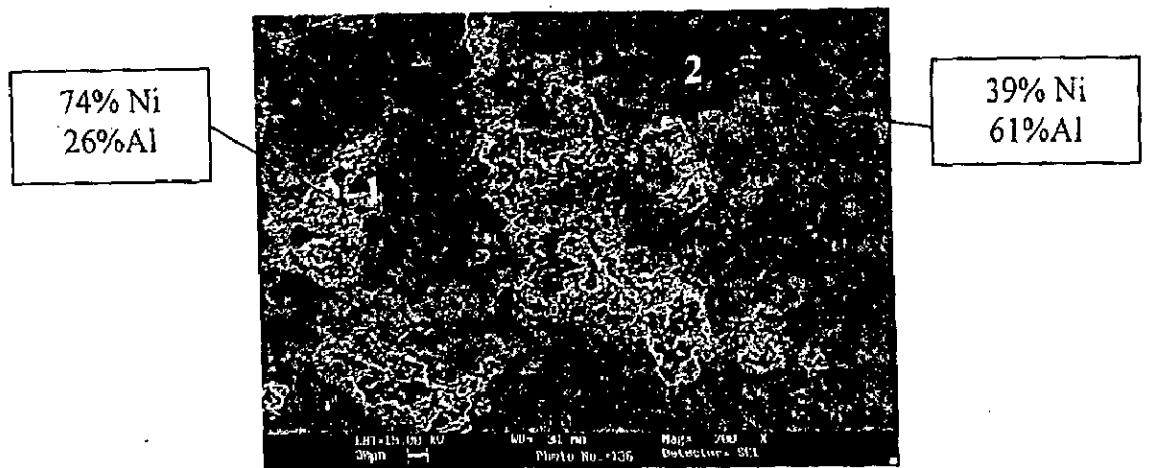


(a)

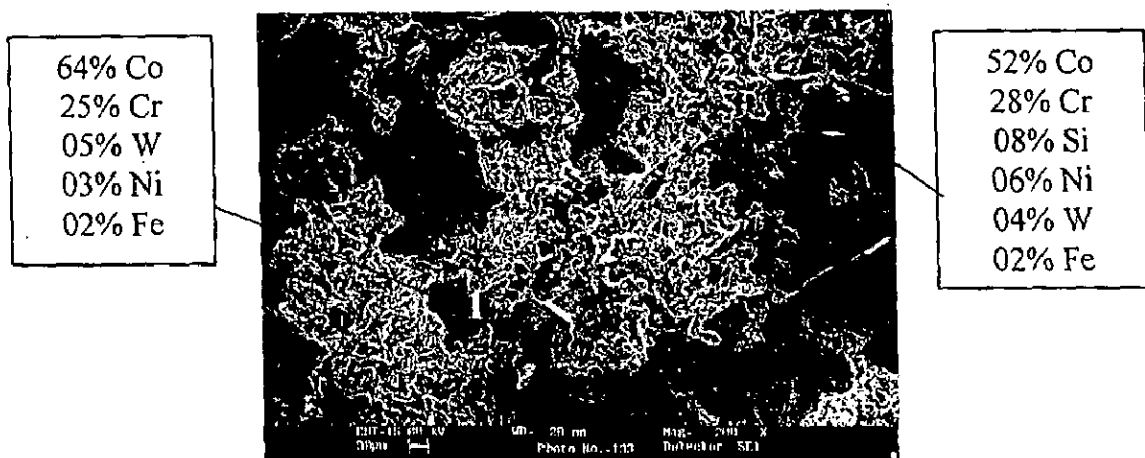


(b)

**Fig. 4.21** SEM/EDAX analysis of the plasma sprayed coatings showing elemental composition (%) at selected points  
 (a) NiCrAlY coating                      (b) Ni-20Cr coating.



(a)



(b)

**Fig. 4.22** SEM/EDAX analysis of the plasma sprayed coatings showing elemental composition (%) at selected points  
 (a)  $\text{Ni}_3\text{Al}$  coating                      (b) Stellite-6 coating.

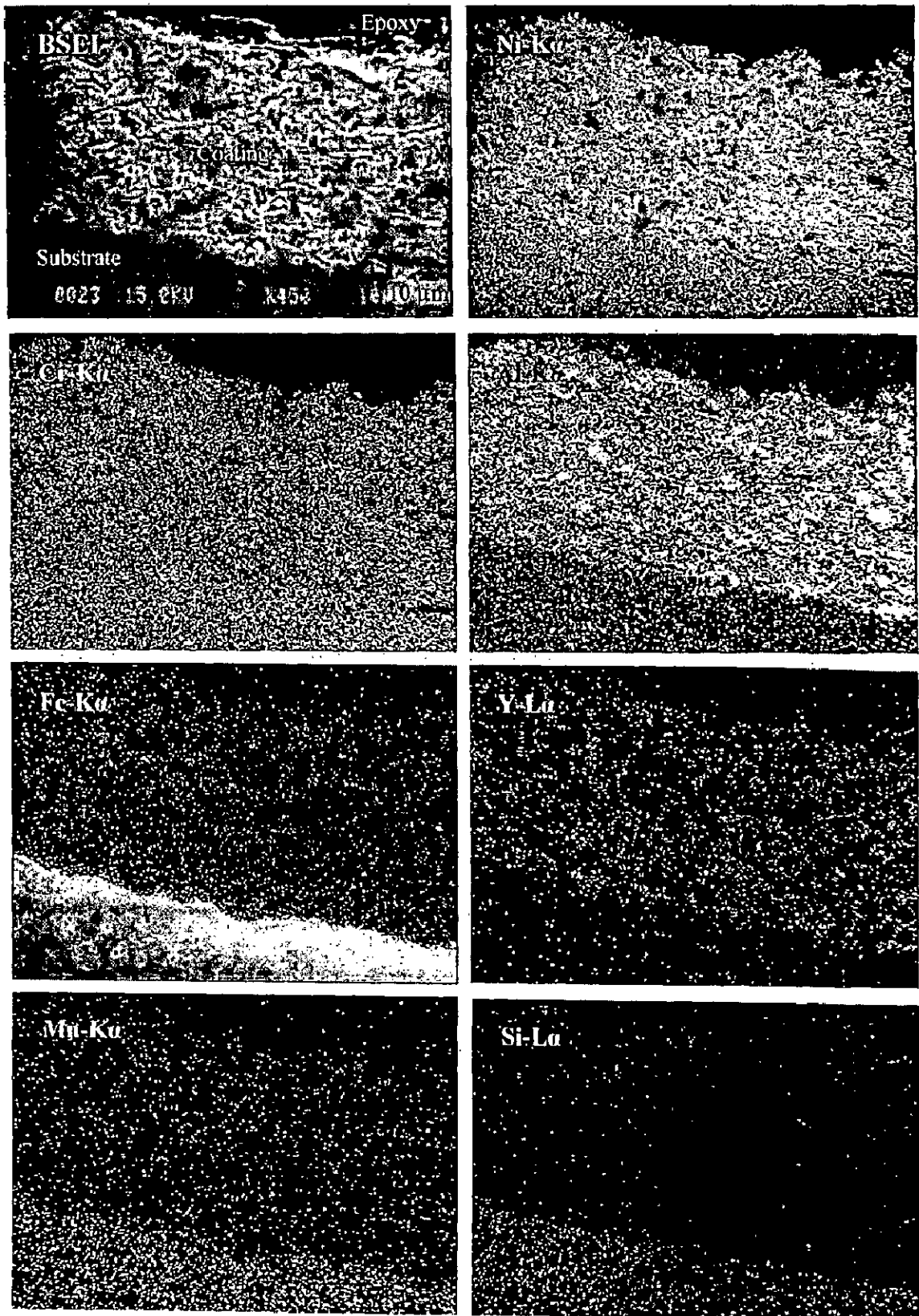


**Fig. 4.23** BSEI and X-ray mappings of the cross-section of plasma spray NiCrAlY coating on the superalloy Superni 601.

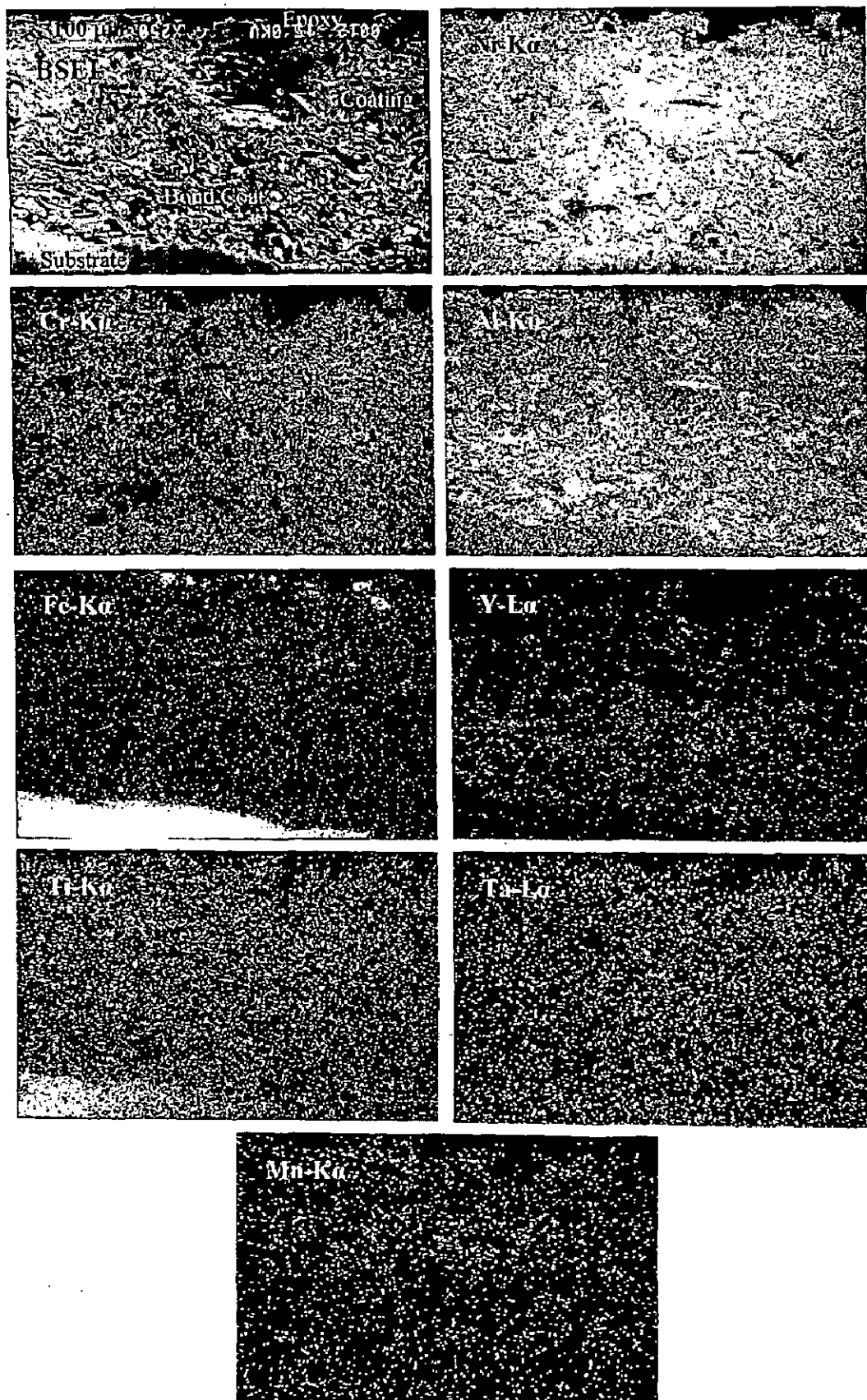


Fig. 4.24 BSEI and X-ray mappings of the cross-section of plasma spray Ni-20Cr coating with bond coat on the superalloy Superni 718.

X-ray mappings for the Ni<sub>3</sub>Al coating as depicted in Fig. 4.25 indicate that Cr has migrated from the bond coat into the Ni<sub>3</sub>Al coat and has reached even to the top surface of the coat. Chromium is generally seen around the aluminium rich areas in the top coat region. Yttrium has also diffused to the top coat in small quantities and is present alongside aluminium rich areas. Fe and Mn have also diffused from the substrate into the top coating in minor concentration and are distributed in an undefined pattern. Further, the Bond coat/substrate interface is distinct, and also clear demarcation is seen between the bond coat and the top coat.

Similar analysis for the plasma sprayed Stellite-6 coating indicates distinct layers of top coat and the bond coat as is obvious from BSEI depicted in Fig. 4.26. Aluminium seems to have diffused into the top coat from the bond coat, where it is present in the form of streaks. In the top region of Stellite-6 coat, there are areas rich in Cr and Co, and are containing some amount of Fe and Ni, and in the regions, where all these elements are absent, Al and Si are seen. Y has diffused from the bond coat to the top coat to a minor extent. Ti and W have shown some diffusion into the bond coat. Ti and Ta have also migrated slightly from the substrate to top as well as bond coat and Ta seems to be co-existing with W. Further, Fe is present at places where W and Ta are absent.

## 4.11 DISCUSSION

Microstructural studies have revealed that the matrix for all the superalloys under study is a solid solution. For the Ni-base superalloys Superni 75 and 718 the matrix is believed to be  $\gamma$ -Ni solid solution, whereas in case of Superni 600 and 601, it is Ni-Cr-Fe solid solution. The conclusions have been made after comparison of the microstructures of the superalloys under study with those of similar international Standard superalloys. The microstructures of the Standard superalloys are taken from Metals Handbook (1972) and ASM Handbook (1995). The formation of carbides has been revealed invariably in all the cases, which could again be characterised with reference to the data available in the said handbooks. Basically strength of the Ni-base superalloys depends on the mechanism of solid solution hardening and precipitation hardening, singly and in combination. The main carbides which have the possibility of their formation by precipitation in the superalloys under study are MC, M<sub>7</sub>C<sub>3</sub> and M<sub>23</sub>C<sub>6</sub>, keeping in view the role of various alloying elements towards formation of particular carbide. Among them, M<sub>23</sub>C<sub>6</sub> has the strongest possibility of formation in all the cases under study, as it is

mainly promoted by Cr (ASM Handbook, 1995). Further,  $M_{23}C_6$  carbide has tendency to precipitate at the grain boundaries. The possible carbides in case of Fe-based superalloy Superfer 800H are  $M_{23}C_6$  and MC. Some large globules as could be seen in Fig. 4.1 (e) might be indicating the presence of MC (TiC) phase.

The plasma spray coatings were obtained at Anod Plasma Ltd. Kanpur (India) using a 40 kW Miller Thermal Plasma Spray apparatus. It was aimed to produce thicker coatings because thicker coatings are generally required for the components of energy generation systems. But self-disintegration of thicker coatings usually restricts the thickness of the coatings (Sidhu et al, 2004). In the present study it was possible to obtain a thickness in range of 200-250  $\mu\text{m}$  for the NiCrAlY, Ni-20Cr and  $\text{Ni}_3\text{Al}$  coatings, whereas somewhat thicker coatings around 350-450  $\mu\text{m}$  could be deposited in case of the Stellite-6. Finally coating thickness of approximately 150  $\mu\text{m}$  for the bond coat and  $\sim 200$   $\mu\text{m}$  for the top coat was selected as threshold limit. After spraying the coating thickness was measured along the cross-section for some randomly selected samples as has been reported in Table 4.2.

The porosity measurements for the plasma sprayed coatings are summarised in Table 4.2. The values of porosity (2.00-4.50%) are in close agreement with the findings of Chen et al (1993), Erickson et al (1998), Hidalgo et al (1998 and 1999), Singh (2003) and Sidhu et al (2004 and 2005), and are reported by the author in his earlier publication (Singh et al, 2005A). Hardness is the most frequently quoted mechanical property of the coatings (Tucker, 1994). The observed microhardness values for the coatings have been compared with those reported by Chen et al (1993), Hsu & Wu (1997), Gu et al (1997), Staia et al (2001), Liang et al (2000), Hidalgo et al (2000), Rinaldi et al (2001), Rosso et al (2001) and Sampath et al (2004), and are found to be in similar range. Moreover, Tucker (1994) has published extensive data on properties of plasma coatings and the values of porosity and microhardness data have been found to be similar to those reported by him. Two very interesting observations could be made after critical examination of the microhardness profiles. Firstly a slight increase in the microhardness values for the substrate superalloys has been observed near the interface between the bond coat and the substrate in all the cases (refer points at a distance of  $-40\mu\text{m}$ ). Secondly it could be seen that the coatings in general, deposited on the superalloy Superni 718 have shown comparatively lower values of microhardness in all the cases. The hardening of the substrates as observed in the current study might have occurred due to the high speed impact of the coating particles during plasma spray deposition. The effect has also been reported by Singh (2003), Hidalgo et al (2000) and Sidhu et al (2004 and 2005).



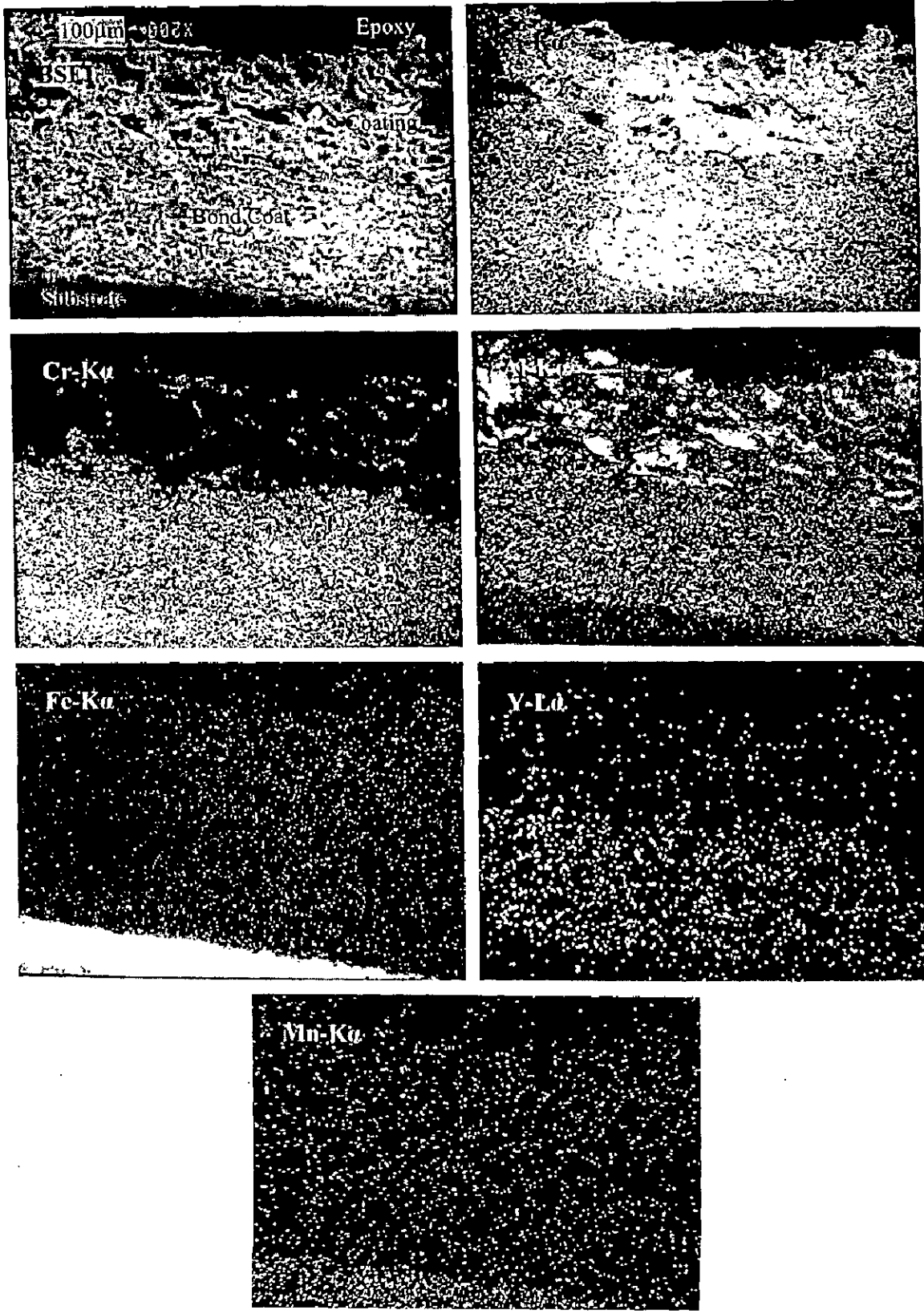


Fig. 4.25 BSEI and X-ray mappings of the cross-section of plasma spray Ni<sub>3</sub>Al coating with bond coat on the superalloy Superni 601.

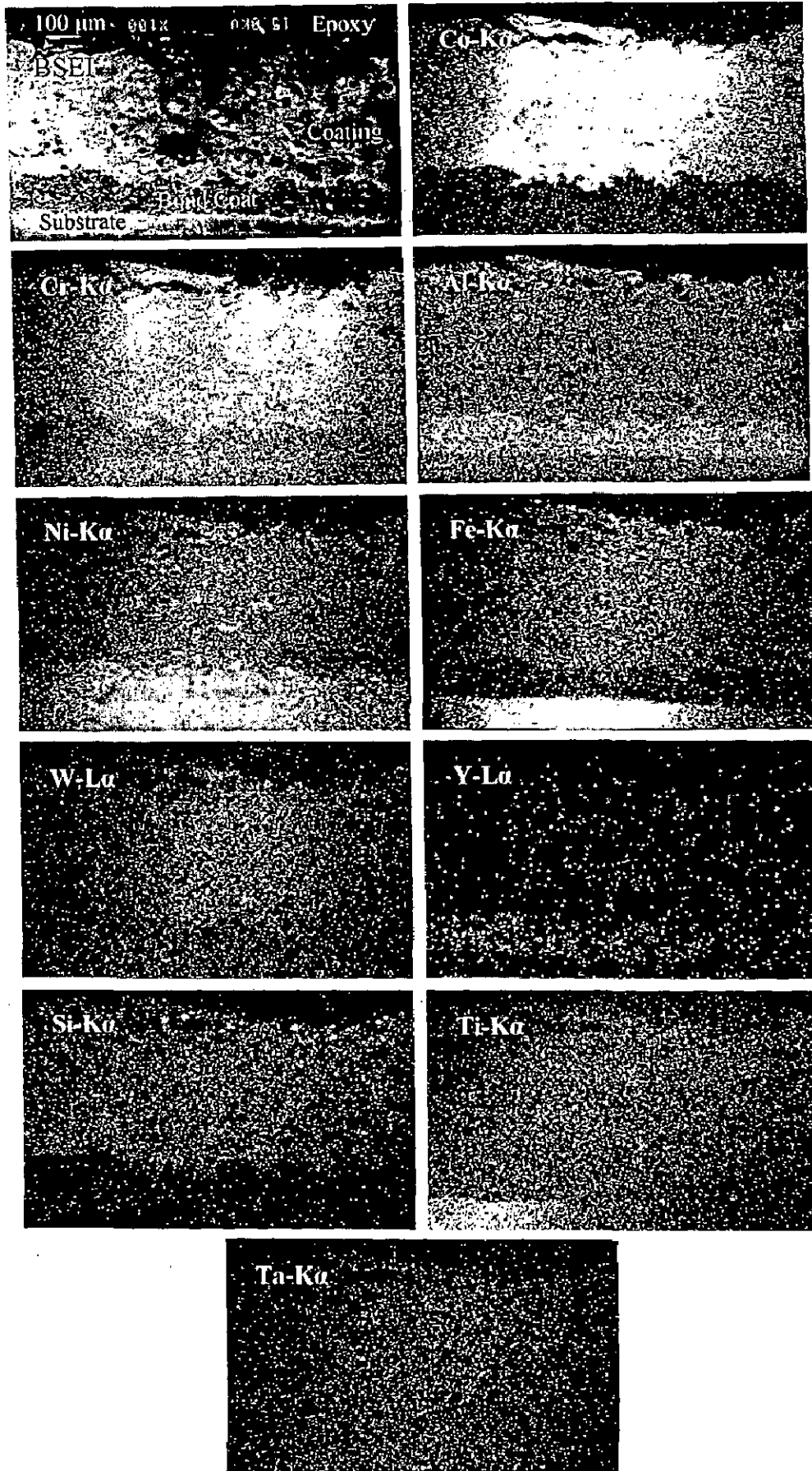


Fig. 4.26 BSEI and X-ray mappings of the cross-section of plasma spray Stellite-6 coating with bond coat on the superalloy Superni 718.

The observed non-uniformity in the hardness values along the thickness of the coatings may be due to the microstructural changes along the cross section of the coatings (Staia et al, 2001). Moreover, the microhardness and other properties of the thermal spray coatings are anisotropic because of their typical splat structure and directional solidification (Tucker, 1994).

Sampath et al (2004) have reported that the deposit microstructures are a direct result of splat morphologies. Microstructures similar to those of present study i.e. lamellar structures with voids and oxide inclusions have also been reported by Vuoristo et al (1994), Bluni and Mardar (1996), Hsu and Wu (1997), Erickson et al (1998), Westergard et al (1998), Ilavsky et al (2000), Rosso et al (2001), Margadant et al (2001), Choi et al (2002), Singh (2003), Sampath et al (2004) and Sidhu et al (2004 and 2005). Wigren and Tang (2001) have also reported that the microstructure of a thermally sprayed coating typically consists of a multiphase matrix (often a mix between hard, soft and amorphous), pores, oxides, delaminations, crack, grit residues and unmelted particles. Further, according to Bluni and Mardar (1996) the oxides may form due to the in-flight oxidation during spraying process and/or preexisting in the feed material. The latter reason for the oxides formation in the structure of coatings under study looks to be more relevant as the chances of in-flight oxidation are meager in case of the shrouded plasma spraying. Further some localized areas having higher densities of open pores and unmelted particles as seen in the micrographs of almost all the coatings have been termed as improperly flattened zone by Choi et al (2002). They opined that such zones are very different from the other lamellar structures, and their formation seems to be connected with both the presence of the partially melted particles and the splashing phenomenon of spreading particles. Splashing occurs not by flowing on the surface but by jetting away from the impinged droplet center to the periphery.

Sampath et al (2004) were of the view that the air plasma spraying and twin-wire arc spraying techniques show pre-ponderance of porosity and interlamellar separations. The distinctive boundaries in the cross-sectional microstructure of the coatings due to different passes of the spray gun have also been observed by Zhang et al (1997) and Sundararajan et al (2003A and 2003B). Zhang et al (1997) further suggested that the distinctive boundaries could be identified as a less dense structure between the passes than within individual passes, owing to the flattened splats having got cooled and solidified before the next pass started. Sampath et al (2004) explained the formation of splats in case of air plasma sprayed coating of Ni-5 wt% Al bond coat. They observed that the core of the splats is predominantly nickel, whereas the aluminium, because of its tendency to oxidise is concentrated towards the outer

surface of the splats i.e. splat boundaries. In the present investigation, EDAX analysis of Ni<sub>3</sub>Al coating, Fig. 4.22 (a) at point 2 showing high percentage of Al (61%) might be indicative of the same phenomena.

The presence of  $\gamma$ -Ni and  $\gamma'$ -Ni<sub>3</sub>Al as main phases in NiCrAlY coatings has also been reported by Singh (2003) and Sidhu et al (2004) for shrouded plasma sprayed NiCrAlY coatings, and Wang et al (2001) and Wang et al (2003) for arc ion plated NiCrAlY coatings. Whereas Choi et al (2002) have identified only  $\gamma$ -Ni phase by XRD in air plasma sprayed Amdry 962. From these phases, it can be inferred that the structure of the NiCrAlY coating consists mainly of  $\gamma$  (nickel solid solution) and  $\gamma'$  (Ni<sub>3</sub>Al). Wu, Y. et al (2001) have also reported the similar structure of plasma sprayed NiCrAlY coatings. The  $\gamma$ -Ni phase shown by XRD of as sprayed Ni-20Cr coating might be indication of formation of nickel solid solution matrix in the coating. SEM/EDAX of the Ni-20Cr coating has revealed this matrix as white phase as can be seen in Fig. 4.21(b). Similar observation has been made by Sundararajan et al (2003A) for air plasma sprayed Ni-20Cr coating where they have indexed XRD pattern for the coating to mainly Ni solid solution  $\gamma$  (fcc) phase.

In case of Ni<sub>3</sub>Al coating, the formation of Ni<sub>3</sub>Al as a main phase has been confirmed by XRD. EDAX analysis of this coating has also shown the presence of Ni and Al. The similar XRD peaks have also been reported by Singh (2003), Sidhu & Prakash (2003), La et al (1999) and Liu and Gao (2001). Further the method of preparation of Ni<sub>3</sub>Al powder for the present study had also been used by Singh (2003), Sidhu & Prakash (2003), Sidhu et al (2004) and La et al (1999). Srinivas et al (2004) have also reported the method of mechanical alloying by a ball mill to formulate Al-Cu-Fe powder. In case of the Stellite-6 coating, the presence of  $\gamma$ -Co (f.c.c.) and M<sub>23</sub>C<sub>6</sub> (Cr<sub>23</sub>C<sub>6</sub>) phases in the St-6 coating indicates the formation of solid solution with  $\gamma$ -Co matrix. These two phases have also been identified by Osma et al (1996) for as-cast Stellite-6. They had also shown similar structure of the St-6 with white dendritic and black interdendritic regions. They further suggested that the spongy appearance of the dendritic regions is a result of ( $\gamma$ -f.c.c) Co solid solution and uniformly distributed intermetallic phase particles.

So far as the interdiffusion of various elements between the substrate and plasma sprayed coatings is concerned, it has been observed from the EPMA (Fig. 4.23 through 4.26) that the diffusion is marginal. While speaking in relative terms, the diffusion between bond coat and top coat is observed to be high as compared to that between bond

coat and the base alloys. Aluminium is found to be the most vulnerable element to the diffusion phenomenon. Cr, Ti, Ta, Fe and Mn are some other elements which are prone to minor diffusion. Mazar et al (1986) have also reported limited interdiffusion in the Ni-Cr-Al-Y/Ni-based, Ni-Cr-Al-Y/Fe-based and Co-Cr-Al-Y/Fe-based systems during studies on the diffusion degradation of these systems. Wu, X. et al (2001) have also observed no obvious diffusion from the coating into the substrate and attributed this to the fact that the interacting process between the molten spraying particles and substrate materials lasted for only a few tenths of a second. Further Nicholls (2000) has opined that diffusion of elements between the substrate and coating can have a major influence on coating performance. Therefore to provide long-term stability at elevated temperatures, it is necessary to develop diffusion-barrier coatings to minimize the interdiffusion between the coating and the substrate. However, he further added that some interdiffusion is necessary to give good adhesion; hence, the diffusion barriers must be tailored to limit the movements of particular problematic elements. Interdiffusion observed in the present study is very minor and might be helpful for providing better adhesion between the substrate, bond coat and the top coat.

# CHAPTER 5

## OXIDATION STUDIES IN AIR

---

Oxidation behaviour of the plasma spray coated as well as uncoated superalloys in air has been described in this chapter. Cyclic oxidation was performed at an elevated temperature of 900°C in air for 50 cycles. The specimens were visually examined at the end of each cycle during the course of study. Efforts have been made to understand the mode of oxidation.

The oxidation products were analysed with XRD, SEM/EDAX and EPMA. The results have been compiled to provide the performance of a particular coating in different sections of the chapter. The thermogravimetric data for each coated superalloy has been plotted alongwith uncoated superalloy in order to present the comparison. The parabolic rate constants and scale thicknesses have been evaluated.

### 5.1 RESULTS

#### 5.1.1 Uncoated Superalloys

##### 5.1.1.1 Visual Examination

Colour of oxide scale formed on the Ni-base superalloys Superni 75, 600, 601 and 718 after air oxidation for 50 cycles at 900°C was dark grey, in general, with some brownish spots. Whereas the scale for oxidised Superfer 800H showed increasing dominance of the brownish spots on the dark grey background with the progress of the study. In case of Superni 75 and 718, greenish tinges were also observed in the scales in the early cycles of study. Few white spots could also be seen on the scales of Superni 75 and Superni 601 from 22<sup>nd</sup> cycle onwards, which vanished towards the end of cycles. Lustrous scales were formed in all the cases upto the mid cycles of study, which eventually went on becoming dull with increasing number of cycles. The scales of the Superni 75, 600, 601 and Superfer 800H showed no spalling and remained intact with the substrates. Whereas in the scale of Superni 718, a very small pit was observed at the end of 7<sup>th</sup> cycle, which showed virtually no growth afterwards. The Macrographs of the oxidized superalloys have been shown in Fig. 5.1, which indicate continuous scales without any cracks.

### 5.1.1.2 Thermogravimetric Data

Weight change ( $\text{mg}/\text{cm}^2$ ) versus number of cycles plots for the superalloys Superni 75, 600, 601, 718 and Superfer 800H oxidised at  $900^\circ\text{C}$  in air upto 50 cycles have been shown in Fig. 5.2. From the plots it can be easily inferred that oxidation rate for the Superni 75 superalloy can be divided into two stages, one being transient oxidation stage and the other is the steady state oxidation stage. During the transient stage (upto first 4 cycles) weight gain has been rapid, whereas during the steady state the weight gain has nearly become constant. In case of all the other oxidised superalloys viz. Superni 600, 601, 718 and Superfer 800H, initial rapid oxidation rate has not been observed and weight gains have shown tendency to reach to steady state with the progress of exposure time, in spite of the fact that some minor deviations are observed. The total weight gain at the end of 50 cycles for the superalloys Superni 75, 600, 601, 718 and Superfer 800H is 3.50, 0.20, 1.73, 2.04 and 1.38  $\text{mg}/\text{cm}^2$  respectively. This shows that the weight gain in case of oxidised Superni 600 is lowest, whereas it is highest in case of Superni 75. In Fig. 5.3, the (weight gain/unit area)<sup>2</sup> versus number of cycles for all the superalloys are plotted to determine the conformance with the parabolic rate law. Although some scatter in the data can be observed in the plots, but it is apparent that these data can be approximated by a parabolic relationship. If the scatter in the measurements is not considered, the values of parabolic rate constant ( $K_p$ ) for the superalloys Superni 600, 601, 718 and Superfer 800H are calculated as 6.11, 16.19, 17.38 and  $8.87 \times 10^{-12} \text{ g}^2 \text{ cm}^{-4} \text{ s}^{-1}$  respectively. Further the value of  $K_p$  as evaluated for Superni 75 shows a transition from  $1.60 \times 10^{-10} \text{ g}^2 \text{ cm}^{-4} \text{ s}^{-1}$  to  $2.17 \times 10^{-12} \text{ g}^2 \text{ cm}^{-4} \text{ s}^{-1}$  after 16<sup>th</sup> cycle.

### 5.1.1.3 Scale Thickness Measurement

The oxide scale thickness for the oxidised specimens was measured from their respective SEM back scattered images as shown in Fig. 5.4 and Fig. 5.9. The average values are 88, 11, 52, 58 and 28  $\mu\text{m}$  respectively for Superni 75, 600, 601, 718 and Superfer 800H. Therefore it can be seen that the scale formed in case of Superni 75 is thickest, whereas it is thinnest in case of Superni 600. The values are almost equal for Superni 601 and 718.

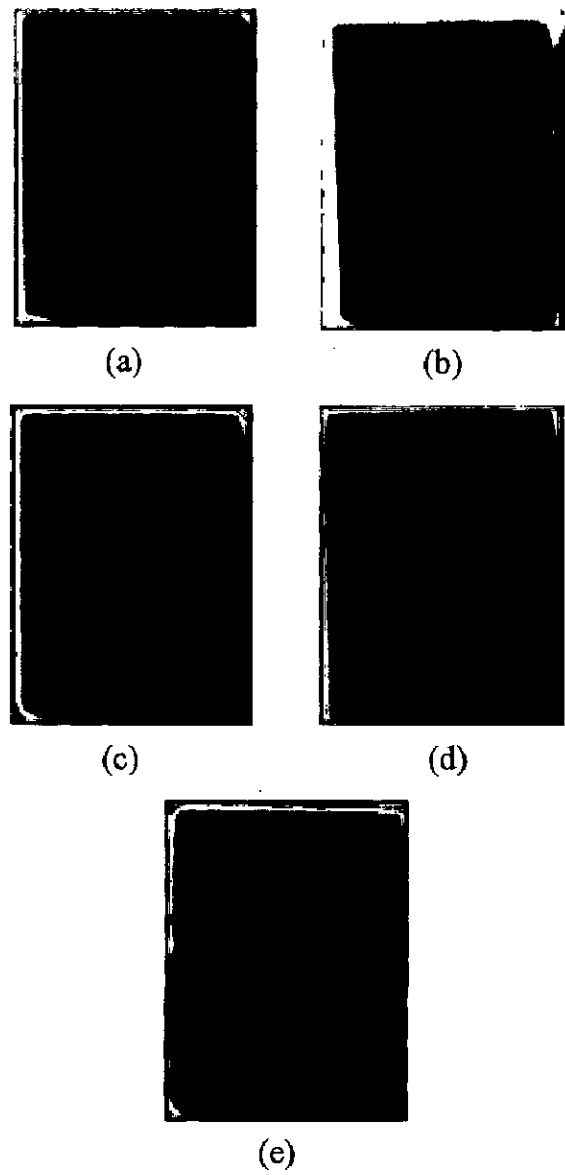


**Fig. 5.1** Macrographs of the uncoated superalloys subjected to cyclic oxidation in air at 900°C for 50 cycles  
(a) Superni 75      (b) Superni 600      (c) Superni 601  
(d) Superni 718      (e) Superfer 800H.



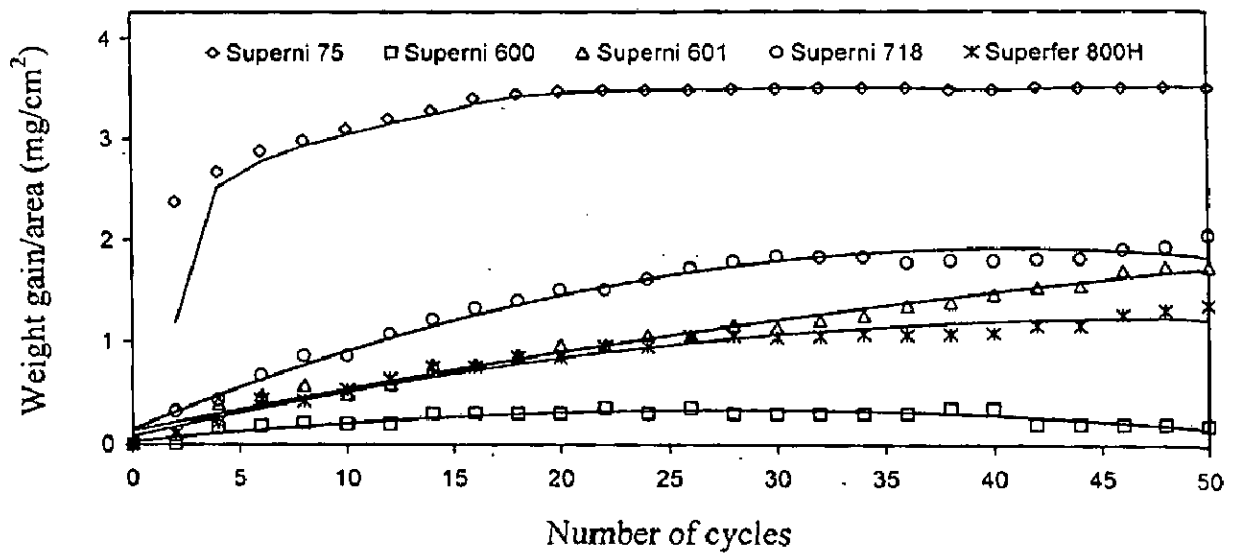


Fig. 5.2 Weight gain vs. number of cycles plot for the uncoated superalloys subjected to cyclic oxidation for 50 cycles in air at 900°C.

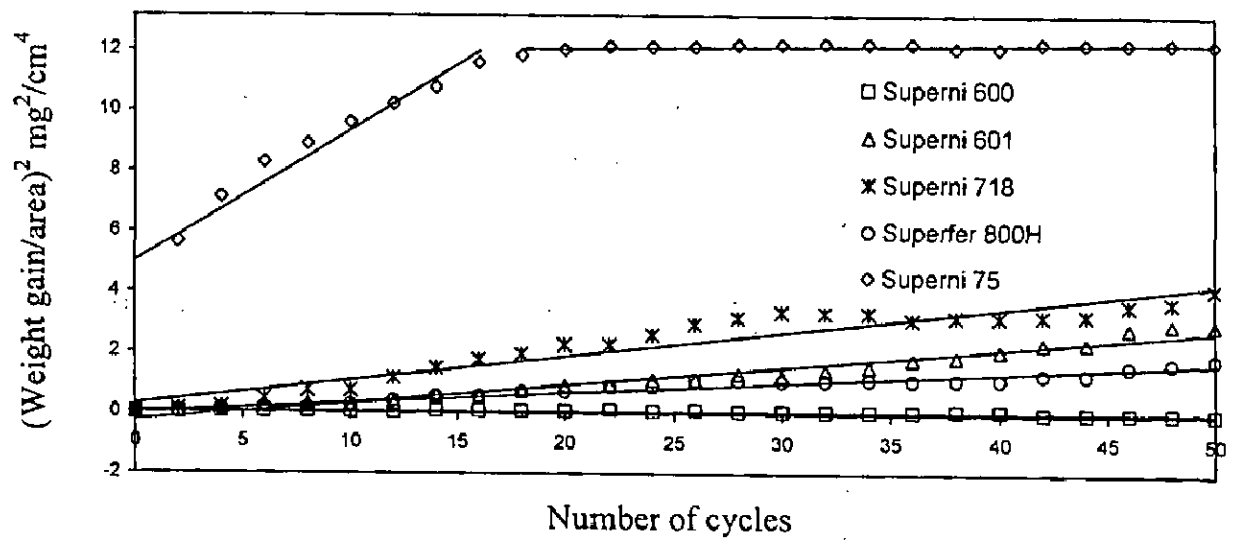
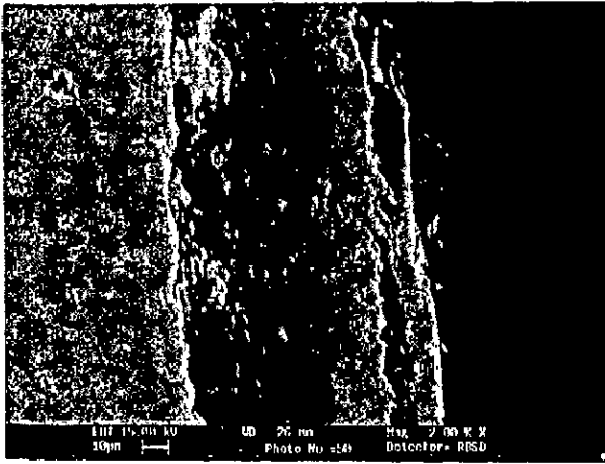
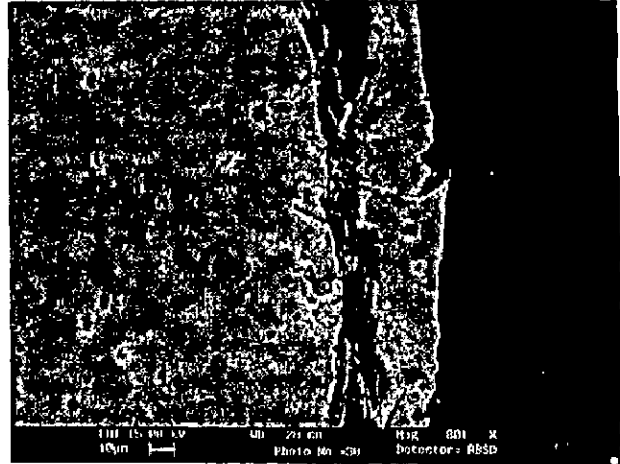


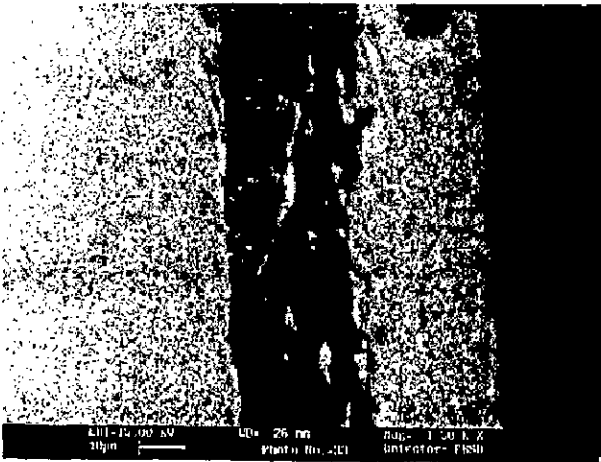
Fig. 5.3 (Weight gain/area)² vs. number of cycles plot for the uncoated superalloys subjected to cyclic oxidation for 50 cycles in air at 900°C.



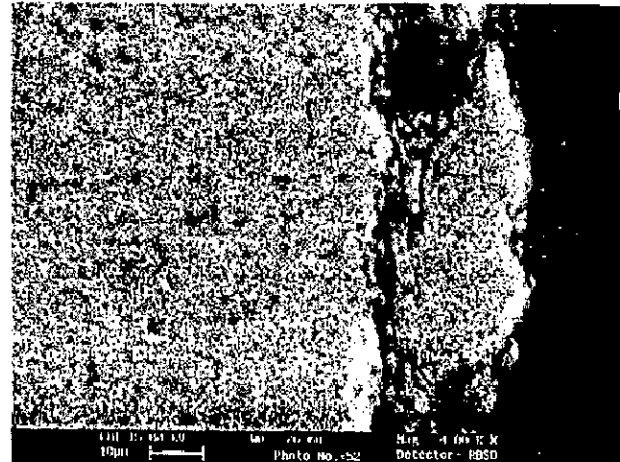
(a)



(b)



(c)



(d)

**Fig. 5.4** SEM back scattered image for the uncoated superalloys after cyclic oxidation in air at 900°C  
 (a) Superni 75 (b) Superni 601 (c) Superni 718  
 (d) Superfer 800H.

#### **5.1.1.4 X-ray Diffraction Analysis**

XRD analysis for the uncoated superalloys after exposure to air at 900°C for 50 cycles has been compiled in Figs. 5.5 and 5.6. As is clear from the diffractograms  $\text{Cr}_2\text{O}_3$  and  $\text{Fe}_2\text{O}_3$  are the phases which are found to be present in all the oxidised superalloys, except for Superni 75 case, where  $\text{Fe}_2\text{O}_3$  is absent. The formation of NiO has been indicated in the scales of Superni 75, 600, 601 and Superfer 800H, whereas  $\text{NiCr}_2\text{O}_4$  has been identified for Superni 75, 600, 718 and Superfer 800H scales.  $\text{Al}_2\text{O}_3$  is found to be present in the scale of Superni 601 and 718, whereas  $\text{NiFe}_2\text{O}_4$  is identified in the Superfer 800H scale.

#### **5.1.1.5 SEM/EDAX Analysis**

##### **(a) Surface Morphology**

SEM/EDAX micrograph of the scale formed after 50 cycles of oxidation in air at 900°C for Superni 75 superalloy indicates mainly white crystalline phase rich in NiO, irregularly dispersed in the black phase (matrix) rich in  $\text{Cr}_2\text{O}_3$ , Fig. 5.7 (a). While SEM micrograph of top surface of the scale in case of Superni 600 superalloy indicates intergranular cracks, which mainly contain  $\text{Cr}_2\text{O}_3$  and NiO, point 1 in Fig. 5.7 (b). Fine globules could mainly be seen dispersed in the black matrix, alongwith the presence of some coarse globules ( $\text{Cr}_2\text{O}_3$ -rich). The matrix is mainly rich in NiO (59%) as indicated by EDAX analysis at point 2. The morphology of scale for the oxidised Superni 601, Fig. 5.7 (c) is similar to that for Superni 75, with  $\text{Cr}_2\text{O}_3$  rich matrix containing a significant amount of MnO (15%), refer point 1. The matrix of the scale of Superni 718 has dominance of  $\text{TiO}_2$  and  $\text{Cr}_2\text{O}_3$  as evident from Fig. 5.8 (a), with relatively large size irregular shaped granules ( $\text{Cr}_2\text{O}_3$ -rich). Whereas the Fig. 5.8 (b) shows globular phase uniformly dispersed in the  $\text{Cr}_2\text{O}_3$ -rich matrix for the oxidised Superfer 800H. The globules are rich in  $\text{Fe}_2\text{O}_3$  as indicated by EDAX analysis at point 2.

##### **(b) Cross-Sectional Analysis**

Oxide scale morphology alongwith variation of elemental composition across the cross-section of superalloy Superni 600 subjected to cyclic oxidation in air at 900°C after 50 cycles has been depicted in Fig. 5.9. The scale is dense and nearly uniform in thickness. The plots show that the scale is consisting of nickel, chromium and iron

alongwith oxygen. The concentration of oxygen is found to increase towards the outer side of the oxide layer. The nickel content in the scale decreases as one moves away from the alloy-scale interface, whereas chromium has shown some increase in its concentration along outward direction. However, iron shows no significant variation in its concentration.

#### **5.1.1.6 EPMA Analysis**

BSEI and X-ray mappings for a part of oxide scale of Superni 75 superalloy after oxidation in air for 50 cycles at 900<sup>0</sup>C are shown in Fig. 5.10, which indicate formation of scale containing mainly chromium and titanium. Whereas BSEI and X-ray mappings for the oxidised Superni 600, Fig. 5.11 show dense but thinner scale as compared to that of Superni 75. The scale consists of two layers; the upper layer is rich in nickel and iron while the lower layer is mainly having chromium and manganese. Further, the scale of the oxidised Superni 601 superalloy is again found to be a dense scale, Fig. 5.12, which is mainly rich in nickel and chromium, alongwith some small amounts of iron and aluminium. Manganese could also be seen in the scale in lesser amounts. A silicon rich nodule is also visible in the scale.

A corresponding analysis for the Superni 718 subjected cyclic oxidation at 900<sup>0</sup>C in air, Fig. 5.13, indicates a dense scale, which is basically nickel rich band where iron and chromium are also present. The scale also contains molybdenum, titanium, aluminium and tantalum. Some islands consisting purely of aluminium, perhaps as inclusions, are seen in the scale. Presence of silicon is further revealed as irregularly dispersed phase in the inner half of the scale at places where some of the elements are found to be absent.

BSEI and X-ray mappings for the oxidised Superfer 800H show iron dominating in continuous scale, which contains substantial amounts of nickel, Fig. 5.14. Chromium and manganese have shown their co-presence in the form of two dense bands, one at the scale/substrate interface and the other at the outermost layer of the scale. Titanium has also indicated the similar tendency. Aluminium is uniformly distributed in the scale with an exception at a few sites, which show depletion of the same. Silicon is distributed as highly concentrated elongated phase in the scale at places, where all other elements are absent.

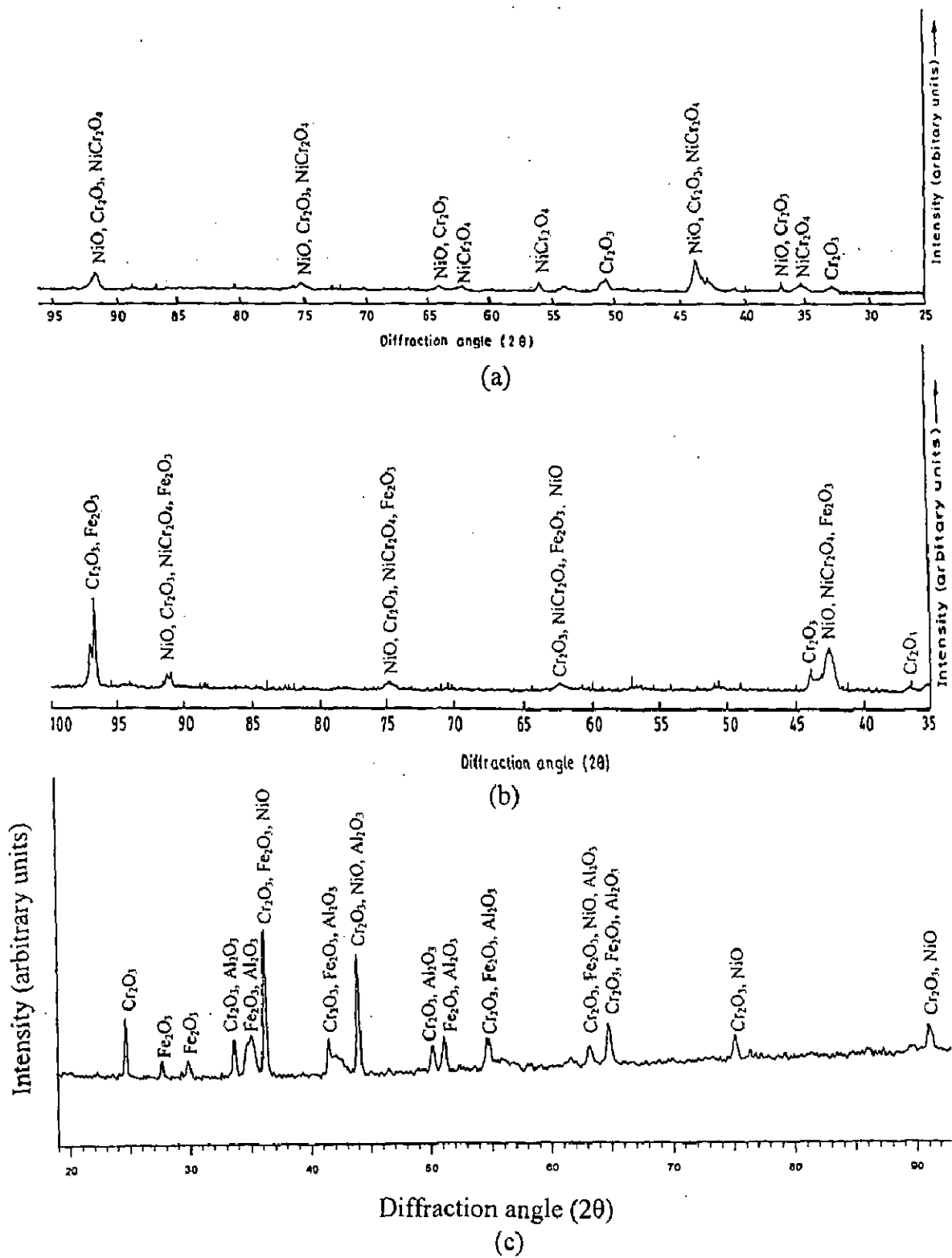
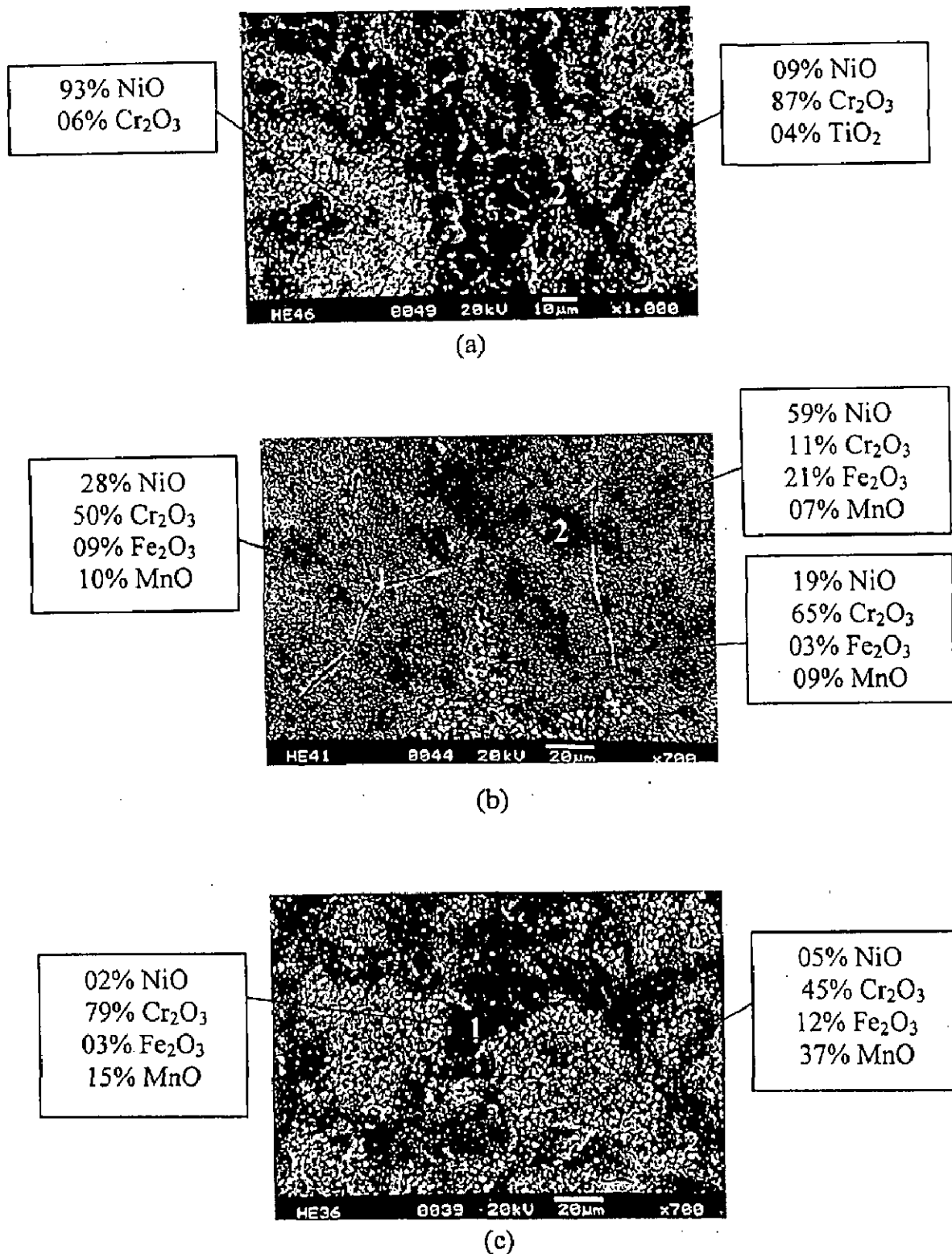
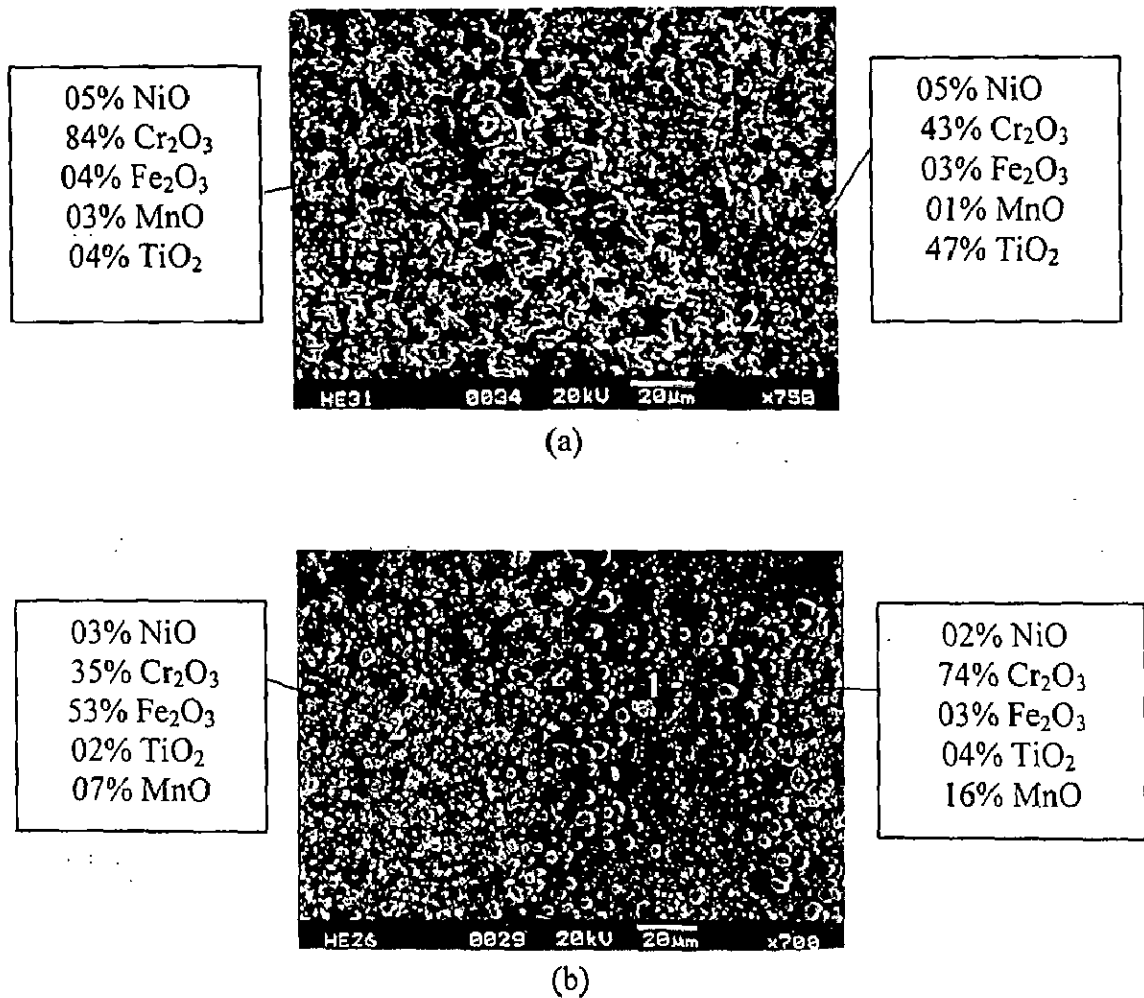


Fig. 5.5 X-ray diffraction patterns for the uncoated superalloys subjected to cyclic oxidation in air at 900°C after 50 cycles  
 (a) Superni 75 (b) Superni 600 (c) Superni 601.





**Fig. 5.7** Surface scale morphology and EDAX analysis for the uncoated superalloys subjected to cyclic oxidation in air at 900°C for 50 cycles (a) Superni 75 (b) Superni 600 (c) Superni 601.



**Fig. 5.8** Surface scale morphology and EDAX analysis for the uncoated superalloys subjected to cyclic oxidation in air at 900°C for 50 cycles  
 (a) Superni 718 (b) Superfer 800H.



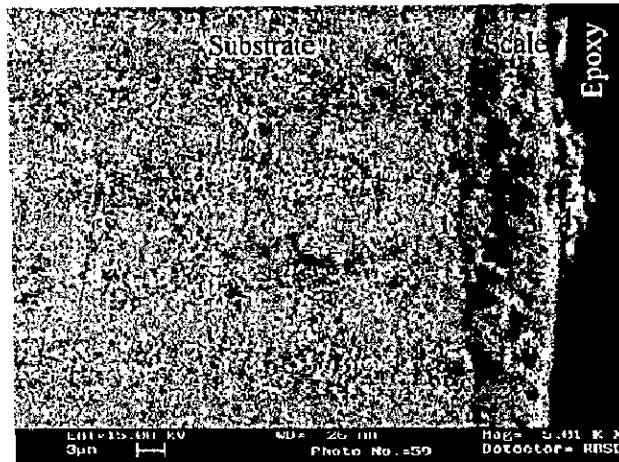
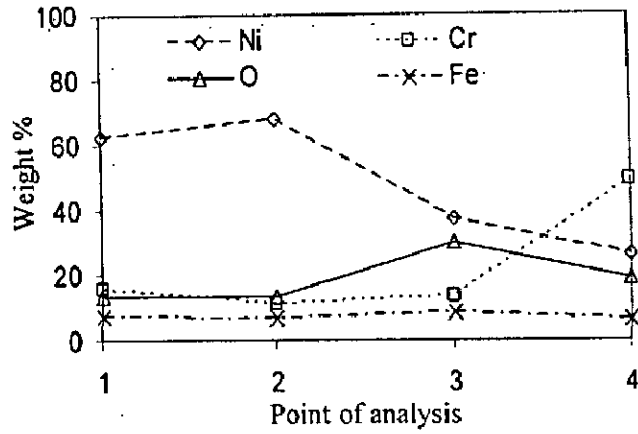


**Fig. 5.9**

Oxide scale morphology and variation of elemental composition across the cross-section of superalloy Superni 600 subjected to cyclic oxidation in air at 900°C after 50 cycles.

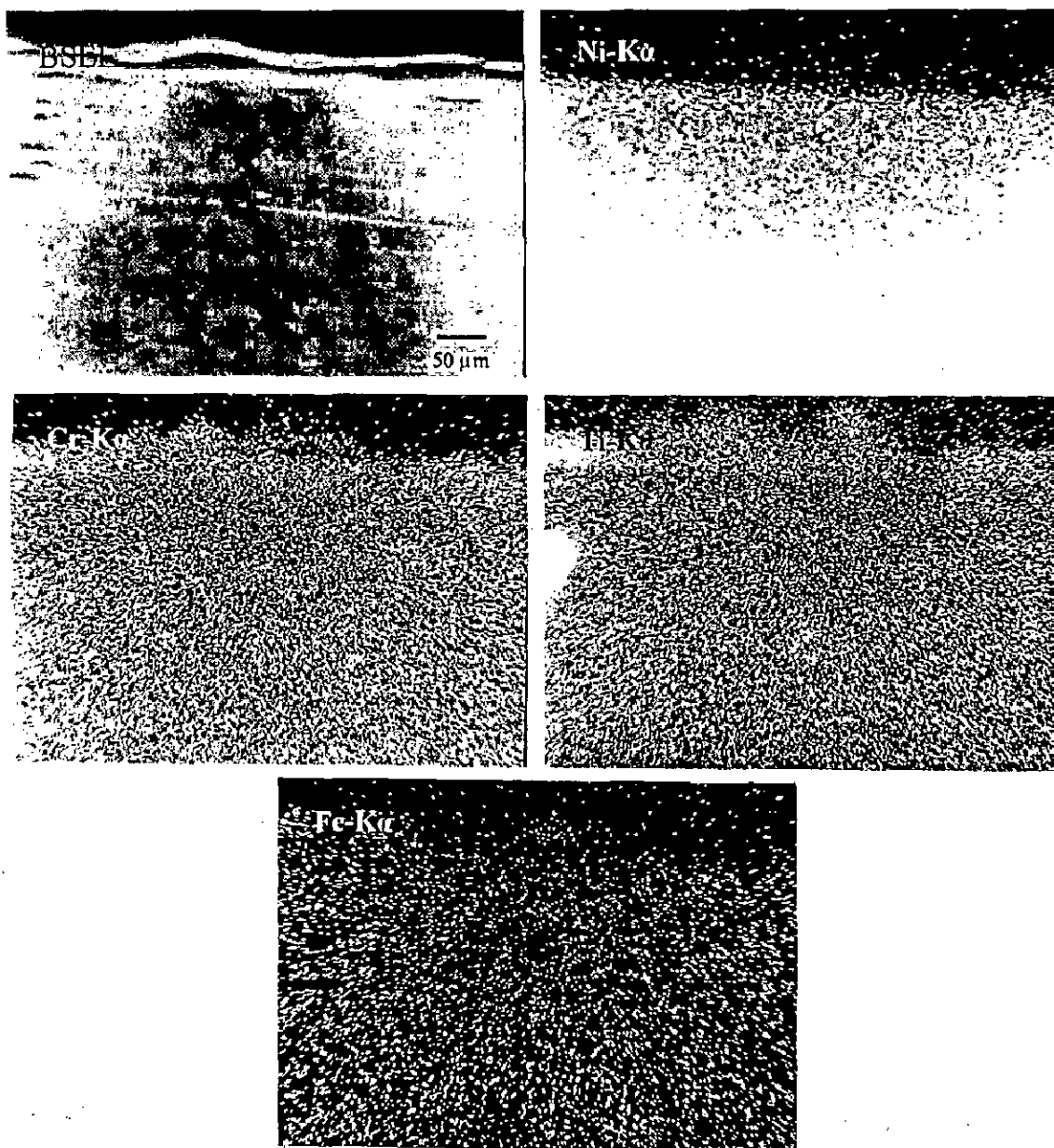


**Fig. 5.10** BSEI and X-ray mappings of the cross-section of Superni 75 subjected to cyclic oxidation at 900°C in air after 50 cycles.

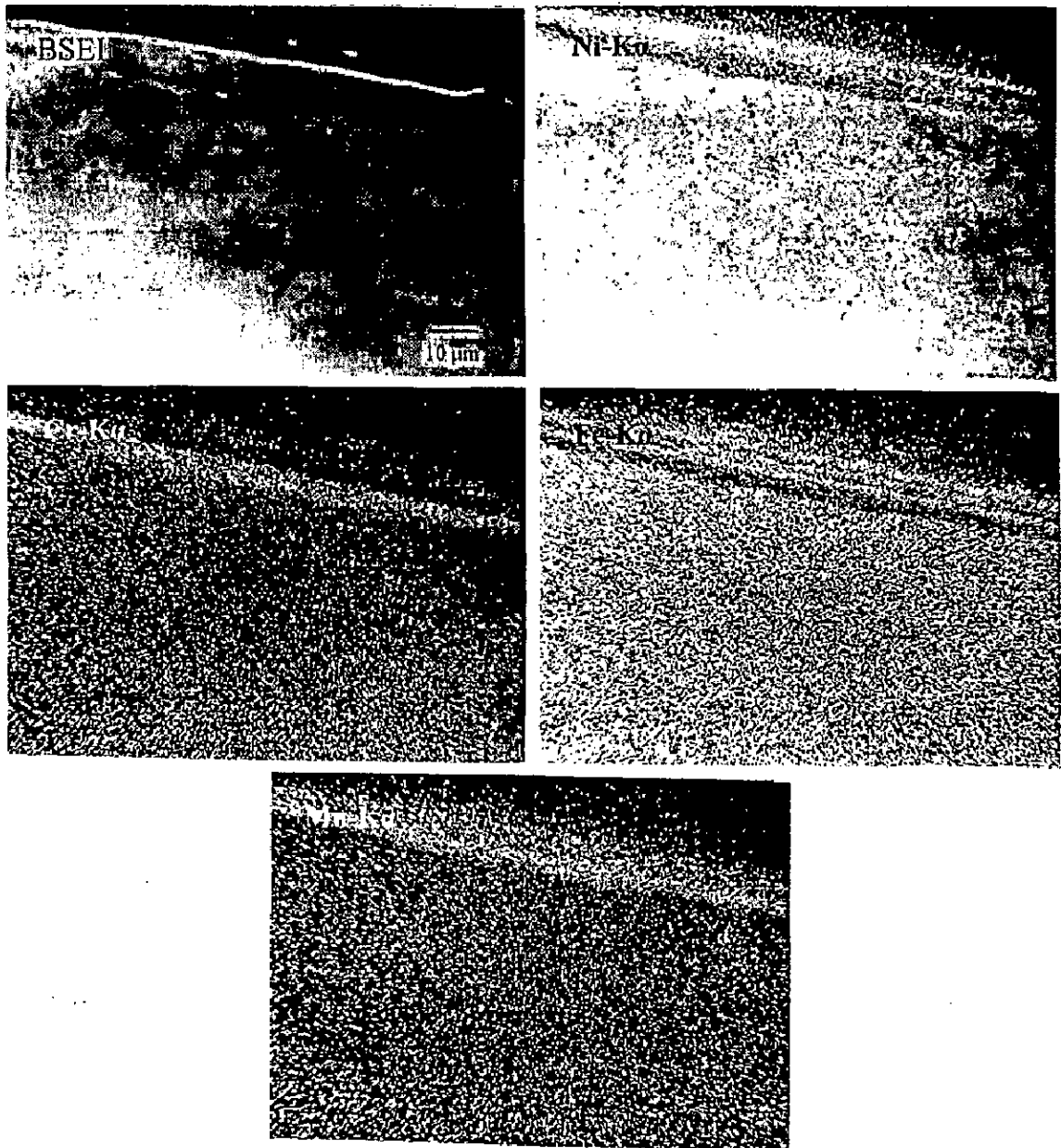


**Fig. 5.11** BSEI and X-ray mappings of the cross-section of Superni 600 subjected to cyclic oxidation at 900°C in air after 50 cycles.

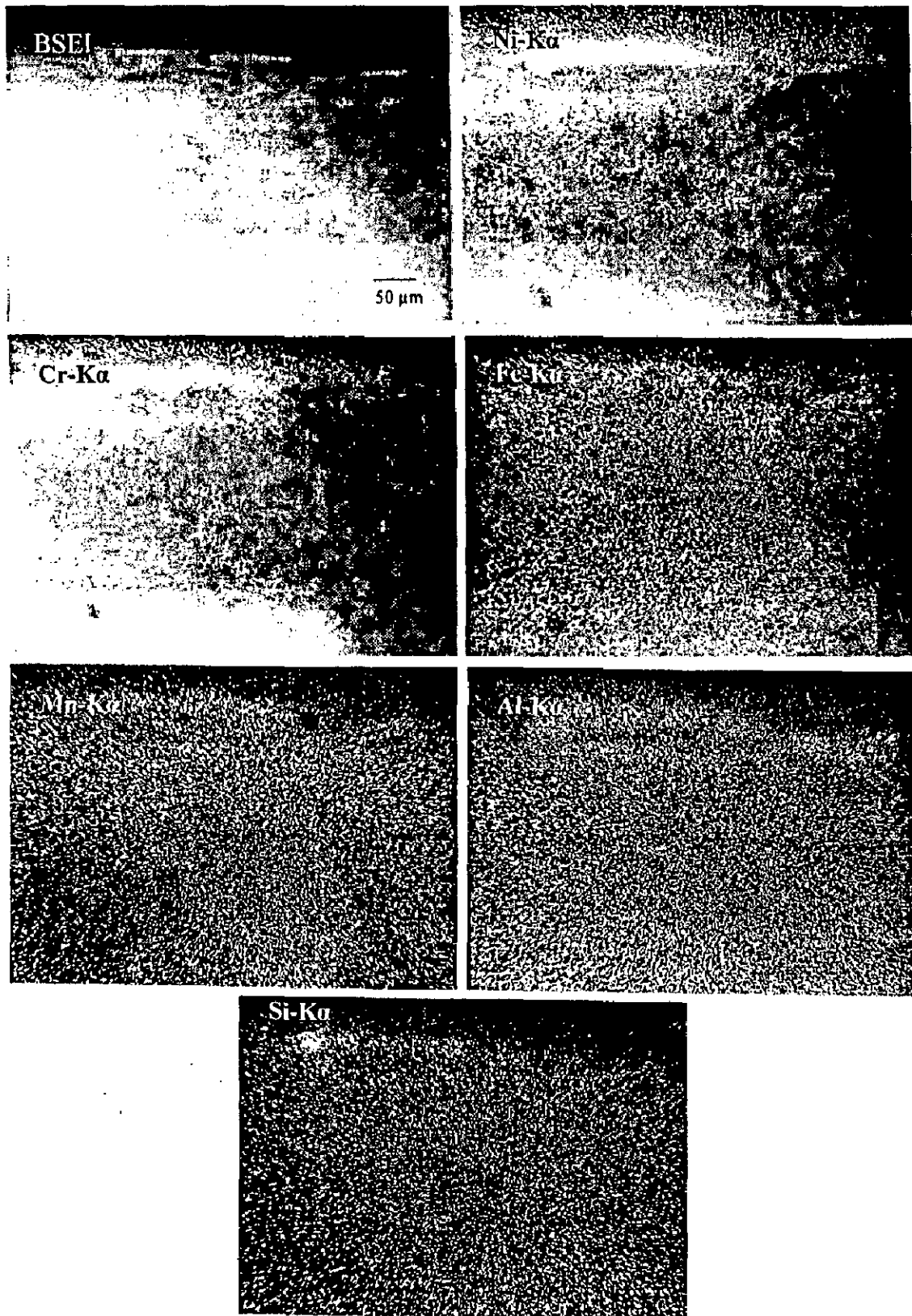


**Fig. 5.12** BSEI and X-ray mappings of the cross-section of Superni 601 subjected to cyclic oxidation at 900°C in air after 50 cycles.

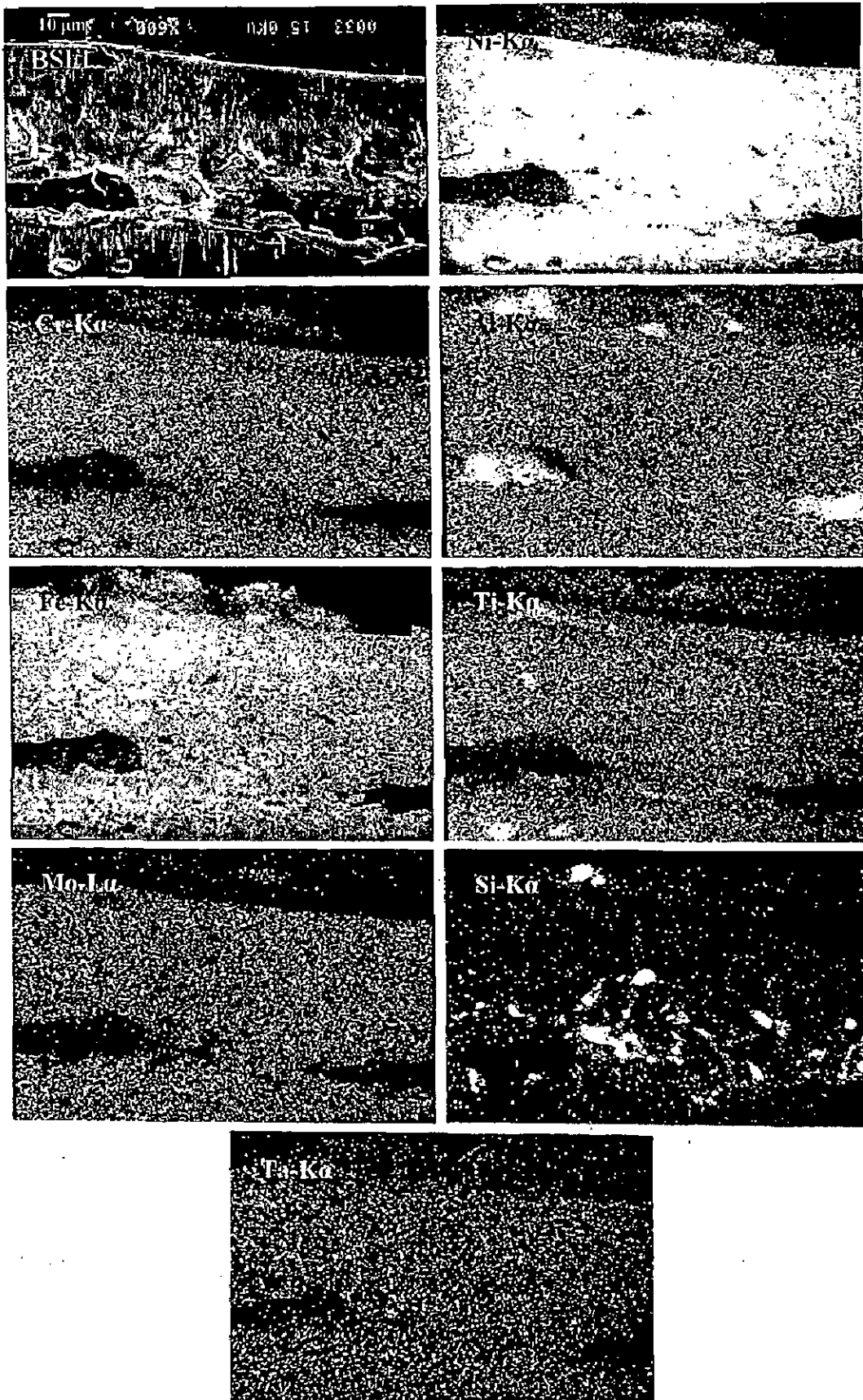


**Fig. 5.13** BSEI and X-ray mappings of the cross-section of Superni 718 subjected to cyclic oxidation at 900°C in air after 50 cycles.

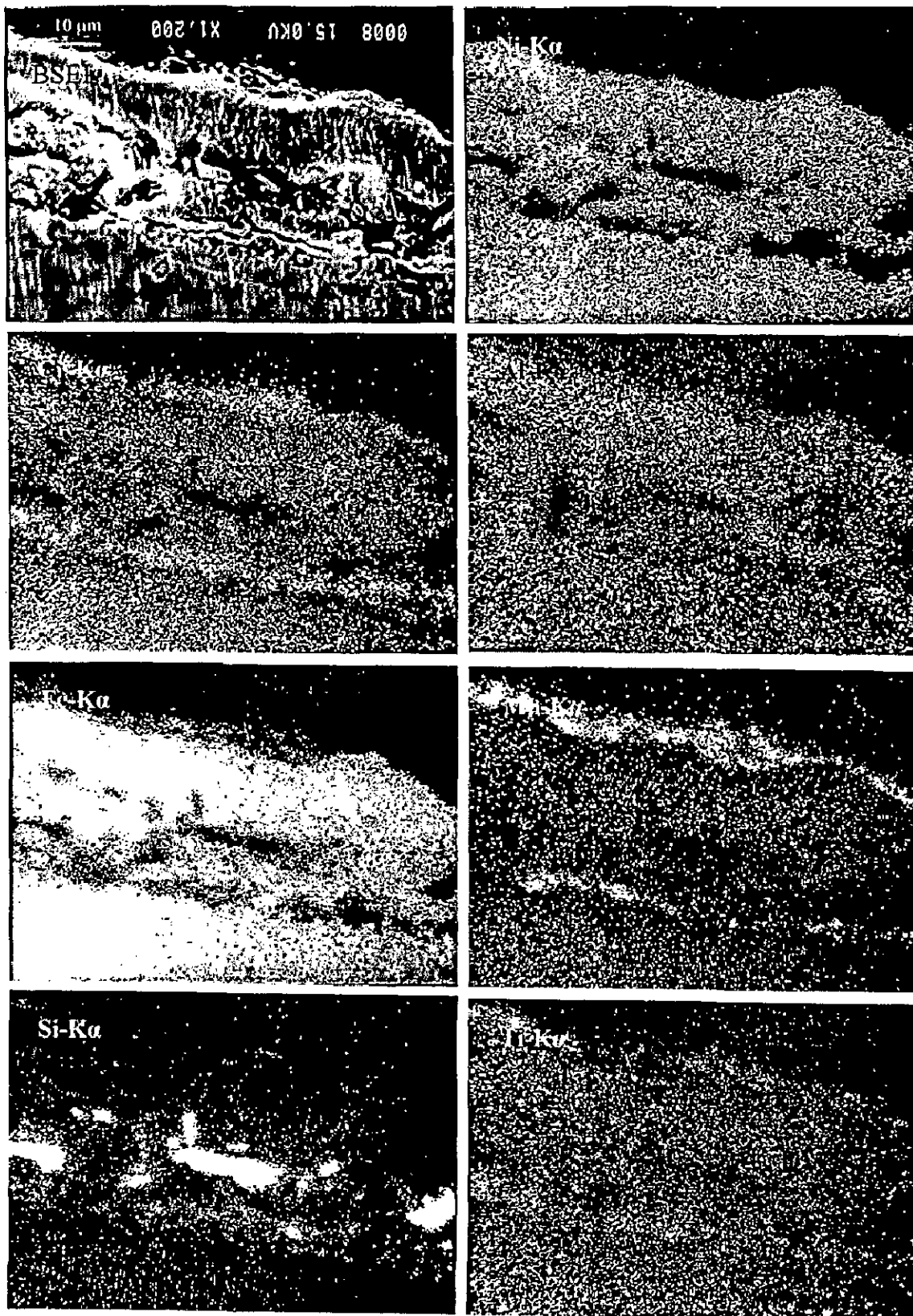


Fig. 5.14 BSEI and X-ray mappings of the cross-section of Superfer 800H subjected to cyclic oxidation at 900°C in air after 50 cycles.

## 5.1.2 NiCrAlY Coating

### 5.1.2.1 Visual Examination

All the plasma spray NiCrAlY coated superalloys have shown the formation of smooth continuous scales without the presence of cracks, when subjected to cyclic oxidation for 50 cycles at 900<sup>0</sup>C as is evident from Fig. 5.15. Colour of the oxide scales for all the coated superalloys at the end of the study was observed to be greenish grey, close to dark green. The colour of scale changed from grey with minor green tinges to greenish grey with the progress of oxidation. The scales were found to be lustrous, with no tendency for spalling. The NiCrAlY coating was found to in good contact with the superalloy substrates over the most of the surface area of the specimens, in general during the course of cyclic oxidation studies, except at some edges. The development of minor superficial cracks in the coating at or near the edges was observed after the very first cycle in all the cases. This cracking resulted in a minor spalling of coating from one or two edges in form of tiny flakes during the subsequent cycles. However this spalling was marginal. These flakes looked like as if they have come out of upper layers of the coatings. In fact this type of minor spalling of the coating from or near some of the edges of the specimens was observed in case of oxidised Ni-20Cr and Ni<sub>3</sub>Al coatings also. Moreover, the extent this minor spallation was observed to be relatively high in case of Ni-20Cr coatings.

In case of NiCrAlY coated Superni 75 and 600 superalloys this minor spalling of coating stopped from 37<sup>th</sup> and 42<sup>nd</sup> cycle respectively, whereas in the Superni 718 and Superfer 800H cases, from 20<sup>th</sup> and 21<sup>st</sup> cycle respectively. The same stopped at the end of 7<sup>th</sup> cycle in the case of Superni 601.

### 5.1.2.2 Thermogravimetric Data

The weight change data for the NiCrAlY coated superalloys cyclically oxidised for 50 cycles at 900<sup>0</sup>C in air has been compiled in Fig. 5.16. All the coated superalloys have shown relatively higher weight gain in the early cycles of study, followed by tendency to show gradual weight gain with further increase in number of cycles. The weight gain shown by the coated superalloy is found to be slightly greater than that

shown by the uncoated superalloy in general in all the cases. The values of the weight gain as measured at the end of 50 cycles are 4.39, 3.82, 4.21, 3.13 and 3.19 mg/cm<sup>2</sup> for the coated Superni 75, 600, 601, 718 and Superfer 800H respectively. To ascertain the rate law for oxidation of the coated superalloys, (weight gain/area)<sup>2</sup> versus number of cycles plots are drawn as shown in Fig. 5.17. The plots show small deviations from the parabolic rate law in all the coated cases. However these data could be approximated by a parabolic relationship. In fact, such minor deviations from parabolic rate law have been observed in all the oxidised coatings viz. NiCrAlY, Ni-20Cr, Ni<sub>3</sub>Al and Stellite-6. Ignoring this scatter in the measurements, the values of the parabolic rate constants ( $K_p$ ) for the NiCrAlY coated superalloys Superni 75, 600, 601, 718 and Superfer 800H are calculated as 4.67, 4.21, 5.87, 2.74 and  $3.81 \times 10^{-11}$  g<sup>2</sup> cm<sup>-4</sup> s<sup>-1</sup> respectively.

### **5.1.2.3 Scale Thickness Measurement**

The scale thickness for NiCrAlY coated superalloys Superni 600, 718 and Superfer 800H after oxidation in air for 50 cycles at 900<sup>0</sup>C was evaluated from the BSE images shown in Fig. 5.18, whereas for the superalloys Superni 75 and 601 from Fig. 5.22 (a) and (b) respectively. The values of oxide scale thickness are 138, 171, 138, 166 and 136 for the coated Superni 75, 600, 601, 718 and Superfer 800H respectively. Evidently, the thickness values for the Superni 75, 601 and Superfer 800H cases are identical, whereas these are nearly same for the Superni 600 and 718.

### **5.1.2.4 X-ray Diffraction Analysis**

X-ray diffractograms for the plasma spray NiCrAlY coated superalloys after cyclic oxidation in air for 50 cycles at 900<sup>0</sup>C are reported in Fig. 5.19 on reduced scales. It can be seen from the diffractograms that all the coated superalloys have indicated the formation of similar phases after oxidation. XRD analysis has revealed the formation of NiO, Al<sub>2</sub>O<sub>3</sub> and NiCr<sub>2</sub>O<sub>4</sub> as main phases after oxidation alongwith some relatively weak peaks of Cr<sub>2</sub>O<sub>3</sub>.



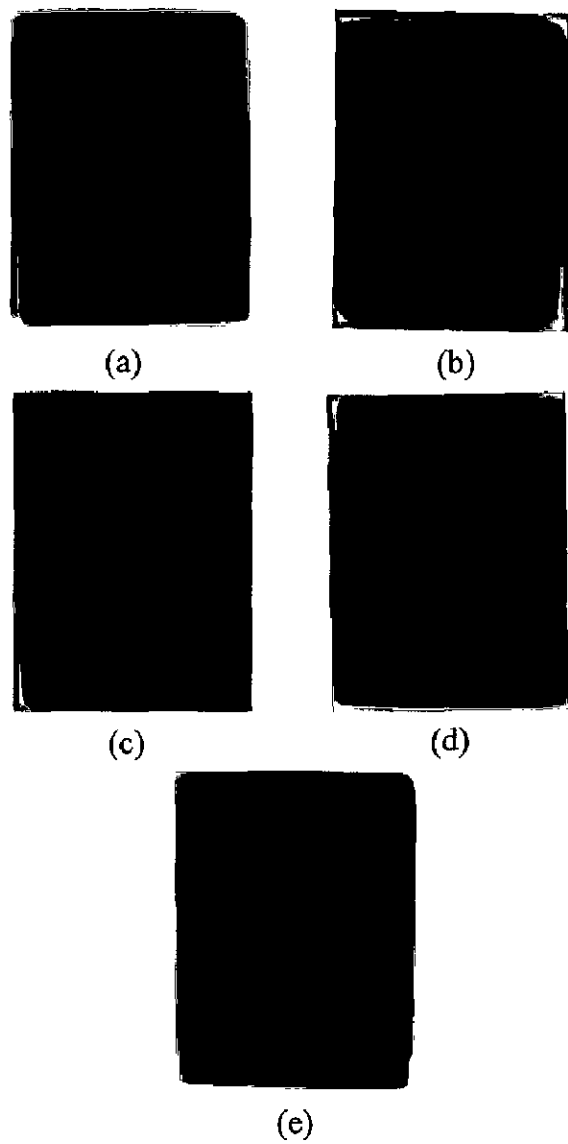


**Fig. 5.15** Macrographs of the NiCrAlY coating with bond coat subjected to cyclic oxidation in air at 900°C for 50 cycles having substrate superalloys  
(a) Superni 75      (b) Superni 600      (c) Superni 601  
(d) Superni 718      (e) Superfer 800H.

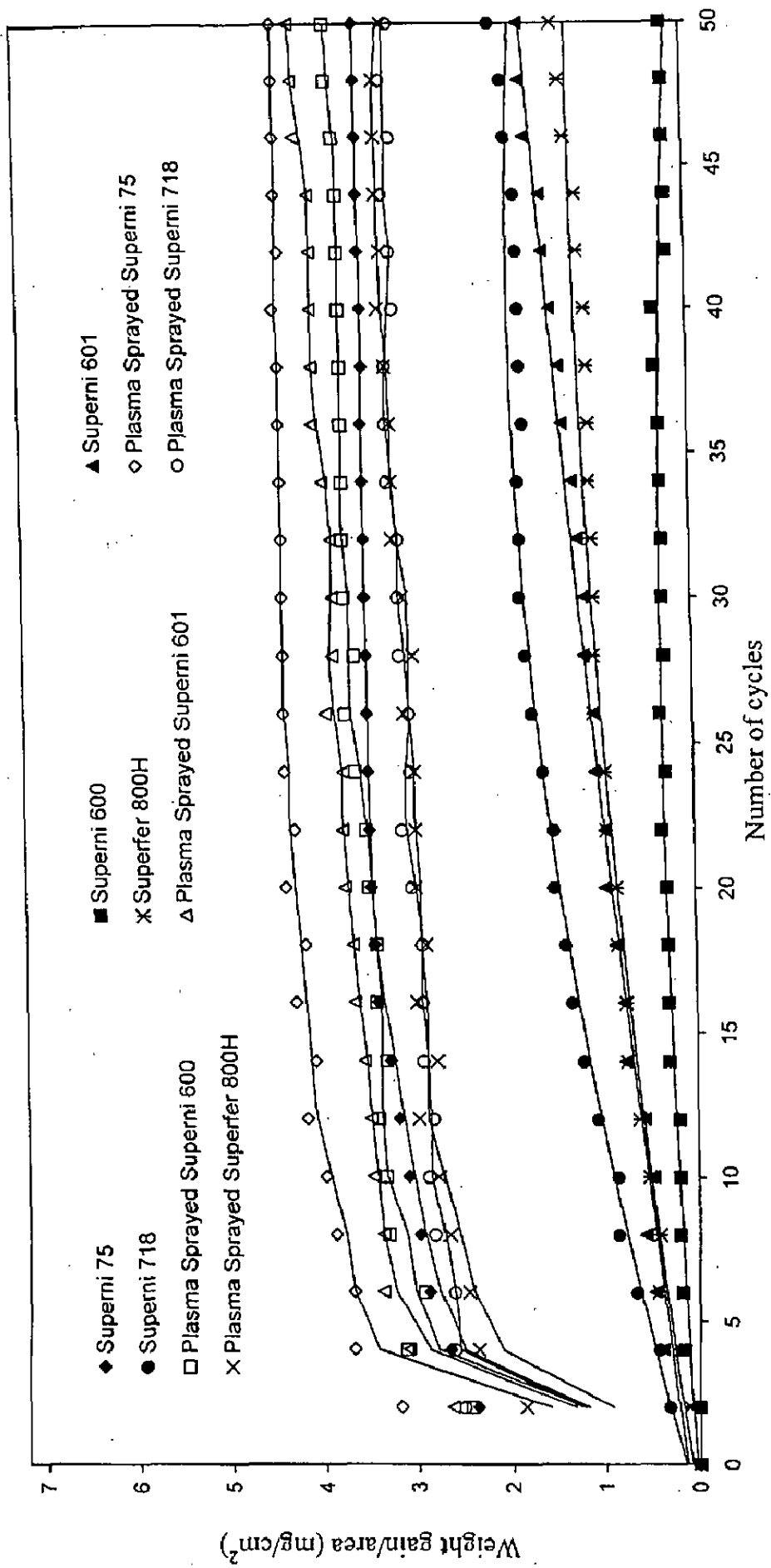


Fig. 5.16 Weight gain vs. number of cycles plots for uncoated and NiCrAlY coated superalloys subjected to cyclic oxidation for 50 cycles in air at 900°C.

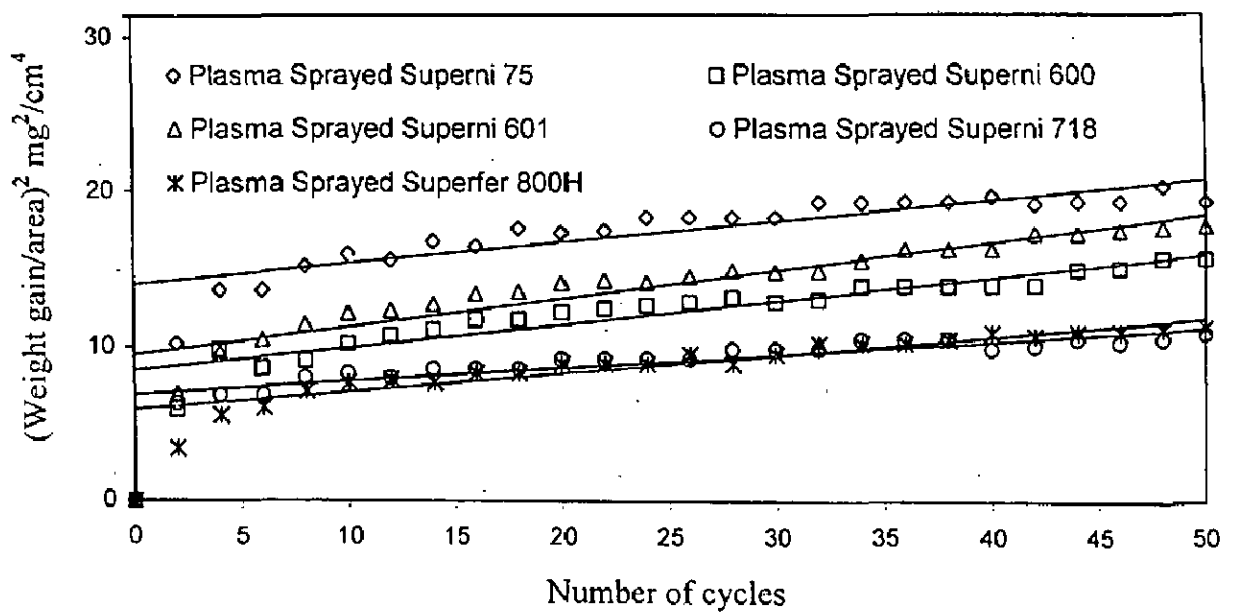
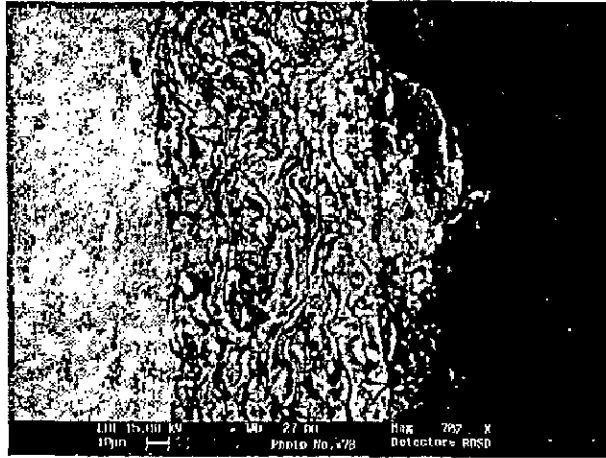
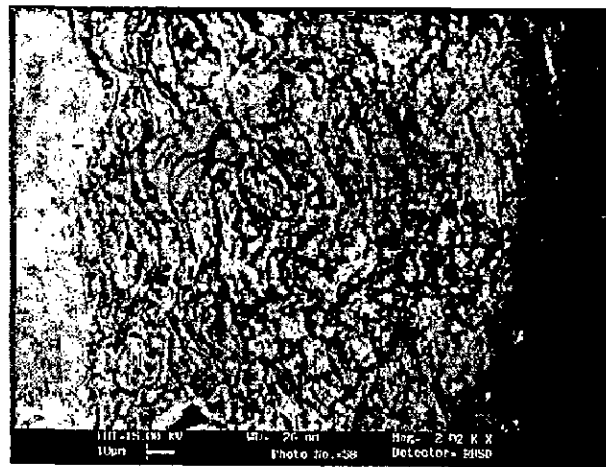


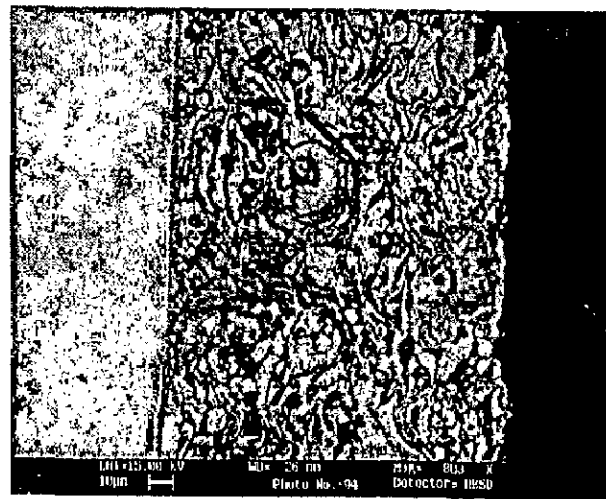
Fig. 5.17 (Weight gain/area)<sup>2</sup> vs. number of cycles plots for the NiCrAlY coated superalloys subjected to cyclic oxidation for 50 cycles in air at 900°C.



(a)



(b)



(c)

**Fig. 5.18** SEM back scattered images for the NiCrAlY coated superalloys after cyclic oxidation in air for 50 cycles at 900°C  
 (a) Superni 600      (b) Superni 718      (c) Superfer 800H.

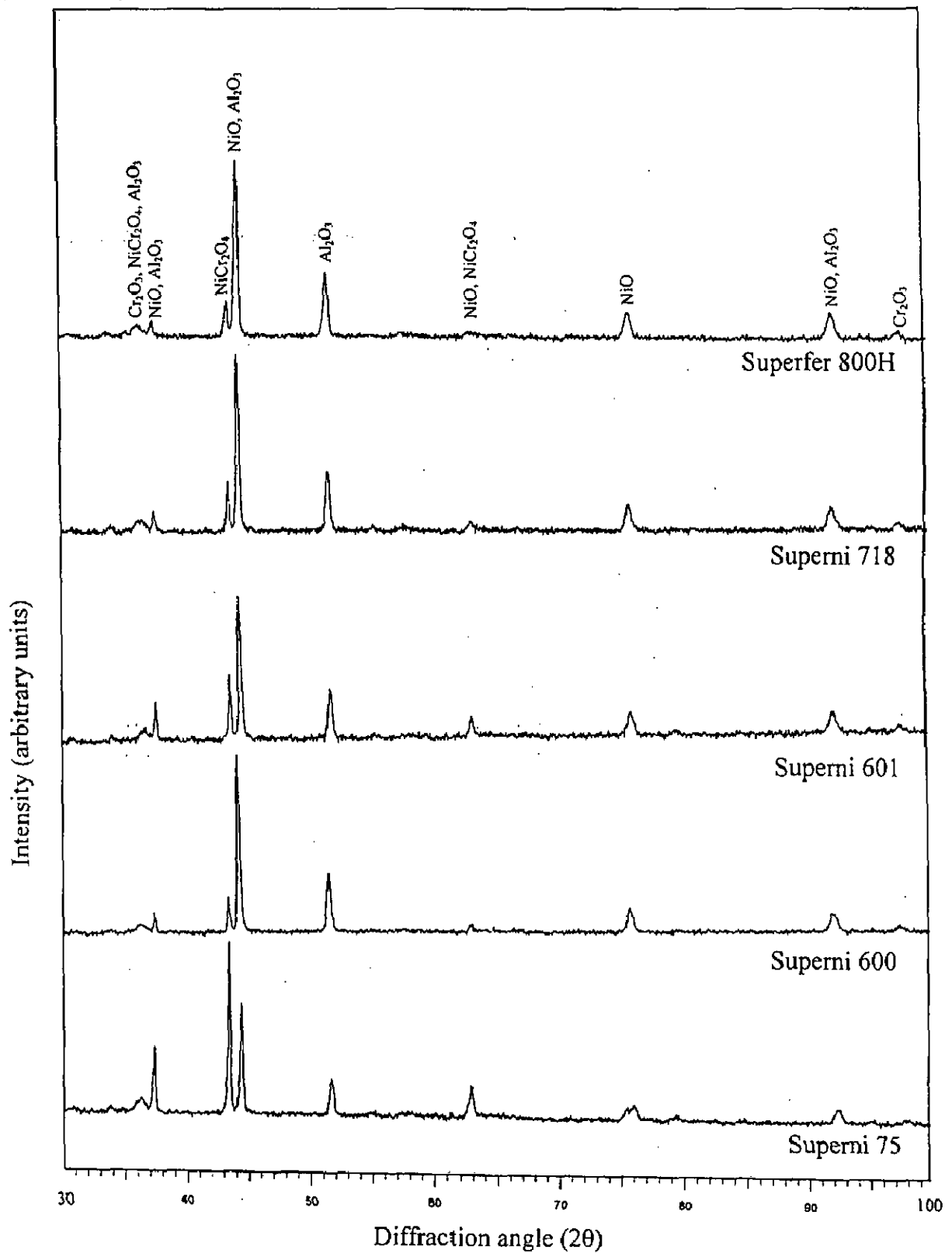


**Fig. 5.19** X-ray diffraction patterns for the NiCrAlY coated superalloys subjected to cyclic oxidation in air at 900°C after 50 cycles.

### 5.1.2.5 SEM/EDAX Analysis

#### (a) Surface Morphology

SEM micrographs shown in Fig. 5.20 and 5.21 point out similar morphologies of the oxide scales for all the NiCrAlY coated superalloys. EDAX micrograph shown in Fig. 5.20 (a) for the coated Superni 75 indicates the oxide scale contains NiO with little amount of oxides of Cr and Al. Whereas in case of Superni 600 coated specimen, the white NiO and Cr<sub>2</sub>O<sub>3</sub> rich areas can be observed to be dispersed in the scale. The presence of small amount of Fe<sub>2</sub>O<sub>3</sub> (2%) at point 2, Fig. 5.20 (b) indicates the probable diffusion of Fe from the base superalloy. The scale for the coated Superni 601 has white phase just similar in composition to that for Superni 600, whereas the black phase is rich in NiO as shown at point 1, Fig. 5.20 (c). Further, the coated Superni 718 scale contains a nickel oxide rich (82%) white phase as shown in Fig. 5.21 (a), which also have oxides of yttrium, iron and tantalum. Al<sub>2</sub>O<sub>3</sub> can be seen in a significant amount (18%) in the black matrix phase. The scale of coated Superfer 800H shows formation of comparatively large quantities of aluminium oxide as indicated at points 1 and 2 in Fig. 5.21 (b), in comparison to those shown by the Ni-base superalloys. Iron oxide has also been identified in the scale by EDAX.

#### (b) Cross-Sectional Analysis

The scale for oxidised superalloy Superni 75, Fig. 5.22 (a) consists mainly of nickel, but in the topmost layer more of aluminium is present. There is relatively small amount of chromium in the scale along with some yttrium. The presence of oxygen at points 3, 4 and 5 indicates that the coating might have got oxidised at these points. Whereas the absence of oxygen at point 2 shows that the Ni-rich splat has not got oxidised. Further, it can be observed that concentration of oxygen is high at the points where aluminum is high and vice-versa. The structure of the scale seems to be lamellar, where there are alternate Ni-rich and Al-rich layers.

Corresponding analysis for the oxidised Superni 601, Fig. 5.22 (b) shows the outermost layer of the scale to be consisting mainly of the oxides of chromium and aluminium alongwith small amounts of oxides of nickel and yttrium. Aluminium has shown fluctuations in composition along the thickness of the scale. There are alternate layers rich in Ni and Al respectively. The nickel rich splat as represented by point 3 seems to be in unoxidised state as oxygen is absent at this point. In both the cases discussed under this section, chromium has shown slight variation in its concentration along the thickness of the scales, and the base alloys have not suffered internal oxidation.

### 5.1.2.6 EPMA Analysis

BSEI and elemental X-ray mappings for the coated superalloy of grade Superni 75 (Fig. 5.23) exposed to cyclic oxidation for 50 cycles at 900°C indicate that oxygen co-exists with aluminium throughout the scale, and yttrium is also seen alongside aluminium. Wherever nickel is present, oxygen is absent, thereby indicating that splats of nickel have not got oxidised, although oxygen seems to have penetrated along the splat boundaries and reacted with aluminium. Some iron is present in the top layers of the scale. Chromium has shown its presence along the interface between the scale and base alloy in the form of stringers, and the places devoid of nickel are rich in chromium. Moreover at most of these places, Cr has got oxidised.

A scale consisting mainly of nickel with uniform distribution of chromium and aluminium could be seen for the coated Superni 600 as has been depicted in Fig. 5.24. Aluminium is present in high concentrations at the places where nickel is absent. Yttrium has shown tendency towards clustering, while iron has indicated diffusion in the scale which is very intensive near the coating/substrate interface. Aluminium seems to have diffused to the substrate superalloy from the coating.

Corresponding analysis for the coated Superni 601 as depicted in Fig. 5.25 reveals a scale with an outer layer consisting mainly of aluminium and nickel, with some diffused iron in the form of clusters. Yttrium is absent in this outermost layer. In the intermediate portion of the scale Ni, Cr, Al and Y are co-existing. Minor movement of basic elements of the substrate superalloy such as manganese and silicon has also been noticed into the scale. Diffusion of iron throughout the scale has also been noticed, which is more prominent near the substrate/coating interface.

EPMA analysis for the oxidised NiCrAlY coated Superni 718, Fig. 5.26 indicates that the scale mainly contains nickel, chromium, aluminium, and there is a presence of some small clusters of iron and silicon in top layers of the scale. The iron and silicon seem to have diffused into the scale from the substrate. Yttrium is seen in the form of clusters throughout the scale. Titanium has shown significant diffusion into the scale from the base alloy and, it is present in little high concentration at the scale/substrate interface.

The EPMA for the oxidised Superfer 800H case reveals a lamellar scale consisting of nickel rich splats, which also contain chromium, Fig. 5.27. Aluminium and yttrium are present at the splat boundaries in the scale, and alongside these splat boundaries oxygen has also penetrated indicating the formation of oxides. Iron has shown diffusion into the scale from the substrate and exists along the chromium rich streaks in the inner layers of the scale.

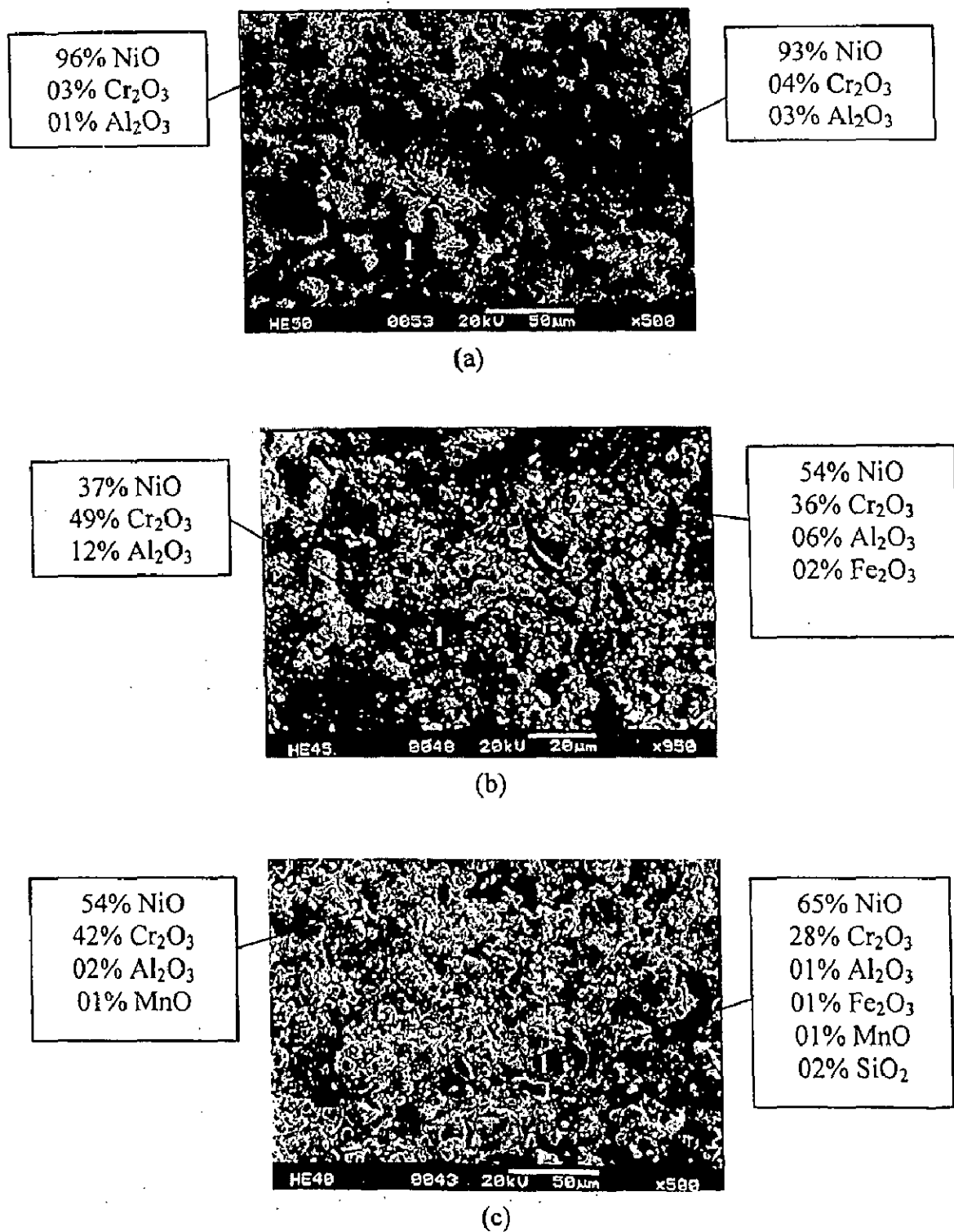


**Fig. 5.20** Surface scale morphology and EDAX analysis for the plasma sprayed NiCrAlY coated superalloys subjected to cyclic oxidation in air at 900°C for 50 cycles  
 (a) Superni 75                      (b) Superni 600                      (c) Superni 601.



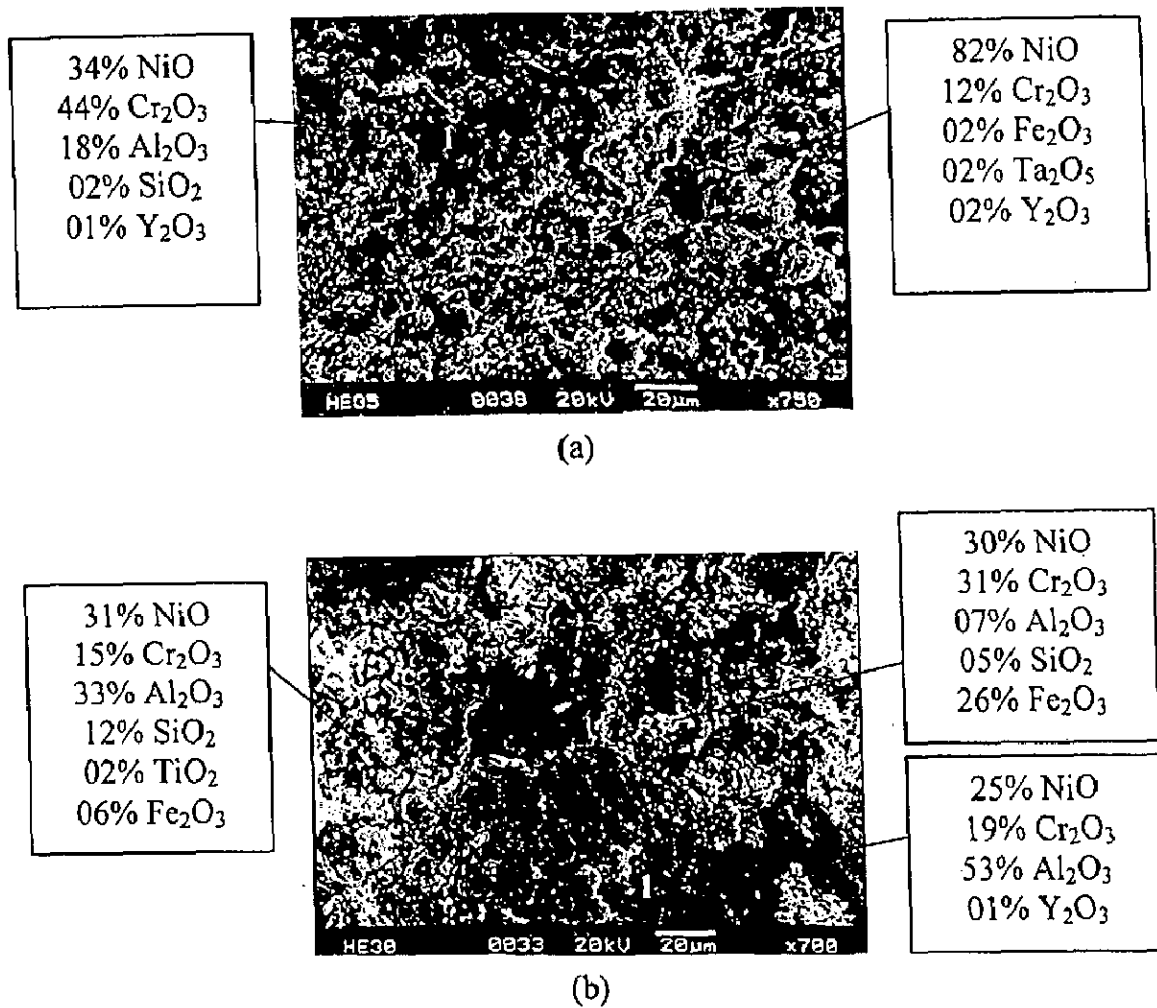
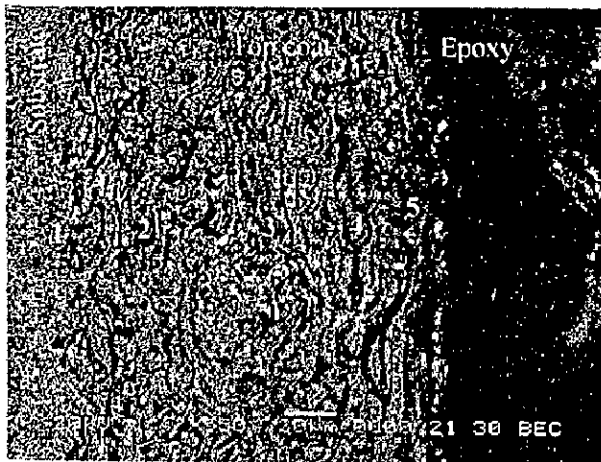
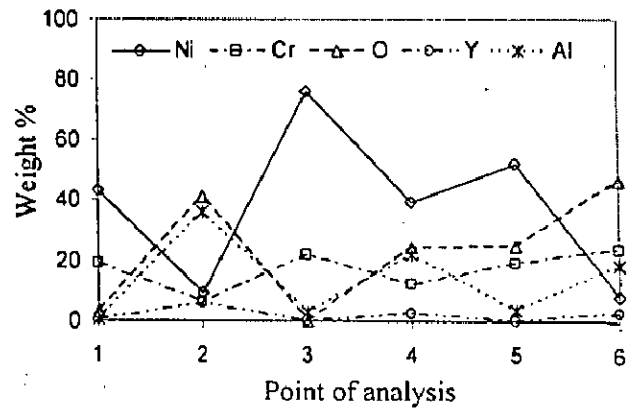
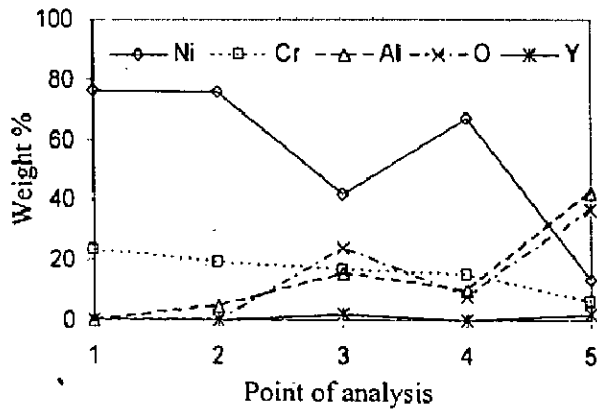
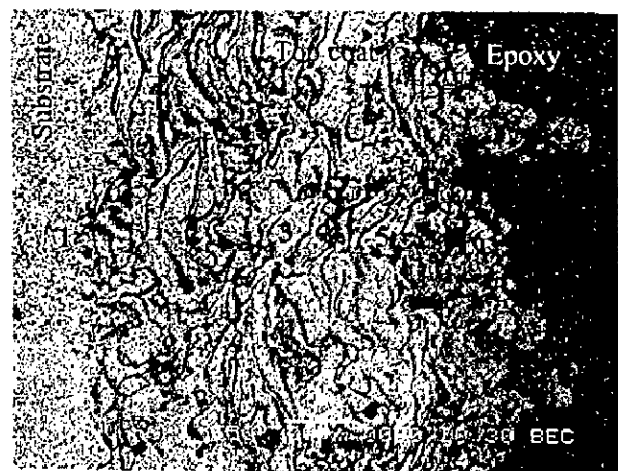


**Fig. 5.21** Surface scale morphology and EDAX analysis for the plasma sprayed NiCrAlY coated superalloys subjected to cyclic oxidation in air at 900°C for 50 cycles  
 (a) Superni 718      (b) Superfer 800H.



(a)



(b)

**Fig. 5.22** Oxide scale morphology and variation of elemental composition across the cross-section of NiCrAlY coated superalloys subjected to cyclic oxidation in air at 900°C after 50 cycles  
 (a) Superni 75                      (b) Superni 601.

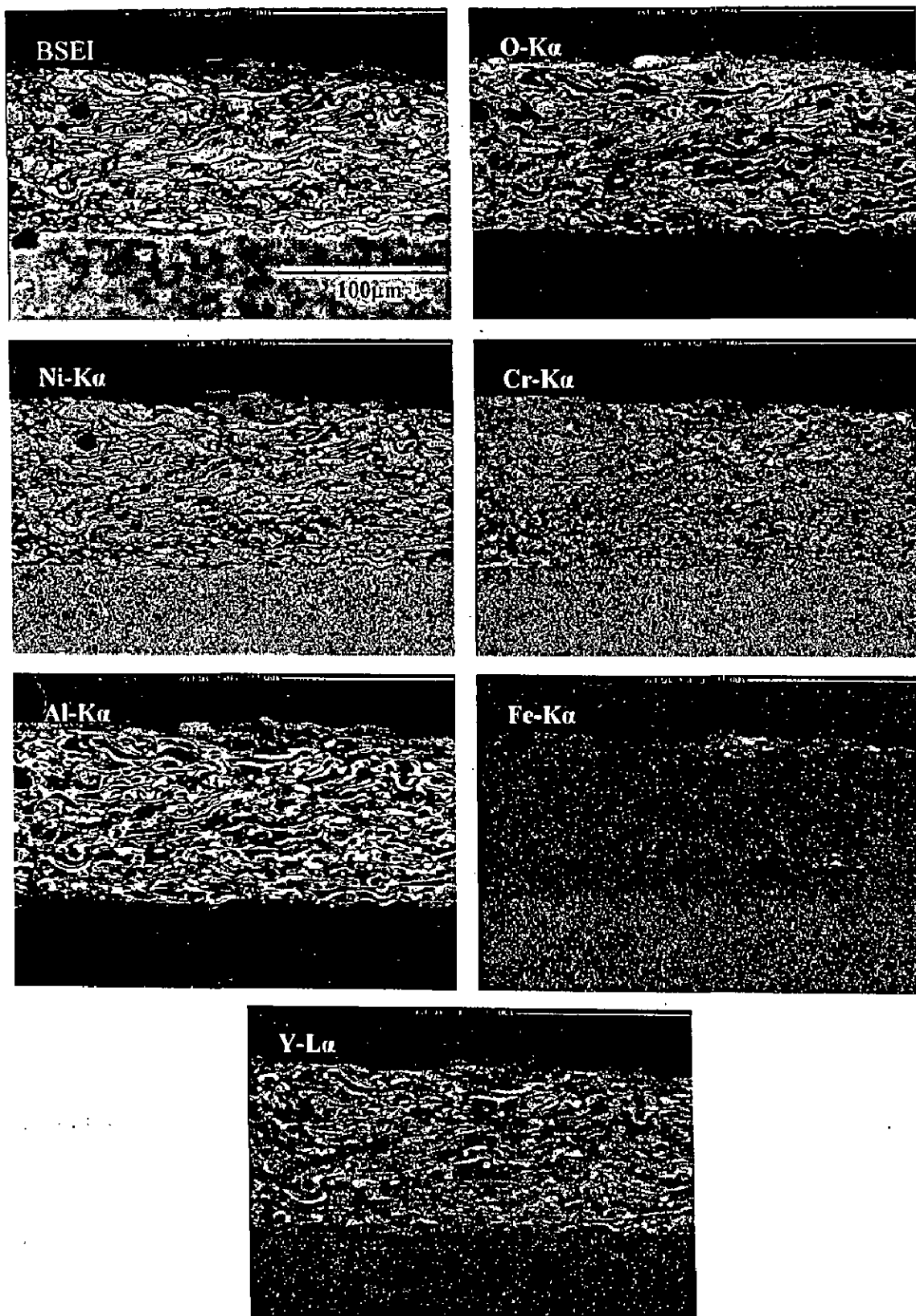


**Fig. 5.23** BSEI and X-ray mappings of the cross-section of NiCrAlY coated superalloy Superni 75 subjected to cyclic oxidation at 900°C in air after 50 cycles.

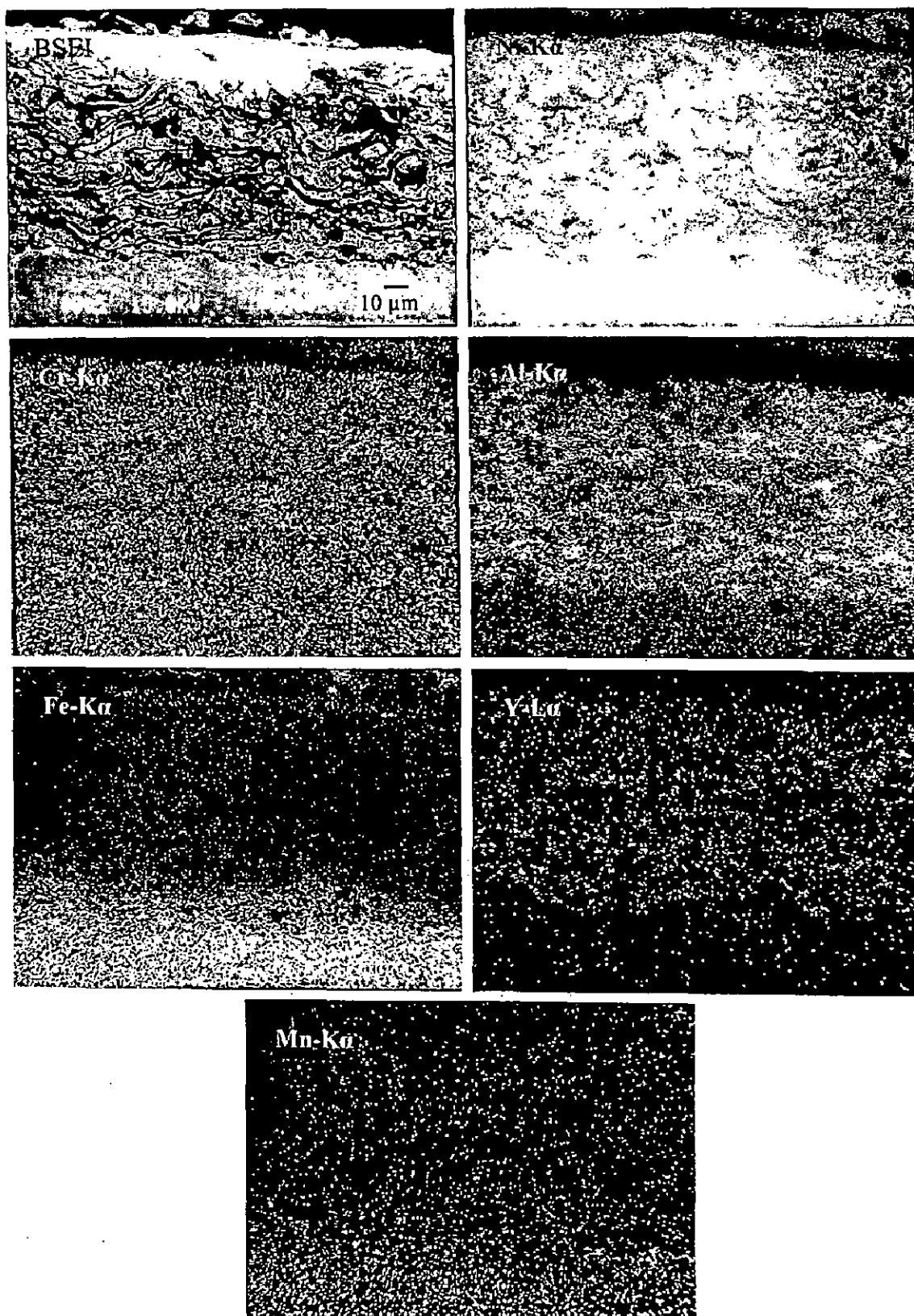


**Fig. 5.24** BSEI and X-ray mappings of the cross-section of NiCrAlY coated superalloy Superni 600 subjected to cyclic oxidation at 900°C in air after 50 cycles.

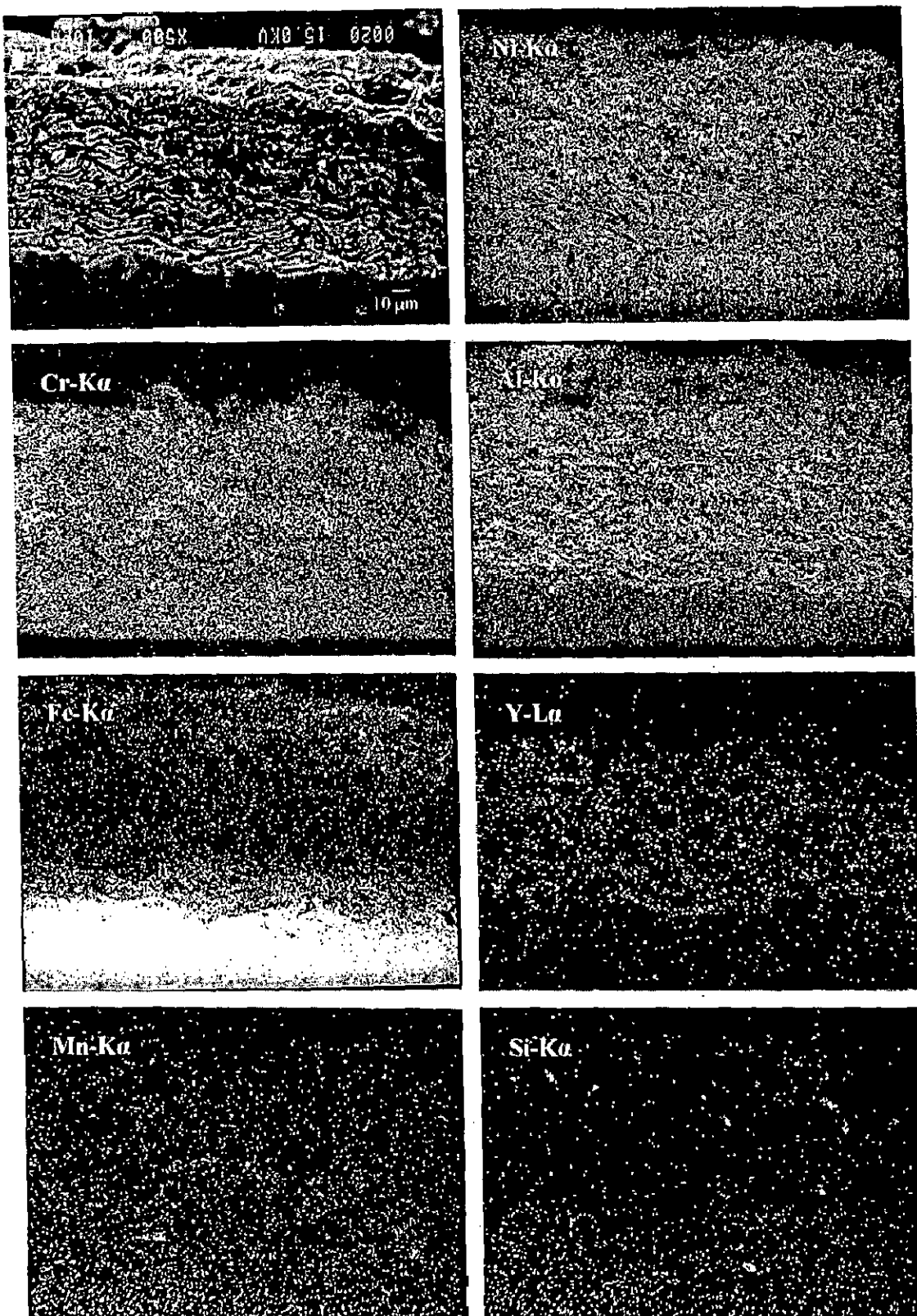


Fig. 5.25 BSEI and X-ray mappings of the cross-section of NiCrAlY coated superalloy Superni 601 subjected to cyclic oxidation at 900°C in air after 50 cycles.

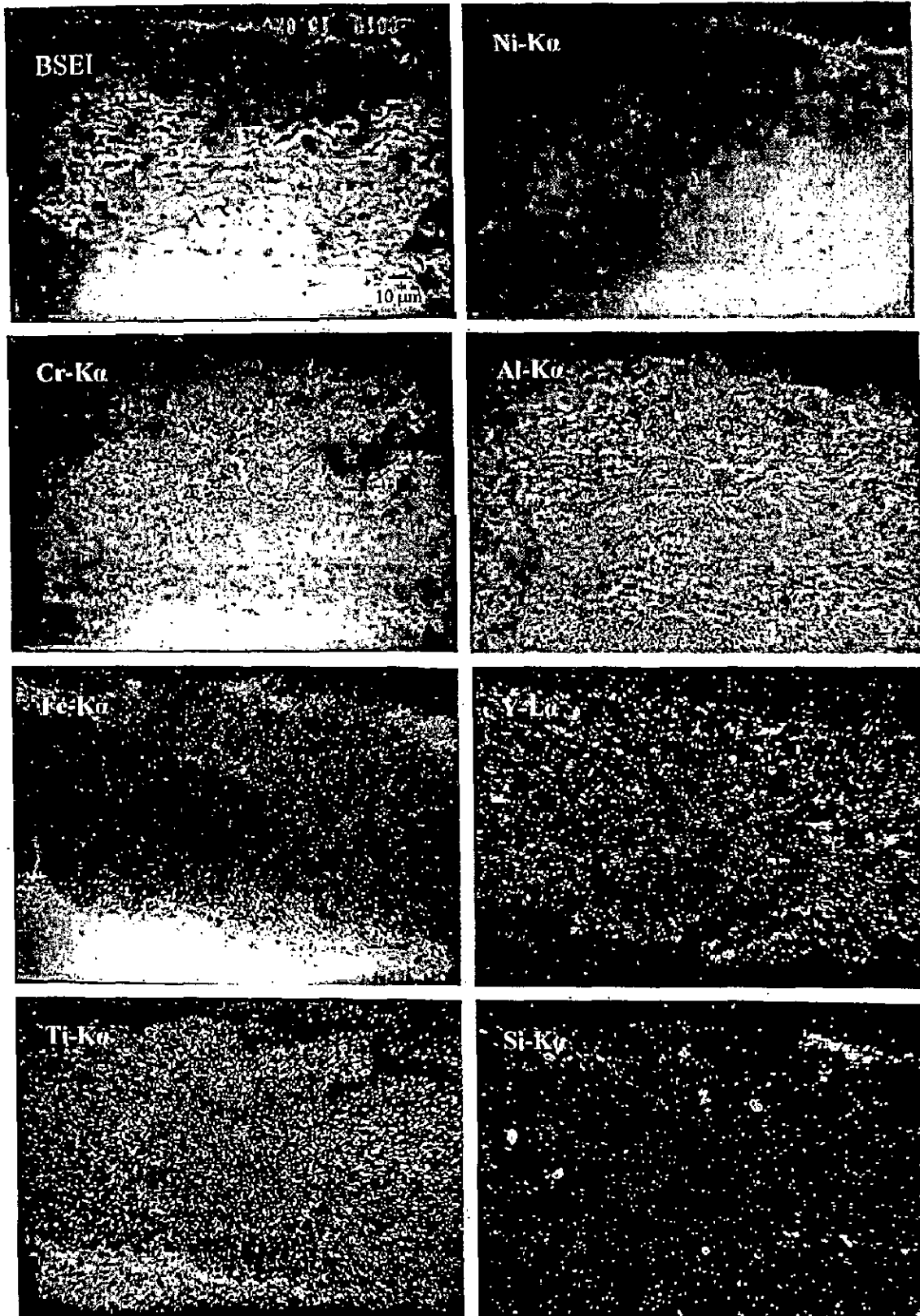
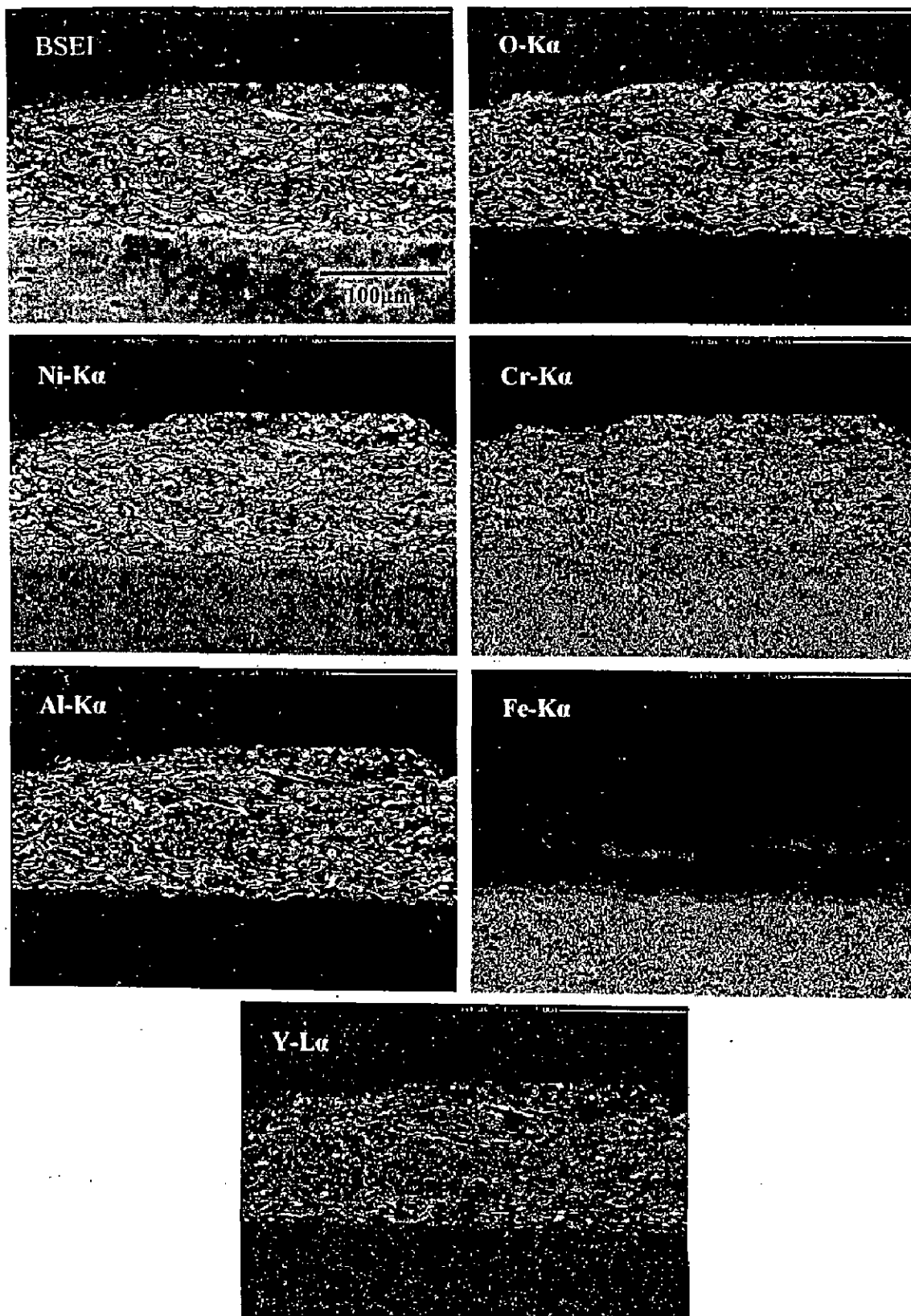


Fig. 5.26 BSEI and X-ray mappings of the cross-section of NiCrAlY coated superalloy Superni 718 subjected to cyclic oxidation at 900°C in air after 50 cycles.



**Fig. 5.27** BSEI and X-ray mappings of the cross-section of NiCrAlY coated superalloy Superfer 800H subjected to cyclic oxidation at 900°C in air after 50 cycles.

### 5.1.3 Ni-20Cr Coating

#### 5.1.3.1 Visual Examination

The colour of oxide scale during initial cycles of air oxidation at 900°C for this coating was grey, which went on turning towards green as the number of cycles increased, leaving a dark green scale at the end of 50 cycles in all the cases. The scales were having smooth surfaces with lustrous appearance, as can be seen in Fig. 5.28. The scales for the coated Superni 75 and Superni 718 showed little tendency for spalling in the form of fine powder during the first half of the study. The Ni-20Cr coating has shown good adherence to all the superalloys, in general during the course of cyclic oxidation studies. The minor spalling of coating from and near the edges (Section 5.1.2.1) stopped in all the cases after about 30 cycles, except for the coated Superni 718, where it continued till the end of study.

#### 5.1.3.2 Thermogravimetric Data

Cumulative weight change ( $\text{mg}/\text{cm}^2$ ) variation as a function of time expressed in number of cycles for the Ni-20Cr coated superalloys is shown in Fig. 5.29. It can be inferred from the plots that the coated superalloys, in general show tendency to approach a gradual weight gain after a high rate of increase in the initial cycles of study. The weight gains after 50 cycles of oxidation for the coated Superni 75, 600, 601, 718 and Superfer 800H are found to be 14.83, 13.98, 12.45, 9.71 and 9.45  $\text{mg}/\text{cm}^2$  respectively. This shows that the Ni-20 Cr coated superalloys have conceived more weight gain as compared to their uncoated counterparts, in general after a cyclic oxidation of 50 cycles. Further as shown in Fig. 5.30, the oxidation process has followed the parabolic rate law for all the coated superalloys. The values of the parabolic rate constants ( $K_p$ ) are found to be 8.84, 7.93, 4.87, 1.98 and  $2.92 \times 10^{-10} \text{ g}^2 \text{ cm}^{-4} \text{ s}^{-1}$  respectively for the coated Superni 75, 600, 601, 718 and Superfer 800H.

#### 5.1.3.3 Scale Thickness Measurement

Scale thicknesses measured from the back scattered electron images (Fig. 5.31, Fig. 5.35 and 5.36) for Ni-20Cr coated superalloys Superni 75, 600, 601, 718 and Superfer 800H oxidised in air at 900°C are 254, 286, 337, 247 and 251  $\mu\text{m}$  respectively.



#### 5.1.3.4 X-ray Diffraction Analysis

All the coated superalloys after oxidation in air at 900<sup>0</sup>C for 50 cycles have shown the formation of common phases as is evident from Fig. 5.32. NiO has been identified as the main phase alongwith phases like Cr<sub>2</sub>O<sub>3</sub> and NiCr<sub>2</sub>O<sub>4</sub>.

#### 5.1.3.5 SEM/EDAX Analysis

##### (a) Surface Morphology

SEM/EDAX analysis for the plasma spray Ni-20Cr coated superalloys after oxidation in air for 50 cycles at 900<sup>0</sup>C has been reported in Fig. 5.33 and 5.34. The oxide scales for the coated Ni-base superalloys have shown the dominance of nickel oxide, whereas that of Fe-base superalloy Superfer 800H has shown significant amounts of chromium oxide alongwith nickel oxide. SEM micrograph for the coated Superni 75 indicates large size nodular phase, which contains NiO and Cr<sub>2</sub>O<sub>3</sub>, dispersed in NiO rich dark phase matrix [Fig. 5.33 (a)], whereas the scales are consisting mainly of NiO crystals in the corresponding cases of Superni 600 and 601. Surface EDAX of the oxidised Ni-20Cr coated Superni 718 also indicates NiO rich scale. While for the oxidised Superfer 800H case, the scale consists of white nodules, having oxides of Ni and Cr in proportion to the coating composition, whereas the subscale region shows lower amount of NiO and a high amount of Cr<sub>2</sub>O<sub>3</sub>, Fig. 5.34 (b).

##### (b) Cross-Sectional Analysis

BSEI micrograph shown in Fig. 5.35 (a) reveals an intact scale for Ni-20Cr coated Superni 75 exposed to cyclic oxidation for 50 cycles at 900<sup>0</sup>C. EDAX analysis indicates the probable formation of oxides of nickel and chromium at point 6. The point 5 shows that aluminium has diffused from the bond coat into the top scale to form aluminium oxide. Alternate Ni-rich and Al-rich layers are present in the scale. All the elements have shown random fluctuation in their concentrations along the thickness of the scale. Further the substrate alloy has not got oxidised as no oxygen is found at point 1.

Two distinct layers could be seen in the oxide scale of oxidised Ni-20Cr coated Superni 600, Fig. 5.35 (b), upper one being dense and thick. This upper layer is found to be rich in nickel as is apparent from the compositions at point 4 and 5 and contains some chromium also. At point 4, the nickel seems to be in un-oxidised state as oxygen is absent

at this point. Chromium has not shown much variation in its concentration level along the thickness of the scale. In the bond coat region of the scale, the dark phase is rich in aluminium and oxygen, while the light grey phase mainly contains nickel. The presence of oxygen at points 2 to 5, as indicated in Fig. 5.36 (a), shows that the oxygen has penetrated into the top as well as bond coat in case of Ni-20Cr coated Superni 601. The uppermost layer of the scale consists mainly of nickel, oxygen and chromium. Further, Al-rich locations in the inner scale are found to have high amounts of oxygen.

In the corresponding case of coated Superfer 800H, top layer of the scale has mainly nickel and chromium present in it, Fig. 5.36 (b). A lamellar crack parallel to top surface of the scale is clearly visible. Oxygen can be seen diffused upto the base alloy at point 1. The presence of aluminium at point 4 indicates its diffusion from the bond coat into the top coat area. At this point the concentration of nickel has shown sharp decline. Oxygen and aluminium co-exist at most of the places in the scale, and wherever nickel is high, oxygen is low in concentration.

#### **5.1.3.6 EPMA Analysis**

EPMA along the cross-section of oxidised Ni-20Cr coated Superni 75 specimen shown in Fig. 5.37 indicates the presence of mainly nickel and chromium in the upper part of the scale. At places where Ni and Cr are absent in the lower part of scale, high concentration of Al and Y can be observed. A thin layer consisting of titanium and chromium could be seen at the bond coat/substrate interface. Al and Y are present at the boundaries of Ni-rich splats in the bond coat area. Iron has diffused even to the uppermost layer of the scale as streaks of iron are present there.

From the corresponding analysis for the coated Superni 600 shown in Fig. 5.38, it can be clearly seen that Ni and Cr are distributed throughout the scale, but there are small pockets, where Ni is totally absent. Similarly there are larger pockets where Cr is deficient. Some of these Cr- and Ni-depleted zones have higher concentration of aluminium, which has perhaps diffused from the bond coat into the upper region of the scale. Iron has also migrated from the substrate into the scale and is present in the form of small streaks, especially along the bond coat/top coat interface. Mn has also got concentrated at the substrate/scale interface. There is indication of Y diffusing from the bond coat to the upper region of the scale.

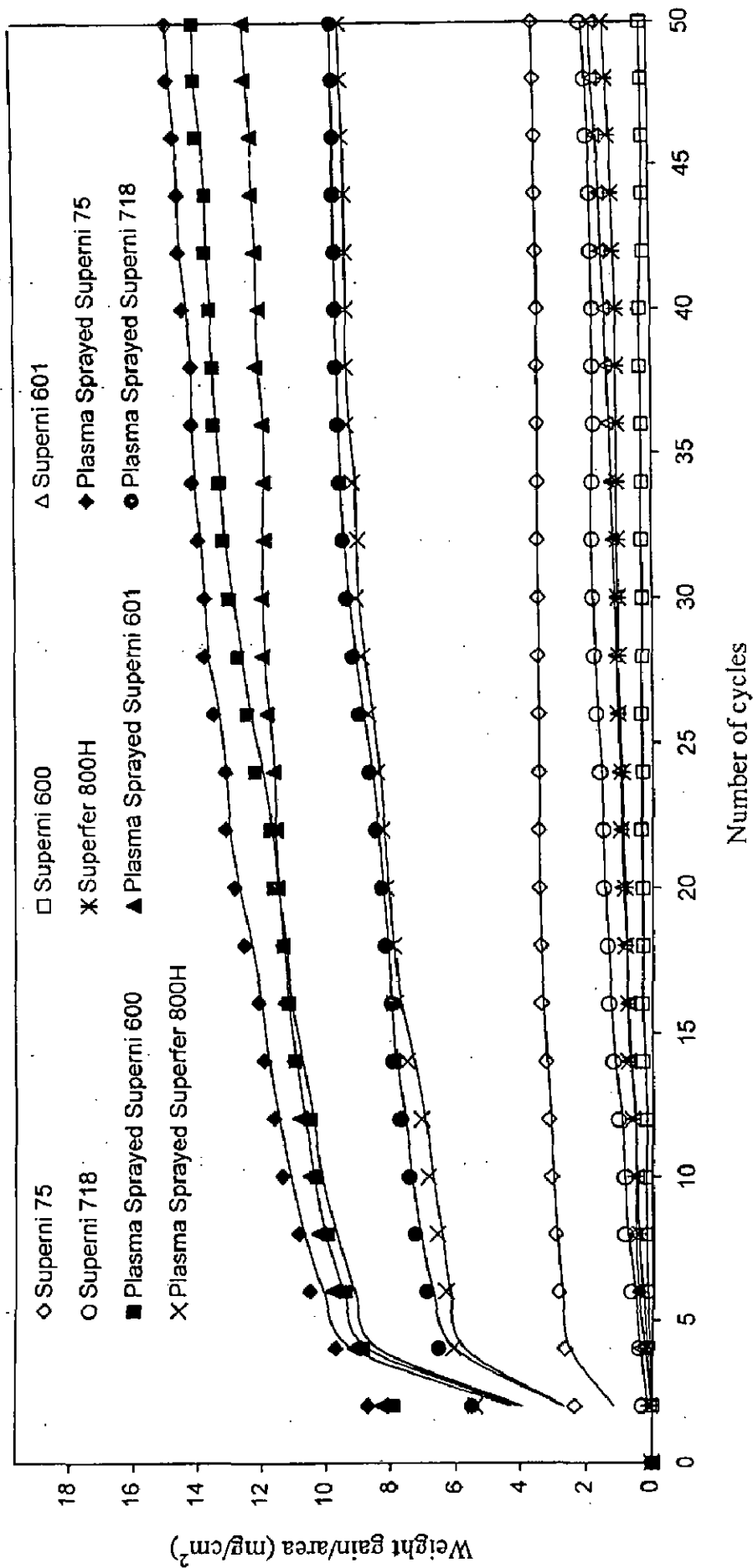
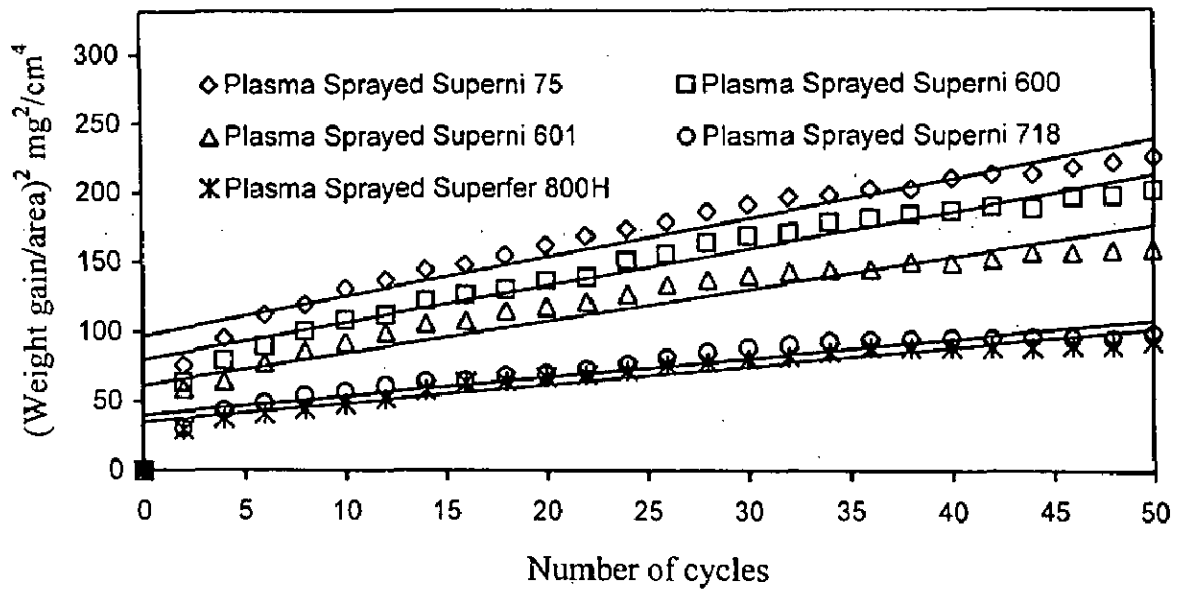
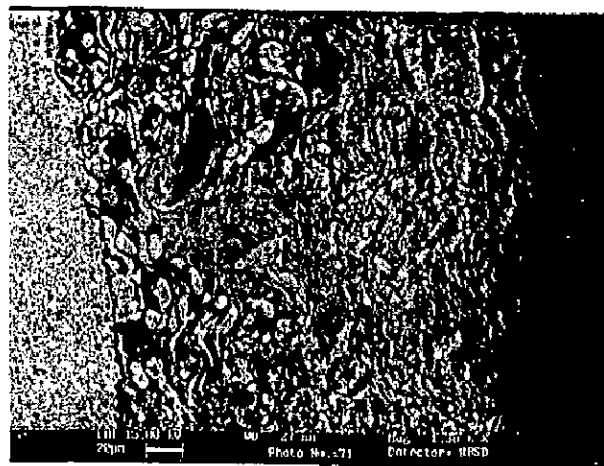


Fig. 5.29 Weight gain vs. number of cycles plots for uncoated and Ni-20Cr coated superalloys subjected to cyclic oxidation for 50 cycles in air at 900°C.



**Fig. 5.30** (Weight gain/area)<sup>2</sup> vs. number of cycles plots for the Ni-20Cr coated superalloys subjected to cyclic oxidation for 50 cycles in air at 900°C.



**Fig. 5.31** SEM back scattered images for the Ni-20Cr coated superalloy Superni 718 after cyclic oxidation in air for 50 cycles at 900°C.

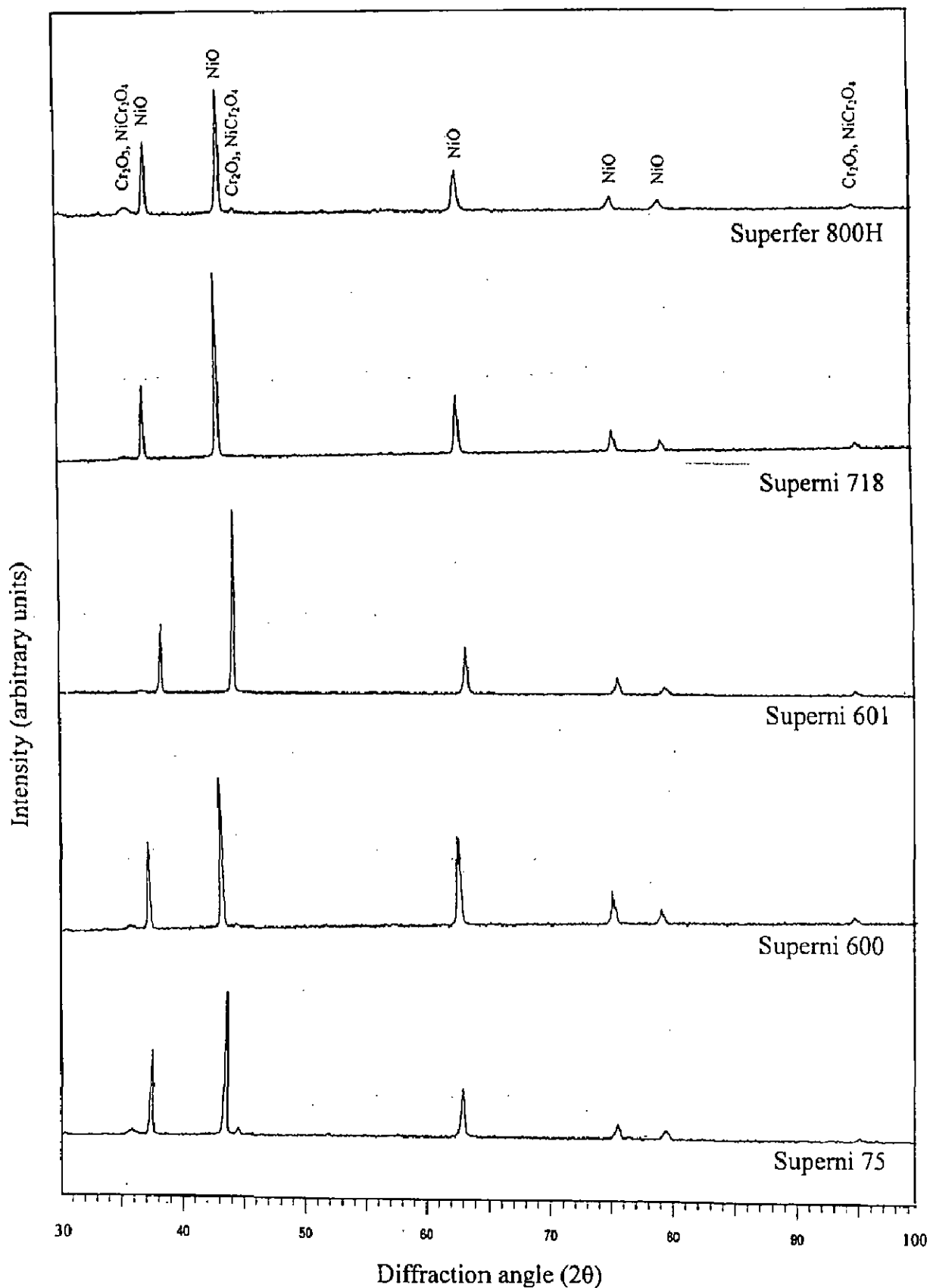


**Fig. 5.32** X-ray diffraction patterns for the Ni-20Cr coated superalloys subjected to cyclic oxidation in air at 900°C after 50 cycles.

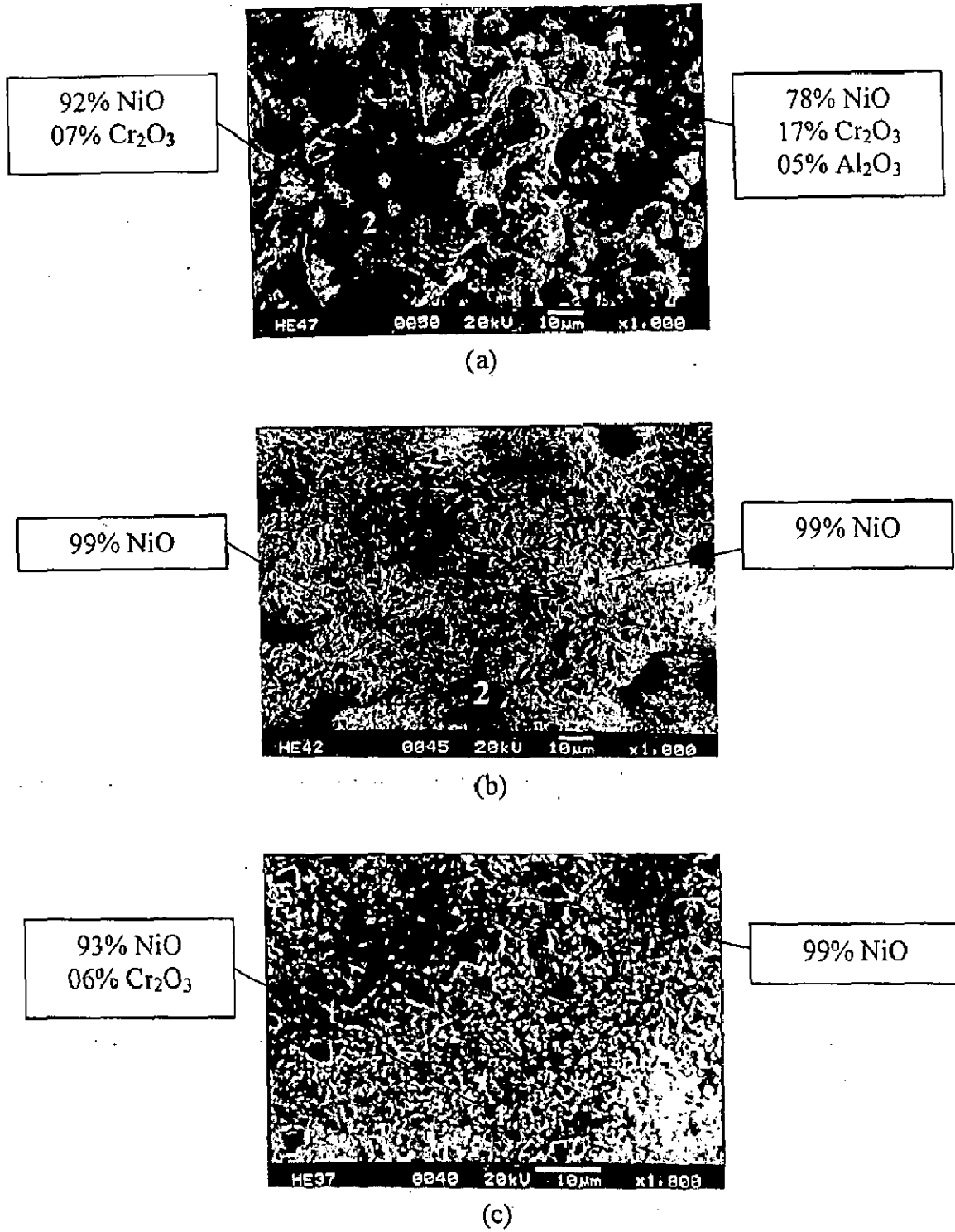


**Fig. 5.33** Surface scale morphology and EDAX analysis for the plasma sprayed Ni-20Cr coated superalloys subjected to cyclic oxidation in air at 900°C for 50 cycles  
 (a) Superni 75      (b) Superni 600      (c) Superni 601.

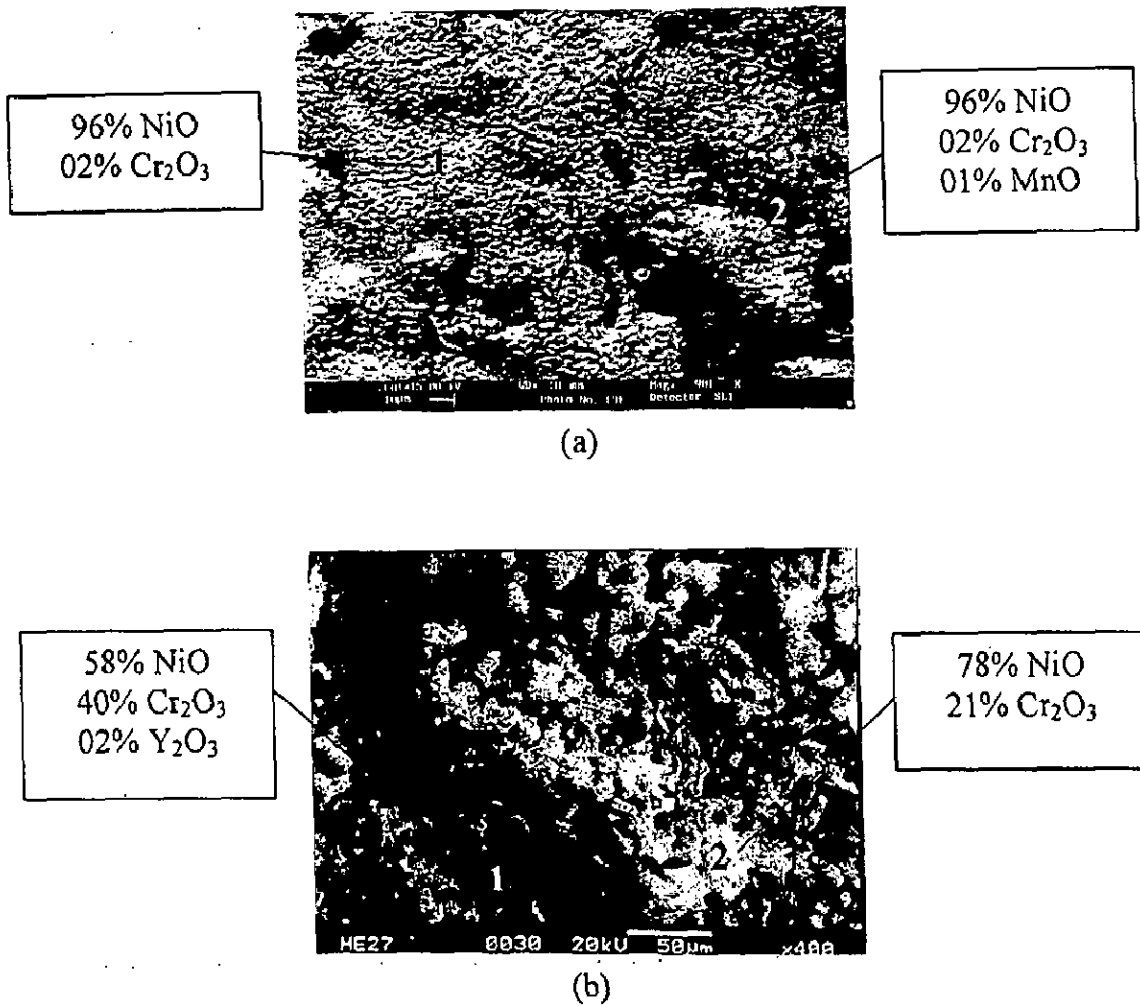
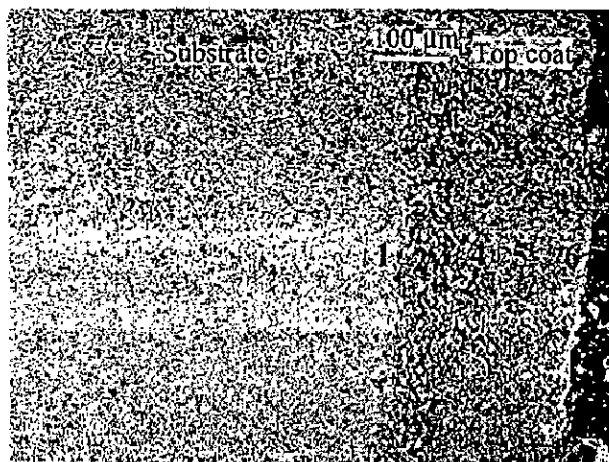
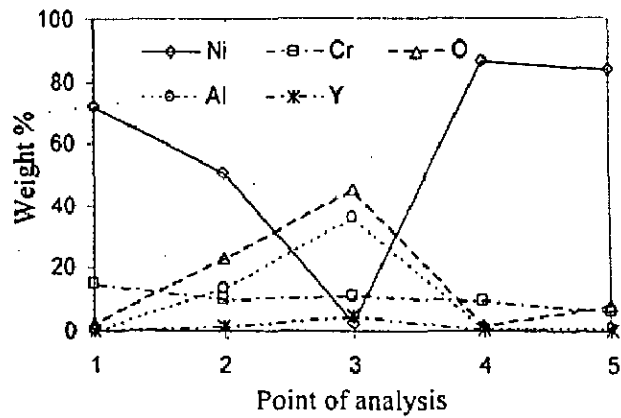
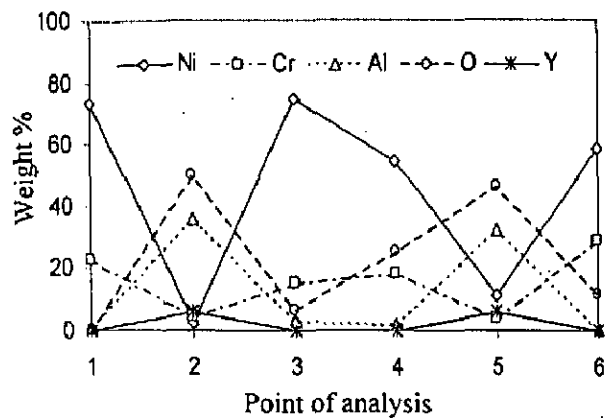
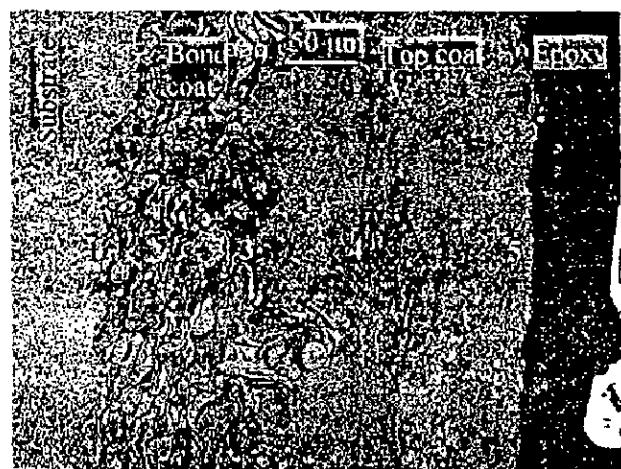


**Fig. 5.34** Surface scale morphology and EDAX analysis for the plasma sprayed Ni-20Cr coated superalloys subjected to cyclic oxidation in air at 900°C for 50 cycles  
 (a) Superni 718      (b) Superfer 800H.



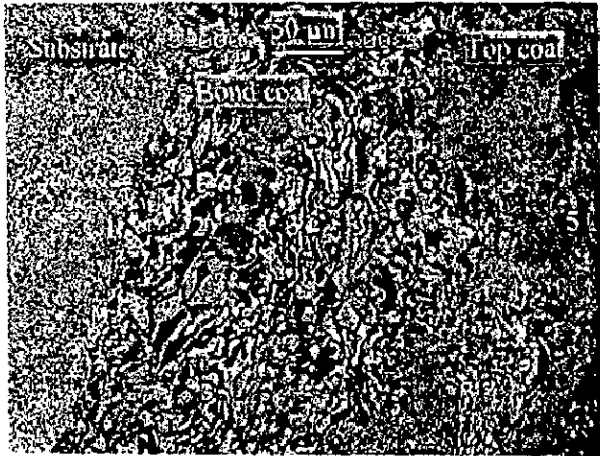
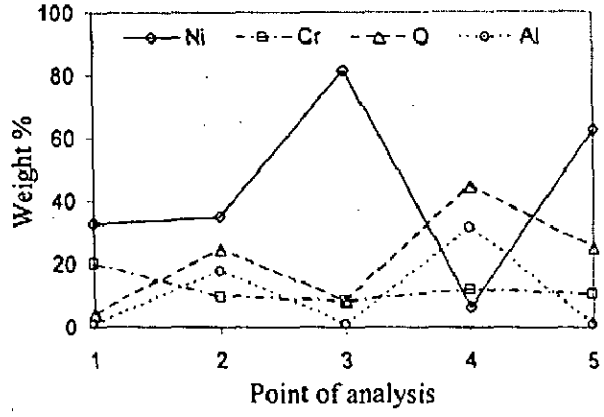
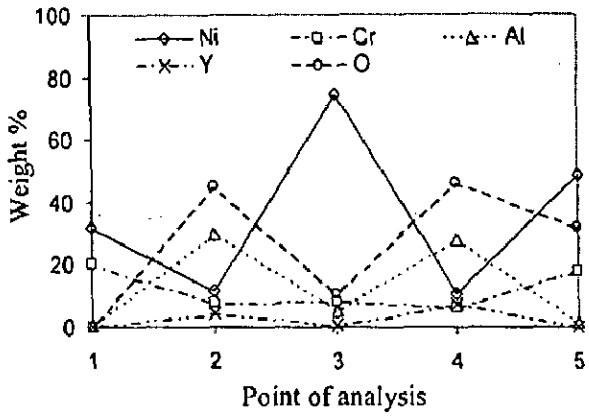
(a)



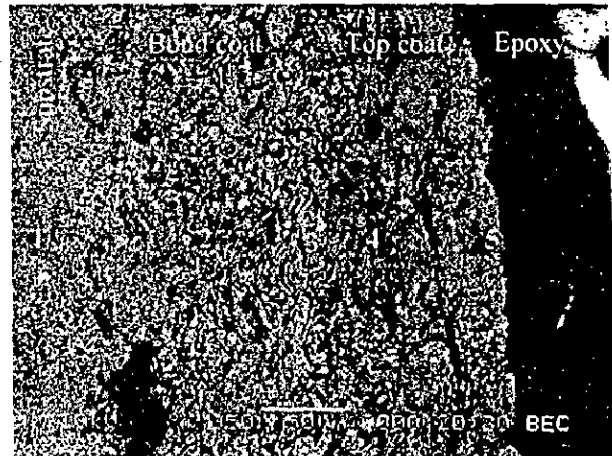
(b)

**Fig. 5.35** Oxide scale morphology and variation of elemental composition across the cross-section of Ni-20Cr coated superalloys subjected to cyclic oxidation at 900°C in air after 50 cycles  
 (a) Superni 75 (b) Superni 600.





(a)



(b)

**Fig. 5.36** Oxide scale morphology and variation of elemental composition across the cross-section of Ni-20Cr coated superalloys subjected to cyclic oxidation in air at 900°C after 50 cycles.  
 (a) Superni 601      (b) Superfer 800H.

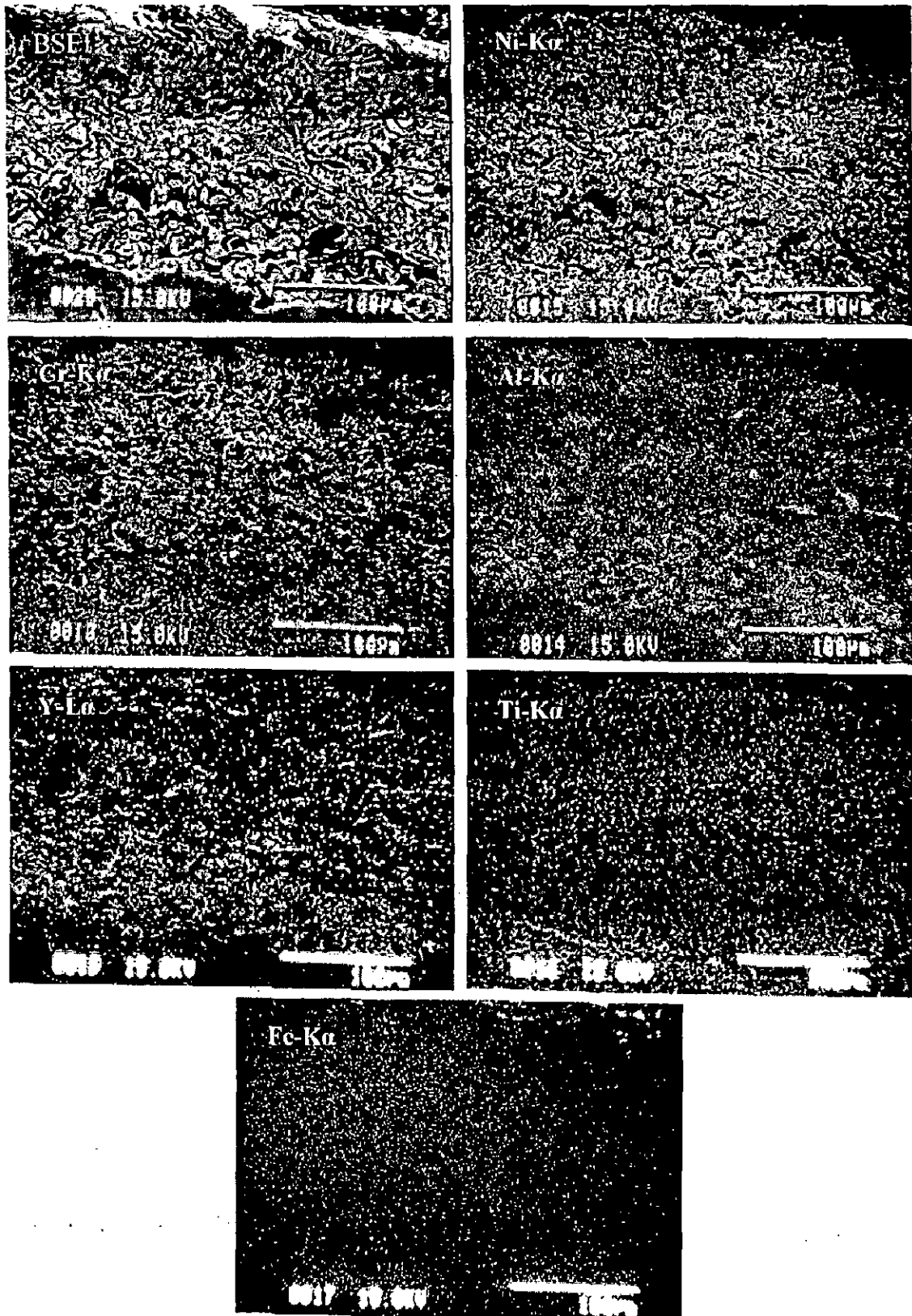


Fig. 5.37 BSEI and X-ray mappings of the cross-section of Ni-20Cr coated superalloy Superni 75 subjected to cyclic oxidation at 900°C in air after 50 cycles.

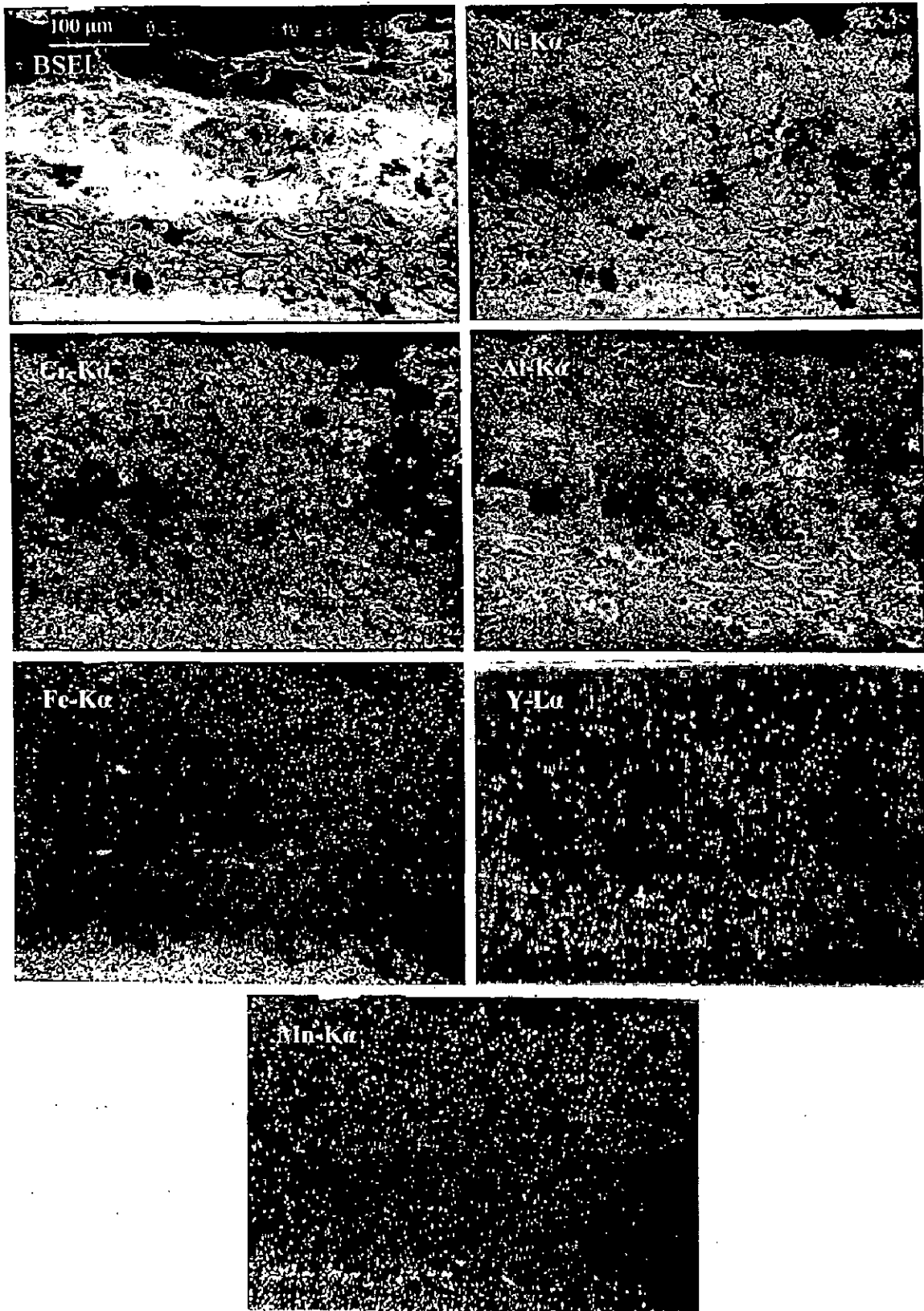


Fig. 5.38 BSEI and X-ray mappings of the cross-section of Ni-20Cr coated superalloy Superni 600 subjected to cyclic oxidation at 900°C in air after 50 cycles.

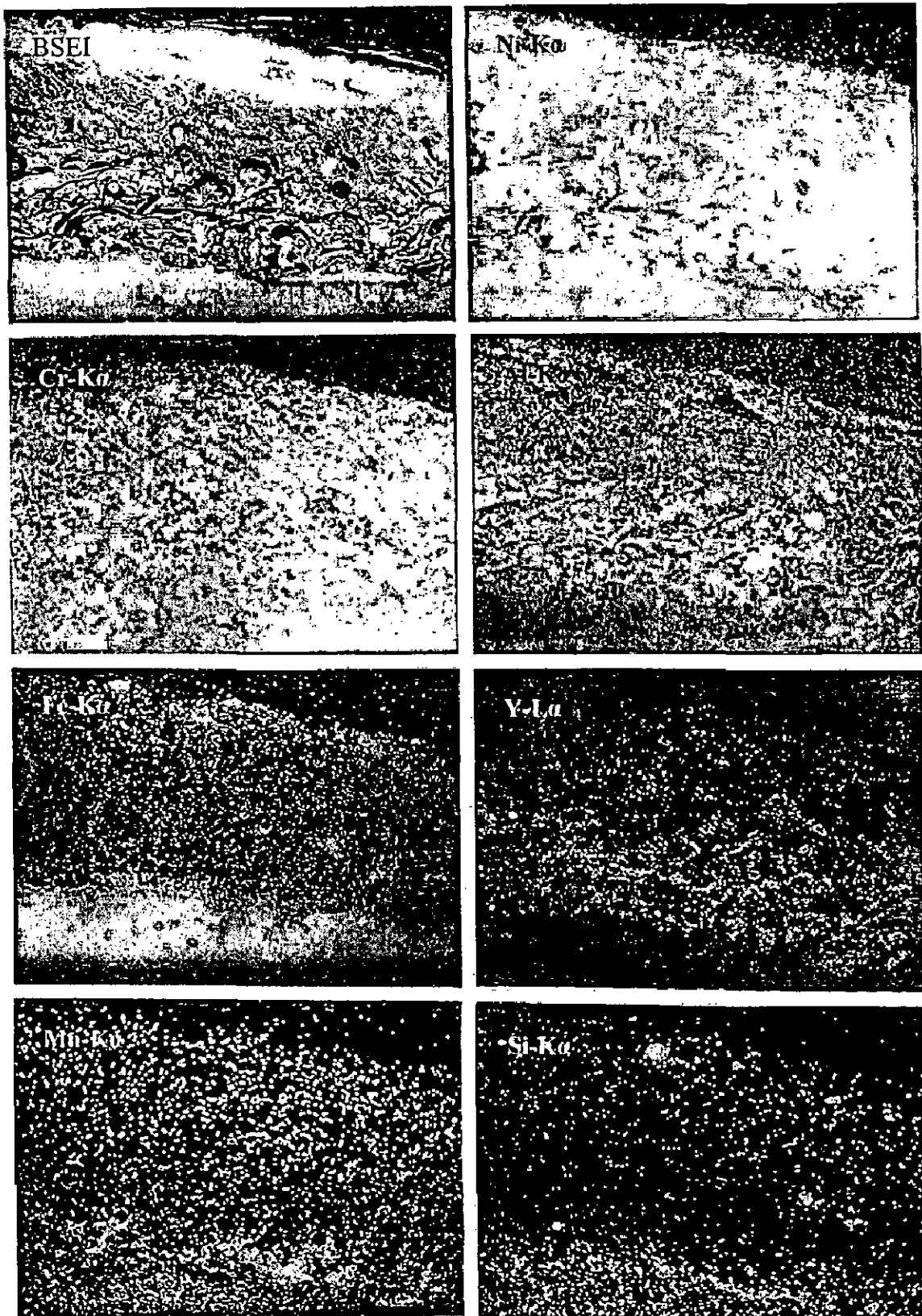


Fig. 5.39 BSEI and X-ray mappings of the cross-section of Ni-20Cr coated superalloy Superni 601 subjected to cyclic oxidation at 900°C in air after 50 cycles.

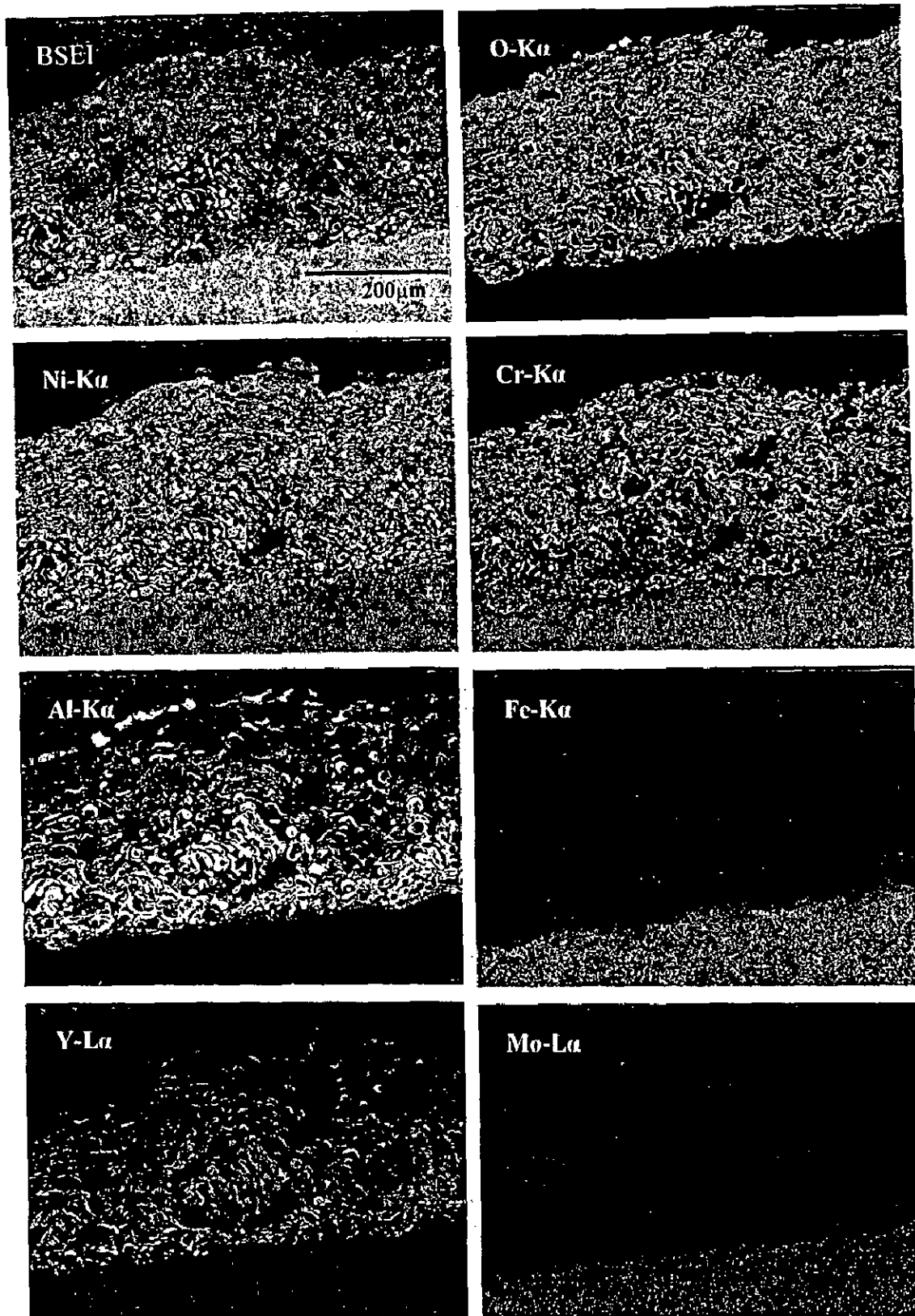


Fig. 5.40 BSEI and X-ray mappings of the cross-section of Ni-20Cr coated superalloy Superni 718 subjected to cyclic oxidation at 900°C in air after 50 cycles.

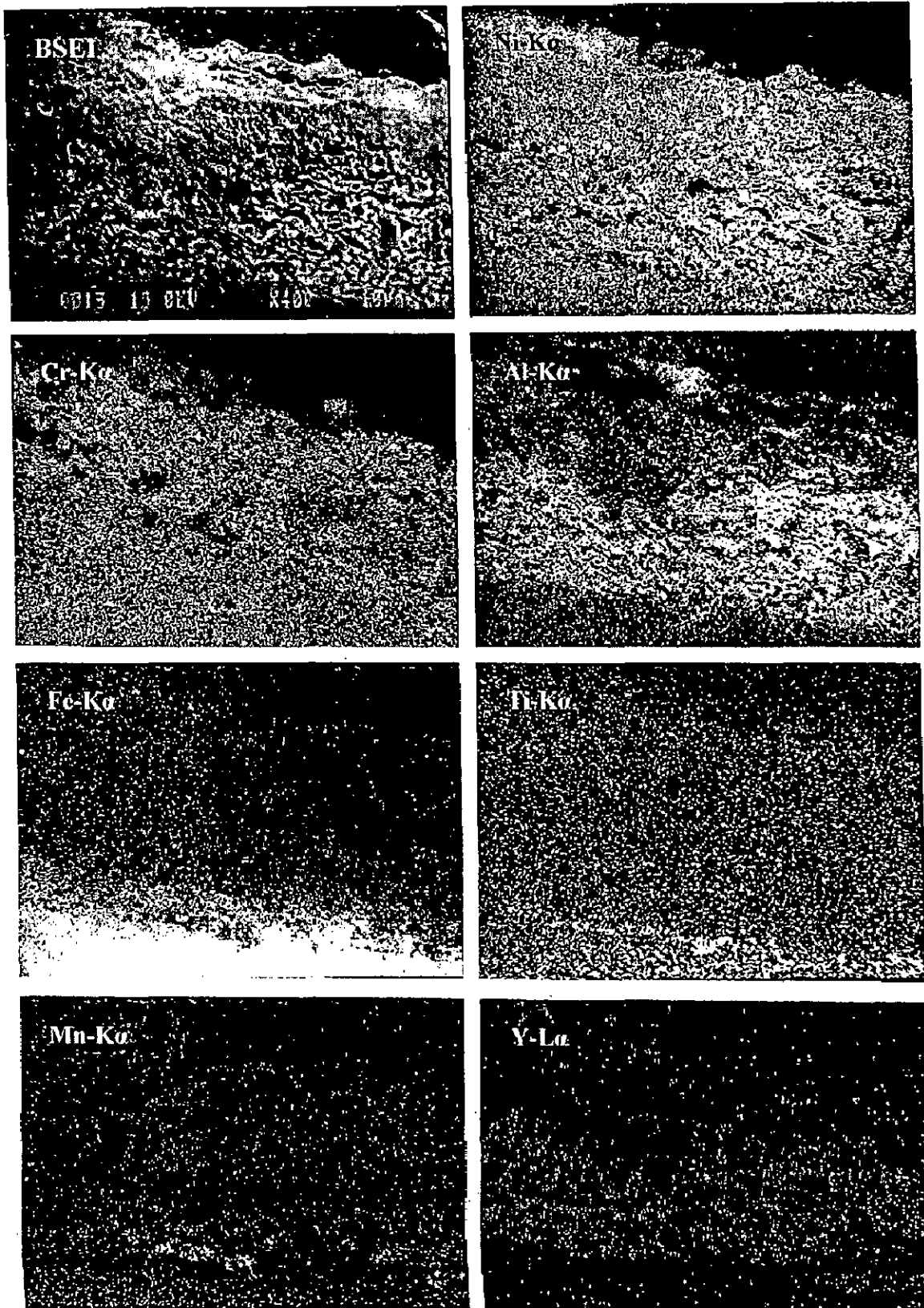


Fig. 5.41 BSEI and X-ray mappings of the cross-section of Ni-20Cr coated superalloy Superfer 800H subjected to cyclic oxidation at 900°C in air after 50 cycles:

## 5.1.4 Ni<sub>3</sub>Al Coating

### 5.1.4.1 Visual Examination

The plasma spray Ni<sub>3</sub>Al coated superalloys have shown the development of a dull green scale when subjected to cyclic oxidation for 50 cycles at 900<sup>o</sup> (Fig. 5.42). Overall the scale was smooth without cracks, with no tendency of spalling during the course of study. The coating was found to be successful in maintaining its contact to the substrate superalloys during the cyclic oxidation studies in general, although it suffered minor spallation along or near the edges of the specimens (Section 5.1.2.1), which was observed to be insignificant. This spalling tendency stopped towards the end of 50 cycles in all the cases except Superni 601, in which it stopped by 32<sup>nd</sup> cycle. Further, the relative extent of this minor spalling was observed to be least in case of Superfer 800H, where it was confined to only one edge of the specimen.

### 5.1.4.2 Thermogravimetric Data

Weight gain/area data for all the Ni<sub>3</sub>Al coated superalloys subjected to cyclic oxidation is plotted against number of cycles in Fig. 5.43. It can be inferred from the plots that all the coated superalloys showed an initial high rate of oxidation followed by a constant rate. The cumulative weight gains after 50 cycles of oxidation are found to be 11.31, 11.58, 11.51, 11.82 and 8.30 mg/cm<sup>2</sup> for the coated superalloys Superni 75, 600, 601, 718 and Superfer 800H respectively. When these data are compared with the data obtained for the oxidised base superalloys, the weight gains for the coated superalloys are found to be greater than those for the corresponding base superalloys. Further, it is evident that the oxidation weight gain data for all the coated Ni-base superalloys are almost same and the values are greater than that for the Fe-base superalloy. The (weight gain/unit area)<sup>2</sup> versus number of cycles plots (Fig. 5.44) confirm that the parabolic law is followed to a fairly acceptable limit in all the cases. The values of parabolic rate constant, K<sub>p</sub> for coated superalloys are evaluated as 4.81, 5.01, 4.41, 5.68 and 2.78 x10<sup>-10</sup> g<sup>2</sup> cm<sup>-4</sup> s<sup>-1</sup> for Superni 75, 600, 601, 718 and Superfer 800H respectively.

### 5.1.4.3 Scale Thickness Measurement

The oxide scale thickness after cyclic oxidation in air at 900<sup>o</sup>C for the superalloys coated with Ni<sub>3</sub>Al was evaluated from the back scattered SEM images shown in Fig. 5.45 and Fig. 5.49. The values are 261, 255, 248, 256 and 252 μm for Superni 75, 600, 601, 718

and Superfer 800H respectively. It is evident that the scale is approximately of same thickness in all the cases.

#### **5.1.4.4 X-ray Diffraction Analysis**

X-ray diffractograms for the plasma spray Ni<sub>3</sub>Al coated superalloys after cyclic oxidation of 50 cycles in air at 900<sup>0</sup>C are shown in Fig. 5.46 on reduced scales, which indicate the formation of phases like nickel oxide (NiO) and aluminum oxide (Al<sub>2</sub>O<sub>3</sub>) alongwith a spinel NiAl<sub>2</sub>O<sub>4</sub> in oxide scales for all the cases.

#### **5.1.4.5 SEM/EDAX Analysis**

##### **(a) Surface Morphology**

SEM/EDAX analysis for all the coated superalloys as given in Fig. 5.47 and Fig. 5.48 indicates that top scale is mainly nickel oxide (white phase) and the structure of the scale is massive, in general. In the sub scale (black phase), which can be the spalled region in the scales of the coated Superni 75 and Superni 600, amount of NiO has decreased and that of Al<sub>2</sub>O<sub>3</sub> increased. A dense uniform scale is seen in the case of oxidised coated Superni 601, which shows no indication of cracking and spalling and is only containing NiO. Further in case of coated Superni 718, the scale is massive and again contains mainly nickel oxide, but there is a spot containing large amount of silica (83%), point 2 in Fig. 5.48 (a) and other constituents, which may diffuse from the substrate. This might be attributed to the ingress of oxygen through porosity in the coating and subsequent oxidation of intermetallics from the base alloy. The scale again is mainly nickel oxide in the case of oxidised Ni<sub>3</sub>Al coated Superfer 800H, which is a dense scale, Fig. 5.48 (b).

##### **(b) Cross-Sectional Analysis**

BSEI micrograph and elemental variation across the cross-section for coated Superni 75 superalloy after cyclic oxidation in air at 900<sup>0</sup>C has been shown in Fig. 5.49 (a). Upper portion of the scale has a massive structure with a lamellar crack just below the top surface. The top layer of the scale is rich in aluminium oxide and also contains some amount of nickel and chromium. As we go below this layer, scale is rich in Ni, containing small amount of Al, point 5 in Fig. 5.49 (a). The scale has retained the lamellar structure of its bond coat, where the splats containing mainly nickel (point 2) are present, with aluminium and oxygen at the splat boundaries.



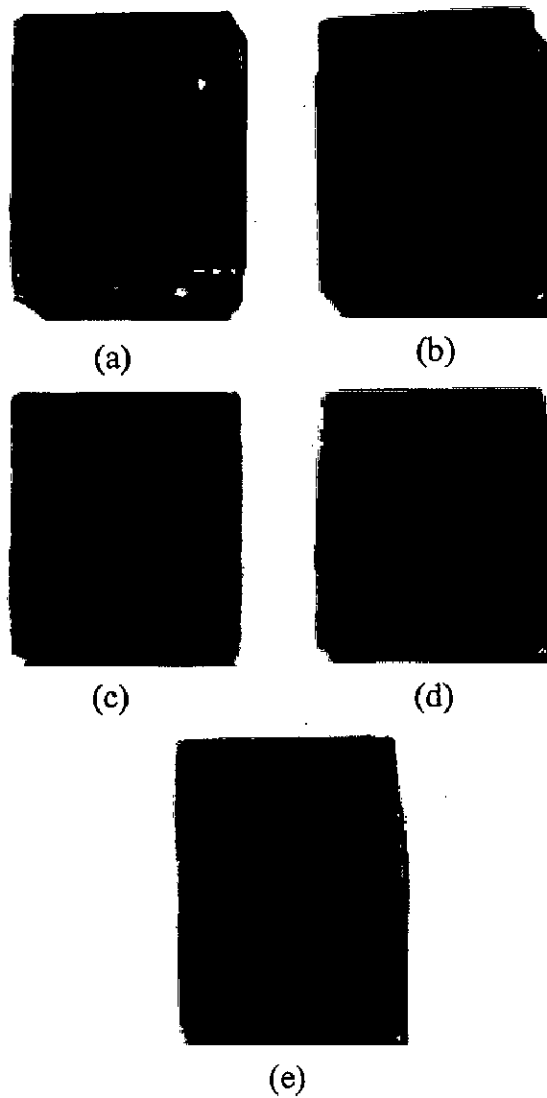


**Fig. 5.42** Macrographs of the  $\text{Ni}_3\text{Al}$  coating with bond coat subjected to cyclic oxidation in air at  $900^\circ\text{C}$  for 50 cycles having substrate superalloys  
(a) Superni 75      (b) Superni 600      (c) Superni 601  
(d) Superni 718      (e) Superfer 800H.

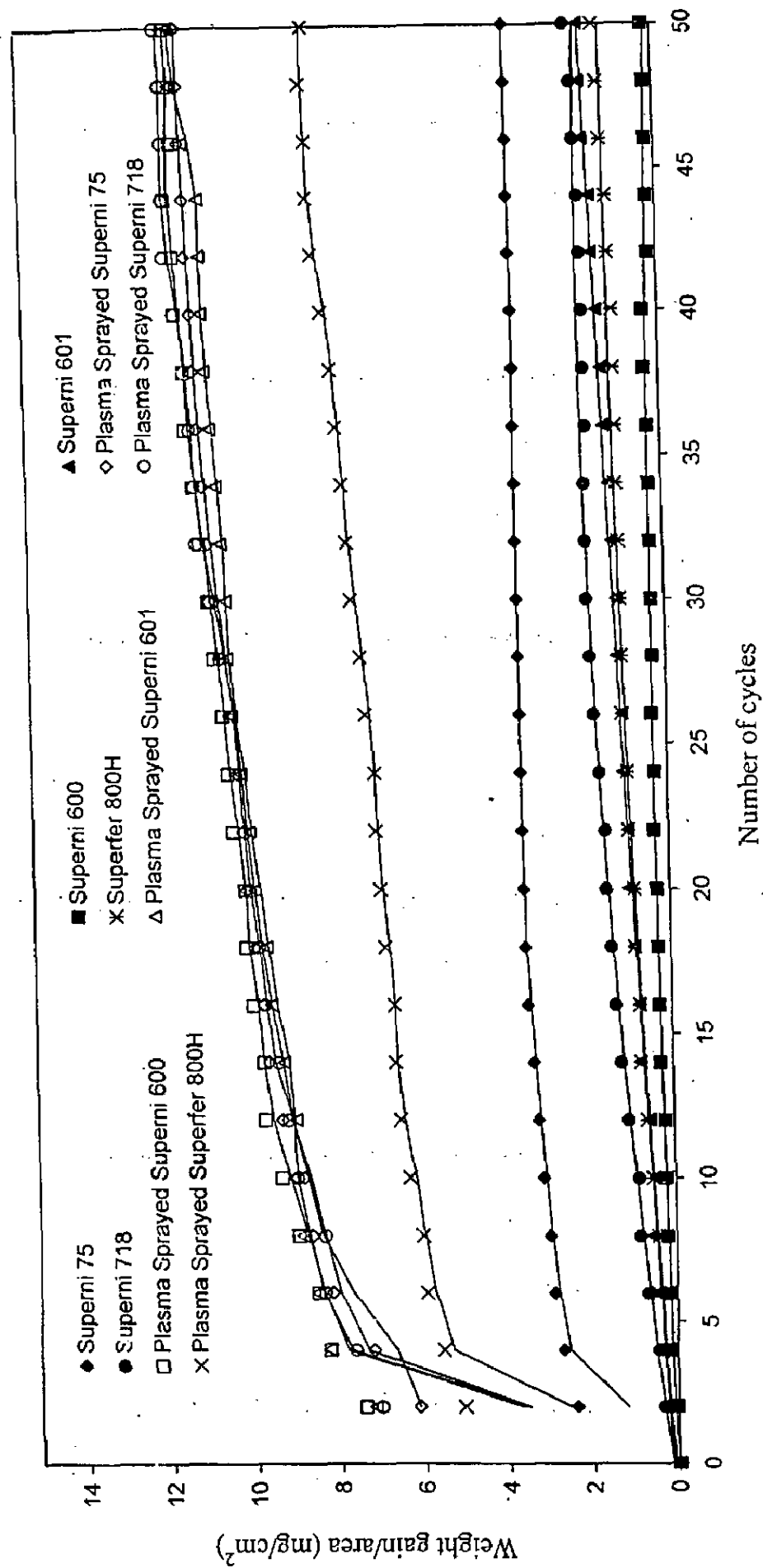


Fig. 5.43 Weight gain vs. number of cycles plots for uncoated and Ni<sub>3</sub>Al coated superalloys subjected to cyclic oxidation for 50 cycles in air at 900°C.

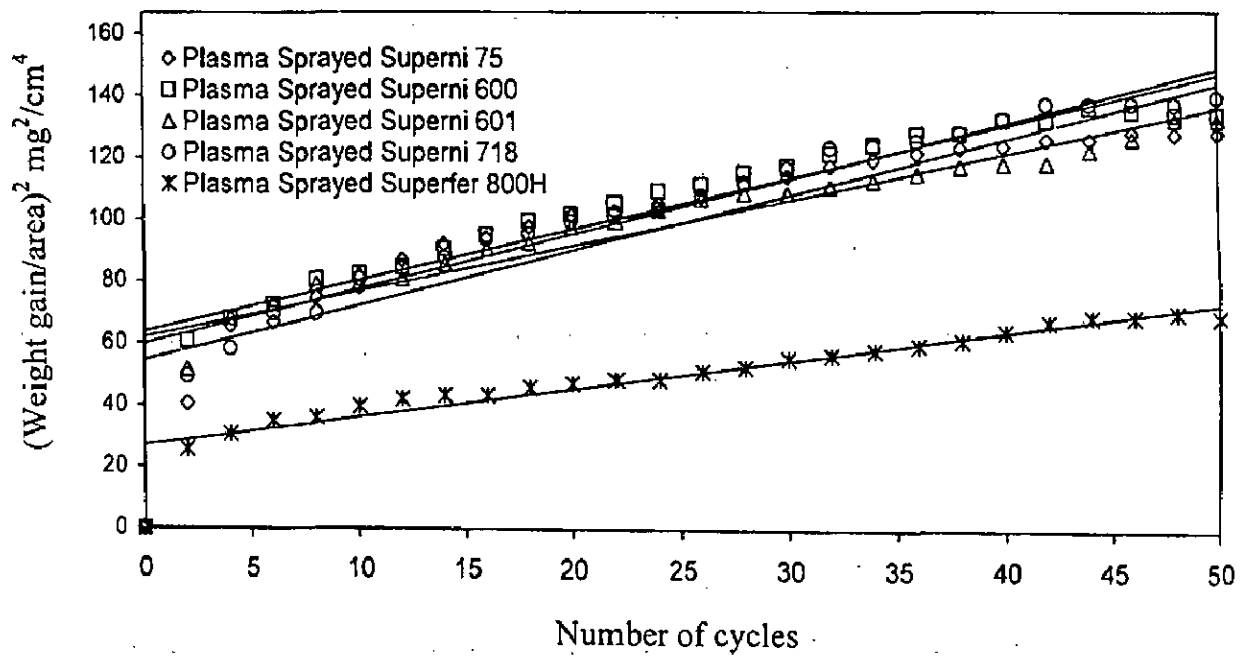
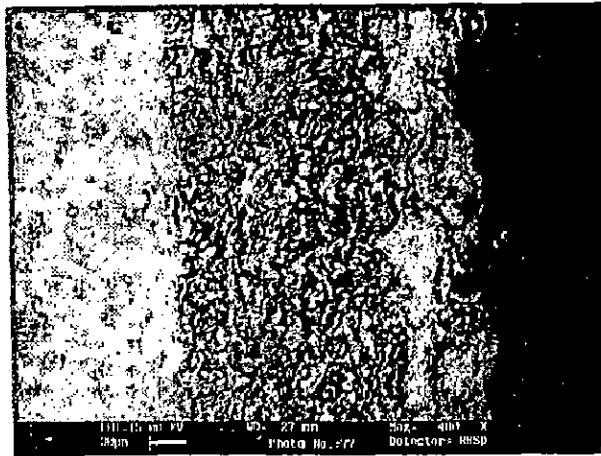
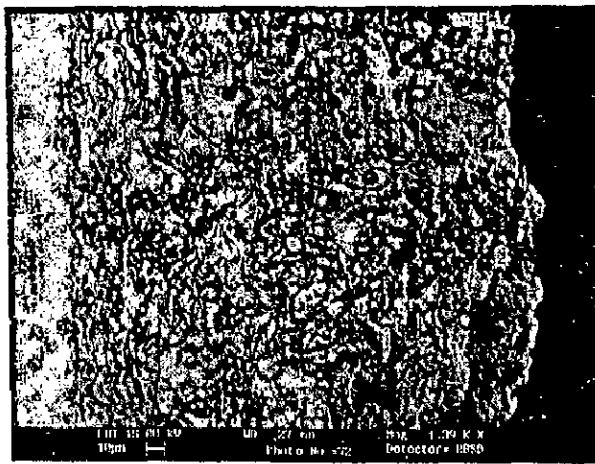


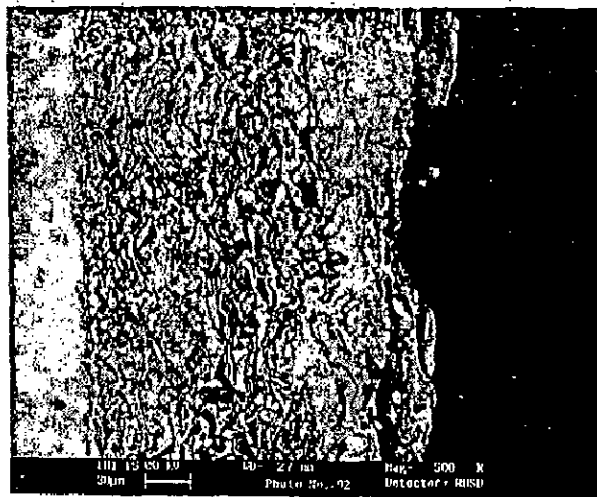
Fig. 5.44  $(\text{Weight gain/area})^2$  vs. number of cycles plots for the  $\text{Ni}_3\text{Al}$  coated superalloys subjected to cyclic oxidation for 50 cycles in air at  $900^\circ\text{C}$ .



(a)



(b)



(c)

Fig. 5.45 SEM back scattered images for the Ni<sub>3</sub>Al coated superalloys after cyclic oxidation in air for 50 cycles at 900<sup>o</sup>C  
(a) Superni 600 (b) Superni 601 (c) Superni 718.

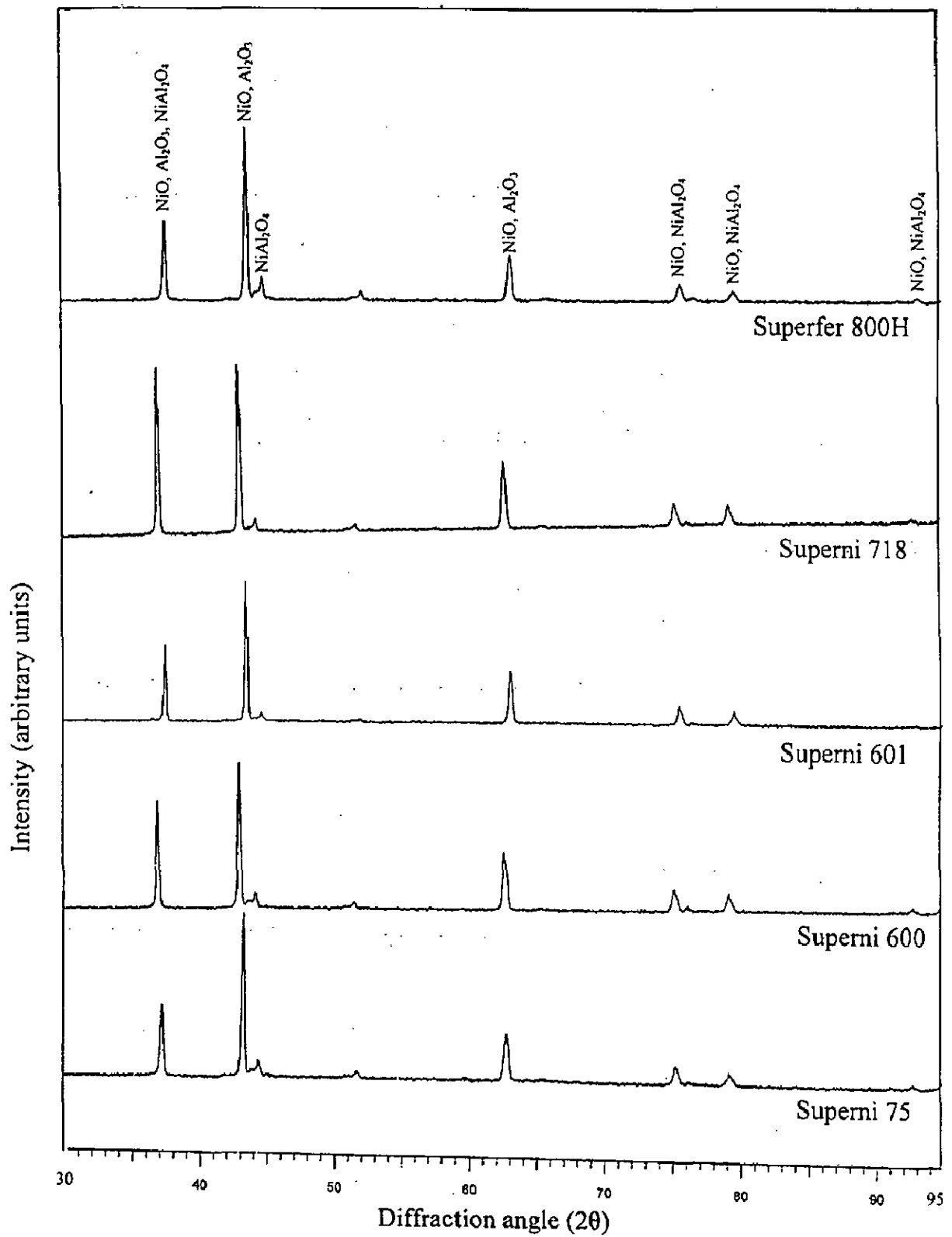
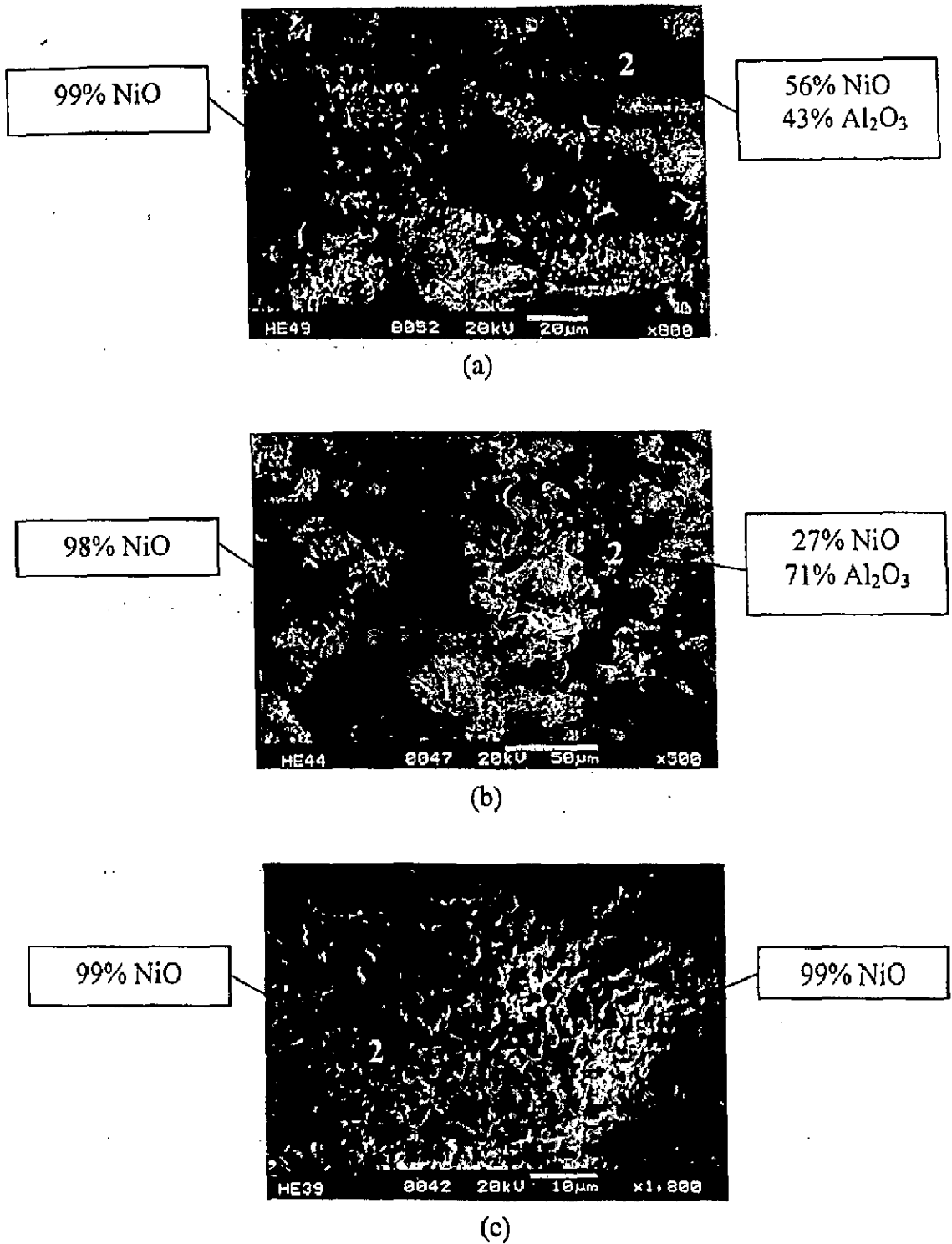
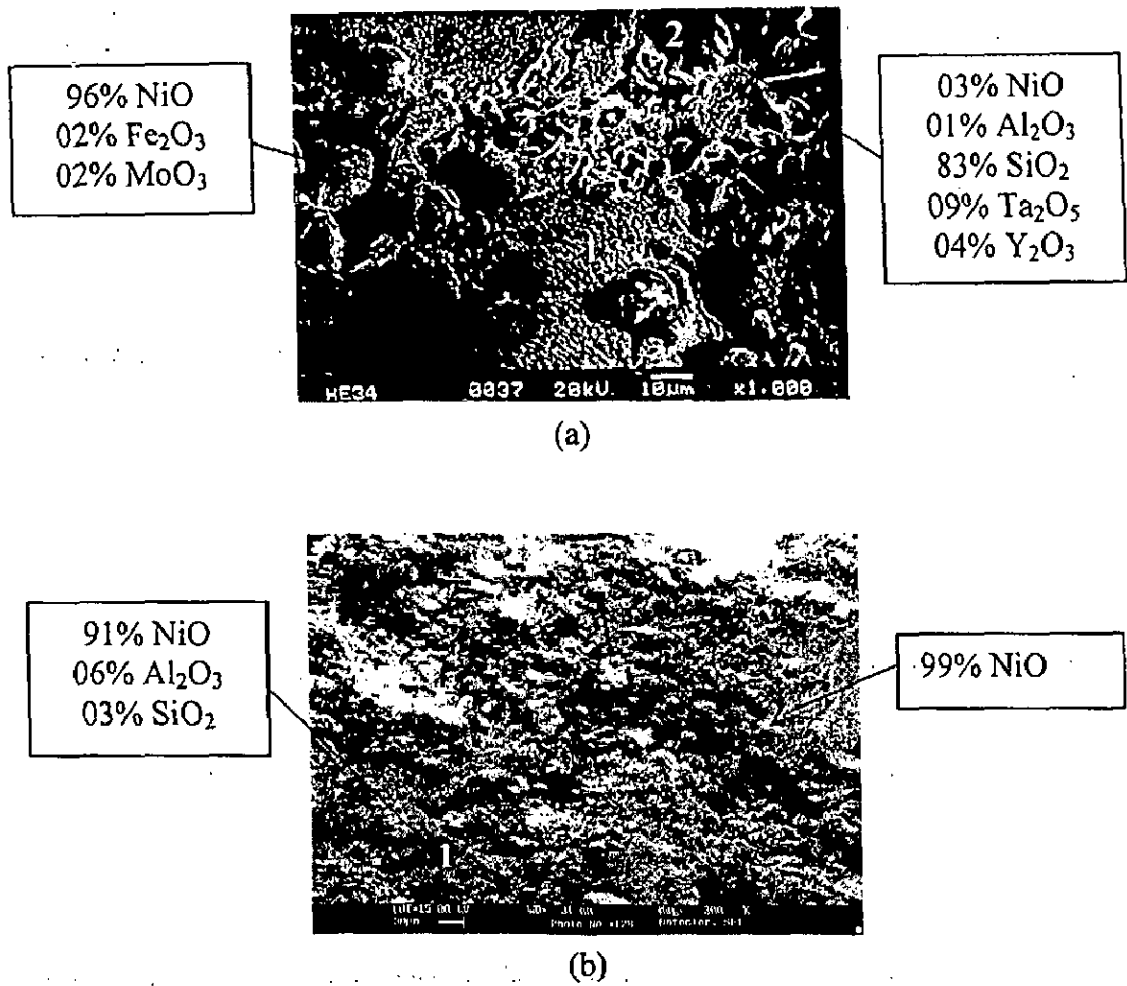


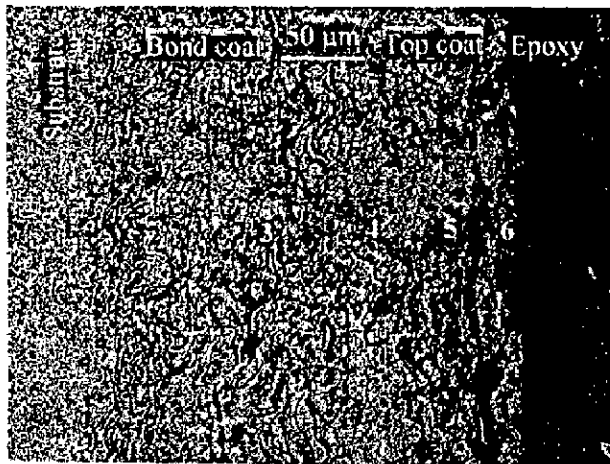
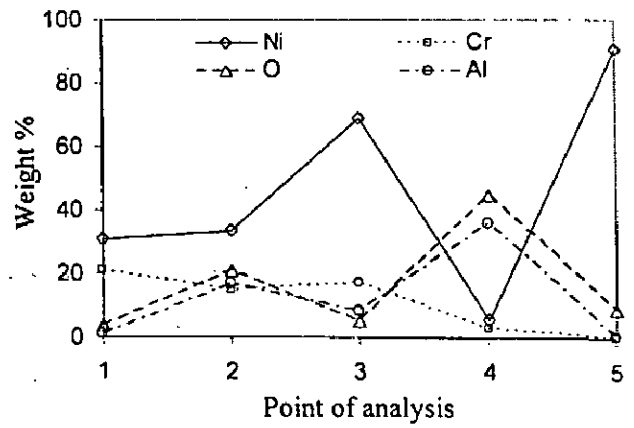
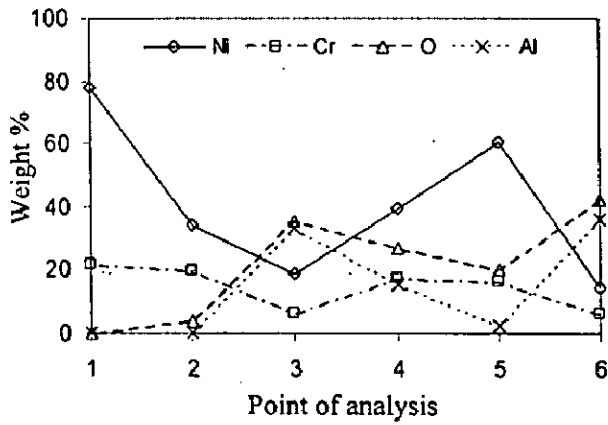
Fig. 5.46 X-ray diffraction patterns for the Ni<sub>3</sub>Al coated superalloys subjected to cyclic oxidation in air at 900°C after 50 cycles.



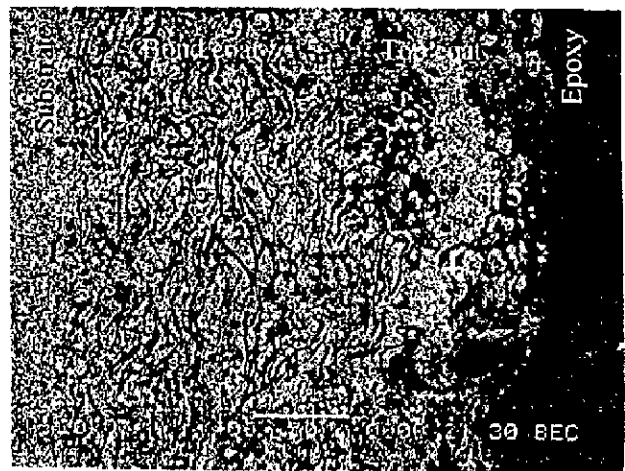
**Fig. 5.47** Surface scale morphology and EDAX analysis for the plasma sprayed  $\text{Ni}_3\text{Al}$  coated superalloys subjected to cyclic oxidation in air at  $900^\circ\text{C}$  for 50 cycles  
 (a) Superni 75                      (b) Superni 600                      (c) Superni 601.



**Fig. 5.48** Surface scale morphology and EDAX analysis for the plasma sprayed  $\text{Ni}_3\text{Al}$  coated superalloys subjected to cyclic oxidation in air at  $900^\circ\text{C}$  for 50 cycles  
 (a) Superni 718      (b) Superfer 800H.



(a)



(b)

**Fig. 5.49** Oxide scale morphology and variation of elemental composition across the cross-section of  $\text{Ni}_3\text{Al}$  coated superalloys subjected to cyclic oxidation at  $900^\circ\text{C}$  in air after 50 cycles  
 (a) Superni 75 (b) Superfer 800H.



The oxide scale morphology indicated in Fig. 5.49 (b) for the coated and oxidised Superfer 800H shows two distinct layers; the outer layer is massive whereas the inner one has lamellar structure. Bond coat has retained its identity. The top scale is mainly nickel, whereas inner layers have lamellar structure with alternate layers of mainly Ni and Al. The penetration of oxygen to the substrate is negligible. Some diffusion of chromium can be observed at point 4 from the bond coat.

#### 5.1.4.6 EPMA Analysis

EPMA analysis for the Ni<sub>3</sub>Al coated Superni 75 oxidised for 50 cycles at 900<sup>0</sup>C, Fig. 5.50 reveals an upper sublayer in the oxide scale, which consists mainly of nickel oxide, with some dispersed aluminium oxide at places where former is absent. Under this sublayer, there is an intermediate band which mainly consists of unreacted nickel, and contains some aluminium oxide as well as chromium oxide stringers. This chromium might have diffused from the bond coat. Yttrium has also diffused to this band. Bond coat seems to have retained its lamellar structure, with alternate layers of nickel and aluminium present in it. Chromium is co-existing mainly with nickel, whereas yttrium with aluminium and oxygen in the bond coat. However, chromium has also shown tendency to form a thin continuous streak at the bond coat/substrate interface, and also it has formed some stringers of its oxide along the splat boundaries.

Similar analysis of the coated superalloy Superni 600 given in Fig. 5.51 indicates an oxide scale, the upper layers of which are containing high concentrations of nickel, and at the top of scale some clusters of aluminium co-exist with nickel. There are some places where aluminium is present and Ni is absent. Chromium and yttrium are mainly restricted to bond coat region of the scale, however some Cr streaks are present in the upper layers of the scale. Iron has diffused from the substrate and small clusters are seen at the top of the scale.

BSEI and Elemental X-ray mappings as shown in Fig. 5.52 across the cross-section of oxidised Superni 601 Ni<sub>3</sub>Al coated superalloy exposed to air at 900<sup>0</sup>C indicate formation of two layered scale with different structures, the upper one contains mainly nickel and aluminium, where aluminium seems to have got oxidised and most of the nickel is unreacted. However, some formation of nickel oxide is also indicated particularly in the top most layer of the scale. Chromium and yttrium are present in patches in the upper region of the scale, indicating their diffusion from the bond coat. Bond coat consists mainly of nickel rich splats, circumscribed by aluminium, yttrium and oxygen containing

boundaries. There is a Cr rich band just above the base superalloy, which is accompanied by Cr depleted thin layer in the alloy substrate. Iron has shown some diffusion to the scale, which is prominent near the bond coat and superalloy interface.

EPMA analysis for the coated Superni 718 after 50 cycles of oxidation at 900°C, Fig. 5.53 shows a massive upper region in the scale and the bond coat has retained its structure. The top scale mainly consists of Ni, with some presence of clusters of Fe and Cr in its outer layers. Aluminium stringers are also visible in this top scale. There is a chromium rich middle scale, containing Ni and Al. Further, Al, Y and Fe seem to be distributed along the splat boundaries in the bond coat region of the scale. Titanium and tantalum have indicated diffusion from the base alloy into the scale.

Nickel is revealed as the main constituent of the scale for oxidised Ni<sub>3</sub>Al coated superalloy Superfer 800H, refer Fig. 5.54. The upper scale has some Al-rich pockets, where Ni is present in lower concentrations. Whereas at some other places, where aluminium is present in lower concentrations, Ni is revealed in high amounts. Chromium is mainly confined to the bond coat; however some amount of Cr is present in the upper layer of the scale. Iron has also diffused from the substrate to the top scale. Manganese and titanium are concentrated along the bond coat/base alloy interface and are also dispersed throughout the scale cross-section perhaps along the splat boundaries alongwith Al and Y. Silicon is also visible in the form of small clusters in the outer layers of the scale.

## **5.1.5 Stellite-6 Coating**

### **5.1.5.1 Visual Examination**

A dark grey scale was noticed in case of all the plasma spray Stellite-6 coated superalloys, when exposed to cyclic oxidation in air at 900°C for 50 cycles are shown in Fig. 5.55. With the progress of study the originally grey colour oxide scale became darker gradually. The surface contact of this coating with all the substrate superalloys was found to be excellent, best among all the coatings studied under cyclic oxidation conditions. No superficial cracking or spalling of the oxide scale or coating took place in case of Stellite-6 coated Superni 75, 600 and 718 superalloys. Whereas little tendency towards minor cracking of the coating near the edges was noticed in case of Superni 601 and Superfer 800H substrates. Two superficial cracks were seen initiating from two different edges in the coating of Superni 601, one from the end of 7<sup>th</sup> cycle and second from 21<sup>st</sup> cycle.

Similar phenomenon of initiation of two minor superficial cracks from the edges was observed in case of Superfer 800H substrate, the starting cycles being 22<sup>nd</sup> and 31<sup>st</sup>. Little growth in the length and width of these cracks could be seen with the progress of study, which did not grow any further after 46<sup>th</sup> cycle.

#### **5.1.5.2 Thermogravimetric Data**

Thermogravimetric measurements taken throughout the 50 cycles are plotted relative to the number of cycles with an aim to understand the kinetics of oxidation. It can be inferred from Fig. 5.56 that the Stellite-6 coating has shown large weight gains in the early cycles of study in general in all the cases. During the subsequent cycles of exposure the weight gain trends have shown the tendency to get stabilized in all the cases. The overall weight gains after 50 cycle of exposure were observed to be 12.07, 10.63, 12.17, 12.78 and 13.04 mg/cm<sup>2</sup> for coated Superni 75, 600, 601, 718 and Superfer 800H respectively. It can be seen that the weight gain values are not very different irrespective of type of the base superalloy. So far as the kinetics of the oxidation is concerned it can be approximated by the parabolic rate law in all the cases, Fig. 5.57. The calculated values of parabolic rate constant ( $K_p$ ) for the Stellite-6 coated Superalloys Superni 75, 600, 601, 718 and Superfer 800H are 4.89, 3.74, 5.32, 5.69 and  $6.40 \times 10^{-10} \text{ g}^2 \text{ cm}^{-4} \text{ s}^{-1}$  respectively.

#### **5.1.5.3 Scale Thickness Measurement**

SEM back scattered images for the Stellite-6 coated superalloys after oxidation in air at 900<sup>o</sup>C for 50 cycles are shown in Figs. 5.58, 5.62 and 5.63. The average values of scale thickness are found to be 519, 554, 638, 603 and 680  $\mu\text{m}$  respectively for the coated Superni 75, 600, 601, 718 and Superfer 800H.

#### **5.1.5.4 X-ray Diffraction Analysis**

X-ray diffraction patterns for the plasma spray Stellite-6 coated superalloys after cyclic oxidation (50 cycles) in air at 900<sup>o</sup>C have been compiled in Fig. 5.59 on a reduced scale. All the coated superalloys have indicated the formation of oxides of cobalt and chromium, and their spinel after oxidation. The main XRD phases identified for the coated superalloys are CoO, CoCr<sub>2</sub>O<sub>4</sub> and Cr<sub>2</sub>O<sub>3</sub>.

### 5.1.5.5 SEM/EDAX Analysis

#### (a) Surface Morphology

SEM/EDAX analysis of the oxide scale developed on the surfaces of Stellite-6 coated superalloys after oxidation for 50 cycles at 900°C has been shown in Fig. 5.60 and Fig. 5.61. The scale for the coated Superni 75 seems to be consisting of large size nodules mainly containing Cr<sub>2</sub>O<sub>3</sub> and CoO, whereas the adjoining area is enriched with Al<sub>2</sub>O<sub>3</sub> and Cr<sub>2</sub>O<sub>3</sub>, which may be a sublayer. For the coated Superni 600 case, the scale is again having nodular structure, which is mainly Cr<sub>2</sub>O<sub>3</sub> with a little amount of CoO. In the regions between the nodules, the amount of Cr<sub>2</sub>O<sub>3</sub> decreases and that of Al<sub>2</sub>O<sub>3</sub> increases and they are in similar amounts. Similarly, in corresponding case of coated Superni 601, nodules are containing mainly Cr<sub>2</sub>O<sub>3</sub> with some CoO and NiO. Whereas in between region of the nodules concentration of Cr<sub>2</sub>O<sub>3</sub> decreases and CoO increases, refer Fig. 5.60 (c). In corresponding case of coated Superni 718 superalloy, nodules are primarily Cr<sub>2</sub>O<sub>3</sub> with good amount of CoO, while inter nodular regions contain mainly Al<sub>2</sub>O<sub>3</sub> with Cr<sub>2</sub>O<sub>3</sub> and oxides of Ta and W. In the scale of oxidised Stellite-6 coated Superfer 800H, the nodules are rich in Cr<sub>2</sub>O<sub>3</sub> and contain substantial amounts of CoO, whereas in inter nodular regions; Al<sub>2</sub>O<sub>3</sub> is again dominating with large percentage of Cr<sub>2</sub>O<sub>3</sub>, Fig. 5.61 (b).

#### (b) Cross-sectional Morphology

Oxide scale morphology and variation of elemental composition across the cross-section of Stellite-6 coated superalloy Superni 75 subjected to cyclic oxidation in air at 900°C after 50 cycles has been shown in Fig. 5.62 (a). The outer layer of the scale is rich in cobalt and chromium with small quantities of tungsten and nickel, but contains very little amount of oxygen at point 5 and 6. This lack of oxygen at point 5 and 6 may be indicative of the fact that Co-rich splats have not got oxidised. The presence of oxygen at points 2 to 6 shows that the whole coating has been penetrated, but there are no signs of internal oxidation of the base alloy. Further, the variation in oxygen content may be attributed to ingress of oxygen across the splat boundaries, both in the top as well as bond coat.

Whereas similar analysis for the coated Superni 601 compiled in Fig. 5.62 (b) shows the outer most layer of the scale (point 6) to be rich in chromium (41%) and oxygen with lesser amounts of cobalt. Whereas at points 4 and 5 where cobalt is present in rich concentrations, oxygen is indicated in small quantities. Tungsten and nickel have also shown their presence in the outer layer of the scale in very small quantities. Absence of oxygen at point 1 indicates that the base superalloy has remained unaffected. Bond coat has retained its identity, and amount of oxygen decreases as one moves into the bond coat.

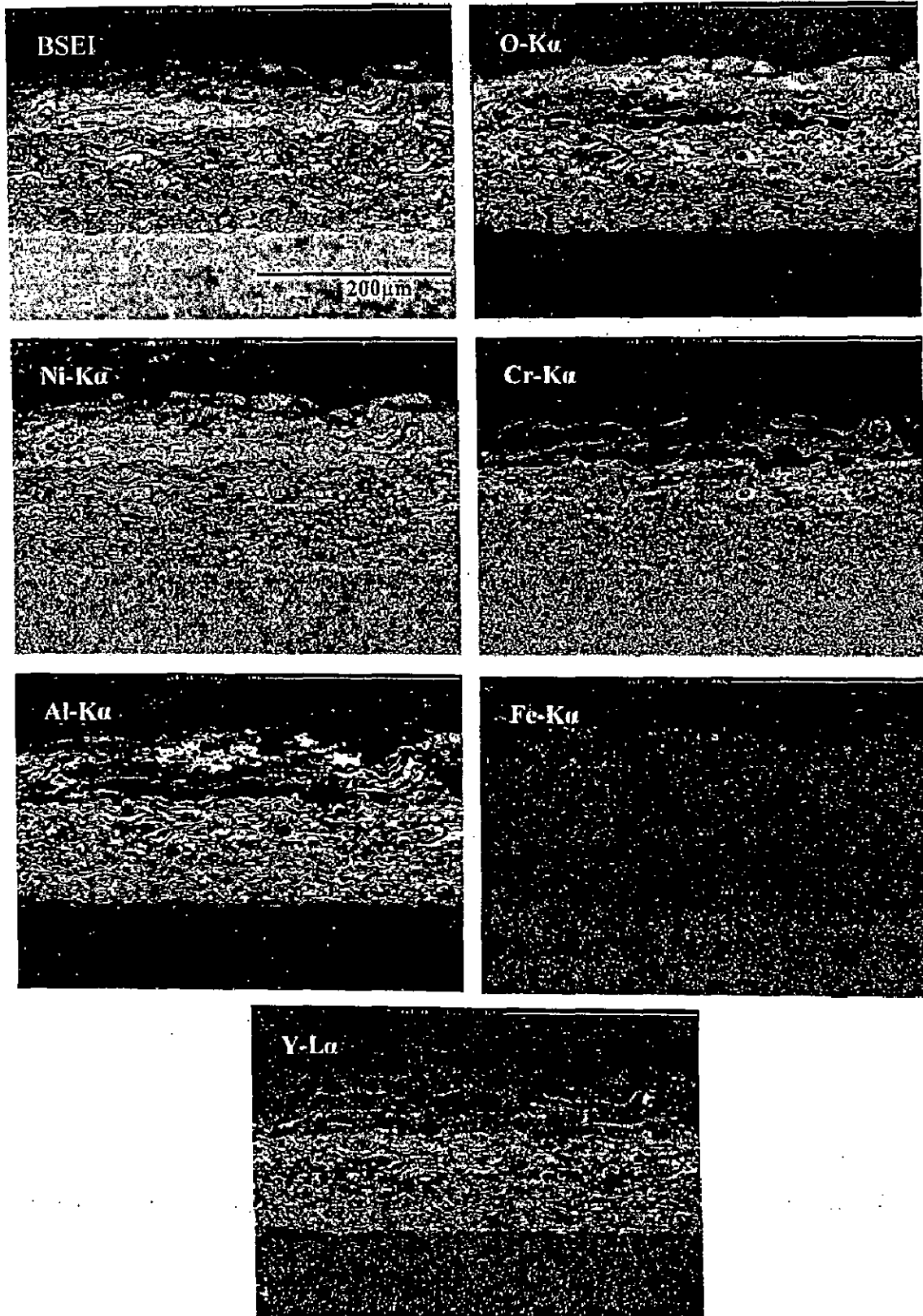
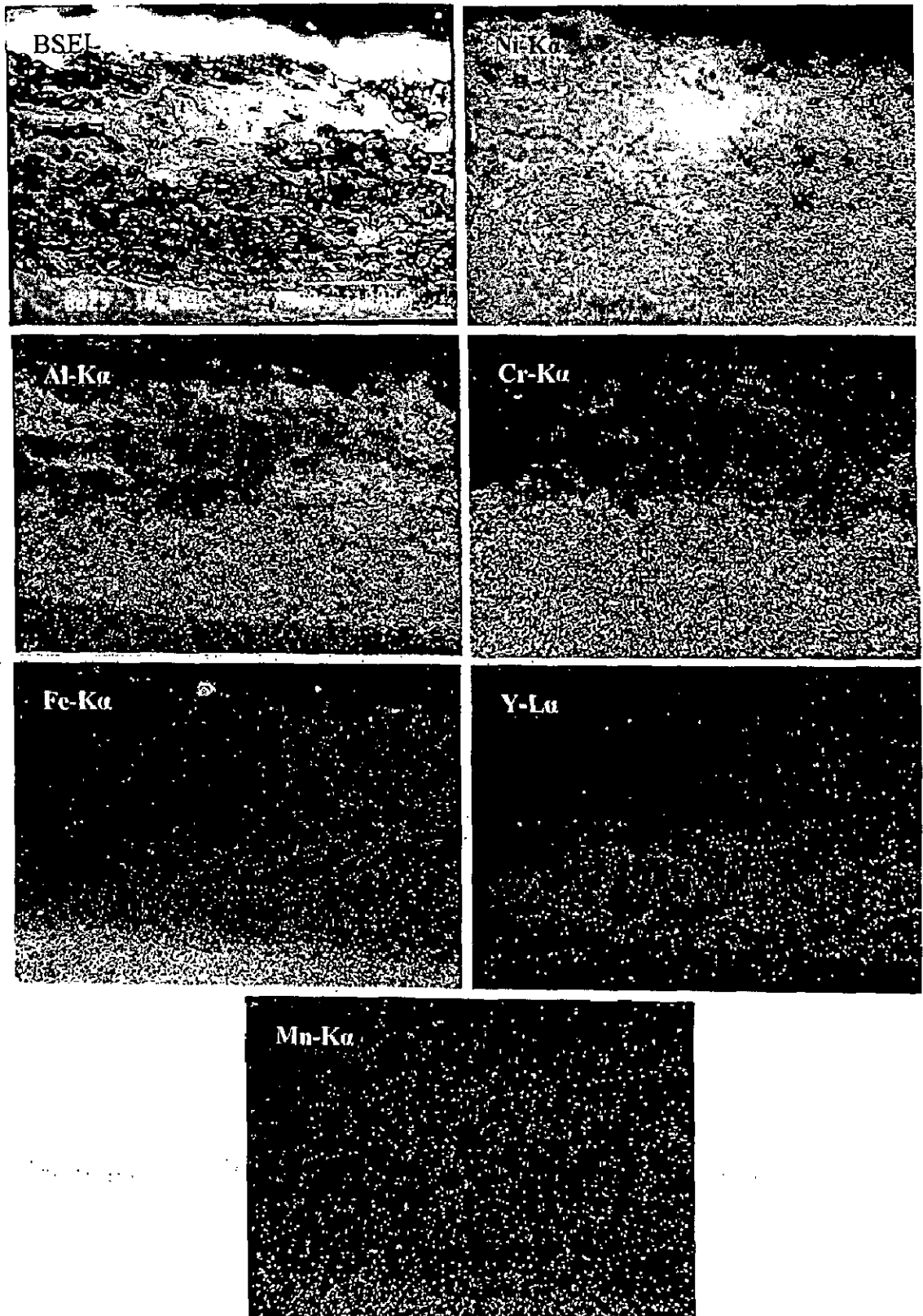
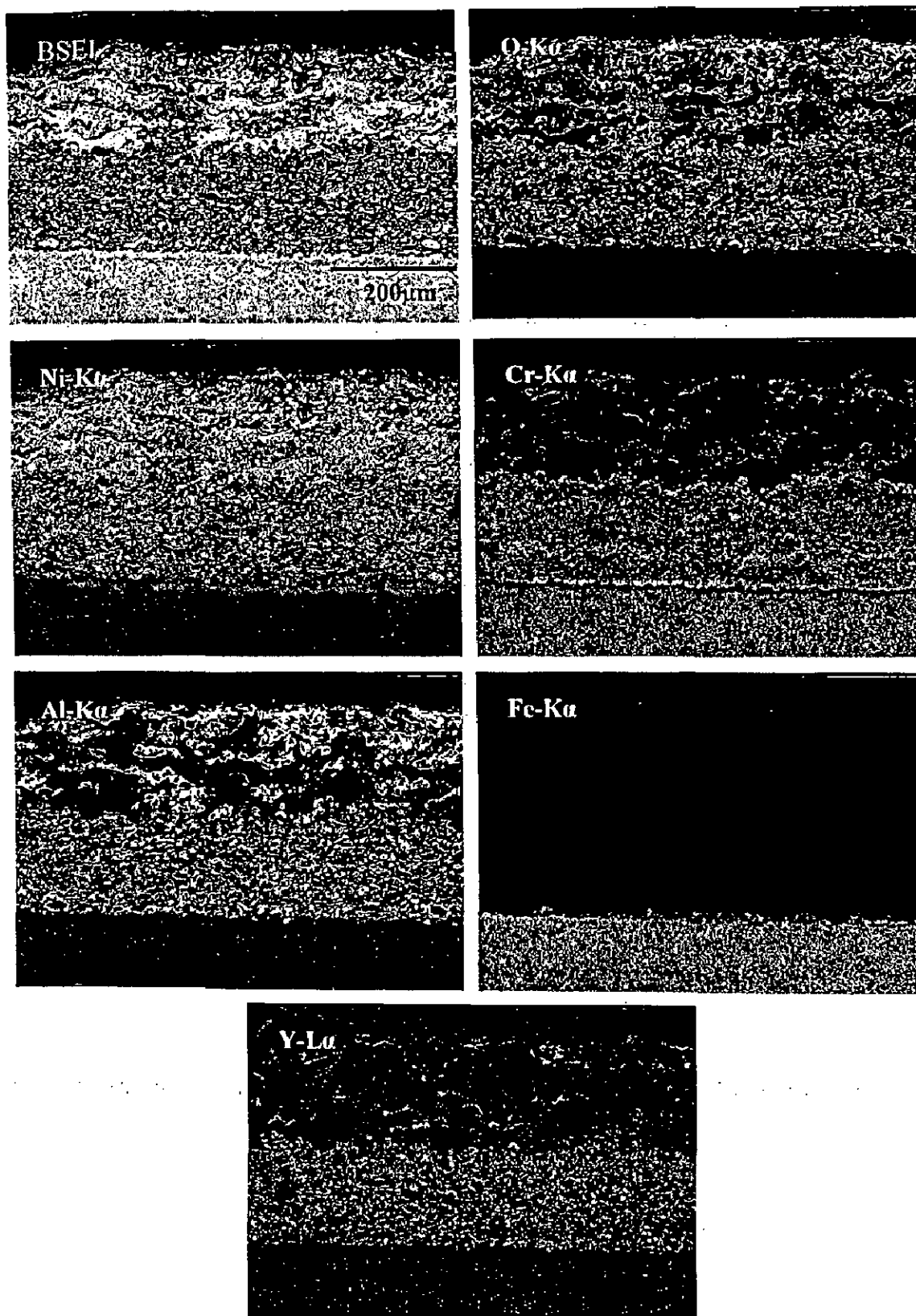


Fig. 5.50 BSEI and X-ray mappings of the cross-section of  $\text{Ni}_3\text{Al}$  coated superalloy Superni 75 subjected to cyclic oxidation at  $900^\circ\text{C}$  in air after 50 cycles.



**Fig. 5.51** BSEI and X-ray mappings of the cross-section of  $\text{Ni}_3\text{Al}$  coated superalloy Superni 600 subjected to cyclic oxidation at  $900^\circ\text{C}$  in air after 50 cycles.



**Fig. 5.52** BSEI and X-ray mappings of the cross-section of  $\text{Ni}_3\text{Al}$  coated superalloy Superni 601 subjected to cyclic oxidation at  $900^\circ\text{C}$  in air after 50 cycles.

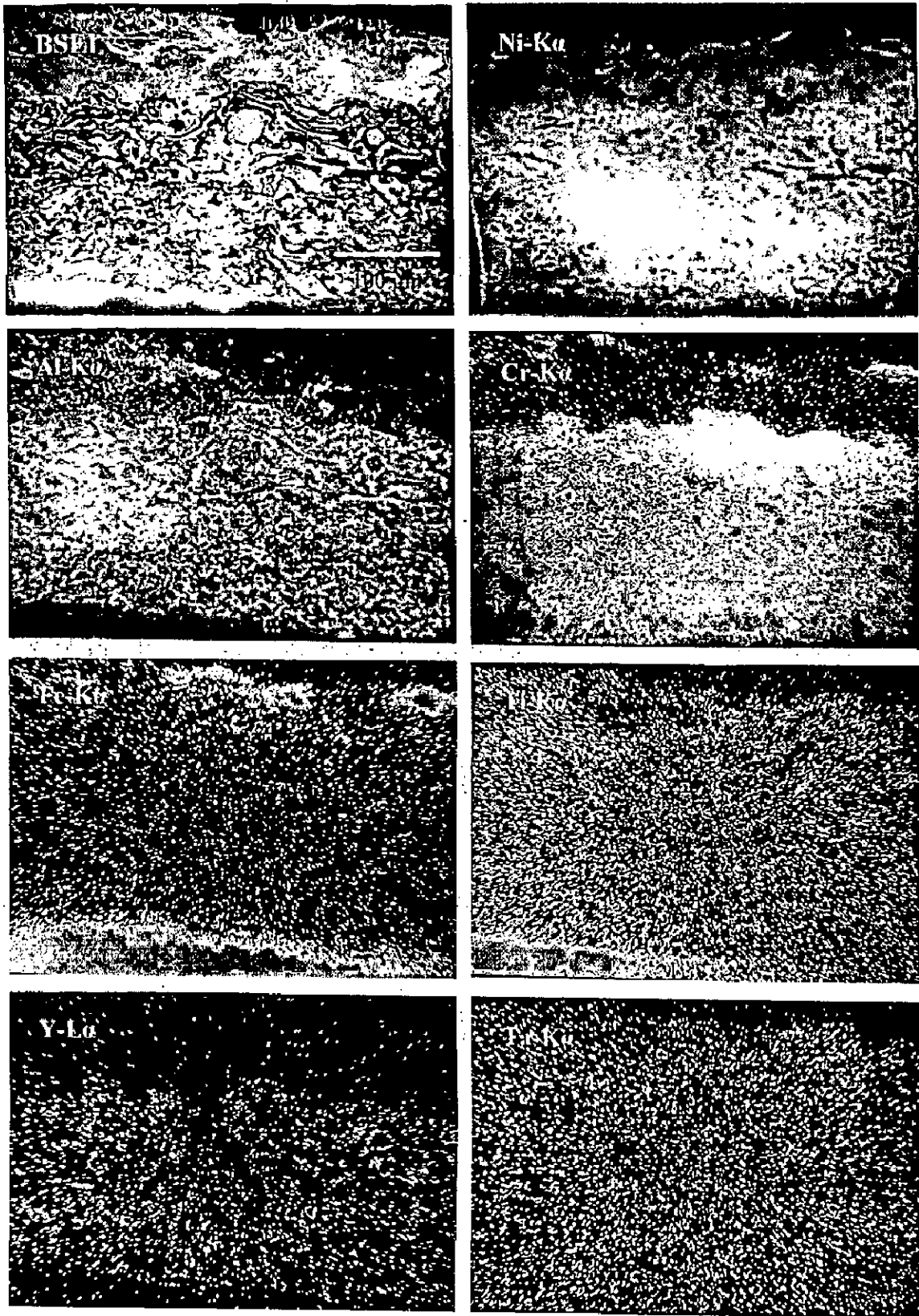
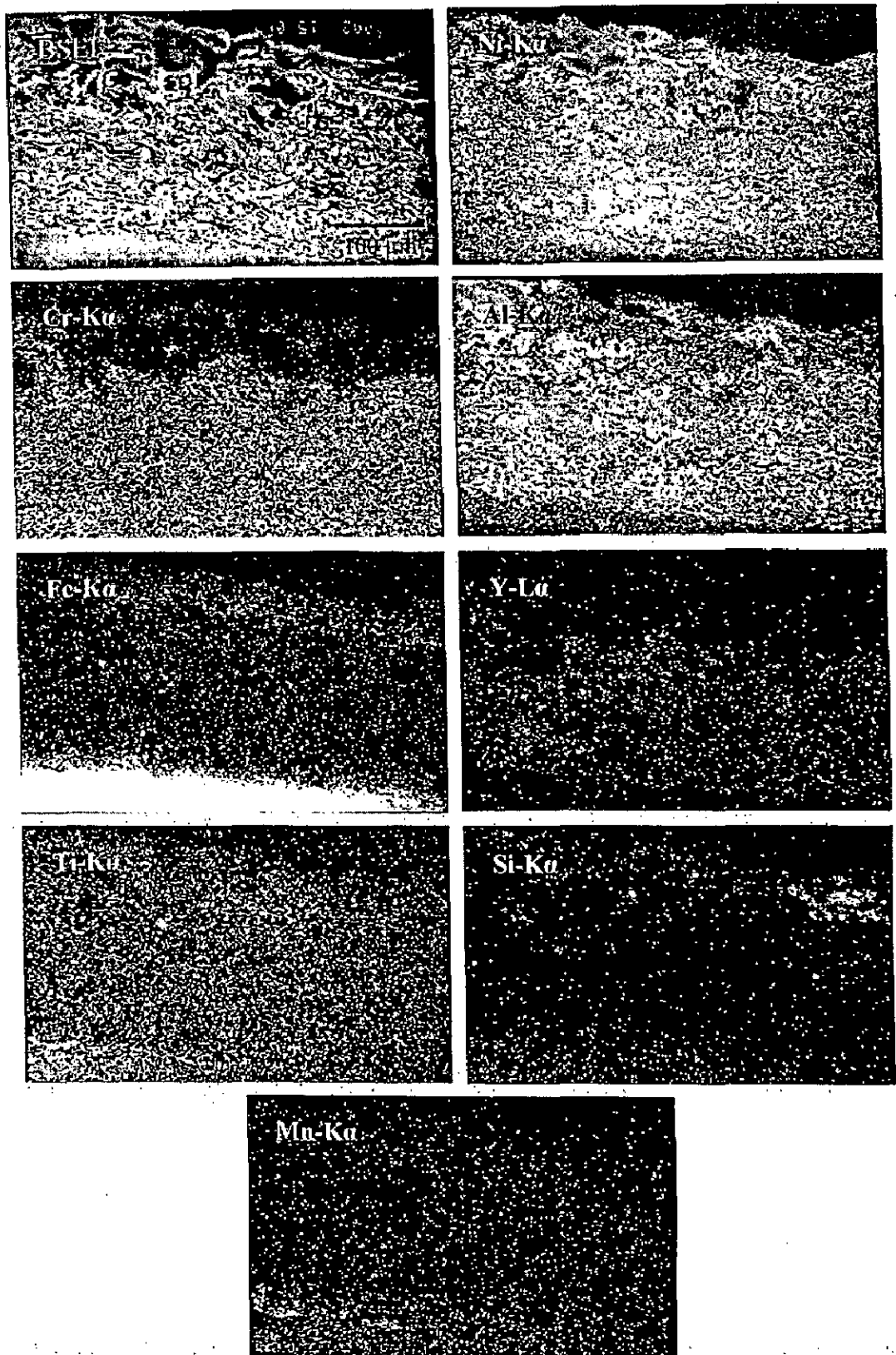
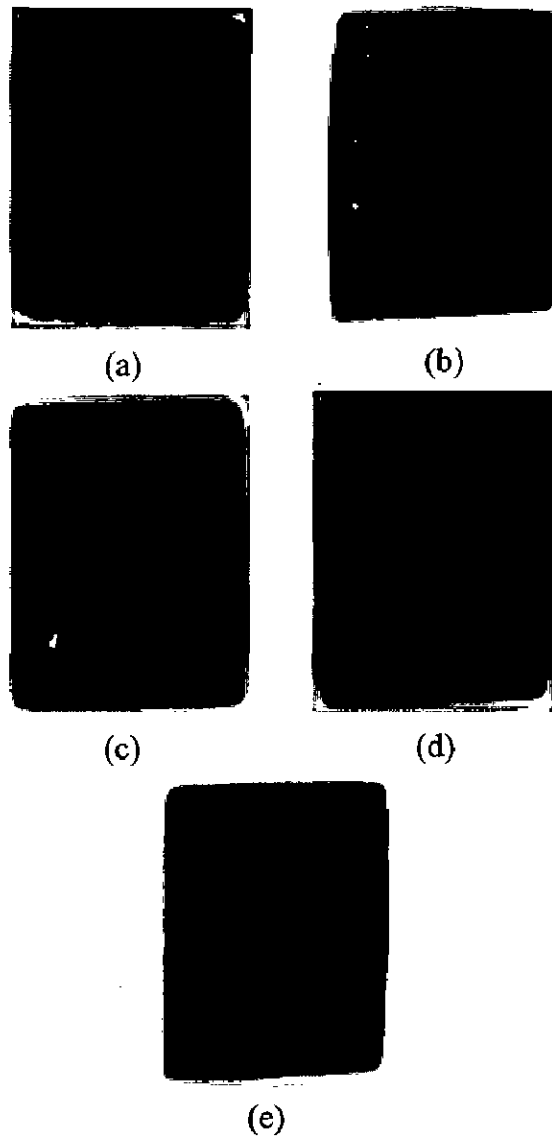


Fig. 5.53 BSEI and X-ray mappings of the cross-section of  $\text{Ni}_3\text{Al}$  coated superalloy Superni 718 subjected to cyclic oxidation at  $900^\circ\text{C}$  in air after 50 cycles.





**Fig. 5.54** BSEI and X-ray mappings of the cross-section of Ni<sub>3</sub>Al coated superalloy Superfer 800H subjected to cyclic oxidation at 900°C in air after 50 cycles.



**Fig. 5.55** Macrographs of the Stellite-6 coating with bond coat subjected to cyclic oxidation in air at 900°C for 50 cycles having substrate superalloys  
(a) Superni 75      (b) Superni 600      (c) Superni 601  
(d) Superni 718      (e) Superfer 800H.

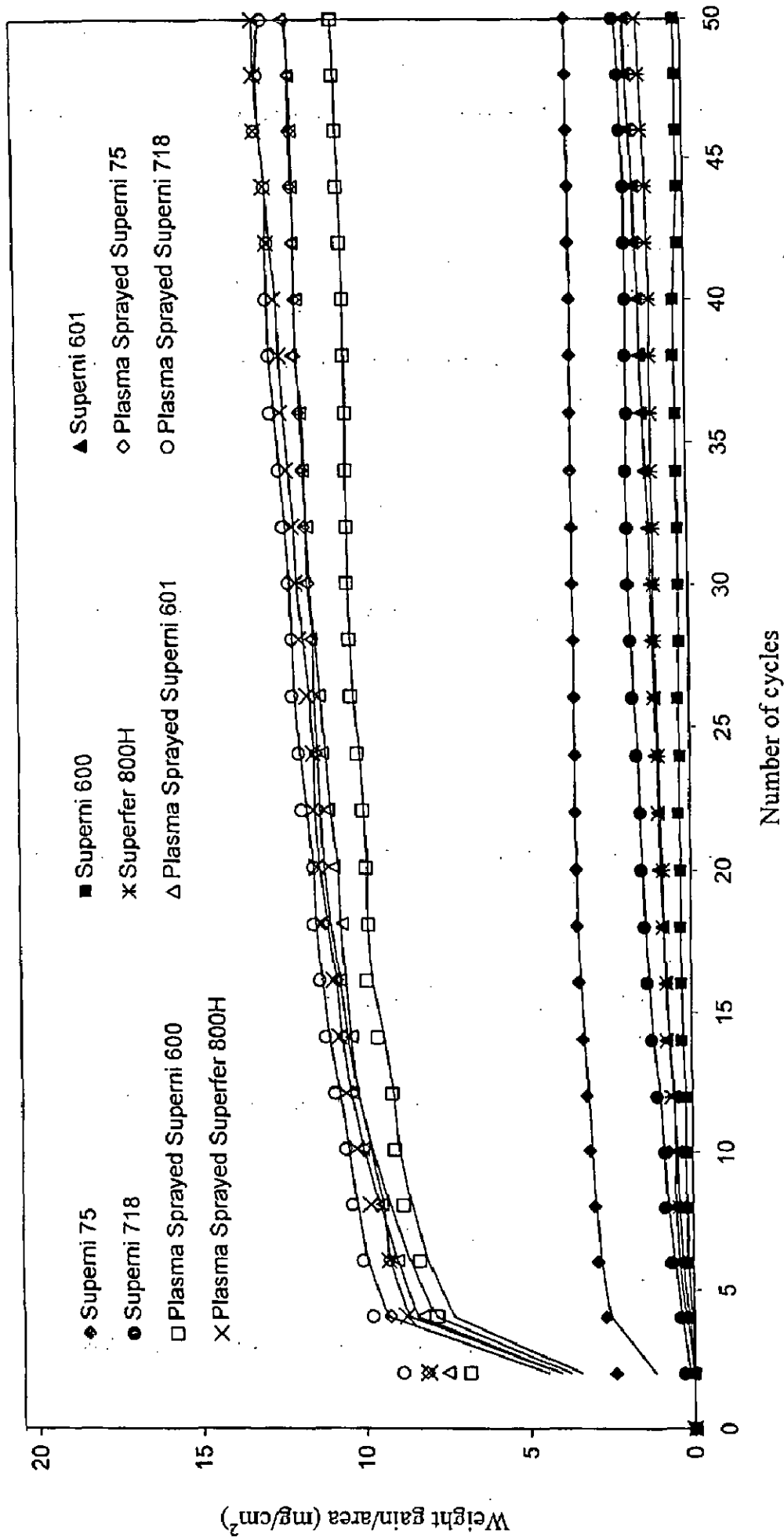


Fig. 5.56 Weight gain vs. number of cycles plot for uncoated and Stellite-6 coated superalloys subjected to cyclic oxidation for 50 cycles in air at 900°C.

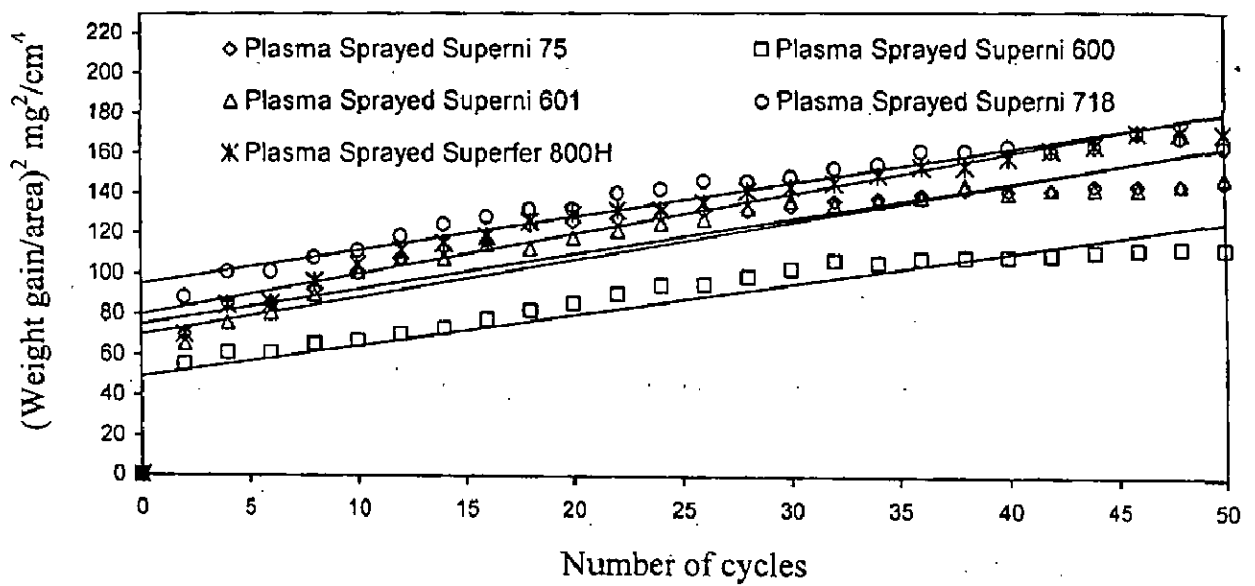
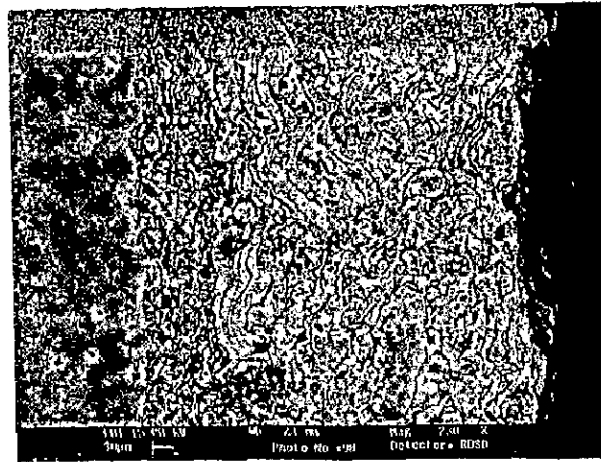
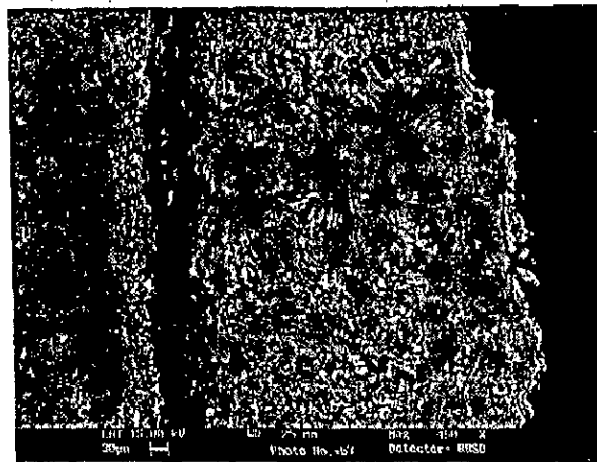


Fig. 5.57  $(\text{Weight gain/area})^2$  vs. number of cycles plots for the Stellite-6 coated superalloys subjected to cyclic oxidation for 50 cycles in air at  $900^\circ\text{C}$ .



(a)



(b)

**Fig. 5.58** SEM back scattered images for the Stellite-6 coated superalloys after cyclic oxidation in air for 50 cycles at 900°C  
(a) Superni 600      (b) Superfer 800H.

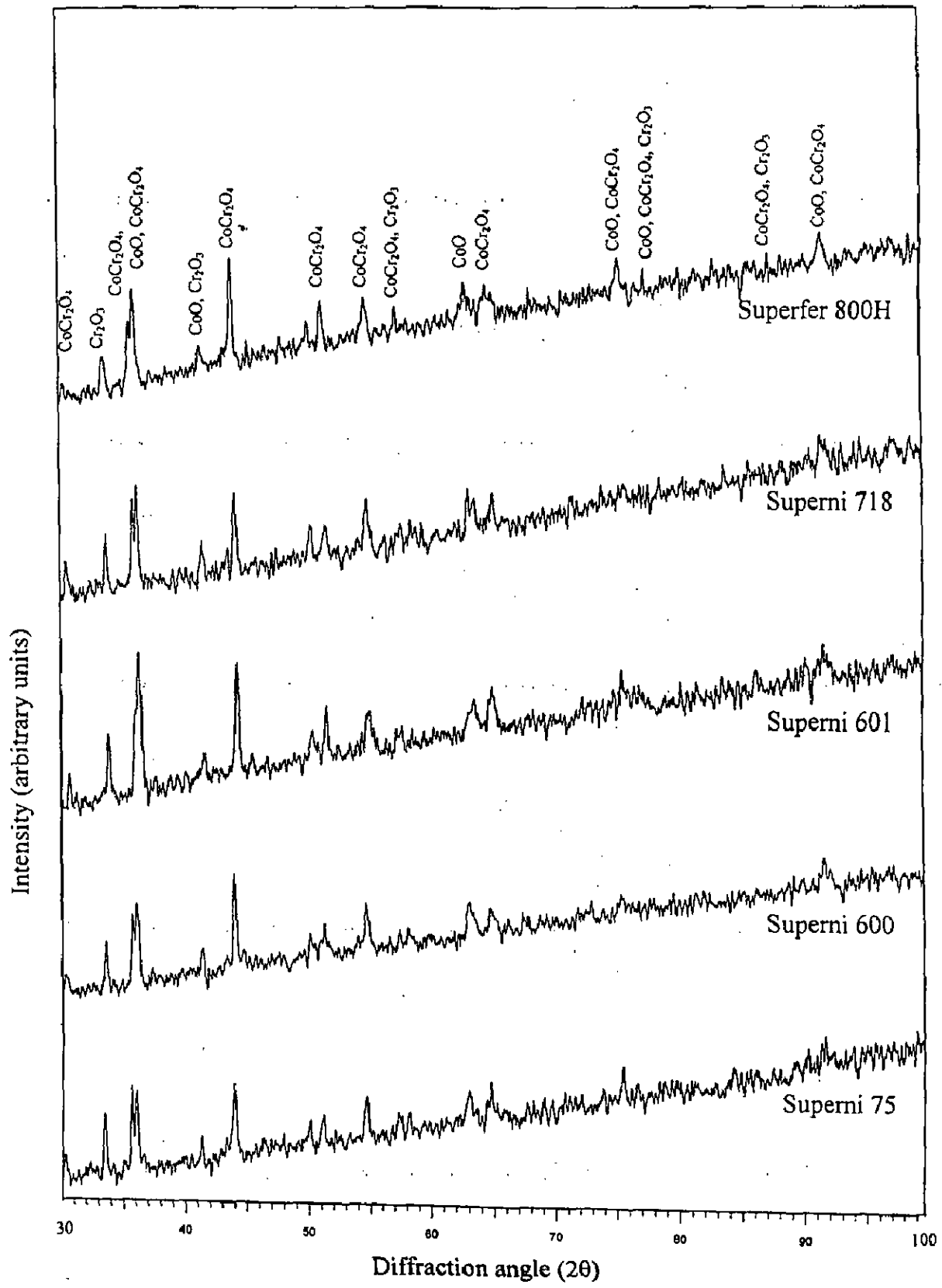


**Fig. 5.59** X-ray diffraction patterns for the Stellite-6 coated superalloys subjected to cyclic oxidation in air at 900°C after 50 cycles.

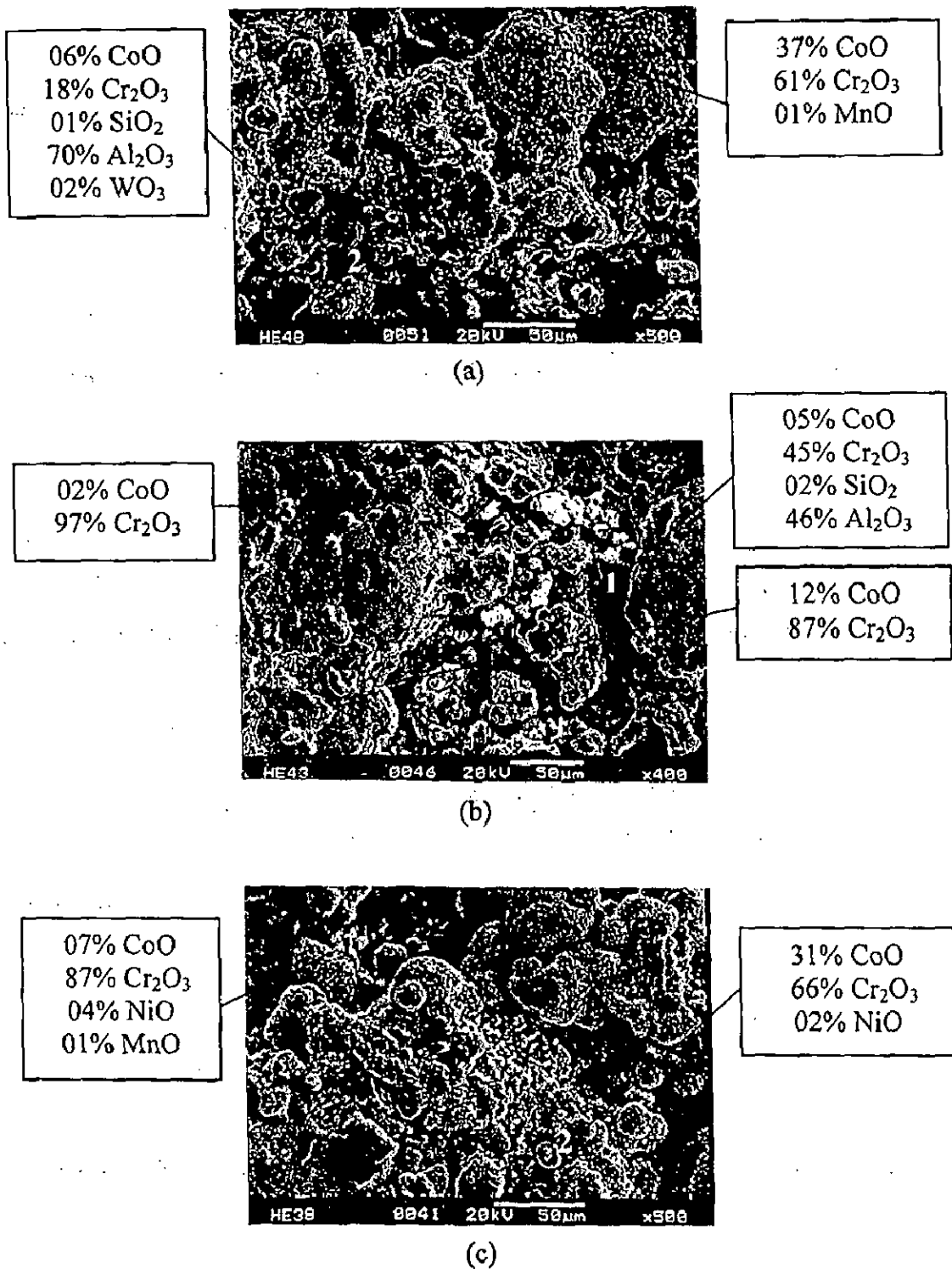


**Fig. 5.60** Surface scale morphology and EDAX analysis for the plasma sprayed Stellite-6 coated superalloys subjected to cyclic oxidation in air at 900°C for 50 cycles  
 (a) Superni 75 (b) Superni 600 (c) Superni 601.

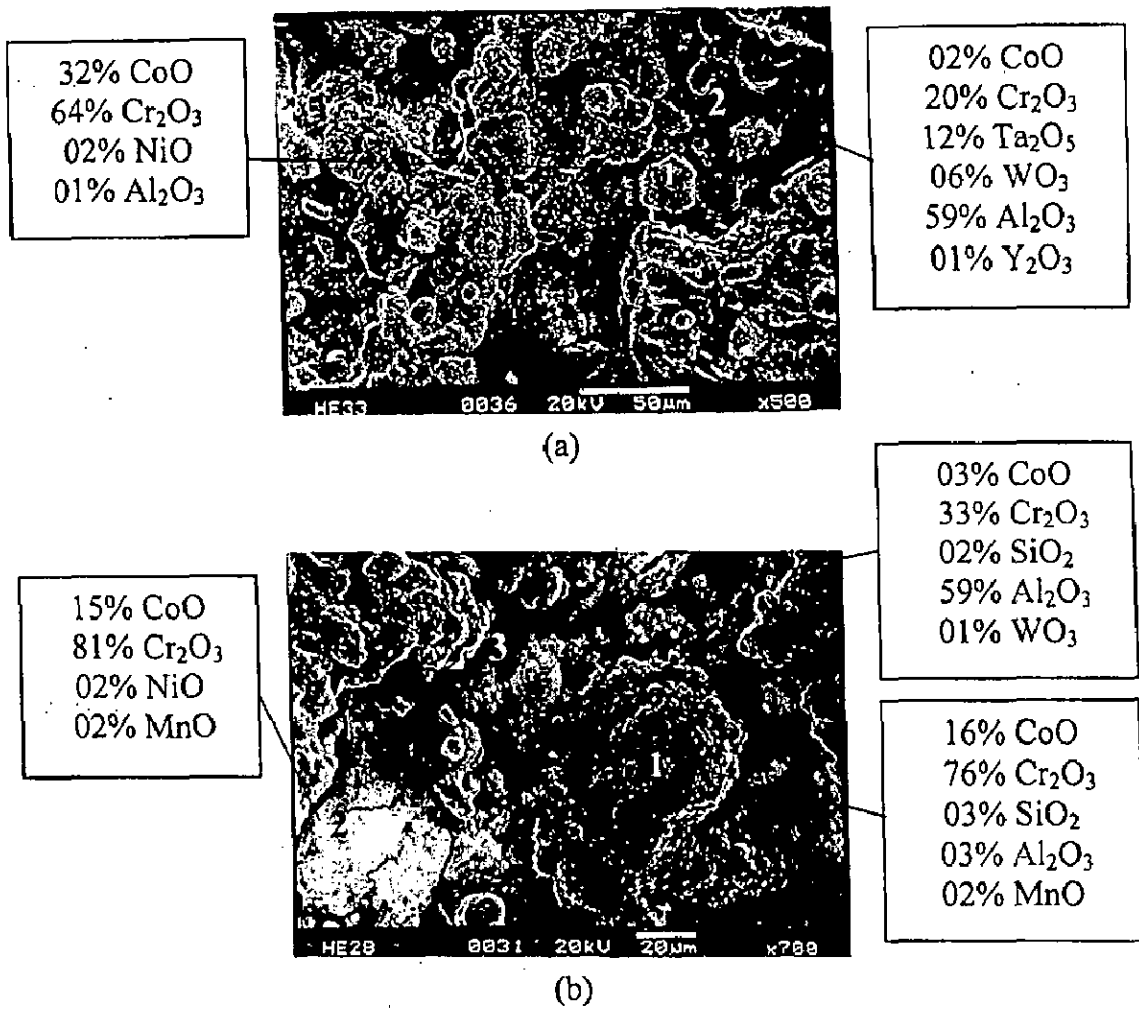
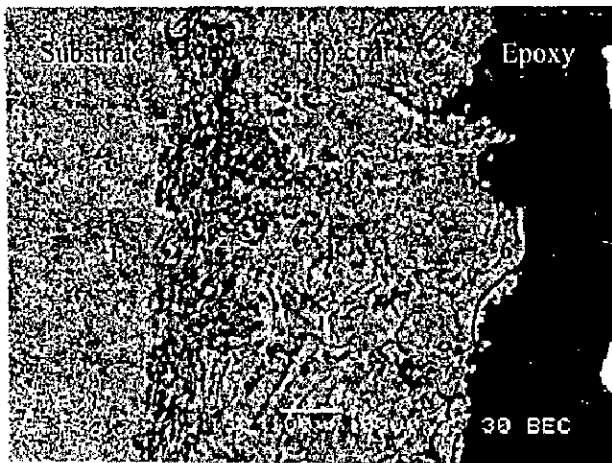
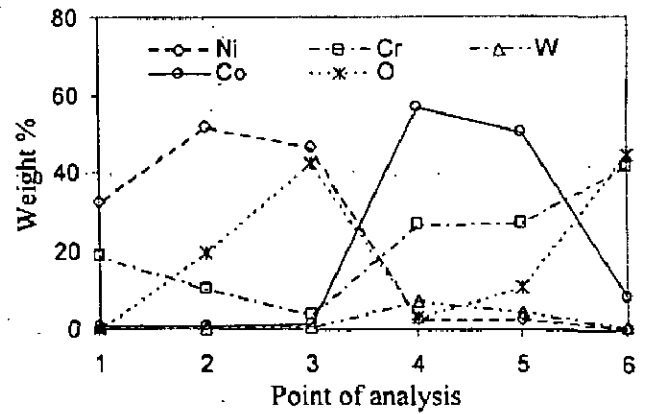
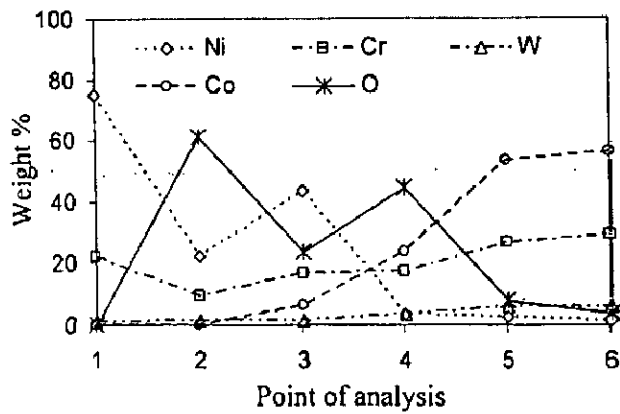
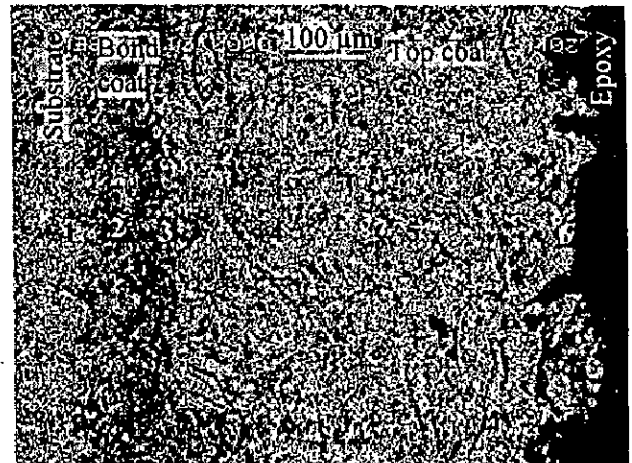


**Fig. 5.61** Surface scale morphology and EDAX analysis for the plasma sprayed Stellite-6 coated superalloys subjected to cyclic oxidation in air at 900°C for 50 cycles  
 (a) Superni 718      (b) Superfer 800H.





(a)



(b)

**Fig. 5.62** Oxide scale morphology and variation of elemental composition across the cross-section of Stellite-6 coated superalloys subjected to cyclic oxidation in air at 900°C after 50 cycles  
 (a) Superni 75 (b) Superni 601.

BSEI for the oxidised Stellite-6 coated Superni 718 shows a structure similar to the previous two cases as has been shown in Fig. 5.63. The outer layer contains mainly cobalt and chromium with some oxygen, where meager quantities of tungsten and nickel are also revealed. At point 5 in the top scale, only chromium and oxygen are mainly indicated. Oxygen is decreasing with decrease in the concentration of Cr; but it is present in high concentration with Ni at point 3. At point 4, there is high concentration of Co with very small amount of oxygen. As we move into the bond coat, concentration of nickel and oxygen is quite high, which further decreases where Al is indicated in high concentrations (point 2). Chromium amounts slightly decrease as one move towards substrate and bond coat interface. Oxygen has decreased after point 3 and it is negligible at a point in the substrate.

#### **5.1.5.6 EPMA Analysis**

BSEI and X-ray maps, Fig. 5.64 for the Stellite-6 coated Superni 75 superalloy after exposure to cyclic oxidation for 50 cycles at 900<sup>o</sup>C indicate cobalt, chromium and tungsten rich scale, where nickel, silicon and iron are also present. Some small clusters of nickel are also revealed in the upper scale. Aluminium has diffused from the bond coat and is present in small quantities at the top of the scale. Yttrium is mainly confined to the bond coat. Titanium has come at the substrate/scale interface in the form of small streaks. Silicon seems to be confined to splat boundaries in the top scale.

EPMA for Superni 600 Stellite-6 coated superalloy presented in Fig. 5.65 indicates the formation of a scale consisting of two layered structure. The top scale is consisting mainly of cobalt and chromium and there is a presence of Ni, W, Fe and Si. Aluminium and yttrium seem to be diffusing upwards in the upper scale from the bond coat likely along the splat boundaries. Fe and Co have shown some diffusion into the bond coat. Manganese is also seen in the scale.

In the case of oxidised Stellite-6 coated superalloy Superni 601, the upper layer contains cobalt and chromium as the main constituents with evenly distributed aluminium, refer Fig. 5.66. Traces of Ni, Fe, W and Si are also indicated in this layer. The sublayer represents the thinner bond coat region of the scale, which contains all the basic elements of the bond coat viz. Ni, Cr, Al and Y. So far as diffusion of the elements from the substrate is concerned, it is found to be less probable as evident from the

mappings for the different elements. Whereas, diffusion of aluminium from the bond coat has occurred in significant amounts into the top coat. Some regions which are devoid of Co are having high concentration of Ni.

In the corresponding case of coated Superni 718, Fig. 5.67, the upper scale has mainly cobalt alongwith chromium. Nickel, tungsten and iron are also analysed in the upper band alongwith with traces of diffused aluminium from the bond coat. Some clots of silicon are also seen dispersed in this band. Whereas in the bond coat area nickel and aluminium are revealed as main constituents with comparatively less concentration of chromium.

EPMA analysis of oxidised Superfer 800H superalloy coated with Stellite-6 reveals a thin streak at the top of the scale, consisting of the oxides of chromium and aluminium as is shown in Fig. 5.68. Below this streak, the scale indicates a splat type lamellar structure for the top and bond coat regions. In the top scale, splats consisting of Co, W and Cr are the areas where oxygen is not present, thereby indicating that these splats have not got oxidised. Oxygen is present at the splat boundaries, where mainly Cr, and at some places Al and Y have got oxidised in the top scale. Chromium has shown some depletion from the bond coat and formed a very thin and continuous streak of its oxide at the bond coat/substrate interface. The bond coat shows prominently the presence of Al, O and Y along the splat boundaries, whereas the splats are not oxidised.

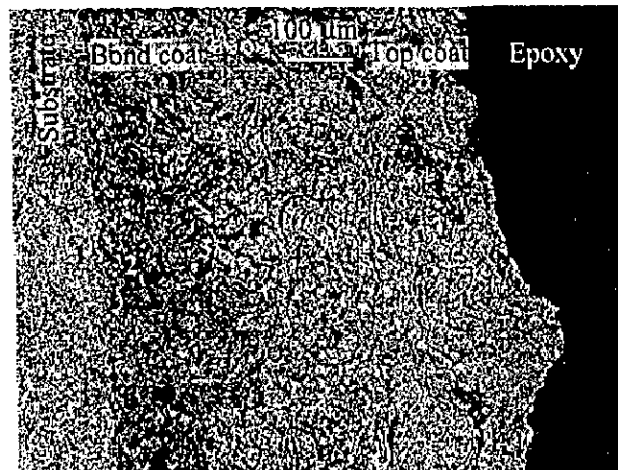
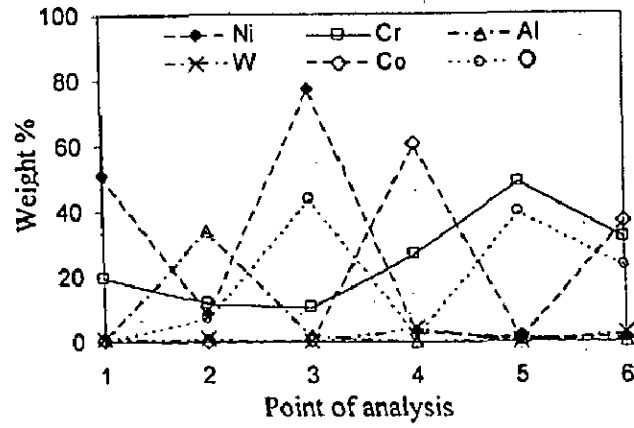


Fig. 5.63

Oxide scale morphology and variation of elemental composition across the cross-section of Stellite-6 coated superalloy Superni 718 subjected to cyclic oxidation in air at 900°C after 50 cycles.

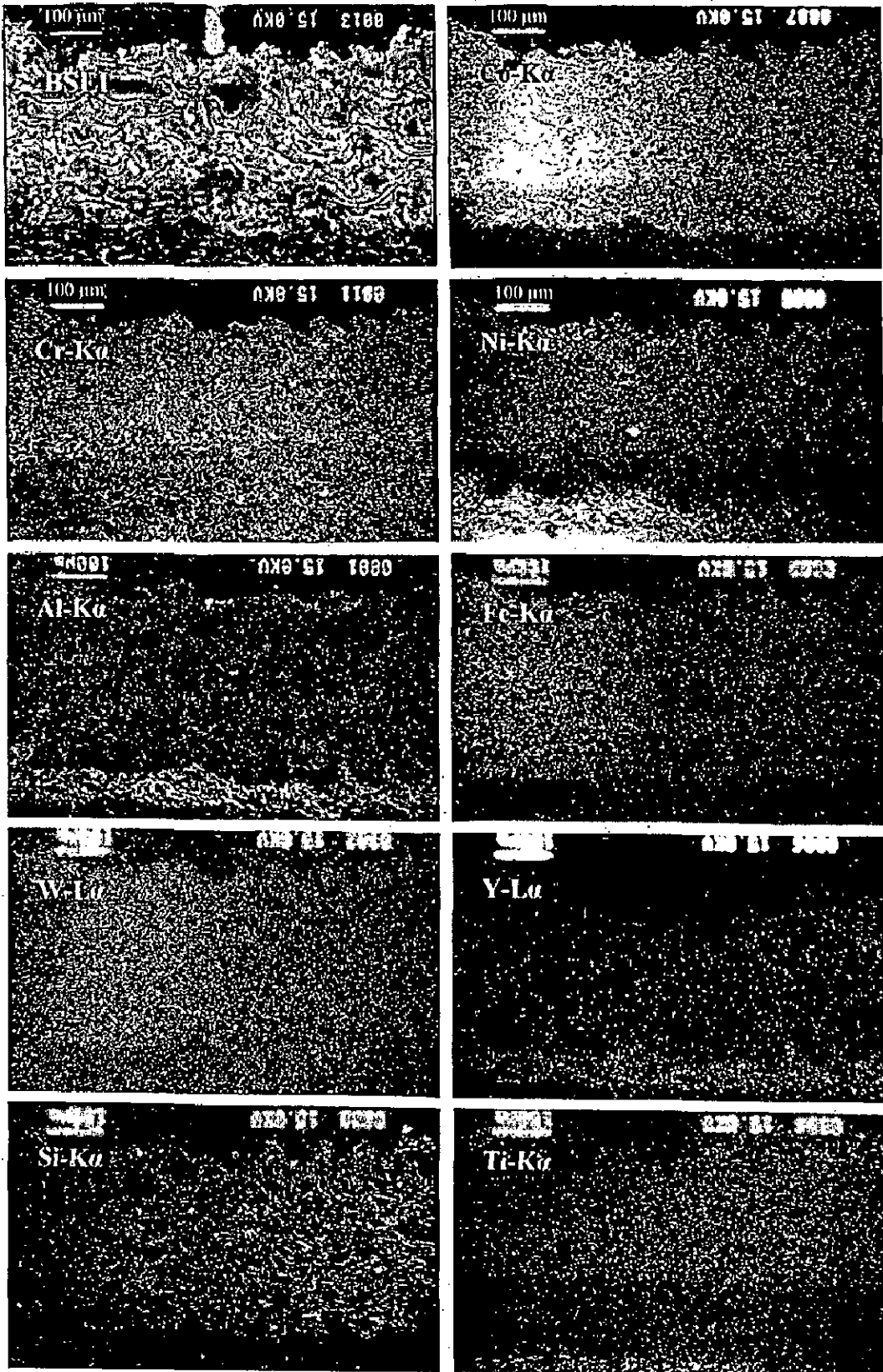


Fig. 5.64 BSEI and X-ray mappings of the cross-section of Stellite-6 coated superalloy Superni 75 subjected to cyclic oxidation at 900°C in air after 50 cycles.

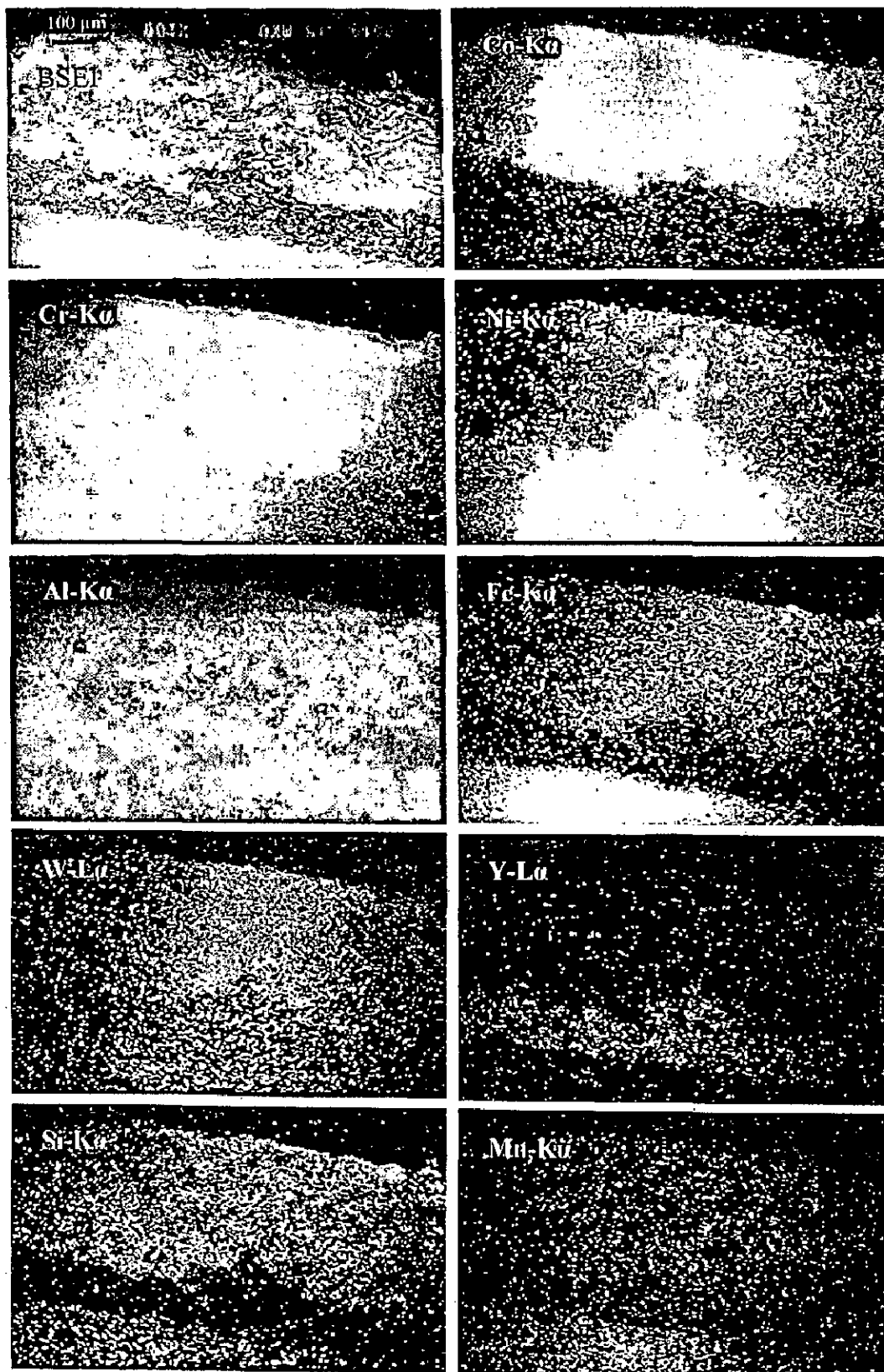
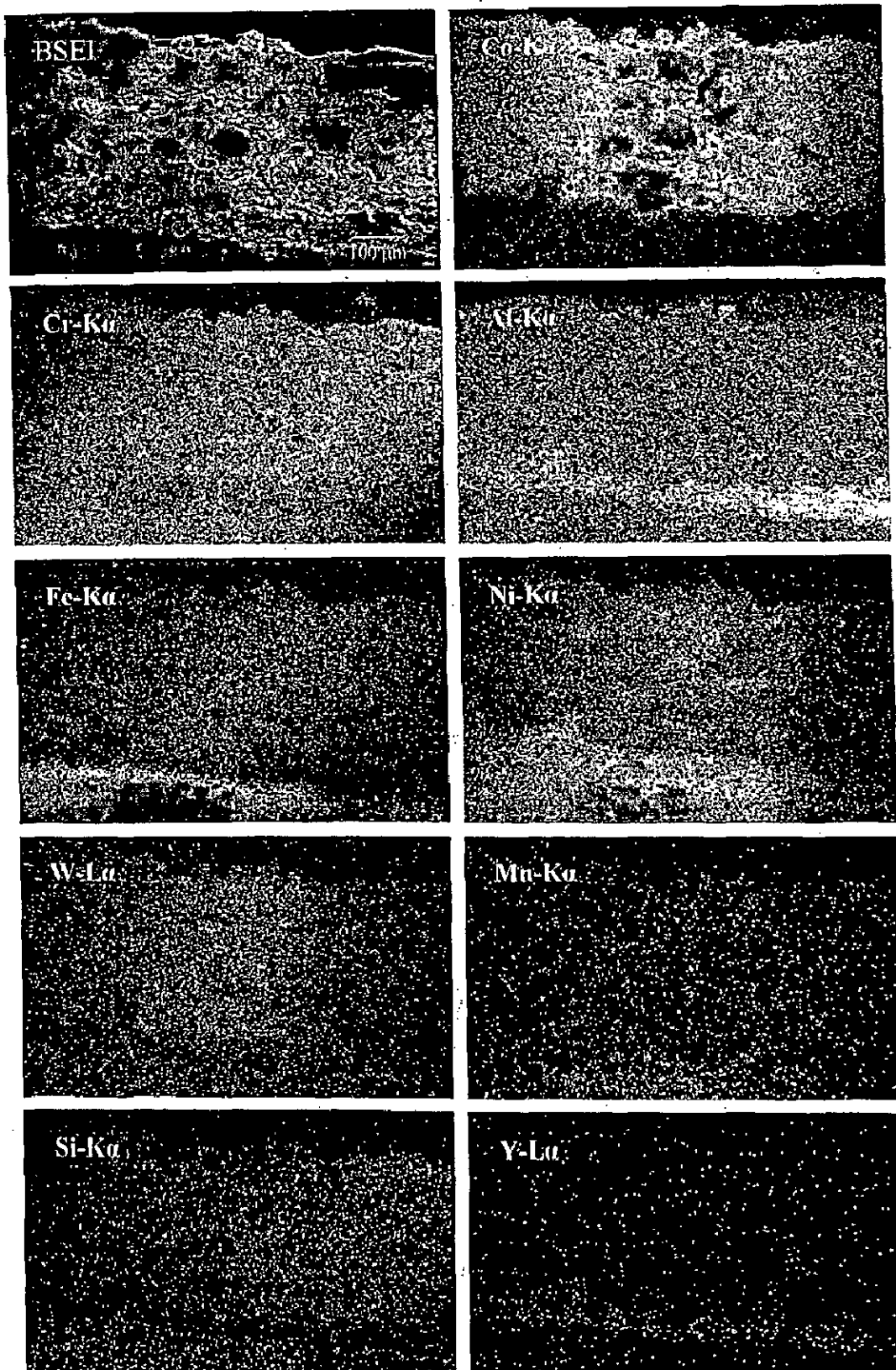


Fig. 5.65 BSEI and X-ray mappings of the cross-section of Stellite-6 coated superalloy Superni 600 subjected to cyclic oxidation at 900°C in air after 50 cycles.



**Fig. 5.66** BSEI and X-ray mappings of the cross-section of Stellite-6 coated superalloy Superni 601 subjected to cyclic oxidation at 900°C in air after 50 cycles.

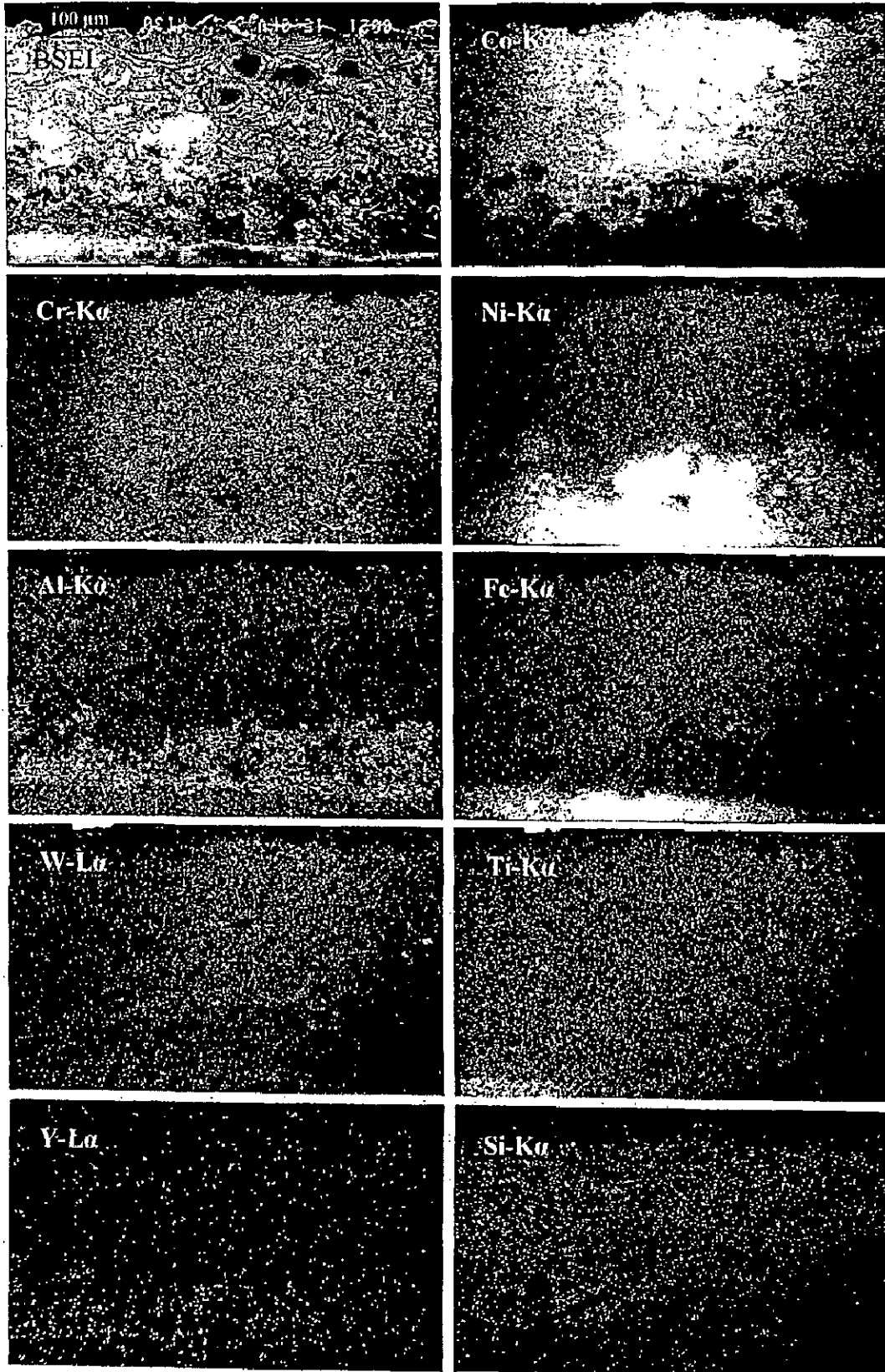


Fig. 5.67 BSEI and X-ray mappings of the cross-section of Stellite-6 coated superalloy Superni 718 subjected to cyclic oxidation at 900°C in air after 50 cycles.



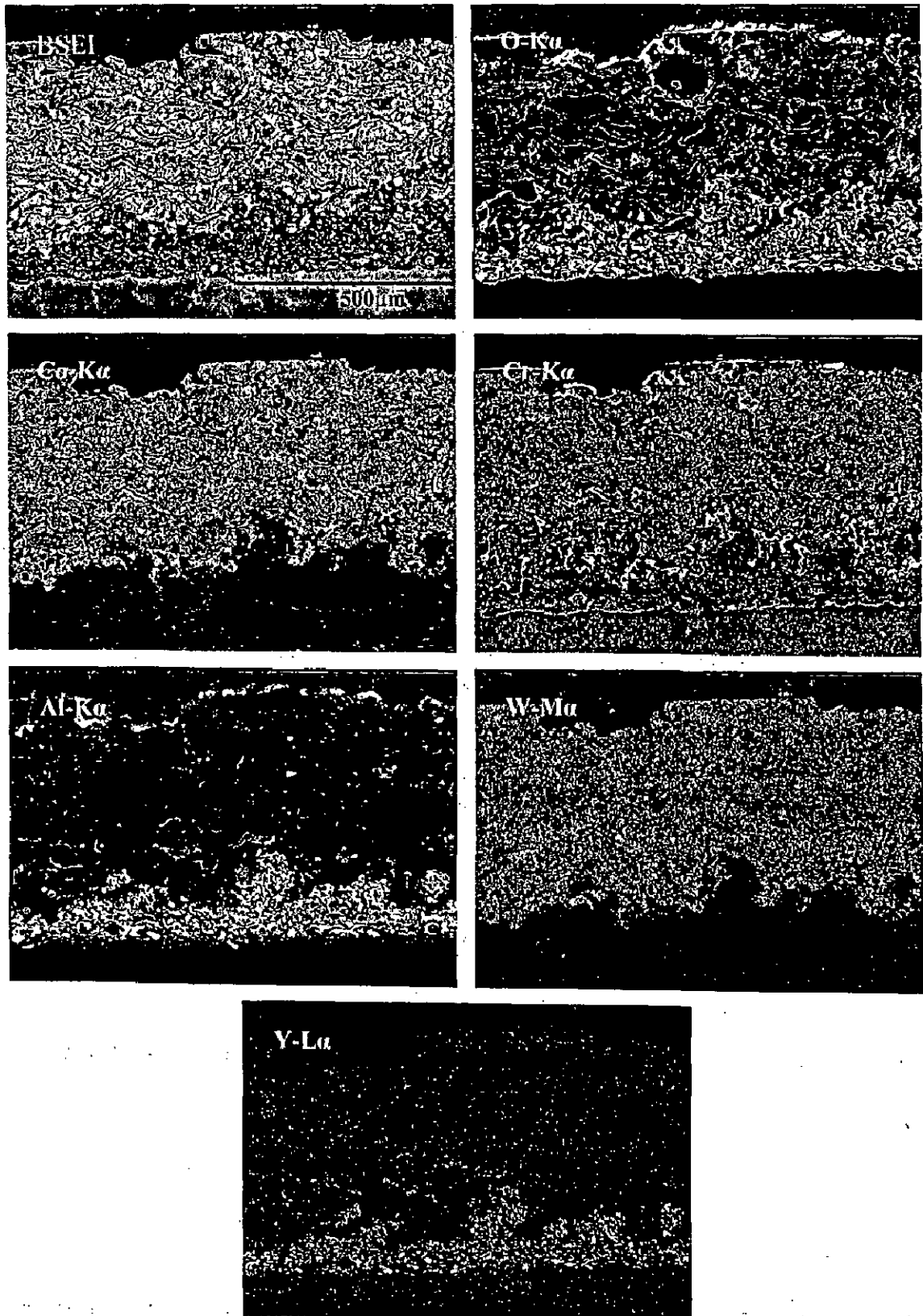


Fig. 5.68 BSEI and X-ray mappings of the cross-section of Stellite-6 coated superalloy Superfer 800H subjected to cyclic oxidation at 900°C in air after 50 cycles.

## 5.2 SUMMARY OF RESULTS

The results of oxidation studies in air for coated and uncoated superalloys are summarised in Table 5.1 to understand the comparative behaviour of different coatings.

**Table 5.1** Summary of the results for coated and uncoated superalloys oxidised in air at 900°C for 50 cycles.

Base super-alloy	Coating	Weight gain mg/cm <sup>2</sup>	Scale thickness $\mu\text{m}$	$K_p \times 10^{-10}$ g <sup>2</sup> cm <sup>-4</sup> s <sup>-1</sup>	Main XRD phases	Remarks
Superni 75	Uncoated	3.50	88	1.60 (upto 16 <sup>th</sup> cycle), then 0.02	Cr <sub>2</sub> O <sub>3</sub> , NiO, NiCr <sub>2</sub> O <sub>4</sub>	No spalling, intact and continuous scale, relatively discontinuous layer of Cr in scale (EPMA)
	NiCrAlY	4.39	138	0.47	NiO, Al <sub>2</sub> O <sub>3</sub> , NiCr <sub>2</sub> O <sub>4</sub> and Cr <sub>2</sub> O <sub>3</sub>	Intact scale without any spalling, integrity between coating and base alloy preserved after oxidation
	Ni-20Cr	14.83	254	8.84	NiO, Cr <sub>2</sub> O <sub>3</sub> and NiCr <sub>2</sub> O <sub>4</sub>	Smooth and lustrous scale with minor spalling tendency, sound contact between coating and base alloy maintained after oxidation
	Ni <sub>3</sub> Al	11.31	261	4.81	NiO, Al <sub>2</sub> O <sub>3</sub> and NiAl <sub>2</sub> O <sub>4</sub>	Smooth scale without cracks and spalling, the coating found integral with base alloy after exposure, perceptible Cr-rich streak at the interface between bond coat/substrate (EPMA)
	Stellite-6	12.07	519	4.89	CoO, CoCr <sub>2</sub> O <sub>4</sub> and Cr <sub>2</sub> O <sub>3</sub>	Dark grey scale without any spallation, contact between coating/base alloy was found to be excellent during and after cyclic oxidation, no minor superficial cracks observed along the edges

Superni 600	Uncoated	0.20	11	0.06	Cr <sub>2</sub> O <sub>3</sub> , Fe <sub>2</sub> O <sub>3</sub> , NiO and NiCr <sub>2</sub> O <sub>4</sub>	No spalling, intact and fine grained scale, with intergranular cracks (SEM), and Cr-rich intact layer in the scale (EPMA)
	NiCrAlY	3.82	171	0.42	NiO, Al <sub>2</sub> O <sub>3</sub> , NiCr <sub>2</sub> O <sub>4</sub> and Cr <sub>2</sub> O <sub>3</sub>	Intact scale without any spalling, integrity between coating and base alloy preserved after oxidation
	Ni-20Cr	13.98	286	7.93	NiO, Cr <sub>2</sub> O <sub>3</sub> and NiCr <sub>2</sub> O <sub>4</sub>	Smooth and lustrous scale with no spallation, sound contact between coating and base alloy maintained after oxidation
	Ni <sub>3</sub> Al	11.58	255	5.01	NiO, Al <sub>2</sub> O <sub>3</sub> and NiAl <sub>2</sub> O <sub>4</sub>	Smooth scale without cracks and spalling, the coating found integral with base alloy after exposure
	Stellite-6	10.63	554	3.74	CoO, CoCr <sub>2</sub> O <sub>4</sub> and Cr <sub>2</sub> O <sub>3</sub>	Dark grey scale without any spallation, contact between coating/base alloy was found to be excellent during and after cyclic oxidation, no minor superficial cracks observed along the edges
Superni 601	Uncoated	1.73	52	0.16	Cr <sub>2</sub> O <sub>3</sub> , Fe <sub>2</sub> O <sub>3</sub> , NiO and Al <sub>2</sub> O <sub>3</sub>	No spalling, intact and continuous scale
	NiCrAlY	4.21	138	0.59	NiO, Al <sub>2</sub> O <sub>3</sub> , NiCr <sub>2</sub> O <sub>4</sub> and Cr <sub>2</sub> O <sub>3</sub>	Intact scale without any spalling, integrity between coating and base alloy preserved after oxidation
	Ni-20Cr	12.45	337	4.87	NiO, Cr <sub>2</sub> O <sub>3</sub> and NiCr <sub>2</sub> O <sub>4</sub>	Smooth and lustrous scale with no spallation, sound contact between coating and base alloy maintained after oxidation
	Ni <sub>3</sub> Al	11.51	248	4.41	NiO, Al <sub>2</sub> O <sub>3</sub> and NiAl <sub>2</sub> O <sub>4</sub>	Smooth scale without cracks and spalling, the coating found integral with base alloy after exposure, visible Cr-rich streak at the interface between bond coat/substrate (EPMA)
	Stellite-6	12.17	638	5.32	CoO, CoCr <sub>2</sub> O <sub>4</sub> and Cr <sub>2</sub> O <sub>3</sub>	Dark grey scale without any spallation, contact between coating/base alloy was found to be excellent during and after cyclic oxidation with no minor spallation at/near edges

Superni 718	Uncoated	2.04	58	0.17	Cr <sub>2</sub> O <sub>3</sub> , Fe <sub>2</sub> O <sub>3</sub> , NiCr <sub>2</sub> O <sub>4</sub> and Al <sub>2</sub> O <sub>3</sub>	No spalling, intact and continuous scale, a very small pit on scale
	NiCrAlY	3.13	166	0.27	NiO, Al <sub>2</sub> O <sub>3</sub> , NiCr <sub>2</sub> O <sub>4</sub> and Cr <sub>2</sub> O <sub>3</sub>	Intact scale without any spalling, integrity between coating and base alloy preserved after oxidation
	Ni-20Cr	9.71	247	1.98	NiO, Cr <sub>2</sub> O <sub>3</sub> and NiCr <sub>2</sub> O <sub>4</sub>	Smooth and lustrous scale with a little spallation, sound contact between coating and base alloy maintained after oxidation
	Ni <sub>3</sub> Al	11.82	256	5.68	NiO, Al <sub>2</sub> O <sub>3</sub> and NiAl <sub>2</sub> O <sub>4</sub>	Smooth scale without cracks and spalling, the coating found integral with base alloy after exposure
	Stellite-6	12.78	603	5.69	CoO, CoCr <sub>2</sub> O <sub>4</sub> and Cr <sub>2</sub> O <sub>3</sub>	Dark grey scale without any spallation, contact between coating/base alloy was found to be excellent during and after cyclic oxidation, no minor superficial cracks observed along the edges
Superfer 800H	Uncoated	1.38	28	0.09	Cr <sub>2</sub> O <sub>3</sub> , Fe <sub>2</sub> O <sub>3</sub> , NiO, NiCr <sub>2</sub> O <sub>4</sub> and NiFe <sub>2</sub> O <sub>4</sub>	No spalling, intact and continuous scale
	NiCrAlY	3.19	136	0.38	NiO, Al <sub>2</sub> O <sub>3</sub> , NiCr <sub>2</sub> O <sub>4</sub> and Cr <sub>2</sub> O <sub>3</sub>	Intact scale without any spalling, integrity between coating and base alloy preserved after oxidation
	Ni-20Cr	9.45	251	2.92	NiO, Cr <sub>2</sub> O <sub>3</sub> and NiCr <sub>2</sub> O <sub>4</sub>	Smooth and lustrous scale with no spallation, sound contact between coating and base alloy maintained after oxidation
	Ni <sub>3</sub> Al	8.30	252	2.78	NiO, Al <sub>2</sub> O <sub>3</sub> and NiAl <sub>2</sub> O <sub>4</sub>	Smooth scale without cracks and spalling, the coating found integral with base alloy after exposure
	Stellite-6	13.04	680	6.40	CoO, CoCr <sub>2</sub> O <sub>4</sub> and Cr <sub>2</sub> O <sub>3</sub>	Dark grey scale without any spallation, contact between coating/base alloy was found to be excellent during and after cyclic oxidation with no minor spallation at/near edges

## 5.3 DISCUSSION

### 5.3.1 Uncoated Superalloys

In general, the superalloys under study that is Superni 75, 600, 601, 718 and Superfer 800H have shown good oxidation resistance. The oxide scales showed no tendency towards cracking or spalling during the course of 50 cycles oxidation study in air at 900°C. Based on the thermogravimetric data the oxidation rates can be arranged in following order:

Superni 75 > Superni 718 > Superni 601 > Superfer 800H > Superni 600

Therefore it can be inferred that the relative oxidation resistance of Superni 75 is minimum among the superalloys under study, while Superni 600 has shown maximum oxidation resistance. The weight gain for the former case is about 18 times of that for the latter case. It is obvious from the EPMA analysis for the superalloys, Fig. 5.10 to Fig. 5.14 that the chromium has formed protective layers in the respective oxide scales after 50 cycle oxidation. The continuous chromia layer in turn might have blocked the diffusion of any species through it to reach the substrate superalloys and hence provided oxidation resistance to the superalloys under study. As is evident from the X-ray mappings for different cases, the scale formed in case of Superni 600 is relatively intact, thin and uniform, and contains a continuous band of Cr just at the scale/substrate interface. The relatively higher oxidation resistance of this superalloy might partly be attributed to the presence of this chromia layer. Whereas the chromia layer seems to be somewhat discontinuous in case of Superni 75; refer Fig. 5.10, therefore could not provide the required protection leading to the development of minimum oxidation resistance.

It has been observed that the superalloys have followed parabolic law of oxidation in general with slight deviations. Hussain et al (1994) have also established the validity of parabolic rate law for a Fe-based superalloy Incoloy 800H, similar to Superfer 800H, whereas Delaunay et al (2000) for Inconel 718 superalloy (akin to Superni 718) at 900°C and Zhao et al (2005) for a new Ni-based superalloy at 950°C. The small deviations from the parabolic rate law have also been observed by Levy et al (1989) during their studies on the oxidation and hot corrosion of some Ni-base advanced superalloys at 704 to 1093°C. Greene and Finfrock (2001) have also reported some scatter in the mass gain per unit area versus time of oxidation data for Inconel 718.

The XRD analysis for the oxidised superalloys revealed the presence of Cr<sub>2</sub>O<sub>3</sub> and Fe<sub>2</sub>O<sub>3</sub> phases for all the cases, except for Superni 75 case, where Fe<sub>2</sub>O<sub>3</sub> is absent. The

formation of NiO has been indicated in the scales of Superni 75, 600, 601 and Superfer 800H, whereas  $\text{NiCr}_2\text{O}_4$  has been identified for Superni 75, 600, 718 and Superfer 800H scales.  $\text{Al}_2\text{O}_3$  is found to be present in the scale of Superni 601 and 718, whereas  $\text{NiFe}_2\text{O}_4$  is identified in the Superfer 800H scale. These XRD results are well supported by the surface EDAX and EPMA analysis in the present study. So far as the literature is concerned, Deb et al (1996) have also reported the formation of phases like NiO and  $\text{Cr}_2\text{O}_3$  during their oxidation studies on a cast Ni-base superalloy and have proposed formation of a continuous outer layer of  $\text{Cr}_2\text{O}_3$ , while Li et al (2003A) have observed  $\text{NiCr}_2\text{O}_4$  phase also for a single crystal Ni-base superalloy oxidised at  $900^\circ\text{C}$  in air. Whereas  $\text{Cr}_2\text{O}_3$  and  $\text{Al}_2\text{O}_3$  phases are also indicated by Bai et al (2004) for another Ni-base superalloy IN-738LC. Furthermore, the X-ray mappings as revealed by the EPMA, Fig.5.14 for the oxidised superalloy Superfer 800H are in good agreement with those reported by Polman et al (1990) for a similar superalloy Incoloy 800H.

A schematic diagram Fig. 5.69 has been suggested to explain the oxidation phenomenon for the case of Superni 600 in the light of explanations regarding oxidation put forward by Stott (1998), which can be taken as a representative case for all the superalloys under study. In the initial stage of oxidation process, when the alloy surface adsorb the oxygen molecules, small impinging nuclei of all the thermodynamically stable oxides such as those of Ni, Cr, Fe and Mn develop on the surface of the alloy. These nuclei then coalesce rapidly to give a transient layer of various oxides in a very short time as the temperature of study becomes very high. As the concentration of Ni is highest in the superalloy Superni 600, the amount of nickel oxide in this layer will be the highest, whereas chromium oxide will be the second dominating phase, followed by oxides of Fe and Mn. In this transient layer, mixed type oxide such as  $\text{NiCr}_2\text{O}_4$  may also form by reaction of oxides of Ni and Cr. As the oxidation progresses, this transient layer continues to grow with NiO at the top of the scale alongwith iron oxide, while the thermodynamically favored chromia attempt to establish a complete layer at the base of this transient layer alongwith MnO. With the progress of exposure, this transient layer continues to grow and sufficient nuclei of the various oxides develop to coalesce to form their complete layers. Once a continuous layer  $\text{Cr}_2\text{O}_3$  is formed at the alloy/scale interface, the rate of oxidation is then controlled by transport of reactants across this layer, which is much slower process than across the initially formed NiO-rich layer. Thereafter, oxidation process enters a steady state.

### 5.3.2 NiCrAlY Coating

It has been observed that all the plasma sprayed NiCrAlY coated superalloys in general followed a parabolic rate law of oxidation. This indicates that the scales formed have shown the tendency to act as diffusion barriers. Li et al (2003C) and Wang et al (2003) have also observed similar behaviour for the MCrAlY coatings. The minor deviations from the parabolic rate law as shown by the coated specimens are in agreement with the findings of Choi et al (2002) and Liu et al (1998). Choi et al (2002) attributed this scatter in data to the formation and rapid growth of inhomogeneous oxides during oxidation process.

The sequence of oxidation rates based on weight gain values for the coated superalloys after 50 cycles of oxidation is:

Superni 75 >Superni 601>Superni 600> Superfer 800H > Superni 718

However this order is in relative terms, otherwise the oxidation rates for the different coated superalloys do not vary much as their respective cumulative weight gains after 50 cycles lie in a narrow range of 3.13-4.39 mg/cm<sup>2</sup>, which is not very significant and it can be inferred that the coated superalloys have shown almost similar oxidation resistance.

Surface XRD analysis has indicated the formation of protective oxides such as NiO, Cr<sub>2</sub>O<sub>3</sub> and  $\alpha$ -Al<sub>2</sub>O<sub>3</sub> in the scales of NiCrAlY coated specimens. EDAX as well as EPMA analysis further support the formation of these phases. These oxides particularly Cr<sub>2</sub>O<sub>3</sub> and  $\alpha$ -Al<sub>2</sub>O<sub>3</sub> may partially inhibit oxidation of the substrate alloys by blocking the diffusion of reacting species towards the substrate alloys, as has been suggested by Nicoll and Wahl (1983), Stroosnijder et al (1994) and Toma et al (1999). Presence of the spinel NiCr<sub>2</sub>O<sub>4</sub> in the oxide scales also helps to develop oxidation resistance as these spinel phases usually have much smaller diffusion coefficients of the cations and anions than those in their parent oxides (Chatterjee et al, 2001).

Wang et al (2002) and Wang et al (2003) have also reported the formation of Cr<sub>2</sub>O<sub>3</sub> and Al<sub>2</sub>O<sub>3</sub> phases for the arc ion plated NiCrAlY coating, when oxidised at 900<sup>o</sup>C, whereas Toma et al (1999) have reported similar phases for oxidised VPS MCrAlY coatings, and Choi et al (2002) for oxidised air plasma spray NiCrAlY coatings. The formation of identical phases for oxidised NiCrAlY coating has also been observed by Liu et al (1998), Chan et al (2000), Wu, Y. N. et al (2001) and Wu, X. et al (2001). The EPMA analysis further indicates the diffusion of some of the basic elements of the superalloy substrates such as Fe, Ti and Si etc. into the scales invariably in all the cases, which has also been observed by Han et al (1997) and Wang et al (2001).

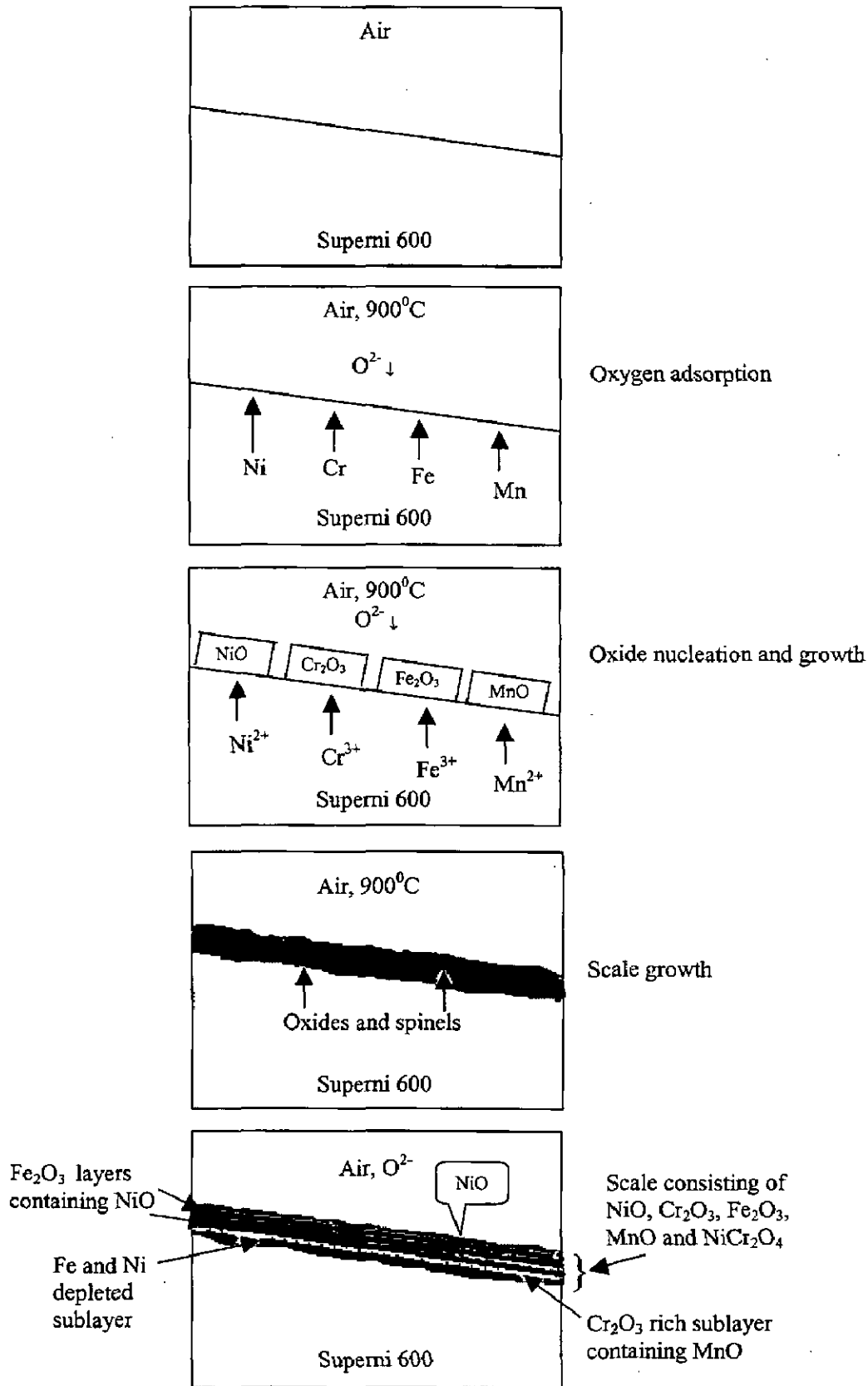


**Fig. 5.69** Schematic diagram showing probable oxidation mechanism for the uncoated superalloy Superni 600 exposed to air at 900°C for 50 cycles.



It could be seen from the respective EPMA analysis that there is no sign of depletion of basic elements from the substrate alloys. This indicates that the coating has been successful in acting as a reservoir for the formation of protective oxides/spinels, consequently may increase the service life of the substrate alloy. Moreover, it is clear from the back scattered images for the coated superalloys subjected to oxidation for 50 cycles that the substrates have not been affected by internal oxidation and the coatings appear to be integral with the substrates. This is further confirmed by the cross-sectional EDAX analysis for the coated Superni 75 and 601, which shows that the oxygen has not penetrated into the substrate alloys. Similarly oxygen mappings for Superni 75 and Superfer 800H also indicate that the oxygen is restricted only to the coatings.

The surface scales for the NiCrAlY coatings, in fact for all the coating viz. Ni-20Cr, Ni<sub>3</sub>Al and Stellite-6 cases, in general, have shown excellent spallation resistance against the cyclic oxidation in air, which indicates further effectiveness of the coatings under study as the cycle-oxidation behaviour of an alloy is dictated mainly by scale spallation resistance as per the opinion of Stott (1992). Therefore, it can be inferred that the necessary protection has been provided by the coating to the substrate superalloys, in spite of the fact that the coated superalloys have shown high overall weight gains as compared to that shown by their uncoated counterparts.

The NiCrAlY coatings subjected to cyclic oxidation in air have shown relatively high weight gains in the early cycles of the exposure. In fact, similar observation has been made for all the types of coatings (NiCrAlY, Ni-20Cr, Ni<sub>3</sub>Al and Stellite-6) under present study during air as well as Na<sub>2</sub>SO<sub>4</sub>-60%V<sub>2</sub>O<sub>5</sub> induced oxidation. These initial high oxidation rates in general might partially be attributed to the rapid formation of oxides at the coating splat boundaries and within open pores due to the penetration of the oxidizing species along the splat boundaries/open pores in the early cycles of the study. Once the oxides are formed at places of porosity and splat boundaries, the coating becomes dense and the diffusion of oxidizing species to the internal portions of the coatings gets slowed down and the growth of the oxides becomes limited mainly to the surface of the specimens. This, in turn, will make the weight gain and hence the oxidation rate steady with the further progress of exposure time.

The EPMA analysis as shown in Fig. 5.23 and Fig. 5.27 for the NiCrAlY coated Superni 75 and Superfer 800H respectively and, the cross sectional EDAX for the Superni 601, Fig. 5.22 (b) indicate that the oxide formed at these splat boundaries and within the pores is mainly aluminium oxide, co-existing with yttrium oxide. Identical findings have also been reported by Bluni and Mardar (1996), Niranatlumpong et al (2000) and Choi et al (2002). Moreover, aluminium oxide has been reported to be a protective oxide and blocks the diffusion paths to protect the base alloy, whereas yttrium oxide can improve mechanical adherence of  $Al_2O_3$  to the coating and also reduce the growth rate of scales (Saxena, 1986, Stott, 1989A and Tawancy et al, 1994). As the NiCrAlY coating has shown the lesser weight gain in comparison to the various other coatings tested in the present study, the presence of Y in the coating might have played its role in reducing the scale growth rate. The plausible mode of the oxidation for the NiCrAlY coated Superni 75 may be described as shown in Fig. 5.70.

Greenish look in the oxide scales for the NiCrAlY, Ni-20Cr and  $Ni_3Al$  coatings might be due to NiO, as has been suggested by Bornstein et al (1975). As mentioned earlier in the results for the NiCrAlY, Ni-20Cr and  $Ni_3Al$  coatings, the presence of NiO phase has been confirmed by X-ray diffractograms and is well supported by surface EDAX analysis.

Development of some superficial minor cracks near or along the edges of the coated specimens, during oxidation experimentation in both the given environments, was observed for almost all the types of investigated coatings, which led to minor spalling of coatings. However this spallation of the coatings was restricted to the edges only. This cracking and subsequent minor spalling may be attributed to the thermal shocks due to differences in the heat expansion coefficients of the oxides, coatings and the substrate (Table A.2) (Rapp et al, 1981 and Liu et al, 2001). Furthermore, the stress concentration factor at the sharp edges of the specimens might have also contributed to this minor cracking and spalling. It is pertinent to mention here that the edges of the specimens were kept sharp deliberately to add one more severe condition to the accelerated testing of the coatings. Otherwise in actual designs the sharp edges are always avoided to eliminate stress concentration.

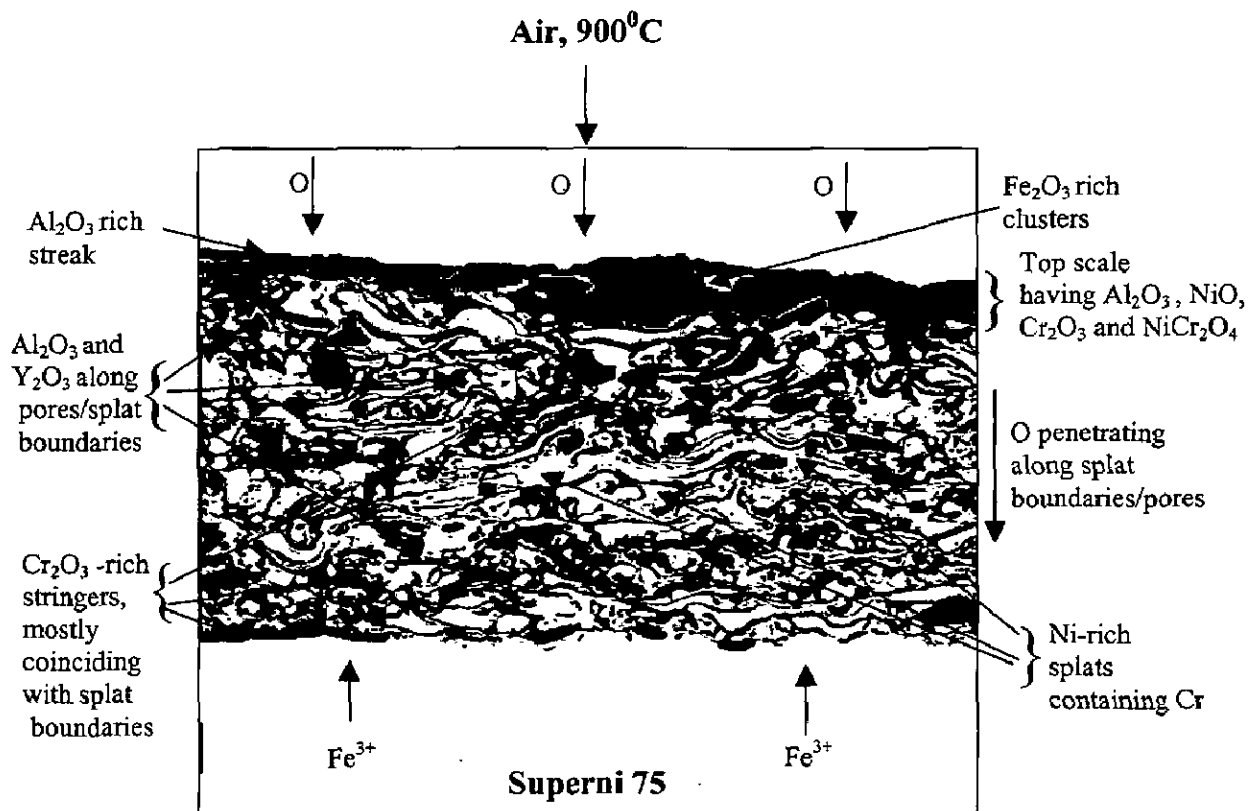


**Fig. 5.70** Schematic diagram showing probable oxidation mode for the NiCrAlY coated Superni 75 exposed to air at 900°C for 50 cycles.

### 5.3.3 Ni-20Cr Coating

Ni-20Cr coated superalloys have shown higher overall weight gains as compared to their uncoated counterparts and have followed nearly parabolic rate kinetics. From the Fig. 5.29, it is evident that the coated superalloys Superni 75, 600 and 601 have shown cumulative weight gain values which are not very significantly apart, whereas same is true for Superni 718 and Superfer 800H cases. Furthermore the coated Superni 718 and Superfer 800H seems to have better oxidation resistance in comparison to the coated Superni 75, 600 and 601. The superalloys can be arranged in the following order with regard to their oxidation resistance:

Superfer 800H > Superni 718 > Superni 601 > Superni 600 > Superni 75

The coating was found to be successful in retaining its surface contact with the substrate superalloys in general. Moreover, possible reasons behind the minor cracking/spalling of coatings have already been discussed in the Section 5.3.2. The formation of NiO, Cr<sub>2</sub>O<sub>3</sub> and NiCr<sub>2</sub>O<sub>4</sub> peaks in the scale of coated superalloys, as confirmed by the XRD analysis, indicates towards the protective nature of this coating. EDAX analysis for the surface of oxidised Ni-20Cr coated superalloys has revealed the presence of NiO in the top scale, which is further strengthened by the greenish colour of the scale. Cross-sectional EDAX analysis for Superni 75, 600, 601 and Superfer 800H also indicate the formation of NiO as main phase in the top scales. The XRD and EDAX results are further endorsed by EPMA analysis in the respective cases. The results are consistent with the findings of Hampikian and Potter (1992), Link et al (1998), Calvarin et al (2000), He et al (2000), Sundararajan et al (2003A).

The dark phase as indicated in the bond coat regions of scales, Fig. 5.35 to 5.36, is found to be containing high amounts of aluminium in general. These regions might be representing the splat boundaries or voids, where aluminium due to its high affinity for oxidation might have got oxidised preferentially as the oxygen penetrate along the splat boundaries. Yttrium could also be seen co-existing with Al almost in all the cases, which is further supported by the respective X-ray mappings. EPMA analysis for the Superni 718 case, Fig. 5.40 indicates that both Al and Y might have got oxidised to block the splat boundaries and minute pores. This may serve as a barrier to the oxidizing species and signifies the usefulness of the coating to protect the substrate superalloys.

Moreover, it is clear from the cross-sectional EDAX that oxygen has not reached the substrate in case of Superni 75 and 601, whereas the amount of oxygen approaching substrates in case of Superni 600 and Superfer 800H is negligible. Oxygen map (Fig.

5.40) for the coated Superni 718 also indicate that the internal oxidation of the substrate alloy has not taken place. This again reflects the beneficial effect of the coating. The proposed mode of attack for the Ni-20Cr coated superalloy Superni 718 has been represented schematically in Fig. 5.71.

The formation of small quantities of  $Al_2O_3$ ,  $Y_2O_3$  and MnO in the scales of Superni 75, Superfer 800H and Superni 718 respectively as indicated by surface EDAX may be due to the diffusion of aluminium and yttrium from the bond coat and manganese from the substrate to the upper coating due to porosity of the coatings as suggested by Niranatlumpong et al (2000) and Belzunce et al (2001). The presence of Al and Y is further authenticated by cross-sectional EDAX in most of the cases. Sundararajan et al (2003A and 2004) have also reported the diffusion of Fe from the substrate to the thermal sprayed Ni-20Cr coating similar to the present study. Diffusion of Mn and Si into the Ni-20 Cr coating to form small streaks as indicated by EPMA analysis in some cases is similar to the findings of Sundararajan et al (2004) regarding the segregation of these elements during oxidation of similar coating at 750<sup>0</sup>C.

#### 5.3.4 Ni<sub>3</sub>Al Coating

The oxidation of Ni<sub>3</sub>Al coated superalloys proceeded by a diffusion controlled mechanism as has been indicated by the parabolic nature of the weight gain versus number of cycles plots, Fig.5.44. All the coated superalloys followed the parabolic rate law for the whole range of the study. The behaviour is in good agreement with findings of Liu and Gao (2001) and Singh and Prakash (2003). It is interesting to note that the Ni<sub>3</sub>Al coated Ni-based superalloys have shown very similar overall weight gains (in a very narrow range of 11.31-11.82 mg/cm<sup>2</sup>), from which it can be inferred that the coated Ni-based superalloys have shown nearly similar oxidation resistance. Whereas, the coated Fe-based superalloy has shown better oxidation resistance as compared to the coated Ni-based superalloys as the overall weight gain is only 8.30 mg/cm<sup>2</sup> in the former case.

Further, as already mentioned the coating has maintained its integrity with all the superalloy substrates under study during the cyclic oxidation run, as can be seen from the respective back scattered images. The base alloys have not suffered internal oxidation. This is obvious from the elemental EDAX analysis across the cross-section in case of Superni 75 and Superfer 800H as oxygen has not penetrated the Superni 75 base alloy, whereas the extent of this penetration is marginal for Superfer 800H. This indicates the protective nature of the coatings. Further justification for the usefulness of coatings has already been discussed in general, in Section 5.3.2.

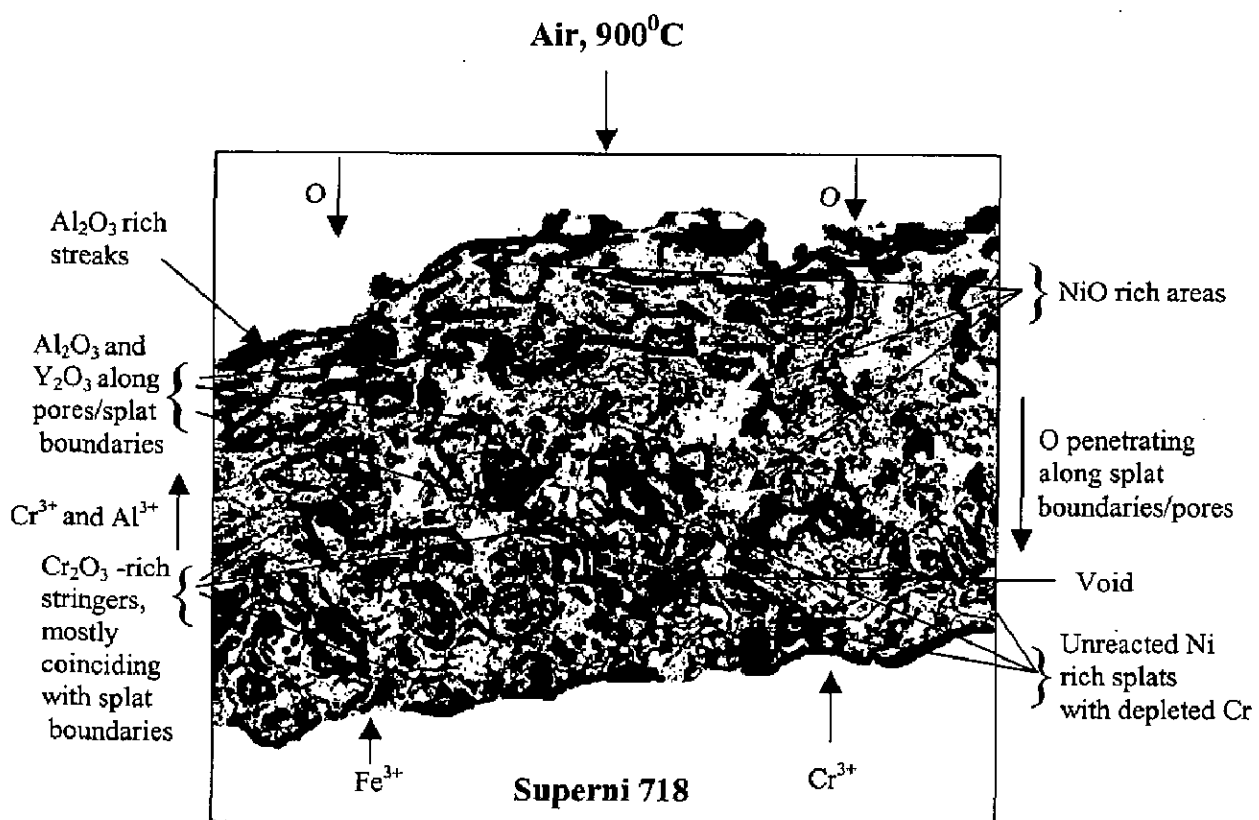


**Fig. 5.71** Schematic diagram showing probable oxidation mode for the Ni-20Cr coated Superni 718 exposed to air at 900<sup>o</sup>C for 50 cycles.

Ni<sub>3</sub>Al has been reported as NiO former by McCarron et al (1976), which has also been observed in the present study for all the Ni<sub>3</sub>Al coated superalloys. Apart from XRD, EDAX and EPMA analysis, the presence of green colour scale further confirms the formation of NiO as reported by Bornstein et al (1975) and Singh (2003). The presence of nickel oxide on surface of nickel aluminide coatings on mild steel has also been observed by Malik et al (1992) during their studies performed at 800<sup>0</sup>C in air. The formation of NiO as a main phase alongwith NiAl<sub>2</sub>O<sub>4</sub> spinel, similar to the current study, has also been reported by Liu and Gao (2001) for Ni<sub>3</sub>Al alloy after oxidation at 900<sup>0</sup>C for 50 hours. They inferred that during oxidation, the alloy grain boundaries promoted the formation of Al<sub>2</sub>O<sub>3</sub>, which further reacts with NiO in the vicinity to form NiAl<sub>2</sub>O<sub>4</sub> spinel. La et al (1999) also observed the formation of NiAl<sub>2</sub>O<sub>4</sub> phase during oxidation of Ni<sub>3</sub>Al coating prepared by the SHS casting on carbon steel.

Elemental X-ray maps of Ni<sub>3</sub>Al coated superalloys indicate the top scale to be consisting mainly of Ni with some Al in dispersed form. Similar type of scale has also been observed by Elrefaie et al (1985). A little high concentration of Cr is seen just at the bond coat and base superalloy interface in all the cases. This is found to be very prominent in case of coated Superni 75 and 601, where Cr rich thin band has formed, refer Fig. 5.50 and 5.52 respectively. This Cr-rich streak might be indicative of formation of chromia layer, which might also have protected the base alloy from being affected. Therefore the bond coat also seems to be contributing towards oxidation resistance, although its major role is to provide good adherence and reduce the effect of thermal expansion coefficients between the coating and the base alloy.

Iron has got diffused into the coating/scale almost in all the cases, but the extent of diffusion is high in case of Superni 718 and Superfer 800H. This may be attributed to the relatively high iron content in these alloys. Sundararajan et al (2005) have also reported the diffusion of Cr from air plasma sprayed Ni-50Cr bond coat to the Al top coat during oxidation in the temperature range of 600-750<sup>0</sup>C similar to the present work. Chan et al (2000) have reported NiAl<sub>3</sub> powder coating onto surface of APS NiCrAlY overlay coating by Argon Shrouded Plasma Spray process and observed interdiffusion occurring between these two coatings during 1 hour heat treatment at 900<sup>0</sup>C, which formed  $\alpha$ -Cr and  $\beta$ -NiAl phases. Based on the above discussion, probable oxidation mode for Ni<sub>3</sub>Al coated Superni 601, as a representative case has been proposed as depicted in Fig. 5.72.

### 5.3.5 Stellite-6 Coating

The Stellite-6 coated superalloys, in general have shown parabolic oxidation behaviour in all the cases. It is evident from Fig. 5.56 that the weight changes indicated by the coated superalloys after 10<sup>th</sup> cycle are not very significant, which shows that the coating may act as a diffusion barrier to any oxidizing species during long term exposures and justifies its use as a protective coating to an extent. Singh (2003) have also reported parabolic behaviour for similar coating on boiler steels, when oxidised at 900<sup>o</sup>C for 50 cycles. Based on the overall weight gains, the oxidation rates for the stellite-6 coated superalloys can be sequenced as follows:

Superfer 800H >Superni 718>Superni 601> Superni 75 > Superni 600

Similar to other coatings, it has again been observed that the major chunk of the overall weight gain was conceived only during initial cycles of study. Considerable effort has been made to explain this rapid initial weight gain in the proceeding sub-sections of this section. However in this case, the oxide formed at the splat boundaries looks to be mainly chromium oxide in the top scale, as can be perceived from EPMA for the coated Superfer 800H, Fig. 5.68, instead of aluminium oxide. Whereas in the bond coat region, the splat boundaries are again blocked mainly by aluminium oxide similar to the other coatings. Further, in almost all the Stellite-6 coated cases, aluminium has indicated significant diffusion into the top scale with a tendency to form thin streak in the outer most layer of the scales, which is obvious from the aluminium maps in the respective cases. This can further contribute to enhance the oxidation resistance of this coating.

Furthermore, this coating has retained continuous surface contact with its respective substrate alloys throughout the oxidation experimentation, which seems to be the best amongst the coatings under study, as it has shown negligible tendency to crack and no spalling of the coating or scale has been observed. Moreover, it can be seen from the cross-sectional EDAX analysis for the oxidised Stellite-6 coated Superni 75, 601, 718, Figs. 5.62 (a), (b) and 5.63 respectively that oxygen has not penetrated into the base superalloys, which further indicates the protective nature of this coating. Similar observation can be made for the Superfer 800H case with the help of oxygen map, refer Fig. 5.68, which shows that the substrate has not got oxidised at all. In addition, one can see a thin continuous streak of chromium oxide just at interface between the bond coat and the matrix in this case, which may further increase the oxidation resistance imparted by the coating.



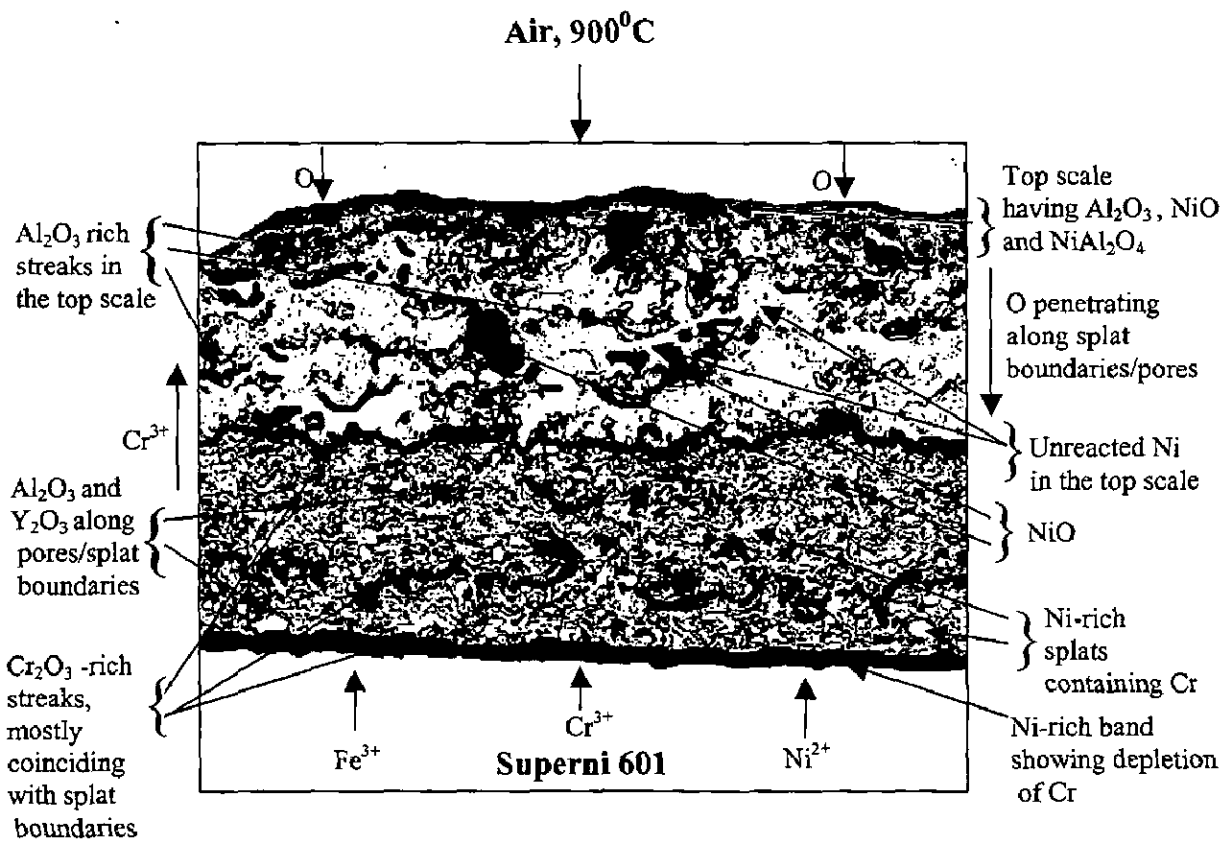


**Fig. 5.72** Schematic diagram showing probable oxidation mode for the Ni<sub>3</sub>Al coated Superni 601 exposed to air at 900°C for 50 cycles.

Overall weight gain values of the coated superalloy are almost identical to the weight gain values reported by Singh (2003) for Stellite-6 coated GrA1 type boiler steel oxidised for 50 cycles at 900°C. The XRD has revealed the oxides of cobalt and chromium along with  $\text{CoCr}_2\text{O}_4$  spinel. Surface as well as cross-sectional EDAX analysis and EPMA also support the formation of these phases. Formation of identical phases has also been reported by Santoro (1979), Luthra (1985) and Singh (2003). The presence of the spinel  $\text{CoCr}_2\text{O}_4$  and  $\text{Cr}_2\text{O}_3$  in top scales may block the diffusion activities through the cobalt oxide (CoO) by suppressing the further formation of CoO (Luthra, 1985). He reported that with an increase in the amount of chromium in cobalt chromium alloy the rate of growth of  $\text{CoCr}_2\text{O}_4$  and  $\text{Cr}_2\text{O}_3$  increases, in competition with CoO and  $\text{Co}_3\text{O}_4$  formation which thereby increases the oxidation resistance of alloys. The probable mode of oxidation for this coated superalloy might be suggested as shown in Fig. 5.73.

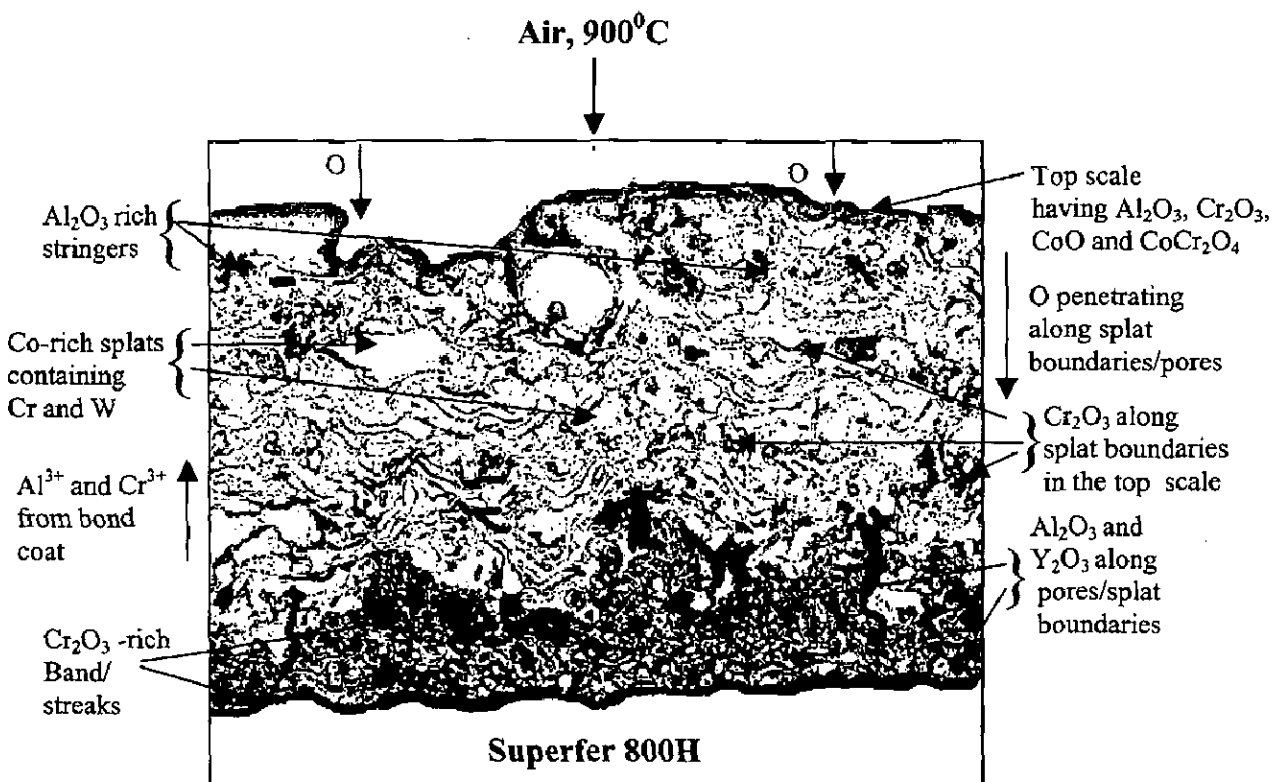


**Fig. 5.73** Schematic diagram showing probable oxidation mode for the Stellite-6 coated Superfer 800H exposed to air at 900°C for 50 cycles.

# CHAPTER 6

## OXIDATION STUDIES IN MOLTEN SALT ENVIRONMENT

---

This chapter describes hot corrosion behaviour of the bare and plasma spray coated superalloys in an aggressive environment of molten salt ( $\text{Na}_2\text{SO}_4$ -60% $\text{V}_2\text{O}_5$ ) at  $900^\circ\text{C}$  under cyclic conditions. Thermogravimetric data has been presented and the corrosion kinetics has been approximated with the help of the data. The visual observations made during the course of cyclic studies have been detailed. Efforts have also been made to understand the mechanism/mode of corrosion wherever possible.

The corrosion products were analysed with the help of XRD, SEM/EDAX and EPMA. The results for uncoated and coated superalloys have been reported under different subheadings. For comparison, the thermogravimetric data of each coating is plotted along with that of the uncoated superalloys. The parabolic rate constants and scale thicknesses values have been evaluated after 50 cycles of exposure.

### 6.1 RESULTS

#### 6.1.1 Uncoated Superalloys

##### 6.1.1.1 Visual Examination

The macrographs for base superalloys Superni 75, 600, 601, 718 and Superfer 800H after hot corrosion at  $900^\circ\text{C}$  for 50 cycles are shown in Fig. 6.1. For all the hot corroded superalloys a grey colour scale appeared on the surfaces from 1<sup>st</sup> cycle onwards which turned to dark grey with the progress of exposure. The scales formed on Superni 75, 600, 601 and Superfer 800H superalloys were fragile. The scale of Superni 75 showed blistering from the 4<sup>th</sup> cycle onwards and spalling started from 13<sup>th</sup> cycle in the form of tiny flakes, whereas in case of Superni 600 the scale indicated tendency to crack from the 17<sup>th</sup> cycle which resulted in peeling of the scale at many locations, following which the spalling of the scale started from 22<sup>nd</sup> cycle. The Superni 601 superalloy suffered intensive spalling during the early cycles. After the 1<sup>st</sup> cycle a fragile scale could be seen on the surfaces of the specimen with cracks at the edges. The fragile scale could not sustain and started separating from the surfaces in the form of little flakes and by the end of 14<sup>th</sup> cycle uppermost layer of the scale

detached from the surfaces of the specimen. The spalling of the scales continued till the end of 50 cycles with decreasing magnitude in all the above cases. In case of Superni 718, a lustrous grey coloured scale could be seen in the early cycles of study, which showed spalling and minor sputtering (disintegration of the scale accompanied by cracking sound during cooling) from 12<sup>th</sup> cycle onwards. This spalling and sputtering of the scale intensified after 20<sup>th</sup> cycle onwards and reached to an extent that it became impossible for the boat to retain the corrosion products and the same started falling outside the boat. During cooling period of following cycles the sputtered scale could also be seen on the cooling mat in the form of tiny flakes outside the boat. This spalling and sputtering went on till the end of 42<sup>nd</sup> cycle, beyond which it stopped and the weight change became nearly uniform. The Superfer 800H specimen exhibited spalling right from the 2<sup>nd</sup> cycle onwards which intensified as the period of study progressed with lot of corrosion products collected in the boat. Sputtering of the scale was also observed from 7<sup>th</sup> cycle onwards. In the case of Superni 601, 718 and Superfer 800H surfaces of the scale become uneven and pits were observed at places from where spalling had taken place.

#### **6.1.1.2 Thermogravimetric Data**

Thermogravimetric data has been compiled in Fig. 6.2 in the form of a plot between weight gain per unit area expressed in  $\text{mg}/\text{cm}^2$  and number of cycles for hot corroded superalloys Superni 75, 600, 610, 718 and Superfer 800H. The values of overall weight gain after 50 cycles of hot corrosion for the superalloys Superni 75, 600, 601 and Superfer 800H are found to be 6.82, 14.34, 24.91 and 52.10  $\text{mg}/\text{cm}^2$  respectively. Evidently Fe-based superalloy Superfer 800H has shown maximum weight gain whereas Ni-base Superni 75 a minimum. Therefore in terms of weight gain Superni 75 has proved to be the most corrosion resistant alloy in the aggressive environment under study. So far as the Superni 718 is concerned, the overall weight gain could be measured accurately only upto 20 cycles, beyond which intense spalling and sputtering made it difficult to measure the overall weight gain. The value of weight gain upto 20 cycles is found to be 11.51  $\text{mg}/\text{cm}^2$  in this case. Further, the weight gain square ( $\text{mg}^2/\text{cm}^4$ ) data were plotted as a function of time (number of cycles) as shown in Fig. 6.3 to establish the rate law for the hot corrosion. It is clear that in spite of some fluctuations in the data, the data conforms to the parabolic rate law to an acceptable limit for all the superalloys.

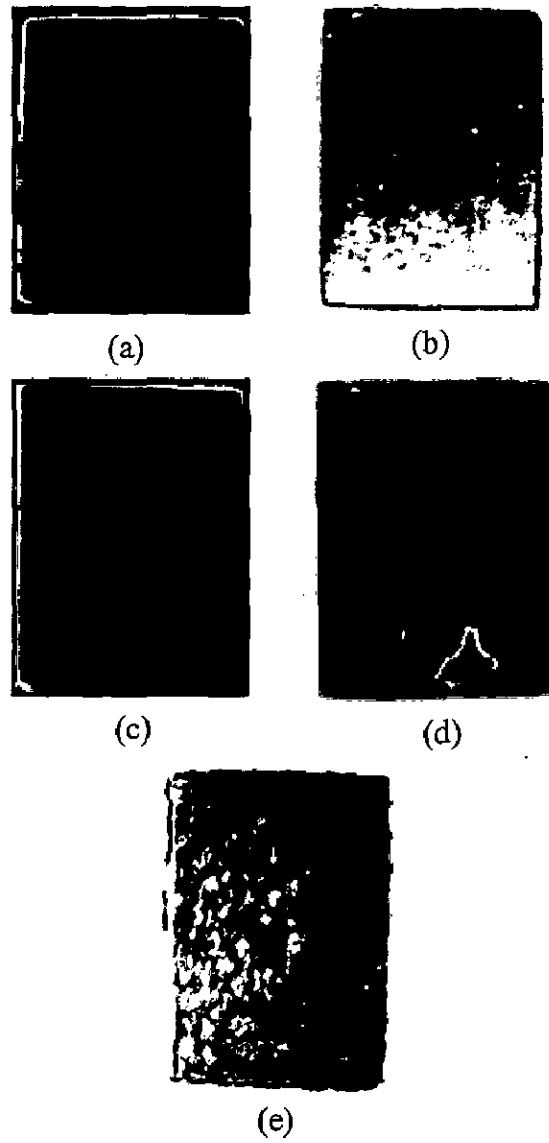


**Fig. 6.1** Macrographs of the uncoated superalloys subjected to cyclic oxidation in  $\text{Na}_2\text{SO}_4$ -60% $\text{V}_2\text{O}_5$  at  $900^\circ\text{C}$  for 50 cycles  
 (a) Superni 75      (b) Superni 600      (c) Superni 601  
 (d) Superni 718      (e) Superfer 800H.

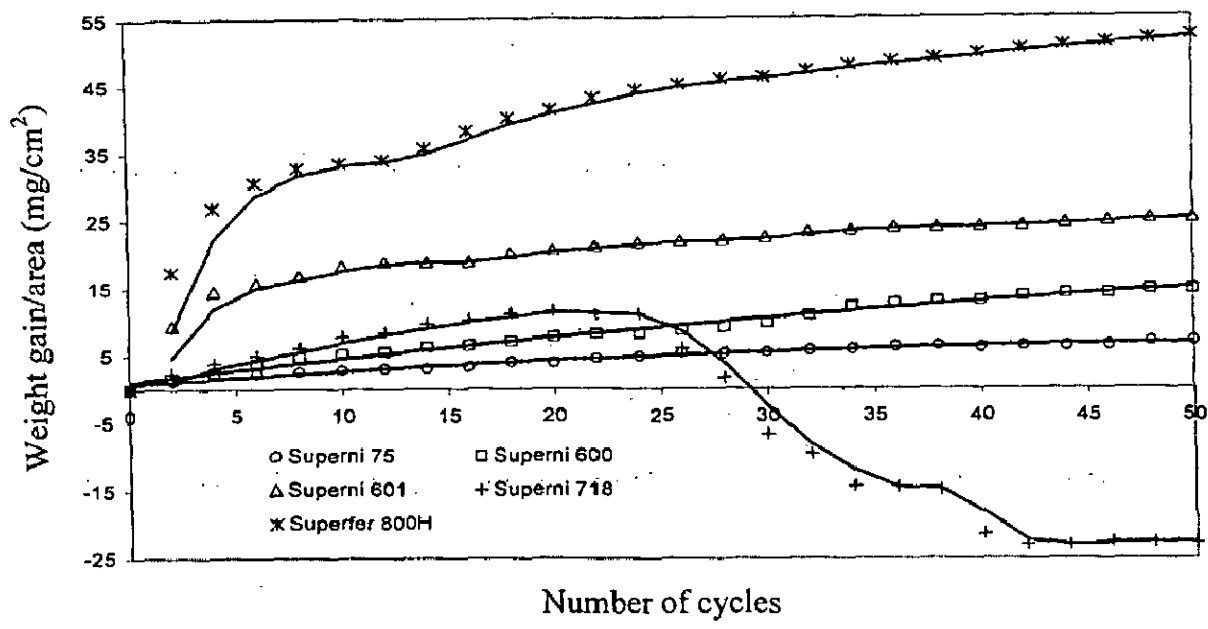


Fig. 6.2 Weight gain vs. number of cycles plot for the uncoated superalloys subjected to cyclic oxidation for 50 cycles in  $\text{Na}_2\text{SO}_4$ -60% $\text{V}_2\text{O}_5$  at  $900^\circ\text{C}$ .

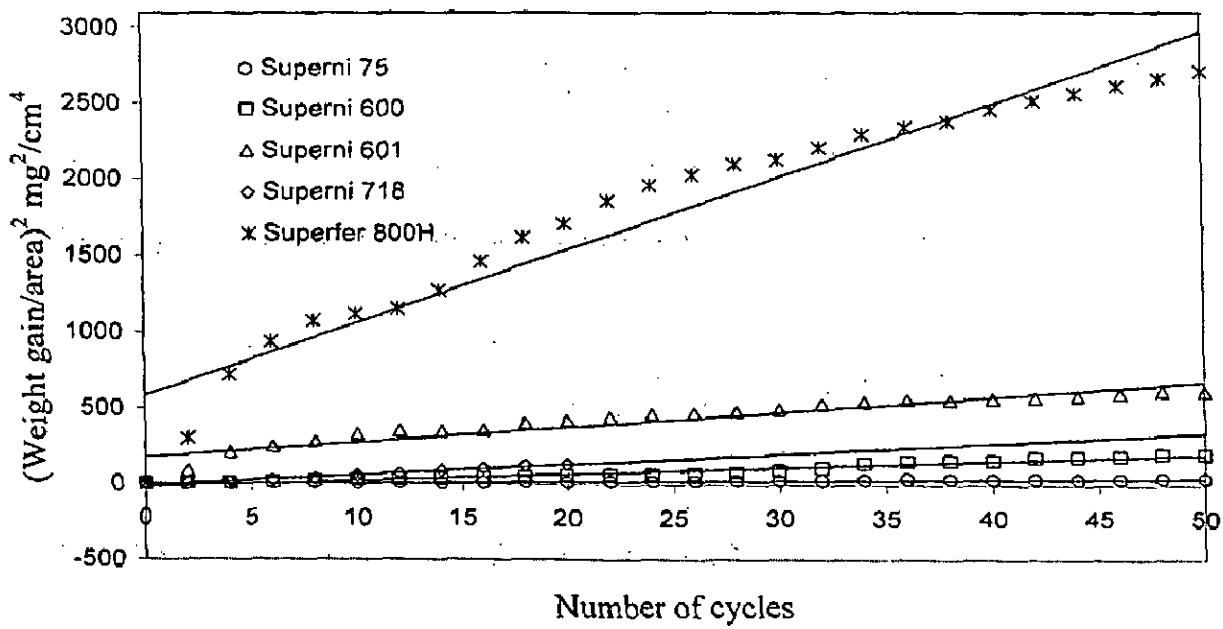


Fig. 6.3  $(\text{Weight gain/area})^2$  vs. number of cycles plot for the uncoated superalloys subjected to cyclic oxidation for 50 cycles in  $\text{Na}_2\text{SO}_4$ -60% $\text{V}_2\text{O}_5$  at  $900^\circ\text{C}$ .

The parabolic rate constants,  $K_p$  for Superni 75, 600, 610 and Superfer 800H superalloys calculated on the basis of 50 cycles data are 2.65, 12.54, 28.08 and  $130.00 \times 10^{-10} \text{ g}^2 \text{ cm}^{-4} \text{ s}^{-1}$  respectively, where for Superni 718 it is  $19.85 \times 10^{-10} \text{ g}^2 \text{ cm}^{-4} \text{ s}^{-1}$  for 20 cycles.

#### **6.1.1.3 Scale Thickness Measurement**

The scale thickness values were measured from SEM back scattered images shown in Fig. 6.4. These values represent the average thickness of oxide scales left with their respective substrates after 50 cycles of exposure to hot corrosion in the given environment. The average values of scale thickness are evaluated to be 53, 147, 38, 48 and 73  $\mu\text{m}$  for the corroded superalloys Superni 75, 600, 601, 718 and Superfer 800H respectively.

#### **6.1.1.4 X-ray Diffraction Analysis**

X-ray diffractograms of the scales for Superni 75, 600 and 601 are given in Fig. 6.5, where those for Superni 718 and Superfer 800H are reported in Fig. 6.6 after exposure to molten salt ( $\text{Na}_2\text{SO}_4\text{-}60\%\text{V}_2\text{O}_5$ ) at  $900^\circ\text{C}$  for 50 cycles on a reduced scale. It is evident from the diffraction patterns that Superni 75 and Superni 600 have shown formation of similar phases after hot corrosion in the given environment. For these two superalloys  $\text{NiO}$ ,  $\text{Fe}_2\text{O}_3$ ,  $\text{NiCr}_2\text{O}_4$  and  $\text{Ni}(\text{VO}_3)_2$  are indicated as the main phases. Whereas in case of hot corroded Superni 601, an additional phase  $\text{FeV}_2\text{O}_4$  is revealed instead of  $\text{Ni}(\text{VO}_3)_2$ . The phases identified in case of Superni 718 after exposure to hot corrosion, Fig. 6.5 (a), are similar to those analysed in case of Superni 601. Further in case of hot corroded Superfer 800H; phases identified are again similar to Superni 601 and 718 cases with the exception of  $\text{NiCr}_2\text{O}_4$  phase being replaced by  $\text{NiFe}_2\text{O}_4$ . Comparatively weak peaks of  $\text{Cr}_2\text{O}_3$  are indicated invariably in all the cases.

#### **6.1.1.5 SEM/EDAX Analysis**

##### **(a) Surface Morphology**

SEM micrographs for Superni 75, 600 and 601 base superalloys after exposure to  $\text{Na}_2\text{SO}_4\text{-}60\%\text{V}_2\text{O}_5$  environment at  $900^\circ\text{C}$  are shown in Fig. 6.7, whereas those for Superni 718 and Superfer 800H in Fig. 6.8 alongwith with EDAX compositions. SEM micrographs



indicate coarse grained crystalline structures for Superni 75 and 600. The main constituent of the scales for these two cases is NiO as can be seen from the EDAX analysis made at certain points in the respective cases. The white crystalline phase in case of Superni 75 is rich in NiO with small quantities of Fe<sub>2</sub>O<sub>3</sub> and Cr<sub>2</sub>O<sub>3</sub>, while the black matrix has comparatively lower amount of NiO with relatively high Cr<sub>2</sub>O<sub>3</sub> content. But in case of hot corroded Superni 600, white phase as well as the black matrix contains equal quantities of NiO. A massive and dense scale has been observed for corroded Superni 601 which is rich in NiO (black matrix), with substantial amounts of Fe<sub>2</sub>O<sub>3</sub> and Cr<sub>2</sub>O<sub>3</sub>. The uppermost layer of the scale (white phase) has dominance of Fe<sub>2</sub>O<sub>3</sub> and contains relatively less quantity of NiO; refer point 2 in Fig. 6.7 (c). The amount of Cr<sub>2</sub>O<sub>3</sub> has also got nearly doubled at this point. Further, the scale of hot corroded Superni 718 superalloy has oxides of Ni, Cr and Fe present in it, Fig. 6.8 (a). The top scale is having similar amounts of NiO and Cr<sub>2</sub>O<sub>3</sub> with 27% Fe<sub>2</sub>O<sub>3</sub>, while in the black phase, the amount of Cr<sub>2</sub>O<sub>3</sub> has decreased and that of Fe<sub>2</sub>O<sub>3</sub> has increased marginally. A corresponding SEM micrograph in the case of Superfer 800H indicates that spalling of the scale might have taken place, Fig. 6.8 (b). From the EDAX analysis, it can be seen that the scale for this Fe-base superalloy is consisting mainly of Fe<sub>2</sub>O<sub>3</sub> with oxides of Ni and Cr present in it. Further the composition of the scale is nearly uniform as can be perceived from the EDAX analysis at point 1 and 2, Fig. 6.8 (b).

#### (b) Cross-Sectional Analysis

Cross-sectional micrograph showing oxide morphology for the base superalloy Superni 718 corroded in molten salt for 50 cycles at 900<sup>o</sup>C is shown in Fig. 6.9. It shows an oxide scale with variable thickness, which is revealed as dark grey area. EDAX analysis presents a comparative estimate of elemental compositions at some points in the substrate as well as in the scale. As shown in Fig. 6.9, oxygen is found to be absent at points 1, 2 and 3 from which it can be concluded that the oxygen has not penetrated into the substrate. The point analysis across the scale indicates the presence of mainly nickel and iron with comparatively small amounts of chromium, oxygen and molybdenum at point 4. EDAX analysis at point 5 shows a sharp decline in the concentration of nickel, where oxygen level has increased substantially. The amount of Cr has also increased at point 5. Further small amount of vanadium is also present in the top of scale. There is clear indication of penetration of the scale into the substrate.

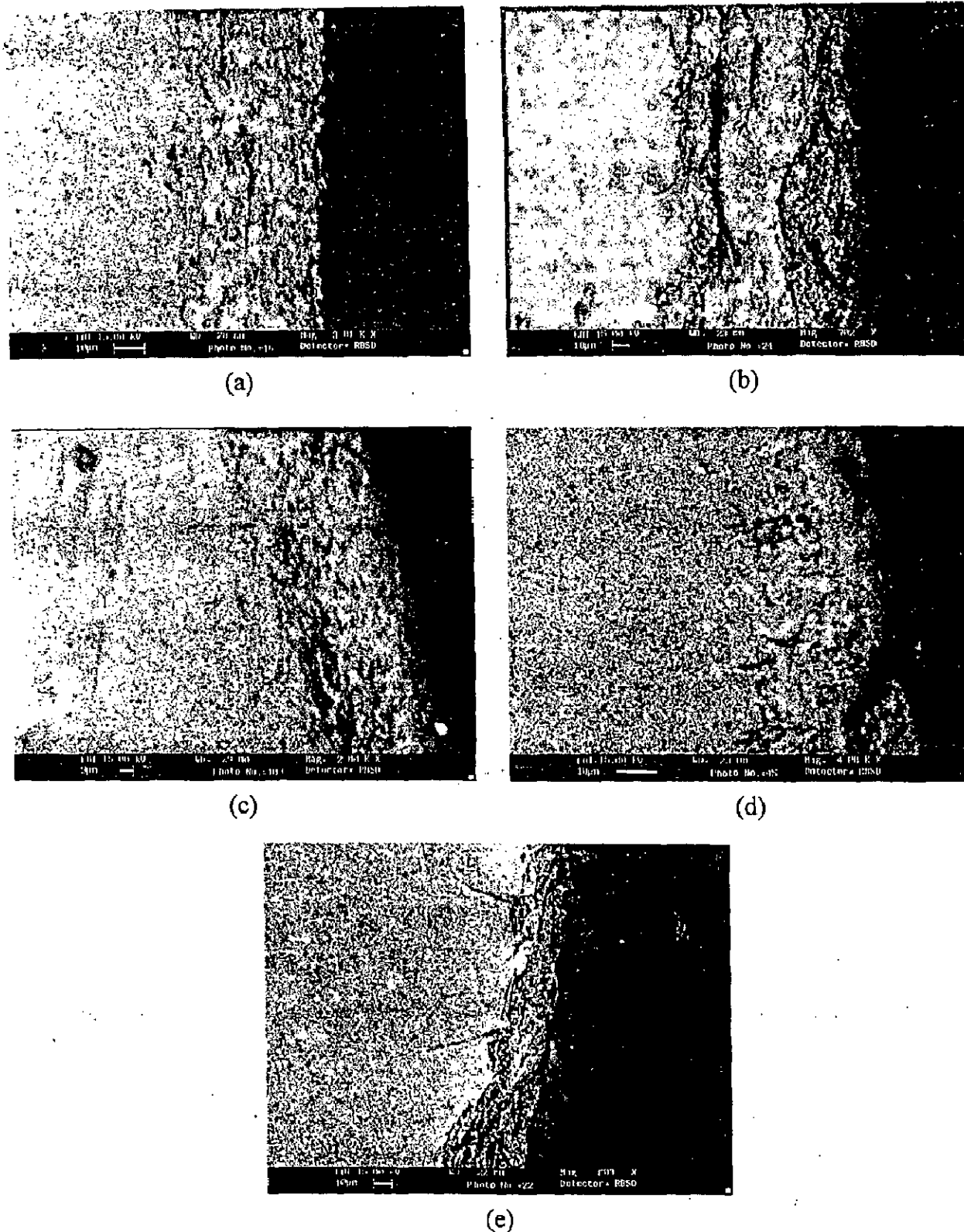


Fig. 6.4 SEM back scattered image for the uncoated superalloys after cyclic oxidation in  $\text{Na}_2\text{SO}_4$ -60% $\text{V}_2\text{O}_5$  for 50 cycles at  $900^\circ\text{C}$

(a) Superni 75            (b) Superni 600            (c) Superni 601  
(d) Superni 718            (e) Superfer 800H.

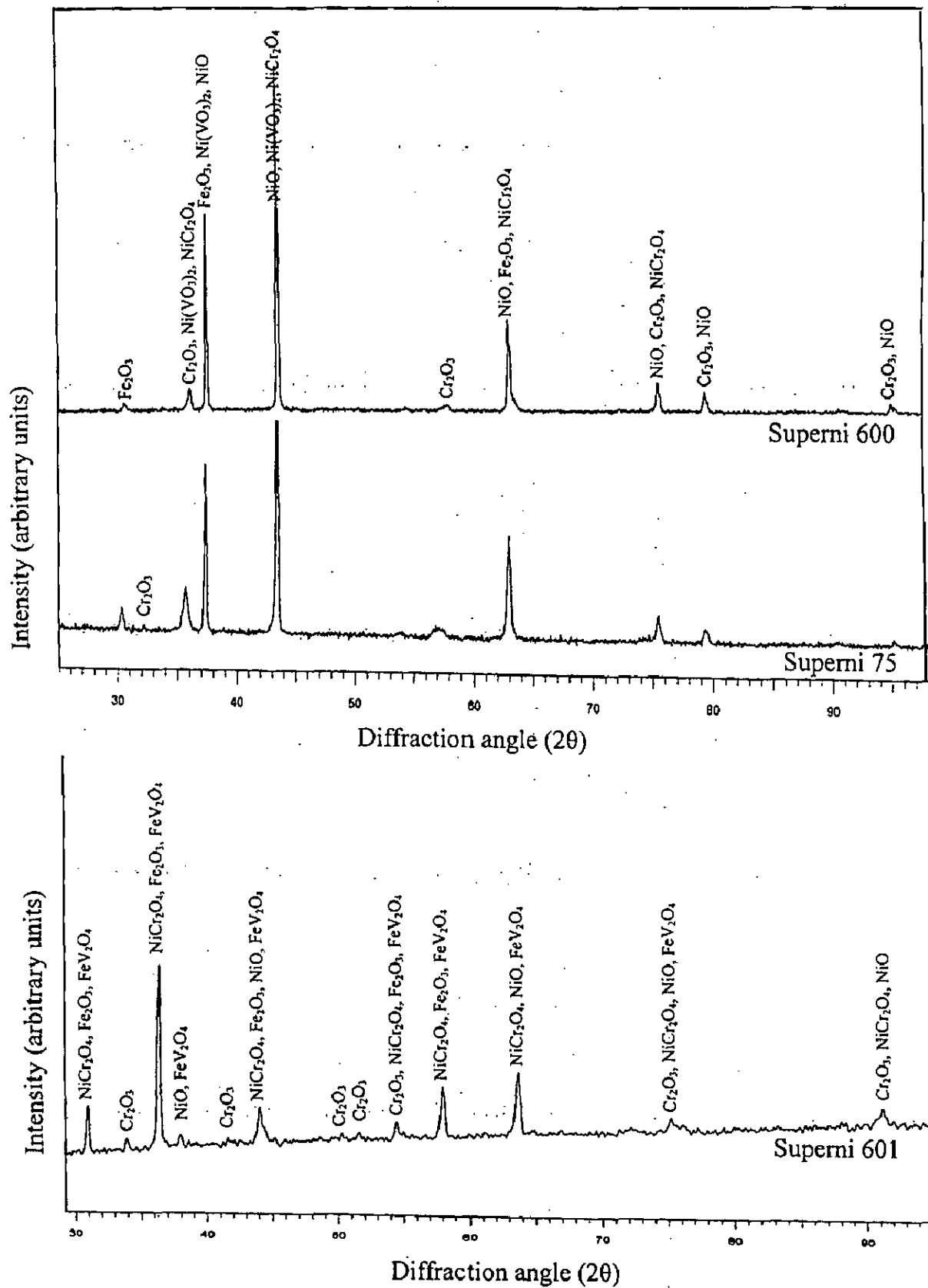


Fig. 6.5 X-ray diffraction patterns for the uncoated superalloys subjected to cyclic oxidation in Na<sub>2</sub>SO<sub>4</sub>-60%V<sub>2</sub>O<sub>5</sub> at 900°C after 50 cycles.

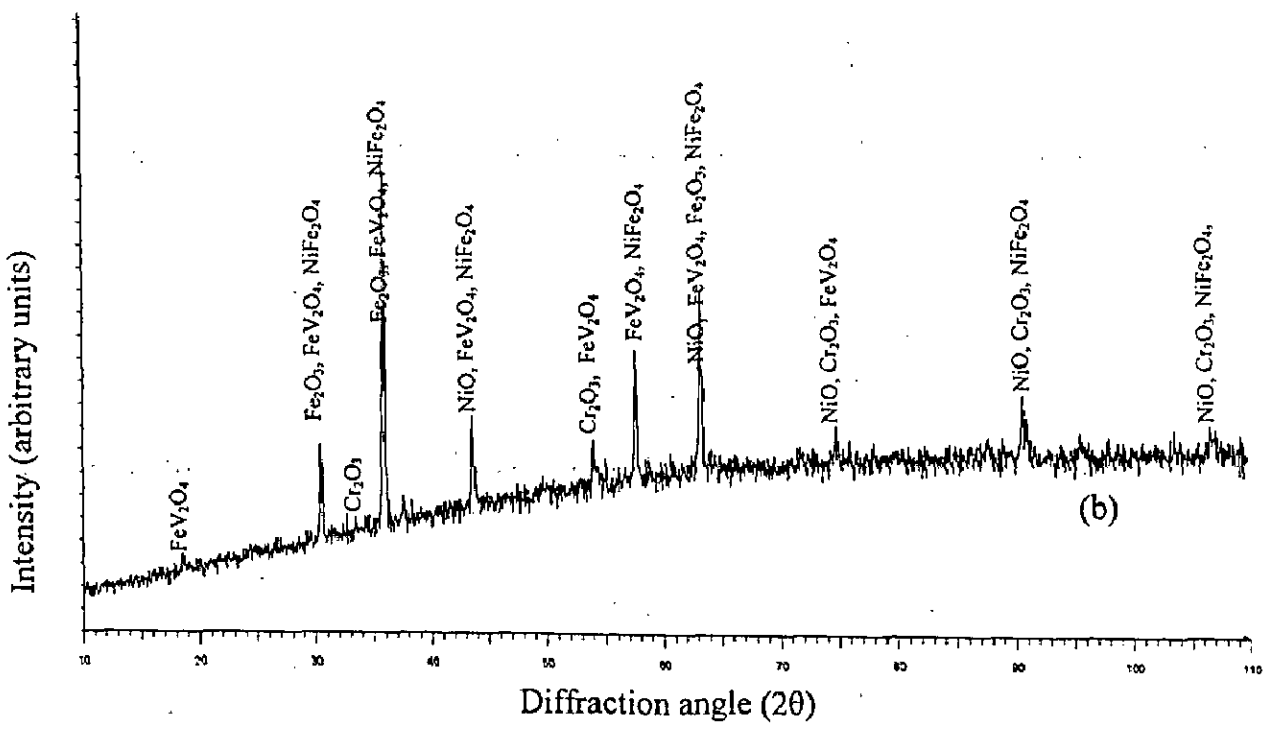
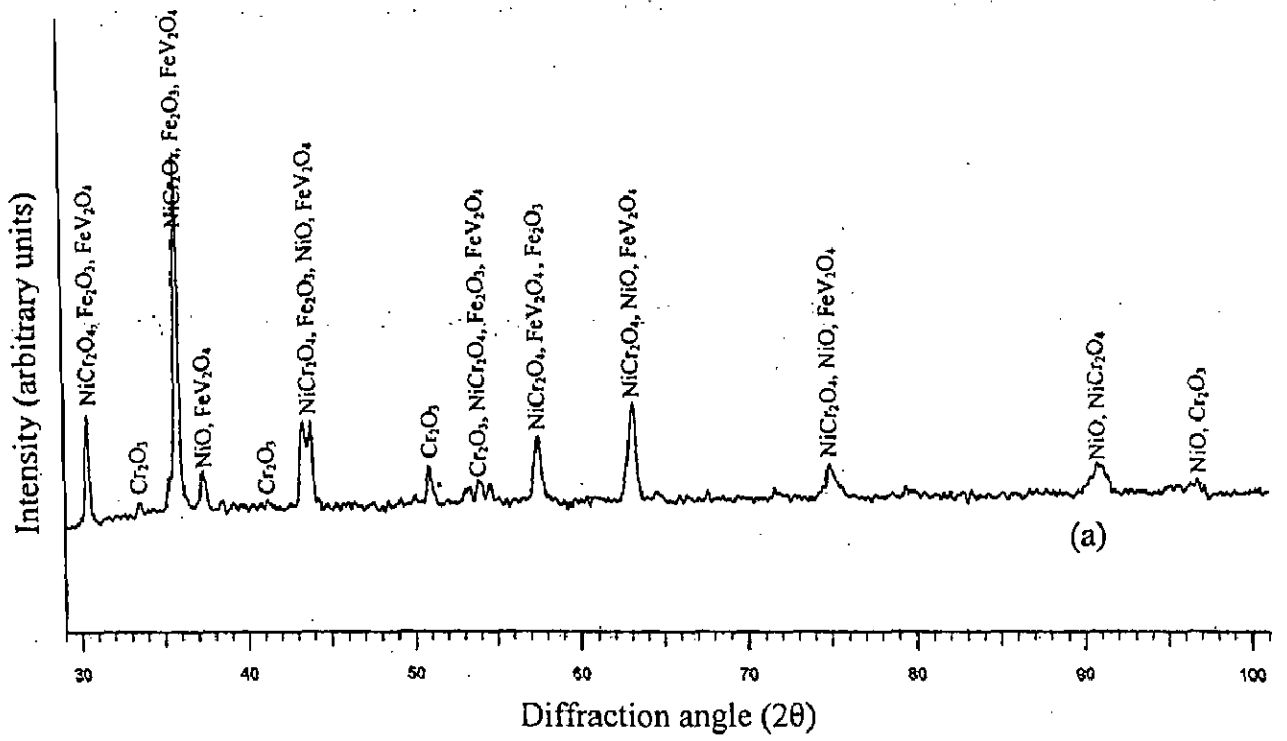


Fig. 6.6 X-ray diffraction patterns for the uncoated superalloys subjected to cyclic oxidation in  $\text{Na}_2\text{SO}_4$ -60% $\text{V}_2\text{O}_5$  at  $900^\circ\text{C}$  after 50 cycles  
 (a) Superni 718 (b) Superfer 800H.

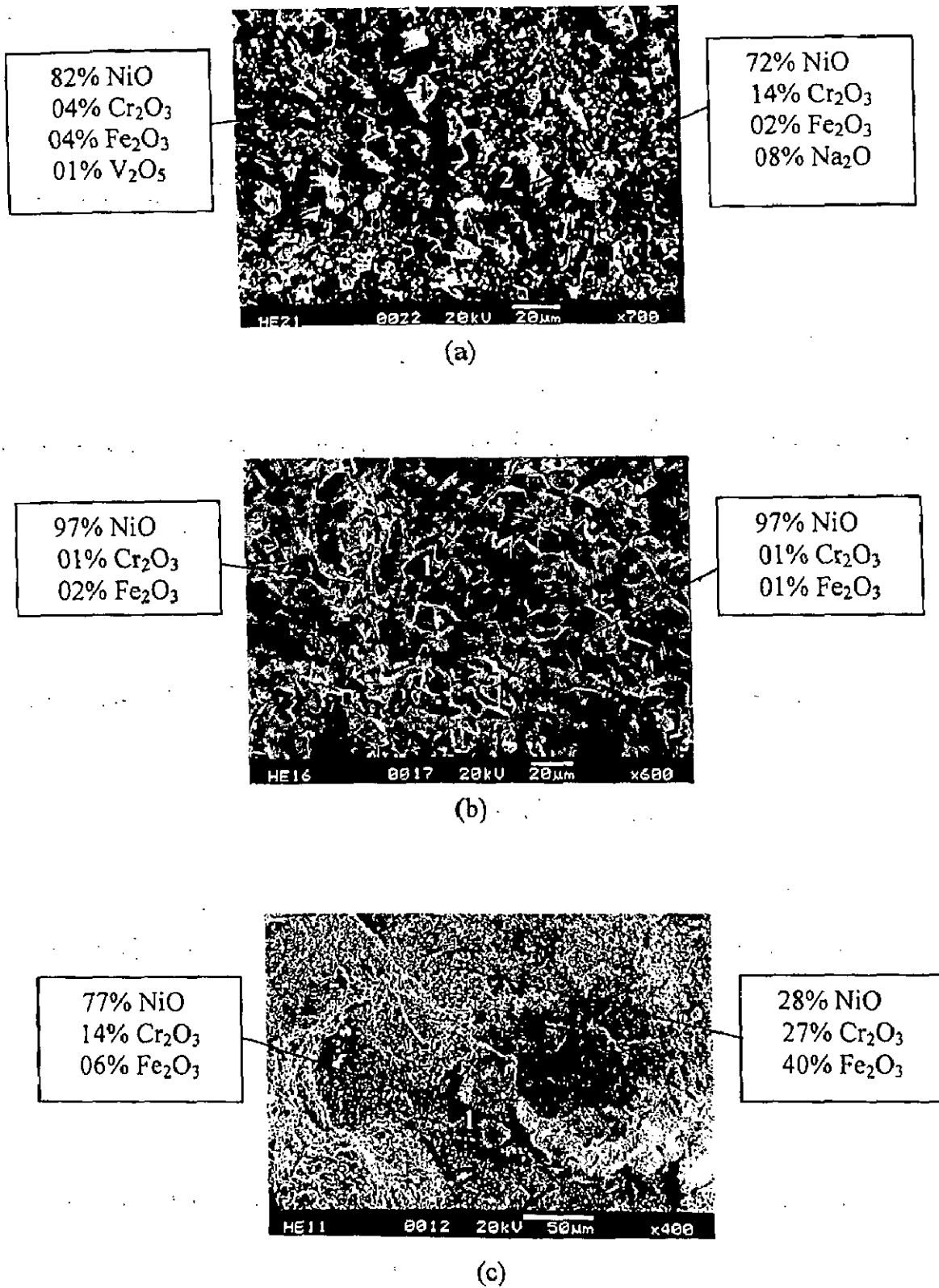
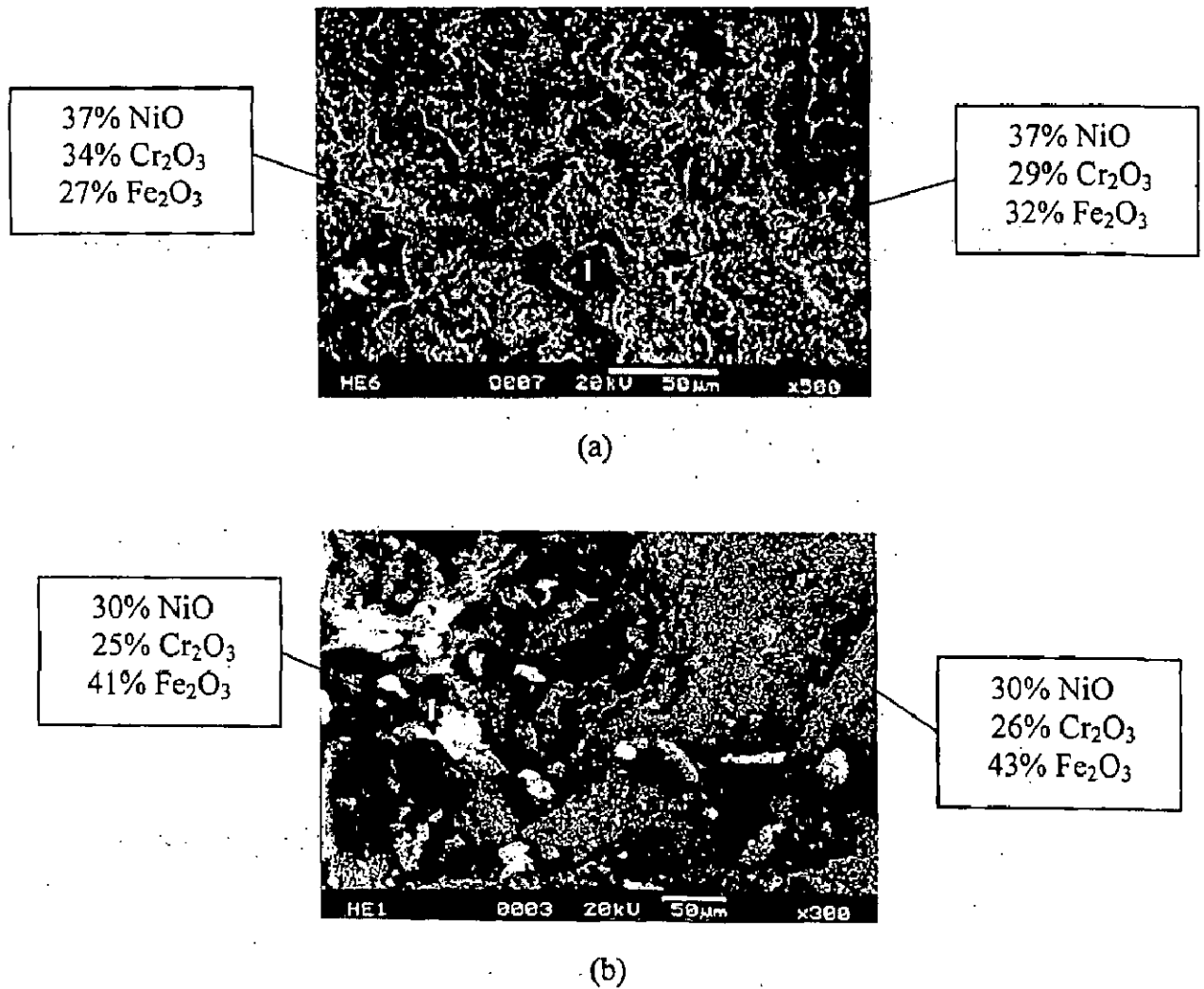
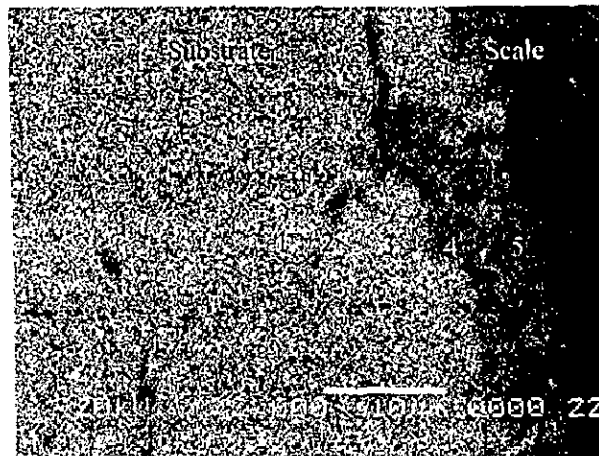
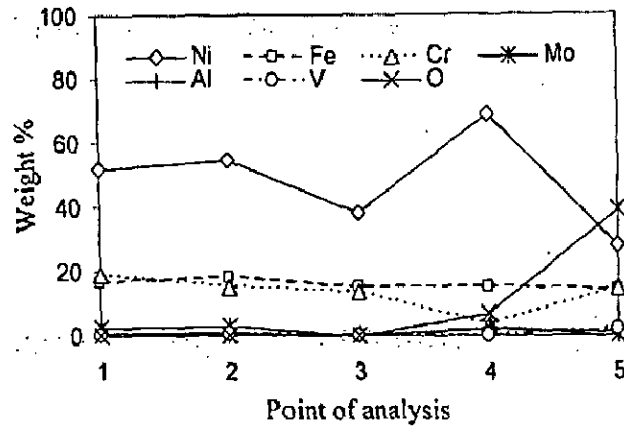


Fig. 6.7 Surface scale morphology and EDAX analysis for the uncoated superalloys subjected to cyclic oxidation in  $\text{Na}_2\text{SO}_4\text{-60}\%\text{V}_2\text{O}_5$  at  $900^\circ\text{C}$  for 50 cycles  
 (a) Superni 75 (b) Superni 600 (c) Superni 601.



**Fig. 6.8** Surface scale morphology and EDAX analysis for the uncoated superalloys subjected to cyclic oxidation in  $\text{Na}_2\text{SO}_4$ -60% $\text{V}_2\text{O}_5$  at  $900^\circ\text{C}$  for 50 cycles  
 (a) Superni 718      (b) Superfer 800H.



**Fig. 6.9**

Oxide scale morphology and variation of elemental composition across the cross-section of uncoated superalloy Superni 718 subjected to cyclic oxidation in  $\text{Na}_2\text{SO}_4\text{-60\%V}_2\text{O}_5$  at  $900^\circ\text{C}$  after 50 cycles.

#### 6.1.1.6 EPMA Analysis

BSEI and X-ray mappings for the superalloy Superni 75 after 50 cycles of hot corrosion in an environment of  $\text{Na}_2\text{SO}_4$ -60% $\text{V}_2\text{O}_5$  at  $900^\circ\text{C}$ , Fig. 6.10 indicate a scale consisting mainly of nickel and chromium. The scale also contains titanium and iron dispersed throughout its cross-section. Further it can be seen that the scale has relatively high concentration of nickel in its upper region, where chromium concentration is low. Whereas chromium has formed a continuous band in the lower portion of the scale. Nickel and iron are present in relatively small quantities in this band. Some Cr-depleted areas can also be seen just below the scale/base alloy substrate, where mainly nickel is present.

Whereas EPMA analysis for the hot corroded Superni 600, Fig. 6.11 reveals an oxide scale which is mainly having nickel and iron present in it. At most of the places nickel and iron are co-existing, while at other places where chromium is present in rich concentrations, nickel and iron are absent. There is a vanadium rich band slightly above the scale/substrate interface, which contains iron, nickel and chromium also. The area just below the scale/substrate interface, which represents the internal penetration zone, has mainly nickel present in it with depletion of iron. There are some Cr-rich stringers present in this internal penetration zone perhaps along the grain boundaries, where nickel is depleted of. Mn has shown tendency to get concentrated in these stringers. Traces of Mn and Na are present throughout the scale.

A similar analysis of the oxide scale for the superalloy Superni 601 after cyclic corrosion for 50 cycles is shown in Fig. 6.12. The scale mainly consists of different sub-layers. The upper layer is rich in iron with clusters of aluminium, and also contains some nickel and chromium. The middle layer of the scale has high chromium concentration alongwith some aluminium rich areas. Iron is absent in this layer. Nickel has shown its presence in the form of a dense band just below the scale/substrate interface.

X-ray mappings for Superni 718 superalloy (Fig. 6.13) indicate a top layer mainly containing nickel and iron, with some chromium present in it. Vanadium is also present in high concentrations in this top layer. Below this top layer, there is a sublayer rich in chromium and vanadium. Titanium has shown its presence in this layer, particularly in the form of some stringers penetrating into the alloy substrate. Ni and Fe are absent along these stringers. Aluminium and silicon can also be observed throughout the scale cross-section. Molybdenum has shown tendency to concentrate in



the substrate just below the interface between scale and substrate. Si is present in high concentration at the top of the scale and also in the form of globules in the base alloy.

BSEI and X-ray mappings for the superalloy Superfer 800H exposed to Na<sub>2</sub>SO<sub>4</sub>-60%V<sub>2</sub>O<sub>5</sub> at 900<sup>o</sup>C for 50 cycles are shown in Fig. 6.14. The scale is rich in Cr with the presence of Ni, Fe, Al, Ti and Mn. Nickel, aluminium and titanium are present in the scale in substantial concentrations, whereas manganese and vanadium are present in very small quantities. There are some patches containing aluminium, where all other elements are absent. At some other places in the scale there are small streaks containing Fe and Ti, where Ni is absent. Silicon is found dispersed into the scale with some tendency to form clusters, one being very prominent near the scale/substrate interface. Traces of sulphur could also be seen in the scale.

## **6.1.2 NiCrAlY Coating**

### **6.1.2.1 Visual Examination**

Macrographs for the corroded surfaces of plasma spray NiCrAlY coated Superni 75, 600, 601, 718 and Superfer 800H superalloys after an exposure to Na<sub>2</sub>SO<sub>4</sub>-60%V<sub>2</sub>O<sub>5</sub> environment for 50 cycles at 900<sup>o</sup>C are shown in Fig. 6.15. It was observed that for all the coated superalloys, colour of the scale changed to dull green from dark grey with the progress of the study. The behaviour of the NiCrAlY coated superalloys was found to be similar. Small superficial cracks were observed at or near some of edges of the specimens during the very first few cycles of exposure leading to minor spalling of the coating from the edges in form of tiny flakes, which stopped towards the end of exposure time in the range of 44<sup>th</sup>-47<sup>th</sup> cycle. However, magnitude of this spallation of the coating was marginal. The spalled flakes came out from the outer layers of the coatings. However, only some edges along the length of the specimens were affected by spalling while others were found be unaffected. Similar tendency towards slight spallation of the coating from or/and near the edges was also shown by all the other coatings viz. Ni-20Cr, Ni<sub>3</sub>Al and Stellite-6 under current investigation during oxidation in the given molten salt environment.

Slight spalling of the scale was indicated in the cases of NiCrAlY coated Superni 75, 600 and 718 in the form of green powder towards the end of exposure from the spots from which coating was detached due to the superficial cracking. Whereas the coated Superni 601 and Superfer 800H showed little spalling of the scales in general from 24<sup>th</sup> and 45<sup>th</sup> cycle onwards respectively.

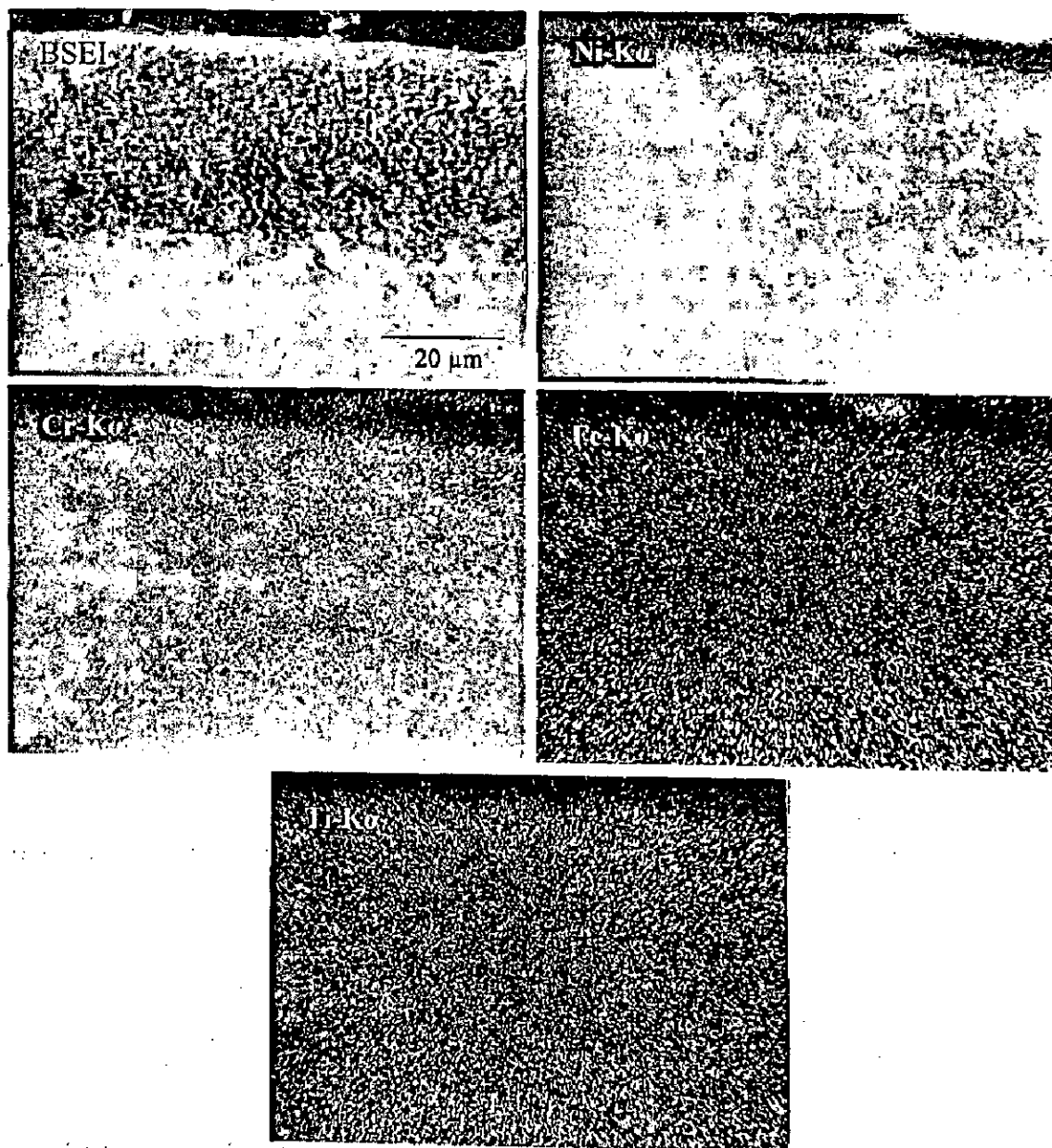
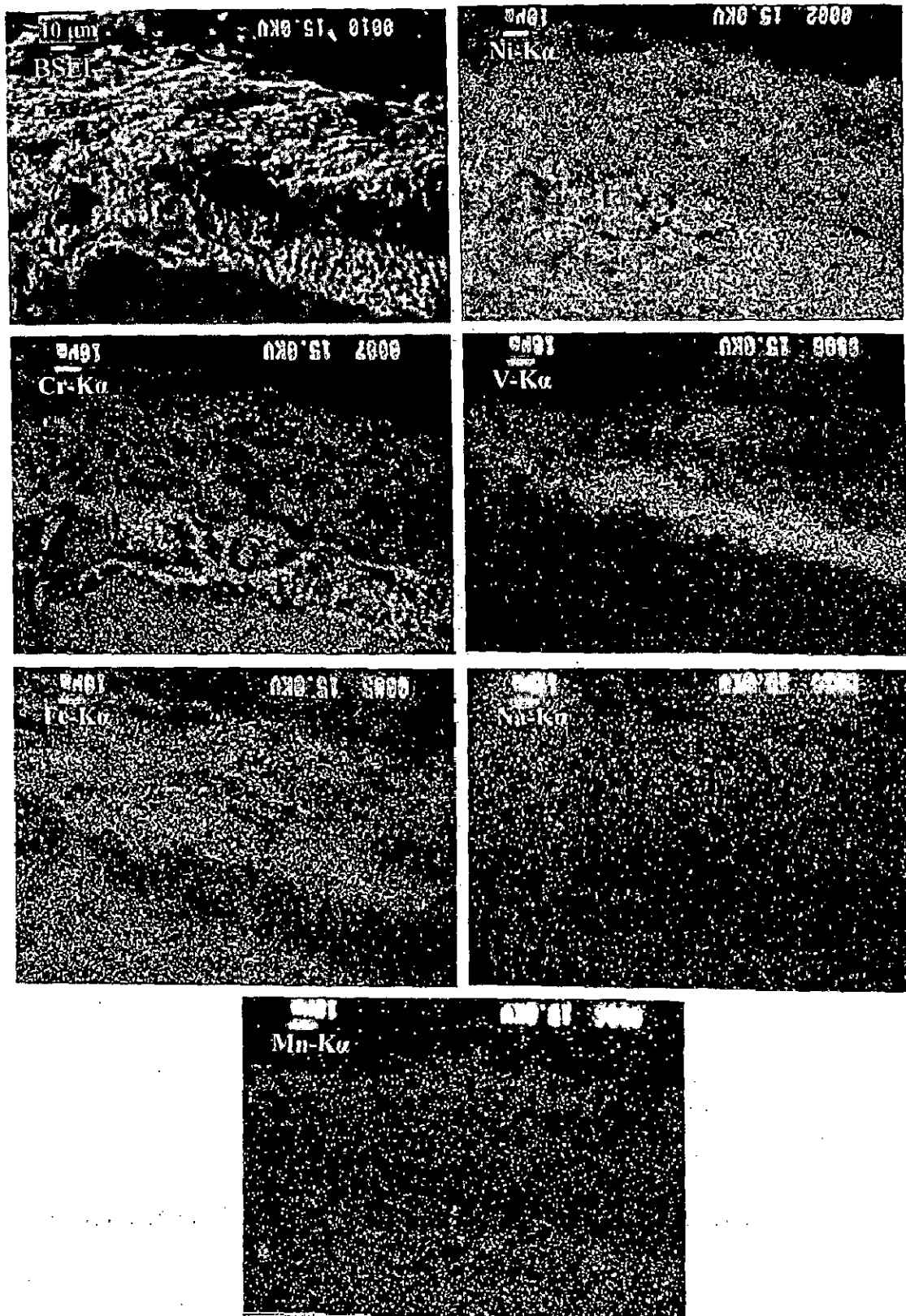


Fig. 6.10 BSEI and X-ray mappings of the cross-section of Superni 75 subjected to cyclic oxidation in  $\text{Na}_2\text{SO}_4\text{-}60\%\text{V}_2\text{O}_5$  at  $900^\circ\text{C}$  after 50 cycles.



**Fig. 6.11** BSEI and X-ray mappings of the cross-section of Superni 600 subjected to cyclic oxidation in  $\text{Na}_2\text{SO}_4$ -60% $\text{V}_2\text{O}_5$  at  $900^\circ\text{C}$  after 50 cycles.

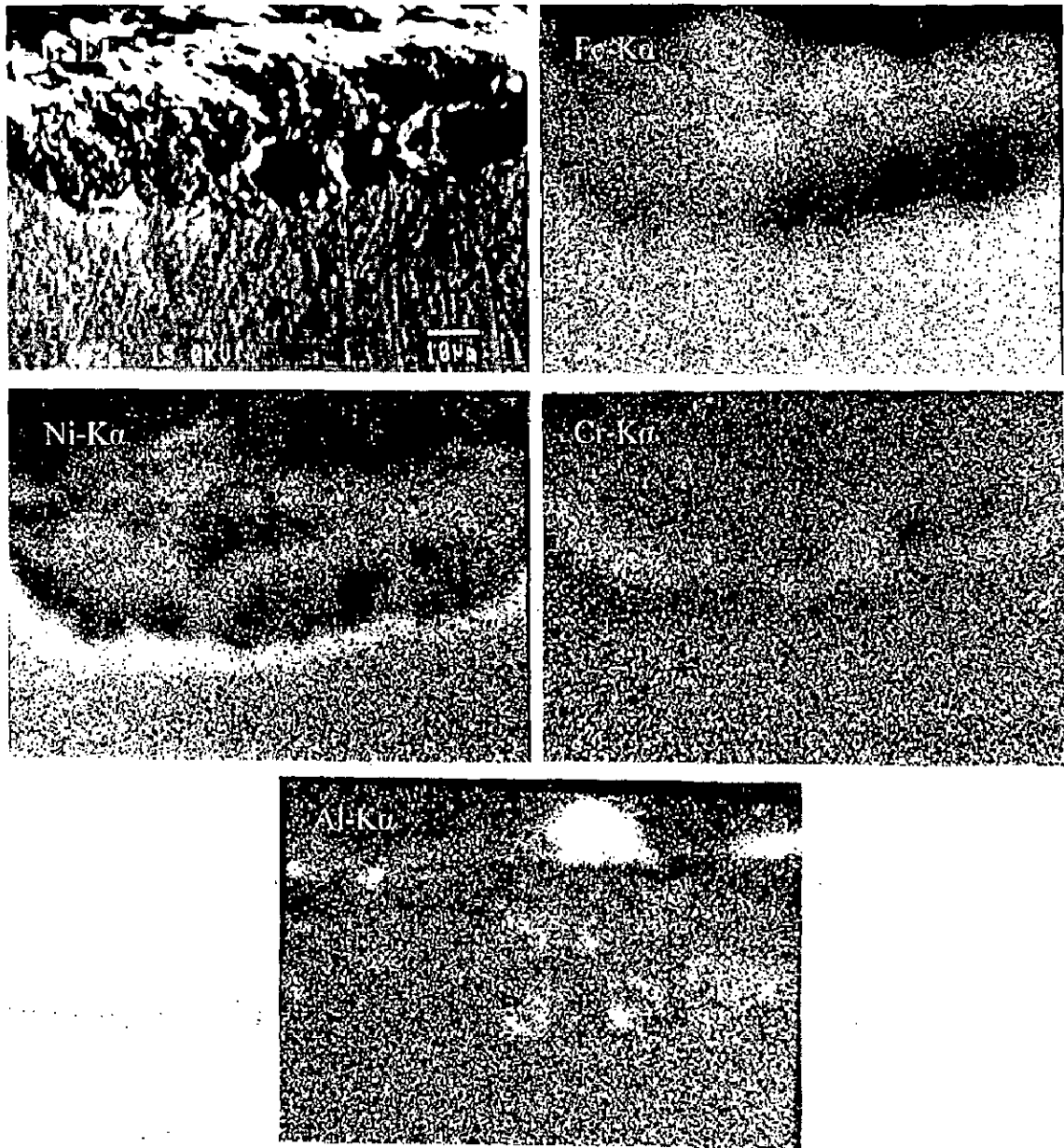


Fig. 6.12 BSEI and X-ray mappings of the cross-section of Superni 601 subjected to cyclic oxidation in  $\text{Na}_2\text{SO}_4$ -60% $\text{V}_2\text{O}_5$  at 900°C after 50 cycles.

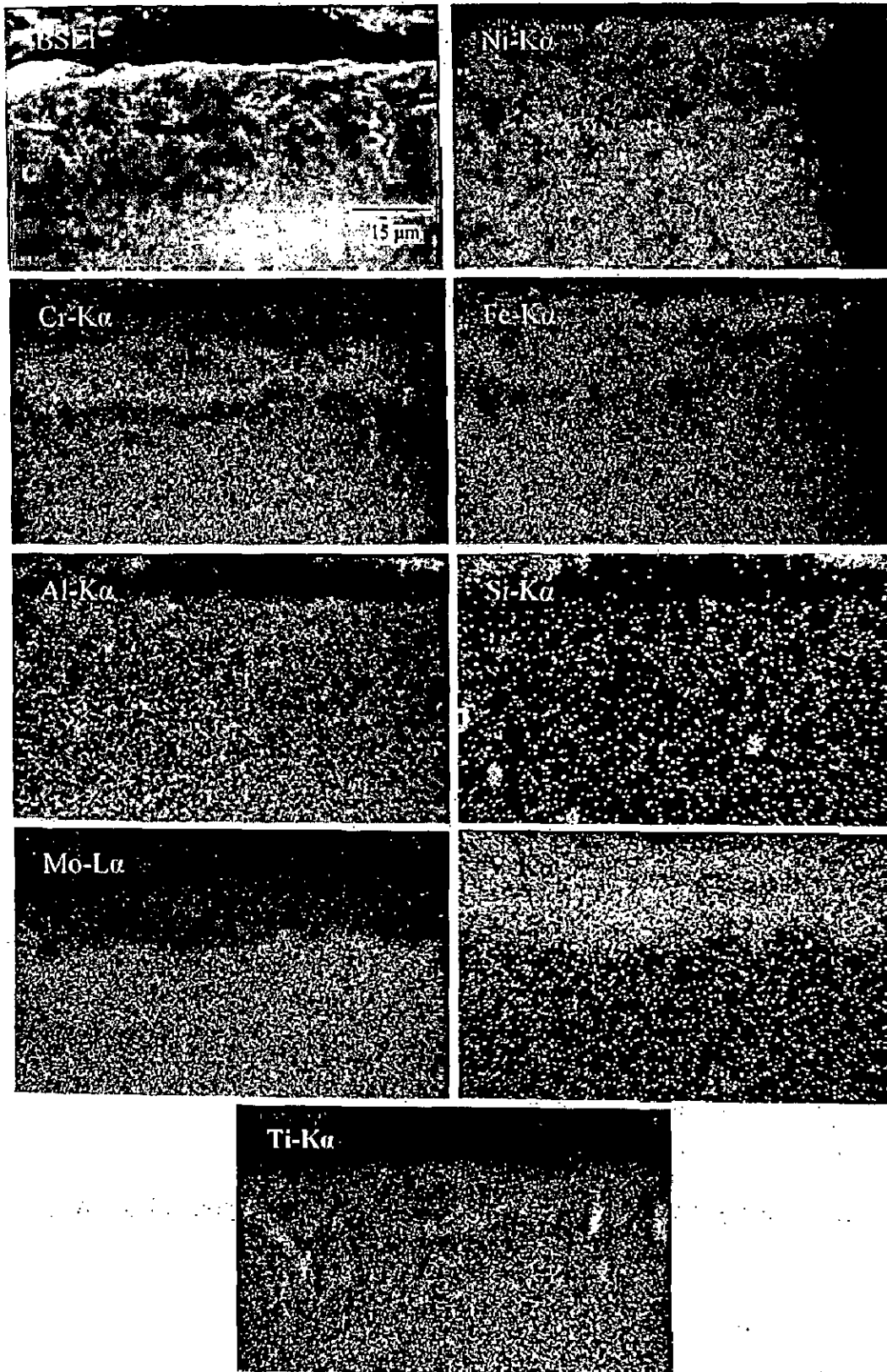


Fig. 6.13 BSEI and X-ray mappings of the cross-section of Superni 718 subjected to cyclic oxidation in  $\text{Na}_2\text{SO}_4\text{-60\%V}_2\text{O}_5$  at  $900^\circ\text{C}$  after 50 cycles.

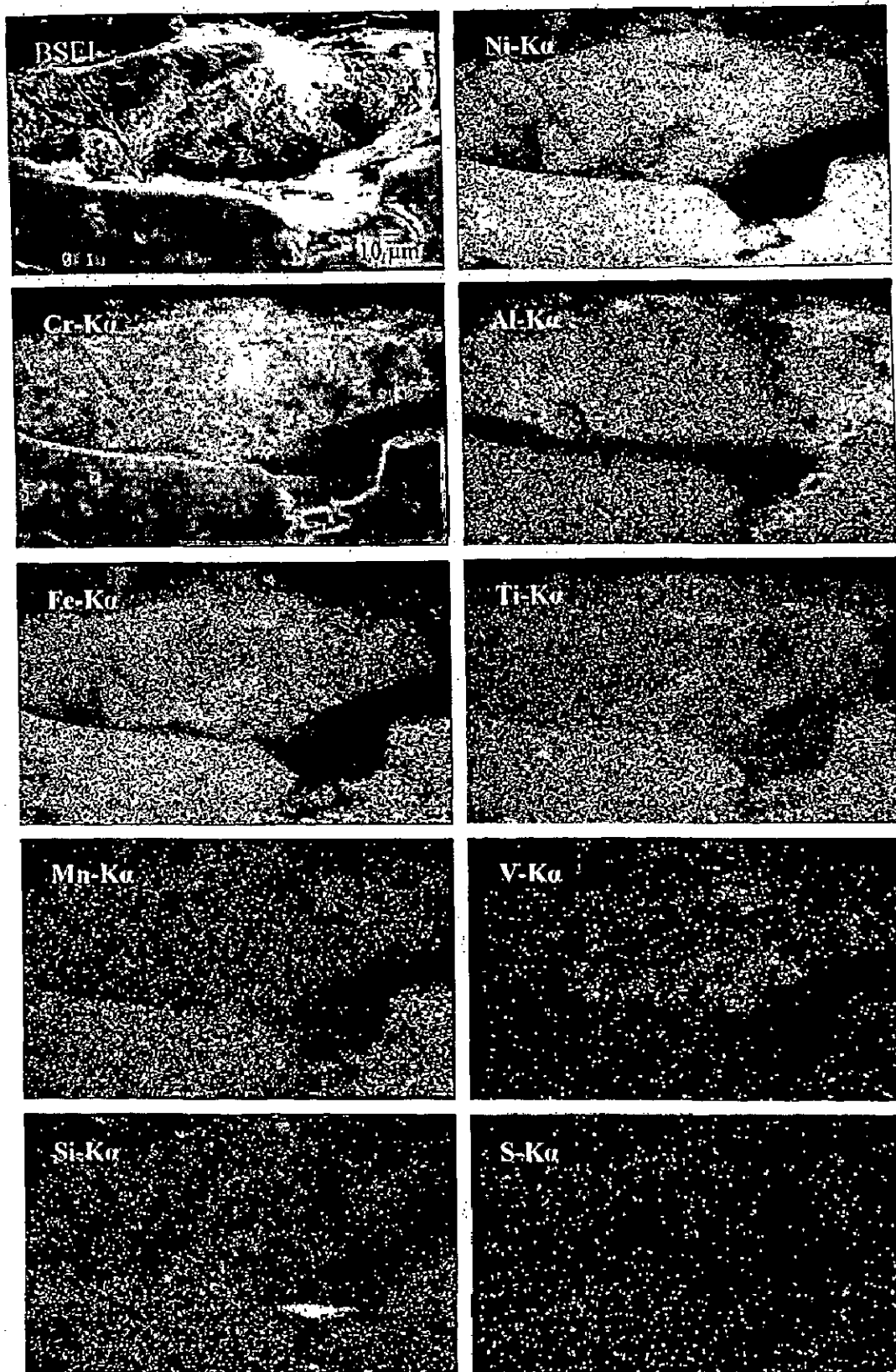
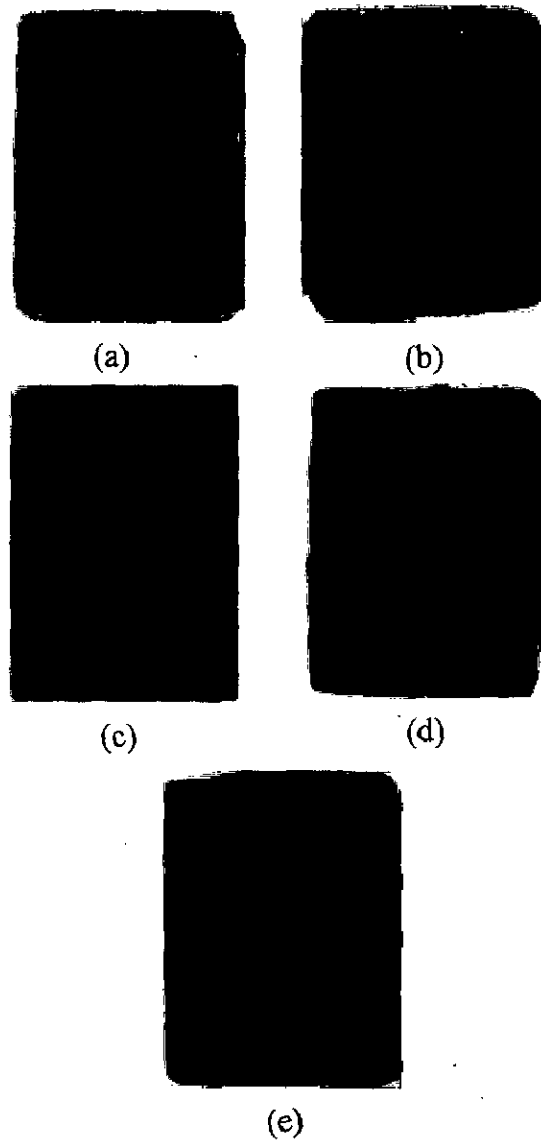


Fig. 6.14 BSEI and X-ray mappings of the cross-section of Superfer 800H subjected to cyclic oxidation in  $\text{Na}_2\text{SO}_4$ -60% $\text{V}_2\text{O}_5$  at  $900^\circ\text{C}$  after 50 cycles.



**Fig. 6.15**

Macrographs of the NiCrAlY coating with bond coat subjected to cyclic oxidation in  $\text{Na}_2\text{SO}_4\text{-60\%V}_2\text{O}_5$  at  $900^\circ\text{C}$  for 50 cycles having substrate superalloys.

- |                 |                    |                 |
|-----------------|--------------------|-----------------|
| (a) Superni 75  | (b) Superni 600    | (c) Superni 601 |
| (d) Superni 718 | (e) Superfer 800H. |                 |

### 6.1.2.2 *Thermogravimetric Data*

Weight gain ( $\text{mg}/\text{cm}^2$ ) data plotted versus time expressed in number of cycles for Superni 75, 600, 601, 718 and Superfer 800H superalloys with and without the coating of NiCrAlY is reported in Fig. 6.16. It can be inferred from the plots that the necessary protection against hot corrosion has been provided by the NiCrAlY coating as the weight gain values for the coated superalloys are smaller than those for respective uncoated superalloys in all the cases. With regard to the resistance imparted by the coating to the base superalloys, the reduction in weight gain is found to be nearly same in case of Superni 600 and Superni 601. This coating has provided best protection to the Fe-base superalloy Superfer 800H as the weight gain in this case has reduced to around 1/9 of that conceived by the uncoated superalloy. In case of bare Superni 718, although the overall weight gain could not be measured for the 50 cycles due to intense spalling and sputtering, yet the weight gain by the uncoated Superni 718 upto 20 cycles is higher than that gained by its coated counterpart after 50 cycles. The plasma spray NiCrAlY coated Superni 75, 600 and Superfer 800H superalloys have shown identical weight gain values, whereas the values are nearly same for Superni 601 and Superni 718. Moreover the coated Superni 601 and Superni 718 superalloys have shown relatively less resistance to hot corrosion as compared to that shown by coated Superni 75, 600 and Superfer 800H superalloys. Moreover all the coated superalloys have nearly followed the parabolic behaviour upto 50 cycles as can be inferred from square of weight change ( $\text{mg}^2/\text{cm}^4$ ) vs. number of cycles plots in Fig. 6.17. The parabolic rate constants ( $K_p$  in  $10^{-10} \text{ g}^2 \text{ cm}^{-4} \text{ s}^{-1}$ ) for the coated superalloys Superni 75, 600, 601, 718 and Superfer 800H are evaluated as 1.48, 1.71, 2.82, 4.88 and 1.38 respectively.

### 6.1.2.3 *Scale Thickness Measurement*

SEM back scattered images across the cross-sections of NiCrAlY coated superalloys Superni 75, 601 and 718 after hot corrosion for 50 cycles at  $900^\circ\text{C}$  are shown in Fig. 6.18, while corresponding images for the coated Superni 600 and Superfer 800H are depicted in Fig. 6.22 (a) and (b) respectively. These micrographs are obtained for the locations at which the scale thickness was the least. The average scale thickness values measured for the coated Superni 75, 600, 601, 718 and Superfer 800H are 139, 144, 165, 179 and 253  $\mu\text{m}$  respectively. Evidently the scale thickness is highest in case of NiCrAlY coated Fe-base superalloy Superfer 800H.



#### 6.1.2.4 X-ray Diffraction Analysis

X-ray diffractograms for the corroded surfaces of NiCrAlY coated superalloys after cyclic studies in molten salt are shown in Fig. 6.19 on reduced scales. All the corroded superalloys indicated the formation of similar phases. The main phases revealed by XRD analysis are NiO, Al<sub>2</sub>O<sub>3</sub> and NiCr<sub>2</sub>O<sub>4</sub> for all the NiCrAlY coated superalloys. Some relatively low intensity peaks pertaining to Cr<sub>2</sub>O<sub>3</sub> phase could also be analysed in all the cases, few of these peaks are visible in respective diffractograms whereas others are not discernible due to reduced scales.

#### 6.1.2.5 SEM/EDAX Analysis

##### (a) Surface Morphology

SEM micrograph and EDAX analysis for NiCrAlY coated superalloys after hot corrosion in molten salt for 50 cycles at 900<sup>o</sup>C are given in Fig. 6.20 and Fig. 6.21. The micrographs in case of coated Superni 75, 600 and 718 superalloys indicate the presence of irregular shaped crystals dispersed throughout their scales, whereas in case of coated Superni 601 and Superfer 800H the scales are fine grained. In the Superni 75, the white phase, which is indicative of the uppermost layer of the scale, consists mainly of NiO and contains small quantities of oxides of Na, Cr, Al and V. The sub-scale (black phase) of the scale is found to have substantial amounts of oxides of Al, Ni, Cr and Na. Whereas in the case of coated Superni 600, the scale is also rich in NiO in the upper layer, but the sub-scale is having mainly Cr<sub>2</sub>O<sub>3</sub>, with NiO and Al<sub>2</sub>O<sub>3</sub> as other prominent phases. The scale for the coated Superni 601 shows the growth of dense white areas, which contain substantial amounts of NiO, Cr<sub>2</sub>O<sub>3</sub> and Al<sub>2</sub>O<sub>3</sub> as revealed by EDAX analysis at point 2, Fig. 6.20 (c). The spalled region of the scale mainly contains NiO, where the amounts of Cr<sub>2</sub>O<sub>3</sub> and Al<sub>2</sub>O<sub>3</sub> have got reduced. Further a continuous and smooth scale with uniform composition could be seen for hot corroded NiCrAlY coated Superni 718 superalloy, which has NiO as its main constituent, Fig. 6.21 (a). Similarly in the case of Superfer 800H [Fig. 6.21(b)], a Cr<sub>2</sub>O<sub>3</sub>-rich uniform composition and continuous surface scale is revealed.

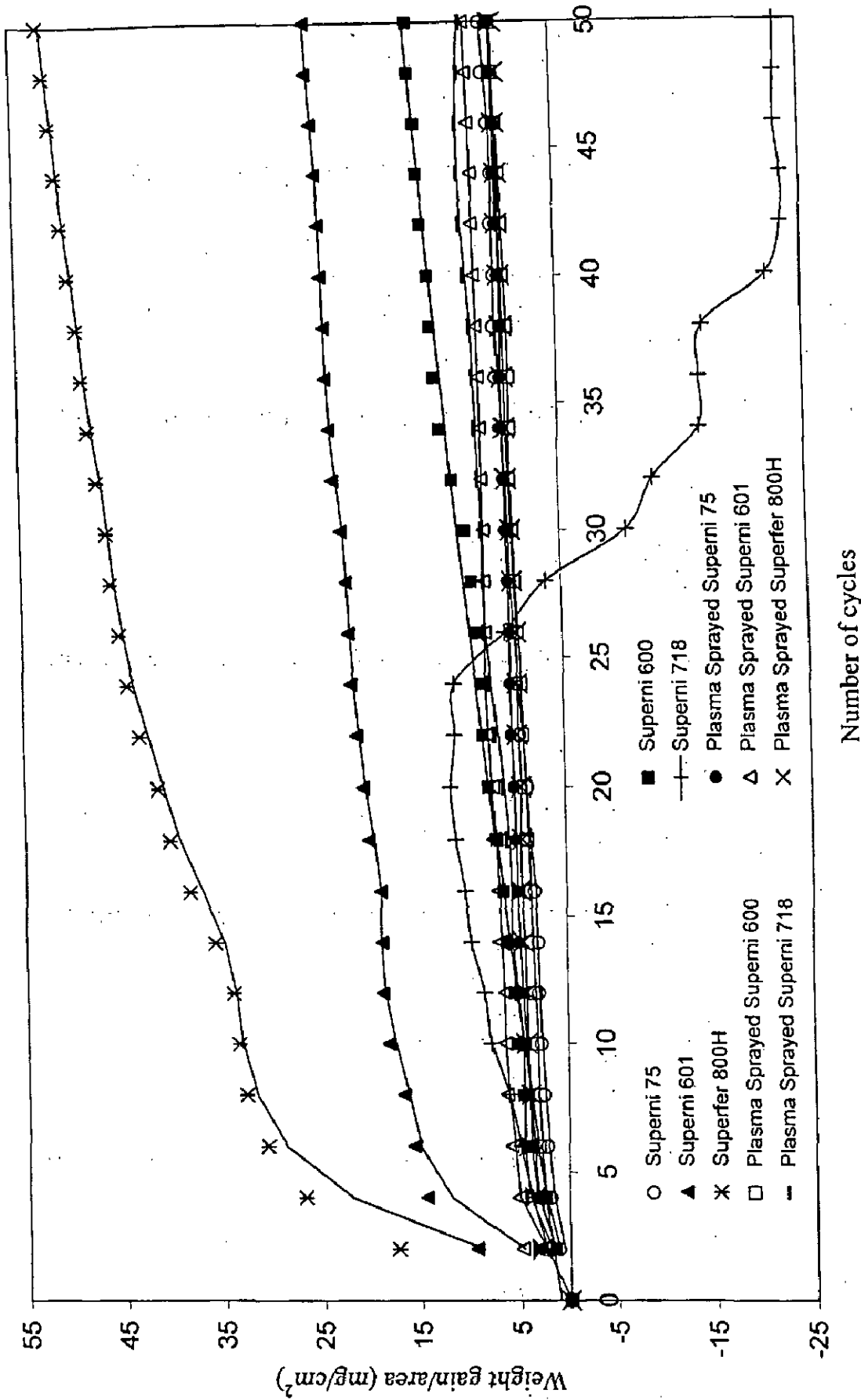


Fig. 6.16 Weight gain vs. number of cycles plot for uncoated and NiCrAlY coated superalloys subjected to cyclic oxidation for 50 cycles in  $\text{Na}_2\text{SO}_4\text{-60\%V}_2\text{O}_5$  at  $900^\circ\text{C}$ .

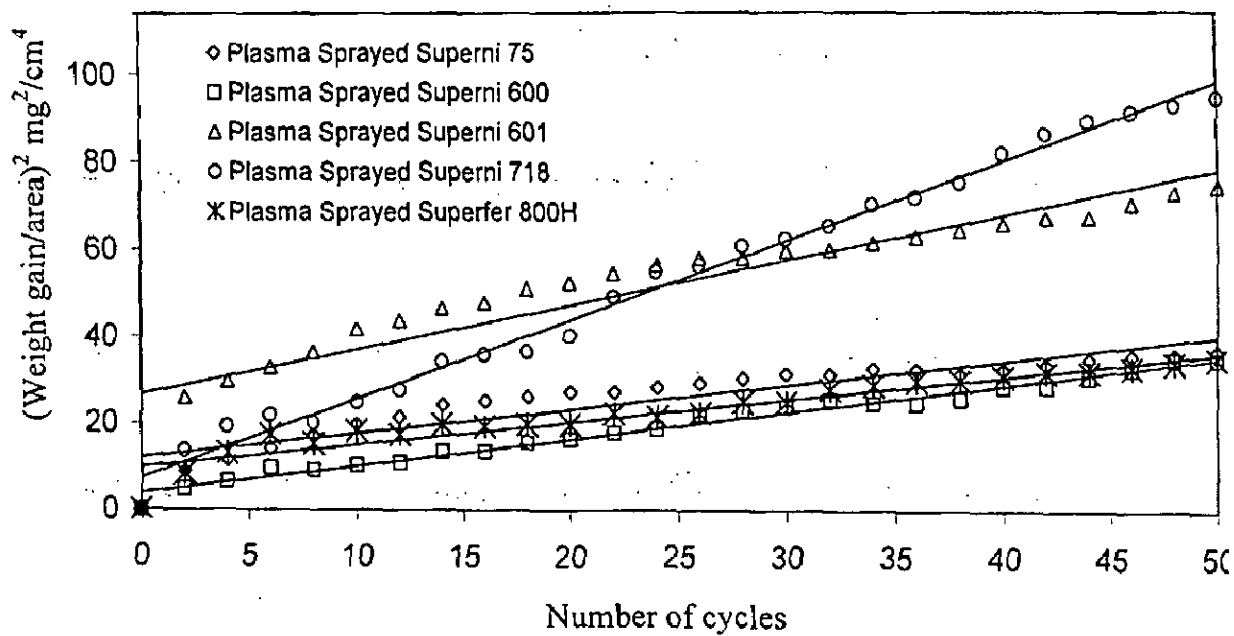
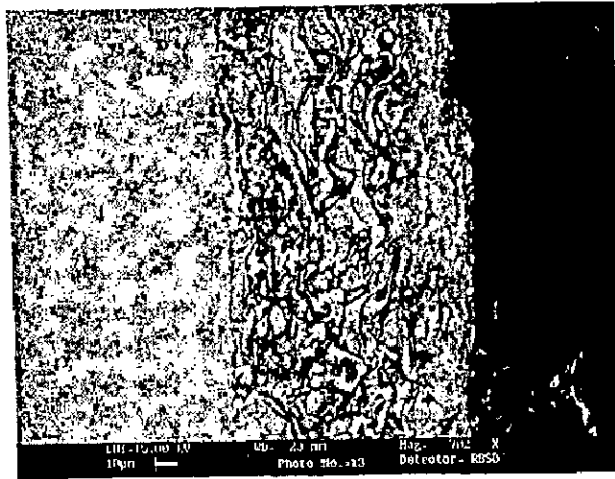
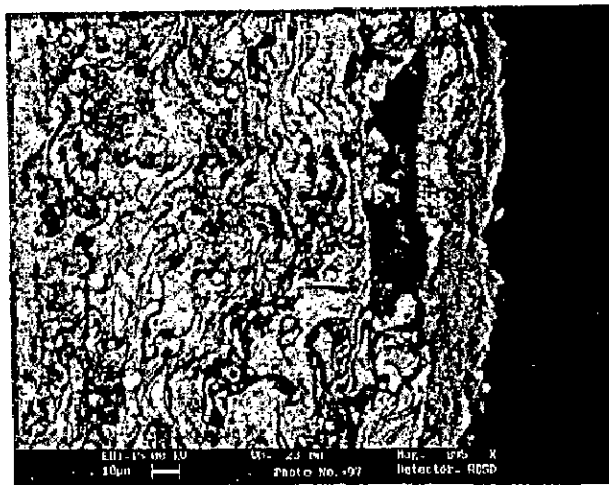


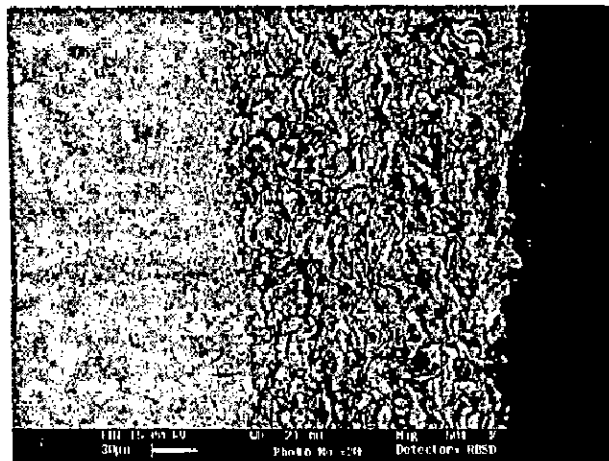
Fig. 6.17  $(\text{Weight gain/area})^2$  vs. number of cycles plot for the NiCrAlY coated superalloys subjected to cyclic oxidation for 50 cycles in  $\text{Na}_2\text{SO}_4$ -60% $\text{V}_2\text{O}_5$  at  $900^\circ\text{C}$ .



(a)



(b)



(c)

**Fig. 6.18**

SEM back scattered images for the NiCrAlY coated superalloys after cyclic oxidation in  $\text{Na}_2\text{SO}_4$ -60% $\text{V}_2\text{O}_5$  for 50 cycles at  $900^\circ\text{C}$ :

(a) Superni 75

(b) Superni 601

(c) Superni 718.

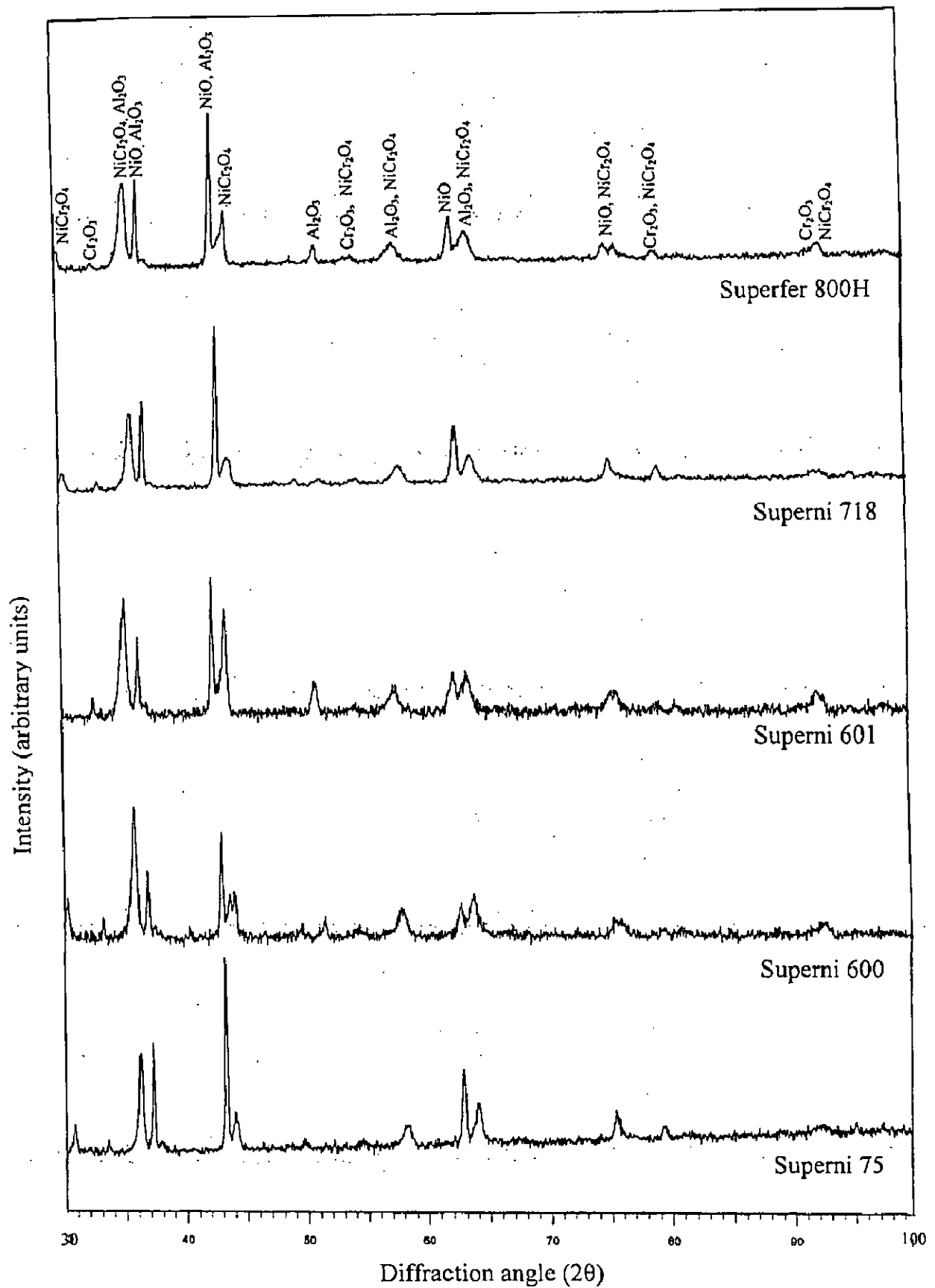
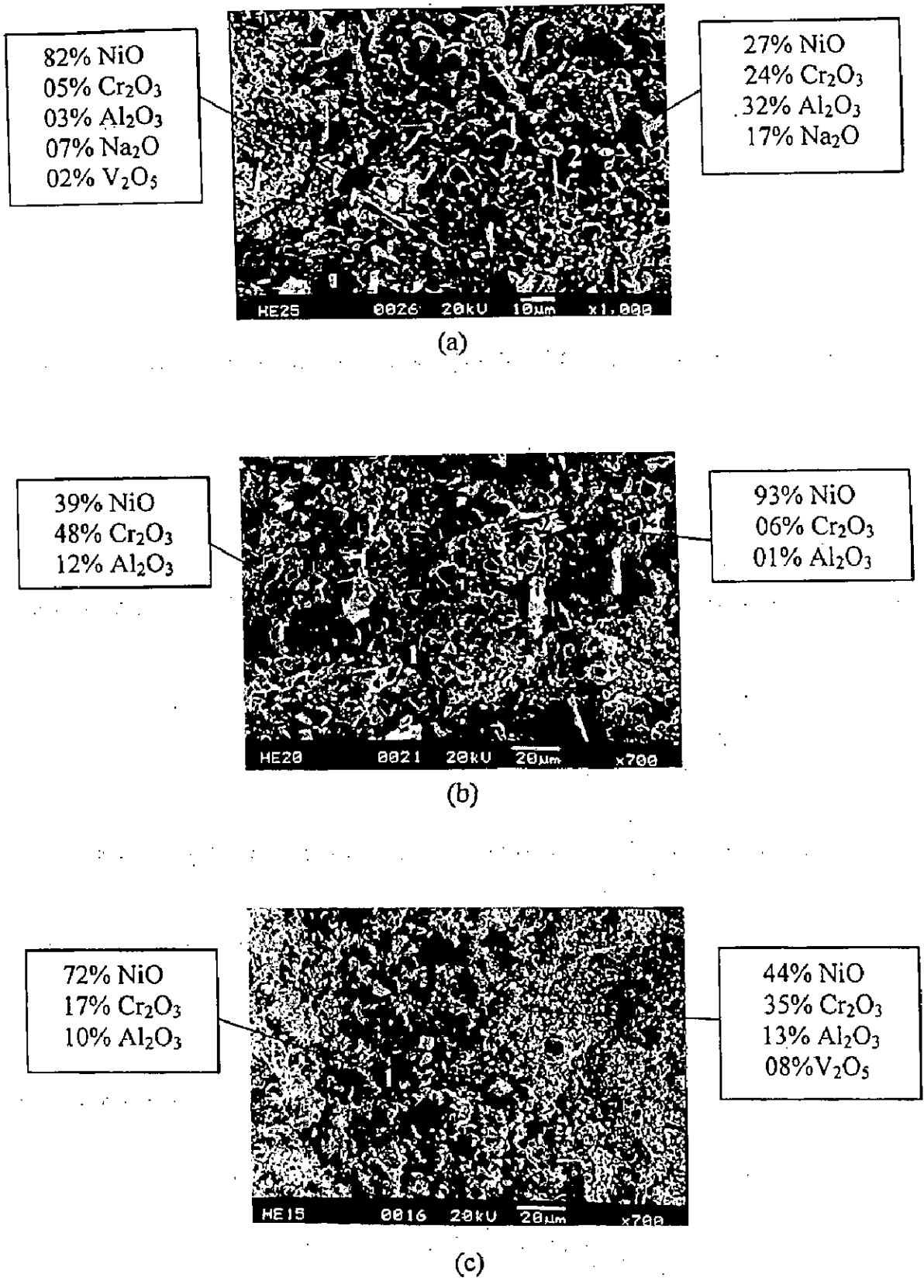
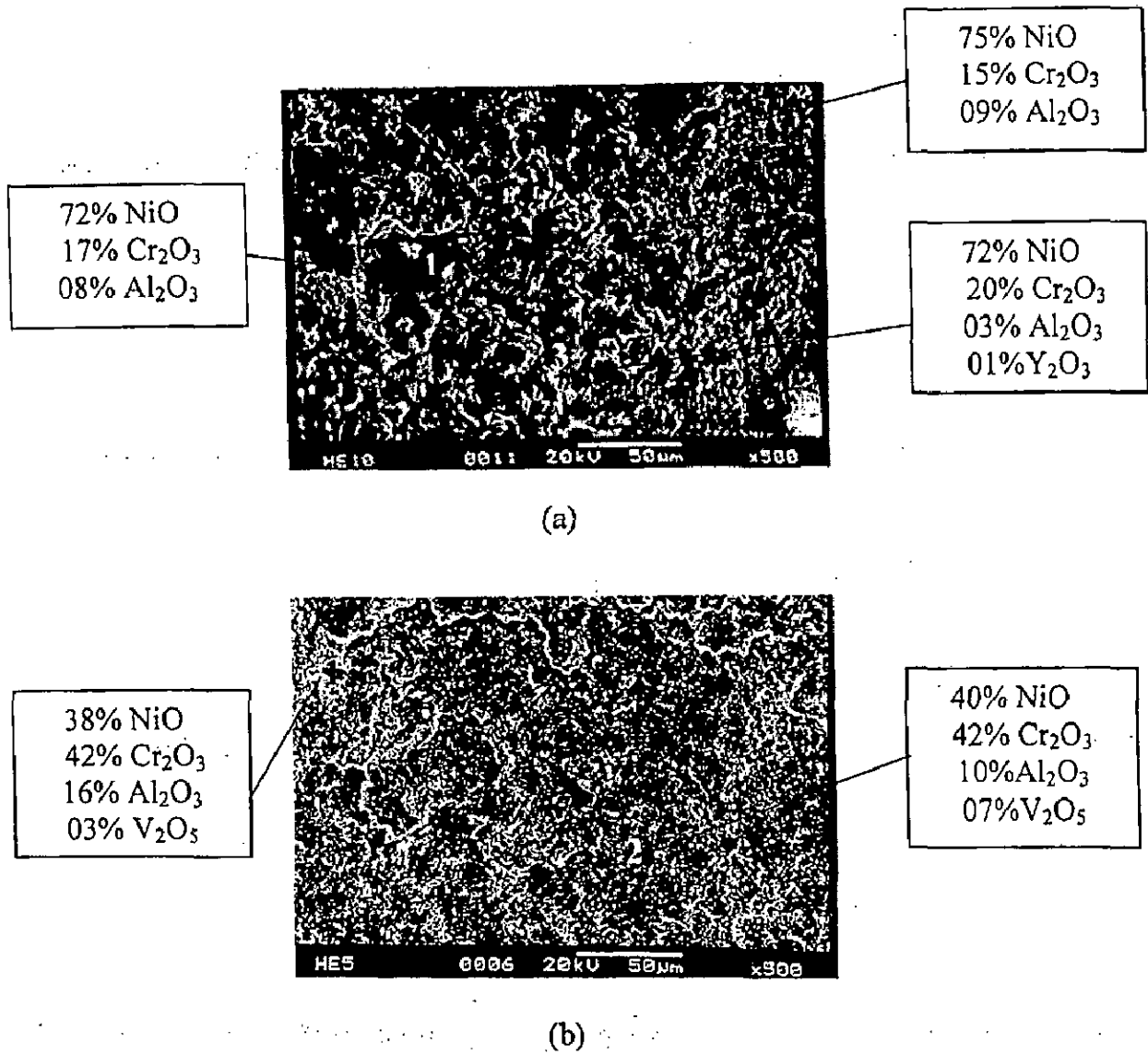


Fig. 6.19 X-ray diffraction patterns for the NiCrAlY coated superalloys subjected to cyclic oxidation in Na<sub>2</sub>SO<sub>4</sub>-60%V<sub>2</sub>O<sub>5</sub> at 900°C after 50 cycles.



**Fig. 6.20** Surface scale morphology and EDAX analysis for the plasma spray NiCrAlY coated superalloys subjected to cyclic oxidation in Na<sub>2</sub>SO<sub>4</sub>-60%V<sub>2</sub>O<sub>5</sub> at 900<sup>o</sup>C for 50 cycles  
 (a) Superni 75      (b) Superni 600      (c) Superni 601.



**Fig. 6.21** Surface scale morphology and EDAX analysis for the plasma spray NiCrAlY coated superalloys subjected to cyclic oxidation in Na<sub>2</sub>SO<sub>4</sub>-60%V<sub>2</sub>O<sub>5</sub> at 900°C for 50 cycles  
 (a) Superni 718 (b) Superfer 800H.

## (b) Cross-Sectional Analysis

BSEI and elemental variation for the cross-section of NiCrAlY coated superalloy Superni 600 subjected to  $\text{Na}_2\text{SO}_4$ -60% $\text{V}_2\text{O}_5$  induced corrosion for 50 cycles at  $900^\circ\text{C}$  are shown in Fig. 6.22 (a). The micrograph shows presence of some lamellar cracks in the upper layers of the scale, while the inner layers of the scale are seen to have retained lamellar structure of sprayed coating. The point wise EDAX analysis shows extensive variations in the concentrations of nickel and oxygen along the thickness of the scale, while the concentration of chromium does not show much variation. The scale in general has indicated the presence of nickel, chromium and aluminium alongwith oxygen at the points of analysis with a comparatively less nickel in the outermost layers of the scale (points 4 and 6). Ni-rich areas in the scale are depleted of Al and vice-versa. At point 6 the presence of vanadium has also been revealed. EDAX analysis at point1 further reveals that oxygen has reached to the substrate, although in small concentration.

An analogous analysis for the hot corroded NiCrAlY coated superalloy Superfer 800H; Fig. 6.22 (b) reveals a scale which has mostly lamellar structure along its cross-section. The scale is found to have alternate Ni-rich and Al-rich layers present in it along its thickness. Whereas, chromium is present in somewhat uniform concentration along the cross-section, except at point 4. At this point a decrease in the amount of Cr and Al is noticed and scale consists mainly of Ni and O. The outer layer of the scale is found to be consisting mainly of Ni and O with small quantities of Cr and Al. The substrate superalloy is found to be unaffected.

### 6.1.2.6 EPMA Analysis

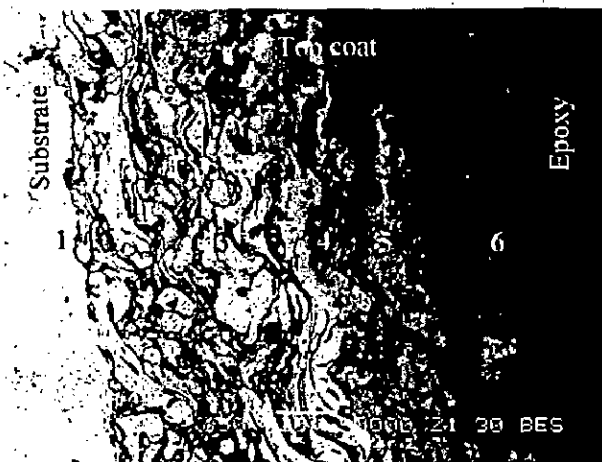
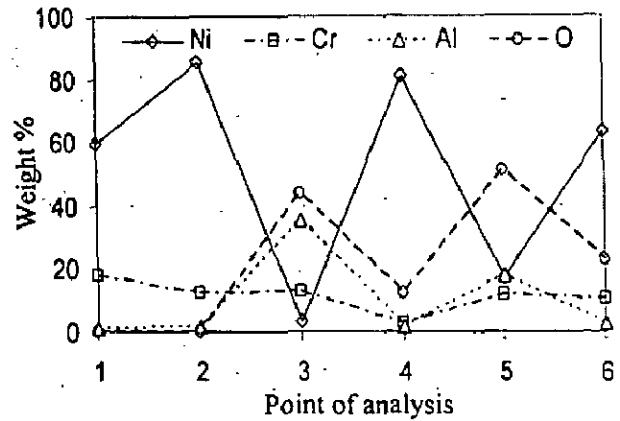
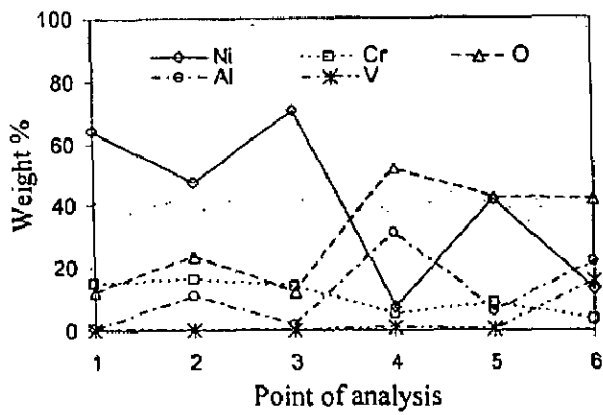
EPMA analysis for the NiCrAlY coated Superni 75 superalloy after exposure to oxidation in  $\text{Na}_2\text{SO}_4$ -60% $\text{V}_2\text{O}_5$  environment for 50 cycles at  $900^\circ\text{C}$  has been compiled in Fig. 6.23 and 6.24. The scale shows a lamellar structure, where the topmost layer mainly consists of aluminium, and also contains Fe and V, Fig. 6.23. Just below this top layer, there is a band having little high concentration of chromium. The inner layers of the scale are consisting of Ni, Cr, Al and Y, with alternate Ni-rich and Al-rich phases present in them. Iron and titanium have diffused from the substrate into the scale in an evenly manner. Titanium has also shown tendency to develop a thin streak at the scale/substrate interface. Traces of sulphur are also seen throughout the scale. Further, it is interesting to note the diffusion of



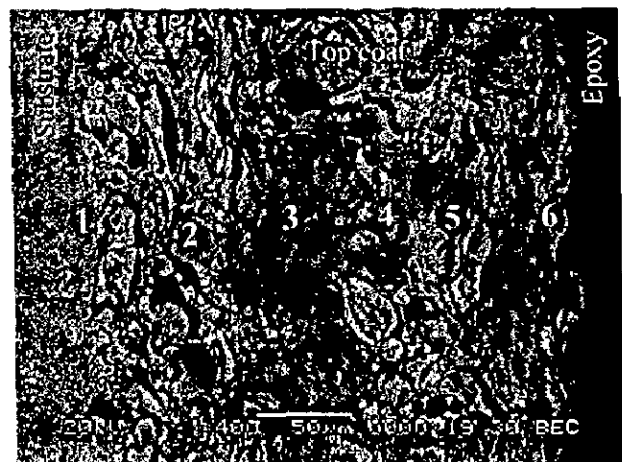
aluminium into the substrate from the coating. Fig. 6.24 shows EPMA analysis for the same specimen at some other cross-section, which indicates that oxygen has penetrated throughout the scale along the splat boundaries to oxidise aluminium. Whereas the splats, consisting of nickel and chromium seem to be in an un-oxidised state. However, some chromium rich stringers can also be observed along the splat boundaries as well as the scale/substrate interface. Further, the top layer of the scale has oxide of mainly chromium, where nickel and aluminium are also seen in mild concentrations.

BSEI micrograph as shown in Fig. 6.25 indicates an oxide scale which has a thin outermost layer, which consists mainly of chromium oxide, alongwith some nickel and aluminium oxides. Just under this layer, there is an intermediate band which is mainly of aluminium oxide. In the remaining scale, the coating seems to have retained its original morphology, where Ni-rich and Al-rich layers are present at alternate positions. The presence of oxygen alongwith aluminium indicates that oxidation of the latter might have taken place, whereas the Ni-rich areas are in unreacted state. Chromium is mainly co-existing with nickel, but it has also formed some clusters in the aluminium rich areas. Vanadium and sulphur have penetrated into the scale. Furthermore, the concentration of vanadium shows a decline as one move towards the base alloy. Whereas sulphur has diffused even into the base alloy and is mainly present in the vicinity of the interface of the scale and the substrate. Iron shows some movement into the entire scale, which is more prominent near the coating/substrate interface.

X-ray mappings for NiCrAlY coated superalloy Superni 601 indicate Al-containing continuous top layer, having Ni and Cr rich areas. Iron has also diffused into this layer. The top layer is followed by a dense underlayer that mainly consists of nickel, Fig. 6.26. The presence of aluminium is indicated at places in the form of streaks in the middle scale where nickel and chromium are absent. On some other places in the middle scale, only chromium is present and Ni is absent. Yttrium is found to be dispersed as clusters throughout the coat, except in the outer layers of the scale, where only traces of it are seen. The diffusion of the iron into the bond coat from the substrate is also indicated. Mn is present at the substrate/scale interface forming small streaks. V can mainly be seen in the top scale.



(a)



(b)

Fig. 6.22 Oxide scale morphology and variation of elemental composition across the cross-section of NiCrAlY coated superalloys subjected to cyclic oxidation in  $\text{Na}_2\text{SO}_4\text{-60\%V}_2\text{O}_5$  at  $900^\circ\text{C}$  after 50 cycles  
 (a) Superni 600 (b) Superfer 800H.

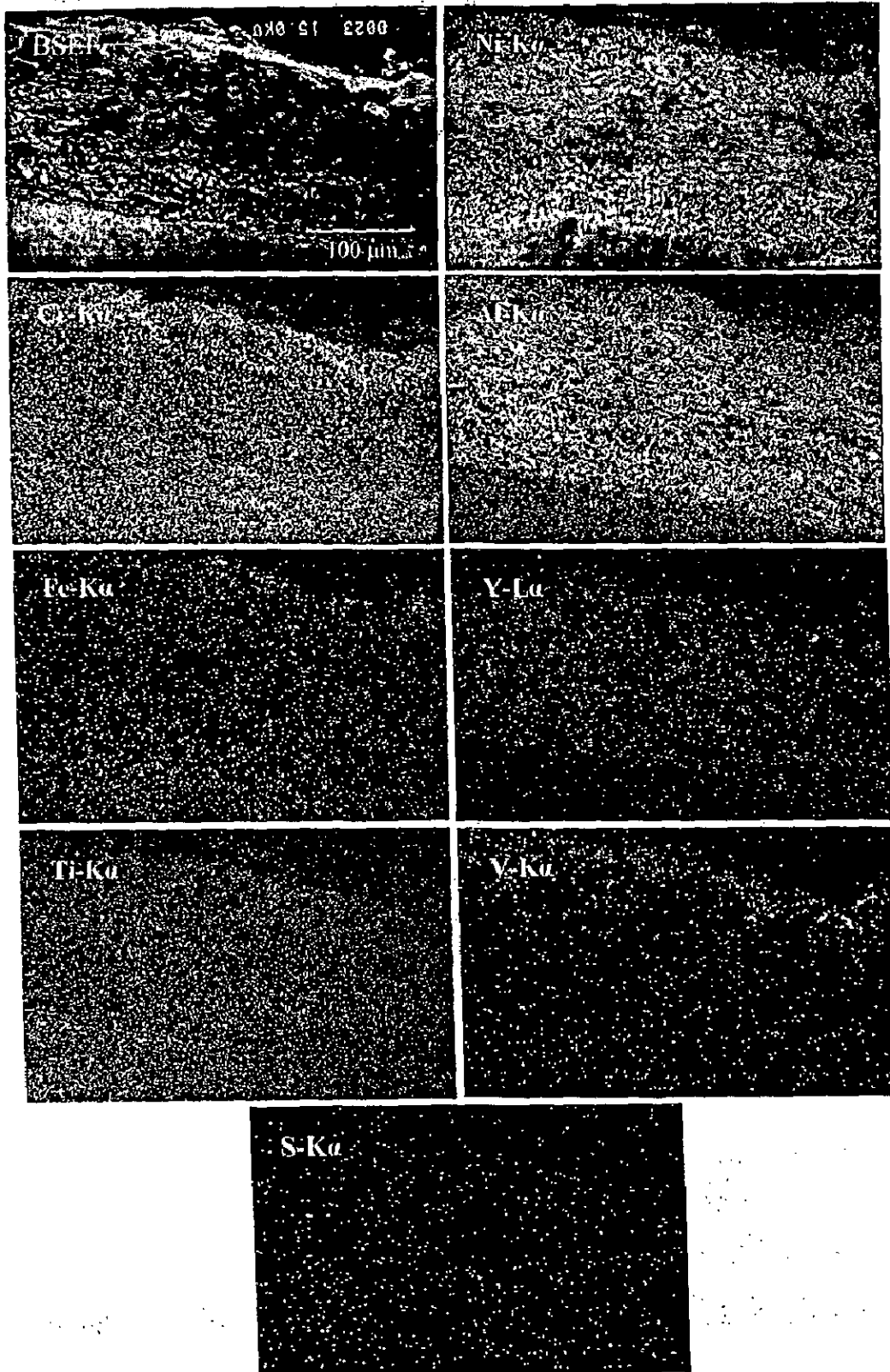
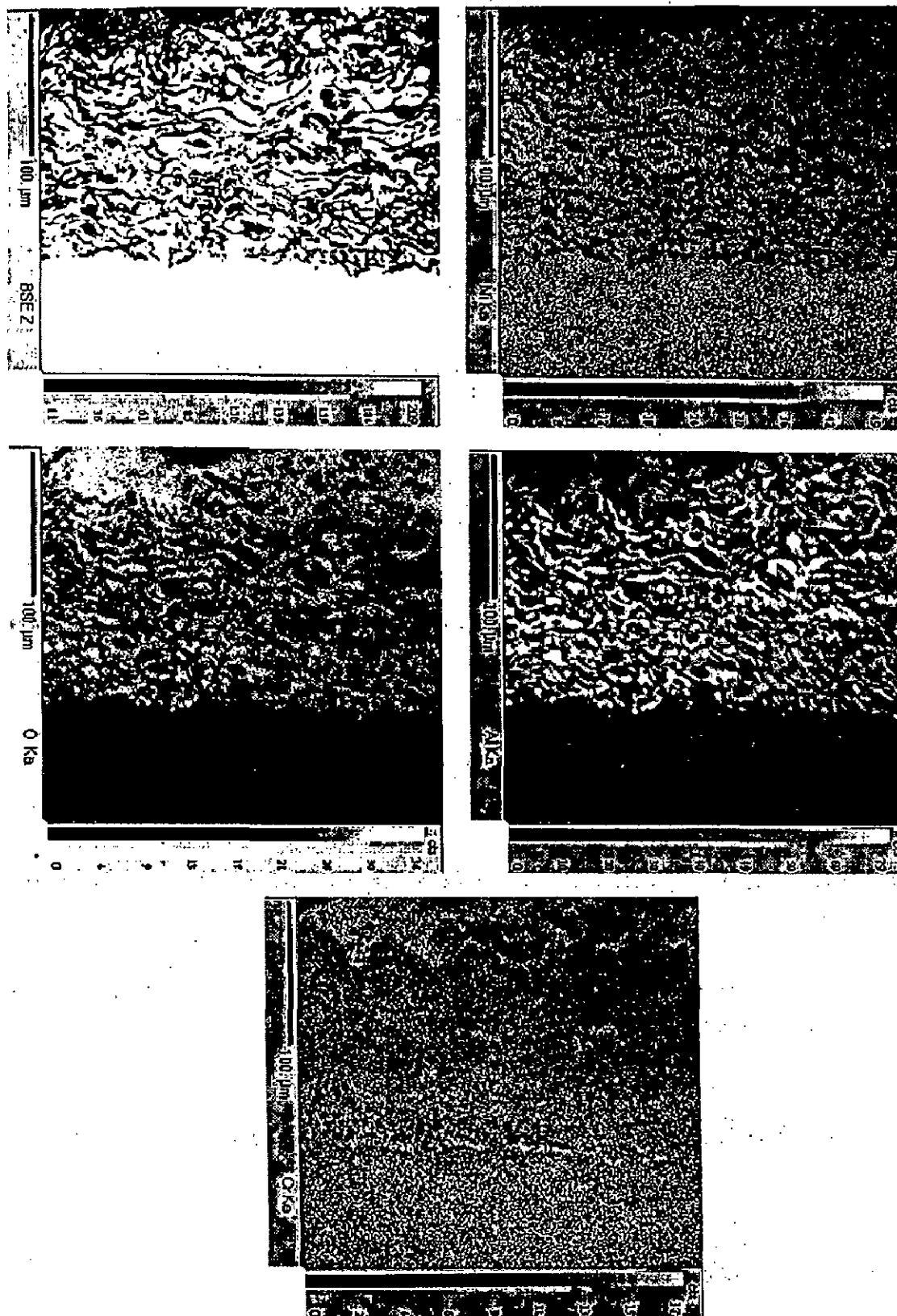
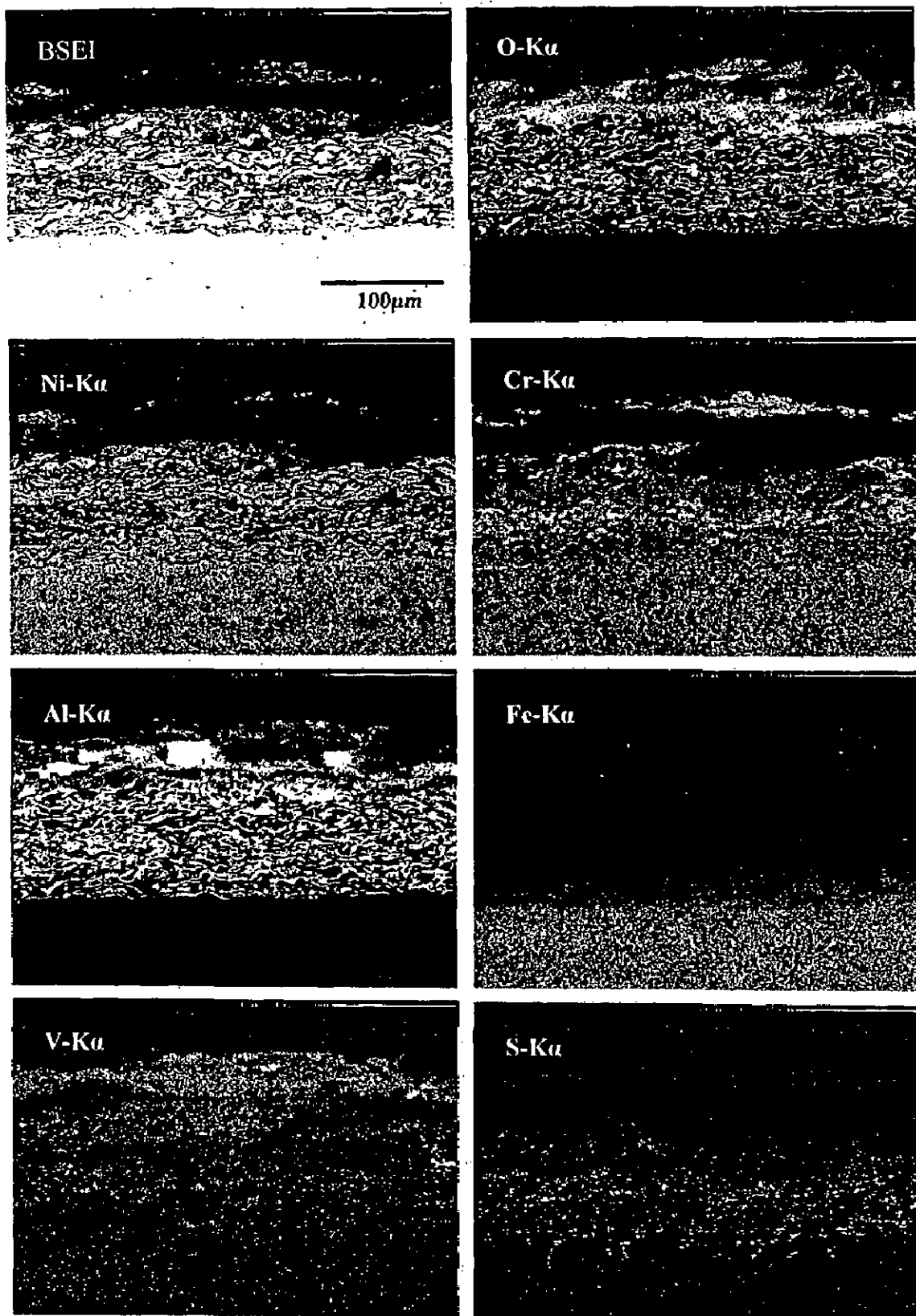


Fig. 6.23 BSEI and X-ray mappings of the cross-section of NiCrAlY coated superalloy Superni 75 subjected to cyclic oxidation in  $\text{Na}_2\text{SO}_4\text{-}60\%\text{V}_2\text{O}_5$  at  $900^\circ\text{C}$  after 50 cycles.



**Fig. 6.24** BSEI and X-ray mappings of the cross-section of NiCrAlY coated superalloy Superni 75 subjected to cyclic oxidation in  $\text{Na}_2\text{SO}_4\text{-60\%V}_2\text{O}_5$  at  $900^\circ\text{C}$  after 50 cycles showing oxygen distribution also.



**Fig. 6.25** BSEI and X-ray mappings of the cross-section of NiCrAlY coated superalloy Superni 600 subjected to cyclic oxidation in  $\text{Na}_2\text{SO}_4$ -60% $\text{V}_2\text{O}_5$  at 900°C after 50 cycles.

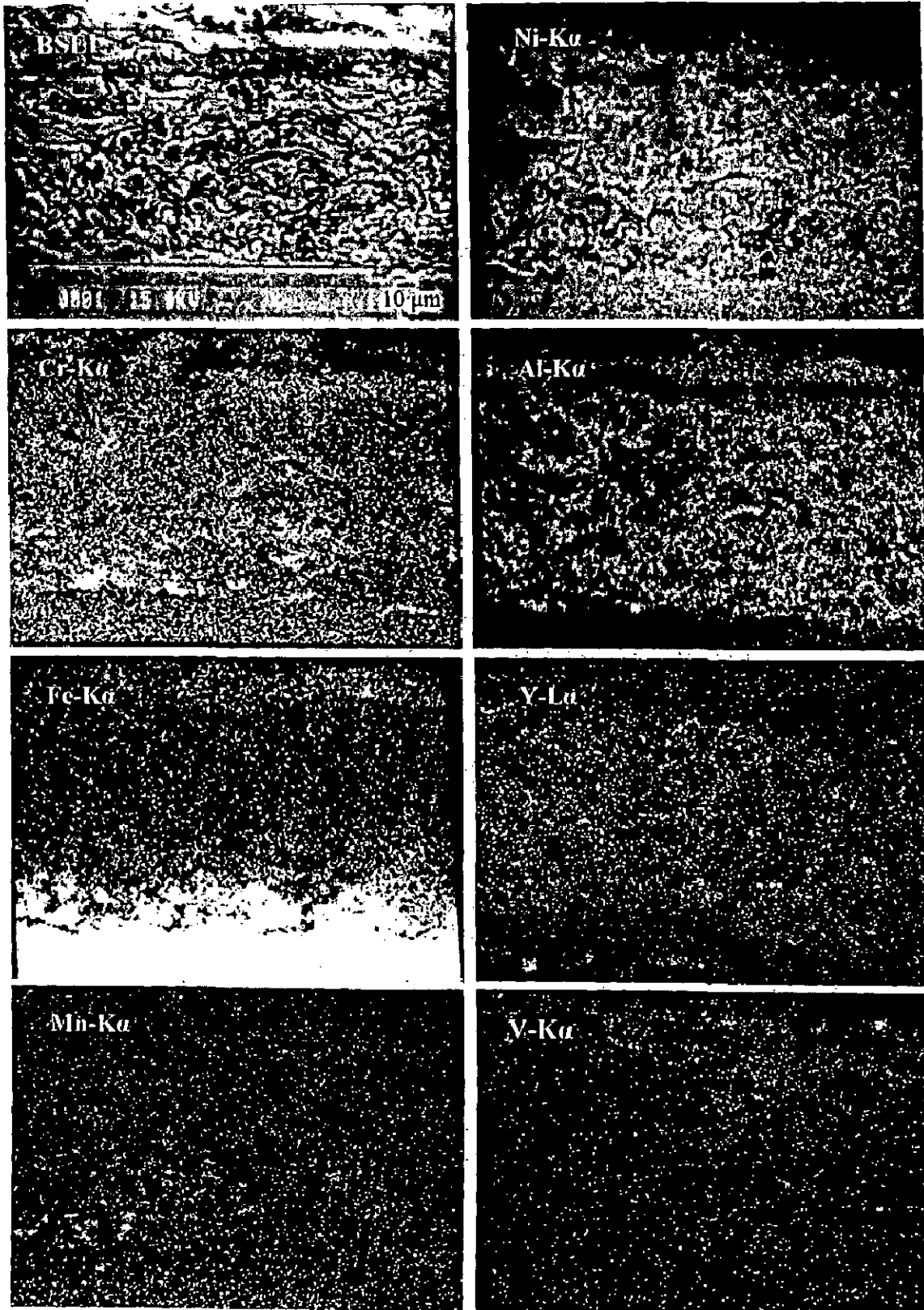


Fig. 6.26 BSEI and X-ray mappings of the cross-section of NiCrAlY coated superalloy Superni 601 subjected to cyclic oxidation in  $\text{Na}_2\text{SO}_4$ -60% $\text{V}_2\text{O}_5$  at 900°C after 50 cycles.

BSEI for the hot corroded NiCrAlY coated Superni 718 specimen, Fig. 6.27 shows a lamellar structure of scale, with a dense layer at the top of the scale. X-ray mappings confirm that this layer mainly contains nickel and aluminium in the form of thin streaks. Chromium is also present in substantial concentrations in the layer. Vanadium and silicon are seen in the outer layers of the scale and formed some clusters also. In rest of the scale nickel can be seen at the places where aluminium is absent and vice-versa. Cr has also shown higher concentrations in the Ni-rich areas. Iron, titanium and tantalum have diffused from the base alloy upwards and got dispersed uniformly in the scale. The iron diffusion is high near the coating/substrate interface. A continuous streak consisting of high amount of Ti can be seen just above the scale/base superalloy interface, where Cr is also present.

A corresponding analysis for the coated Superfer 800H (Fig. 6.28) indicates a scale consisting of a top layer containing oxides of nickel, chromium and aluminium. While the coating has retained its lamellar structure in the lower portion of the scale, where Ni-rich splats are encircled by oxides of aluminium. Cr is also seen forming stringers along the splat boundaries and pores/voids, and seems to have got oxidised. Diffusion of iron from the substrate to the lower layers of the scale is also evident. Vanadium has diffused into the entire scale, and its concentration is high in the top layers. Whereas sulphur has penetrated into the base superalloy to get segregated with chromium at the places, where Ni and Fe are absent.

### **6.1.3 Ni-20Cr Coating**

#### **6.1.3.1 Visual Examination**

The colour of scales after first cycle was grey which gradually turned to dark green for all the plasma spray Ni-20Cr coated superalloys with the advancement of cyclic hot corrosion study, except for the Ni-20Cr coated Superni 718 (Fig. 6.29). The colour of the scale in latter case was grey upto the end of study although greenish tinges dominated the grey colour during first 9 cycles. The scales were found to be smooth and intact, in general. Spalling of the scales was not observed for the Ni-20Cr coated and corroded superalloys, but marginal spalling of the coatings was observed near and/or the edges, as already mentioned in Section 6.1.2.1. The initiation of the said superficial cracks started from 4<sup>th</sup>, 34<sup>th</sup>, 16<sup>th</sup>, 18<sup>th</sup> and 12<sup>th</sup> cycle respectively for the coated Superni 75, 600, 601, 718 and Superfer 800H. The extent

of this slight spallation was comparatively more in case of coated Superni 601 and Superfer 800H, whereas it was lowest in case of coated Superni 600.

### 6.1.3.2 Thermogravimetric Data

Weight change ( $\text{mg}/\text{cm}^2$ ) variations as a function of time expressed in number of cycles for the Ni-20Cr coated superalloys after hot corrosion in  $\text{Na}_2\text{SO}_4$ -60% $\text{V}_2\text{O}_5$  at  $900^\circ\text{C}$  for 50 cycles are shown in Fig. 6.30. Evidently the Superni 600, 601 and Superfer 800H superalloys with plasma sprayed coating conceived lesser overall weight gains as compared to their uncoated counterparts in the given molten salt environment, whereas in case of Superni 75 the weight gain in coated condition is two folds of that in uncoated condition. Further the values of overall weight gains for the coated Superni 600, 601 and Superfer 800H are comparable that means these coated superalloys have revealed approximately similar hot corrosion resistance. Besides, the plots in Fig. 6.30 point out that the plasma sprayed Ni-20Cr coating is relatively more effective in imparting hot corrosion resistance to the Fe-base superalloy than to the Ni-base superalloys under study. This coating has reduced the overall weight gain by around 80% in case of Superfer 800H, whereas by around 20% and 57% for Superni 600 and 601 cases respectively, leaving aside the case of Superni 718, where intense spalling and sputtering restricted the total weight gain measurements to 20 cycles only.

To establish the rate law for the cyclic corrosion, square of weight gain/area data is plotted versus number of cycles in Fig. 6.31, which reveals some scatter in the data invariably in all the cases. Still the corrosion kinetics could be approximated by parabolic rate law in case of Superni 600, 601, 718 and Superfer 800H with  $K_p$  values calculated as 5.05, 4.72, 8.32 and  $5.04 \times 10^{-10} \text{ g}^2 \text{ cm}^{-4} \text{ s}^{-1}$  respectively. While the coated Superni 75 indicates inconsistency in the parabolic rate constant, which has value of  $22.95 \times 10^{-10} \text{ g}^2 \text{ cm}^{-4} \text{ s}^{-1}$  upto first 16 cycles and then changes to  $9.36 \times 10^{-10} \text{ g}^2 \text{ cm}^{-4} \text{ s}^{-1}$  for 17<sup>th</sup> to 38<sup>th</sup> cycle. This follows another transition to somewhat lower value of  $4.49 \times 10^{-10} \text{ g}^2 \text{ cm}^{-4} \text{ s}^{-1}$  in the remaining cycles. It is worth mentioning here that the last value of parabolic rate for the coated Superni 75 is comparable with those for the coated Superni 600, 601 and Superfer 800H.



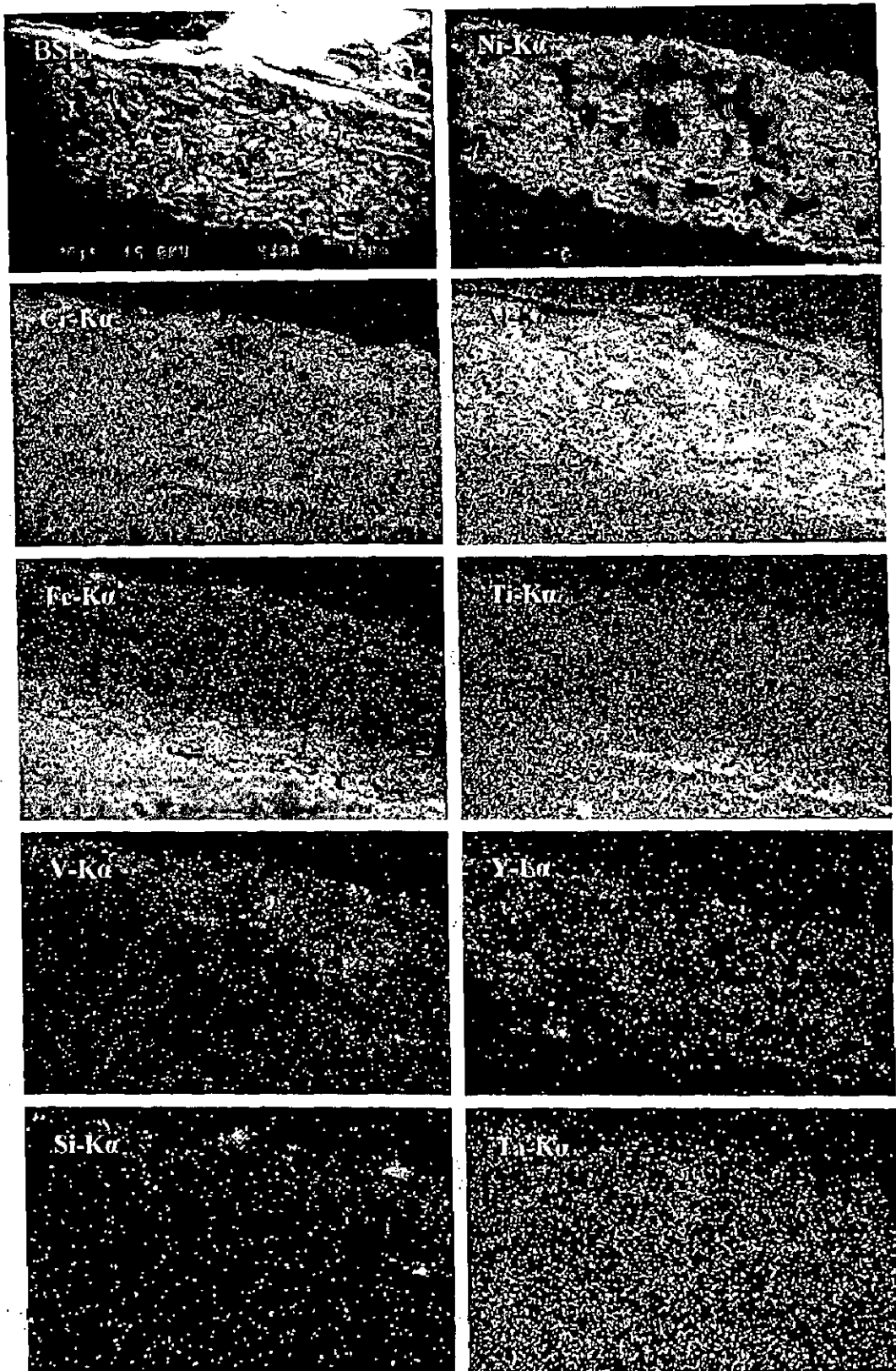


**Fig. 6.27** BSEI and X-ray mappings of the cross-section of NiCrAlY coated superalloy Superni 718 subjected to cyclic oxidation in  $\text{Na}_2\text{SO}_4$ -60% $\text{V}_2\text{O}_5$  at 900°C after 50 cycles.

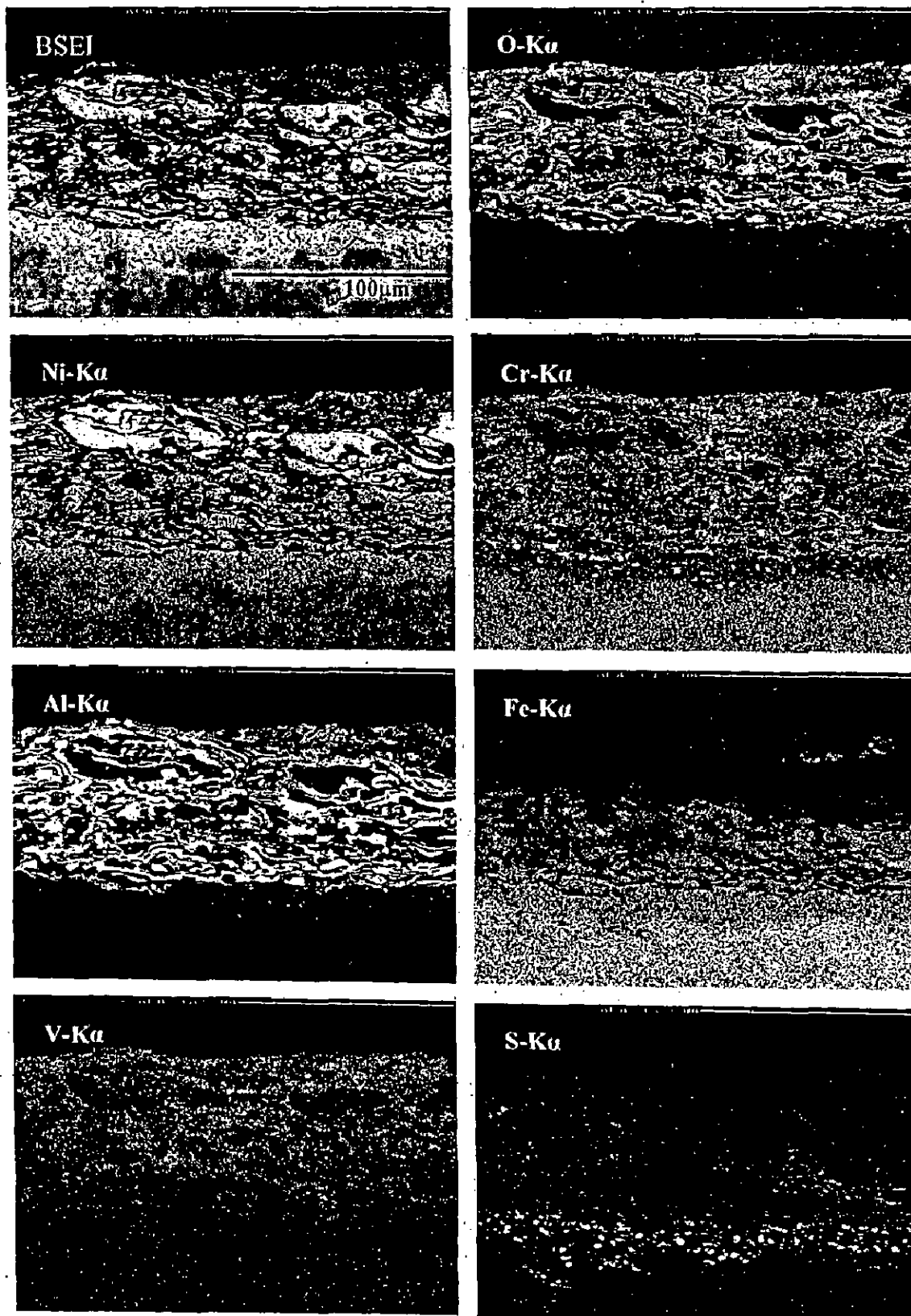
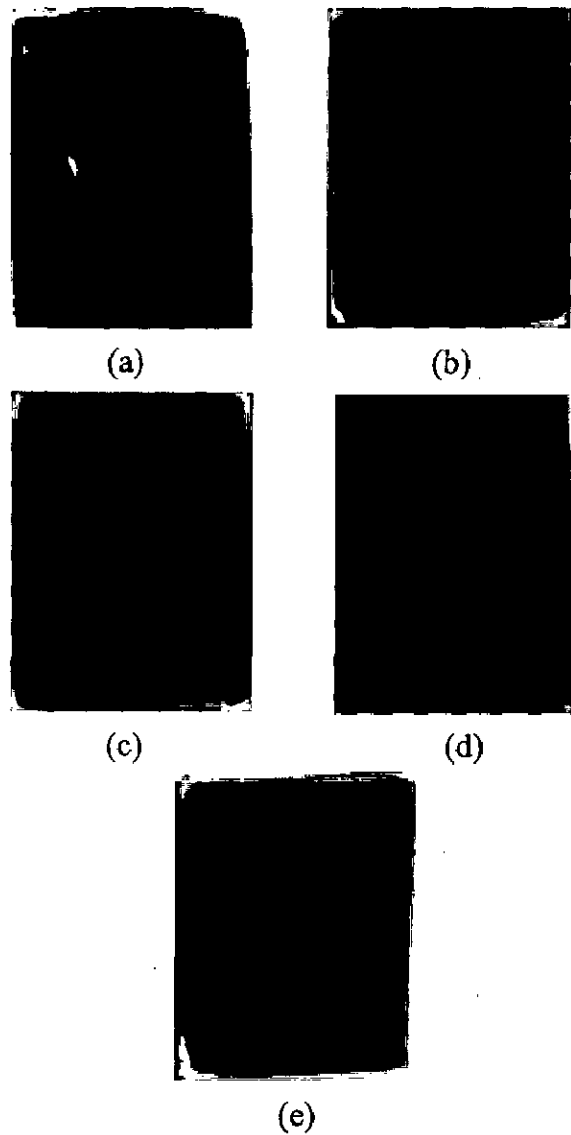
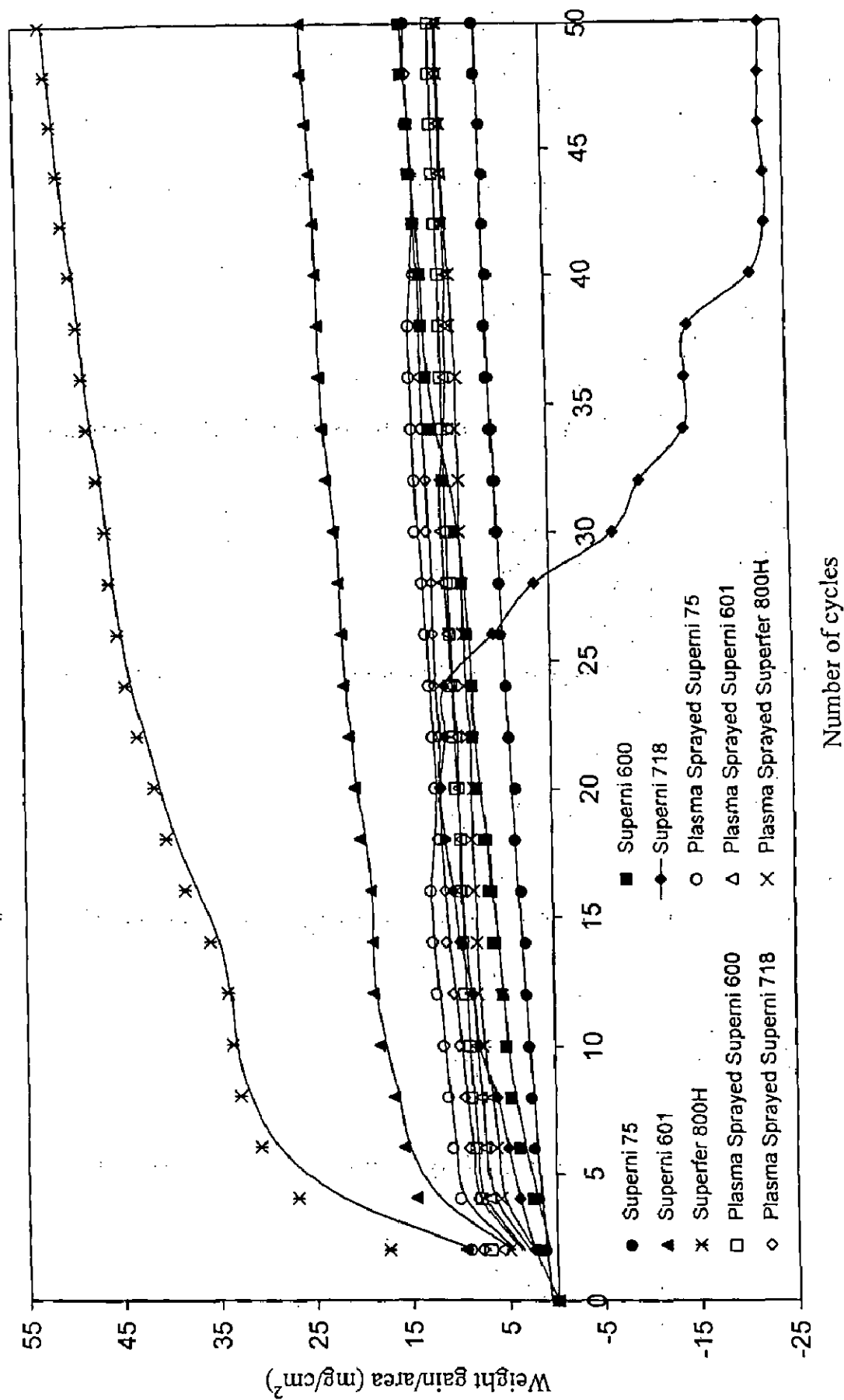


Fig. 6.28 BSEI and X-ray mappings of the cross-section of NiCrAlY coated superalloy Superfer 800H subjected to cyclic oxidation in  $\text{Na}_2\text{SO}_4$ -60% $\text{V}_2\text{O}_5$  at 900°C after 50 cycles.



**Fig. 6.29** Macrographs of the Ni-20Cr coating with bond coat subjected to cyclic oxidation in  $\text{Na}_2\text{SO}_4\text{-60\%V}_2\text{O}_5$  at  $900^\circ\text{C}$  for 50 cycles having substrate superalloys  
 (a) Superni 75      (b) Superni 600      (c) Superni 601  
 (d) Superni 718      (e) Superfer 800H



Number of cycles

Fig. 6.30 Weight gain vs. number of cycles plot for uncoated and Ni-20Cr coated superalloys subjected to cyclic oxidation for 50 cycles in  $\text{Na}_2\text{SO}_4\text{-60\%V}_2\text{O}_5$  at  $900^\circ\text{C}$ .

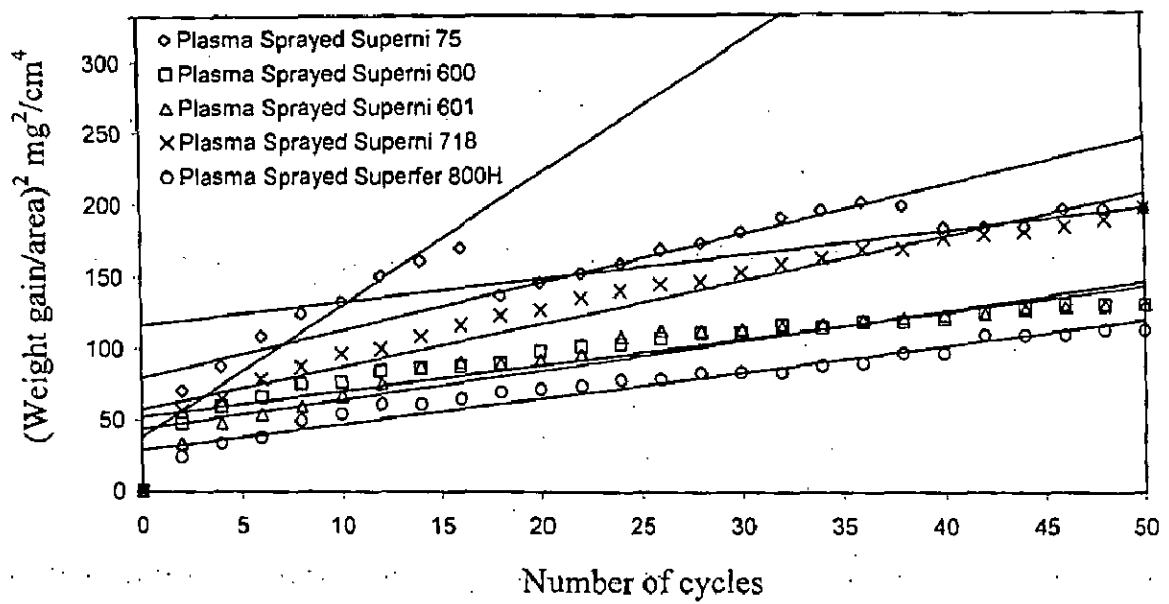


Fig. 6.31  $(\text{Weight gain/area})^2$  vs. number of cycles plot for the Ni-20Cr coated superalloys subjected to cyclic oxidation for 50 cycles in  $\text{Na}_2\text{SO}_4$ -60% $\text{V}_2\text{O}_5$  at  $900^\circ\text{C}$ .

### 6.1.3.3 Scale Thickness Measurement

Backscattered electron images along the smallest cross-section of Ni-20Cr coating on Superni 75, 600, 601, 718 and Superfer 800H substrate superalloys after cyclic hot corrosion are shown in Fig. 6.35 through Fig. 6.37. Average scale thickness as measured from BSE Images is 199, 269, 188, 196 and 158  $\mu\text{m}$  respectively for the coated Superni 75, 600, 601, 718 and Superfer 800H substrate superalloys. Evidently, Ni-20Cr coated Fe-base superalloy has indicated a minimum scale thickness in the present study.

### 6.1.3.4 X-ray Diffraction Analysis

XRD profiles for the scales of Ni-20Cr coated superalloys after hot corrosion in molten salt at  $900^{\circ}\text{C}$  for 50 cycles shows common phases for all the substrate superalloys as can be seen in Fig. 6.32. The profiles are shown on reduced scales. Nickel oxide (NiO) is revealed as a prominent phase for Ni-20Cr coated superalloys. In addition to NiO, some weak peaks of  $\text{Cr}_2\text{O}_3$  and  $\text{NiCr}_2\text{O}_4$  are also observed.

### 6.1.3.5 SEM/EDAX Analysis

#### (a) Surface Morphology

SEM micrograph alongwith EDAX measurements at some selected points for the oxide scale of Ni-20 Cr coated Superni 75 exposed to hot corrosion in the molten salt at  $900^{\circ}\text{C}$  after 50 cycles is depicted in Fig. 6.33 (a). The micrograph reveals a spongy scale, with a white phase consisting mainly of NiO (74%), with substantial amounts of  $\text{Cr}_2\text{O}_3$  and  $\text{Al}_2\text{O}_3$  present in it. Whereas in the black matrix the amount of NiO is 36% alongwith significant concentrations of  $\text{Cr}_2\text{O}_3$  and  $\text{Al}_2\text{O}_3$ . The presence of Al and Y on the surface of the scale indicates the probable diffusion of these elements from the bond coat. Analogous SEM micrograph for the coated Superni 600, Fig. 6.33 (b) shows a blocky morphology which is a typical structure for NiO (Susan and Marder, 2002). Small amount of  $\text{V}_2\text{O}_5$  is also present in the subscale, refer point 1. The granular scale in the case of coated Superni 601 is again having mainly NiO in its top most layer, Fig. 6.33 (c). The black patches present in the scale have shown a decline in the concentration of NiO, with increased content of  $\text{Cr}_2\text{O}_3$  and  $\text{Al}_2\text{O}_3$ .

A similar analysis for the coated Superni 718 case, Fig. 6.34 (a) indicates a scale consisting of distorted granules. EDAX analysis again predicts NiO as the main constituent of the scale. Further the SEM micrograph for the coated Superfer 800H

scale shows a big black region in the scale, Fig. 6.34 (b), which contains nearly equal amounts of  $\text{Cr}_2\text{O}_3$  and  $\text{NiO}$ , while the top scale is seen to have  $\text{NiO}$  as the main phase. The presence of small quantities of oxides of Fe and Si in the top scale indicates the diffusion of these elements from the substrate.

#### (b) Cross-Sectional Analysis

SEM/EDAX analysis along the cross-sections of Ni-20Cr coated Superni 75, 600, 601, 718 and Superfer 800H specimens corroded in  $\text{Na}_2\text{SO}_4$ -60% $\text{V}_2\text{O}_5$  environment at  $900^\circ\text{C}$  is shown in Fig. 6.35 to Fig. 6.37 respectively. In case of the coated Superni 75, the outermost layer of the scale is found to be rich in nickel, chromium and oxygen as shown at point 6, Fig. 6.35 (a). EDAX analysis at points 2-6 shows a significant diffusion of iron from the substrate across the thickness of scale. Further, oxygen is found to be present at the points 4 and 6 only, alongwith nickel, chromium and aluminium, and proportionately less iron. The presence of aluminium at point 6 reveals the probable diffusion of the same from the bond coat. The scale contains nearly uniform quantities of chromium along its thickness as revealed from EDAX analysis at points 2 to 6, while other elements show fluctuations in their concentrations.

BSEI for the coated Superni 600, Fig. 6.35 (b) shows a scale which has a massive structure in its outermost region, while the inner region of the scale is having lamellar structure resembling with the as sprayed morphology of the bond coat (Chapter 4). EDAX analysis indicates that the outer layers are having mainly oxides of Ni and Cr, while small amounts of aluminium are also present in them. The presence of Al in the top layers points out the diffusion of the same from the bond coat. Further the dark phase in the bond coat region of the scale has high Al content as compared to the white phase, which is Ni-rich. Presence of oxygen at point 1 indicates that oxygen has penetrated the substrate. However, the concentration of oxygen is observed to be decreasing as one move towards the bond coat/base alloy interface.

Duplex scale has been observed in case of coated Superni 601, Fig. 6.36 (a) where oxygen content increases as one moves towards outer layers of the scale, except at point 2, where oxygen is present in higher amount. The top layers of the scale are again having oxides of mainly Ni and Cr. Aluminium has diffused into the top scale from the bond coat to form its oxide as revealed from EDAX analysis at point 5 and 6. Further, the points at which nickel is present in large quantities

aluminium is found in feeble amounts as analysed at points 3 and 4. Bond coat has retained its structure, where black phase is having high aluminium concentration and the white phase contains mainly Ni. Oxygen has even reached to the substrate and internal oxidation is perceptible.

Analogous analysis for the coated Superni 718, Fig. 6.36 (b) shows an intact scale, the outermost layers of which contain oxides of mainly Ni, Cr and some Al. The presence of Al in these layers indicates that the diffusion of aluminium has taken place from the bond coat. The bond coat seems to have retained its identity. Further, in the layers of the scale, Ni-rich areas are depleted of Al and vice-versa. Cr is found almost in uniform amount along the cross-section of the scale, with an exception at point 6. At point 6, the amount of chromium has increased substantially. Iron has also shown diffusion into the scale from the base superalloy as iron is found to be present at points 2 and 3. Oxygen has penetrated upto the substrate.

A corresponding analysis for the coated Superfer 800H superalloy again shows two distinct regions in the scale, Fig. 6.37. The inner region seems to have retained its identity, while outer region has become massive in appearance. The top scale is again found to be consisting of oxides of mainly Ni and with some Cr. Diffusion of Al from the bond coat to the top scale has also been noticed. Chromium has shown uniformity in its concentration along the cross-section of the scale. Traces of iron are also found in the scale, which point out the migration of the same from the substrate to the scale.

In general it has been observed that the scales for all the Ni-20Cr coated superalloys under study show domination of nickel alongwith some chromium and oxygen in their outermost layers. Moreover, the scales have shown good adherence to their respective substrates.

#### **6.1.3.6 EPMA Analysis**

Elemental X-ray mappings for Ni-20Cr coated Superni 75 superalloy, Fig. 6.38 after hot corrosion in molten salt at 900<sup>o</sup>C for 50 cycles indicate formation of a scale with its top layers containing mainly nickel, while chromium is found to be co-existing with nickel at most of places in this layer. At the places in this top layer where nickel is absent, aluminium has got diffused from the bond coat. Yttrium has also diffused to these places and co-exists with aluminium. In the bond coat region of the scale, aluminium and nickel are present at alternate positions. Some diffusion of titanium from the substrate into the scale is also noticed especially near the bond



coat/substrate interface, where a thin streak of titanium is evident. Traces of vanadium are present in the upper region of the scale.

EPMA for the cross-section of Ni-20Cr coated Superni 600 superalloy corroded for 50 cycles in the given environment shows a dense layer in the upper portion of the scale (Fig. 6.39), which is rich in nickel and contains chromium also. Aluminium and yttrium have also shown their co-presence in the form of clusters in some regions of this layer, which indicate their diffusion from the bond coat. This might have caused some aluminium depleted areas in the bond coat region as is evident from the X-ray mapping for Al. There are some other places in the scale which are depleted of nickel and are having higher concentration of Cr. Iron has migrated from the substrate into the scale especially near the substrate/coating interface. Similar observations can be made from the EPMA analysis of the same specimen at some different place, Fig. 6.40 using oxygen detection crystal. From the oxygen map, it can be clearly inferred that oxidation has taken place in the bond coat along the splat boundaries, where mostly aluminium and chromium are present. In the top scale, aluminium has diffused and it is present in the form of streaks, perhaps along the splat boundaries, where nickel is absent. Nickel present in the splats at some places has not got oxidised, whereas in one part of the upper scale, Ni and Cr have got oxidised.

A corresponding analysis for the oxidised Ni-20Cr coated Superni 601 specimen, Fig. 6.41 shows an oxide scale with an uppermost layer consisting mainly of nickel. Presence of Al, Cr, Fe, Si and Mn has also been revealed in this layer in the form of clusters. There is an underlayer containing mainly nickel and chromium just below the uppermost layer. The presence of a Ni-rich area normal to the substrate surface in the middle of the scale where Cr is depleted indicates that crack might have formed and got healed by diffusion of Ni from the bond coat. Aluminium has diffused to the places where nickel and chromium are absent in the upper coat. Yttrium is observed to be mainly confined to the bond coat, with a minor diffusion of the same into the top coat and it co-exists with aluminium. Presence of vanadium in the top coat as well as bond coat has also been confirmed by X-ray mappings. Diffusion of iron into the bond coat is very intensive near the bond coat/base alloy interface. Further, silicon and manganese have also migrated into entire cross-section of the scale with a tendency to form small streaks.

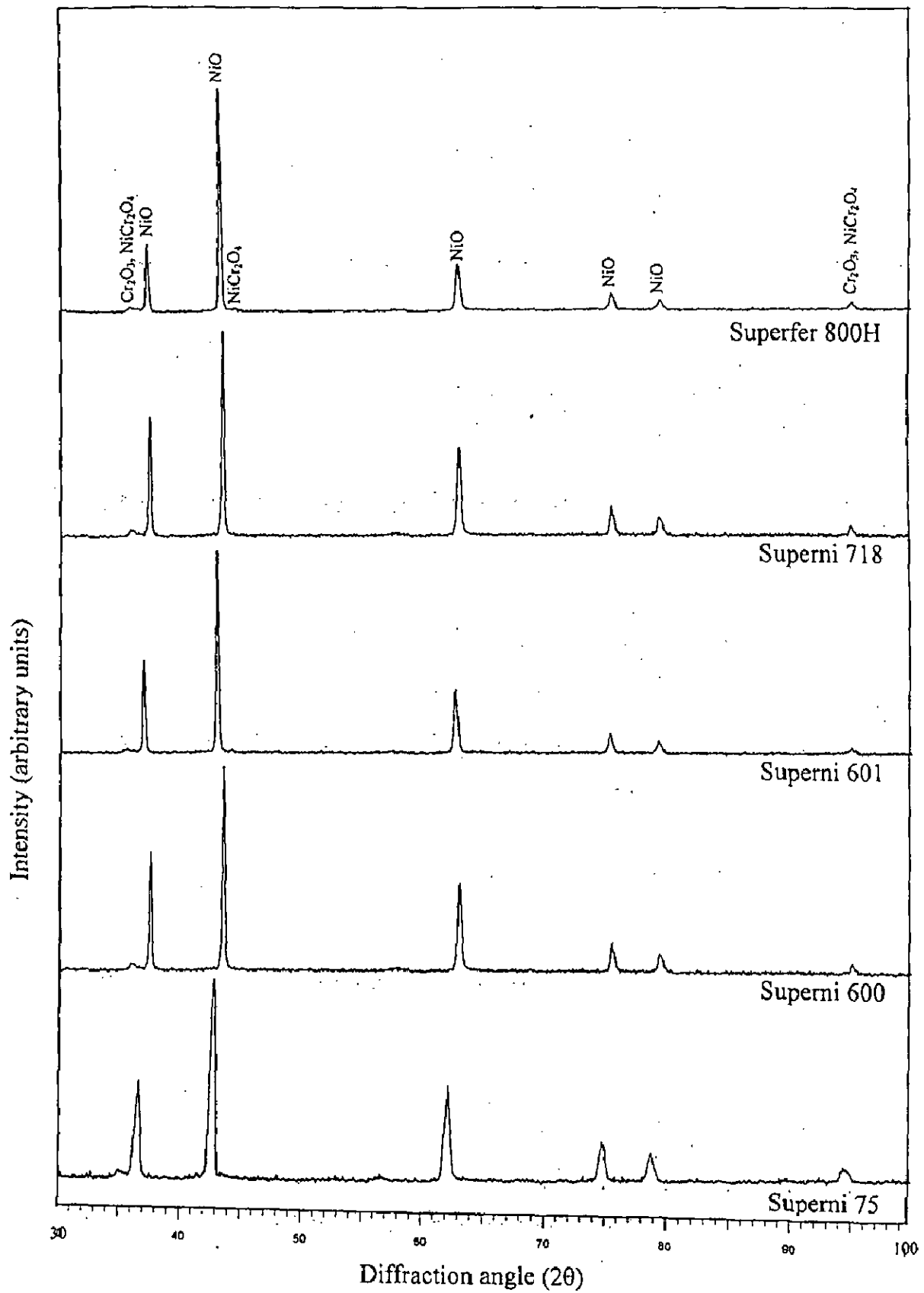
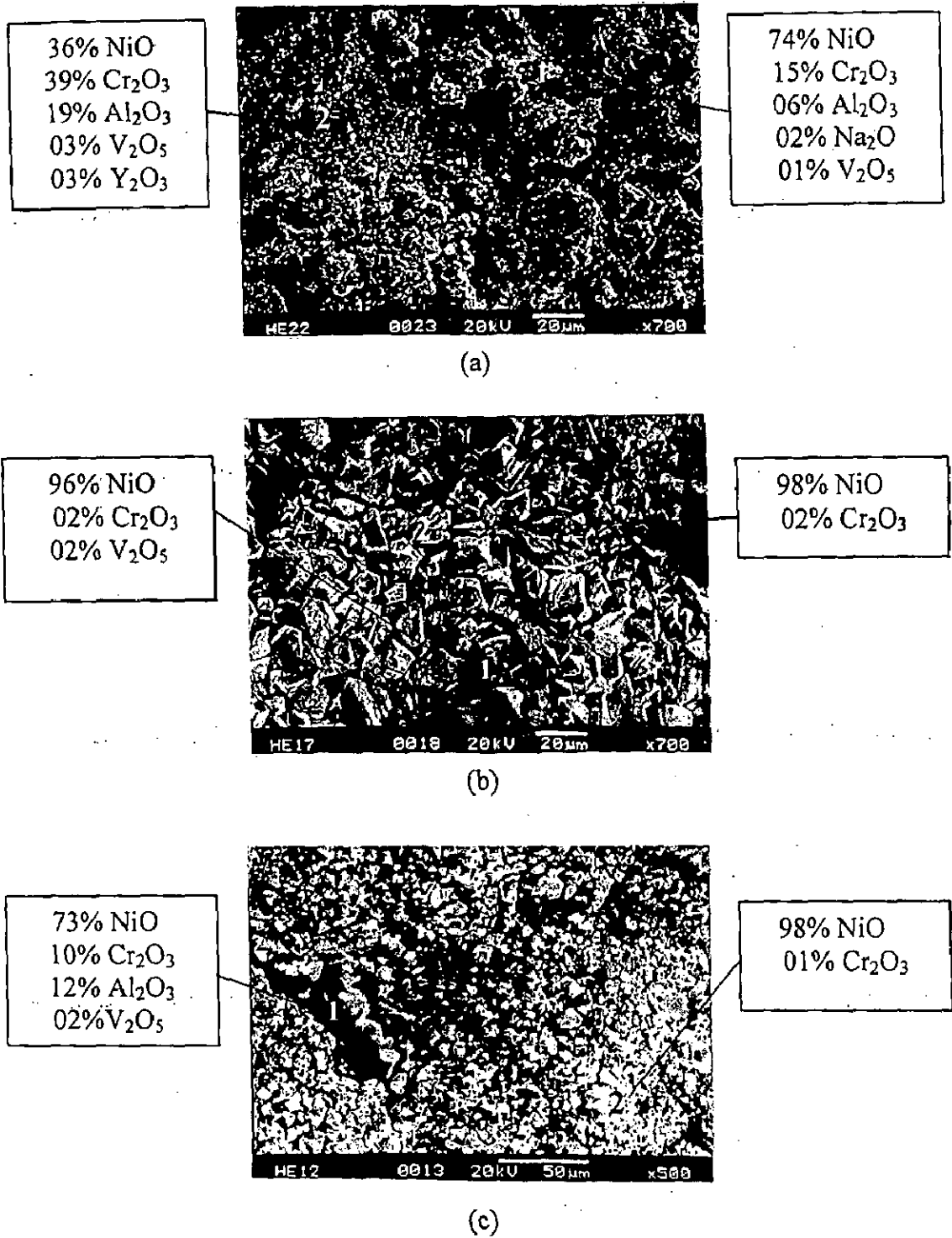
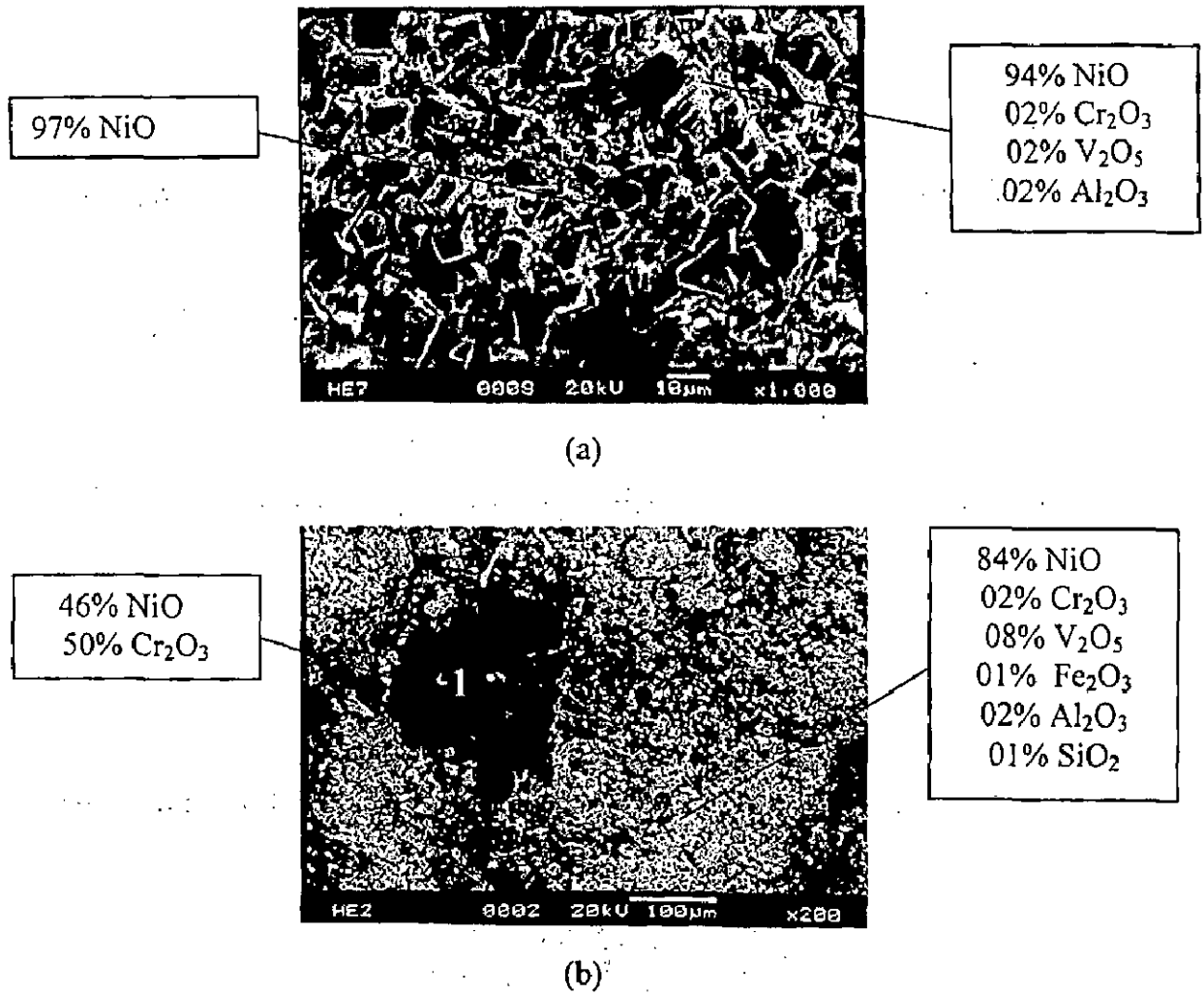


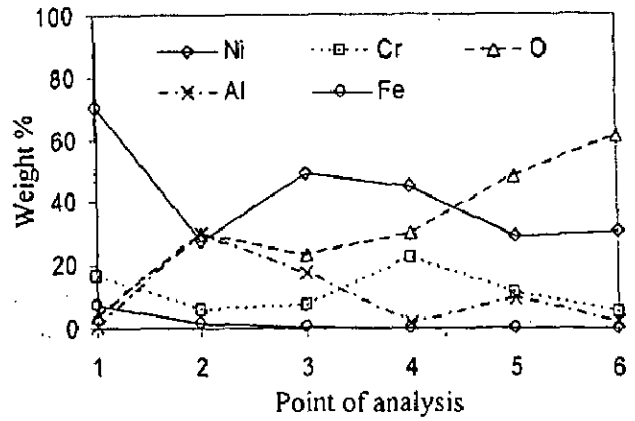
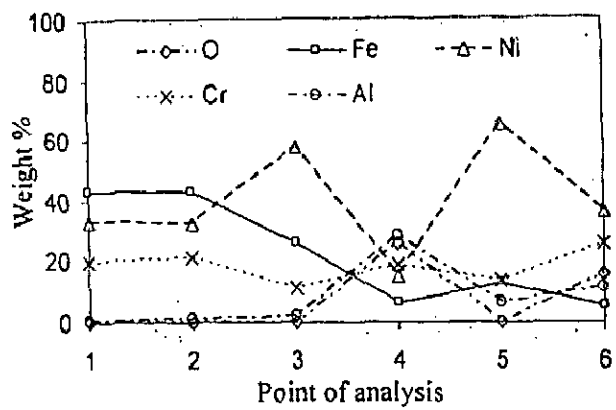
Fig. 6.32 X-ray diffraction patterns for the Ni-20Cr coated superalloys subjected to cyclic oxidation in Na<sub>2</sub>SO<sub>4</sub>-60%V<sub>2</sub>O<sub>5</sub> at 900°C after 50 cycles.



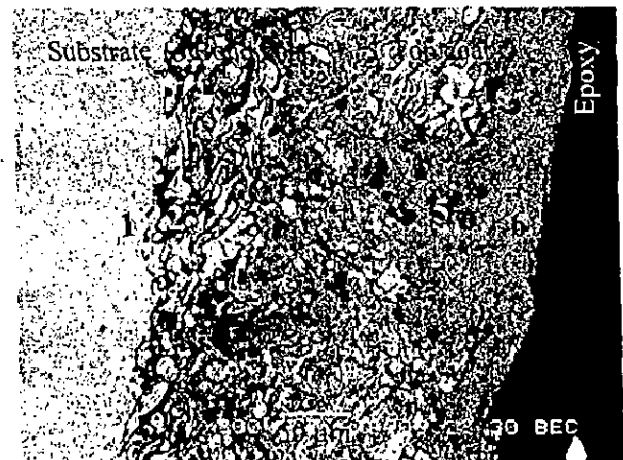
**Fig. 6.33** Surface scale morphology and EDAX analysis for the plasma spray Ni-20Cr coated superalloys subjected to cyclic oxidation in Na<sub>2</sub>SO<sub>4</sub>-60%V<sub>2</sub>O<sub>5</sub> at 900°C for 50 cycles  
 (a) Superni 75 (b) Superni 600 (c) Superni 601.



**Fig. 6.34** Surface scale morphology and EDAX analysis for the plasma spray Ni-20Cr coated superalloys subjected to cyclic oxidation in  $\text{Na}_2\text{SO}_4$ -60% $\text{V}_2\text{O}_5$  at  $900^\circ\text{C}$  for 50 cycles  
 (a) Superni 718      (b) Superfer 800H.

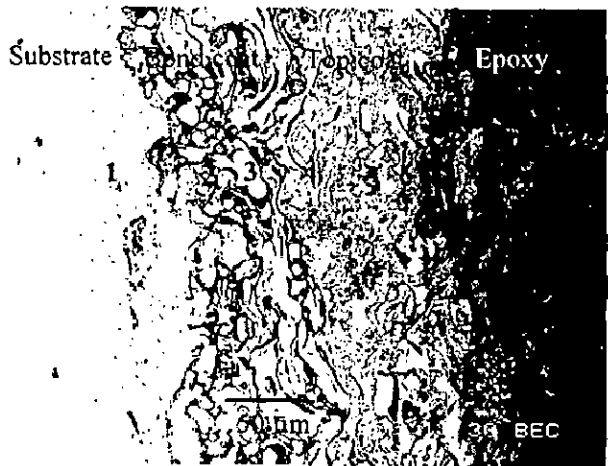
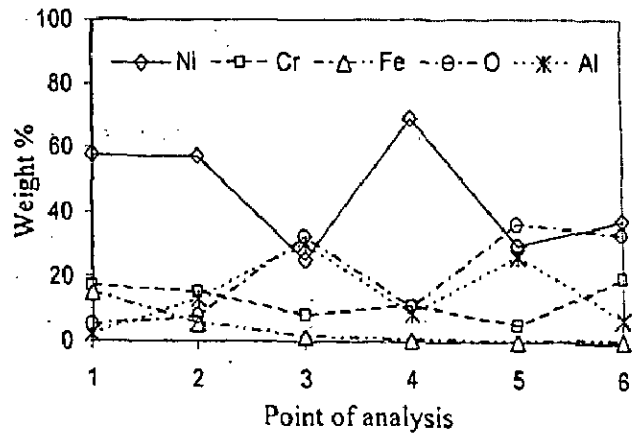
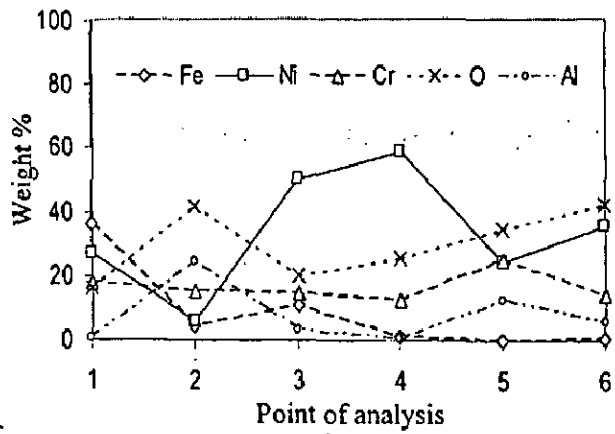


(a)

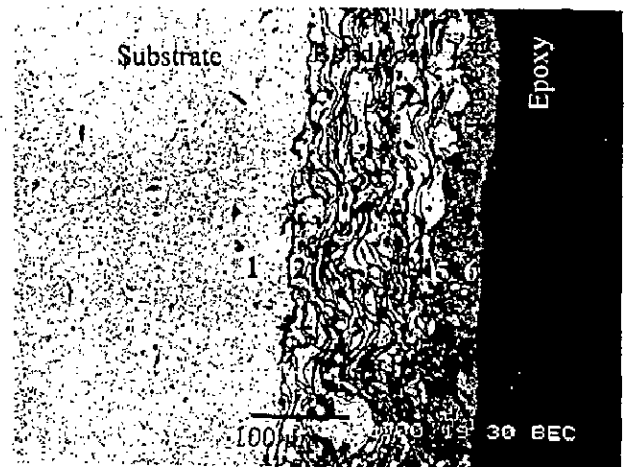


(b)

**Fig. 6.35** Oxide scale morphology and variation of elemental composition across the cross-section of Ni-20Cr coated superalloys subjected to cyclic oxidation in  $\text{Na}_2\text{SO}_4\text{-60}\%\text{V}_2\text{O}_5$  at  $900^\circ\text{C}$  after 50 cycles  
 (a) Superni 75      (b) Superni 600.



(a)



(b)

**Fig. 6.36** Oxide scale morphology and variation of elemental composition across the cross-section of Ni-20Cr coated superalloys subjected to cyclic oxidation in  $\text{Na}_2\text{SO}_4\text{-60\%V}_2\text{O}_5$  at  $900^\circ\text{C}$  after 50 cycles  
 (a) Superni 601 (b) Superni 718.

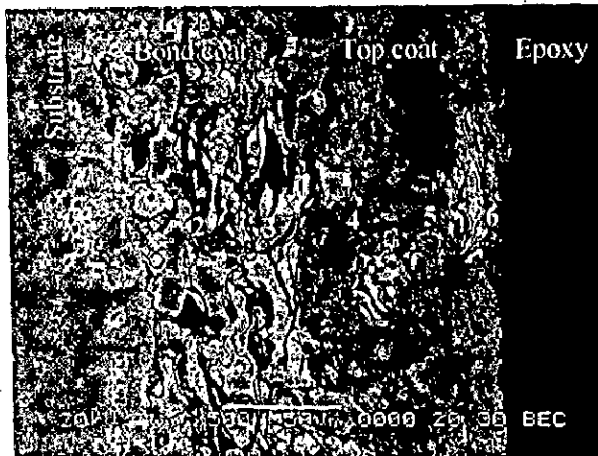
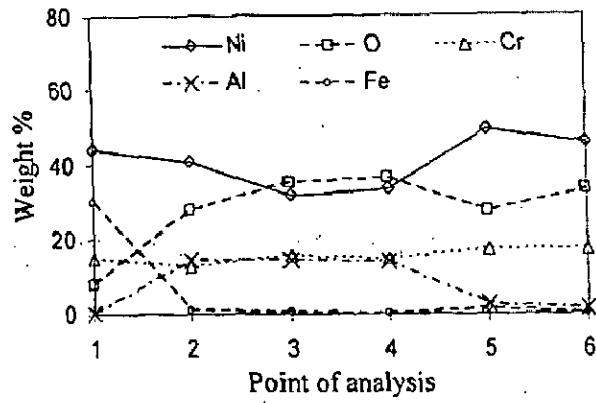


Fig. 6.37 Oxide scale morphology and variation of elemental composition across the cross-section of Ni-20Cr coated superalloy Superfer 800H subjected to cyclic oxidation in  $\text{Na}_2\text{SO}_4\text{-60}\%\text{V}_2\text{O}_5$  at  $900^\circ\text{C}$  after 50 cycles.

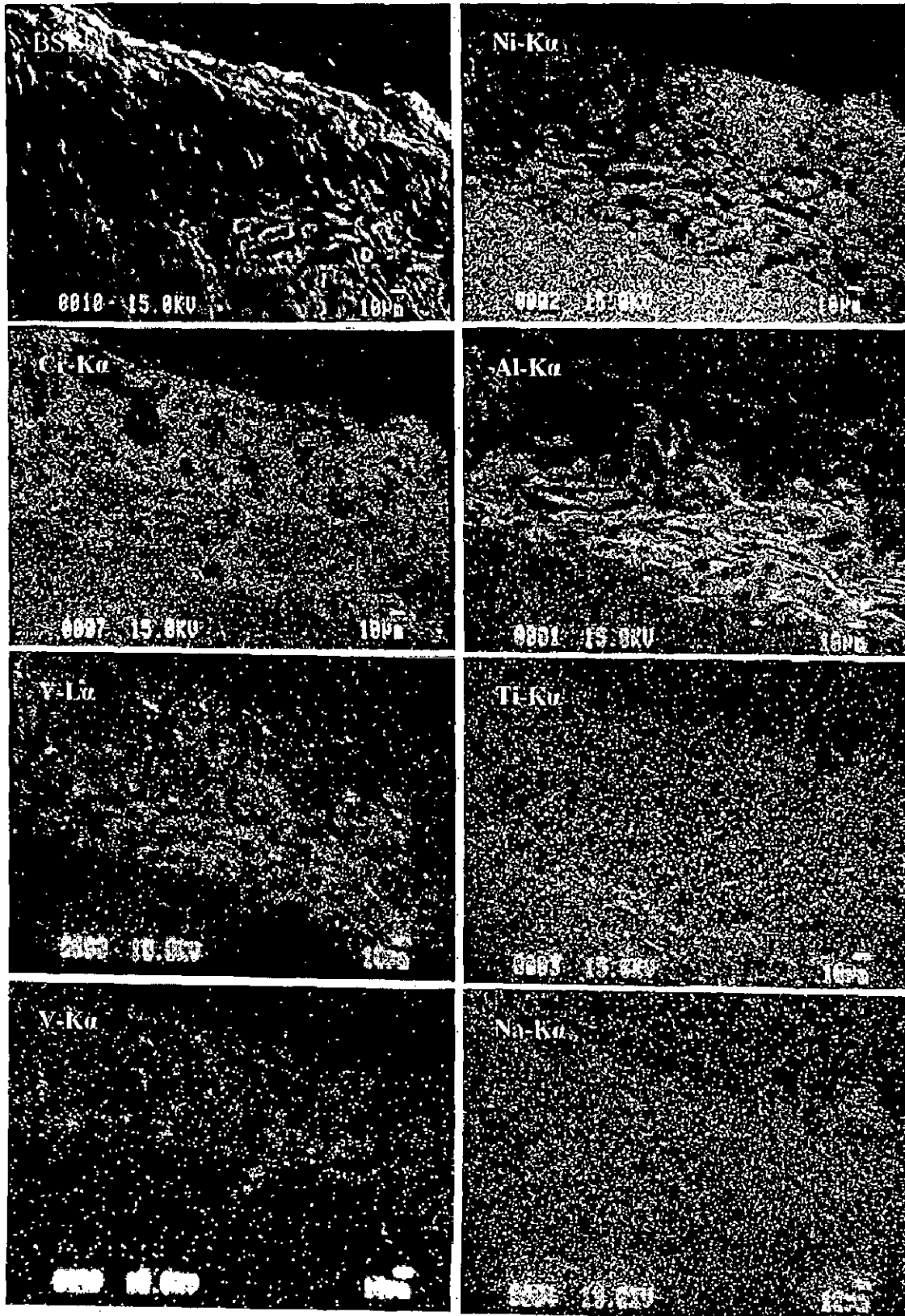


Fig. 6.38 BSEI and X-ray mappings of the cross-section of Ni-20Cr coated superalloy Superni 75 subjected to cyclic oxidation in  $\text{Na}_2\text{SO}_4$ -60% $\text{V}_2\text{O}_5$  at 900°C after 50 cycles.



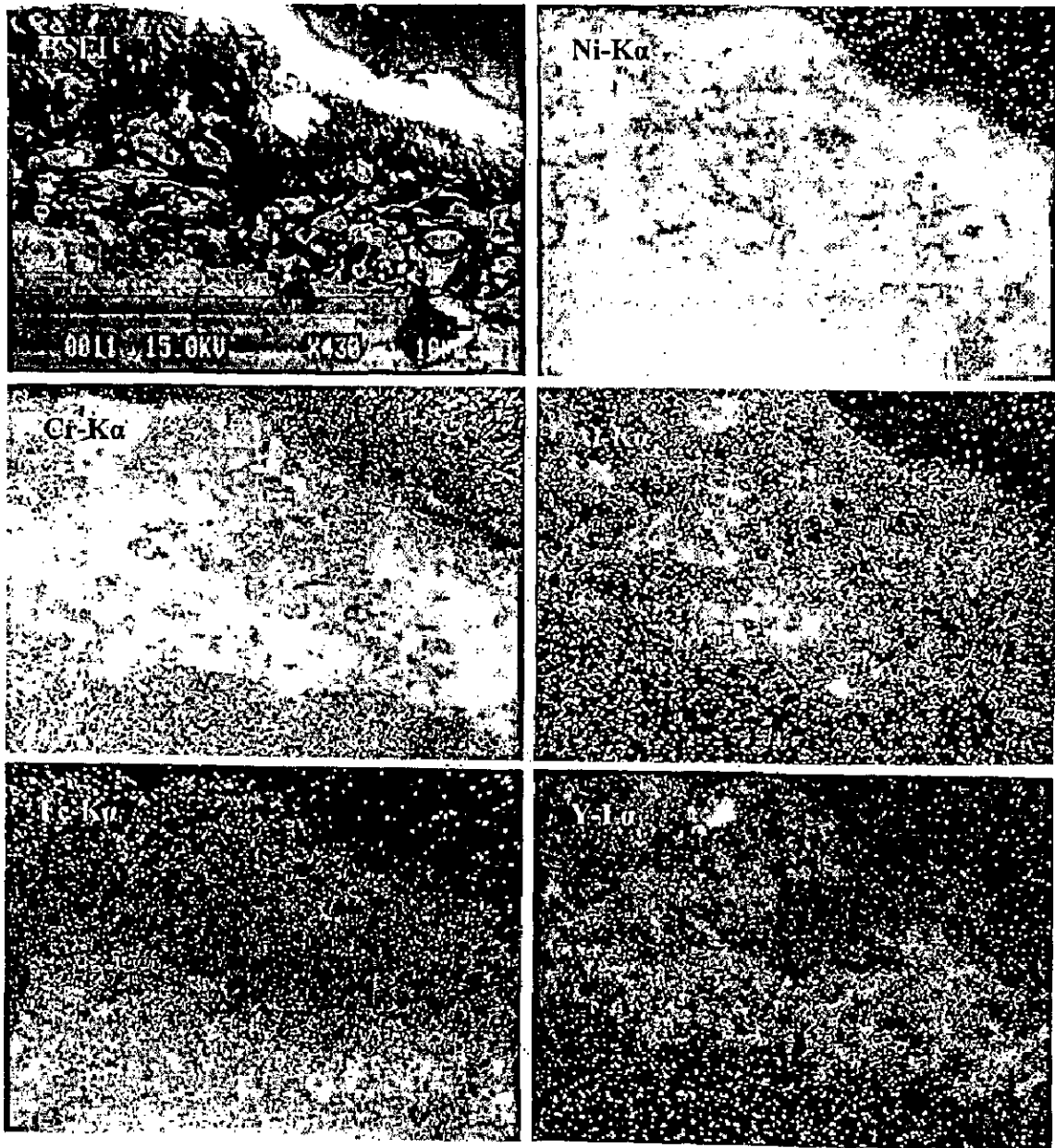


Fig. 6.39 BSEI and X-ray mappings of the cross-section of Ni-20Cr coated superalloy Superni 600 subjected to cyclic oxidation in  $\text{Na}_2\text{SO}_4$ -60% $\text{V}_2\text{O}_5$  at 900°C after 50 cycles.

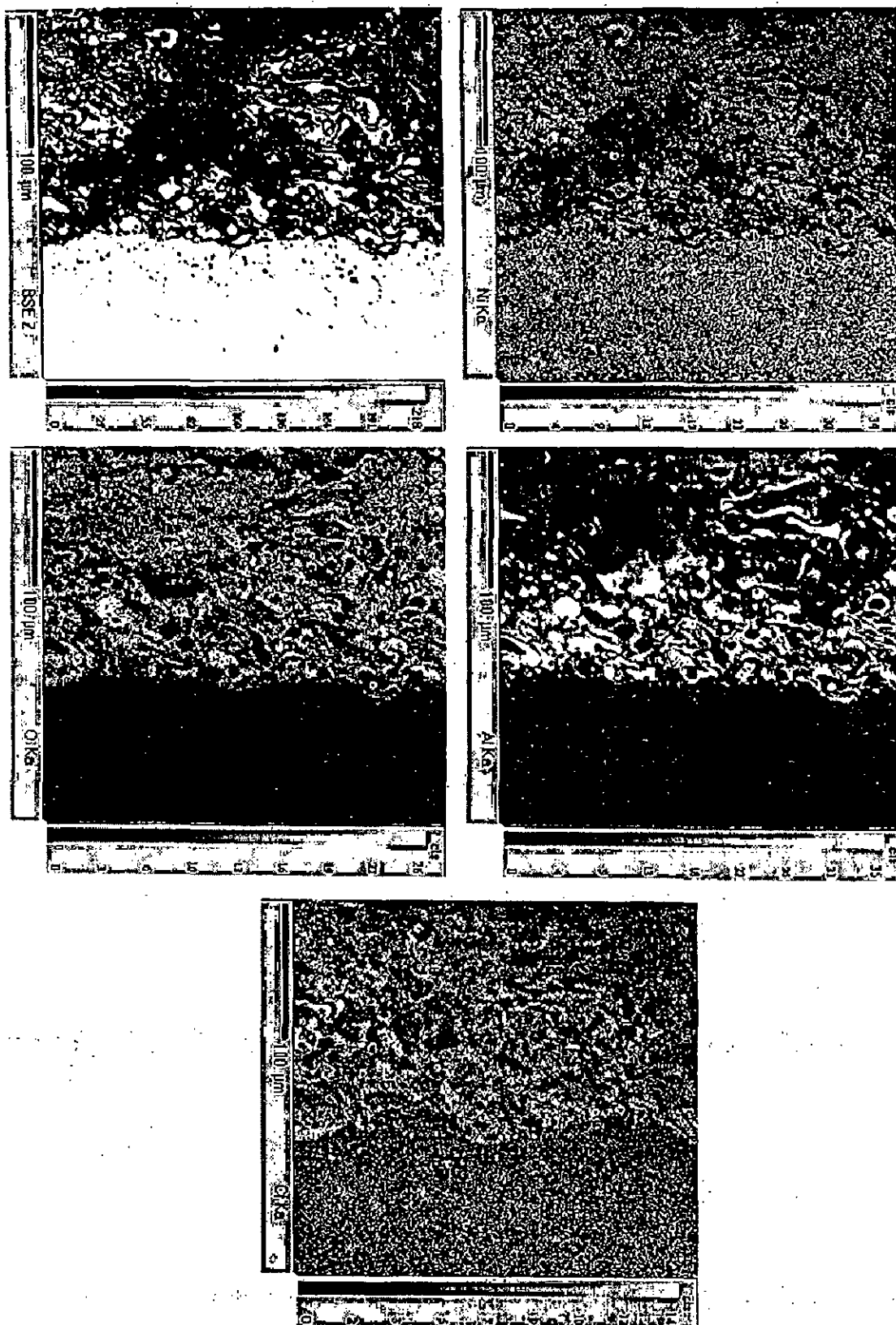


Fig. 6.40 BSEI and X-ray mappings of the cross-section of Ni-20Cr coated superalloy Superni 600 subjected to cyclic oxidation in  $\text{Na}_2\text{SO}_4$ -60% $\text{V}_2\text{O}_5$  at  $900^\circ\text{C}$  after 50 cycles showing oxygen distribution also.

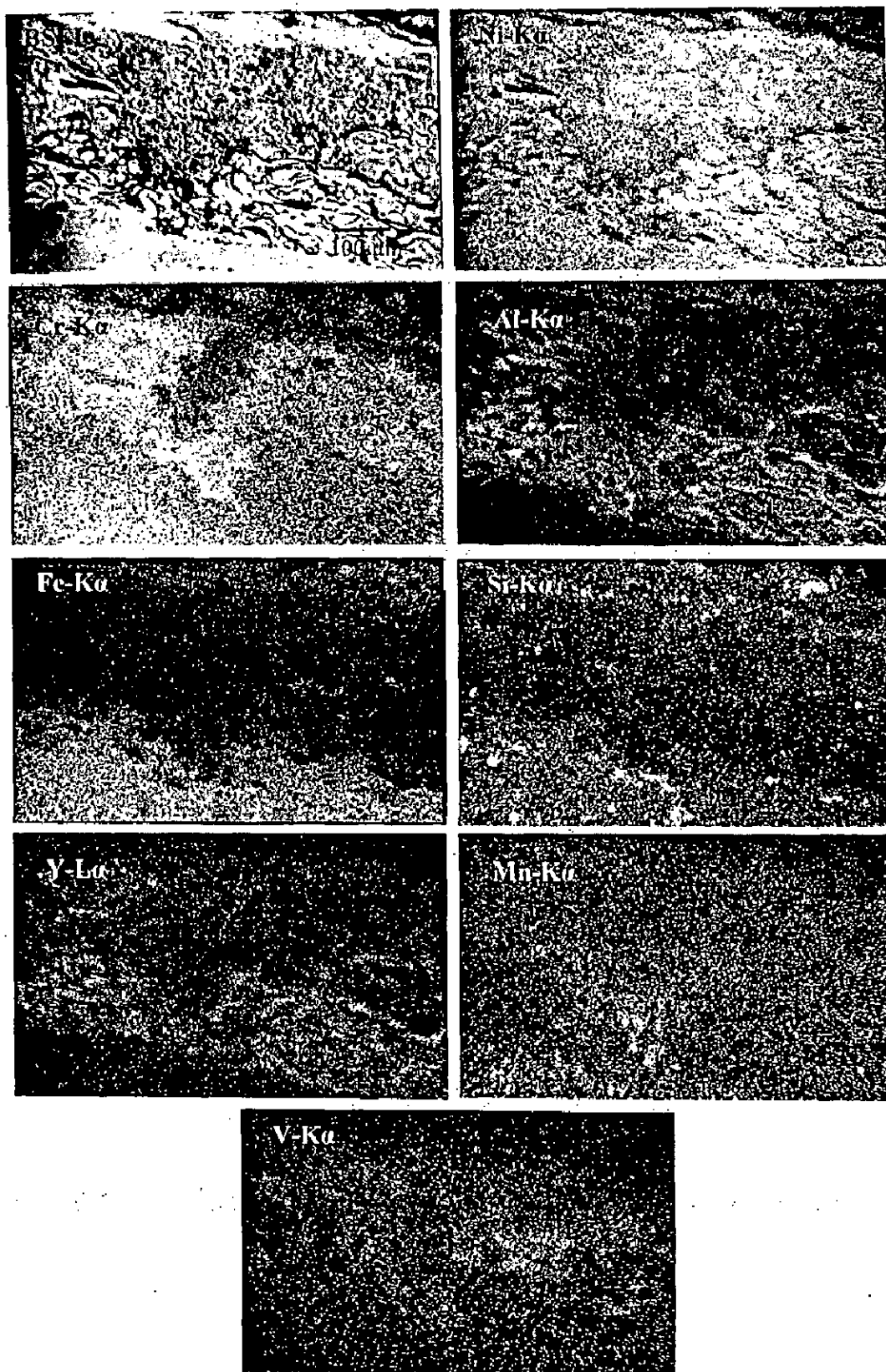


Fig. 6.41 BSEI and X-ray mappings of the cross-section of Ni-20Cr coated superalloy Superni 601 subjected to cyclic oxidation in  $\text{Na}_2\text{SO}_4\text{-60\%V}_2\text{O}_5$  at  $900^\circ\text{C}$  after 50 cycles.

Further, minor spalling of the scales was also observed in the form of green powder in all the cases. In case of Superni 75 and 600 this spalling took place from the places from where the coating was detached due to cracks. Whereas the spalling of the scale in general was observed in case of Superni 718 and Superfer 800H by the end of 48<sup>th</sup> and 26<sup>th</sup> cycle respectively.

#### 6.1.4.2 Thermogravimetric Data

The weight gain/unit area data for the uncoated and Ni<sub>3</sub>Al coated superalloys subjected to molten salt (Na<sub>2</sub>SO<sub>4</sub>-60%V<sub>2</sub>O<sub>5</sub>) oxidation for 50 cycles at 900°C is plotted as a function of time expressed in number of cycles in Fig. 6.45. Clearly the overall weight gain at the end of 50 cycles is reduced after the application of plasma spray Ni<sub>3</sub>Al coating in case of Superni 601 and Superfer 800H, whereas nothing can be concluded in case of Superni 718 as in the latter case, intense sputtering and spalling made it difficult to take the overall weight change upto 50 cycles. The overall weight gain for the coated Superfer 800H superalloy is found to around 29% of that for the uncoated superalloy, whereas for the coated Superni 601 the corresponding value is in the order of 68%. Furthermore the cumulative weight gain due to cyclic hot corrosion in case of Superni 75 and 600 has increased after the use of the coating. Besides the Ni<sub>3</sub>Al coated Superni 75 has shown highest resistance to corrosion among the Ni<sub>3</sub>Al coated superalloys on the basis of weight gain at the end of 50 cycles.

In Fig. 6.46, the weight gain/unit area square data has been plotted against the number of cycles, which indicate that the oxidation phenomena can be approximated by parabolic rate law for the coated superalloys. The coated superalloys Superni 601, 718 and Superfer 800H have parabolic rate constants ( $K_p$ ) as 12.63, 18.50,  $9.06 \times 10^{-10}$  g<sup>2</sup> cm<sup>-4</sup> s<sup>-1</sup> respectively upto 50 cycles, whereas the coated Superni 75,  $10.15 \times 10^{-10}$  g<sup>2</sup> cm<sup>-4</sup> s<sup>-1</sup> upto 42 cycles, beyond which parabolic rate law no longer holds good. Furthermore, the coated Superni 600 has shown reduction in the value of  $K_p$  from  $25.00 \times 10^{-10}$  g<sup>2</sup> cm<sup>-4</sup> s<sup>-1</sup> (upto 36 cycles) to  $7.74 \times 10^{-10}$  g<sup>2</sup> cm<sup>-4</sup> s<sup>-1</sup> towards the end of exposure time. It is pertinent to mention here that the value of  $K_p$  for the Ni<sub>3</sub>Al coated Superni 718 (50 cycles) is lower than that for uncoated Superni 718 (20 cycles).

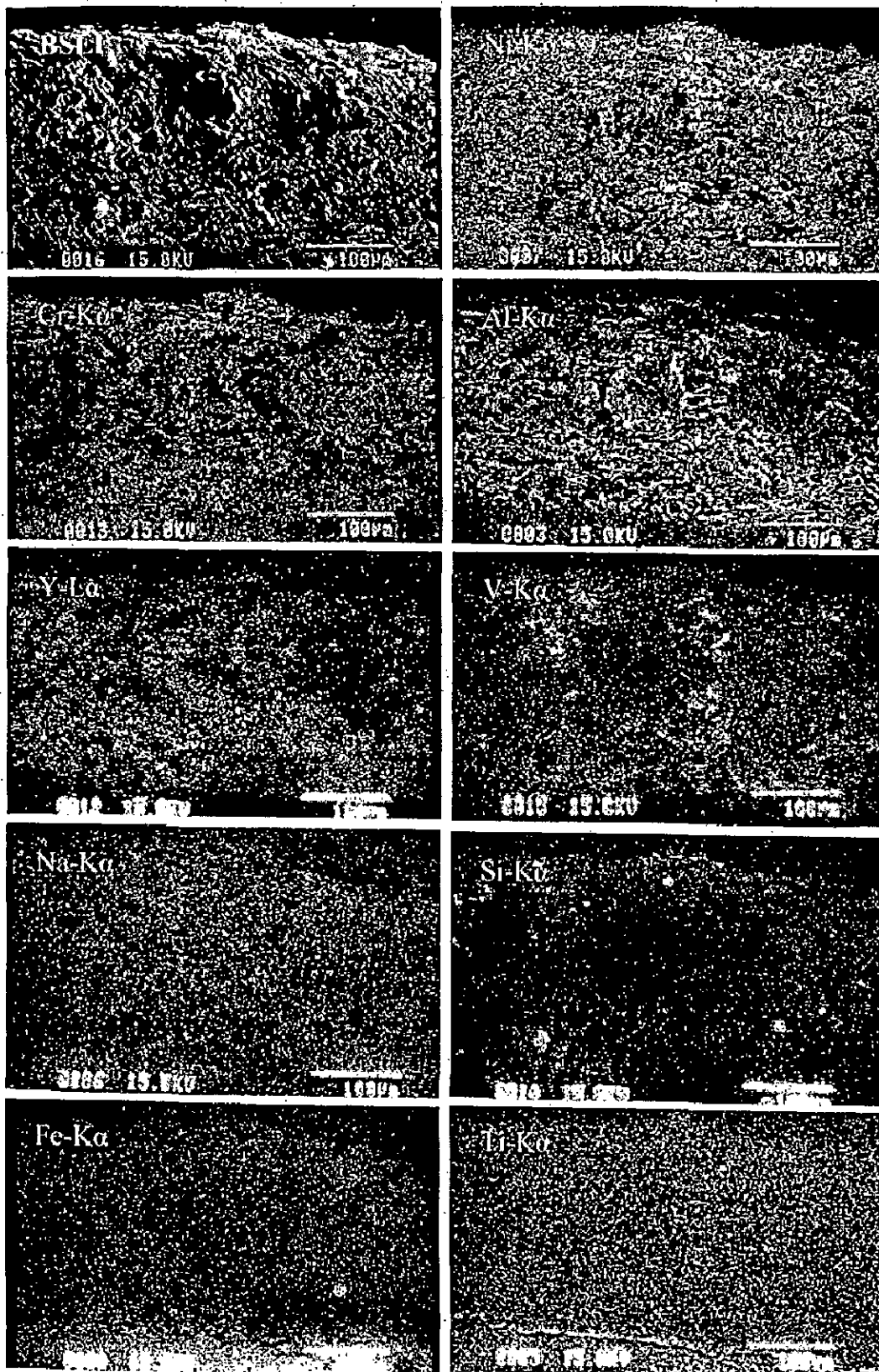


Fig. 6.42 BSEI and X-ray mappings of the cross-section of Ni-20Cr coated superalloy Superni 718 subjected to cyclic oxidation in  $\text{Na}_2\text{SO}_4$ -60% $\text{V}_2\text{O}_5$  at 900°C after 50 cycles.

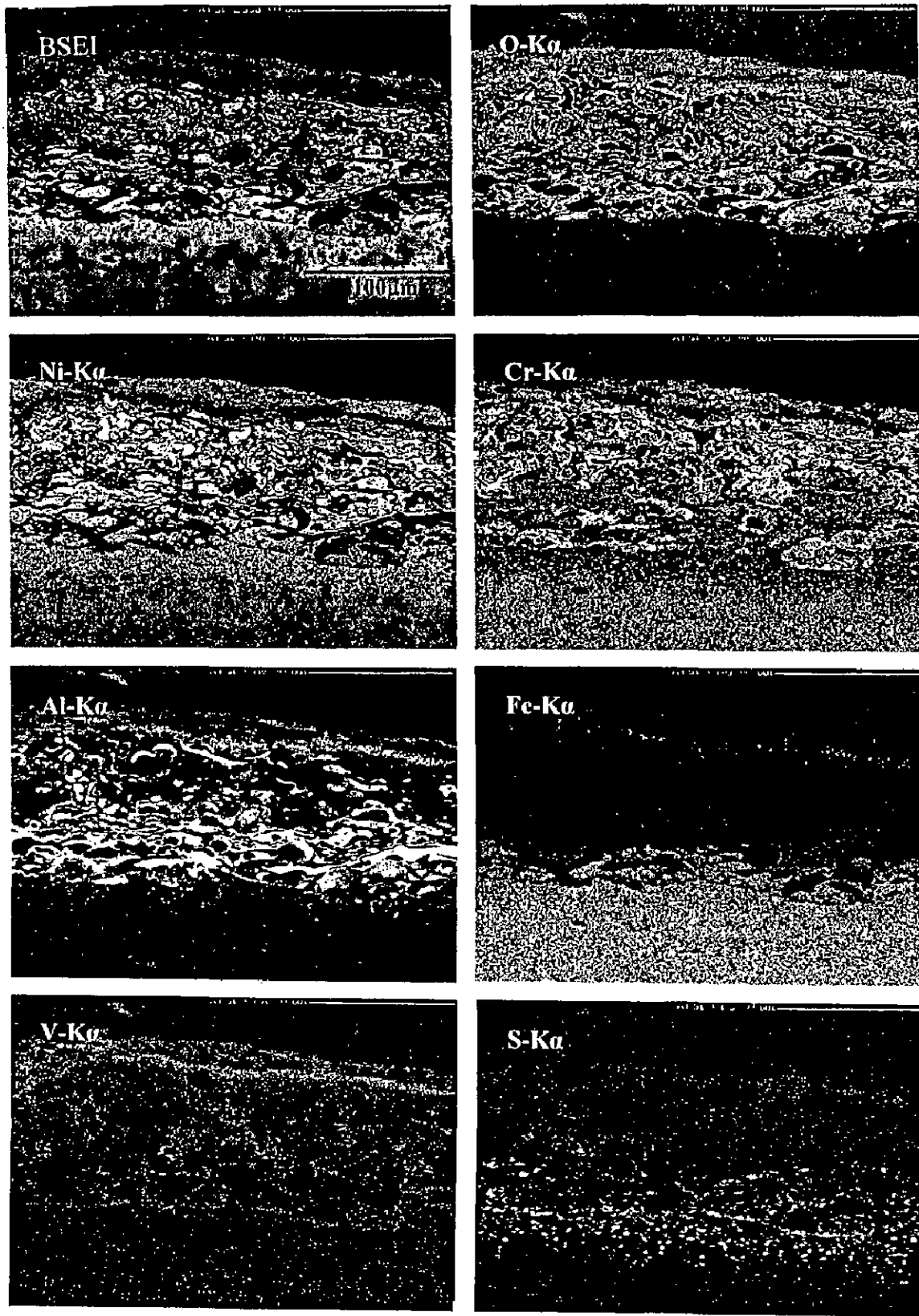
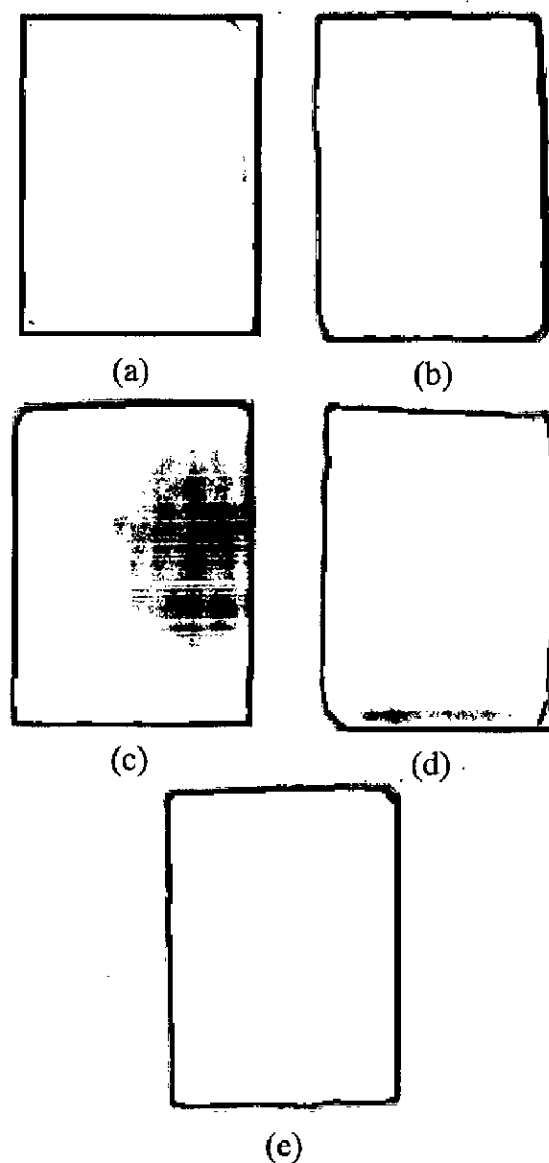


Fig. 6.43 BSEI and X-ray mappings of the cross-section of Ni-20Cr coated superalloy Superfer 800H subjected to cyclic oxidation in  $\text{Na}_2\text{SO}_4$ -60% $\text{V}_2\text{O}_5$  at 900°C after 50 cycles.



**Fig. 6.44** Macrographs of the  $\text{Ni}_3\text{Al}$  coating with bond coat subjected to cyclic oxidation in  $\text{Na}_2\text{SO}_4\text{-60\%V}_2\text{O}_5$  at  $900^\circ\text{C}$  for 50 cycles having substrate superalloys  
(a) Superni 75                      (b) Superni 600                      (c) Superni 601  
(d) Superni 718                      (e) Superfer 800H.

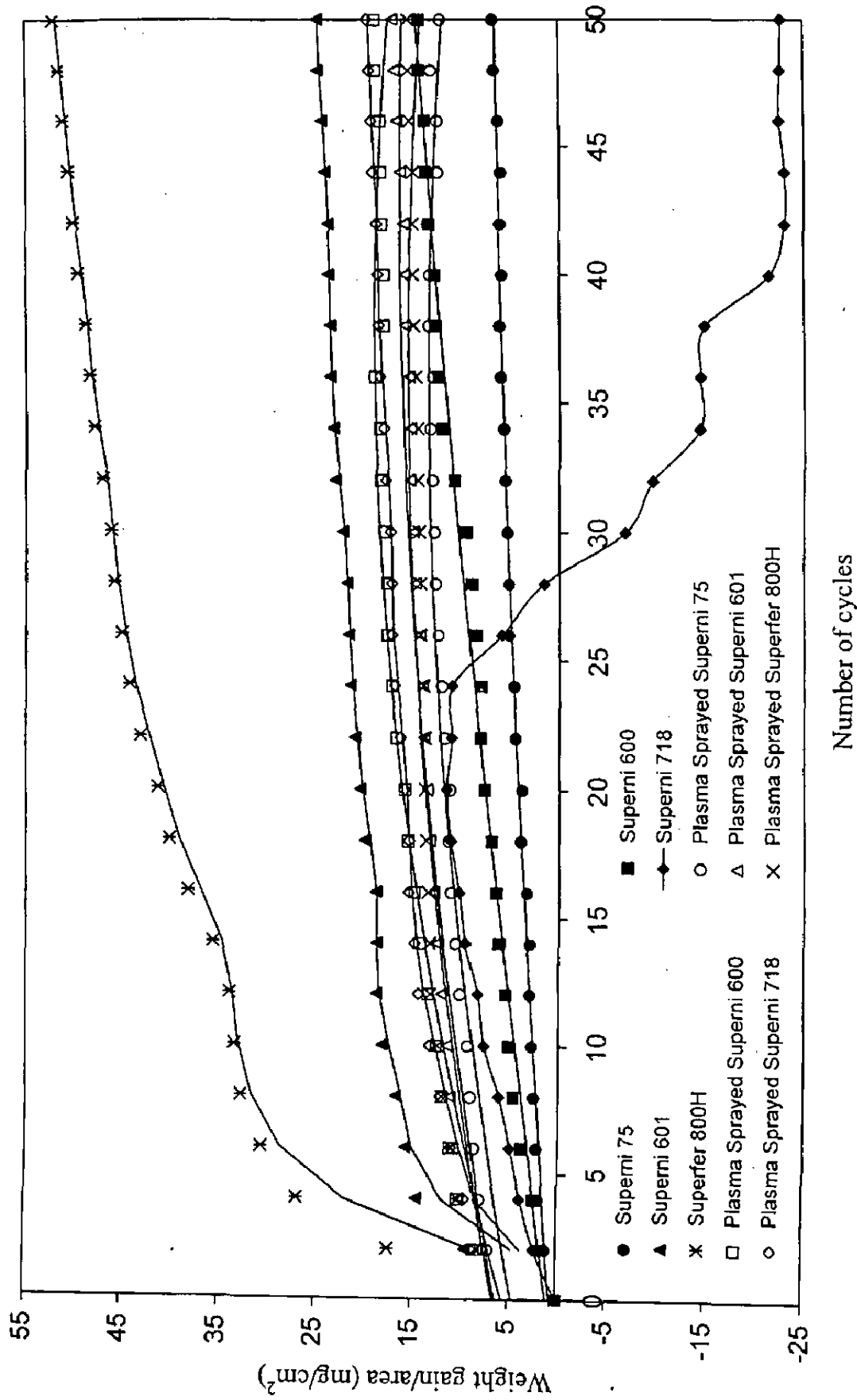


Fig. 6.45 Weight gain vs. number of cycles plot for uncoated and Ni<sub>3</sub>Al coated superalloys subjected to cyclic oxidation for 50 cycles in Na<sub>2</sub>SO<sub>4</sub>-60%V<sub>2</sub>O<sub>5</sub> at 900°C.



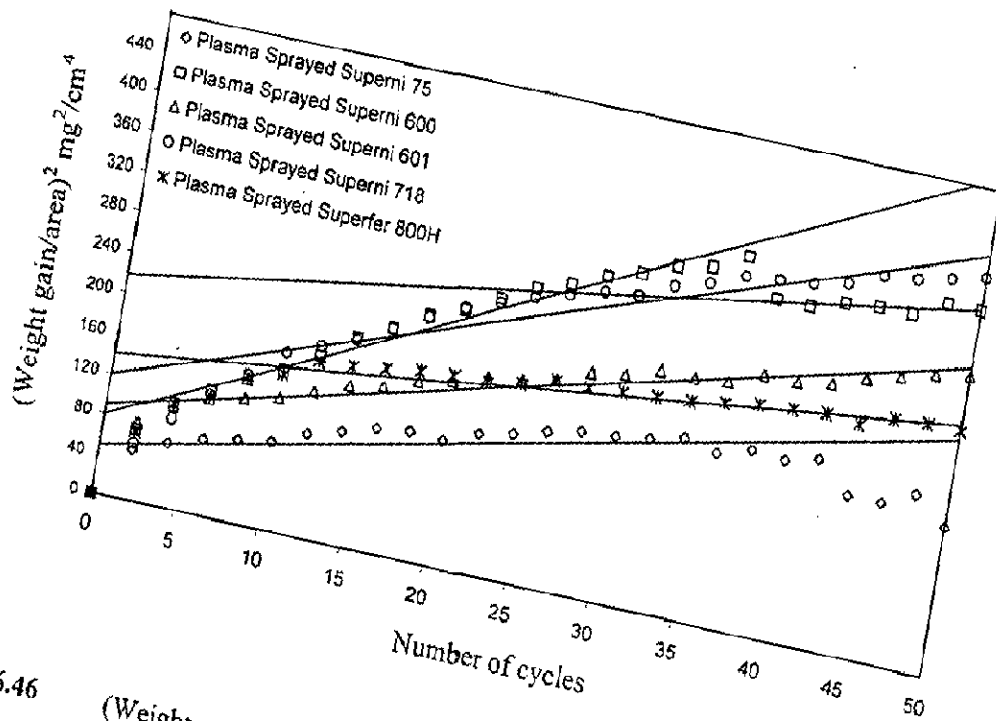


Fig. 6.46

(Weight gain/area)<sup>2</sup> vs. number of cycles plot for the Ni<sub>3</sub>Al coated superalloys subjected to cyclic oxidation for 50 cycles in Na<sub>2</sub>SO<sub>4</sub>-60%V<sub>2</sub>O<sub>5</sub> at 900°C.

#### **6.1.4.3 Scale Thickness Measurement**

SEM back scattered micrographs for the corroded cross-sections of Ni<sub>3</sub>Al coated superalloys Superni 75 and 601 are shown in Fig. 6.47, whereas those for the Ni<sub>3</sub>Al coated superalloys Superni 600, 718 and Superfer 800H are shown in Fig. 6.51 (b), Fig. 6.52 (a) and (b) respectively. The scale thickness values for the coated Superni 75 and 600 are very similar and are measured as 285 and 287  $\mu\text{m}$  respectively. A minimum scale thickness of 151  $\mu\text{m}$  has been obtained by the coated Superni 718. Whereas the corresponding values are 240 and 178  $\mu\text{m}$  respectively for the coated Superni 601 and Superfer 800H.

#### **6.1.4.4 X-ray Diffraction Analysis**

X-ray diffractograms for the Ni<sub>3</sub>Al coated superalloys after 50 cycles of hot corrosion in Na<sub>2</sub>SO<sub>4</sub>-60%V<sub>2</sub>O<sub>5</sub> at 900<sup>0</sup>C are shown in Fig. 6.48 on reduced scales. Identical phases have been revealed in the surface scale of all the five coated superalloys. The XRD analysis revealed the formation of nickel oxide (NiO) as a main phase, whereas aluminum oxide (Al<sub>2</sub>O<sub>3</sub>) and NiAl<sub>2</sub>O<sub>4</sub> phases are also indicated by relatively low intensity peaks in the respective diffraction patterns.

#### **6.1.4.5 SEM/EDAX Analysis**

##### **(a) Surface Morphology**

After hot corrosion in Na<sub>2</sub>SO<sub>4</sub>-60%V<sub>2</sub>O<sub>5</sub> environment at 900<sup>0</sup>C for 50 cycles the scales of Ni<sub>3</sub>Al coated superalloys in general contain high amounts of nickel oxide (NiO) as is evident from SEM/EDAX analysis shown in Fig. 6.49 and Fig. 6.50. The scale in the case of coated Superni 75 has spongy appearance, Fig. 6.49 (a) and is mainly consisting of NiO and at some places there is small concentration of Cr<sub>2</sub>O<sub>3</sub> and V<sub>2</sub>O<sub>5</sub> present in it. The scale for the coated Superni 600 superalloy has shown a fine grained morphology, where some spalling of the scale has also been noticed, which is revealed as black areas in the micrograph, Fig. 6.49 (b). The scale is mainly NiO. A small quantity of V<sub>2</sub>O<sub>5</sub> is detected by EDAX analysis at a point in the subscale. Whereas scale has distorted grains for the coated Superni 601 superalloy and is again consisting mainly of NiO. Small quantities of Na<sub>2</sub>O and V<sub>2</sub>O<sub>5</sub> are found in the top scale, while the subscale contains Cr<sub>2</sub>O<sub>3</sub> in small

concentrations. Further, the top most layer of the scale for the coated Superni 718 is mainly NiO. At some spots, the presence of  $V_2O_5$ ,  $Cr_2O_3$  and  $Y_2O_3$  has also been indicated, which may perhaps be the spalled regions, Fig. 6.50 (a). The presence of Y at this point indicates that diffusion of Y has taken place from the bond coat. Similar analysis for the coated Superfer 800H scale shows that the top scale is NiO again, whereas the sublayer has small quantities of  $Y_2O_3$ ,  $V_2O_5$  and  $Al_2O_3$  present in it also.

#### (b) Cross-Sectional Analysis

Cross-sectional BSEI and EDAX analysis for the  $Ni_3Al$  coated Superni 75 after an exposure to  $Na_2SO_4$ -60% $V_2O_5$  environment at  $900^{\circ}C$  for 50 cycles are shown in Fig. 6.51 (a). It is evident from the micrograph that the scale has two distinct zones present in it. The outer zone of the scale looks to be massive with some lamellar cracks. EDAX analysis at two points i.e. 5 and 6 shows that this region mainly consists of nickel oxide, and contains aluminium oxide also. The presence of chromium in this zone indicates that diffusion of the same has taken place from the bond coat into the top coat. The portion of the scale between the top zone and the substrate seem to have retained its as-sprayed lamellar structure (Chapter 4). The EDAX measurements at points 2 and 3 further reveals the presence of perhaps unreacted Ni, Cr and Al in a composition similar to that of bond coat alloy powder. Besides it is clear from the analysis along cross-section of the scale that wherever concentration of nickel increases, there is reduction in aluminium concentration and vice-versa. Moreover the absence of oxygen in the substrate shows that it has remained unaffected.

Back scattered electron image in the case of coated Superni 600, Fig. 6.51 (b) again shows a duplex scale. The outer massive portion of the scale is mainly consisting of oxides of nickel, while small amounts of aluminium are also visible throughout this portion indicating probable formation of alumina. The diffusion of chromium into the top scale from the bond coat has also been confirmed by the analysis. The presence of oxygen in the bond coat indicates that bond coat might also have got partially oxidised.

Oxide scale morphology for the coated Superni 718 is again similar to those exhibited by the coated Superni 75 and 600 cases. In the massive top scale, there is richness of Ni accompanied by depletion of aluminium and vice-versa, as is clear from the

EDAX analysis at points 4, 5 and 6 in Fig. 6.52 (a). Migration of chromium from the bond coat to the top scale is evident in this case also. Oxygen is seen penetrating even upto the base superalloy. Besides, the dark black phases in the scale are found to have high amounts of aluminium with a low in concentration of nickel.

The presence of oxygen throughout the cross-section of oxide scale for the corroded Ni<sub>3</sub>Al coated superalloy Superfer 800H, Fig. 6.52 (b) indicates that whole of the coating might have got oxidised alongwith internal oxidation of some portion of the base alloy. The morphology of the scale is again similar to that of the other Ni<sub>3</sub>Al coated superalloys described in this section. It is worth mentioning that the diffusion of chromium from the bond coat into the top scale has not been indicated in this case. Whereas minor diffusion of Fe into the bond coat and the top scale can be observed from the EDAX analysis, which is very prominent at a point 2, near the scale/base alloy interface.

#### **6.1.4.6 EPMA Analysis**

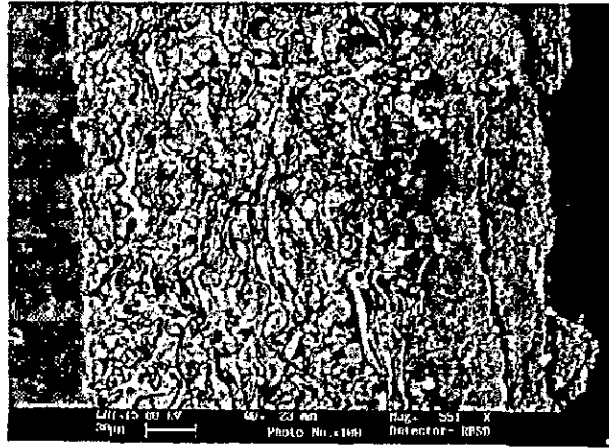
Elemental X-ray mappings for the corroded cross-section of Ni<sub>3</sub>Al coated Superni 75 superalloys are shown in Fig. 6.53. The upper zone of the scale is consisting mainly of nickel with some aluminium. At some places in this zone where nickel is absent, aluminium is present and vice-versa. Small amounts of vanadium and chromium are also present in this portion. Just below this top zone of the scale, a band with high concentration of chromium can be seen. In the bond coat region of the scale Ni, Cr, Al and Y are mainly revealed and bond coat seem to have retained its original structure. Titanium and iron have shown their presence throughout the scale indicating diffusion from the substrate superalloy and a thin streak of titanium has formed at the bond coat/base alloy interface. Minor diffusion of Y is also indicated into the top scale, where it is present in form of small clusters.

A similar analysis for the coated Superni 600 indicate a nickel oxide rich band at the top of the scale, which contains dispersed aluminium oxide at the places, where nickel is depleted of (Fig. 6.54). Vanadium has also diffused in this band and is present at the places where both nickel as well as aluminium are absent. Chromium diffusion from the bond coat into the top scale is minor. In rest of the scale which corresponds the bond coat, nickel rich splat containing chromium are visible, which are mainly surrounded by aluminium oxide. Chromium oxide has also formed stringers around most of these splats and seems to co-exist with aluminium oxide. Sulphur has penetrated into the base alloy perhaps along the grain boundaries.

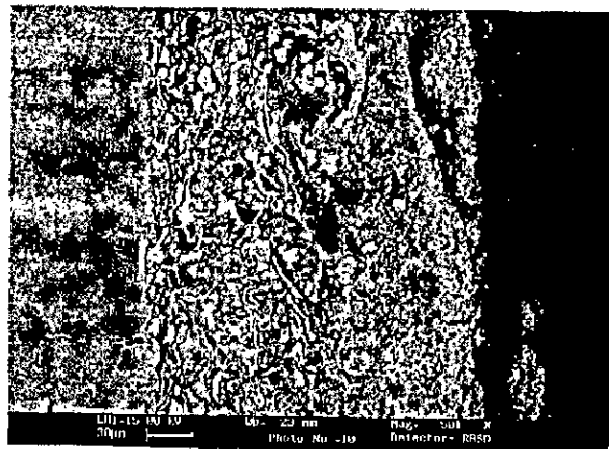
EPMA analysis of the Ni<sub>3</sub>Al coated Superni 601 specimen after exposure to the given environment, Fig. 6.55 reveals that the top region of the scale mainly consists of nickel. At the places in this top scale, where nickel is depleted, aluminium is present in higher concentrations in the form of small streaks. Chromium has shown tendency to diffuse into the lower layers of this top region of the scale, especially at the places where aluminium is in low concentrations. Some elongated clusters of vanadium and silicon are also revealed at the top of the scale. Nickel and aluminium are present at alternate locations in the bond coat, while chromium seems to be co-existing with nickel, and yttrium has shown its presence alongwith aluminium. Iron and manganese have also migrated to the scale from the substrate superalloy and a high concentration of iron is observed just above the scale/base alloy interface.

The topmost band of the scale for hot corroded Superni 718 case (Fig. 6.56) is mainly nickel oxide and contains streaks of aluminium oxide at the places where nickel is absent. V is also seen in this layer in the form of stringers. In the bond coat region of the scale, nickel and aluminium oxide are present at alternate positions. While chromium is seen forming thin band in the middle of scale by diffusing upwards just below interface between the bottom and top coat. This might have resulted in observed Cr-depleted band in the upper layer of bond coat. There is a little high concentration of nickel just below the bond coat in the form of a continuous layer, which is depleted of Cr. Sulphur is present with nickel in a band, which is depleted of chromium. Iron has shown minor diffusion into the scale, whereas molybdenum diffusion into the topmost layers of the scale is substantial.

Corresponding analysis for the Superfer 800H case (Fig. 6.57) reveals that the upper scale is consisting mainly of nickel oxide, and the bond coat has retained its identity. Ni in the bond coat has remained un-oxidised, and aluminium oxide is present along the Ni-rich splats. Chromium has migrated to the upper layers from the bond coat, leaving behind a band depleted of Cr. There is also indication of diffusion of Cr from the substrate with lower region of bond coat, which is obvious from Cr-depleted band in the base alloy, and this band has got enriched with nickel. S is present in the form of thin parallel layers below the substrate/bond coat interface. There is some ingress of vanadium into the scale and it is present as clusters in the top scale. Iron has migrated from the base alloy through the bond coat and is present in the upper scale, and at some places, it co-exists with vanadium.



(a)



(b)

**Fig. 6.47** SEM back scattered images for the Ni<sub>3</sub>Al coated superalloys after cyclic oxidation in Na<sub>2</sub>SO<sub>4</sub>-60%V<sub>2</sub>O<sub>5</sub> for 50 cycles at 900<sup>o</sup>C  
(a) Superni 75      (b) Superni 601.

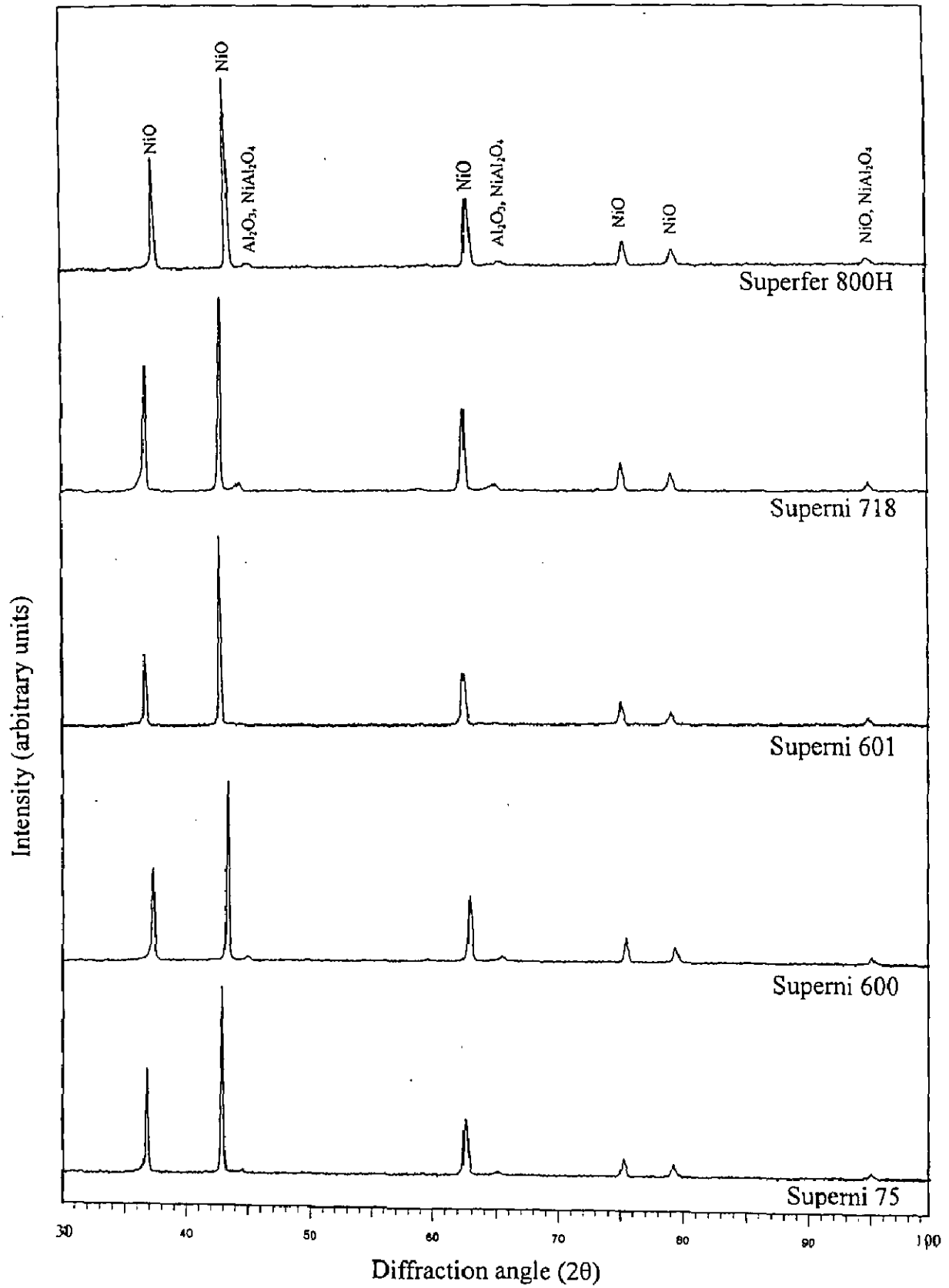


**Fig. 6.48** X-ray diffraction patterns for the Ni<sub>3</sub>Al coated superalloys subjected to cyclic oxidation in Na<sub>2</sub>SO<sub>4</sub>-60%V<sub>2</sub>O<sub>5</sub> at 900°C after 50 cycles.

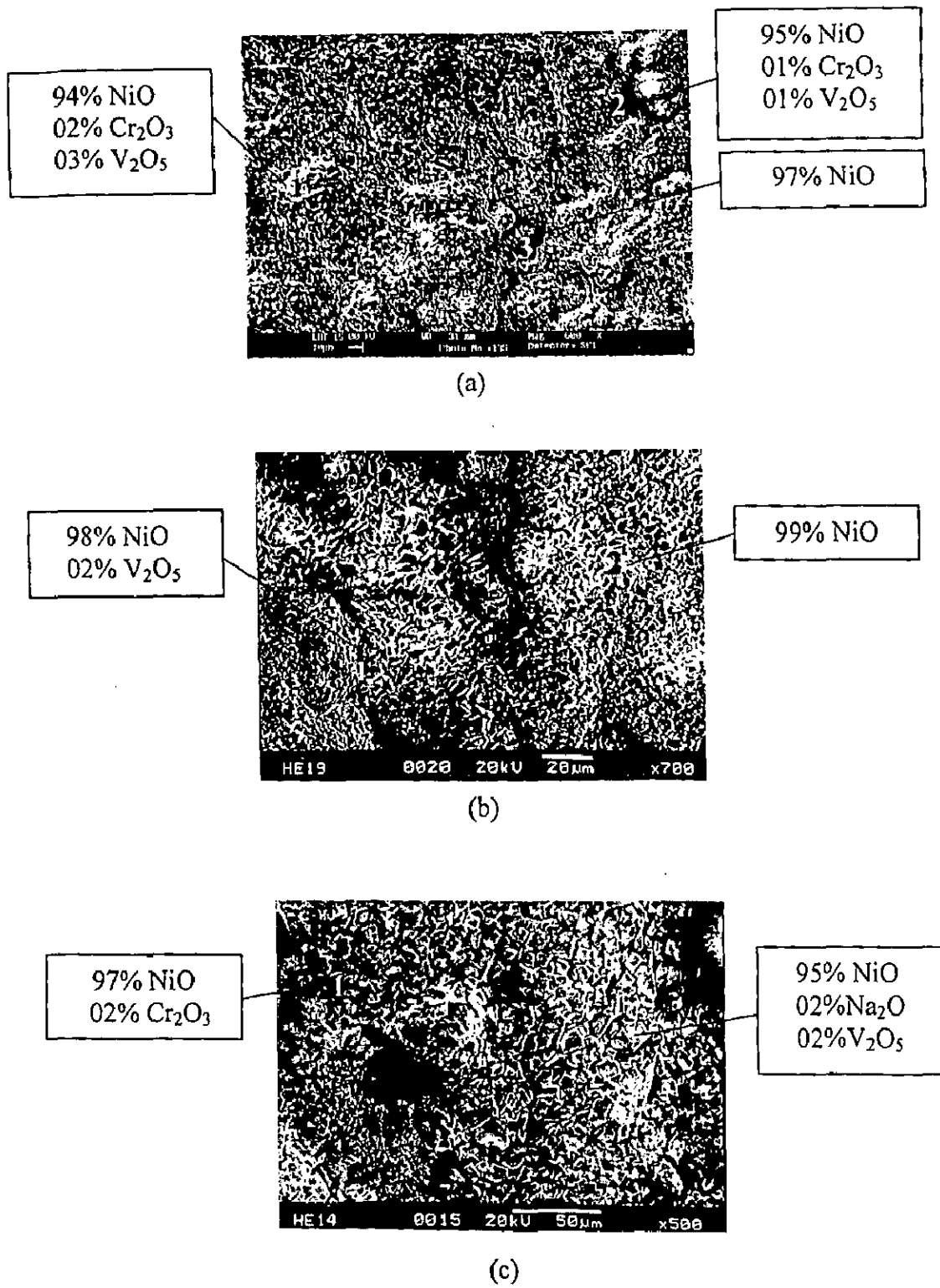
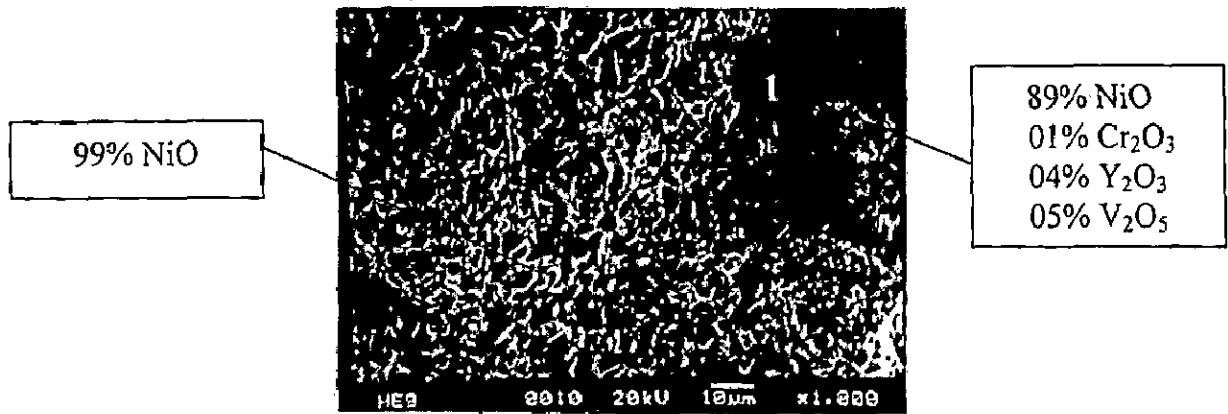
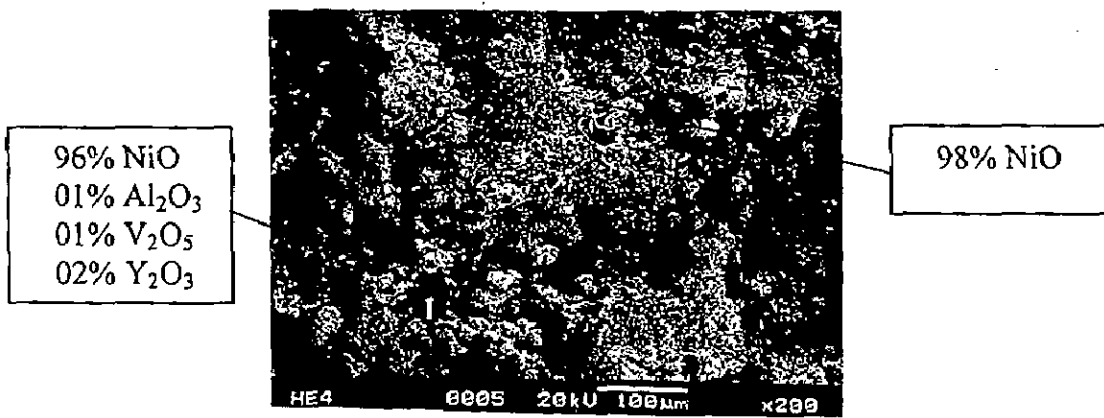


**Fig. 6.49** Surface scale morphology and EDAX analysis for the plasma spray Ni<sub>3</sub>Al coated superalloys subjected to cyclic oxidation in Na<sub>2</sub>SO<sub>4</sub>-60%V<sub>2</sub>O<sub>5</sub> at 900°C for 50 cycles  
 (a) Superni 75                      (b) Superni 600                      (c) Superni 601.



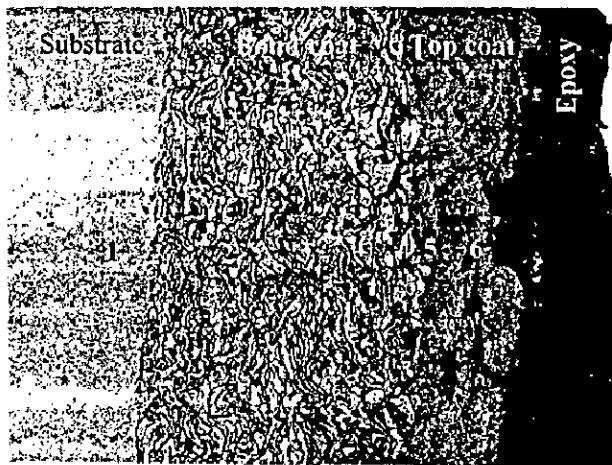
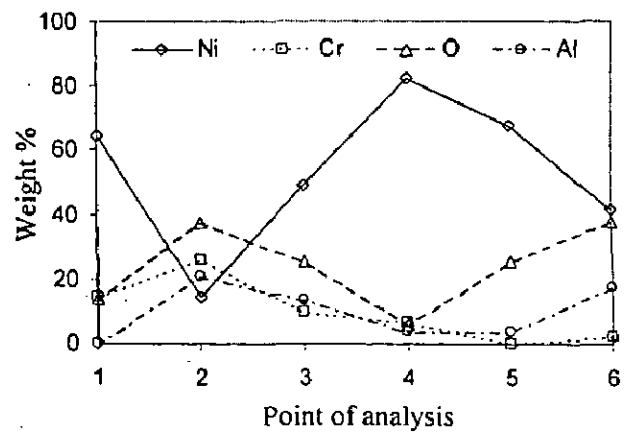
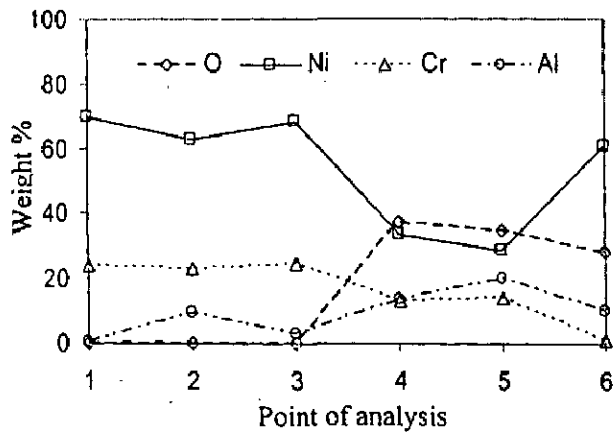


(a)

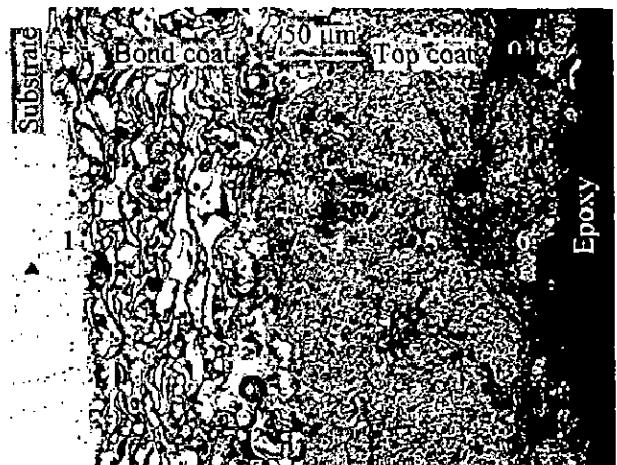


(b)

**Fig. 6.50** Surface scale morphology and EDAX analysis for the plasma spray Ni<sub>3</sub>Al coated superalloys subjected to cyclic oxidation in Na<sub>2</sub>SO<sub>4</sub>-60%V<sub>2</sub>O<sub>5</sub> at 900°C for 50 cycles  
 (a) Superni 718      (b) Superfer 800H.

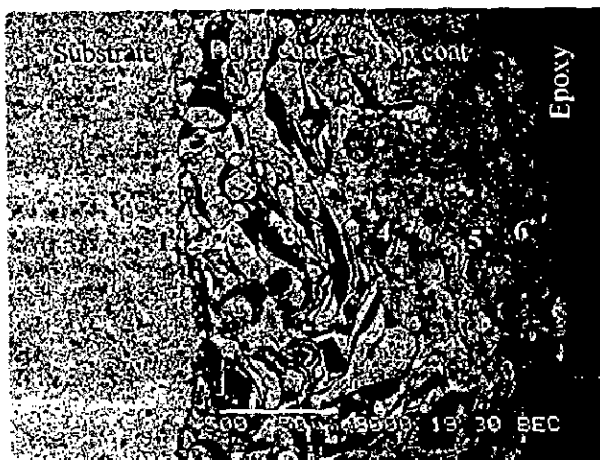
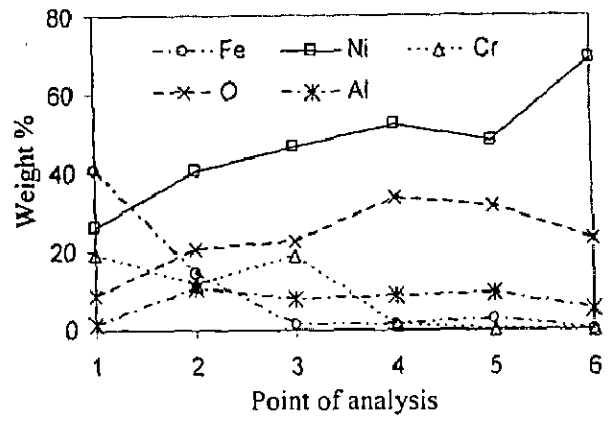
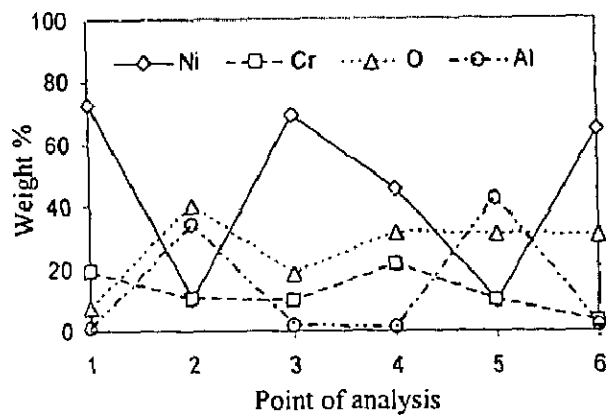


(a)

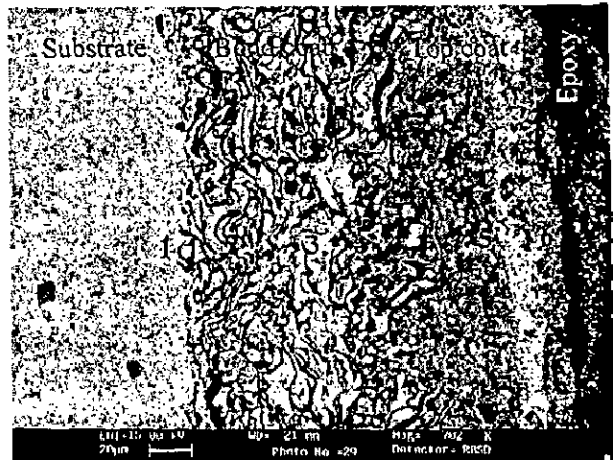


(b)

**Fig. 6.51** Oxide scale morphology and variation of elemental composition across the cross-section of  $\text{Ni}_3\text{Al}$  coated superalloys subjected to cyclic oxidation in  $\text{Na}_2\text{SO}_4$ -60% $\text{V}_2\text{O}_5$  at  $900^\circ\text{C}$  after 50 cycles  
 (a) Superni 75      (b) Superni 600.



(a)



(b)

**Fig. 6.52** Oxide scale morphology and variation of elemental composition across the cross-section of  $\text{Ni}_3\text{Al}$  coated superalloys subjected to cyclic oxidation in  $\text{Na}_2\text{SO}_4\text{-60\%V}_2\text{O}_5$  at  $900^\circ\text{C}$  after 50 cycles  
 (a) Superni 718      (b) Superfer 800H.

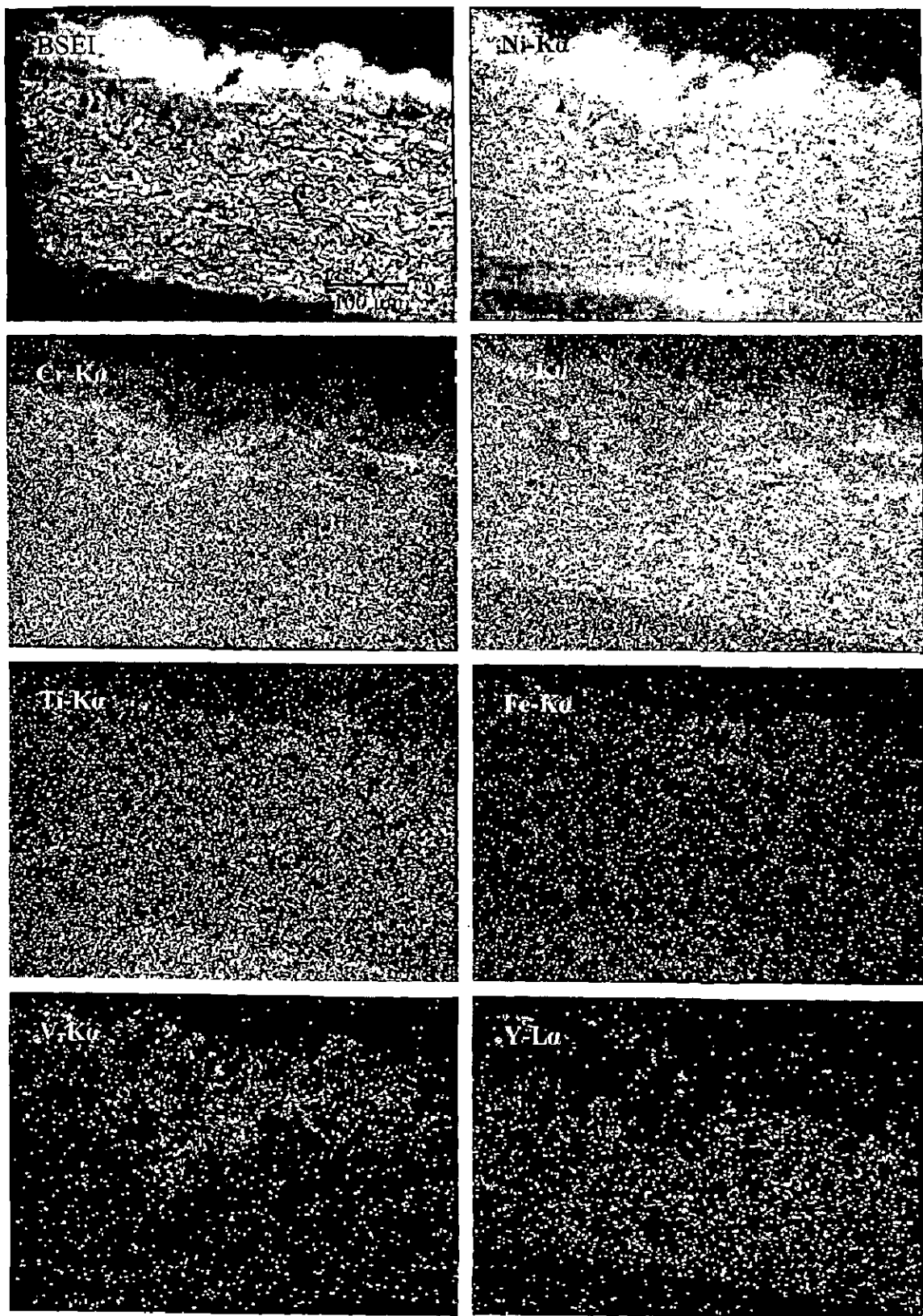


**Fig. 6.53** BSEI and X-ray mappings of the cross-section of Ni<sub>3</sub>Al coated superalloy Superni 75 subjected to cyclic oxidation in Na<sub>2</sub>SO<sub>4</sub>-60%V<sub>2</sub>O<sub>5</sub> at 900°C after 50 cycles.

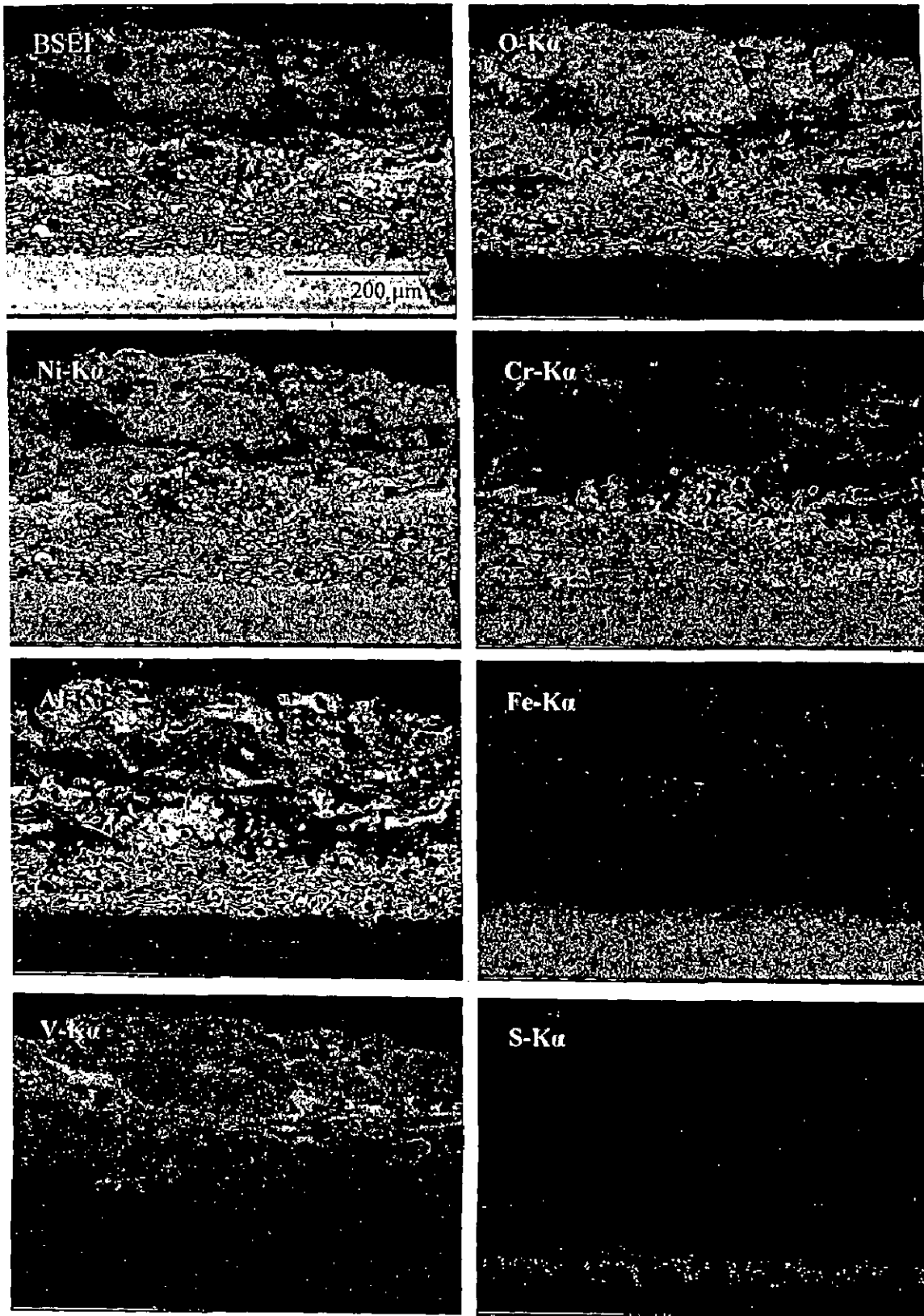


**Fig. 6.54** BSEI and X-ray mappings of the cross-section of  $\text{Ni}_3\text{Al}$  coated superalloy Superni 600 subjected to cyclic oxidation in  $\text{Na}_2\text{SO}_4$ -60% $\text{V}_2\text{O}_5$  at  $900^\circ\text{C}$  after 50 cycles.

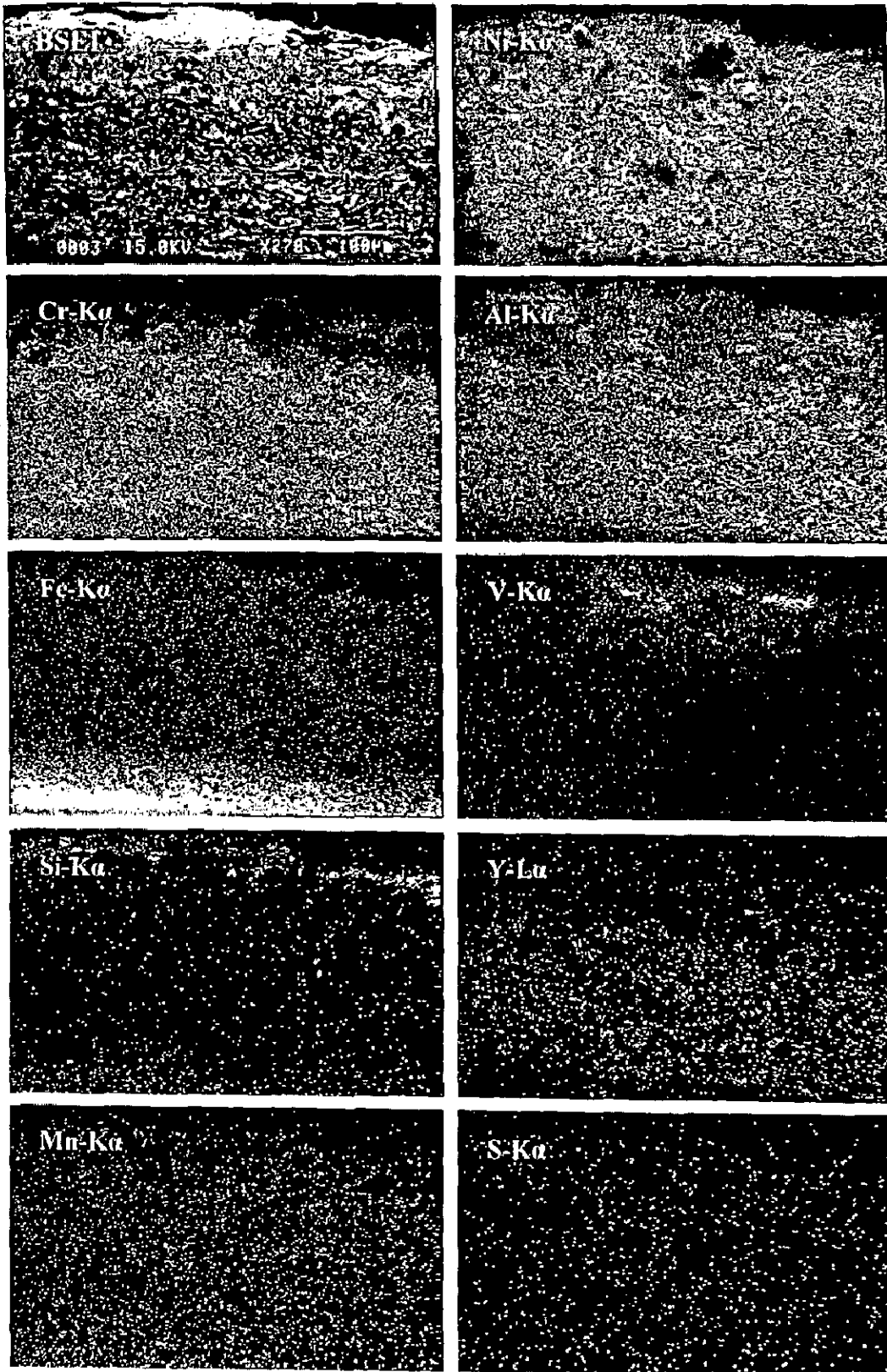
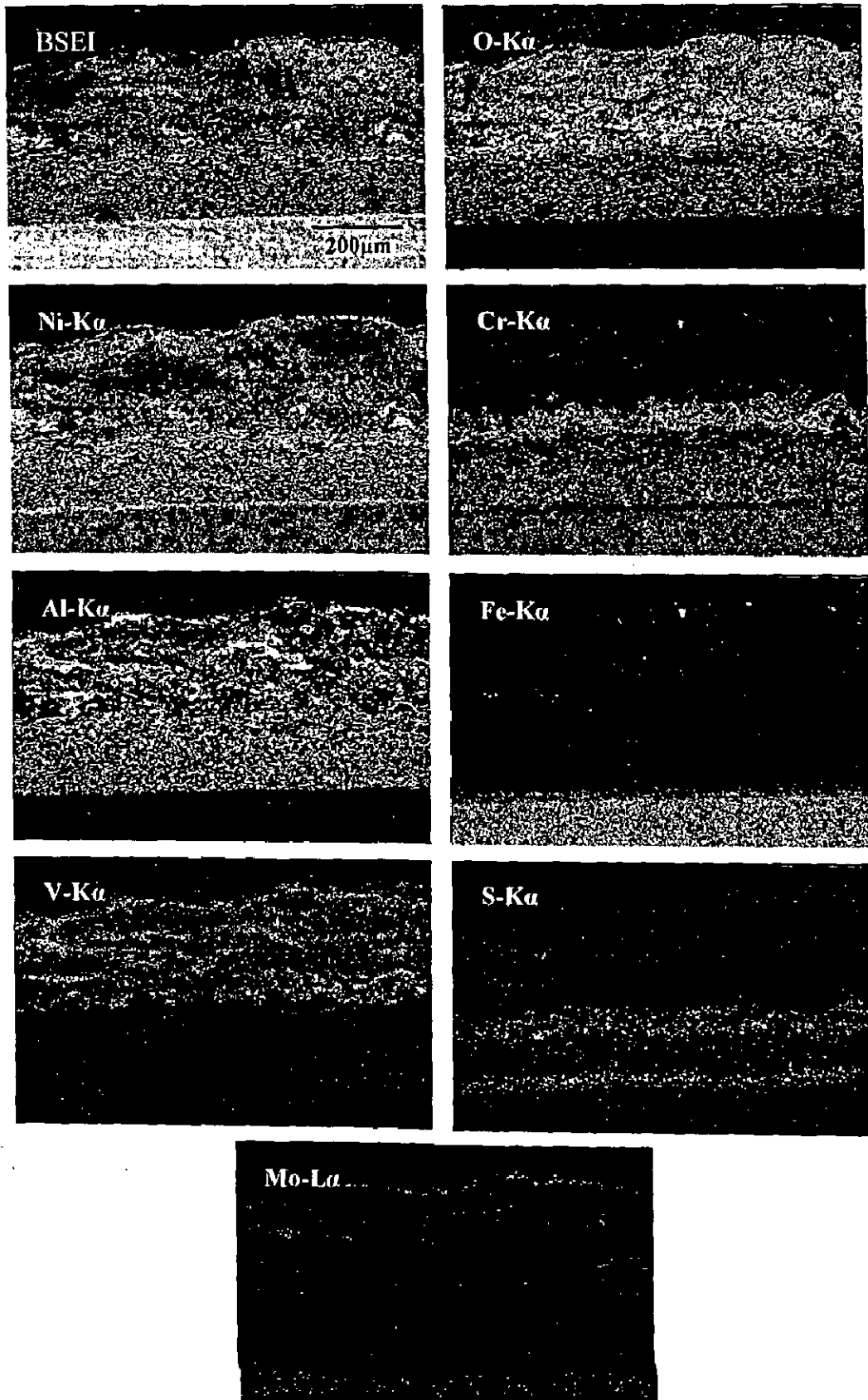


Fig. 6.55 BSEI and X-ray mappings of the cross-section of Ni<sub>3</sub>Al coated superalloy Superni 601 subjected to cyclic oxidation in Na<sub>2</sub>SO<sub>4</sub>-60%V<sub>2</sub>O<sub>5</sub> at 900°C after 50 cycles.



**Fig. 6.56** BSEI and X-ray mappings of the cross-section of  $\text{Ni}_3\text{Al}$  coated superalloy Superni 718 subjected to cyclic oxidation in  $\text{Na}_2\text{SO}_4\text{-60\%V}_2\text{O}_5$  at  $900^\circ\text{C}$  after 50 cycles.

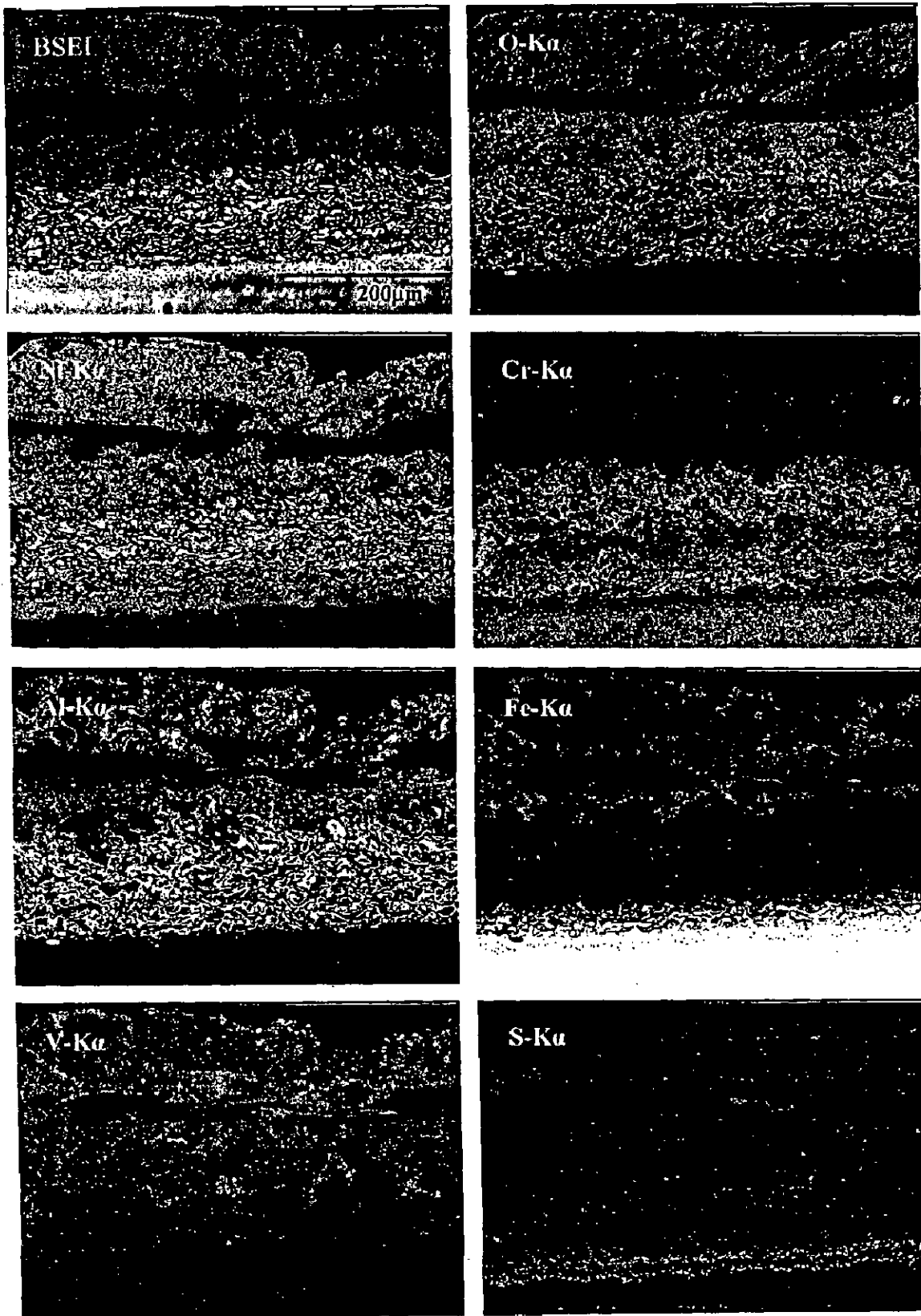


Fig. 6.57 BSEI and X-ray mappings of the cross-section of  $\text{Ni}_3\text{Al}$  coated superalloy Superfer 800H subjected to cyclic oxidation in  $\text{Na}_2\text{SO}_4$ -60% $\text{V}_2\text{O}_5$  at  $900^\circ\text{C}$  after 50 cycles.



## 6.1.5 Stellite-6 Coating

### 6.1.5.1 Visual Examination

Macro morphologies of the oxide scales for the plasma spray Stellite-6 coated superalloys after hot corrosion in  $\text{Na}_2\text{SO}_4\text{-}60\%\text{V}_2\text{O}_5$  at  $900^\circ\text{C}$  for 50 cycles are depicted in Fig. 6.58. Colour of the oxide scales for all the coated superalloys was grey after the first cycle which turned to dark grey during first 8 to 9 cycles, and subsequently showed the formation of silver grey areas on the dark grayish background with the progress of cycles. The superficial cracking at or near some of the edges started from the end of 15<sup>th</sup>, 41<sup>st</sup> and 13<sup>th</sup> cycle respectively for the coated superalloys Superni 600, 718 and Superfer 800H, which resulted in minor spallation of the coating from/near edges (Section 6.1.2.1). The relative magnitude of loss to the coating due to said spalling was highest for Superfer 800H substrate, where the top layer of the main coating flaked off from one of its flat surface over a small area, while it remained intact with all the other surfaces. Whereas the coating in case of Superni 75 and 601 did not suffer spallation, although superficial minor cracks were seen near one edge by the end of 22<sup>nd</sup> and 23<sup>rd</sup> cycle in the respective cases.

Further the minor spalling of the scale was observed invariably for all the coated superalloys which once started continued upto the termination of the study in the form of fine blackish powder. This spalling initiated from 27<sup>th</sup>, 11<sup>th</sup>, 36<sup>th</sup>, 24<sup>th</sup> and 7<sup>th</sup> cycle for the coated superalloys Superni 75, 600, 601, 718 and Superfer 800H respectively.

### 6.1.5.2 Thermogravimetric Data

Weight changes expressed in  $\text{mg}/\text{cm}^2$  have been plotted in Fig. 6.59 as a function of time expressed in number of cycles for the Stellite-6 coated as well as uncoated superalloys subjected to cyclic oxidation in  $\text{Na}_2\text{SO}_4\text{-}60\%\text{V}_2\text{O}_5$  environment at  $900^\circ\text{C}$  for 50 cycles. The overall weight gains after 50 cycles are measured to be 23.64, 28.08, 28.02, 22.96 and 31.44  $\text{mg}/\text{cm}^2$  for the Stellite-6 coated Superni 75, 600, 601, 718 and Superfer 800H respectively. Therefore it can be inferred that among the Stellite-6 coated superalloys, the coated Superni 718 has shown the highest corrosion resistance to the given environment. Further, Stellite-6 coating is found to be successful in decreasing the weight gain in case of Superfer 800H substrate only, which is 60% of the weight gain

in the corresponding uncoated case. Otherwise the higher overall weight gains are indicated by coated Superni 75, 600 and 601 specimens as compared to ones for the base alloys, whereas nothing can be concluded regarding Superni 718 on the basis of weight gain data as the data could not be obtained upto 50 cycles for the uncoated case. The cumulative weight gains shown by the coated Superni 75 and 718 as well as Superni 600 and 601 superalloys are nearly same.

The squares of total weight gain values per unit area ( $\text{mg}^2/\text{cm}^4$ ) are plotted in Fig. 6.60 against the number of cycles to understand the kinetics of corrosion for the Stellite-6 coated superalloys. The coated superalloys in general followed the parabolic rate law for the whole range of cyclic study with parabolic rate constant ( $K_p$ ) values as 26.92, 43.26, 42.36, 30.38 and  $50 \times 10^{-10} \text{ g}^2 \text{ cm}^{-4} \text{ s}^{-1}$  respectively for the coated Superni 75, 600, 601, 718 and Superfer 800H. It is worth mentioning that this coating has shown the minimum deviations from parabolic rate law in comparison to those shown by the NiCrAlY, Ni-20Cr and Ni<sub>3</sub>Al coatings.

#### **6.1.5.3 Scale Thickness Measurement**

The BSEI for the corroded Stellite-6 coated Superni 75, 600, 601, 718 and Superfer 800H are shown in Figs. 6.64 to 6.66 respectively. The thickness values evaluated from these BSE images are found to be 435, 603, 591, 496 and 549  $\mu\text{m}$  respectively for the coated Superni 75, 600, 601, 718 and Superfer 800H respectively.

#### **6.1.5.4 X-ray Diffraction Analysis**

XRD profiles for the scales of Stellite-6 coated superalloys after hot corrosion in molten salt at  $900^\circ\text{C}$  for 50 cycles shows the formation of common phases for all the substrate superalloys as can be seen in Fig. 6.61. These profiles are shown on reduced scales. CoO and  $\text{CoCr}_2\text{O}_4$  are revealed as the main phases in the scales. Whereas some weak peaks indicating the presence of  $\text{Cr}_2\text{O}_3$  are also visible in the respective diffractograms.

#### **6.1.5.5 SEM/EDAX Analysis**

##### **(a) Surface Morphology**

SEM morphology and EDAX analysis for Stellite-6 coated Superni 75, 600 and 601 superalloys after cyclic hot corrosion are shown in Fig. 6.62, whereas those for Superni 718 and Superfer 800H in Fig. 6.63. Scale for the coated Superni 75 consists of

irregular shaped grains (splats) along which there are white layers, and very fine globules are present throughout the scale. The scale mainly contains CoO with some Cr<sub>2</sub>O<sub>3</sub>, Fig. 6.62 (a). NiO and Al<sub>2</sub>O<sub>3</sub> are also present in small percentages.

Oxide scale for the coated Superni 600 also contains globules distributed across the scale, somewhere irregular shape splats are seen with black colour inside and white phase along the boundaries, Fig. 6.62 (b). The black region contains lower amount of CoO and higher amount of Cr<sub>2</sub>O<sub>3</sub>. In the black region the CoO precipitates have got nearly halved, while Cr<sub>2</sub>O<sub>3</sub> got doubled as compared to the white region. SEM micrograph, Fig. 6.62 (c) shows a scale having spongy appearance in the case of coated Superni 601. The top scale is again having the dominance of CoO, and also has Cr<sub>2</sub>O<sub>3</sub> and NiO in noticeable amounts. While NiO is found to be absent in the spalled region of the scale and the concentration of CoO, in turn has increased, refer point 1.

The scale for the coated Superni 718 superalloy, Fig. 6.63 (a) is found to have CoO and Cr<sub>2</sub>O<sub>3</sub> as its main constituents in its white region. An increase in the concentration of cobalt oxide can be seen in the black region of scale, where the concentration of Cr<sub>2</sub>O<sub>3</sub> has reduced by 50%. Further migration of aluminum from the bond coat to the top coat to form alumina in the spalled region of the scale (black region) is also observed. Contrary to the stellite-6 coated Ni-base superalloys, the Fe-based Superfer 800H has shown dominance of Cr<sub>2</sub>O<sub>3</sub> in its scale, Fig. 6.63 (b). CoO content is nearly uniform throughout the scale. The black region (matrix) has relatively higher concentration of chromia, and white phase along the grain boundaries contains lesser amounts of Cr<sub>2</sub>O<sub>3</sub>.

#### (b) Cross-Sectional Analysis

Scale morphologies and EDAX analysis of the cross-sections of plasma spray Stellite-6 coated Superni 75, 600, 601, 718 and Superfer 800H superalloys after 50 cycles of hot corrosion are reported in Fig. 6.64 to Fig. 6.66 respectively. It is obvious from the respective figures that the scale morphologies are very similar in all the cases and show two layers having different structures. The top and bond coats have retained their original structures. EDAX analysis done at a point (point 6) near the outermost layer of the scale indicates that this layer mainly consists of cobalt, chromium and oxygen in all the cases. In the case of coated Superni 75, Co-rich splat present in the inner layers of the top scale is found to have remained un-oxidised, point 4, Fig. 6.64 (a).

Whereas at point 5 near the cobalt splat boundary, amount of oxygen has increased, and aluminium is also found in substantial amounts. Further, light grey phase (point 3) in the bond coat consists mainly of nickel and oxygen, whereas the dark phase is rich in chromium and oxygen. Whereas, in the case of Superni 600, Co-rich areas in the top scale are found to have low oxygen content and vice-versa. In the bond coat, aluminium and oxygen are co-existing at the places, where nickel is present in low concentration.

The splats in case of oxidised Stellite-6 coated Superni 601 are again found to be rich in Co (point 4), which are perhaps encircled by Cr-rich oxygen containing boundaries (point 5). Alternate layers rich in Al and Ni seem to be present in the bond coat. Further, aluminium rich layers are observed to contain increased oxygen content. The scale in case of Superni 718 substrate, again have Co-rich un-oxidised splats in inner layers of the top scale (point 3 and 4), which perhaps are surrounded by Cr-rich streaks (point 5). Ni-rich splats are found to be present in the bond coat, which have not suffered oxidation. EDAX analysis at points 2 and 3 in case of Fe-base superalloy, Fig. 6.66 predicts significant amount of iron in the bond coat, which may perhaps have diffused from the substrate. The splats are again Co-rich (point 5), and relatively high Al content is perceptible along the splat boundaries (point 4) in the top scale.

Moreover, aluminium has diffused to the top scale in minor quantities in all the cases, as has been indicated by the EDAX measurements, except in the coated Superni 600 case. Oxygen has also penetrated into the substrate in case of coated Superni 75, 601 and Superfer 800H superalloys. The scales are found to be in good contact with their respective substrates.

#### **6.1.5.6 EPMA Analysis**

BSEI and elemental X-ray mappings for the cross-section of Superni 75 Stellite-6 coated superalloy corroded in an environment of  $\text{Na}_2\text{SO}_4$ -60% $\text{V}_2\text{O}_5$  at  $900^\circ\text{C}$  for 50 cycles are shown in Fig. 6.67. The top zone of the scale is consisting mainly of Co and Cr with comparatively small quantities of Si, W and Fe. Bond coat has maintained its identity, and there is some migration of Al and Y into the top scale from the bond coat. Vanadium is present in the top scale, which seems to have got penetrated along the splat boundaries. Nickel has migrated to uppermost layers of the scale.

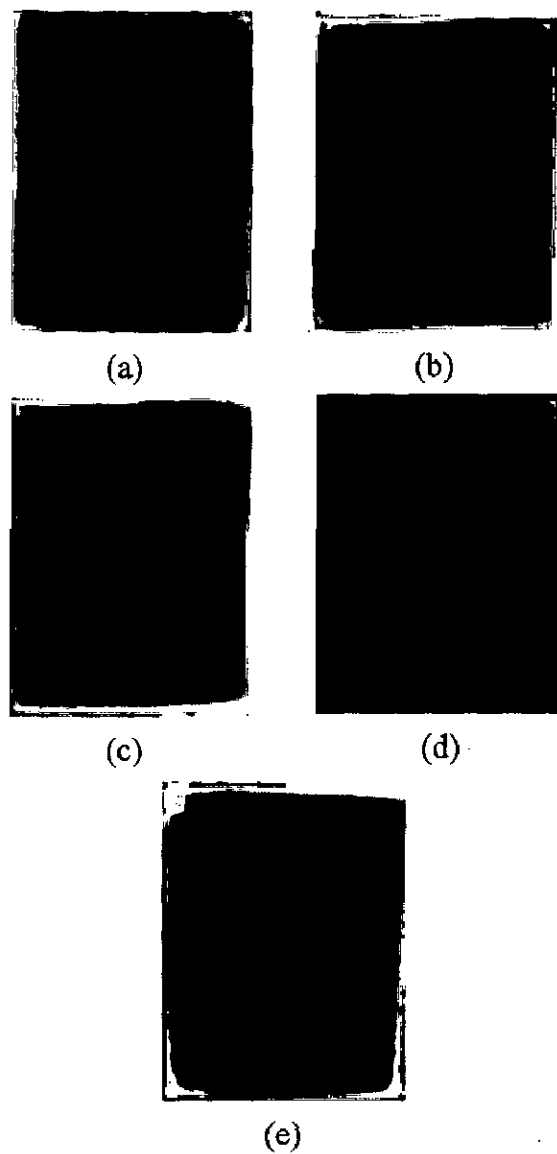
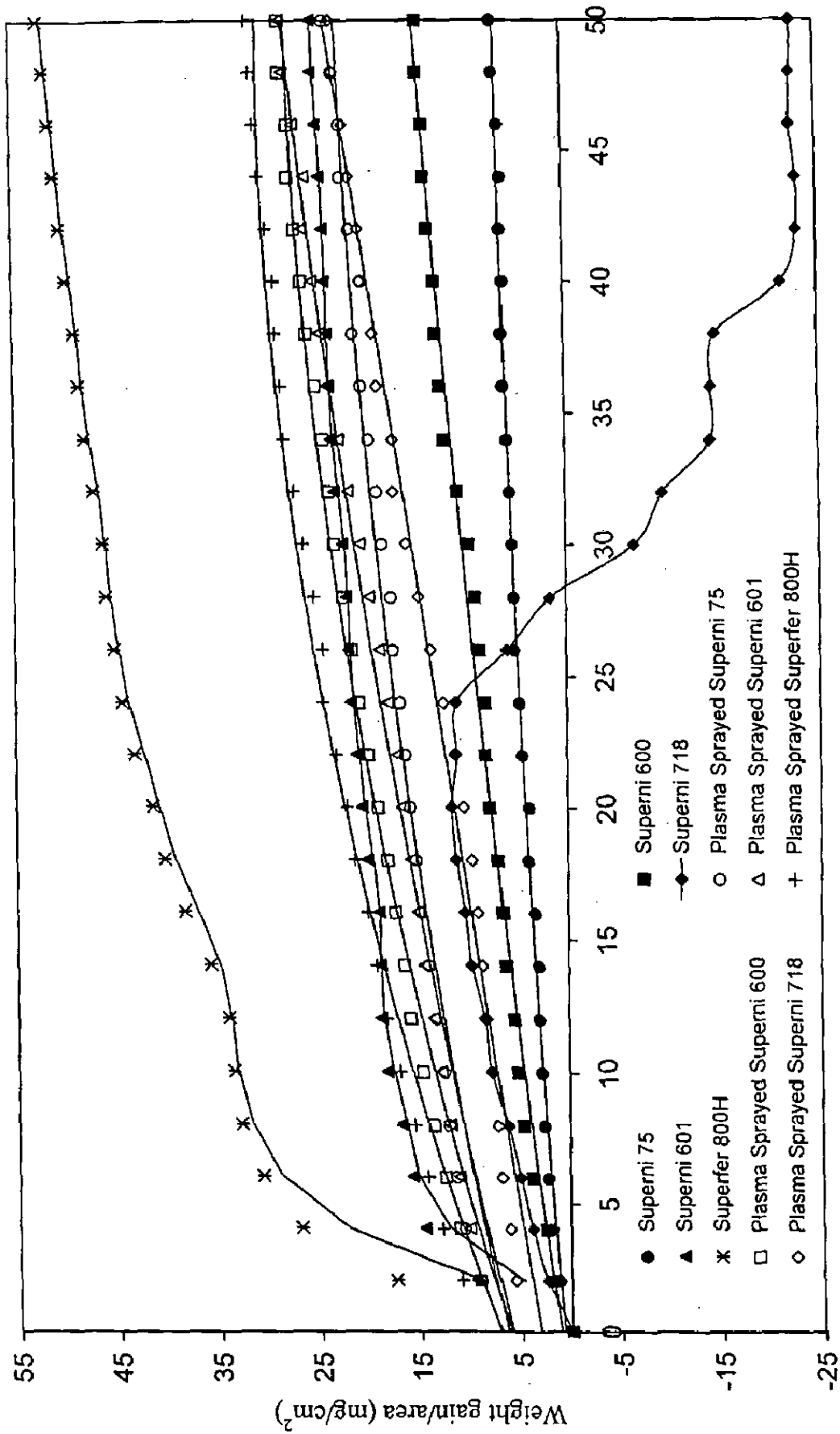


**Fig. 6.58**

Macrographs of the Stellite-6 coating with bond coat subjected to cyclic oxidation in  $\text{Na}_2\text{SO}_4\text{-60}\%\text{V}_2\text{O}_5$  at  $900^\circ\text{C}$  for 50 cycles having substrate superalloys

- |                 |                    |                 |
|-----------------|--------------------|-----------------|
| (a) Superni 75  | (b) Superni 600    | (c) Superni 601 |
| (d) Superni 718 | (e) Superfer 800H. |                 |



Number of cycles

Fig. 6.59 Weight gain vs. number of cycles plot for uncoated and Stellite-6 coated superalloys subjected to cyclic oxidation for 50 cycles in  $\text{Na}_2\text{SO}_4\text{-60}\%\text{V}_2\text{O}_5$  at  $900^\circ\text{C}$ .

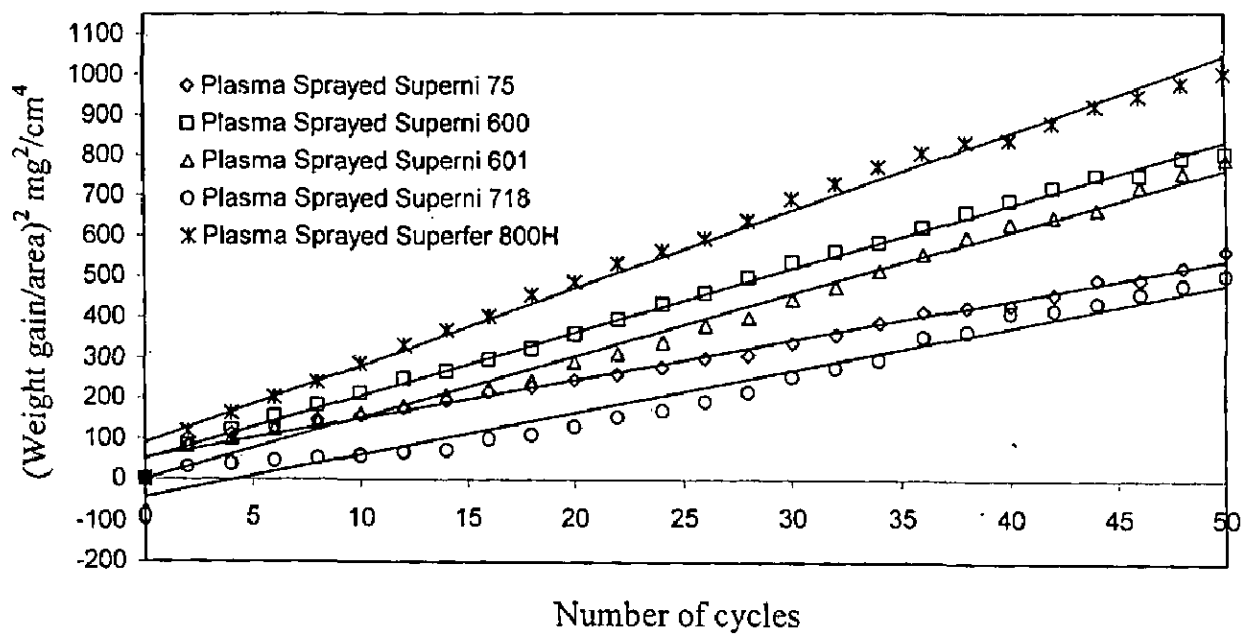
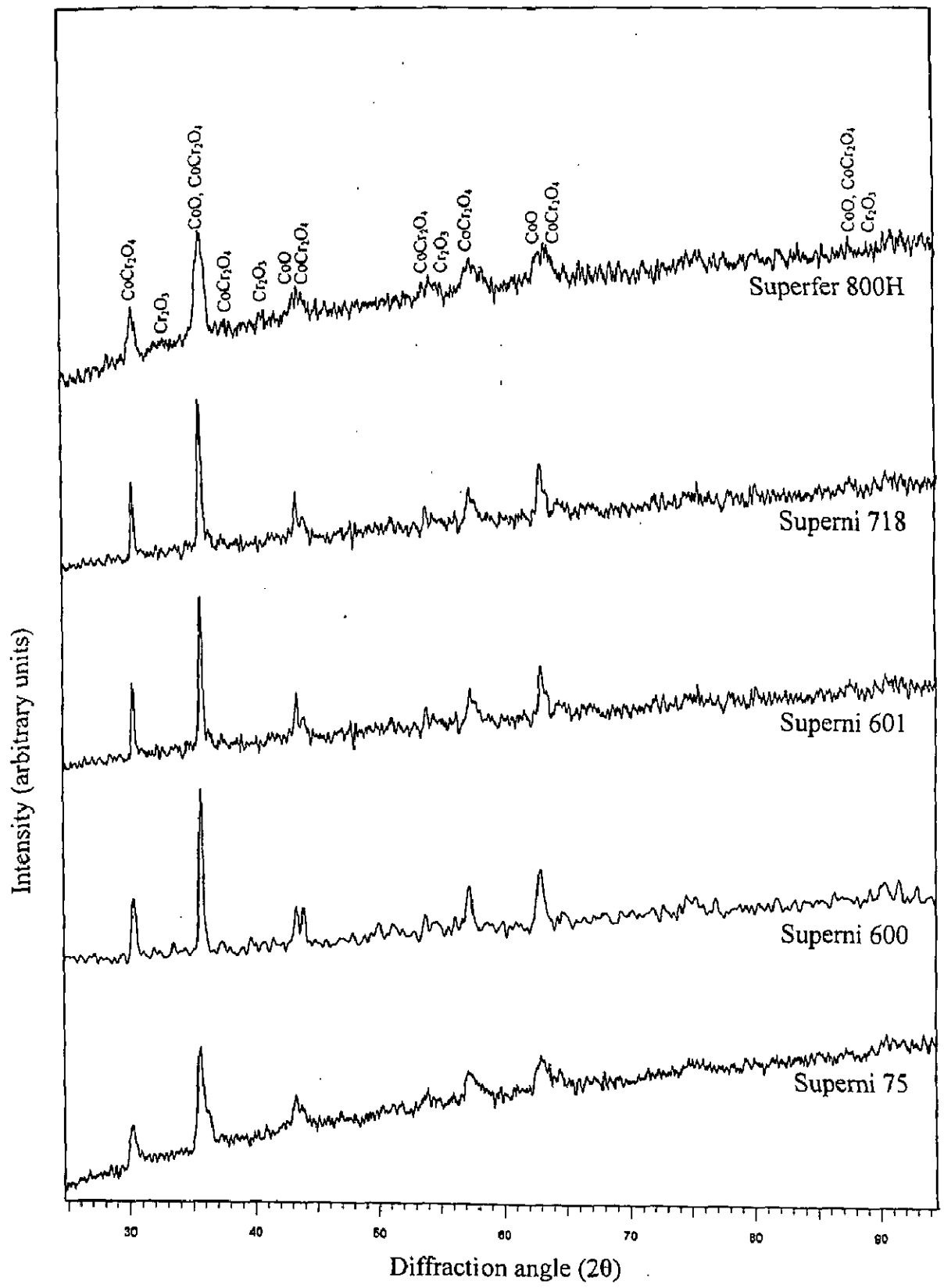
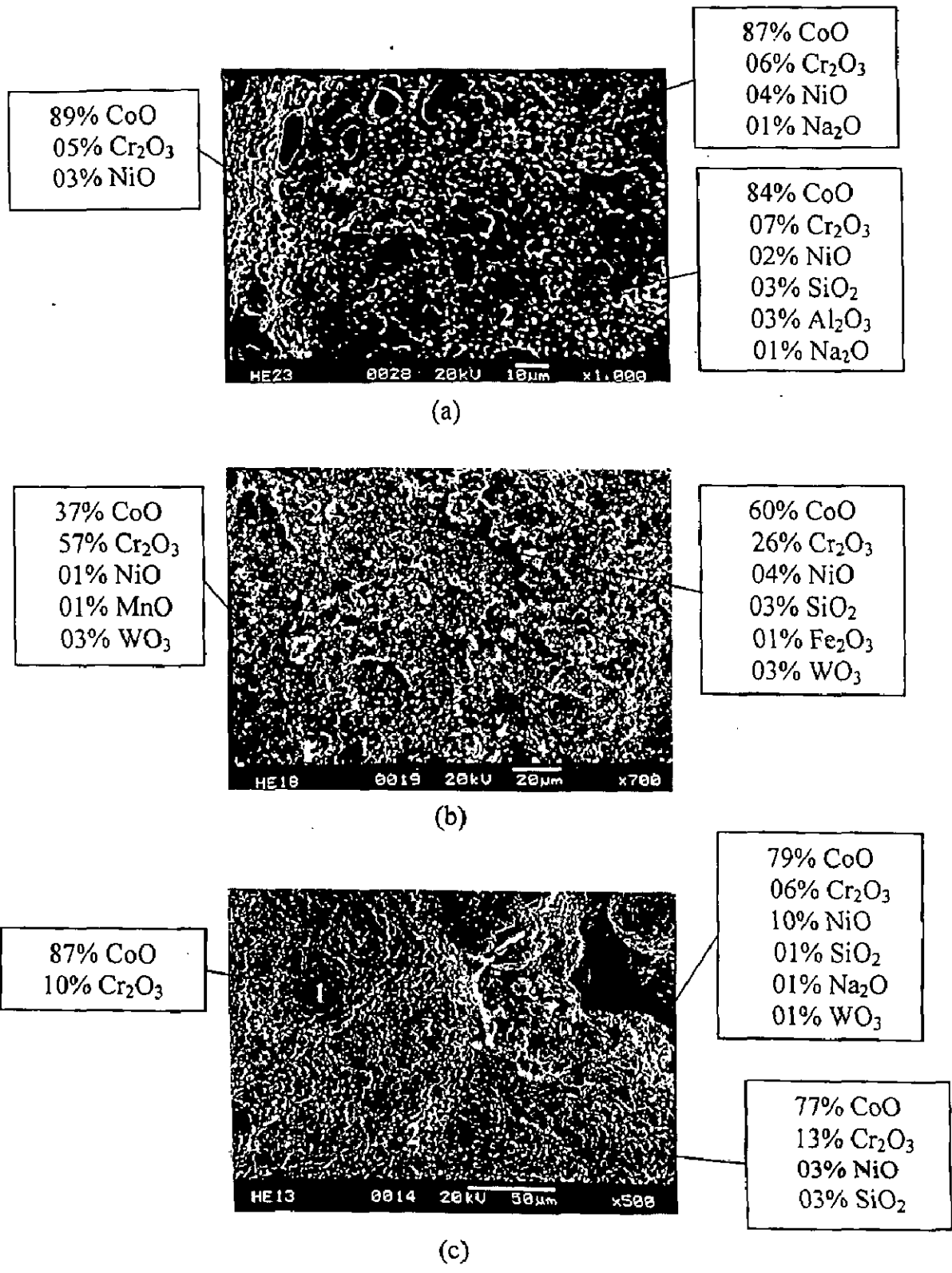


Fig. 6.60 (Weight gain/area)<sup>2</sup> vs. number of cycles plot for the Stellite-6 coated superalloys subjected to cyclic oxidation for 50 cycles in Na<sub>2</sub>SO<sub>4</sub>-60%V<sub>2</sub>O<sub>5</sub> at 900°C.

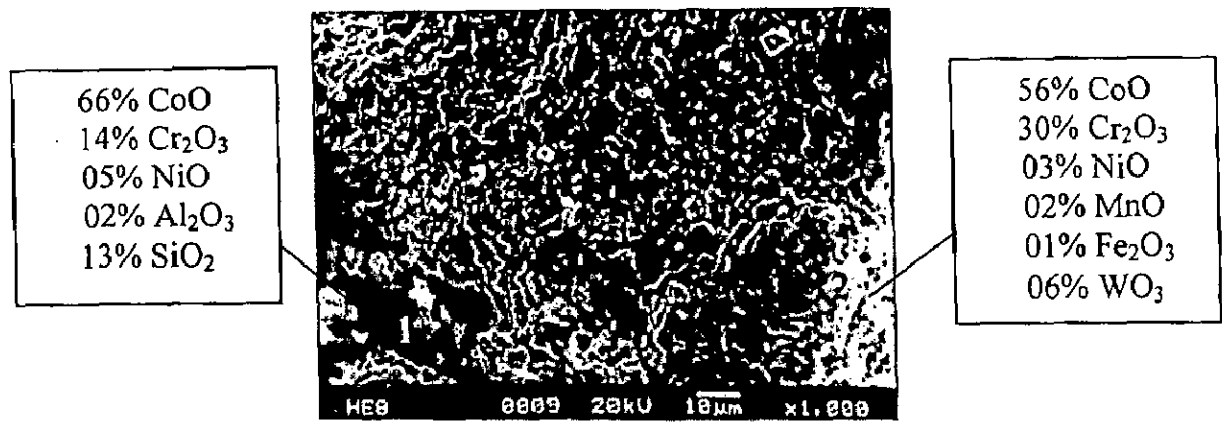


**Fig. 6.61** X-ray diffraction patterns for the Stellite-6 coated superalloys subjected to cyclic oxidation in Na<sub>2</sub>SO<sub>4</sub>-60%V<sub>2</sub>O<sub>5</sub> at 900°C after 50 cycles.

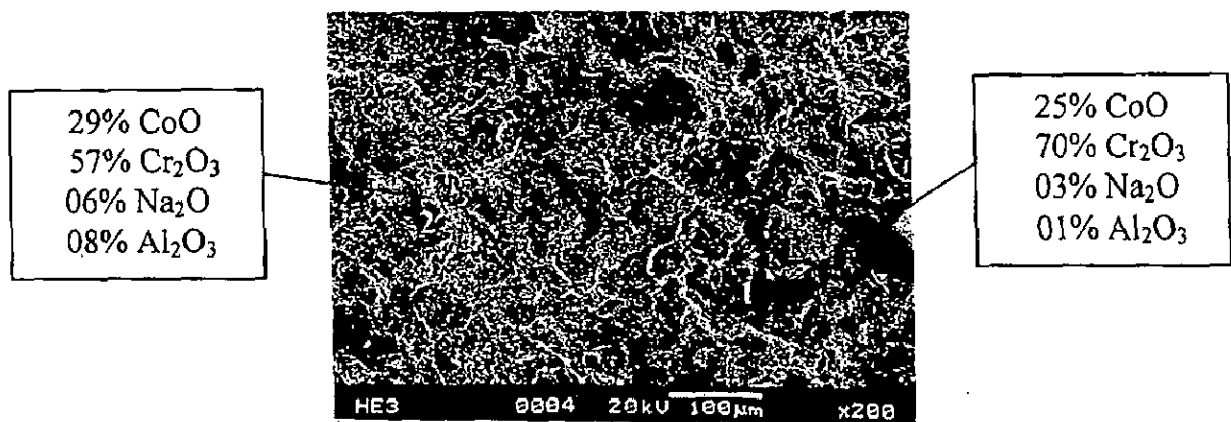




**Fig. 6.62** Surface scale morphology and EDAX analysis for the plasma spray Stellite-6 coated superalloys subjected to cyclic oxidation in Na<sub>2</sub>SO<sub>4</sub>-60%V<sub>2</sub>O<sub>5</sub> at 900<sup>o</sup>C for 50 cycles  
 (a) Superni 75                      (b) Superni 600                      (c) Superni 601.

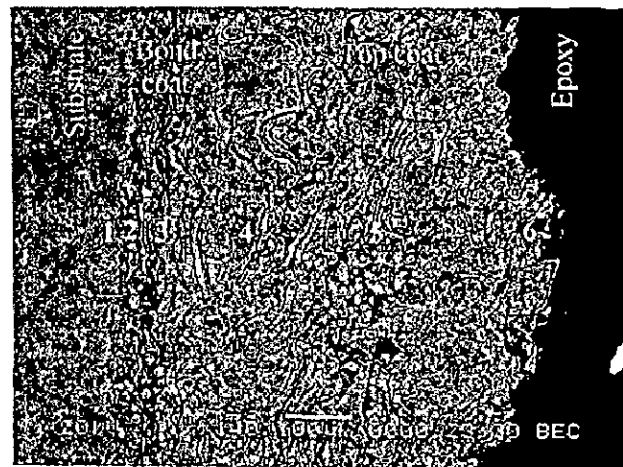
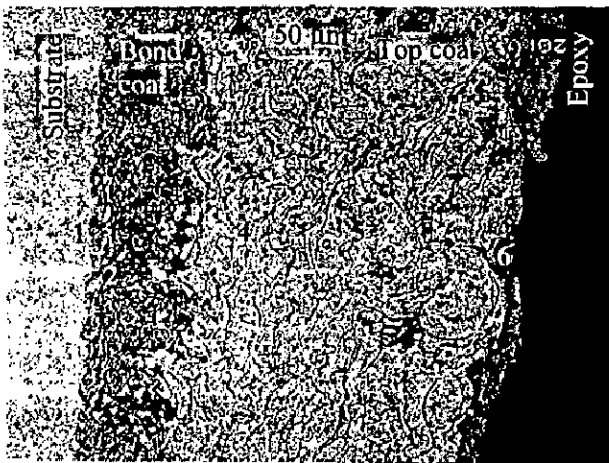
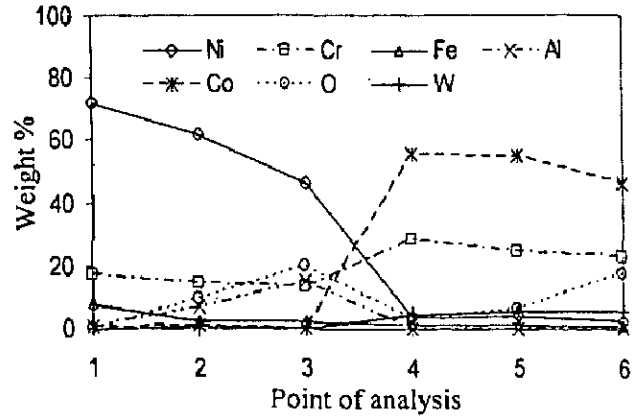
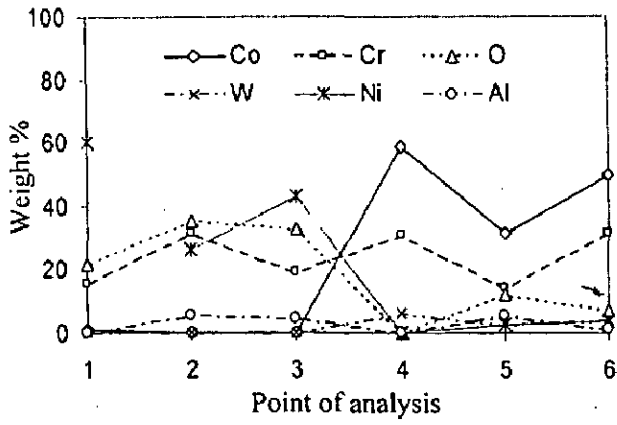


(a)



(b)

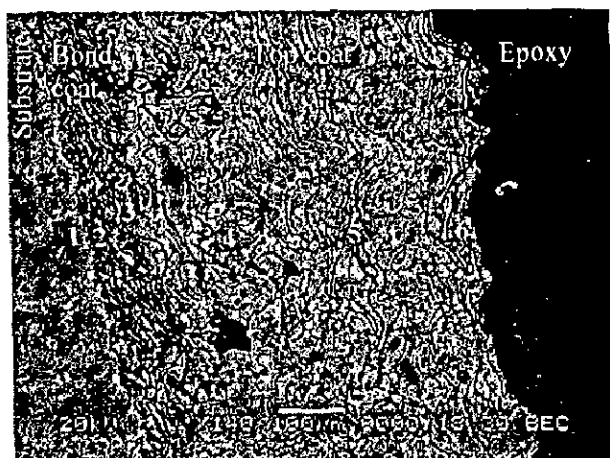
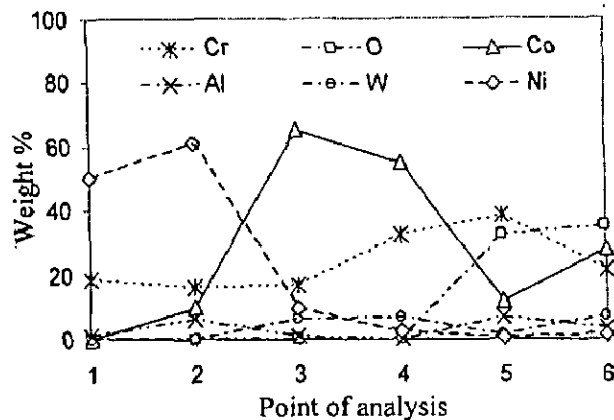
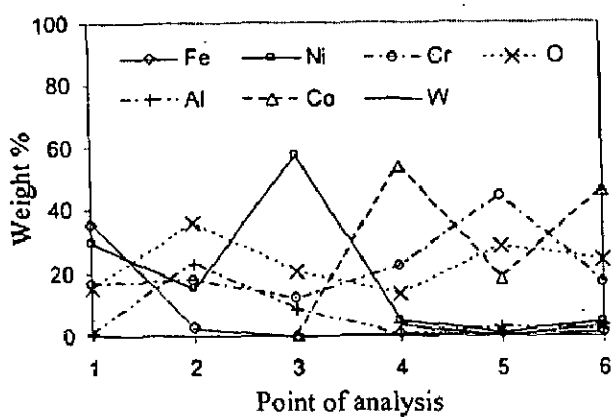
**Fig. 6.63** Surface scale morphology and EDAX analysis for the plasma spray Stellite-6 coated superalloys subjected to cyclic oxidation in Na<sub>2</sub>SO<sub>4</sub>-60%V<sub>2</sub>O<sub>5</sub> at 900<sup>o</sup>C for 50 cycles  
(a) Superni 718                      (b) Superfer 800H.



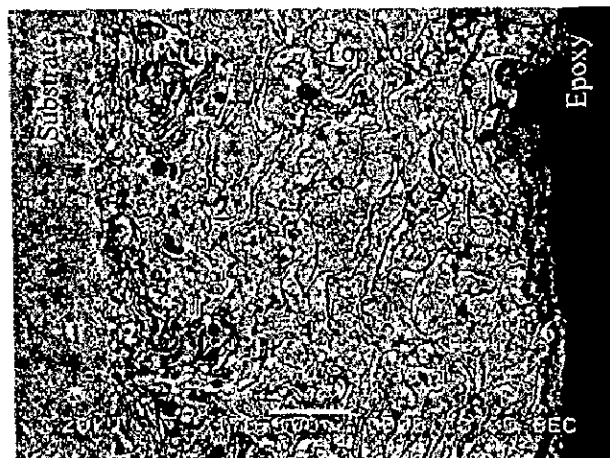
(a)

(b)

**Fig. 6.64** Oxide scale morphology and variation of elemental composition across the cross-section of Stellite-6 coated superalloys subjected to cyclic oxidation in  $\text{Na}_2\text{SO}_4$ -60% $\text{V}_2\text{O}_5$  at 900°C after 50 cycles  
 (a) Superni 75      (b) Superni 600.



(a)



(b)

**Fig. 6.65** Oxide scale morphology and variation of elemental composition across the cross-section of Stellite-6 coated superalloys subjected to cyclic oxidation in  $\text{Na}_2\text{SO}_4$ -60% $\text{V}_2\text{O}_5$  at 900°C after 50 cycles  
 (a) Superni 601      (b) Superni 718.

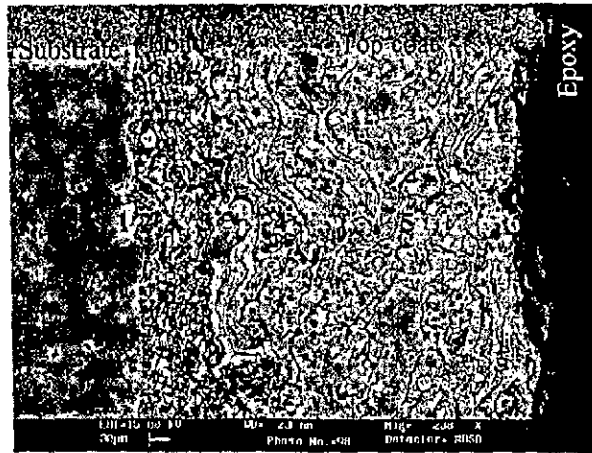
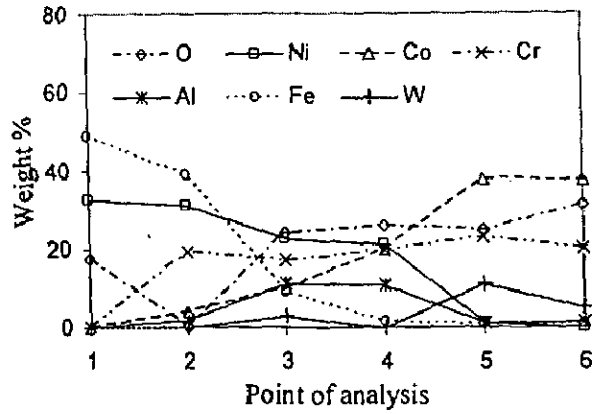
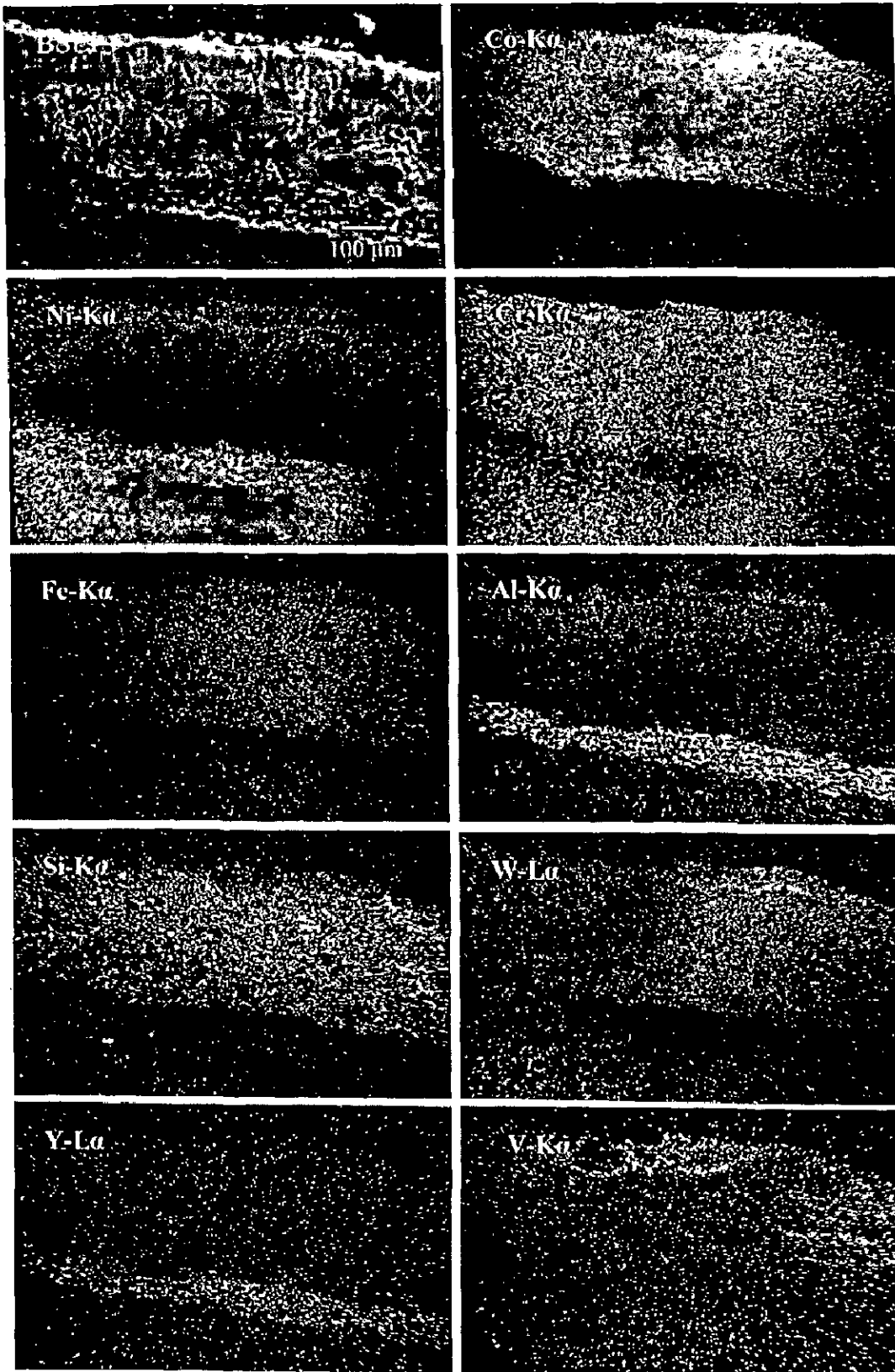


Fig. 6.66 Oxide scale morphology and variation of elemental composition across the cross-section of Stellite-6 coated superalloy Superfer 800H subjected to cyclic oxidation in  $\text{Na}_2\text{SO}_4$ -60% $\text{V}_2\text{O}_5$  at  $900^\circ\text{C}$  after 50 cycles.



**Fig. 6.67** BSEI and X-ray mappings of the cross-section of Stellite-6 coated superalloy Superni 75 subjected to cyclic oxidation in  $\text{Na}_2\text{SO}_4$ -60% $\text{V}_2\text{O}_5$  at 900°C after 50 cycles.

EPMA analysis for the corroded Stellite-6 coated Superni 600 superalloy is depicted in Fig. 6.68. Top layer is mainly consisting of cobalt and chromium having small amounts of W, Ni, Si, Fe and Mn. A nearly continuous streak of aluminium at the outer most part of the scale and some clusters of aluminium in the middle layers of the scale are noticeable, which reflect the possibility of diffusion of aluminium from the bond coat into the top coat. These clusters of aluminium are present at the places where all other elements are depleted of. Bond coat has retained its identity, where some diffusion of W is noticed. Furthermore, EPMA done with oxygen detection crystal at some other location for the same scale, Fig. 6.69, clearly indicates that oxygen is present along the splat boundaries in the top scale co-existing with chromium at most of the places, and the splats have remained un-oxidised. Similarly in the bond coat, nickel rich splats have not suffered oxidation, and oxygen is indicated along the splat boundaries, where aluminium and chromium might have got oxidised.

A corresponding analysis for the Stellite-6 coated superalloy Superni 601 (Fig. 6.70) indicates a dense layer consisting mainly of chromium and cobalt, which also contain tungsten, aluminium and silicon, alongwith some Ni and Fe. Further Al has formed a thin streak at the top of the scale. The presence of aluminium in the top scale indicates diffusion of the same from the bond coat. Small stringers of Fe and Si are also seen at the top of the scale. Minor diffusion of iron into the bond coat is also noticed. Yttrium is mainly confined to the bond coat and co-exists with aluminium.

X-ray mappings for St-6 coated Superni 718 (Fig. 6.71) indicate a dense top scale consisting mainly of chromium and cobalt, which also contain tungsten and silicon. Aluminium, nickel and iron are also present in the upper scale in small quantities. Minor diffusion of iron into the bond coat is also visible. Bond coat has retained its identity. Y has shown minor diffusion into the top scale from the bond coat.

An analogous analysis for the coated Superfer 800H superalloy has been compiled in Fig. 6.72. The Stellite-6 top coat and the bond coat can be clearly distinguished in the BSEI micrograph. Top scale is mainly rich in Cr and Co along with some amount of W. Whereas iron and nickel are present throughout the top scale. Titanium is present in the top scale in an evenly manner. Aluminium has shown diffusion into the top scale from the bond coat. The presence of vanadium has also been revealed in the top portion of the scale, thereby indicating ingress of the same. Y is mainly confined to the bond coat. Two

continuous bands, one rich in nickel and other in chromium are indicated in the bond region of the scale just above the bond coat/substrate interface. Minor diffusion of Fe and Ti in the lower scale that is in the bond coat from the substrate is also indicated.



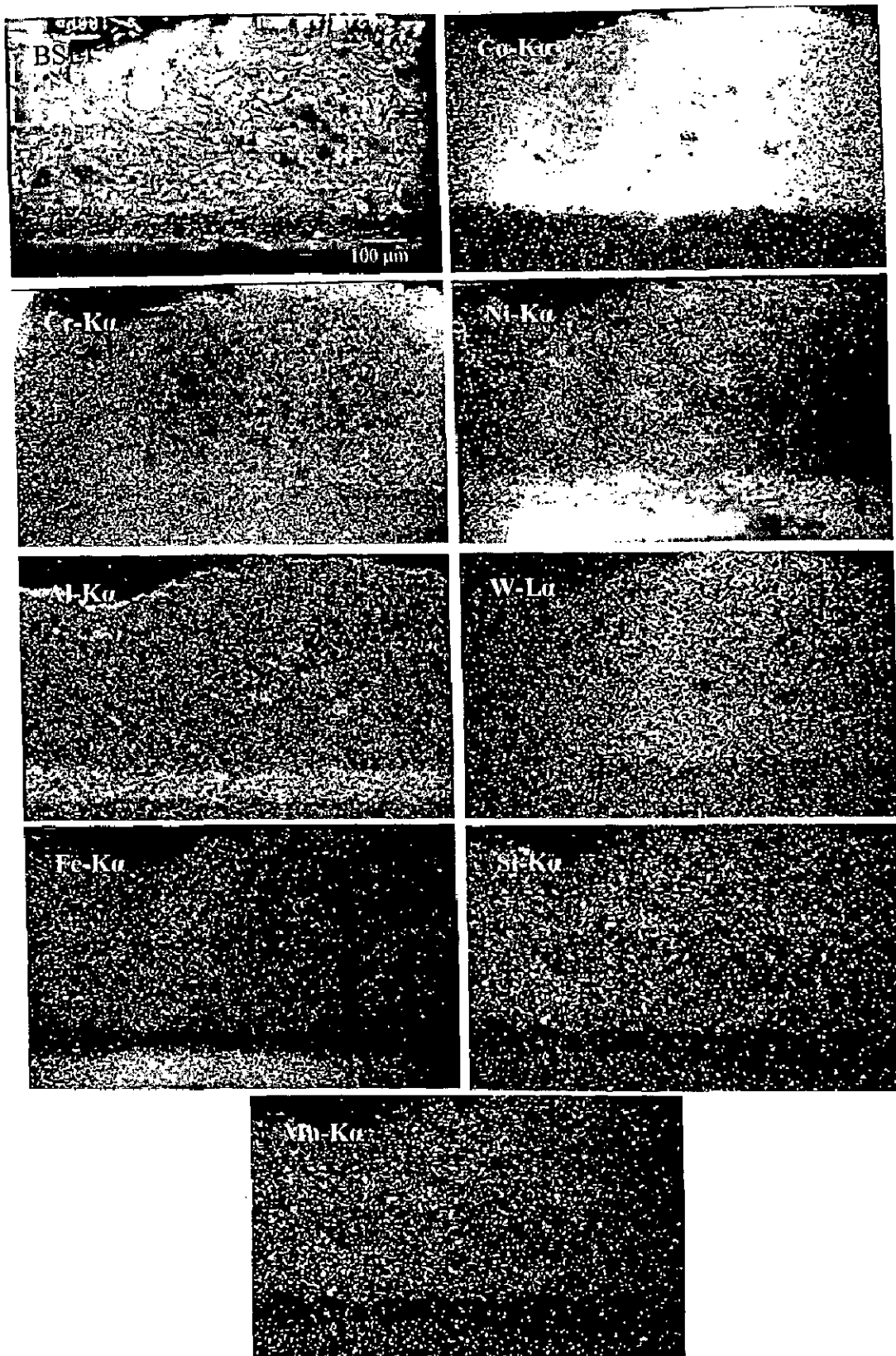
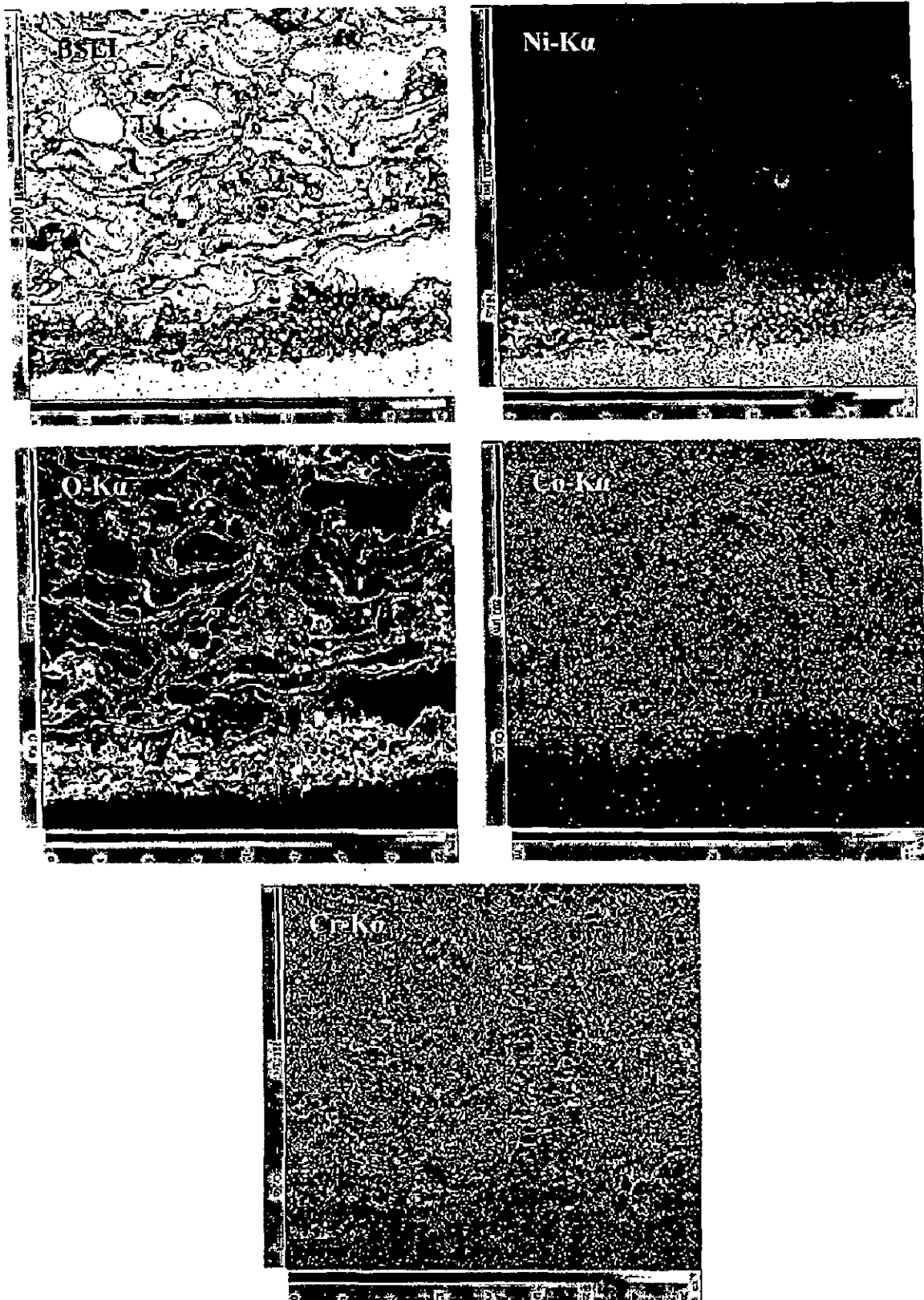
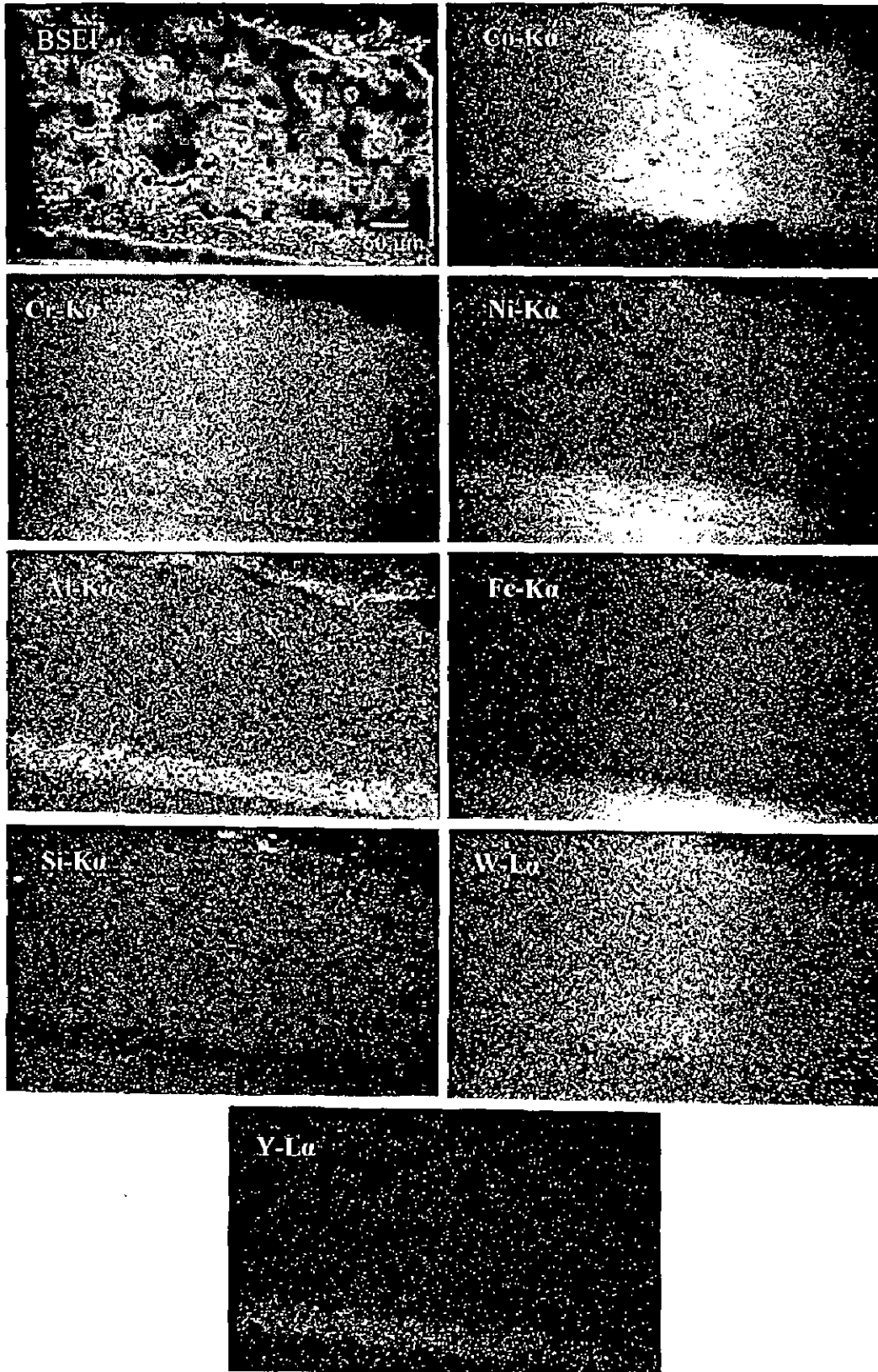


Fig. 6.68 BSEI and X-ray mappings of the cross-section of Stellite-6 coated superalloy Superni 600 subjected to cyclic oxidation in  $\text{Na}_2\text{SO}_4\text{-60\%V}_2\text{O}_5$  at  $900^\circ\text{C}$  after 50 cycles.



**Fig. 6.69** BSEI and X-ray mappings of the cross-section of Stellite-6 coated superalloy Superni 600 subjected to cyclic oxidation in  $\text{Na}_2\text{SO}_4$ -60% $\text{V}_2\text{O}_5$  at  $900^\circ\text{C}$  after 50 cycles showing oxygen distribution also.



**Fig. 6.70** BSEI and X-ray mappings of the cross-section of Stellite-6 coated superalloy Superni 601 subjected to cyclic oxidation in  $\text{Na}_2\text{SO}_4$ -60% $\text{V}_2\text{O}_5$  at 900°C after 50 cycles.

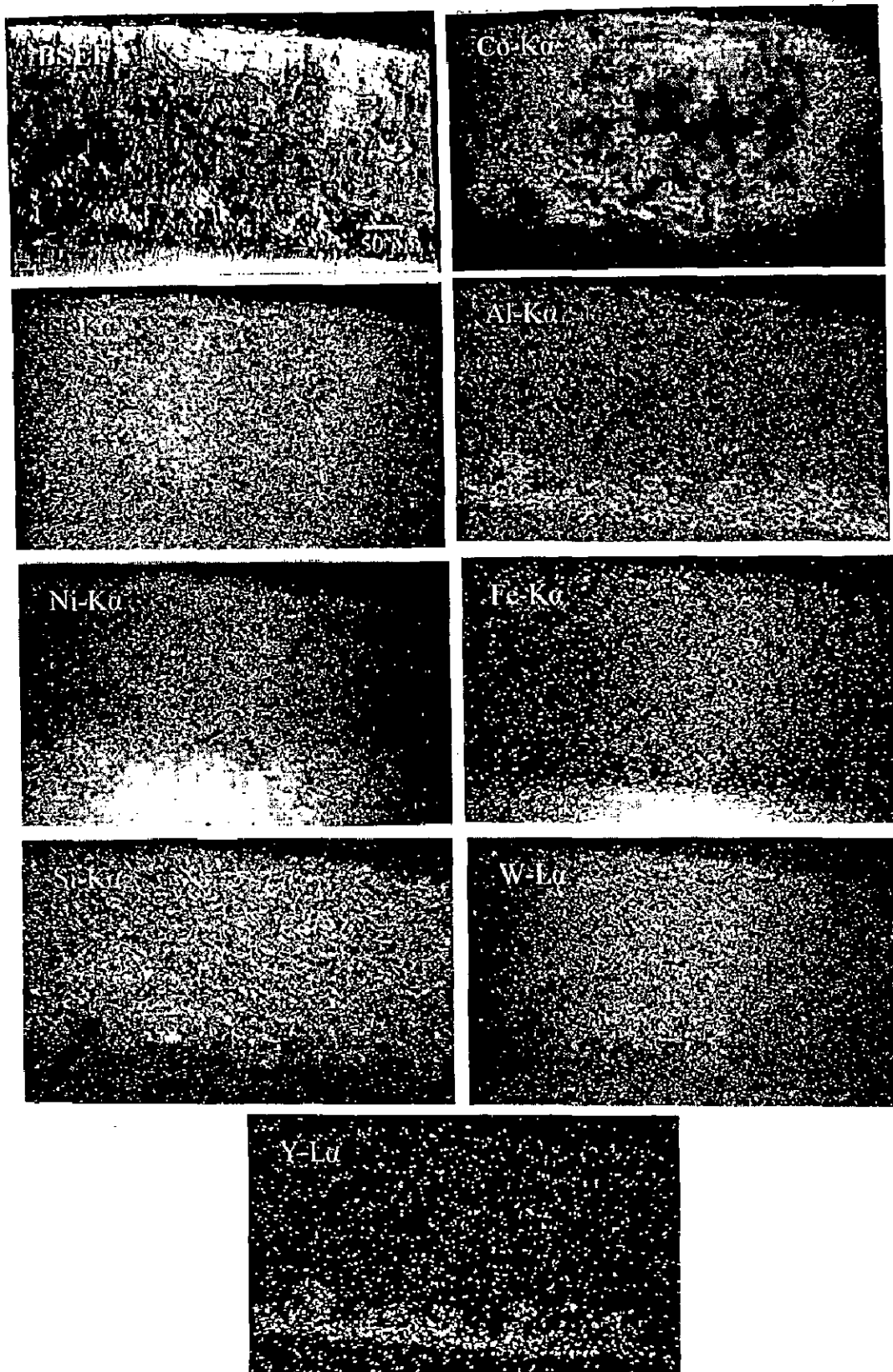


**Fig. 6.71** BSEI and X-ray mappings of the cross-section of Stellite-6 coated superalloy Superni 718 subjected to cyclic oxidation in  $\text{Na}_2\text{SO}_4$ -60% $\text{V}_2\text{O}_5$  at 900°C after 50 cycles.

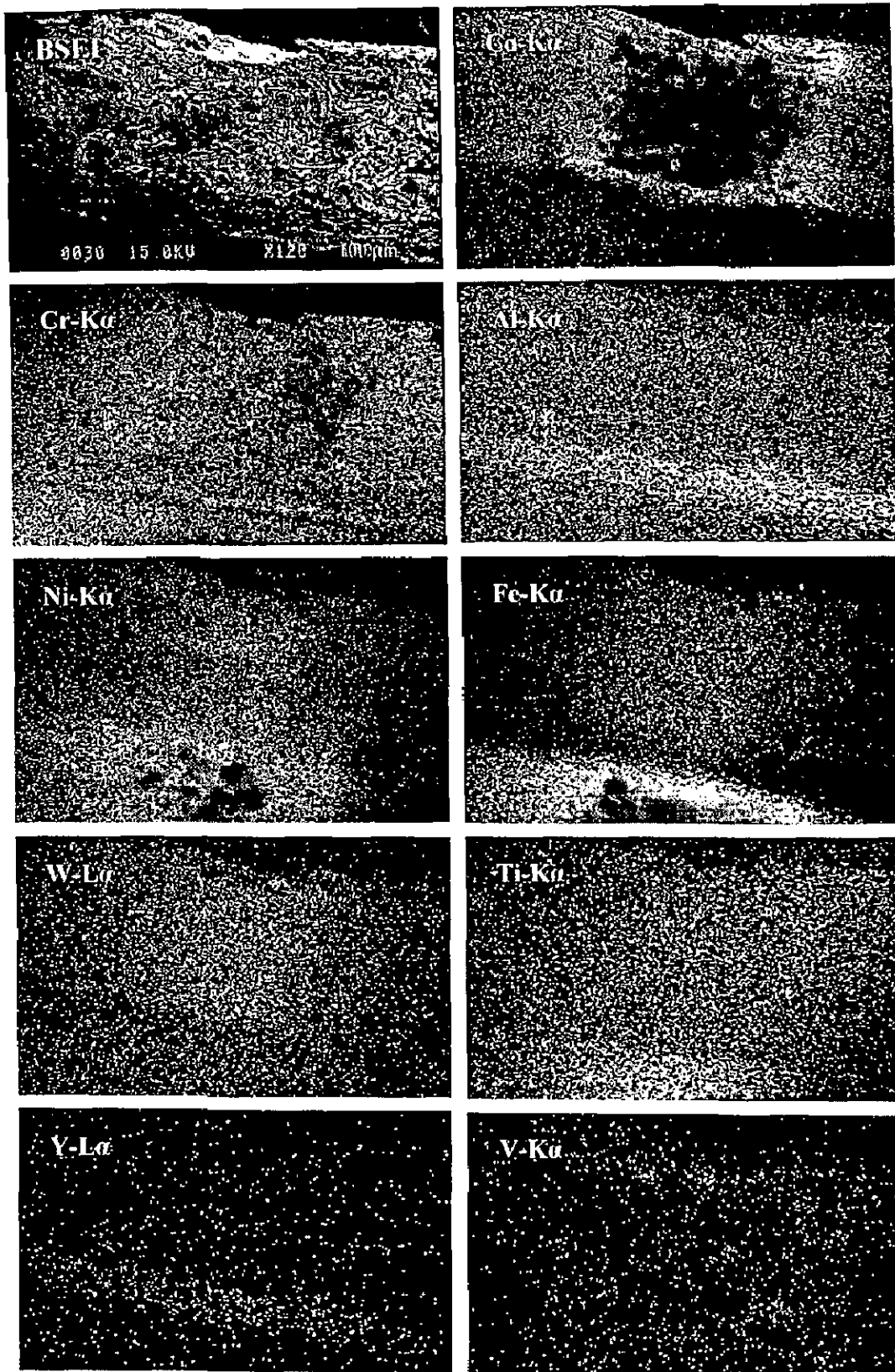


Fig. 6.72 BSEI and X-ray mappings of the cross-section of Stellite-6 coated superalloy Superfer 800H subjected to cyclic oxidation in  $\text{Na}_2\text{SO}_4$ -60% $\text{V}_2\text{O}_5$  at 900°C after 50 cycles.

## 6.2 SUMMARY OF RESULTS

Results as obtained after hot corrosion of coated and uncoated superalloys in molten salt environment are summarised in Table 6.1. These tabulated results are ready reference to compare the hot corrosion behaviour of coated and uncoated superalloys.

**Table 6.1** Summary of the results for coated and uncoated superalloys oxidised in molten salt ( $\text{Na}_2\text{SO}_4\text{-60\%V}_2\text{O}_5$ ) at  $900^\circ\text{C}$  for 50 cycles.

Base super-alloy	Coating	Weight gain $\text{mg/cm}^2$	Scale thickness $\mu\text{m}$	$K_p \times 10^{-10}$ $\text{g}^2\text{cm}^{-4}\text{s}^{-1}$	Main XRD phases	Remarks
Superni 75	Uncoated	6.82	53	2.65	NiO, $\text{Fe}_2\text{O}_3$ , $\text{NiCr}_2\text{O}_4$ , $\text{Ni}(\text{VO}_3)_2$ and $\text{Cr}_2\text{O}_3$	Fragile dark grey scale, blistering from 4 <sup>th</sup> cycle and spallation from 13 <sup>th</sup> cycle upto the end of study with reducing magnitude
	NiCrAlY	5.87	139	1.48	NiO, $\text{Al}_2\text{O}_3$ , $\text{NiCr}_2\text{O}_4$ and $\text{Cr}_2\text{O}_3$	Intact greenish scale, indicated minor spalling towards end, integrity between coating and base alloy preserved after corrosion run
	Ni-20Cr	13.98	199	22.95 (upto 16 <sup>th</sup> cycle), 9.36 (upto 38 <sup>th</sup> cycle) and 4.49	NiO, $\text{Cr}_2\text{O}_3$ and $\text{NiCr}_2\text{O}_4$	Smooth and intact greenish scale without spalling, sound contact between coating and base alloy maintained after exposure
	$\text{Ni}_3\text{Al}$	12.15	285	10.15 (upto 42 cycles)	NiO, $\text{Al}_2\text{O}_3$ and $\text{NiAl}_2\text{O}_4$	Green scale with minor spallation in a powder form, the coating found integral with base alloy after exposure over most of the surface area
	Stellite-6	23.64	435	26.92	$\text{CoO}$ , $\text{CoCr}_2\text{O}_4$ and $\text{Cr}_2\text{O}_3$	Dark grey scale with indications of slight spallation from 27 <sup>th</sup> cycle in the form of fine black powder, contact between coating/base alloy was found to be excellent during and after cyclic oxidation, even minor spalling of the coating along the edges was not seen

Superni 600	Uncoated	14.34	147	12.54	NiO, Fe <sub>2</sub> O <sub>3</sub> , NiCr <sub>2</sub> O <sub>4</sub> , Ni(VO <sub>3</sub> ) <sub>2</sub> and Cr <sub>2</sub> O <sub>3</sub>	Fragile dark grey scale, cracks started from 17 <sup>th</sup> cycle and spallation from 22 <sup>nd</sup> cycle upto the end of study with reducing magnitude
	NiCrAlY	5.87	144	1.71	NiO, Al <sub>2</sub> O <sub>3</sub> , NiCr <sub>2</sub> O <sub>4</sub> and Cr <sub>2</sub> O <sub>3</sub>	Intact greenish scale, indicated minor spalling towards end, integrity between coating and base alloy preserved after corrosion run
	Ni-20Cr	11.42	269	5.05	NiO, Cr <sub>2</sub> O <sub>3</sub> and NiCr <sub>2</sub> O <sub>4</sub>	Smooth and intact greenish scale without spalling, sound contact between coating and base alloy maintained after exposure
	Ni <sub>3</sub> Al	18.90	287	25.00 (upto 36 <sup>th</sup> cycle); then 7.74	NiO, Al <sub>2</sub> O <sub>3</sub> and NiAl <sub>2</sub> O <sub>4</sub>	Green scale with minor spallation in a powder form, the coating found integral with base alloy after exposure over most of the surface area
	Stellite-6	28.08	603	43.26	CoO, CoCr <sub>2</sub> O <sub>4</sub> and Cr <sub>2</sub> O <sub>3</sub>	Dark grey scale with indications of slight spallation from 11 <sup>th</sup> cycle in the form of fine black powder, contact between coating/base alloy was found to be very good during and after cyclic corrosion
Superni 601	Uncoated	24.91	38	28.08	NiO, Fe <sub>2</sub> O <sub>3</sub> , NiCr <sub>2</sub> O <sub>4</sub> , FeV <sub>2</sub> O <sub>4</sub> and Cr <sub>2</sub> O <sub>3</sub>	Fragile and uneven dark grey scale, cracks started from 1 <sup>st</sup> cycle at the edges accompanied by intensive spalling upto 14 <sup>th</sup> cycle, which continued upto the end of study with reducing magnitude
	NiCrAlY	8.56	165	2.82	NiO, Al <sub>2</sub> O <sub>3</sub> , NiCr <sub>2</sub> O <sub>4</sub> and Cr <sub>2</sub> O <sub>3</sub>	Intact greenish scale, indicated minor spalling from 24 <sup>th</sup> cycle in powder form, integrity between coating and base alloy preserved after corrosion run

	Ni-20Cr	10.79	188	4.72	NiO, Cr <sub>2</sub> O <sub>3</sub> and NiCr <sub>2</sub> O <sub>4</sub>	Smooth and intact greenish scale without spalling, sound contact between coating and base alloy maintained after exposure
	Ni <sub>3</sub> Al	17.15	240	12.63	NiO, Al <sub>2</sub> O <sub>3</sub> and NiAl <sub>2</sub> O <sub>4</sub>	Green scale with minor spallation in a powder form, the coating found integral with base alloy after exposure over most of the surface area
	Stellite-6	28.02	591	42.36	CoO, CoCr <sub>2</sub> O <sub>4</sub> and Cr <sub>2</sub> O <sub>3</sub>	Dark grey scale with indications of slight spallation from 36 <sup>th</sup> cycle in the form of fine black powder, contact between coating/base alloy was found to be excellent during and after cyclic corrosion, even minor spalling of the coating along the edges was not seen
Superni 718	Uncoated	11.51 (upto 20 cycles only)	48	19.85 (upto 20 cycles only)	NiO, Fe <sub>2</sub> O <sub>3</sub> , NiCr <sub>2</sub> O <sub>4</sub> , FeV <sub>2</sub> O <sub>4</sub> and Cr <sub>2</sub> O <sub>3</sub>	Fragile and uneven scale with intensive spalling and sputtering from 12 <sup>th</sup> cycle, which further intensified from 20 <sup>th</sup> cycle onwards, subsequently slowed down after 42 <sup>nd</sup> cycle
	NiCrAlY	8.86	179	4.88	NiO, Al <sub>2</sub> O <sub>3</sub> , NiCr <sub>2</sub> O <sub>4</sub> and Cr <sub>2</sub> O <sub>3</sub>	Intact greenish scale, indicated minor spalling towards end, integrity between coating and base alloy preserved after corrosion run
	Ni-20Cr	14.03	196	8.32	NiO, Cr <sub>2</sub> O <sub>3</sub> and NiCr <sub>2</sub> O <sub>4</sub>	Smooth and intact greenish scale without spalling, sound contact between coating and base alloy maintained after exposure
	Ni <sub>3</sub> Al	19.73	151	18.50	NiO, Al <sub>2</sub> O <sub>3</sub> and NiAl <sub>2</sub> O <sub>4</sub>	Green scale with minor spallation in a powder form from 48 <sup>th</sup> cycle, the coating found integral with base alloy after exposure over most of the surface area



	Stellite-6	22.96	496	30.38	CoO, CoCr <sub>2</sub> O <sub>4</sub> and Cr <sub>2</sub> O <sub>3</sub>	Dark grey scale with indications of slight spallation from 24 <sup>th</sup> cycle in the form of fine black powder, contact between coating/base alloy was found to be very good during and after cyclic corrosion
Superfer 800H	Uncoated	52.10	73	130.00	NiO, Fe <sub>2</sub> O <sub>3</sub> , NiFe <sub>2</sub> O <sub>4</sub> , FeV <sub>2</sub> O <sub>4</sub> and Cr <sub>2</sub> O <sub>3</sub>	Uneven scale, spalling from 2 <sup>nd</sup> cycle alongwith some sputtering tendency from 7 <sup>th</sup> cycle, continued till the end of study
	NiCrAlY	5.71	253	1.38	NiO, Al <sub>2</sub> O <sub>3</sub> , NiCr <sub>2</sub> O <sub>4</sub> and Cr <sub>2</sub> O <sub>3</sub>	Intact greenish scale, indicated minor spalling from 45 <sup>th</sup> cycle in powder form, integrity between coating and base alloy preserved after corrosion run
	Ni-20Cr	10.63	158	5.04	NiO, Cr <sub>2</sub> O <sub>3</sub> and NiCr <sub>2</sub> O <sub>4</sub>	Smooth and intact greenish scale without spalling, sound contact between coating and base alloy maintained after exposure
	Ni <sub>3</sub> Al	15.50	178	9.06	NiO, Al <sub>2</sub> O <sub>3</sub> and NiAl <sub>2</sub> O <sub>4</sub>	Green scale with minor spallation in a powder form from 26 <sup>th</sup> cycle onwards, the coating found integral with base alloy after exposure over most of the surface area
	Stellite-6	31.44	549	50.00	CoO, CoCr <sub>2</sub> O <sub>4</sub> and Cr <sub>2</sub> O <sub>3</sub>	Dark grey scale with indications of slight spallation from 7 <sup>th</sup> cycle in the form of fine black powder, contact between coating/base alloy was found to be very good during and after cyclic corrosion over the most of the surface area

## 6.3 DISCUSSION

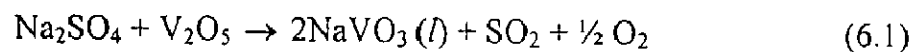
### 6.3.1 Uncoated Superalloys

In general the uncoated superalloys have indicated accelerated oxidation in  $\text{Na}_2\text{SO}_4$ -60% $\text{V}_2\text{O}_5$  environment at  $900^\circ\text{C}$  in comparison to that in air. The Fe-base superalloy Superfer 800H has shown least resistance to the hot corrosion amongst the Superalloys Superni 75, 600, 601 and Superfer 800H. The weight gain values for the fifth superalloy Superni 718 could not be compared with the rest of cases, as data is available for 20 cycles only for this superalloy. On the basis of cumulative weight gain data for 50 cycles, corrosion rate of the superalloys under study can be arranged in the following order:

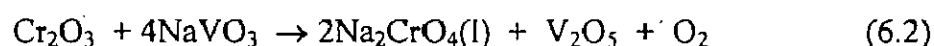
$$\text{Superfer 800H} > \text{Superni 601} > \text{Superni 600} > \text{Superni 75}$$

The superior corrosion resistance shown by Ni-base superalloys, Superni 75 and 600 might be ascribed to the formation of  $\text{Cr}_2\text{O}_3$  and nickel vanadate (Kerby and Wilson, 1973 and Gitanjaly, 2003).  $\text{Ni}(\text{VO}_3)_2$  acts as a diffusion barrier for the oxidizing species as has been reported by Seierstein and Kofstad (1987). Gitanjaly (2003) has also reported similar sequence for the corrosion rates of Superfer 800H, Superni 601 and Superni 75 based on the weight change data for 30 cycles. Further, it has been observed that all the superalloys under study, in general have obeyed parabolic rate law of oxidation upto 50 cycles, except Superni 718. In the latter case intensive spalling and sputtering made it difficult to evaluate overall weight gain upto 50 cycles. However the superalloy has followed a parabolic rate law upto 20 cycles.

It has been observed that the rate of weight gain was relatively high in all the cases during the initial period of exposure, which may partially be attributed to the formation of  $\text{NaVO}_3$  (m. p.  $\approx 610^\circ\text{C}$ ) as a result of following reaction at  $900^\circ\text{C}$  (Kolta et al, 1972):



This  $\text{NaVO}_3$  acts as a catalyst and also serves as oxygen carrier to the base alloy, therefore will lead to rapid oxidation of the basic elements of the superalloys to form protective oxide scales. Simultaneously, the protective scale is destroyed or eliminated by molten salts and consequently the metal surface is exposed to direct action of aggressive environment as has been indicated in the current investigation also. Seiersten and Kofstad (1987) as well as Swaminathan et al (1993) have suggested simultaneous growth of oxides and their dissolution in molten salt as per following reaction:



After a period of high corrosion rate it has been observed that the rate of corrosion tends to be almost uniform with the further progress of study. This can be ascribed to the slower growth rate of chromia scale. Furthermore, the formation of nickel vanadate or iron-vanadate in the scales with the progress of study might have also contributed to slower oxidation rate as these vanadates are capable of decreasing the short circuit diffusion of ions as has been suggested by Swaminathan et al (1993) and Tiwari and Prakash (1997).

Whereas superalloy of grade Superni 718 underwent extensive spalling and sputtering of its scales. In addition to the above mentioned mechanism, the accelerated hot corrosion of this superalloy might have also been occurred due to the presence of higher amount of molybdenum (3.05%) in it. The molybdenum might have resulted in the formation of  $MoO_3$ , which according to Peters et al (1976) may react with  $Na_2SO_4$  to form a low melting point phase  $Na_2MoO_4$  by the following reaction:



This might have caused alloy induced acidic fluxing, subsequently giving rise to accelerated spalling of the scale. Identical findings have also been reported by Bourhis and John (1975), Pettit and Meier (1985), Misra (1986), Shih et al (1989) and Singh (2003). Fig. 6.73 shows the plausible mechanism governing the corrosion process for superalloy Superni 718 in an environment of  $Na_2SO_4$ -60% $V_2O_5$ .

The surface XRD has indicated the formation of  $Fe_2O_3$  and NiO phase in all the cases alongwith some weak intensity peaks of  $Cr_2O_3$ . The presence of spinel  $NiCr_2O_4$  has also been confirmed in all the Ni-base superalloys, where in case of Fe-base superalloy,  $NiFe_2O_4$  spinel has been indicated by the analysis. Formation of nickel vanadate has been revealed in case of Superni 75 and 600, while that of iron-vanadate in case of superalloys Superni 601, 718 and Superfer 800H. These X-ray diffraction results are well supported by SEM/EDAX and EPMA results. The studies conducted by Iyer et al (1987), Swaminathan et al (1993), Tiwari (1997), Tiwari and Prakash (1996), Deb et al (1996), Tiwari and Prakash (1997) and Gitanjaly (2003) on similar superalloys also endorse formation of identical phases.

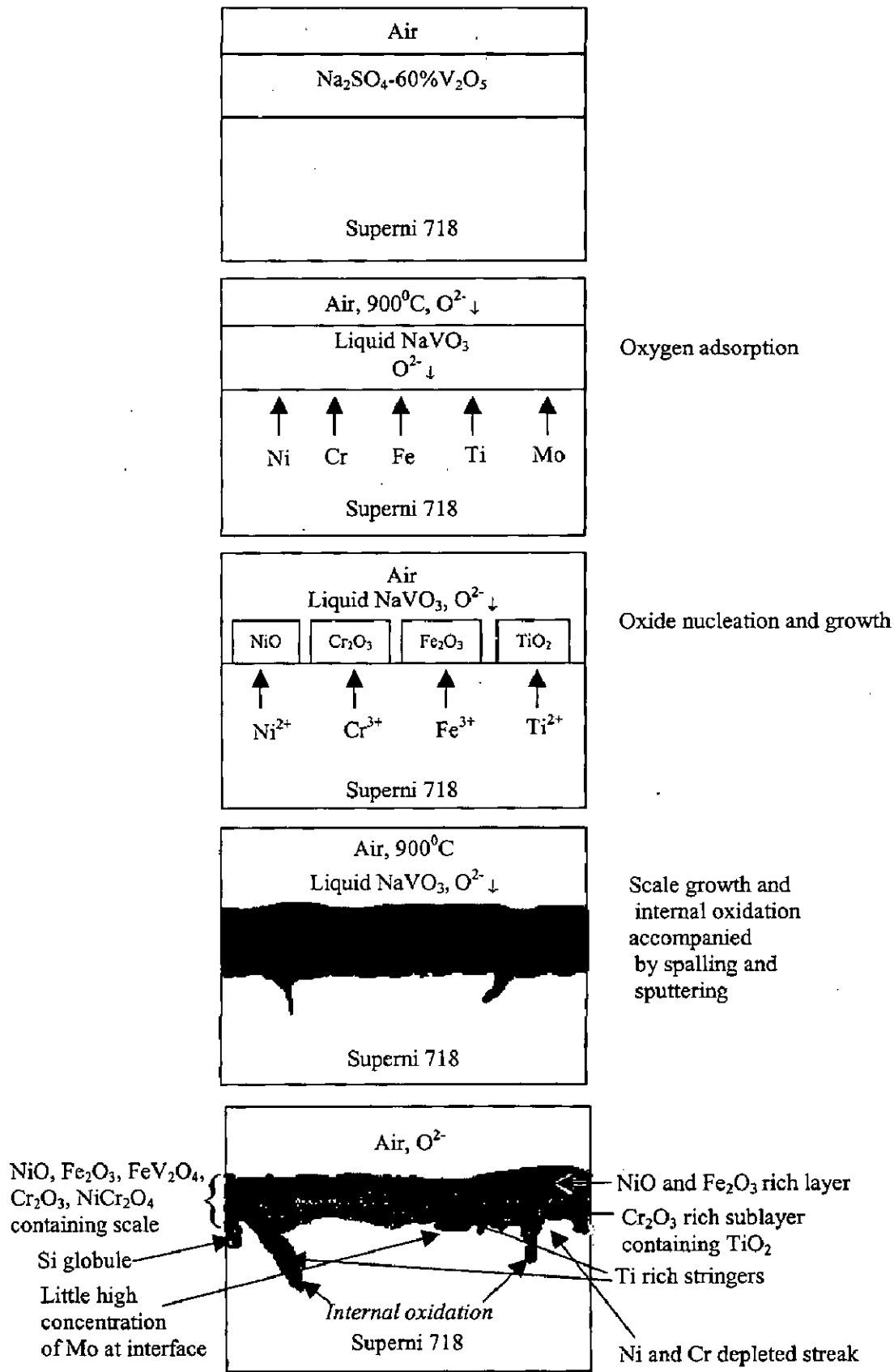


**Fig. 6.73** Schematic diagram showing probable hot corrosion mechanism for the uncoated superalloy Superni 718 exposed to  $\text{Na}_2\text{SO}_4\text{-60\%V}_2\text{O}_5$  at  $900^\circ\text{C}$  for 50 cycles.

### 6.3.2 NiCrAlY Coating

The greenish look of the surface scale of NiCrAlY, Ni-20Cr and Ni<sub>3</sub>Al coated superalloys exposed to cyclic oxidation in Na<sub>2</sub>SO<sub>4</sub>-60%V<sub>2</sub>O<sub>5</sub> environment might be attributed to the formation of NiO as has been proposed by Bornstein et al (1975). The weight gain data for the NiCrAlY coated superalloys shows that the coating has been successful in reducing the overall weight gain in general, Fig. 6.16 and therefore it can be inferred that the necessary protection has been provided by the NiCrAlY coating to the base superalloys. The relative corrosion rates of the NiCrAlY coated superalloys based on the thermogravimetric data, although not very significantly apart, can be arranged in the following order:

Superni 718 > Superni 601 > Superni 75 > Superni 600 > Superfer 800H

The protection from hot corrosion might partially be due to the oxides of aluminium, chromium and nickel, and spinel of Ni and Cr present in the top scales as revealed by the surface XRD analysis. The presence of these phases is further supported by the surface and cross-sectional EDAX analysis and by EPMA. The formation of identical phases for MCrAlY coating has also been reported by Wu, Y. N. et al (2001) and Wu, X. et al (2001), Singh (2003) and the author (Singh et al, 2005B and 2005C). Longa & Takemoto (1992) have also identified NiO and NiCr<sub>2</sub>O<sub>4</sub> alongwith relatively small quantities of Cr<sub>2</sub>O<sub>3</sub> phase for NiCrAl flame sprayed coatings on steel substrates when oxidised in an environment of Na<sub>2</sub>SO<sub>4</sub>-85%V<sub>2</sub>O<sub>5</sub> at 900°C. They suggested that preferential NiO and spinel formation prevent the exclusive development of chromia layer that is why continuous Cr<sub>2</sub>O<sub>3</sub> was not present in the surface layer, which seems to be true for the current investigation also, refer respective Cr-maps. The formation of NiO layers in the scale has also been reported by Seiersten and Kofstad (1987) for APS NiCrAlY coating on a Ni-base superalloy Inconel 600 when exposed to 800°C in molten salt environment. Further, it is obvious from the oxygen maps in case of Superni 75, 600 and Superfer 800H as depicted in Fig. 6.24, Fig. 6.25 and Fig. 6.28 respectively that the base superalloys have not undergone internal oxidation.

Only slight spalling of the scales was observed in the form of green powder in case NiCrAlY and Ni<sub>3</sub>Al coated cases, while in case of Stellite-6 coated specimens, this micro-spalling was in the form of blackish powder. However the scales in general showed no tendency towards cracking and were found intact. Similar minor spalling of the scale was observed by Chan et al (2000) for oxidised APS NiCrAlY coating. These spallation zones were invariably observed in areas of local convex curvature. This accords well with the earlier work of Strawbridge et al (1997), where spallation was

associated with the development of out-of-plane tensile stresses in the region of convex curvature during cooling.

All the coatings under study viz. NiCrAlY, Ni-20Cr, Ni<sub>3</sub>Al and Stellite-6 were successful in maintaining their continuous surface contact with base superalloys, when subjected to molten salt induced corrosion. As explained in the Section 6.1.2.1, only some of the edges of the specimens were affected and few superficial cracks were developed along/near them. This resulted in minor spalling of the coating from/near the edges, the extent of which insignificant in context of the overall surface area of the specimens. This phenomenon was observed almost in all the coated cases. This tendency may be attributed to the different values of thermal expansion coefficients of the oxide scale, coatings, and the base superalloys (Table A.2) (Rapp et al, 1981 and Liu et al, 2001), and the sharp edges of the coated specimens, which has already been discussed in the Chapter 5.

Oxidation of the coatings under study in the given molten salt environment might partly be attributed to the porosity and splat structure of plasma spray coatings as has already been discussed in Chapter 5. However, as the environment of study in this case contains molten salt, therefore the elements such as V, S and oxygen may diffuse along these splats or pores, instead of only air as was observed during air oxidation. Such a tendency has been observed for almost all types of the coatings under study, which can be perceived from V and S maps in the respective cases.

EPMA analysis for the NiCrAlY coated Superni 600 and Superfer 800H, Fig. 6.25 and 6.28 respectively indicates that sulphur has penetrated into the substrate alloys and there it is co-existing with Cr and might form CrS. The oxidation of this CrS might yield a protective scale of Cr<sub>2</sub>O<sub>3</sub> as per the views of Khanna and Jha (1998). Whereas diffusion of vanadium has been restricted to the scales and it is concentrated mainly in the top scales. However, once the splat boundaries and pores present in the coating are blocked due to formation of oxides, they will no more provide path to transportation of reacting species towards the base alloy. The presence of Fe in the scales as has been revealed by EPMA analysis for the coated cases might be attributed to the diffusion of iron from the substrate across the scale. The extent of this diffusion seems to be increasing with increase in iron content in the base superalloys. Fig. 6.74 shows the schematically representation of the probable hot corrosion mode for the NiCrAlY coated Superni 75.

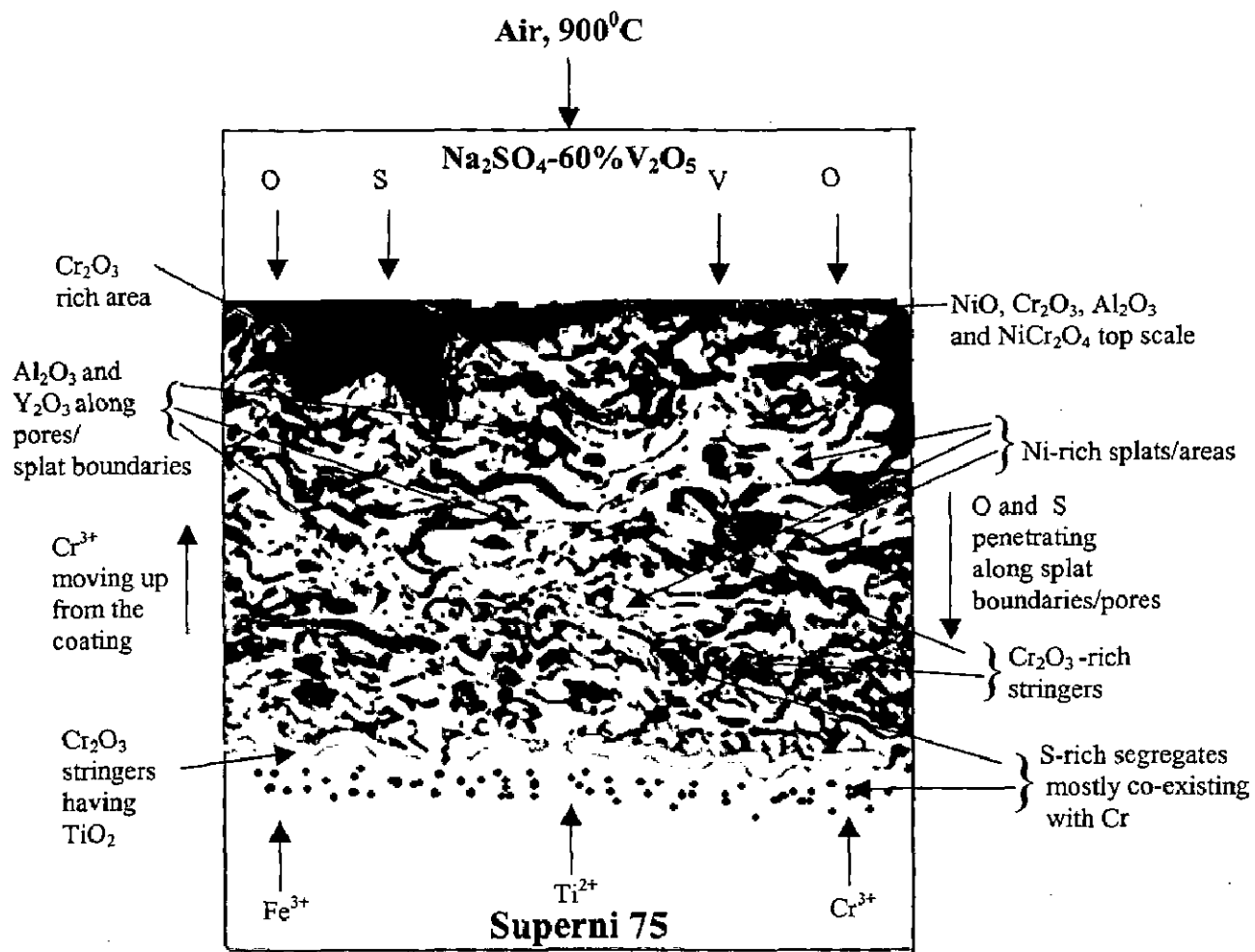


**Fig. 6.74** Schematic diagram showing probable hot corrosion mode for the NiCrAlY coated Superni 75 exposed to Na<sub>2</sub>SO<sub>4</sub>-60%V<sub>2</sub>O<sub>5</sub> at 900°C for 50 cycles.

### 6.3.3 Ni-20Cr Coating

The Ni-20Cr coating has been found to be successful in reducing the weight gain in case of superalloys Superni 600, 601 and Superfer 800H, therefore it can be inferred that these coated superalloys have indicated better corrosion resistance than their respective uncoated superalloys. So far as the reduction in weight gain after application of this coating is concerned, one can observe that the coating has performed best in case of Superfer 800H substrate, where it has decreased the overall weight gain by 80% approximately. Whereas in case of Superni 718, the weight gain value for 20 cycles for the uncoated case ( $11.51 \text{ mg/cm}^2$ ) is close to the corresponding value for 50 cycles for the coated case ( $14.03 \text{ mg/cm}^2$ ). From this comparison the effectiveness of the coating to reduce the weight gain in this case can be inferred. The overall weight gain in case of coated Superni 75 alloy is twice that of uncoated alloy, but it is still less than that for the coated Superni 718. However, the kinetics of oxidation after the 38<sup>th</sup> cycle indicates a comparable value of  $K_p$  with those of other coated superalloys 600, 601 and Superfer 800H, which foretells that the oxidation rate in the Superni 75 case might have reached nearly to those of the latter cases by the end of exposure. Moreover, the coatings have shown tendency to act like diffusion barriers to the corroding species as the parabolic rate law has been followed in all the cases. In the order of overall weight gain after 50 cycles, the Ni-20Cr coated specimens can be arranged in the following order:

Superni 718 > Superni 75 > Superni 600 > Superni 601 > Superfer 800H

Therefore it can be inferred that the coated Fe-based superalloy has shown best corrosion resistance to the given environment. This might also be attributed to the presence of a nearly continuous chromia layer present in the top scale along with layers of oxides Ni and Al, Fig. 6.43. While the relatively low corrosion resistance of the coated Superni 718 and 75 could also be anticipated from the comparatively discontinuous distribution of Cr, Ni and Al in the scale, Fig. 6.42 and 6.38 respectively. The titanium has shown considerable diffusion into the coatings and formed nearly continuous band at the interface between the bond coat and the substrate superalloys, which might also be detrimental to the corrosion resistance in these cases (Li and Gleeson, 2004). Further, the scales appear to be in good contact with the substrate superalloys for all the cases as can be perceived from respective BSEI micrographs depicted in Fig. 6.35 to Fig. 6.37.

The XRD analysis for the hot corroded Ni-20Cr coated superalloys have shown the formation of protective phases like NiO,  $\text{Cr}_2\text{O}_3$  and  $\text{NiCr}_2\text{O}_4$  in the oxide scales, which are further endorsed by EPMA and EDAX analysis. These results are in good agreement with the findings of Longa-Nava et al (1996), Li et al (2000), Nickel et al (2002) and Singh (2003). The diffusion of aluminium from the bond coat into the top



scale as indicated by X-ray mappings as well as cross-sectional EDAX in all the cases was also noticed by Singh (2003). Longa-Nava et al (1996) have concluded from the studies on low pressure plasma sprayed Ni-20Cr coatings that the formation of chromate solute anions can prevent sulphidation of the alloy. Longa & Takemoto (1992) have also identified phases like  $\text{Cr}_2\text{O}_3$ , NiO and  $\text{NiCr}_2\text{O}_4$  for NiCr flame sprayed coatings on steel substrates when oxidised in an environment of  $\text{Na}_2\text{SO}_4$ -85% $\text{V}_2\text{O}_5$  at 900°C. Further they attributed the better adhesion of the coating to the diffusion of Fe, which has also been observed in the current study.

It has been observed from the EPMA analysis, Fig. 6.43 for the Ni-20Cr coated Superfer 800H that sulphur has reached mainly below the interface between the bond coat and the base alloy, and it co-exists with Cr, similar to NiCrAlY coating. Whereas V has mainly restricted to the coating. Longa & Takemoto (1992) and Singh (2003) have also reported the diffusion of molten salt into the coating. Based upon the above discussion, plausible hot corrosion mode for the Ni-20Cr coated Superni 600 has been proposed as shown in Fig. 6.75.

#### 6.3.4 $\text{Ni}_3\text{Al}$ Coating

All the  $\text{Ni}_3\text{Al}$  coated superalloys have shown conformance to parabolic law of oxidation upto 50 cycles with an exception of Superni 75, which has shown comparatively higher deviations after 42 cycles. This is in good agreement with the observations of Lu et al (2004), who have also reported parabolic oxidation behaviour for a directionally solidified  $\text{Ni}_3\text{Al}$  base alloy named IC-6 in a gas environment containing 1%  $\text{H}_2\text{S}$ , 0.1%  $\text{H}_2$  plus 5 ppm  $\text{O}_2$  balanced by argon at 700°C.

Sequence of corrosion resistance based upon overall weight gain for the coated superalloys was as follows:

Superni 75 > Superfer 800H > Superni 601 > Superni 600 > Superni 718

The plausible reason behind the lower oxidation resistance as shown by coated Superni 718 might be due to the presence of Mo and slightly high concentration of Ti in the substrate superalloy. It is obvious from the X-ray map for Mo in Fig. 6.56 that Mo has diffused to the top of the scale. McCarron et al (1976) have concluded that Ti alloyed with  $\text{Ni}_3\text{Al}$  definitely reduces the hot corrosion resistance of  $\text{Ni}_3\text{Al}$ . The better corrosion resistance of the coated Superni 75 might partially be attributed to the fact that oxygen could not penetrate the whole thickness of the coating as shown in Fig.6.51 (a), refer points 1, 2 and 3, thereby contributing to low weight gain in this case.



The XRD analysis of the hot corroded samples has revealed the presence of NiO as the main phase alongwith protective phases like  $\text{Al}_2\text{O}_3$  and  $\text{NiAl}_2\text{O}_4$  in the oxide scales. EDAX and EPMA analysis have further supported the formation of these phases. McCarron et al (1976) have also reported  $\text{Ni}_3\text{Al}$  to be NiO former. According to Natesan (1988) the corrosion of  $\text{Ni}_3\text{Al}$  at  $900^\circ\text{C}$  and above produces scales containing an outer layer of NiO, an inner layer of  $\text{Al}_2\text{O}_3$  and an intermediate layer of the Ni-Al spinel  $\text{NiAl}_2\text{O}_4$ . This might be the reason behind indication of weak peaks of  $\text{Al}_2\text{O}_3$  and  $\text{NiAl}_2\text{O}_4$  in the XRD diffraction. Moreover, Malik et al (1992) and Sidhu & Prakash (2003) also reported NiO and  $\text{Al}_2\text{O}_3$  phases in their studies on  $\text{Ni}_3\text{Al}$  coatings on boiler steels, whereas Liu and Gao (2001) during investigation on oxidation of  $\text{Ni}_3\text{Al}$  alloy at  $900^\circ\text{C}$ . The presence of  $\text{NiAl}_2\text{O}_4$  and NiO was also noticed by Lee & Lin (2002) during their hot corrosion studies on  $\text{Ni}_3\text{Al}$  intermetallic compound at 800 and  $1000^\circ\text{C}$  and by Singh et al (2005B and 2005C). Moreover, Lee and Lin (2002) inferred that the  $\text{NiAl}_2\text{O}_4$  might provide better hot corrosion resistance than NiO since the solubility of  $\text{NiAl}_2\text{O}_4$  spinel is thermodynamically lesser than that of NiO in the molten salt. Further the respective EPMA, Fig. 6.53 to Fig. 6.57 indicates the formation of NiO at the top of the scales with dispersed  $\text{Al}_2\text{O}_3$ , which was also observed by Elrefaie et al (1985).

The penetration of vanadium into the scale as has been revealed invariably in all the cases is in good agreement with the observations of Niu et al (1994), where they observed that  $\text{Ni}_3\text{Al}$  alloy suffered accelerated hot corrosion due to penetration of molten salt through the scale. Further, it is obvious from the EPMA analysis, Fig. 6.54, 6.56 and 6.57 for the coated Superni 600, 718 and Superfer 800H respectively that sulphur has reached even below the interface between the bond coat and the base alloy. The diffusion of nickel downwards into the substrate from coating has been indicated in case of Superfer 800H, Fig.6.57 similar to the findings of Singh (2003). Schematic diagram, Fig. 6.76 shows the probable oxidation mode for the  $\text{Ni}_3\text{Al}$  coated Superni 600 subjected to molten salt environment for 50 cycles at  $900^\circ\text{C}$ .

### 6.3.5 Stellite-6 Coating

The overall weight gain values in the case of Stellite-6 coated superalloys have shown the following trend:

Superfer 800H > Superni 600  $\approx$  Superni 601 > Superni 75 > Superni 718

This coating was found to be successful in reducing the overall weight gain in case of Superfer 800H superalloy and hence was successful in reducing the corrosion rate for this Fe-based superalloy. Whereas nothing could be concluded in case of Superni 718 on the basis of thermogravimetric data. In all the other cases, the coated superalloys have conceived more overall weight gains as compared to their uncoated counterparts. Further similar to all the other coated cases, the major portion of the overall weight gain has been conceived in the early cycles of study and the weight have become nearly steady as the exposure time is increased. This indicates that the corrosion behaviour is governed by parabolic rate law. The possible reasons for this initial high weight gains have been already discussed, in general, in Chapter 5. However, in this case, as is obvious from Cr-maps in Fig. 6.69, the splat boundaries seem to be blocked by chromium oxide in the upper coat of Stellite-6, contrary to all other types of coating, where aluminium oxide is present instead of chromium oxide. Whereas in the bond coat regions, the oxide along the splat boundaries/pores appears to be that of mainly aluminium. The blockage of these boundaries and pores might improve the oxidation resistance of the coating. Also this coating was found successful in maintaining its integrity with its respective superalloy substrates in general as can be visualized from the back-scattered images reported in Fig. 6.64 to 6.66.

The XRD analysis revealed the oxides of mainly cobalt and chromium along with the spinel of cobalt-chromium, which are reported to protective in nature against corrosion. Formation of these phases has also been supported by the surface as well cross-sectional EDAX analysis, and EPMA. CoO, CoCr<sub>2</sub>O<sub>4</sub> and Cr<sub>2</sub>O<sub>3</sub> phases has also been reported by Santoro (1979), Luthra (1985) and Singh (2003). As proposed by Luthra (1985) formation of spinel CoCr<sub>2</sub>O<sub>4</sub> may block the diffusion activities through the cobalt oxide (CoO) thereby suppressing the further formation of this oxide. He further opined that increase in the growth of CoCr<sub>2</sub>O<sub>4</sub> and Cr<sub>2</sub>O<sub>3</sub> in competition with CoO and Co<sub>3</sub>O<sub>4</sub> formation increases the corrosion resistance of alloys.

The presence of vanadium as has been revealed by X-ray maps in case of Superni 75 and Superfer 800H might be due to penetration of molten salt along the splat boundaries and pores present in the coatings in the initial stage of hot corrosion, similar to the observations of Singh (2003). Fig. 6.77 shows probable mode of corrosion phenomena for the Stellite-6 coated Superni 600.

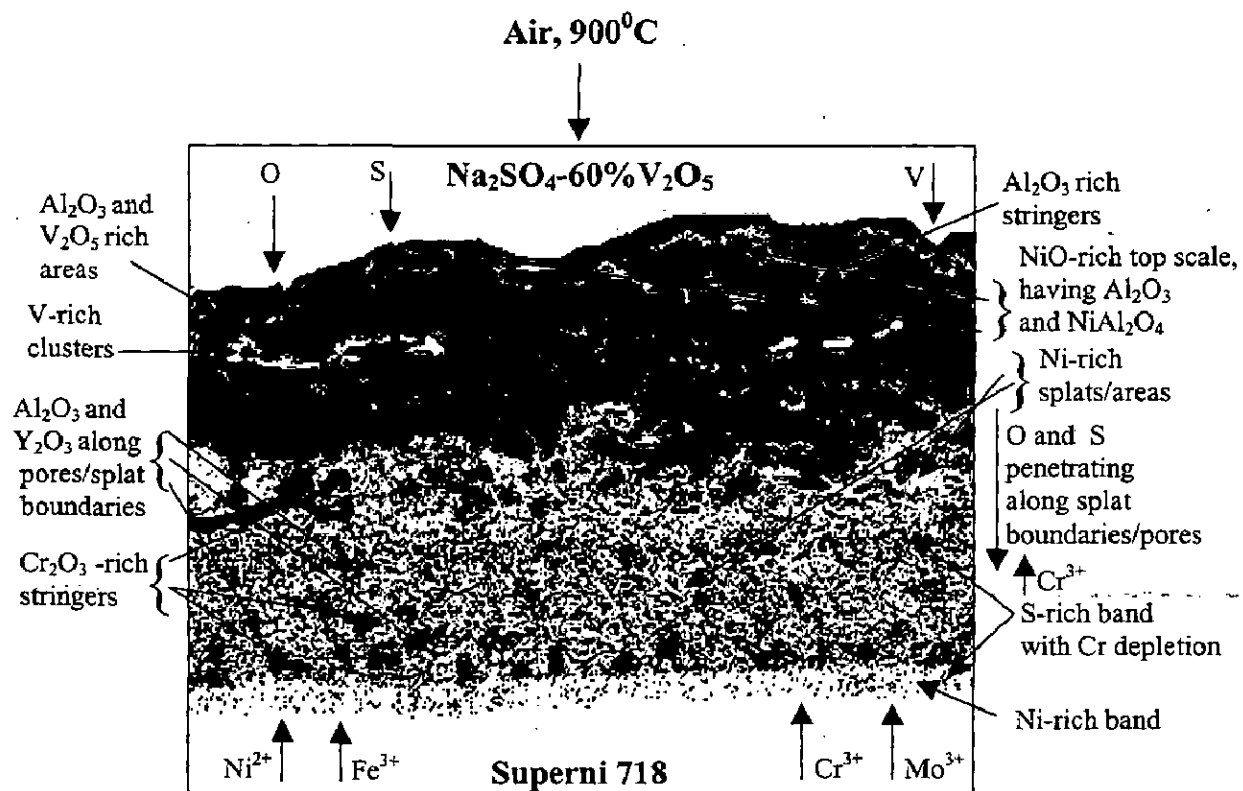


**Fig. 6.76** Schematic diagram showing probable hot corrosion mode for the Ni<sub>3</sub>Al coated Superni 718 exposed to Na<sub>2</sub>SO<sub>4</sub>-60%V<sub>2</sub>O<sub>5</sub> at 900°C for 50 cycles.

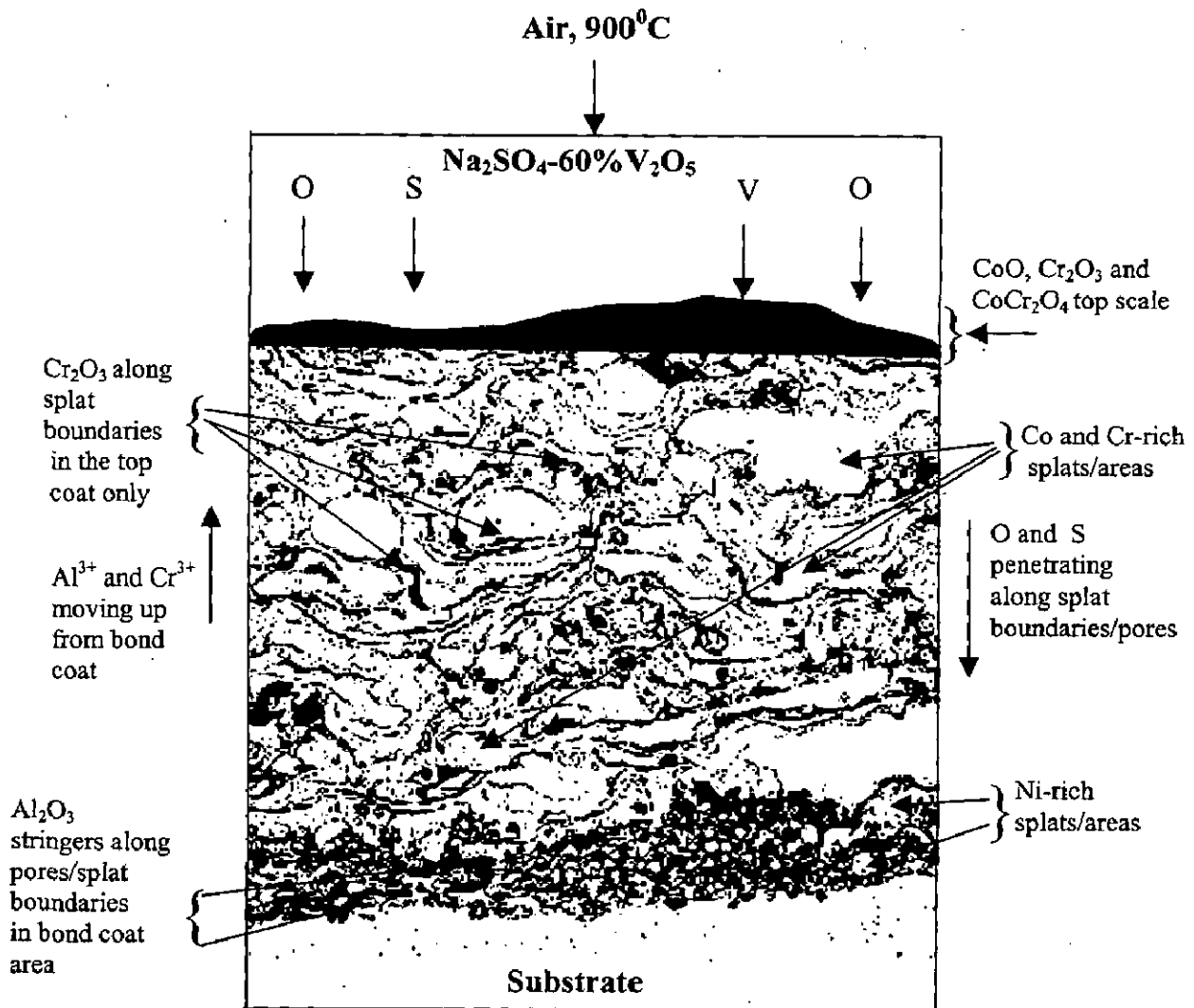


**Fig. 6.77** Schematic diagram showing probable hot corrosion mode for the Stellite-6 coated Superni 600 exposed to Na<sub>2</sub>SO<sub>4</sub>-60%V<sub>2</sub>O<sub>5</sub> at 900<sup>0</sup>C for 50 cycles.

# CHAPTER 7

## COMPARATIVE DISCUSSION

---

In this chapter, an attempt has been made to present the results of the current investigation giving comparative performance of the superalloys and superalloys coated with various coatings by the plasma spray process. The performance of these uncoated and coated superalloys in air and aggressive environment of  $\text{Na}_2\text{SO}_4$ -60% $\text{V}_2\text{O}_5$  under cyclic conditions at an elevated temperature of  $900^\circ\text{C}$  has been discussed.

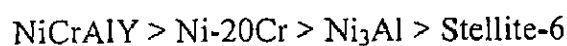
The bar charts showing the overall weight gains in air and molten salt environments after 50 cycles for the coated and uncoated superalloys are presented in Figs. 7.1 and 7.2 respectively. From the bar charts, it can be inferred that the superalloys under study have shown low oxidation resistance against the given molten salt environment as compared to that against the air under cyclic conditions. Superni 75 has indicated a minimum resistance to air oxidation amongst the superalloys under study (Fig. 7.1) on one hand, while on the other; it has shown highest oxidation resistance to molten salt attack (Fig. 7.2). Superni 600 has been found to be most resistant to the air oxidation among all the superalloys. Whereas, the Fe-based superalloy Superfer 800H showed minimum resistance to the molten salt corrosion in comparison to the superalloys Superni 75, 600 and 601 on the basis of weight gain data, while Superni 718 suffered accelerated hot corrosion in the form of intense spalling and sputtering of its scale to an extent that cumulative weight gain could be determined upto only 20 cycles of the study. The accelerated corrosion of the alloy Superni 718 might be attributed to presence of 3.05% molybdenum content in the basic composition of this alloy as has already been explained in Chapter 2 and 6.

From the bar charts, it can be inferred that NiCrAlY coating has provided maximum resistance to oxidation in air and molten salt environment. This coating in as-sprayed condition had a lamellar structure consisting of splats, which were rich in Ni, with splat boundaries containing mainly Al, Y with some Cr. During oxidation under cyclic conditions in air, oxygen penetrated along the interconnected splat boundaries and

pores and oxidised mainly Al and Y, alongwith Cr at some locations. This might be responsible for blocking/slowing down the transport of oxygen along the splat boundaries and pores, thereby making the oxidation rate to reach steady state in this case. Similarly in case of molten salt induced oxidation, although there is higher overall weight gain as compared to air oxidation, cross-sectional analysis of corroded scale again indicated the presence of as-coated structure in general. Oxygen, aluminium and yttrium (alongwith Cr at some places) were again found along the Ni-rich un-oxidised splats, although there is indication of sulphur reaching the substrate alloys, which might have moved along the splat boundaries/pores in the earlier stage of hot corrosion. The protection shown by this coating might also be contributed by the simultaneous formation of an additional protective oxide  $\alpha\text{-Al}_2\text{O}_3$  alongwith  $\text{Cr}_2\text{O}_3$  and  $\text{NiCr}_2\text{O}_4$ . According to Toma et al (1999),  $\alpha\text{-Al}_2\text{O}_3$  grows very slowly and is thermodynamically stable.

Moreover, the presence of yttrium in the NiCrAlY coating could have played its role in reducing the scale growth rate and hence the overall weight gain as per the views of Saxena (1987), Stott (1989A) and Tawancy et al (1994). Tawancy et al (1994) suggested that Y could be oxidised into Y-rich oxide “pegs” within the  $\alpha\text{-Al}_2\text{O}_3$  scale, improving its mechanical adherence to the coating. Secondly the presence of small concentrations of Y within the scale in solid solution could have reduced the scale growth rate. Thirdly, the segregation of yttrium to the grain boundaries of the  $\alpha\text{-Al}_2\text{O}_3$  scale could also reduce its growth rate (Stott, 1989A) as well as improve its elevated temperature mechanical strength. While according to Nicholls and Hancock (1989), Y could segregate to fill voids or pores along the grain boundaries of the scale, improving its cohesion. Moreover, among all the NiCrAlY coated superalloys under study, the NiCrAlY coated Superfer 800H alloy have shown a maximum oxidation resistance both to air as well as molten salt environments.

The sequence for the overall protective behaviour of coatings in molten salt environment has been observed as given below:





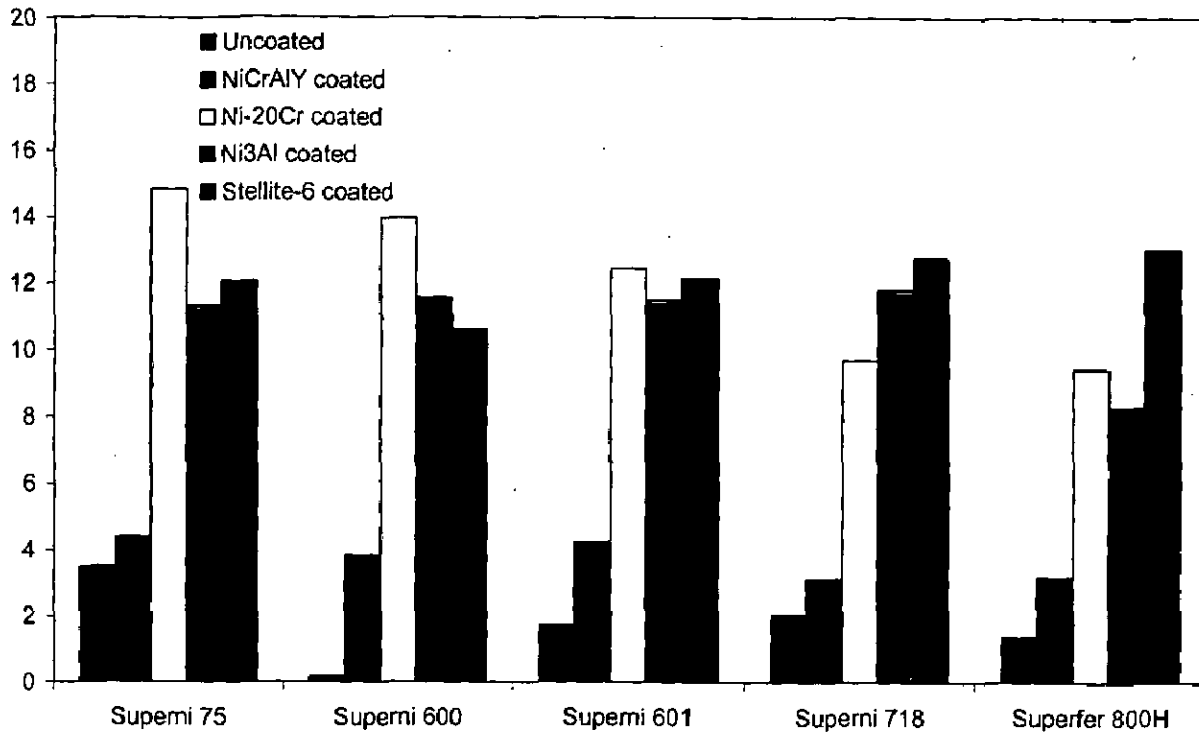
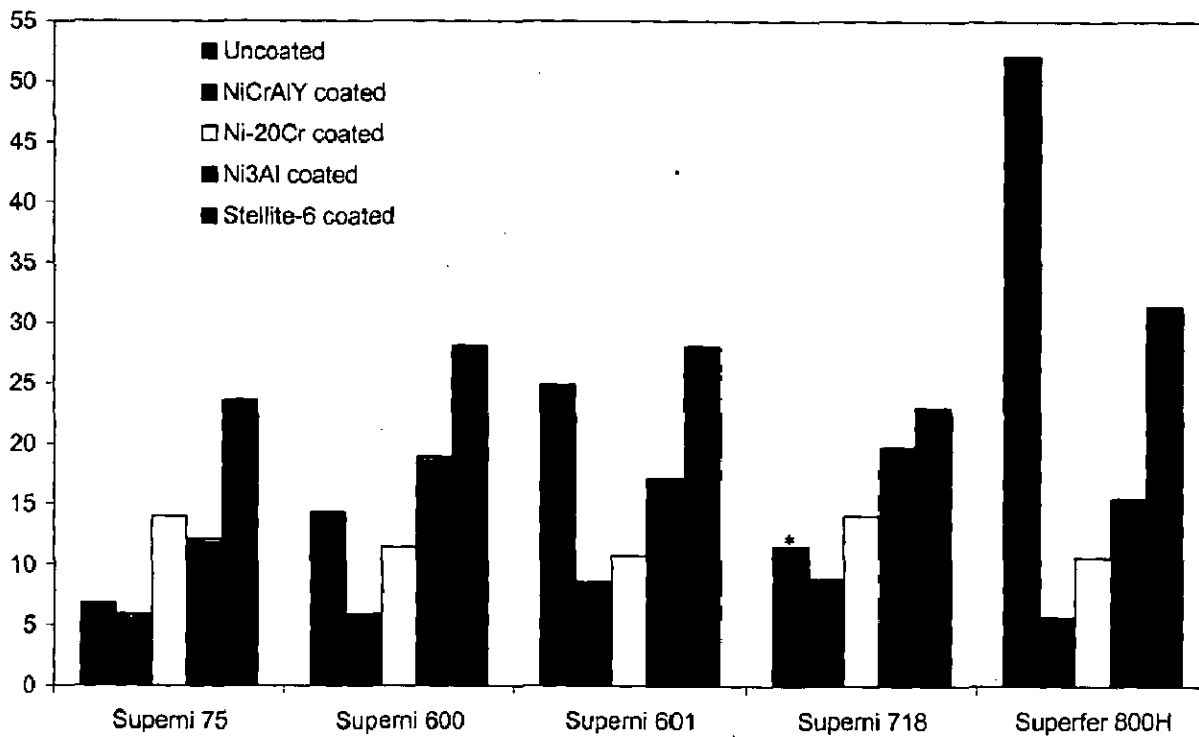


**Fig. 7.1** Bar charts showing cumulative weight gain ( $\text{mg}/\text{cm}^2$ ) for the coated and uncoated superalloys subjected to cyclic oxidation in air at  $900^\circ\text{C}$  for 50 cycles.



\*Extensive spalling made it difficult to monitor the weight gain after 20 cycles

**Fig. 7.2** Bar charts showing cumulative weight gain ( $\text{mg}/\text{cm}^2$ ) for the coated and uncoated superalloys subjected to cyclic oxidation in  $\text{Na}_2\text{SO}_4$ -60% $\text{V}_2\text{O}_5$  environment at  $900^\circ\text{C}$  for 50 cycles.

Lu et al (2004) have also reported after the comparative study that IC-6 alloy (Ni<sub>3</sub>Al based alloy) behaved similar to Ni-Cr alloys in terms of high temperature sulphidation and oxidation resistance, whereas this is inferior to MCrAlY coating materials. Comparatively lowest corrosion resistance of the Co-based (Stellite-6) coating might be ascribed to low content of Cr (19%) in its basic composition, which is not sufficient to resist the onset of basic fluxing as has been suggested by Whittle (1972). He suggested that 25-30% chromium is needed to establish a protective layer in Co-base alloys because diffusion coefficient for chromium in cobalt is about an order of magnitude less than that in nickel. Tewari (1997) and Gitanjali (2003) have also observed that Co-based superalloys have inferior corrosion resistance than Ni-base superalloys in an environment of Na<sub>2</sub>SO<sub>4</sub>-60%V<sub>2</sub>O<sub>5</sub> at 900<sup>o</sup>C.

So far as behaviour of the different coatings in the air is concerned, NiCrAlY coatings gave the best protection to the superalloys under study. Whereas the performance of other coatings could not be sequenced in general, it was observed to vary with the change in substrate superalloy. Comparing the oxidation resistance of Ni-20Cr, Ni<sub>3</sub>Al and Stellite-6 coatings in the air, sequences observed for the different coated superalloys are as follows:

Ni <sub>3</sub> Al > Stellite-6 > Ni-20Cr	for	Superni 75 and Superni 601
Stellite-6 > Ni <sub>3</sub> Al > Ni-20Cr	for	Superni 600
Ni-20Cr > Ni <sub>3</sub> Al > Stellite-6	for	Superni 718
Ni <sub>3</sub> Al > Ni-20Cr > Stellite-6	for	Superfer 800H

Therefore Ni<sub>3</sub>Al appears to be better coating against air oxidation in comparison to Ni-20Cr and Stellite-6 coatings. This resistance might also be imparted by the presence of thin continuous streaks of Cr at the interface between the bond coat and the base alloys as can be visualised in the respective cases, Fig. 5.50 and 5.52. On the contrary the relatively low oxidation resistance shown by Ni-20Cr and Stellite-6 coatings might partially be due to absence of such continuous chromia layers, with an exemption of oxidised Stellite-6 coated Superfer 800H, where continuous layer could be seen at bond coat/substrate interface.

Effect of the base superalloys was considerable in most of the coated cases on the oxidation behaviour in air and molten salt environments, except in case of air oxidation of the Ni<sub>3</sub>Al coated Ni-base superalloys, and NiCrAlY coated superalloys, where the oxidation rates were not significantly apart. Smeggil and Bornstein (1983) and Singh (2003) have also observed the effects of substrate alloying elements on the oxidation and

hot corrosion resistance for diffusion aluminide and plasma sprayed coatings respectively.

So far as the comparison of performance of a particular coating in the different environments is concerned, it has been observed that the coatings have shown more cumulative weight gains in the molten salt than those in the air in all the cases as is obvious from Figs. 7.1 and 7.2, with an exemption of Ni-20Cr coating. In the latter case, Ni-20Cr coated superalloys Superni 75, 600 and 601 coated have shown more weight gain during air oxidation than that during molten salt environment. Similar observation has also been made by Singh (2003) during his studies on oxidation behaviour of Ni-20Cr coating on boiler tube steels in the similar environments. The effect of molten salt induced oxidation was relatively high in case of Stellite-6 coating, followed by NiCrAlY, Ni<sub>3</sub>Al and Ni-20Cr coatings on the basis of ratio of the overall weight gain in the molten salt atmosphere to the weight gain in air oxidation.

NiCrAlY coating may be recommended as the best coating for the superalloys under current investigation so far as hot corrosion and oxidation resistance are concerned based upon the findings of the current study. This coating was also successful in maintaining integrity with its respective substrates throughout the exposure time to both the environments of the study, without any significant spalling of its oxide scales. However, while selecting a particular coating for a specific application, various other factors such as substrate compatibility, adhesion, porosity, the possibility of repair or recoating, interdiffusion, the effect of thermal cycling, resistance to wear and cost should also be considered (Sidky and Hocking, 1999).

# CHAPTER 8

## CONCLUSIONS

---

The conclusions from the present investigation regarding oxidation behaviour of NiCrAlY, Ni-20Cr, Stellite-6 and Ni<sub>3</sub>Al coatings formulated by argon shrouded plasma spray process on five types of superalloys namely Superni 75, Superni 600, Superni 601, Superni 718 and Superfer 800H are presented in this chapter. The oxidation studies were conducted in air as well as molten salt (Na<sub>2</sub>SO<sub>4</sub>-60%V<sub>2</sub>O<sub>5</sub>) environments under cyclic conditions in a laboratory furnace at an elevated temperature of 900<sup>0</sup>C for an oxidation run of 50 cycles in all the cases. NiCrAlY was firstly deposited as a bond coat in all the coatings. All the coating powders were commercially available except Ni<sub>3</sub>Al, which was prepared from stoichiometric mixture of nickel-aluminium. Salient conclusions from the present study are enumerated below:

- (1) Ni<sub>3</sub>Al coating was successfully obtained on the given Ni- and Fe-based superalloys by shrouded plasma spray process using stoichiometric mixture of nickel and aluminium. The formation of Ni<sub>3</sub>Al was confirmed by X-ray diffractograms.
- (2) NiCrAlY, Ni-20Cr and Stellite-6 could be successfully obtained by shrouded plasma spray process on the given superalloys. All the coatings showed some porosity (2.00-4.50%).
- (3) In the present study it was possible to obtain a thickness in range of 200-250 μm for the NiCrAlY, Ni-20Cr and Ni<sub>3</sub>Al coatings, whereas somewhat thicker coatings around 350-450 μm could be deposited in case of the Stellite-6. The thicker coatings beyond the above mentioned range were found to disintegrate by themselves.
- (4) The cross-sectional microhardness of the coatings was found to be variable with the distance from the coating-substrate interface. So far as the upper values of the hardness range are concerned, Stellite-6 coating showed an upper limit of 490 Hv (maximum among all the coatings), while Ni<sub>3</sub>Al coatings exhibited an upper limit of 223 Hv (minimum among all the coatings).
- (5) In almost all the coating formulations, a slight increase in microhardness values for the substrate superalloys was observed near the bond coat/substrate interface.

- (6) The interdiffusion of various elements amongst the substrate and plasma sprayed coatings was observed to be marginal as has been indicated by EPMA. The diffusion between the bond coat and top coat was relatively high. Aluminium was found to be the most vulnerable element to the diffusion phenomenon.
- (7) Superni 600 has shown a maximum resistance to cyclic oxidation in air at 900<sup>0</sup>C amongst the given superalloys, which might be attributed to the presence of a continuous band of Cr just at the scale/substrate interface in the oxidised superalloy, as was revealed by EPMA.
- (8) Superni 75 has indicated lowest resistance to air oxidation under cyclic condition at 900<sup>0</sup>C in comparison to all the investigated superalloys, where chromia layer present in scale was found to be relatively discontinuous (EPMA).
- (9) The oxidation rates for the investigated superalloys based on the overall weight gains after 50 cycles of oxidation in the Na<sub>2</sub>SO<sub>4</sub>-60%V<sub>2</sub>O<sub>5</sub> environment could be arranged in the following order:
- Superfer 800H > Superni 601 > Superni 600 > Superni 75
- (10) Superni 718 suffered accelerated hot corrosion in the given molten salt environment in the form of intense spalling and sputtering of its scale, which may be ascribed to the presence of 3.05% molybdenum in its basic composition, which might have caused severe hot corrosion by acidic fluxing (Peters et al, 1976, Fryburg et al, 1984 and Pettit and Meier, 1985).
- (11) Rate of oxidation was observed to be high in the early cycles of the study in both the given environments for all types of coatings, which may be attributed to the fact that during transient period of oxidation, the oxidizing species might have penetrated in the coating along the interconnected network of pores and splat boundaries to cause rapid oxidation. However, once all these possible diffusion paths are blocked by the formation of the oxides, the oxidation then becomes limited mainly to the surface of the coatings, thereby enters in a steady state.
- (12) All the coatings after exposure to air as well as molten salt induced oxidation have shown the presence of mainly oxides as has been indicated by surface XRD and EDAX analysis. The phases revealed are oxides of chromium and/or aluminium, and spinels containing nickel-chromium/cobalt-chromium/nickel-aluminium type mixed oxides. These oxides especially Al<sub>2</sub>O<sub>3</sub> and Cr<sub>2</sub>O<sub>3</sub> offer a better protection against oxidation/hot corrosion due to their low growth rate, strongly bounded compositions and ability to act as effective barriers against

ionic migration (Stott, 1989B). The spinel phases may further enhance the oxidation resistance due to their much smaller diffusion coefficients of the cations and anions than those in their parent oxides (Chatterjee et al, 2001).

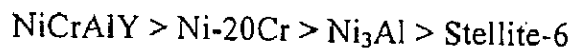
- (13) In case of NiCrAlY coatings, the splat structure could be clearly seen after air as well as molten salt oxidation with the help of EPMA/Cross-sectional EDAX analysis, where the splats (Ni-rich) were in un-oxidised state. The ingress of corrosive species in the initial stages along the splat boundaries resulted in formation of oxides of mainly aluminium, alongwith those of yttrium and chromium.
- (14) Bond coat was found to have retained its identity in case of Ni-20Cr, Ni<sub>3</sub>Al and Stellite-6 coated samples in both the environments of current investigation. The Ni-rich splats present in the bond coats were found to be, by and large, in un-oxidised state, whereas oxides of aluminium, yttrium and chromium were observed to be formed along the pores and splat boundaries.
- (15) In case of Stellite-6 coating, chromium and oxygen were found to co-exist along the splat boundaries in both the environments of study, whereas cobalt rich splats remained un-oxidised.
- (16) During oxidation studies in air, all the coatings have shown overall weight gains higher than their uncoated counterpart superalloys. However, in all the coated cases, the oxidation behaviour was found to be governed by parabolic rate law. Moreover, the internal oxidation of the substrate superalloys has not been observed in general.
- (17) In case of studies in air, the NiCrAlY coated superalloys showed minimum rate of oxidation amongst the all the coated superalloys, where the performance sequence for all the other coatings was dependent on the type of the base superalloy as below:

Ni <sub>3</sub> Al > Stellite-6 > Ni-20Cr	for	Superni 75 and Superni 601
Stellite-6 > Ni <sub>3</sub> Al > Ni-20Cr	for	Superni 600
Ni-20Cr > Ni <sub>3</sub> Al > Stellite-6	for	Superni 718
Ni <sub>3</sub> Al > Ni-20Cr > Stellite-6	for	Superfer 800H

- (18) Ni<sub>3</sub>Al appeared to be a better coating against air oxidation in comparison to Ni-20Cr and Stellite-6 coatings. This resistance might partly be imparted by the presence of thin continuous streaks of Cr at the bond coat/base alloy interface, especially in case of Ni<sub>3</sub>Al coated Superni 75 and 601 (EPMA). On the contrary

the relatively low oxidation resistance shown by Ni-20Cr coatings may partially be attributed to absence of such continuous chromia layers.

- (19) In case of Stellite-6 coated Superfer 800H, EPMA indicated a thin and continuous layer of chromium oxide at the bond coat/base alloy interface during air oxidation, which may also serve to protect the substrate alloy during long term use. However, in other Stellite-6 coated superalloys, no such continuous layer of chromia was seen during air oxidation.
- (20) In the molten salt environment, the coatings were found to be successful in reducing the overall weight gains in most of the cases, hence the corrosion rates. The coatings could be arranged as follows on the basis of their performance in developing hot corrosion resistance:



- (21) The NiCrAlY coated Superfer 800H superalloy showed the highest oxidation resistance to both air and molten salt environments. The best protection indicated by NiCrAlY coating, in general, might also be attributed the simultaneous formation of an additional protective oxide  $\alpha\text{-Al}_2\text{O}_3$  alongwith  $\text{Cr}_2\text{O}_3$  and  $\text{NiCr}_2\text{O}_4$ , which grows very slowly and is thermodynamically stable. Moreover, the presence of yttrium in the coating might also have reduced the scale growth rates and hence the overall weight gains.
- (22) Better performance of Ni-20Cr coating on the Superfer 800H in the molten salt environment might also be due to presence of nearly continuous band of chromia present in the top scale.
- (23) Relatively lower oxidation resistance of the Stellite-6 coated superalloys in the molten salt environment might also be ascribed to low Cr (19%) content in the coating composition, which should be 25-30% for the Co base alloys to resist basic fluxing as per the views of Whittle (1972).
- (24) Protection imparted by Stellite-6 coating to Superni 601 and Superfer 800H in the given molten salt environment might partly be due to the presence of continuous Cr-rich layers above the bond coat/substrate interface as was revealed by EPMA.
- (25) The effect of the base superalloys was considerable in most of the cases on the oxidation behaviour in air and molten salt, except in case of air oxidation of the  $\text{Ni}_3\text{Al}$  coated Ni-base superalloys, and NiCrAlY coated superalloys, where the oxidation rates were not significantly apart.

- (26) Ni-20Cr coated superalloys Superni 75, 600 and 601 have shown more overall weight gains during air oxidation than those during molten salt environment.
- (27) In most of the cases of coated superalloy samples subjected to molten salt environment, sulphur has penetrated into the base superalloys, while vanadium remained mainly in the top scales (EPMA). The ingress of S and V might have occurred along the coating splat boundaries/pores during transient period of oxidation.
- (28) Titanium has shown significant diffusion into the scales in case of NiCrAlY, Ni-20Cr and Ni<sub>3</sub>Al coated Superni 75, 718 and Superfer 800H during molten salt as well as air oxidation, with a tendency to form thin streaks at the interface between the bond coat and substrates.
- (29) Diffusion of iron into the scales of NiCrAlY, Ni-20Cr and Ni<sub>3</sub>Al coatings has also shown by EPMA in most of the cases after exposure to oxidation/hot corrosion, which is relatively high in case of molten salt induced oxidation. The magnitude of the iron migration into the scales was higher in case of Fe-based superalloy Superfer 800H, where it has shown its presence, even in the Ni-rich splats near the bond coat/substrate superalloys in some cases.
- (30) The EPMA analysis has indicated diffusion of some of the other basic elements of the superalloy substrates such as Mn, Mo, Ta and Si into the scales in many cases, while diffusion of Cr from the bond coat to the Ni<sub>3</sub>Al coating was also noticed. However, the diffusion stability can be considered a life-limiting factor if coatings are operated at temperatures greater than 1000<sup>0</sup>C for prolonged periods of time (Mazars et al, 1986).
- (31) Only minor spalling of the scales was observed in powder form during the molten salt corrosion for most of the coated cases. The scales in general showed no tendency towards spalling/cracking and were found intact.
- (32) Some superficial minor cracks were observed near/along the sharp edges of the coated specimens during cyclic oxidation in air as well as molten salt environments. This cracking further resulted in disintegration/spalling of the edges of the coatings, which was marginal.
- (33) The temperature, at which the coatings have been found useful for the given superalloys in reducing the corrosion, can enhance the efficiency by a significant fraction particularly in case of boilers.



(34) NiCrAlY coating may be recommended as the best coating for the superalloys under investigation to be used for boilers and gas turbines (in fact other similar high temperature applications) so far as hot corrosion and oxidation resistance are concerned based upon the findings of the current study. Also this coating has been found to be successful in maintaining its integrity with its respective substrates throughout the exposure to both the environments of the study, without any significant spalling of its oxide scales.

## SUGGESTIONS FOR FUTURE WORK

---

1. Behaviour of the coated superalloys should also be evaluated in the actual industrial environments, such as in the actual running boiler for longer durations.
2. All the investigated coatings have been found to be successful in maintaining continuous surface contact with their respective substrate superalloys during oxidation in air as well as in molten salt; however the adhesive strength of the coatings should be evaluated. The detailed bonding study can help to predict the behaviour of these coatings for different erosive-corrosive environments.
3. High temperature erosion behaviour of the coatings may also be investigated.
4. Hot stage microscopy may be used to understand the development of the scale as well as mechanism of transport of species during the oxidation and hot corrosion runs.
5. Studies may be conducted to investigate the hot corrosion behaviour of the thermal spray coatings developed by some other processes such as high-velocity oxy-fuel and detonation spray processes.
6. Cost effectiveness analysis should be done for different types of coatings.
7. Attempts can be made to estimate the useful life of these coated superalloys by extrapolation of the laboratory data by mathematical modeling.
8. Some efforts should be made to eliminate the porosity of these coatings so as to enhance their corrosion resistance. In this regard post coating treatments should be explored.
9. Some other coatings compositions should be tested especially by alloying the coating powders with rare earth elements.

**Table A.1** Summary of oxidation of Fe-, Ni- & Co- base alloys in air,  $\text{Na}_2\text{SO}_4$  and  $\text{V}_2\text{O}_5$  environments

Material	Environment	Brief Details
<b>Oxidation in air</b>		
Iron	Gas mixtures containing Ar, $\text{O}_2$ and $\text{Cl}_2$ , 1100 and 1200K	The rate of oxidation of iron was significantly inhibited by the presence of chlorine in the environment, which has been attributed to the formation of a dense layer of $\text{Fe}_2\text{O}_3$ on the outside of the oxide scale formed in the presence of chlorine (Lee and McNellan, 1990).
Thin films of Fe-20Cr-Al	Thermal-cycling conditions, 1150°C	The films were found to be very susceptible to breakdown oxidation after short periods of exposure to air, due to exhaustion of aluminium in the substrate arising from the large surface area to volume ratio (Stott and Hiramatsu, 2000). It was further observed that when the aluminium concentration in the alloy drops below a critical level, a layer of chromia was able to develop and grow at the alumina-alloy substrate interface. This eventually was suggested to cause breakdown oxidation and formation of iron-rich oxides on the specimen.
Fe-15 wt %Cr-4% wt Al	Isothermal as well as cyclic oxidation, 1000-1300°C	The effect of zirconium and yttrium alloying on the high temperature oxidation of Fe-15 wt %Cr-4% wt Al was investigated. It was observed that the yttrium addition decreased the oxidation rate appreciably at 1000°C in $\text{O}_2$ - $\text{H}_2\text{O}$ atmosphere where it did not affect oxidation rate in $\text{O}_2$ . Whereas under similar conditions 1% Zr addition increased the weight gain both in $\text{O}_2$ and air but in $\text{O}_2$ - $\text{H}_2\text{O}$ weight gain was much less as compared to that of the base alloy. At a temperature of 1200°C in air, the effect of Zr concentration on the oxidation of the alloy was to increase the oxidation rate. Further lower concentration of Zr i.e. 0.2% was found to be beneficial in improving the oxidation resistance under cyclic conditions with reduced spalling of the scale. Alloying with 1% Y was also observed to be equally effective in improving the oxidation resistance at 1200°C (Pandey, 1983).
Ni-10Cr-5Al, Ni-20Cr-5Al and Ni-30Cr-5Al alloys	Isothermal oxidation in Air, 1000°C	The oxide formed adjacent to the alloy was $\alpha$ - $\text{Al}_2\text{O}_3$ such that the higher was the Cr content of the alloy the easier was its formation. The Ni-30Cr-5Al alloy formed a complete layer of $\alpha$ - $\text{Al}_2\text{O}_3$ in the initial stages of oxidation through 'oxygen gettering' by Cr. Further a decrease in scale thickness and an increase in scale adherence were observed with an increase in Cr content from 10 to 30% (Ul-Hamid, 2004).

304 L stainless steel	In steam as well as in air, 1000-1375°C	The oxidation by steam was fast as compared to that by air. The diffusion through Fe-Ni-Cr spinel layer was suggested as the parabolic rate controlling process in case of oxidation by steam. Whereas, in case of oxidation by air the formation of Cr <sub>2</sub> O <sub>3</sub> was reflected as a reason for slow oxidation (Bittel et al, 1969).
Austenitic stainless steel (AISI-316, -321 and -304)	Linear heating rate 6 K min <sup>-1</sup> up to 1150°C and the isothermal holding at 1000°C, with and without superficially applied CeO <sub>2</sub>	In the bare condition 321-grade steel was reported to exhibit best performance whereas in the presence of coatings the performance of 316 and 321 grades was identical (Seal et al, 1994). Roy et al (1995) have also studied the role of the similar type of coatings on AISI 347 and reported identical results.
AISI 316 stainless steel	Under non-isothermal heating followed by isothermal holding at 1423 K	The influence of alloy surface preparation as induced by mechanical polishing and electro polishing on the oxidation behaviour has been reported. The mechanically polished surfaces exhibited a shorter incubation period but better oxidation resistance during isothermal holding as compared to electro polished surfaces. This was attributed to enhanced outward diffusion of Cr favouring formation of continuous band of Cr-rich layers (Kuiry et al, 1994).
Laser surface engineered composite boride coating on plain carbon steel	In air, at 600, 800 and 1000°C for 10, 30 and 50 hours	The effect of long duration exposure at high temperature was investigated (Agarwal et al, 2000). They used thermogravimetric technique to study the kinetics of oxidation at elevated temperature. Oxidation rate for all the samples was observed to be parabolic in nature and oxidation kinetic rate constant was reported to increase with increasing temperature of exposure.
<b>Na<sub>2</sub>SO<sub>4</sub> Induced Hot Corrosion</b>		
Pure Iron & Fe-5Cr Alloy, and Fe-13Cr Alloy	1 atmosphere of oxygen, 900°C	Pure iron did not undergo accelerated oxidation, which has been attributed to the thickening of the scale too rapidly for sulphur to penetrate the oxide and interact directly with the metal. Authors further reported an immediate acceleration in oxidation rate of Fe-5Cr alloy in the presence of Na <sub>2</sub> SO <sub>4</sub> deposits this was attributed to sulphide formation mechanism which initially restricted spinel formation (Trafford & Whittle, 1980A). In their study conducted on Fe-13% Cr alloy, Na <sub>2</sub> SO <sub>4</sub> coating markedly enhanced the oxidation rate and resulted in the formation of thick, compact and stratified scales. They postulated that formation of sulphides in the alloy substrate and mechanical failure of scale was responsible for the enhanced oxidation (Trafford & Whittle, 1980 B).

Pure iron, chromium and manganese and Chromium	Gas mixture, containing O <sub>2</sub> (3.6%), SO <sub>2</sub> (0.25%) and N <sub>2</sub> (bal), 600-800°C	The enhanced corrosion phenomenon was interpreted in terms of low melting liquid sulphates formation. Further the corrosion rate of pure chromium was not appreciably affected by the salt deposit (Nanni et al, 1987).
Pure Iron	Simulated combustion gas containing SO <sub>3</sub> , 600-800°C	The accelerated reaction observed in the presence of Na <sub>2</sub> SO <sub>4</sub> deposits was attributed to the formation of a liquid salt solution between Na <sub>2</sub> SO <sub>4</sub> and the sulphates of the corroded metal with the production of duplex scales consisting of a mixture of metal oxides and sulphides (Gesmundo & Viani, 1988).
Iron	In oxygen, 750°C	The accelerated oxidation of iron in the presence of deposits of Na <sub>2</sub> SO <sub>4</sub> was attributed to the formation of abundant sulphide which had a highly defected lattice and allowed rapid diffusion of a liquid phase. The liquid phase was eutectic melt of Na <sub>2</sub> SO <sub>4</sub> and Na <sub>2</sub> O. Further it was concluded that the accelerated oxidation had most of the characteristics common with usual low temperature hot corrosion except that it occurred under basic conditions developed by the removal of sulphur from the sulphate deposits instead of the usual acidic conditions established by the SO <sub>3</sub> in the atmosphere (Shi, 1993).
Pure Iron and Fe-Al Alloys	Na <sub>2</sub> SO <sub>4</sub> deposit, O <sub>2</sub> -rich atmospheres containing SO <sub>2</sub> -SO <sub>3</sub> at 650 -700°C	The accelerated oxidation of pure iron beneath Na <sub>2</sub> SO <sub>4</sub> deposit was believed to be induced by the formation of eutectic melt of Na <sub>2</sub> SO <sub>4</sub> -iron sulphate. The growth of oxide has been reported to predominant although fluxing contributed a little to the corrosion. In alloys containing Al, fluxing proceeded at a considerable rate in the early stages due to the different oxygen pressure at the oxide/melt interface. Reduction of SO <sub>3</sub> released SO <sub>2</sub> , which caused the formation of sulphides in the scale. Sulphides were supposed to contribute considerably to the acceleration due to their high defect concentration (Shi et al, 1993).
Pure Ni and Al and Fe-Cr, Ni-Cr and Fe-Al alloys	In oxygen and air, 750°C	Shi (1995) studied the possibility of Na <sub>2</sub> SO <sub>4</sub> -Na <sub>2</sub> O eutectic melt formation on the metals deposited with Na <sub>2</sub> SO <sub>4</sub> . In case of Ni, Co, Al, Cr and their alloys he could not detect formation of Na <sub>2</sub> SO <sub>4</sub> -Na <sub>2</sub> O. In case of iron base alloy with high Cr or Al content, where Cr <sub>2</sub> O <sub>3</sub> or Al <sub>2</sub> O <sub>3</sub> were formed, again Na <sub>2</sub> SO <sub>4</sub> -Na <sub>2</sub> O eutectic was not observed. However, at lower Cr or Al content this eutectic melt was suggested to be the possible cause for accelerated rate of corrosion.
Pure Iron	Na <sub>2</sub> SO <sub>4</sub> , Na <sub>2</sub> SO <sub>4</sub> +NaCl, Na <sub>2</sub> SO <sub>4</sub> +V <sub>2</sub> O <sub>5</sub> , combustion gas, 600°C	Iron suffered low temperature hot corrosion in the presence of salt deposits at 600°C. The additions of NaCl and V <sub>2</sub> O <sub>5</sub> to Na <sub>2</sub> SO <sub>4</sub> changed the corrosion kinetics significantly and modified the scale structure (Li et al, 1996).

Binary Iron Aluminide (Fe <sub>3</sub> Al)	In pure oxygen, 1100 K, 1225 K and 1330K	The faster kinetics observed in the initial stages of oxidation was related to the formation of $\theta$ -Al <sub>2</sub> O <sub>3</sub> and slower kinetics in the later stages of oxidation to the formation of $\alpha$ -Al <sub>2</sub> O <sub>3</sub> . The overall rate of hot corrosion was higher than that of oxidation at all temperatures. The presence of $\alpha$ -Fe <sub>2</sub> O <sub>3</sub> in addition to alumina was indicated by XRD. Cross-sectional microscopy revealed that the metal-scale interfaces were pitted in hot corrosion conditions and the pits contained aluminium sulphide. Sulphides were also detected along grain boundaries in the intermetallic near the scale-metal interface (Das et al, 2002).
Ferritic Steels containing Cr, Al & Ti	Fused salt mixture containing Na <sub>2</sub> SO <sub>4</sub> at 927°C and gas mixture CO, CO <sub>2</sub> , CH <sub>4</sub> , H <sub>2</sub> O, H <sub>2</sub> and H <sub>2</sub> S at 600°C	The presence of Ti with 12 % Cr and 3% Al increased the proportion of Fe, which diffused to the outer layer of the scale. The excellent behaviour of steels at temperatures above 600°C was explained by the increase in Al diffusion coefficient with temperature (Coze et al, 1989).
310 Stainless Steel	Various ratios of Na <sub>2</sub> SO <sub>4</sub> /NaCl deposit, in air at 750°C	The weight gain kinetics in simple oxidation was found to follow a steady state parabolic rate law after 3 hours, while the kinetics with the salt deposits displayed a multi-stage growth rates. The most severe corrosion took place with 75% NaCl mixtures. Uniform internal attack was the morphology of NaCl-induced hot corrosion, while the extent of intergranular attack was more pronounced as the content of Na <sub>2</sub> SO <sub>4</sub> in the mixture was increased (Tsaur et al, 2005).
Pure Nickel and Udimet 700	In a high velocity burner rig, 900°C	Corrosion of Ni in the burner rig produced a relatively compact NiO scale along with some internal grain boundary corrosion. Corrosion of Udimet 700 was observed to occur in two stages. During the first stage, the corrosion proceeded by the reaction of Cr <sub>2</sub> O <sub>3</sub> scale with the Na <sub>2</sub> SO <sub>4</sub> and evaporation of the Na <sub>2</sub> CrO <sub>4</sub> reaction product from the surface of the corroding sample. Cr depletion in the alloy occurred and sulphide particles were formed in the Cr depletion zone. Extensive sulphidation occurred during the second stage of corrosion and a thick scale was formed (Misra, 1987).
Pre-oxidised Nickel	In an SO <sub>2</sub> -O <sub>2</sub> gas atmosphere at 900°C	Chromate anion suppressed the sulphidation of Ni probably by precipitating solid Cr <sub>2</sub> O <sub>3</sub> from the melt. Vanadate anions enhanced the onset of the hot corrosion and sulphidation probably via rapid dissolution of the protective oxide scale at cracks/defects or grain boundaries (Otsuka & Rapp, 1990).
Pure Nickel	Under SO <sub>3</sub> + SO <sub>2</sub> + O <sub>2</sub> gas mixture & SO <sub>2</sub> and O <sub>2</sub> atmospheres, 900°C	The corrosion loss in mixed atmosphere containing SO <sub>3</sub> was reported to be larger than those observed in pure SO <sub>2</sub> and O <sub>2</sub> atmospheres. The corrosion loss was found to correspond to the thickness of the oxide layers. High corrosion losses were attributed to the fact that SO <sub>3</sub> strongly acted as an oxidizing agent for the corrosion process (Hara et al 1991).

Ni-23.1 Nb-4.4Al and Ni-19.7Nb-6.0 Cr-2.5Al	Dean rig test, 900°C and 1100°C	Below the outer layer, mainly of NiNb <sub>2</sub> O <sub>6</sub> , high proportion of Al <sub>2</sub> O <sub>3</sub> has been reported to be present. Internal oxidation of the metal producing Al <sub>2</sub> O <sub>3</sub> and Cr <sub>2</sub> O <sub>3</sub> was believed to occur before the development of external Al <sub>2</sub> O <sub>3</sub> layer. In some isolated regions the alloy was found to be much more severely attacked, the pit contained NiNb <sub>2</sub> O <sub>6</sub> , NbCr <sub>2</sub> O <sub>4</sub> and Ni. At 1100°C, more uniform corrosion was observed, the outer layer was mainly NiCr <sub>2</sub> O <sub>4</sub> and beneath it a layer of Cr <sub>2</sub> O <sub>3</sub> containing particles of NbCr <sub>2</sub> O <sub>4</sub> was observed. Internal oxides were mainly Al <sub>2</sub> O <sub>3</sub> and there were massive Ni-rich sulphides ahead of oxidation front (Johnson et al, 1978).
Ni-30Cr and Co-30Cr	600-900°C	The rapid rate of attack was explained on the basis of sulphation of the transient surface oxides (Ni or Co oxides) and the dissolution of these transition metal sulphates into Na <sub>2</sub> SO <sub>4</sub> to yield a liquid phase (Luthra and Shores, 1980).
B-1900	Na <sub>2</sub> SO <sub>4</sub>	Na <sub>2</sub> SO <sub>4</sub> interacted with the alloy to form sodium and sulphur compounds, rapid removal of sulphur from the Na <sub>2</sub> SO <sub>4</sub> by unretarded diffusion of sulphur and precipitation of Cr-rich sulphide phases promoted the formation of Na <sub>2</sub> O. The catastrophic oxidation observed during sulphidation was due to interactions between Na <sub>2</sub> O and the substrate (Bornstein and DeCrescente, 1970).
Ni-base superalloys and seven binary Ni-base alloys	Pure O <sub>2</sub> , 825-1000°C	Based upon the results, it was concluded that the reduction of the oxide ion content of Na <sub>2</sub> SO <sub>4</sub> was a necessity, but not sufficient condition for sulphidation inhibition. The addition of Mo or V to nickel imparted sulphidation resistance in it because their oxides reacted with and decreased the oxide ion content of Na <sub>2</sub> SO <sub>4</sub> . The disagreement in the literature regarding the effect of Molybdenum on hot corrosion was suggested to be largely due to differences in testing techniques and differences in whether the investigators have been more concerned with the initiation or with propagation modes of hot corrosion (Bornstein et al, 1973).
Ni-base superalloys	1 atm O <sub>2</sub> , 650-1000°C (Goebel et al), O <sub>2</sub> , 750-950°C (Misra)	The alloys underwent catastrophic corrosion. The accelerated oxidation occurred as a result of the formation of a liquid flux based on Na <sub>2</sub> SO <sub>4</sub> which dissolved the normally protective oxide scales. Catastrophic or self-sustaining rapid oxidation can occur in alloys which contain Mo, W or V because solution of oxides of these elements with Na <sub>2</sub> SO <sub>4</sub> decrease the oxide ion activity of the molten salts, producing melts which are acidic fluxes for oxide scales (Goebel et al, 1973 and Misra, 1986). The evaporation rate of MoO <sub>3</sub> from Na <sub>2</sub> Mo-MoO <sub>3</sub> melts has been reported to decrease considerably by Misra (1986) when dissolved in Na <sub>2</sub> MoO <sub>4</sub> .

Ni-base industrial superalloys	Static deposits of Na <sub>2</sub> SO <sub>4</sub> or NaCl or both in still air, 850-1000°C	The susceptibility to hot corrosion was found to be correlated to the type of scale produced during simple oxidation. Alloys forming an Al <sub>2</sub> O <sub>3</sub> scale were found to be susceptible to Na <sub>2</sub> SO <sub>4</sub> deposits, independent of their Cr content. The quantity of the Na <sub>2</sub> SO <sub>4</sub> deposits dictated the nature of attack and, under certain conditions, the refractory element alloy additions appeared to play an essential role. Alloys containing Cr <sub>2</sub> O <sub>3</sub> or TiO <sub>2</sub> in the simple oxidation scale proved to be sensitive to NaCl attack (Bourhis and John, 1975).
Ni-15Cr-Mo (Peters et al), Fe-, Ni- and Co-base alloys	900°C (Peters et al), 600°C and above (Pettit and Meier), 975°C in oxygen (Fryburg et al)	The effect of Mo on the hot corrosion of superalloys has also been reported by Peters et al (1976), Pettit and Meier (1985) and Fryburg et al (1984). The alloy containing Mo suffered catastrophic degradation. It has been reported that the MoO <sub>2</sub> reacted with Na <sub>2</sub> SO <sub>4</sub> to produce an acid (SO <sub>2</sub> -rich) salt, leading to acidic fluxing. The MoO <sub>3</sub> incorporated into the Na <sub>2</sub> SO <sub>4</sub> via the formation of compounds such as Na <sub>2</sub> MoO <sub>4</sub> , Na <sub>2</sub> MoO <sub>4</sub> .MoO <sub>3</sub> and Na <sub>2</sub> MoO <sub>4</sub> .2MoO <sub>4</sub> . All these phases were liquid and left a high solubility for Al <sub>2</sub> O <sub>3</sub> and Cr <sub>2</sub> O <sub>3</sub> . Peters et al (1976) added that there is threshold amount of molybdenum below which catastrophic attack is not encountered, e.g. for Ni-15% Cr threshold has been reported to be between 3-4%.
Ni-base Superalloys, B-1900 and NASA-TRW IVA	In pure O <sub>2</sub> , 900°C	After an induction period of little corrosion, local basic fluxing attack of the Cr <sub>2</sub> O <sub>3</sub> / Al <sub>2</sub> O <sub>3</sub> scale spreaded to cover the surface and generated catastrophic linear kinetics. During catastrophic attack of B-1900, the sulphate ions reacted to release SO <sub>2</sub> and formed sulphides in the alloy and salt was converted to Na <sub>2</sub> MoO <sub>4</sub> (Fryburg et al, 1982).
Fe-, Ni- and Co-base alloys	Atmospheres containing O <sub>2</sub> , N <sub>2</sub> and SO <sub>2</sub> , 729-1076°C	The corrosion rate was lowest when the chromium content of the alloy was highest. Further Mo and Cu were found to increase the corrosion rate. The main corrosion products formed in air were NiO and Cr <sub>2</sub> O <sub>3</sub> . In hot corrosion tests NiS and Cr <sub>3</sub> S <sub>8</sub> were found (Pehkonen et al, 1987).
Ni and Ni-base Alloy EI 867 with the Aluminate and Cr-Al Diffusion Coatings	Pure Na <sub>2</sub> SO <sub>4</sub>	Low alloyed aluminate and Cr-Al coatings showed very poor resistance to oxidation. After 24 hrs, these had been almost completely removed. Modification of highly alloyed aluminate coatings with Cr resulted in uniform and relatively slow degradation of the coating. Cr enriched zone is supposed to act as a barrier to the oxidation of refractory metals such as Mo, W and V thus preventing the onset of catastrophic corrosion (Godlewski and Godlewska, 1987).
Ni-16Cr-2Nb, IN 738, Ni-16Cr and Superalloy 537	900 and 1000°C	Na <sub>2</sub> SO <sub>4</sub> coated coupons of Ni-16Cr-2Nb and Ni-16Cr developed dense, protective oxide scales and exhibited good hot corrosion resistance. Alloys 537 and IN 738 experienced a shift from basic fluxing to acidic fluxing and as the temperature was increased, the rate of attack increased significantly (Zho et al, 1987).



Inconel 600 and Incoloy 825	Ar + 1% O <sub>2</sub> , 940°C	Inconel 600 was able to form a protective layer of chromia in Ar + 1% O <sub>2</sub> with or without a thin layer of Na <sub>2</sub> SO <sub>4</sub> at a temperature of 940°C, whereas Incoloy 825 was not able to form chromia in the same environment. This was attributed to the formation of nickel and chromium molybdates due to 3.22% Mo present in the alloy. When O <sub>2</sub> content was only 300ppm, sodium sulphate layer strongly enhanced the corrosion of Inconel 600 and Incoloy 825 (Santorelli et al, 1989).
Review (Shih)	Low-temperature corrosion	Some superalloys containing molybdenum are subjected to sub-melting point hot corrosion when covered with a sulphate, which is associated with the formation of a molybdenum-containing melt resulting from the reaction of MoO <sub>3</sub> with the sulphate (Shih, 1989).
Superalloys HA-188, S-57, IN-617 and TD-NiCrAl	Mach 0.3 burner rig at various temperatures, sea salt concentrations and salt compositions.	Accelerated corrosion of the specimens has been reported in the temperature zones above the calculated dew points of Na <sub>2</sub> SO <sub>4</sub> . It was believed that the corrosion occurred by small amount of salt deposit on those temperature zones during heat-up following each cooling cycle or by small amounts of salt migrating from deposits at cooler zones via a wetting action. Large deposits of salt appear to inhibit corrosion that is why less corrosion was noticed at 900°C when flame was doped with 10 ppm sea salt than when it was doped with 5 ppm sea salt (Santoro, 1979).
Nimonic 105	At 900°C	Hot corrosion did not seem to be very detrimental towards the superalloy. It was concluded that SO <sub>3</sub> pressures below 5x10 <sup>-3</sup> atm did not affect the electrokinetic behaviour, but pressures greater than 5x10 <sup>-3</sup> atmospheres produced higher corrosion rates which was attributed to the acid fluxing by the sulphate melt. Addition of NaCl to the molten Na <sub>2</sub> SO <sub>4</sub> resulted in increased dissolution of Nimonic 105 (Sequeira and Hocking, 1981).
Nimonic 105, 75, 80A and 90	With and without Cr <sub>2</sub> (SO <sub>4</sub> ) <sub>3</sub> , NiSO <sub>4</sub> or CoSO <sub>4</sub> additions, 650-1000°C	Upto 800°C, the lower oxidation rates for Na <sub>2</sub> SO <sub>4</sub> coated alloys were attributed to a scale morphology consisting of inner scales of Cr <sub>2</sub> O <sub>3</sub> acting as a protective oxide film and external scales of NiO. This morphology was observed to be maintained at high temperatures (Malik and Ahmad, 1983).
Alloys B1900 and IN 100 (Al <sub>2</sub> O <sub>3</sub> -formers), Inconel 600, 690, Incoloy 800, IN 738, Nimonic 80A, 100, and 105 (Cr <sub>2</sub> O <sub>3</sub> -formers)	In the presence of Na <sub>2</sub> SO <sub>4</sub> (s) and NaCl (s) separately, and in combination, air, 850 and 1000°C	The Cr <sub>2</sub> O <sub>3</sub> formers got attacked more aggressively by NaCl (s) than Na <sub>2</sub> SO <sub>4</sub> (s). Al <sub>2</sub> O <sub>3</sub> -formers and to some extent NiO-formers were more resistant to NaCl attack than Cr <sub>2</sub> O <sub>3</sub> formers. While Na <sub>2</sub> SO <sub>4</sub> induced corrosion preceded by fluxing and sulphidation reactions, the NaCl induced corrosion was observed to follow a reaction path of fluxing, chloridation and oxidation. The Na <sub>2</sub> SO <sub>4</sub> -NaCl induced corrosion involved combination of reactions occurring in the presence Na <sub>2</sub> SO <sub>4</sub> and NaCl separately (Malik et al, 1988).

Single-crystal Ni-base superalloys and DS Mar M 200	704 and 900°C	All the alloys were severely degraded at 900 and 704°C. There was no significant difference between the hot corrosion of these alloys when tested in air or in oxygen with SO <sub>3</sub> , provided a liquid deposit was present in both cases. It was concluded that all the superalloys under study require a coating if they were to be exposed to any of the hot-corrosion conditions at temperatures of 704°C or higher (Levy et al, 1989).
Inconel 740	850 - 1000°C	The kinetics curves of the alloy at 950°C without Na <sub>2</sub> SO <sub>4</sub> deposit and at 850°C with Na <sub>2</sub> SO <sub>4</sub> deposit obeyed the parabolic law, whereas the uniform parabolic growth behaviour of oxide was not followed at 1000°C without Na <sub>2</sub> SO <sub>4</sub> deposit and at 950°C with Na <sub>2</sub> SO <sub>4</sub> deposit due to oxide spallation at 1000°C and the evaporation of Na <sub>2</sub> CrO <sub>4</sub> melt at 950°C, respectively. The oxide scales were found to be consisting of Cr <sub>2</sub> O <sub>3</sub> , (Ni, Co) Cr <sub>2</sub> O <sub>4</sub> , TiO <sub>2</sub> and Al <sub>2</sub> O <sub>3</sub> and internal oxide scales at all temperatures. The internal sulphidation was suggested to take place due to the existence of Na <sub>2</sub> SO <sub>4</sub> deposit. The complex layered structure of the oxide scales was reported to be in favour of the resistance to oxidation. The accelerated oxidation of the alloy in the presence of Na <sub>2</sub> SO <sub>4</sub> deposit was attributed to the dissolution of Cr <sub>2</sub> O <sub>3</sub> induced by basic fluxing in molten Na <sub>2</sub> SO <sub>4</sub> (Zhao et al, 2004).
Co-Cr, Co-Al and Co-Cr-Al Alloys.	In O <sub>2</sub> -SO <sub>2</sub> -SO <sub>3</sub> , 600 to 750°C	Co-Cr and Co-Cr-Al alloys reacted non-uniformly, usually in the form of pits and Co-Al alloys suffered broad frontal attack. Under all conditions, a thin sulphur-rich band containing sulphides was observed at the alloy/scale interface and cobalt dissolved near the interface and formed Co <sub>3</sub> O <sub>4</sub> /or CoSO <sub>4</sub> (S) (Luthra, 1982).
Co-Cr, Co-Al and Co-Cr-Al Alloys	In O <sub>2</sub> -0.15% (SO <sub>2</sub> +SO <sub>3</sub> ), 750°C	Accelerated oxidation tests at 750°C showed that the corrosion resistance of binary Co-Cr and Co-Al alloys increased with the Cr and Al content of alloys. This protection was offered by the rapid growth of CoCr <sub>2</sub> O <sub>4</sub> /Cr <sub>2</sub> O <sub>3</sub> and CoAl <sub>2</sub> O <sub>4</sub> /Al <sub>2</sub> O <sub>3</sub> oxides in comparison to CoO and Co <sub>3</sub> O <sub>4</sub> . At high enough Cr (≥40%) and Al (≥15%) concentrations, the growth rates were so fast that liquid did not even form, consequently the corrosion rates were very low. Tests on Co-Cr-Al alloys indicated that simultaneous presence of Cr and Al was deleterious to the resistance against low temperature hot corrosion (Luthra, 1985).
Metal oxides such as Co <sub>3</sub> O <sub>4</sub> , NiO, Al <sub>2</sub> O <sub>3</sub> , Cr <sub>2</sub> O <sub>3</sub> , Fe <sub>2</sub> O <sub>3</sub> and SiO <sub>2</sub>	627-927°C (Malik and Mobin) and 827-927°C (Mobin et al) in O <sub>2</sub>	The interaction of the metal oxides with Na <sub>2</sub> SO <sub>4</sub> has been studied. As suggested, the high temperature reaction products usually contain 3-phase structure namely, Na <sub>2</sub> O-MO-M <sub>2</sub> O <sub>3</sub> and metal sulphide and or metal sulphate. The formation of Na <sub>2</sub> O-M <sub>2</sub> O was further reported to be dependent upon the solid state solubility of metal oxide in the molten salt at high temperature and under limited solubility conditions Na <sub>2</sub> O-M <sub>2</sub> O was invariably formed, but as soon as conditions got relaxed the oxide M <sub>2</sub> O <sub>3</sub> precipitated and was observed to form a separate phase (Malik and Mobin, 1987 and Mobin et al, 1996).

V <sub>2</sub> O <sub>5</sub> Induced Hot Corrosion	
Gas-turbine alloys	750°C and above
Review	-----
Technical note (Fairman) Review (Pantony & Vasu)	-----
Pure metals such as iron, cobalt, nickel, molybdenum, titanium, tungsten and 99.5% vanadium rods, and single crystals of chromium	Immersion in the melt, in O <sub>2</sub>

<p>Vanadium pentaoxide coatings had a deleterious effect throughout the useful temperature range of all the alloys up to 1120 hrs in 70-hr cycles. The effect was reported to be more pronounced for iron base alloys at temperatures above 750°C (Harris et al, 1955).</p>
<p>Oxidation of pure Cr in V<sub>2</sub>O<sub>5</sub> occurs with a very rapid diffusion rate and so only the initial stages of the oxidation curve were supposed to be more important. Later slowing down of the oxidation rate could be attributed mainly to the effect of scale thickening. Loose and spongy appearance of the scale was observed at the beginning of the process; V<sub>2</sub>O<sub>5</sub> was present in excess and did dissolve the products of oxidation. At the same point the liquid was saturated with the oxide which subsequently could get precipitated. The presence of various phases in a thin layer of scale would impose such severe strain on the film that cracking and exfoliation could be expected. This would permit liquid phase to reach the metal surface again and the conditions to form a spongy scale were seen to prevail. This mechanism would apply only to iron base alloys, which are susceptible to the catastrophic corrosion (Sachs, 1958).</p>
<p>Fairman (1962) reported that the accelerated oxidation due to V<sub>2</sub>O<sub>5</sub> is most likely to be the consequence of the catalytic action of vanadium pentoxide. It results in splitting the oxygen molecule at the metal surface, so cause rapid corrosion. Pantony &amp; Vasu (1968A) concluded from the theoretical survey of fireside corrosion of boilers and gas-turbines that in residual fuel ash, V<sub>2</sub>O<sub>5</sub> can be the most serious cause of "catastrophic" corrosion.</p>
<p>A diffusion controlled corrosion process given by equation below hold good for the initial stages of vanadic corrosion of all metals under study except nickel and chromium.</p> $\Delta w = Kt$ <p>where <math>\Delta w</math> is the weight change per cm<sup>2</sup> at time <math>t</math>, and <math>k</math> is the velocity constant. Whereas nickel obeyed a logarithmic rate law. The velocity constant was found to be inversely proportional to the depth of melt. On the basis of comparison of activation energies of the various rate processes, a single mechanism underlying the corrosion processes of iron, cobalt, vanadium, titanium, tungsten and molybdenum was suggested, which involves an inward diffusion of oxygen (or other active species) and a sequential outward diffusion of the corrosion products. In case of nickel and chromium, the existence of a coherent corrosion layer separating the slag from nickel and chromium was revealed, which was named as protective barrier for these metals and was found to be absent for other metals under study (Pantony &amp; Vasu, 1968B).</p>

Iron, nickel and several alloys containing iron, nickel, and chromium	Crucible and rotating disk testing	<p>The stainless steels and particularly 440 stainless steel (25 wt% Cr) showed the best corrosion resistance to liquid <math>V_2O_5</math>. The rate of corrosion of Armco iron by liquid <math>V_2O_5</math> has been reported to be controlled initially by the diffusion of oxygen across the metal oxide-liquid vanadate interface. As the available oxygen ions got depleted from the melt, the rate controlling mechanism was observed to be changed to the sorption of oxygen at the liquid vanadate gas phase interface. Whereas in case of nickel, Inconel 600 and the iron alloys, the rates of corrosion were found to be affected by the formation and dissolution of the protective metal oxide layers. They concluded that the presence of Fe and Na in the vanadate melts did not alter the rate controlling process of oxygen diffusion and oxygen sorption, but it increased the non stoichiometry and hence increased the oxygen diffusion. The rate of corrosion was reported to be affected by temperature, oxygen partial pressure and rotational speed, volume of liquid vanadate, composition of the metal and composition of the liquid vanadates. According to them, Inconel showed better corrosion resistance than stainless steels (Kerby and Wilson, 1973).</p>
High temperature alloys	-----	<p>Vanadate-induced corrosion of high temperature alloys has been studied by thermogravimetry in laboratory furnaces (using a limited amount of vanadate deposit), in burner rigs (where small amounts of vanadates are continually being deposited on the surface), or by immersion of specimens in crucibles with molten salt. The reaction products formed during exposure in laboratory furnaces and in burner rigs were qualitatively the same, but the kinetics and reaction rates were differing considerably. The mechanisms were found to be complex (Beltran and Shores, 1972).</p>
50Cr-50Ni alloy	In pure $V_2O_5$ and sodium vanadates, 750-950°C in a rotating disk apparatus	<p>In pure <math>V_2O_5</math> at 810°C, a <math>Cr_2O_3</math> scale has been observed on the alloy which subsequently got dissolved slowly into the liquid melt and was thus proposed as a barrier layer by them. In case of <math>NV_6</math> this barrier layer was not observed. The increased basic character of the melt and its consequently greater fluxing ability toward acidic oxides was thought to be a more important part process than the increased ionic conductivity of <math>NV_6</math> over <math>V_2O_5</math> at this temperature. At 950°C the corrosion in terms of both dissolution rate and corrosion rate was reportedly greater in <math>V_2O_5</math> than in <math>NV_6</math> (Dooley and Wilson, 1975).</p>
Superalloys	700°C	<p>The relationship of the high temperature corrosion of superalloys with contaminants has been reported by Hancock (1987). It was proposed that to compare contaminant conditions the contaminant flux rate (CFR) rather than the contaminant level in the fuel or environment should be considered. He further suggested that at temperatures above 700°C where vanadates cause fluxing of the protective oxide scales, corrosion could be determined by the CFR and temperature rather than by material selection.</p>

Nickel base superalloy	In air, 700°C	Vanadium, present as vanadium pentoxide, attacked the alloy severely at the temperature of investigation. Study of ternary oxide system and spot tests showed that two low melting eutectics, namely, NiO-V <sub>2</sub> O <sub>3</sub> -Cr <sub>2</sub> O <sub>3</sub> melting at 550°C and V <sub>2</sub> O <sub>3</sub> -Cr <sub>2</sub> O <sub>3</sub> -Fe <sub>2</sub> O <sub>3</sub> melting at 480°C, were formed. The formation of these liquid eutectics and the presence of corrosive V <sub>2</sub> O <sub>5</sub> caused severe damage to the superalloy (Iyer et al, 1987).
Nickel base superalloys Nimonic 80A, Hastelloy C-276 and Superni 600	In air, 923, 973 and 1023 K	The hot corrosion kinetics obeyed a parabolic law with two regions at 973 and 1023 K, the corrosion rate falling with the formation of a solid Ni <sub>3</sub> V <sub>2</sub> O <sub>8</sub> layer. The acid-base fluxing mechanism and a second mechanism by which nickel vanadate was precipitated from a nickel vanadium compound located in the short circuit diffusion path has been assumed to be occurring in the growing oxide. The corrosion rate for these alloys got decreased with the formation of a compact solid vanadate layer (Swaminathan et al, 1993).

**Table A.2** Thermal expansion coefficients of substrate steels, coatings and oxides

Alloy or oxide	Thermal expansion coefficient ( $10^{-6}$ per $^{\circ}\text{C}$ )	Reference
Nimonic 75	11	<a href="http://www.matweb.com/">http://www.matweb.com/</a>
Inconel 600	13.3	
Inconel 601	13.75	
Inconel 718	13	
Incoloy Alloy 800H	14.4	
Co-base superalloys	17	<a href="http://www.lucasmilhaupt.com/">http://www.lucasmilhaupt.com/</a>
NiCrAlY	12.7	Taymaz et al (1999)
Ni-20Cr	17.3	Metal Handbook (1961)
S-816 (Co-Cr-Ni based alloy)	15.98	
Ni <sub>3</sub> Al	18.6	Wang et al (2002)
Al <sub>2</sub> O <sub>3</sub>	8.5	Niranatlumpong et al (2000)
Cr <sub>2</sub> O <sub>3</sub>	8.5	
FeAl <sub>2</sub> O <sub>4</sub>	8.5	
FeCr <sub>2</sub> O <sub>4</sub>	8.5	
NiAl <sub>2</sub> O <sub>4</sub>	8.5	
Fe <sub>2</sub> O <sub>3</sub>	12	Huminik (1963)

**Table A.3 Chemical composition (Wt%) of the Ni- and Fe-based superalloys and coatings powders, and environmental conditions employed**

Midhani Grade (Similar Grade)		Superalloys										Coating Powders			Exposure Time	Environment/ Temperature
		Chemical Composition (Wt%)										Coating powder	Composition (wt %)	Particle size (µm)		
		Fe	Ni	Cr	Ti	Al	Mo	Mn	Si	Cu	Ta					
Superni 75 (Nimonic 75)	3	Bal	19.5	0.3	-	-	-	-	-	-	0.1	Ni-22Cr-10Al-1Y (Praxair NI-343) (also sprayed as a bond coat of around 150 µm, for each coating)	Cr (22), Al (10), Y (1), Ni (bal.)	-45 +10	<ul style="list-style-type: none"> <li>• 50 cycles each cycle of 1 hr heating followed by 20 min. cooling at ambient conditions</li> <li>• Air, 900°C</li> <li>• Air, 900°C after thin coat of Na<sub>2</sub>SO<sub>4</sub> 60% V<sub>2</sub>O<sub>5</sub></li> </ul>	
Superni 600 (Inconel 600)	10 max	Bal	15.5	-	-	-	0.5	-	-	-	0.2	Ni-20Cr (Praxair NI-105)	Ni (80), Cr (20)	-45 +5		
Superni 601 (Inconel 601)	Bal	62	23	-	1.48	-	0.8	0.37	0.1	-	0.025	Stellite-6 (Eu Troloy)	Cr (19), C (0.7), Si (2.3), Fe (3), Ni (13.5), B (1.7), W (7.5), Mn (1 max.), Co (bal.)	-180+53		
Superni 718 (Inconel 718)	18.5	Bal	19	0.9	0.5	3.05	0.18	0.18	0.15	5.13	0.04	Nickel and Aluminum	Stoichiometric ratio 3:1 (Ni:Al) Ni (min. assay 99.99%) and Al (min. assay 99.7%) mixed in laboratory ball mill for 8 hrs	Ni-74 Al- fine powder		
Superfer 800H (Incoloy 800H)	Bal	52	21	0.3	0.3	-	1.5 max	1 max	-	-	0.1 max					

## REFERENCES

---

1. Agarwal, A., Katipelli, L. R. and Dahotre, N. B., (2000), "Elevated Temperature Oxidation of Laser Surface Engineered Composite Boride Coating on Steel," *Metall. Mater. Trans. A*, Vol. 31A, No. 2, pp. 461-473.
2. Almeraya, C. F., Martinez, V. A., Gaona, C., Romero, M.A. and Malo, J.M., (1998A), "Hot Corrosion of the Steel SA213-T22 and SA213-TP347H in 80% V<sub>2</sub>O<sub>5</sub>-20% Na<sub>2</sub>SO<sub>4</sub> Mixture," *Revista de Metalurgia*, Vol. 34, No. 1, pp. 11-17.
3. Almeraya, C. F., Martinez, V. A. and Gonzalez, R. J. G., (1998B), "Electrochemical Studies of Hot Corrosion of Type 347H Stainless Steel," *Brit. Corros. J.*, Vol. 33, No. 4, pp. 288-291.
4. Aoh, J.N. and Chen, J.C., (2001), "On the Wear Characteristics of Cobalt-based Hardfacing Layer after Thermal Fatigue and Oxidation," *Wear*, Vol. 250, pp. 611-620.
5. **ASM Handbook**, (1995), "Metallography and Microstructures," Vol. 9, Sixth Printing, ASM Publication, Metals Park Ohio.
6. Bai, C. Y., Luo, Y. J. and Koo, C. H., (2004), "Improvement of High Temperature Oxidation and Corrosion Resistance of Superalloy IN-738LC by Pack Cementation," *Surf. Coat. Technol.*, Vol. 183, No. 1, 2004, pp. 74-88.
7. Barbooti, M. M., Al-Madfai, S. H. and Nassouri, H. J., (1988), "Thermochemical Studies on Hot Ash Corrosion of Stainless Steel 304 and Inhibition by Magnesium Sulphate," *Thermochimica Acta*, Vol. 126, pp. 43-49.
8. Batchelor, A.W., Lam, L.N. and Chandrasekaran, M, (2003), "Ch. 6: Discrete Coatings," in 'Materials Degradation and its Control by Surface Engineering,' 2<sup>nd</sup> Edition, Imperial College Press.
9. Beltran, A.M. and Shores, D.A., (1972), "Ch. 11: Hot Corrosion," in 'The Superalloys,' Eds. Sims, C.T. and Hagel, W.C., Wiley Publ., John Wiley and Sons, N. Y.
10. Belzunce, F. J., Higuera, V. and Poveda, S., (2001), "High Temperature Oxidation of HFPD Thermal-Sprayed MCrAlY Coatings," *Mater. Sci. & Engg. A-Struct.*, Vol. 297, No. 1-2, pp. 162-167.



11. **Bhusari, M.**, (2001), "Plasma Spray: The Job Shop Perspective," Proc. Inter. Thermal Spray Conf., May 28-30, Singapore, pp. 1289-1297.
12. **Bhushan, B.** and Gupta, B. K. (1991), 'Handbook of Tribology: Materials, Coatings and Surface Treatments,' McGraw-Hill, New York.
13. **Bittel, J.T.**, Sjodahl, L.H. and White, J.F., (1969), "Oxidation of 304L Stainless Steel by Steam and by Air," Corros., Vol. 25, No. 1, pp. 7-14.
14. **Bluni, S.T.** and Mardar, A.R., (1996), "Effects of Thermal Spray Coating Composition and Microstructure on Coating Response and Substrate Protection at High Temperatures," Corros., Vol. 52, No. 3, pp. 213-218.
15. **Bornstein, N. S.** and DeCrescente, M.A., (1969), "Relationship Between Compounds of Sodium and Sulfur and Sulfidation," Met. Soc. AIME-Trans., Vol. 245, No. 9, pp. 1947-1952.
16. **Bornstein, N. S.** and DeCrescente, M.A., (1970), "The Role of Sodium and Sulfur in the Accelerated Oxidation Phenomena-Sulphidation," Corros., Vol. 26, No. 7, pp. 209-214.
17. **Bornstein, N. S.** and DeCrescente, M.A., (1971), "The Role of Sodium in the Accelerated Oxidation Phenomenon termed Sulphidation," Metall. Trans., No.2, pp. 2875-2883.
18. **Bornstein, N.S.**, DeCrescente, M.A. and Roth, H.A., (1973), "The Relationship Between Relative Oxide Ion Content of  $\text{Na}_2\text{SO}_4$ , the Presence of Liquid Metal Oxides and Sulfidation Attack," Metall. Trans., Vol. 4, pp. 1799-1810.
19. **Bornstein, N. S.**, Decrescente, M. A. and Roth, H. A., (1975), "Effect of Vanadium and Sodium Compounds on the Accelerated Oxidation of Nickel Base Alloys," Proc. Conf. on Gas Turbine Mater. in the Marine Environment, MMIC-75-27, Columbus, Ohio, USA, pp. 115-160.
20. **Bourhis, Y.** and John C. St., (1975), " $\text{Na}_2\text{SO}_4$ - and NaCl-Induced Hot Corrosion of Six Nickel-Base Superalloys," Oxid. Met., Vol. 9, No. 6, pp. 507-528.
21. **Brasunas, A. deS.**, (1977), "Ch. 13: Alloy Behaviour at High Temperatures," in 'NACE Basic Corrosion Course,' Pub. NACE, Houston, Texas.
22. **Budinski, K. G.**, (1998), 'Engineering Materials, Properties and Selection,' Pub. Prentice-Hall of India, New Delhi, India.
23. **Bull, S.J.**, (1994), "Microstructural Characterisation of Coatings and Thin Films," Surf. Eng., Pub. ASM Inter., Vol.5, pp.660.

24. **Burakowski, T. and Wierzchon, T.**, (1999), 'Surface Engineering of Metals, Principles, Equipment, Technology,' CRC Press, N. W., Boca Raton, Florida.
25. **Burman, C. and Ericsson, T.**, (1983), "Study of Plasma Sprayed FeCrAlY Coatings after Various Post-Treatments," Proc. Sympos. High-Temperature Protective Coatings, March 7-8, Atlanta, GA, USA, Ed. Singhal, S.C., Pub. Metall. Soc of AIME, Warrendale, PA, USA, pp. 51-59.
26. **Calvarin, G., Molins, R. and Huntz, A. M.**, (2000), "Oxidation Mechanism of Ni-20Cr Foils and its Relation to the Oxide-Scale Microstructure," Oxid. Met., Vol. 53, No. 1-2, pp. 25-48.
27. **Cha, S. C. and Wolpert, P.**, (2003), "High-Temperature Erosion and Corrosion Measurement of Thermally Sprayed Materials," Adv. Eng. Mater., Vol. 5, No.4, pp. 213-217.
28. **Chan, W.Y., Evans, H.E., Ponton, C.B., Nicholls, J.R. and Simms, N.J.**, (2000), "Influence of NiAl<sub>3</sub> on the High Temperature Oxidation of a Plasma-Sprayed Overlay Coating," Mater. High Temp., Vol. 17, No. 2, pp. 173-178.
29. **Chatterjee, U. K., Bose, S. K. and Roy, S. K.**, (2001), 'Environmental Degradation of Metals,' Pub. Marcel Dekker, 270 Madison Avenue, New York.
30. **Chattopadhyay, B. and Wood, G.C.**, (1970), "Transient Oxidation of Alloys" Oxid. Met., Vol 2, No. 4, pp. 373-399.
31. **Chen, H. C., Liu, Z. Y. and Chuang, Y. C.**, (1993), "Degradation of Plasma-Sprayed Alumina and Zirconia Coatings on Stainless Steel During Thermal Cycling and Hot Corrosion," Thin Solid Films, Vol. 223, No. 1, pp. 56-64.
32. **Choi, H., Yoon, B., Kim, H. and Lee, C.**, (2002), "Isothermal Oxidation of Air Plasma Spray NiCrAlY Bond Coatings," Surf. Coat. Technol., Vol. 150, No. 2-3, pp. 297-308.
33. **Chuanxian, C., Bingtang, H. and Huiling, L.**, (1984), "Plasma Sprayed Wear-Resistance Ceramic and Cermet Coating Materials," Thin Solid Films, Vol. 118, No. 4, pp. 485-493.
34. **Coze, L. J., Franzoni, U., Cayla, O., Devisme, A. and Lefort, A.**, (1989), "The Development of High-Temperature Corrosion-Resistant Aluminium-Containing Ferritic Steels," Mater. Sci. Eng. A-Struct., Vol.120, pp. 293-300.

35. **Cuevas-Arteaga, C.**, Porcayo-Calderon, J., Izquierdo, G., Martinez-Villafane, A. and Gonzalez-Rodriguez, J.G., (2001), "Study of Hot Corrosion of Alloy 800 using Linear Polarization Resistance and Weight Loss Measurement," *Mater. Sci. Technol.*, Vol.17, No. 7, pp. 880-885.
36. **Darolia, R.**, (1991), "NiAl Alloys for High-Temperature Structural Applications," *JOM*, March, pp. 44-49.
37. **Das, D.**, Balasubramaniam, R. and Mungole, M. N., (2002), "Hot Corrosion of Fe<sub>3</sub>Al," *J. Mater. Sci.*, Vol. 37, No. 6, pp. 1135-1142.
38. **Deb, D.**, Iyer, S. R. and Radhakrishnan, V. M., (1996), "A Comparative Study of Oxidation and Hot Corrosion of a Cast Nickel Base Superalloy in Different Corrosive Environments," *Mater. Lett.*, Vol. 29, pp. 19-23.
39. **Delaunay, F.**, Berthier, C., Lenglet, M. and Lameille, J. M., (2000), "SEM-EDS and XPS Studies of the High Temperature Oxidation Behaviour of Inconel 718," *Mikrochim. Acta*, Vol. 132, pp 337-343.
40. **DeMasi-Marcin, J. T.** and Gupta, D. K., (1994), "Protective Coatings in the Gas Turbine Engine," *Surf. Coat. Technol.*, Vol. 68-69, pp. 1-9.
41. **Dey, G. K.** and Sekhar, J. A., (1998), "Micropyretic Synthesis of Nickel Aluminides," *T. Indian I. Metals*, Vol. 50, No. 1, pp. 79-89.
42. **Dooley, R. B.** and Wilson, J. R., (1975), "The Corrosion of 50Cr-50Ni Alloy in Liquid Vanadate Systems in the Temperature Range 750-950<sup>0</sup>C," *Trans. ASME*, July, pp. 422-428.
43. **Doychak, J.**, (1995), "Ch. 43: Oxidation Behaviour of High-Temperature Intermetallics," in 'Intermetallic Compounds, Principles and Practice, Vol. 1- Principles,' Eds. Westbrook, J.H. and Fleischer, F.L., Pub. John Wiley & Sons Ltd., England.
44. **Eliasz, N.**, Shemesh, G. and Latanision, R.M., (2002), "Hot Corrosion in Gas Turbine Components," *Eng. Fail. Anal.*, Vol. 9, pp. 31-43.
45. **Elrefaie, F. A.**, Manolescu, A. and Smeltzer, W. W., (1985), "Oxidation Properties of Nickel in the Temperature Range 1073-1500 K," *J. Electrochem. Soc.*, Vol. 132, No. 10, pp. 2489-2493.
46. **Erickson, L. C.**, Westergard, R., Wiklund, U., Axen, N., Hawthorne, H. M. and Hogmark, S., (1998), "Cohesion in Plasma-Sprayed Coatings: A Comparison between Evaluation Methods," *Wear*, Vol. 214, pp. 30-37.

47. **Evans, H. E. and Taylor, M. P.**, (2001), "Diffusion Cells and Chemical Failure of MCrAlY Bond Coats in Thermal-Barrier Coating Systems," *Oxid. Met.*, Vol. 55, No. 1-2, pp. 17-34.
48. **Fairman, L.**, (1962), "Technical Note: Mechanism of Accelerated Oxidation by Vanadium-Containing Fuel Ash," *Corros. Sci.*, Vol. 2, pp. 293-296.
49. **Fauchais, P, Vardelle, A. and Vardelle, M.**, (1991), 'Modelling of Plasma Spraying of Ceramic Films and Coatings,' Ed. Vinenzini, Pub. Elsevier State Publishers B.V.
50. **Fauchais, P., Coudert, J. F. and Vardelle, M.**, (1997), "Transient Phenomena in Plasma Torches and in Plasma Sprayed Coating Generation," *J. De Physique IV*, Vol. 7, pp. C4-187-198.
51. **Fauchais, P, Vardelle, A. and, Dussoubs, B.**, (2001), "Quo Vadis Thermal Spray," *J. Therm. Spray Technol*, Vol. 10, No. 1, pp. 44-46.
52. **Fauchais, P, Fukumoto, M., Vardelle, A. and Vardelle, M.**, (2004A), "Knowledge Concerning Splat Formation: An Invited Review," *J. Therm. Spray Technol*, Vol. 13, No. 3, pp 337-360.
53. **Fauchais, P.**, (2004B), "Topical Review: Understanding Plasma Spraying," *J. Phys. D: Appl. Phys.*, Vol. 37, pp. R86-R108.
54. **Fryburg, G. C., Kohl, F. J., Stearns, C. A. and Fielder, W. L.**, (1982), "Chemical Reactions Involved in the Initiation of Hot Corrosion of B-1900 and NASA-TRW VIA," *J. Electrochem. Soc.*, Vol. 129, No. 3, pp. 571-585.
55. **Fryburg, G. C., Kohl, F. J. and Stearns, C. A.**, (1984), "Chemical Reactions Involved in the Initiation of Hot Corrosion of IN-738," *J. Electrochem. Soc.*, Vol. 131, No. 12, pp. 2985-2996.
56. **Gesmundo, F. and Viani, F.**, (1988), "The Mechanism of Low-Temperature Corrosion of Pure Iron and Manganese at 600-800°C," *Mater. Chem. Phys.*, Vol. 20, pp.513-528.
57. **Gill, B. J. and Tucker, R. C. Jr.**, (1986), "Plasma Spray Coating Processes," *Mater. Sci. Technol.*, Vol. 2, No. 3, pp. 207-213.
58. **Gitanjaly and Prakash, S.**, (1999), "Review on Effect of Additives on the Hot Corrosion," 5<sup>th</sup> NACE Proc., New Delhi, India, 22-24<sup>th</sup> Nov., pp. 174-182.
59. **Gitanjaly, Prakash, S. and Singh, S.**, (2002), "Effects of MgO and CaO on Hot Corrosion of Fe Base Superalloy Superfer 800H in Na<sub>2</sub>SO<sub>4</sub>-60%V<sub>2</sub>O<sub>5</sub> Environment," *Brit. Corros. J.*, Vol. 37, No. 1, pp. 56-62.

60. **Gitanjaly**, (2003), 'Role of Inhibitors on Hot Corrosion of Superalloys in  $\text{Na}_2\text{SO}_4\text{-V}_2\text{O}_5$  Environment,' Ph.D. Thesis, Met. Mat. Engg. Deptt., Indian Institute of Technology Roorkee, Roorkee, India.
61. **Godlewski**, K. and **Godlewska**, E., (1987), "The Effect of Chromium on the Corrosion Resistance of Aluminide Coatings on Nickel and Nickel-Based Substrates," *Mater. Sci. Eng.*, Vol. 88, pp. 103-109.
62. **Goebel**, J. A. and **Pettit**, F. S., (1970A), " $\text{Na}_2\text{SO}_4$  - Induced Accelerated Oxidation (Hot Corrosion) of Nickel," *Metall. Trans.*, Vol. 1, pp. 1943-1954.
63. **Goebel**, J. A. and **Pettit**, F. S., (1970B), "The Influence of Sulphides on the Oxidation Behaviour of Nickel-base Alloys," *Metall Trans*, Vol.1, pp.3421-3429.
64. **Goebel**, J. A., **Pettit**, F. S. and **Goward**, G. W., (1973), "Mechanisms for the Hot Corrosion of Nickel-Base Alloys," *Metall. Trans.*, Vol. 4, pp. 261-275.
65. **Goward**, G.W., (1998), "Progress in Coatings for Gas Turbine Airfoils," *Surf. Coat. Technol.*, Vol. 108-109, pp.73-79.
66. **Greene**, G.A. and **Finfrock**, C.C., (2001), "Oxidation of Inconel 718 in Air at High Temperatures," *Oxid. Met.*, Vol. 55, No. 5-6, pp. 505-521.
67. **Gu**, Y.W., **Khor**, K.A., **Fu**, Y.Q. and **Wang**, Y., (1997), "Functionally Graded  $\text{ZrO}_2\text{-NiCrAlY}$  Coatings Prepared by Plasma Spraying using Pre-Mixed, Spheroidized Powders," *Surf. Coat. Technol.*, Vol. 96, No. 2-3, pp 305-312.
68. **Guilemany**, J. M., **Fernandez**, J., **Delgado**, J., **Benedetti**, A. V. and **Climent**, F., (2002), "Effects of Thickness Coating on the Electrochemical Behaviour of Thermal Spray  $\text{Cr}_3\text{C}_2\text{-NiCr}$  Coatings," *Surf. Coat. Technol.*, Vol. 153, No. 2-3, pp. 107-113.
69. **Gupta**, N., (2003), "Technical Talk on Cathodic Protection," *IIM Metal News*, Vol. 16, No. 1, pp. 38.
70. **Gurrappa**, I., (1999), "Hot Corrosion Behavior of CM 247 LC Alloy in  $\text{Na}_2\text{SO}_4$  and  $\text{NaCl}$  Environments," *Oxid. Met.*, Vol. 51, No. 5, pp. 353-382.
71. **Gurrappa**, I., (2001), "Identification of Hot Corrosion Resistant  $\text{MCrAlY}$  Based Bond Coatings for Gas Turbine Engine Applications," *Surf. Coat. Technol.*, Vol. 139, No. 2-3, pp. 272-283.
72. **Hamner**, N. E., (1977), "Ch. 14: Coatings for Corrosion Protection," in 'NACE Basic Corros. Course,' Houston, Texas.

73. **Hampikian, J. M. and Potter, D. I., (1992),** "The Effects of Yttrium Ion Implantation on the Oxidation of Nickel-Chromium Alloys. II. Oxidation of Yttrium Implanted Ni-20Cr," *Oxid. Met.*, Vol. 38, No. 1-2, pp. 139-159.
74. **Han, Y.F., Xing, Z.P., Chaturvedi, M.C. and Xu, Q., (1997),** "Oxidation Resistance and Microstructure of Ni-Cr-Al-Y-Si Coating on Ni<sub>3</sub>Al Based Alloy," *Mater. Sci. Eng. A-Struct.*, Vol. 239, pp. 871-876.
75. **Hancock, P. and Hurst R.C., (1974),** "The Mechanical Properties and Breakdown of Surface Oxide Films at Elevated Temperatures," in 'Advances in Corrosion Science and Technology,' Vol.4, Eds. Fontana, M.G. and Staehle, R.W., Pub. Plenum Press, New York.
76. **Hancock, P., (1987),** "Vanadic and Chloride Attack of Superalloys," *Mater. Sci. Technol.*, Vol. 3, pp. 536-544.
77. **Hara, M., Hisaichi, T., Itoh, K. and Shinata, Y., (1991),** "Effects of SO<sub>3</sub>, SO<sub>2</sub> and O<sub>2</sub> Gasses on Hot Corrosion of Ni and Ni-Cr Alloys in Molten Na<sub>2</sub>SO<sub>4</sub>," *J. Jpn. I. Met.*, Vol. 55, No. 11, pp. 1207-1215.
78. **Harris, G.T., Child, H.C. and Kerr, J.A., (1955),** "Effect of the Composition of Gas-Turbine Alloys on Resistance to Scaling and to Vanadium Pentaoxide Attack," *ISIJ Int.*, Vol. 179, pp. 342-347.
79. **Haugrud, R., (2001),** "On the High-Temperature Oxidation of Fe, Co, Ni and Cu-based Alloys with Addition of a Less Noble Element," *Mater. Sci. Eng. A-Struct.*, Vol. 298, pp. 216-226.
80. **Haugrud, R., (2003),** "On the High-Temperature Oxidation of Nickel," *Corros. Sci.*, Vol. 45, No.1, pp.211-235.
81. **He, Y., Huang, Z., Qi, H., Wang, D., Li, Z. and Gao, W., (2000),** "Oxidation Behaviour of Micro-Crystalline Ni-20Cr-Y<sub>2</sub>O<sub>3</sub> ODS Alloy Coatings," *Mater. Lett.*, Vol. 45, pp. 79-85.
82. **He, J. L., Chen, K. C., Chen, C. C., Leyland, A. and Matthews, A., (2001),** "Cyclic Oxidation Resistance of Ni-Al Alloy Coatings Deposited on Steel by a Cathodic Arc Plasma Process," *Surf. Coat. Technol.*, Vol. 135, pp. 158-165.
83. **Heath, G. R., Heimgartner, P., Irons, G., Miller, R. and Gustafsson, S., (1997),** "An Assessment of Thermal Spray Coating Technologies for High Temperature Corrosion Protection," *Mater. Sci. Forum*, Vol. 251-54, pp. 809-816.

84. **Hidalgo, V. H., Varela, F. J. B. and Rico, E. F., (1997),** "Erosion Wear and Mechanical Properties of Plasma-Sprayed Nickel- and Iron-Based Coatings Subjected to Service Conditions in Boilers," *Trib. Int.*, Vol. 30, No. 9, pp. 641-649.
85. **Hidalgo, V. H., Varela, F. J. B. and Menendez, A. C., (1998),** "Characterization and High Temperature Behaviour of Thermal Sprayed Coatings Used in Boilers," *Proc. 15<sup>th</sup> Int. Thermal Spray Conf.*, May 25-29, Nice, France, pp. 617-621.
86. **Hidalgo, V. H., Varela, F. J. B., Martinez, S.P. and Espana, S. G., (1999),** "Characterization and High Temperature Behaviour of Cr<sub>3</sub>C<sub>2</sub>-NiCr Plasma Sprayed Coatings," *Proc. United Thermal Spray Conf.*, Germany, pp. 683-686.
87. **Hidalgo, V. H., Varela, J. B., Calle, J. M. de la and Menendez, A. C., (2000),** "Characterisation of NiCr Flame and Plasma Sprayed Coatings for Use in High Temperature Regions of Boilers," *Surf. Eng.*, Vol. 16, No. 2, pp. 137-142.
88. **Hocking, M. G., (1993A),** "Coatings Resistant to Erosive/Corrosive and Severe Environments," *Surf. Coat. Technol.*, Vol. 62, pp. 460-466.
89. **Hocking, M. G., (1993B),** "Hot Corrosion of Coatings for Superalloys," *I. O. M., Conf.*
90. **Hodgkiess, T. and Neville, A., (1998),** "An Analysis of Environmental Factors Affecting Corrosion Behavior of Thermal Spray Cermet Coatings," *Proc. of 15<sup>th</sup> Inter. Thermal Spray Conf.*, 25-29<sup>th</sup> May, Nice, France, Vol. 1, pp. 63-68.
91. **Hou, P. Y. and Stringer, J., (1988),** "The Influence of Ion-Implanted Yttrium on the Selective Oxidation of Chromium in Co-25wt.% Cr," *Oxid. Met.*, Vol. 29, No. 1-2, pp. 45-73.
92. **Hsu, I. C. and Wu, S. K., (1997),** "Oxidation Improvement of Ti-48Al-2Cr-2Nb Intermetallics by Air Plasma Sprayed ZrO<sub>2</sub>-Ni-4.5wt%Al Coatings," *Surf. Coat. Technol.*, Vol. 90, pp. 6-13.
93. **Huminik, J., (1963),** 'High-Temperature Inorganic Coatings,' Reinhold Pub. Corp., New York.
94. **Hussain, N., Shahid, K.A., Khan, I.H. and Rahman, S., (1994),** "Oxidation of High-Temperature Alloys (Superalloys) at Elevated Temperatures in Air: I," *Oxid. Met.*, Vol. 41, No. 3-4, pp. 251-269.
95. **Hwang, Y. S. and Rapp, R. A., (1989),** "Thermochemistry and Solubilities of Oxides in Sodium Sulfate-Vanadate Solutions," *Corros.*, Vol. 45, No. 11, pp. 933-937.

96. **Illavsky, J., Pisacka, J., Chraska, P., Margandant, N., Siegmann, S., Wagner, W., Fiala, P. and Barbezat, G.,** (2000), "Microstructure-Wear and Corrosion Relationships for Thermally Sprayed Metallic Deposits," Proc. 1<sup>st</sup> Inter. Thermal Spray Conf., Montreal, Quebec, Canada, May 8-11, pp. 449-454.
97. **Iyer, S. R., Iyer, K. J. L. and Radhakrishnan, V. M.,** (1987), "High Temperature Corrosion of a Ni-Base Superalloy by Vanadium," Proc. of 10<sup>th</sup> ICMC, Madras, India, Vol. IV, pp. 3665-3670.
98. **Johnson, D. M., Whittle, D. P. and Stringer, J.,** (1978), "The Hot Corrosion of Directionally Solidified Ni-Cr-Nb-Al ( $\gamma/\delta$ ) Eutectic Alloys," Oxid. Met., Vol. 12, No. 3, pp. 273-291.
99. **Kai, W., Chang, M.T., Liu, C.D., Chiang, D.L. and Chu, J.P.,** (2002), "The High-Temperature Corrosion of Fe-28Al Base Alloys Containing Cr and Y Additions in H<sub>2</sub>/H<sub>2</sub>S/H<sub>2</sub>O Mixed Gases," Mater. Sci. Eng. A-Struct., Vol. 329-331, pp. 734-744.
100. **Kawahara, Y.,** (1997), "Development and Application of High Temperature Corrosion-Resistant Materials and Coatings for Advanced Waste-to-Energy Plants," Mater. High Temp., Vol.14, No. 3, pp. 261-268.
101. **Kerby, R. C. and Wilson J. R.,** (1973), "Corrosion of Metals by Liquid Vanadium Pentoxide and the Sodium Vanadates," Trans. ASME, January, pp. 36-44.
102. **Khalid, F.A., Hussain, N. and Shahid, K.A.,** (1999), "Microstructure and Morphology of High Temperature Oxidation in Superalloys," Mater. Sc. & Eng. A- Struct., Vol. 265, pp.87-94.
103. **Khanna, A. S. and Jha, S. K.,** (1998), "Degradation of Materials Under Hot Corrosion Conditions," T. Indian I. Metals, Vol. 51, No. 5, pp. 279-290.
104. **Knotek, O.,** (2001), "Chapter 3: Thermal Spraying and Detonation Spray Gun Processes," in 'Handbook of Hard Coatings: Deposition Technologies, Properties and Applications,' Ed. Bunshah, R. F., Noyes Pub. Park Ridge, New Jersey, U. S. A./William Andrew Publishing, LLC, Norwich, New York, U.S.A., pp. 77-107.
105. **Koch, G. H., Brongers, M. P. H., Thompson, N. G., Virmani, Y. P. and Payer, J. H.,** (2002), "Historic Congressional Study: Corrosion Costs and Preventive Strategies in the United States," Supplement to Mater. Perfor., July, pp. 1-11.
106. **Kofstad, P.** (1966), "Ch.1: General Introduction" in 'High Temperature Oxidation of Metals,' John Wiley & Sons Inc. USA.



107. Kofstad, P., (1988), "Chapter 14" in 'High Temperature Corrosion,' Elsevier Applied Science, London & New York, pp. 465.
108. Kolta, G. A., Hewaidy, L. F. and Felix, N. S., (1972), "Reactions Between Sodium Sulphate and Vanadium Pentoxide," *Thermochim. Acta*, Vol. 4, pp. 151-164.
109. Kuiry, C., Seal, S., Bose, S. K. and Roy, S. K., (1994), "Effect of Surface Preparation on the High-Temperature Oxidation Behaviour of AISI 316 Stainless Steel," *ISIJ Int.*, Vol. 34, No. 7, pp. 599-606.
110. Kumar, K. S. and Liu, C. T., (1993), "Ordered Intermetallic Alloys. II. Silicides, Trialuminides, and Others," *JOM*, Vol. 45, No. 6, pp. 28-34.
111. Kwok, C. T., Cheng, F. T. and Man, H. C., (2001), "Laser-Fabricated Fe-Ni-Co-Cr-B Austenitic Alloy on Steels. Part I. Microstructures and Cavitation Erosion Behaviour," *Surf. Coat. Technol.*, Vol. 145, pp. 194-205.
112. La, P., Bai, M., Xue, Q. and Liu, W., (1999), "A Study of Ni<sub>3</sub>Al Coating on Carbon Steel Surface via the SHS Casting Route," *Surf. Coat. Technol.*, Vol. 113, pp. 44-51.
113. Lai, G. Y., (1990), 'High Temperature Corrosion of Engineering Alloys,' ASM Inter. Book, pp. 15-46.
114. Lambert, P., Champagne, B. and Arseneault, B., (1991), "Oxidation and Hot Corrosion in Na<sub>2</sub>SO<sub>4</sub>-10%V<sub>2</sub>O<sub>5</sub> of Ni-17Cr-6Al-0.5Y and Ni-16Cr-5.7Al-0.47Y-5Si, MCrAlY Alloys at 700°C," *Can. Metall. Quart.*, Vol. 30, No. 2, pp. 125-130.
115. Lee, S.Y. and McNallan, M.J., (1990), "Inhibition of Oxidation of Iron in Environments Containing Chlorine at 1100 and 1200 K," *J. Electrochem. Soc.*, Vol. 137, No. 2, pp. 472-479.
116. Lee, W. H. and Lin, R. Y., (2002), "Hot Corrosion Mechanism of Intermetallic Compound Ni<sub>3</sub>Al," *Mater. Chem. Phys.*, Vol. 77, pp. 86-96.
117. Levy, M., Huie, R. and Pettit, F., (1989), "Oxidation and Hot Corrosion of Some Advanced Superalloys at 1300 to 2000°F (704 to 1093°C)," *Corros.*, Vol. 45, No. 8, pp. 661-674.
118. Li, B. and Gleeson, B., (2004), "Effects of Minor Elements on the Cyclic Oxidation Behavior of Commercial Fe-Base 800-Series Alloys," *Oxid. Met.*, Vol. 62, No. 1-2, pp. 45-69.

119. Li, C. L., Zhao, H. X., Matsumura, M., Takahashi, T., Asahara, M. and Yamaguchi, H., (2000), "The Effect of NiCr Intermediate Layer on Corrosion Behavior of Cr<sub>2</sub>O<sub>3</sub> Ceramic Coated Materials," *Surf. Coat. Technol.*, Vol. 124, pp. 53-60.
120. Li, L., Zhu, R. and Gesimundo, F., (1996), "Hot Corrosion of Iron in the Presence of Salt Mixture Deposit containing NaCl and V<sub>2</sub>O<sub>5</sub> at 600°C," *J. Mater. Sci. Technol.*, Vol. 12, No. 6, pp. 445-451.
121. Li, M. H., Sun, X. F., Li, J. G., Zhang, Z. Y., Jin, T., Guan, H.R. and Hu, Z. Q., (2003A), "Oxidation Behaviour of a Single-Crystal Ni-Base Superalloy in Air-I: At 800 and 900°C," *Oxid. Met.*, Vol. 59, No. 5-6, pp.591-605.
122. Li, M. H., Sun, X. F., Jin, T., Guan, H.R. and Hu, Z.Q., (2003B), "Oxidation Behaviour of a Single-Crystal Ni-Base Superalloy in Air-II: At 1000, 1100, and 1150°C," *Oxid. Met.*, Vol. 60, No.1-2, pp.195-210.
123. Li, M. H., Zhang, Z. Y., Sun, X. F., Li, J. G., Yin, F. S., Hu, W. Y., Guan, H. R. and Hu, Z. Q., (2003C), "Oxidation Behaviour of Sputter-Deposited NiCrAlY coating," *Surf. Coat. Technol.*, Vol. 165, No. 3, pp. 241-247.
124. Li, Y., Yuan, C., Guo, J. T. and Yang, H. C., (2003), "Oxidation Kinetics of Cast Ni-Base Superalloy K35," *J. Northeastern Uni.*, Vol. 24, No. 1, pp. 75-78.
125. Liang, G. Y., Wong, T. T., MacAlpine, J. M. K. and Su, J. Y., (2000), "Study of Wear Resistance of Plasma-Sprayed and Laser-Remelted Coatings on Aluminium Alloy," *Surf. Coat. Technol.*, Vol. 127, No. 2, pp. 233-238.
126. Liao, H., Normand, B. and Coddet, C., (2000), "Influence of Coating Microstructure on the Abrasive Wear Resistance of WC/Co Cermet Coatings," *Surf. Coat. Technol.*, Vol. 124, pp. 235-242.
127. Link, R. J., Birks, N., Pettit, F. S. and Dethorey, F., (1998), "The Response of Alloys to Erosion-Corrosion at High Temperatures," *Oxid. Met.*, Vol. 49, No. 3-4, pp. 213-236.
128. Liu, P. S., Liang, K. M., Zhou, H. Y., Gu, S. R., Sun, X. F., Guan, H. R., Jin, T. and Yang, K. N., (2001), "Cyclic Oxidation Behavior of Aluminide Coatings on the Co-Base Superalloy DZ40M," *Surf. Coat. Technol.*, Vol. 145, pp. 75-79.
129. Liu, Z., Gao, W., Dahm, K. L. and Wang, F., (1998), "Oxidation Behaviour of Sputter-Deposited Ni-Cr-Al Micro-Crystalline Coatings," *Acta Mater.*, Vol. 46, No. 5, pp. 1691-1700.

130. Liu, Z. and Gao, W., (2001), "Oxidation Behaviour of Cast Ni<sub>3</sub>Al Alloys and Microcrystalline Ni<sub>3</sub>Al + 5% Cr Coatings with and without Y Doping," *Oxid. Met.*, Vol. 55, No. 5-6, pp. 481-504.
131. Longa-Nava and Takemoto, M., (1992), "High-Temperature Corrosion of Laser-Glazed Alloys in Na<sub>2</sub>SO<sub>4</sub>-V<sub>2</sub>O<sub>5</sub>," *Corros.*, Vol. 48, No. 7, pp. 599-607.
132. Longa-Nava, Y., Zhang, Y. S., Takemoto, M. and Rapp, R. A., (1996), "Hot Corrosion of Nickel-Chromium and Nickel-Chromium-Aluminum Thermal-Spray Coatings by Sodium Sulfate-Sodium Metavanadate Salt," *Corros.*, Vol. 52, No. 9, pp. 680-689.
133. Lovelock, H. L. de V., Kinds, J. and Young, P. M., (1998), "Characterisation of WC-12Co Thermal Spray Powders and HPHVOF Wear Resistant Coatings," *Powder Metall.*, Vol. 41, No. 4, pp. 292-299.
134. Lu, Y., Chen, W. and Eadie, R., (2004), "Evaluation of High Temperature Corrosion Resistance of a Ni<sub>3</sub>Al (Mo) Alloy," *Intermetallics*, Vol. 12, pp. 1299-1304.
135. Luthra, K. L. and Shores, D.A., (1980), "Mechanism of Na<sub>2</sub>SO<sub>4</sub> Induced Corrosion at 600-900 °C," *J. Electrochem. Soc.*, Vol. 127, No. 10, pp. 2202-2210.
136. Luthra, K. L. and Spacil, H.S., (1982), "Impurity Deposits in Gas Turbines from Fuels Containing Sodium and Vanadium," *J. Electrochem. Soc.*, Vol.129, No. 3, pp. 649-656.
137. Luthra, K. L., (1982), "Low Temperature Hot Corrosion of Cobalt-Base Alloys: Part I. Morphology of the Reaction Product," *Metall. Trans. A*, Vol. 13A, pp.1843-1852.
138. Luthra, K. L., (1983), "Mechanisms of Low Temperature Hot Corrosion," in 'High Temperature Corrosion,' Houston, NACE, Ed. Rapp, R.A., pp. 507-518.
139. Luthra, K. L., (1985), "Kinetics of the Low Temperature Hot Corrosion of Co-Cr-Al Alloys," *J. Electrochem. Soc.*, Vol. 132, No. 6, pp. 1293-1298.
140. Malik, A. U. and Ahmad, S., (1983), "Na<sub>2</sub>SO<sub>4</sub>-Induced Corrosion of Some Nimonic Alloys at 650 to 1000°C," *Metallkd.*, Vol. 74, No. 12, pp. 819-824.
141. Malik, A. U. and Mobin, M., (1987), "Studies on Some Solid State Reactions Relevant to Hot Corrosion," *Proc. of 10<sup>th</sup> ICMC, Madras, India, Vol. IV*, pp. 3345-3365.

142. **Malik, A.U., Asrar, N., Ahmad, S. and Siddiqi, N. A. B.,** (1988), "Hot Corrosion Behaviour of Some Industrially Important Nickel-base Alloys in Presence of  $\text{Na}_2\text{SO}_4(\text{S})$  and  $\text{NaCl}(\text{S})$ ," *Metallkd.*, Vol. 79, No.5, pp. 285-295.
143. **Malik, A. U., Ahmad, R., Ahmad, S. and Ahmad S.,** (1992), "High Temperature Oxidation Behaviour of Nickel Aluminide Coated Mild Steel," *Practical Metallography*, Vol. 29, pp. 255-268.
144. **Margadant, N., Siegmann, S., Patscheider, J., Keller, T., Wagner, W., Ilavsky, J., Pisacka, J., Barbezat, G. and Fiala, P.,** (2001), "Microstructure - Property Relationships and Cross-Property-Correlations of Thermal Sprayed Ni-Alloy Coatings," *Proc. Inter. Thermal Spray Conference*, May 28-30, Singapore, pp. 643-652.
145. **Matsuura, K., Ohsasa, K., Sueoka, N. and Kudoh, M.,** (1999), "Nickel Monoaluminide Coating on Ultralow-Carbon Steel by Reactive Sintering," *Metall. Mater. Trans. A*, Vol. 30A, pp. 1605-1611.
146. **Mazar, P., Maresse, D. and Lopvet, C.,** (1986), 'High Temperature Alloys for Gas Turbines,' Eds. Betz, M. et al, Pub. Dordrecht, Netherlands, D. Reidel Publishing Co., pp. 1183-1192.
147. **McCarron, R. L., Lindblad, N. R. and Chatterji, D.,** (1976), "Environment Resistance of Pure and Alloyed  $\gamma'$ - $\text{Ni}_3\text{Al}$  and  $\beta$ - $\text{NiAl}$ ," *Corros.*, Vol. 32, No. 12, pp. 476-481.
148. **Metals Handbook,** (1961), "Properties and Selection of Metals, 8<sup>th</sup> Edition," Vol.1, ASM Publication, Metals Park Ohio.
149. **Metals Handbook,** (1972), 'Atlas of Microstructures of Industrial Alloys,' Vol. 7, ASM Publication, Metals Park OH, USA.
150. **Metals Handbook,** (1975), 'Failure analysis and Prevention,' Vol.10, ASM Publication, Metals Park OH, USA.
151. **Misra, A. K.,** (1986), "Mechanism of  $\text{Na}_2\text{SO}_4$ -Induced Corrosion of Molybdenum Containing Nickel-Base Superalloys at High Temperatures," *J. Electrochem. Soc.*, Vol. 133, No. 5, pp. 1029-1037.
152. **Misra, A.K.,** (1987), " $\text{Na}_2\text{SO}_4$ -Induced Corrosion of Pure Nickel and Superalloy Udimet 700 in a High Velocity Burner Rig at  $900^\circ\text{C}$ ," *Corros. NACE*, Vol. 43, No. 7, pp. 440-449.

153. **Mobin, M., Malik, A. U., Ahmad, S., Hasan, S. K. and Ajmal, M.,** (1996), "Studies on the Interactions of Metal Oxides and  $\text{Na}_2\text{SO}_4$  at 1100 and 1200 K in Oxygen," *Bull. Mater. Sci.*, Vol. 19, No. 5, pp. 807-821.
154. **Nanni, P., Buscaglia, V., Asmundis, C. D. and Roy, S. K.,** (1987), "Sodium Sulphate Induced Hot Corrosion of Pure Fe, Mn and Cr in Combustion Gas," *Proc. of 10<sup>th</sup> ICMC, Madras, India, Vol. IV*, pp. 3413-3422.
155. **Natesan, K.,** (1976), "Corrosion-Erosion Behavior of Materials in a Coal-Gasification Environment," *Corros.*, Vol. 32, No. 9, pp. 364-370.
156. **Natesan, K.,** (1985), "High-Temperature Corrosion in Coal Gasification Systems," *Corros.*, Vol. 41, No. 11, pp. 646-655.
157. **Natesan, K.,** (1988), "Oxidation-Sulfidation Behavior of Ni Aluminide in Oxygen-Sulfur Mixed-Gas Atmospheres," *Oxid. Met.*, Vol. 30, No. 1-2, pp. 53-83.
158. **Natesan, K.,** (1993), "Applications of Coatings in Coal-Fired Energy Systems," *Surf. Coat. Technol.*, Vol. 56, pp. 185-197.
159. **National Materials Advisory Board,** (1996), "Coatings for High-Temperature Structural Materials: Trends and Opportunities," *National Academy Press Washington D.C.*, <http://www.nap.edu/openbook/0309053811/html>, pp 1-85.
160. **Nicholls, J. R. and Hancock, P.,** (1989), in 'The Role of Active Elements in the Oxidation of High Temperature Metals and Alloys,' Ed. Lang, E., Elsevier Applied Science, London, pp. 195.
161. **Nicholls, J. R. and Stephenson, D.J.,** (1995), "Ch. 22: High-Temperature Coatings for Gas Turbines," in 'Intermetallic Compounds, Principles and Practice, Vol. 2-Practice,' Eds. Westbrook, J.H. and Fleischer, F.L., Pub. John Wiley & Sons Ltd., England.
162. **Nicholls, J.R.,** (2000), "Designing Oxidation-Resistant Coatings," *JOM*, January, pp. 28-35.
163. **Nickel, H., Quadackers, W. J. and Singheiser, L.,** (2002), "Analysis of Corrosion Layers on Protective Coatings and High Temperature Materials in Simulated Service Environments of Modern Power Plants Using SNMS, SIMS, SEM, TEM, RBS and X-ray Diffraction Studies," *Anal. Bioanal. Chem.*, Vol. 374, pp. 581-587.
164. **Nicoll, A. R. and Wahl, G.,** (1983), "The Effect of Alloying Additions on M-Cr-Al-Y Systems-An Experimental Study," *Thin Solid Films*, Vol. 95, pp. 21-34.

165. **Nicoll, A. R.**, (1984), "Chapter 13: The Production and Performance Evaluation of High Temperature Coatings," in 'Coatings and Surface Treatment for Corrosion and Wear Resistance,' Eds. Strafford, K. N., Datta, P. K. and Googan, C. G., (1984), Institution of Corros. Sci. and Technol., Birmingham, Pub. Ellis Horwood Ltd., Chichester.
166. **Nicoll, A. R.**, Gruner, H., Wuest, G. and Keller, S., (1986), "Future Developments in Plasma Spray Coating," *Mater. Sci. Technol.*, Vol. 2, No. 3, pp. 214-219.
167. **Niranatlumpong, P.**, Ponton, C. B. and Evans, H. E., (2000), "The Failure of Protective Oxides on Plasma-Sprayed NiCrAlY Overlay Coatings," *Oxid. Met.*, Vol. 53, No. 3-4, pp. 241-258.
168. **Nishimura, C.** and Liu, C. T., (1993), "Reactive Sintering of Ni<sub>3</sub>Al Under Compression," *Acta. Metall. Mater.*, Vol. 41, No. 1, pp. 113-120.
169. **Niu, Y.**, Gesmundo, F., Viani, F. and Wu, W., (1994), "The Corrosion of Ni<sub>3</sub>Al in a Combustion Gas with and without Na<sub>2</sub>SO<sub>4</sub>-NaCl Deposits at 600-800<sup>o</sup>C," *Oxid. Met.*, Vol. 42, No. 3-4, pp. 265-283.
170. **Okafor, I. C. I.** and Reddy, R. G., (1999), "Oxidation Behaviour of High-Temperature Aluminides," *JOM*, Vol. 51, No. 6, pp. 35-39, 47.
171. **Osma, A.**, Kayali, E.S. and Ovecoglu, M.L., (1996), "The Effect of Elevated Temperature and Silicon Addition on a Cobalt-Based Wear Resistant Superalloy," *J. of Mater. Sci.*, Vol. 31, No. 17, pp. 4603-4608.
172. **Otero, E.**, Merino, M. C., Pardo, A., Biezma, M. V. and Buitrago, G., (1987), "Study on Corrosion Products of IN657 Alloy in Molten Salts," *Proc. of 10<sup>th</sup> ICMC, Madras, India*, Vol. IV, pp. 3583-3591.
173. **Otero, E.**, Pardo, A., Hernaez, J. and Perez, F. J., (1990), "The Hot Corrosion of IN-657 Superalloy in Na<sub>2</sub>SO<sub>4</sub>-V<sub>2</sub>O<sub>5</sub> Melt Eutectic," *Corros. Sci.*, Vol. 30, pp. 677-683.
174. **Otero, E.**, Pardo, A., Hernaez, J. and Perez, F. J., (1992), "The Corrosion of Some Superalloys (At 1000 K) in Molten Eutectic Mixture 60% V<sub>2</sub>O<sub>5</sub>-40% Na<sub>2</sub>SO<sub>4</sub>: The Influence of the Oxygen and Carbon Residues," *Corros. Sci.*, Vol. 34, pp. 1747-1757.
175. **Otsuka, N.** and Rapp, R.A., (1990), "Effects of Chromate and Vanadate Anions on the Hot Corrosion of Preoxidized Ni by a Thin Fused Na<sub>2</sub>SO<sub>4</sub> Film at 900<sup>o</sup>C," *J. Electrochem. Soc.*, Vol. 137, No. 1, pp. 53-60.

176. **Pandey, J. L.**, (1983), "Effect of Zirconium and Yttrium Alloying on High Temperature Oxidation of Fe-15wt%Cr-4wt%Al," University of Roorkee, Dept. of Chemistry, Roorkee, India.
177. **Pantony, D.A. and Vasu, K. I.**, (1968A), "Studies in the Corrosion of Metals under Melts-I," *J. Inorg. Nucl. Chem.*, Vol. 10, pp. 423-432.
178. **Pantony, D.A. and Vasu, K.I.**, (1968B), "Studies in the Corrosion of Metals under Melts-III," *J. Inorg. Nucl. Chem.*, Vol. 10, pp. 755-779.
179. **Paul, L. D. and Seeley, R. R.**, (1991), "Oil Ash Corrosion- A Review of Utility Boiler Experience," *Corros.*, Vol. 47, No. 2, pp. 152-159.
180. **Pehkonen, A., Tikkanen, M. H., Ylasaari, S. and Forsen, O.**, (1987), "Behaviour of Some Super Alloys in Different High Temperature Atmospheres," *Proc. of 10<sup>th</sup> ICMC, Madras, India, Vol. IV*, pp. 3781-3787.
181. **Peters, K. R., Whittle, D. P. and Stringer, J.**, (1976), "Oxidation and Hot Corrosion of Nickel-Based Alloys Containing Molybdenum," *Corros. Sci.*, Vol. 16, pp. 791-804.
182. **Pettit, F. S. and Meier, G. H.**, (1985), "Oxidation and Hot corrosion of Superalloys," *Superalloys 85*, Eds. Gell, M., Kartovich, C. S., Bricknel, R. H., Kent W. B. and Radovich, J. F., *Met. Soc. of AIME, Warrendale, Pennsylvania*, pp. 651-687.
183. **Pettit, F. S. and Giggins, C. S.**, (1987), "Hot Corrosion, Ch. 12," in 'Superalloys II,' Eds. Sims, C. T., Stoloff, N. S. and Hagel, W. C., *Pub. Wiley Pub., N. Y.*
184. **Pfender, E.**, (1988), "Fundamental Studies Associated with the Plasma Spray Process," *Surf. Coat. Technol.*, Vol. 34, pp. 1-14.
185. **Polman, E.A., Fransen, T. and Gellings, P.J.**, (1990), "High-Temperature Corrosion and Mechanical Properties of Protective Scales on Incoloy 800H: The Influence of Preoxidation and Ion Implantation," *Oxid. Met.*, Vol. 33, No. 1-2, pp. 135-155.
186. **Porcayo-Calderon, J., Gonzalez-Rodriguez, J.G. and Martinez, L.**, (1998), "Protection of Carbon Steel against Hot Corrosion using Thermal Spray Si- and Cr-Base Coatings," *J. Mater. Eng. Perform.*, Vol. 7, pp. 79-87.
187. **Prakash, S., Singh, S., Sidhu, B. S. and Madeshia, A.**, (2001), "Tube Failures in Coal Fired Boilers," *Proc. National Seminar on Advances in Material and Processing, Nov., 9-10, IITR, Roorkee, India*, pp. 245-253.

188. **Rapp**, R. A., Devan, J. H., Douglass, D. L., Nordine, P. C., Pettit, F. S. and Whittle, D. P., (1981), "High Temperature Corrosion in Energy Systems," *Mater. Sci. Engg.*, Vol. 50, pp. 1-17.
189. **Rapp**, R. A. and Goto, K. S., (1981), "The Hot Corrosion of Metals by Molten Salts," *Sympos. Fused Salts*, Eds. Braunstein, J. and Selman, J. R., The Electrochem. Soc., Pennington, N. J., pp.159.
190. **Rapp**, R. A., (1986), "Chemistry and Electrochemistry of the Hot Corrosion of Metals," *Corros.*, Vol. 42, No. 10, pp. 568-577.
191. **Rapp**, R. A. and Zhang, Y. S., (1994), "Hot Corrosion of Materials: Fundamental Studies," *JOM*, Vol. 46, No. 12, pp. 47-55.
192. **Rapp**, R. A., (2002), "Hot Corrosion of Materials: A Fluxing Mechanism," *Corros. Sci.*, Vol. 44, No. 2, pp. 209-221.
193. **Rinaldi**, C., Ferravante, L., Uberti Paci, F. and Bianchi, P., (2001), "Extensive Characterization of Dense and Corrosion Resistant Coatings Produced by Improved Shrouded Techniques," *Proc. Inter. Thermal Spray Conf.*, May 28-30, Singapore, pp. 1185-1193.
194. **Rosso**, M., Scrivani, A., Ugues, D. and Bertini, S., (2001), "Corrosion Resistance and Properties of Pump Pistons Coated with Hard Materials," *Inter. J. Refractory Metals and Hard Mater.*, Vol.19, pp. 45-52.
195. **Roy**, K., Bottino, C., Rakesh, V. R., Kuiry, S. C. and Bose, S. K., (1995), "Improved High Temperature Oxidation Behaviour of AISI 347 Grade Stainless Steel by Superficial Coating of CeO<sub>2</sub>," *ISIJ Int.*, Vol. 35, No. 4, pp. 433-442.
196. **Sachs**, K., (1958), "Accelerated High Temperature Oxidation due to Vanadium Pentoxide," *Metallurgia*, Apr., pp. 167-173.
197. **Sadique**, S. E., Mollah, A. H., Islam, M. S., Ali, M. M., Megat, M. H. H. and Basri, S., (2000), "High-Temperature Oxidation Behavior of Iron-Chromium-Aluminum Alloys," *Oxid. Met.*, Vol. 54, Nos. 5-6, pp. 385-400.
198. **Saffarian**, H. M., Gan, Q., Hadkar, R. and Warren, G. W., (1996), "Corrosion Behavior of Binary Titanium Aluminide Intermetallics," *Corros.*, Vol. 52, No. 8, pp. 626-633.
199. **Sampath**, S., Jiang, X.Y., Matejicek, J., Prchlik, L., Kulkarni, A. and Vaidya, A., (2004), "Role of Thermal Spray Processing Method on the Microstructure, Residual Stress and Properties of Coatings: An Integrated Study of Ni-5 Wt. % Al Bond Coats," *Mater. Sci. Eng. A-Struct.*, Vol. 364, pp. 216-231.



200. **Santorelli, R., Sivieri, E. and Reggiani, R.C., (1989),** "High-Temperature Corrosion of Several Commercial Fe-Cr-Ni Alloys Under a Molten Sodium Sulphate Deposit in Oxidizing Gaseous Environments," *Mater. Sci. Eng. A-Struct.*, Vol. 120, pp. 283-291.
201. **Santoro, G. J., (1979),** "Hot Corrosion of Four Superalloys: HA-188, S-57, IN-617 and TD-NiCrAl," *Oxid. Met.*, Vol. 13, No. 5, pp. 405-435.
202. **Saunders, S. R. J., Gohil, D. D., Banks, J. P., Sheriff, M. U., Tortorelli, P. F., Van, J. H. D. and Wright, I. G., (1997),** "Behaviour of FeCr Alloy and Iron Aluminides Alloys in Coal Gasification Atmospheres Containing HCl," *Mater. Sci. Forum*, Vol. 251-254, pp. 583-590.
203. **Saunders, S.R.J. and Nicholls, J.R., (1984),** "Hot Salt Corrosion Test Procedures and Coating Evaluation," *Thin Sold Films*, Vol. 119, pp. 247-269.
204. **Saxena, D., (1986),** 'Effect of Zr and Y Addition on High Temperature Sulphidation Behaviour of Fe-15Cr-4Al,' Ph.D. Thesis, Met. Mat. Engg. Dept., University of Roorkee, Roorkee, India.
205. **Schmidt, R. D. and Ferriss, D. P., (1975),** "New Materials Resistant to Wear and Corrosion to 1000<sup>0</sup>C," *Wear*, Vol. 32, pp. 279-289.
206. **Schneibel, J. H. and Becher, P. F., (1999),** "Iron and Nickel Aluminide Composites," *J. Chinese Institute of Engrs.*, Vol. 22, No. 1, pp. 1-12.
207. **Seal, S., Bose, S. K. and Roy, S. K., (1994),** "Improvement in the Oxidation Behaviour of Austenitic Stainless Steels by Superficially Applied, Cerium Oxide Coatings," *Oxid. Met.*, Vol. 41, No. 1-2, pp. 139-178.
208. **Seiersten, M. and Kofstad, P., (1986),** "Sodium Vanadate Induced Corrosion of Ni and NiCrAlY coatings," *Mater. Sci. Technol.*, Vol. 3, No. 7, pp. 576-583.
209. **Seiersten, M. and Kofstad, P., (1987),** "The Effect of SO<sub>3</sub> on Vanadate-Induced Hot Corrosion," *High Temp. Technol.*, Vol. 5, No. 3, pp. 115-122.
210. **Sequeira, C.A.C. and Hocking, M.G., (1981),** "Hot Corrosion of Nimonic 105 in Sodium Sulfate-Sodium Chloride Melts," *Corros.*, Vol. 37, No. 7, pp. 392-406.
211. **Serghini, S. and Dallaire, S., (2000),** "Cyclic and Isothermal Oxidation at 1200°C of HVOF NiCrAlY Sprayed Coatings," *Proc. International Thermal Spray Conference*, May 8-11, Montreal, Quebec, Canada, pp. 1005-1009.
212. **Sharma, R. N., (1996),** "Hot Corrosion Behaviour of Iron- and Nickel-Base Superalloys in Salt Environments at Elevated Temperatures," Ph. D. Thesis, Met. Mat. Engg. Deptt., University of Roorkee, Roorkee, India.

213. **Shi, L.**, (1993), "Accelerated Oxidation of Iron Induced by Na<sub>2</sub>SO<sub>4</sub> Deposits in Oxygen at 750<sup>0</sup>C- A New Type Low-Temperature Hot Corrosion," *Oxid. Met.*, Vol. 40, No. 1-2, pp. 197-211.
214. **Shi, L.**, Zhang, Y. and Shih, S., (1993), "The Low Temperature Hot corrosion of Iron and Iron-Aluminium Alloys," *Corros. Sci.*, Vol. 33, No, 9, pp.1427-1438.
215. **Shi, L.**, (1995), "On the Possibility of a Na<sub>2</sub>SO<sub>4</sub>-Na<sub>2</sub>O Eutectic Melt Developing on Metals Coated with Na<sub>2</sub>SO<sub>4</sub> Deposit in Oxygen/Air at Intermediate Temperatures," *Corros. Sci.*, Vol. 37, No. 8, pp. 1281-1287.
216. **Shih, S.**, Zhang, Y. and Li, X., (1989), "Sub-Melting Point Hot Corrosion of Alloys and Coatings," *Mater. Sci. Eng. A-Struct.*, Vol. 120, pp. 277-282.
217. **Shinata, Y.**, Takahashi, F. and Hashiura, K, (1987), "NaCl-Induced Hot Corrosion of Stainless Steels," *Mater. Sci. Eng.*, Vol. 87, pp. 399-405.
218. **Sidhu, B.S.** and Prakash, S., (2003), "Evaluation of the Corrosion Behaviour of Plasma-Sprayed Ni<sub>3</sub>Al Coatings on Steel in Oxidation and Molten Salt Environment at 900<sup>0</sup>C," *Surf. Coat. Technol.*, Vol. 166, No. 1, pp. 89-100.
219. **Sidhu, B.S.**, Puri, D. and Prakash, S., (2004), "Characterisations of Plasma Sprayed and Laser Remelted NiCrAlY Bond Coats and Ni<sub>3</sub>Al Coatings on Boiler Tube Steels," *Mater. Sci. Eng. A-Struct.*, Vol. 368, No. 1-2, pp. 149-158.
220. **Sidhu, B.S.**, Puri, D. and Prakash, S., (2005), "Mechanical and Metallurgical Properties of Plasma Sprayed and Laser Remelted Ni-20Cr and Stellite-6 Coatings," *J. Mater. Process. Technol.*, Vol. 159, No. 3, pp. 347-355.
221. **Sidky, P.S.** and Hocking, M.G., (1987), "The Hot Corrosion of Ni-Based Ternary Alloys and Superalloys for Application in Gas Turbines Employing Residual Fuels," *Corros. Sci.*, Vol. 27, No. 5, pp. 499-530.
222. **Sidky, P.S.**, Hocking, M.G., (1999), "Review of Inorganic Coatings and Coating Processes For Reducing Wear and Corrosion," *Brit. Corros. J.*, Vol. 34, No. 3, pp. 171-183.
223. **Singh, B.**, (2003), 'Studies on the Role of Coatings in Improving Resistance to Hot Corrosion and Degradation,' Ph.D. Thesis, Met. & Mat. Eng. Dept., Indian Institute of Technology Roorkee, Roorkee.
224. **Singh, H.**, Puri, D. and Prakash, S., (2005A), "Studies of Plasma Spray Coatings on a Fe-base Superalloy, their Structure and High Temperature Oxidation Behaviour," *Anti Corros. Method M.*, Vol. 52, No. 2, pp. 84-95.

225. **Singh, H., Puri, D. and Prakash, S., (2005B),** "Some Studies on Hot Corrosion Performance of Plasma Sprayed Coatings on a Fe-Based Superalloy," *Surf. Coat. Technol.*, Vol. 192, No. 1, pp. 27-38.
226. **Singh, H., Puri, D. and Prakash, S., (2005C),** "Corrosion Behaviour of Plasma Sprayed Coatings on a Ni-base Superalloy in  $\text{Na}_2\text{SO}_4$ -60% $\text{V}_2\text{O}_5$  Environment at  $900^\circ\text{C}$ ," *Metall. Mater. Trans. A*, Vol. 36, No 4, pp. 1007-1015.
227. **Smeggil, J. G. and Bornstein, N. S., (1983),** "Study of Interdiffusion Effects on Oxidation/Corrosion Resistant Coatings for Advanced Single Crystal Superalloys," *Proc. Sympos. High-Temperature Protective Coatings*, March 7-8, Atlanta, GA, USA, Ed. Singhal, S.C., Pub. Metall. Soc of AIME, Warrendale, PA, USA, pp. 61-74.
228. **Srinivas, V., Barua, P., Ghosh, T.B. and Murty, B.S., (2004),** "Oxidation Behaviour of Al-Cu-Fe Nanoquasicrystal Powders," *J. Non-Cryst. Solids*, Vol. 334-335, pp. 540-543.
229. **Staia, M. H., Valente, T., Bartuli, C., Lewis, D.B. and Constable, C.P., (2001),** "Part I: Characterization of  $\text{Cr}_3\text{C}_2$ -25% NiCr Reactive Plasma Sprayed Coatings Produced at Different Pressures," *Surf. Coat. Technol.*, Vol. 146-147, pp. 553-562.
230. **Stott, F. H., (1989A),** in 'The Role of Active Elements in the Oxidation of High Temperature Metals and Alloys,' Ed. Lang, E., Elsevier Applied Science, London, pp. 3.
231. **Stott, F.H., (1989B),** "Influence of Alloy Additions on Oxidation," *Mater. Sci. Technol.*, Vol. 5, pp. 734-740.
232. **Stott, F. H., (1992),** "Developments in Understanding the Mechanisms of Growth of Protective Scales on High-Temperature Alloys," *Mater. Charact.*, Vol. 28, No. 3, pp. 311-325.
233. **Stott, F. H., (1998),** "The Role of Oxidation in the Wear of Alloys," *Trib. Int.*, Vol. 31, No. 1-3, pp. 61-71.
234. **Stott, F. H. and Hiramatsu, N., (2000),** "Breakdown of Protective Scales during the Oxidation of Thin Foils of Fe-20Cr-5Al Alloys at High Temperature", *Mater. High Temp.*, Vol. 17, No. 1, pp. 93-99.
235. **Strawbridge, A., Evans, H. E. and Ponton, C. B., (1997),** "Spallation of Oxide Scales from NiCrAlY Overlay Coatings," *Mater. Sci. Forum*, Vol. 251-254, pp. 365-374.

236. **Streiff, R.**, (1987), "The Effect of Laser Surface Treatment of High-Temperature Oxidation and Corrosion Resistance of Materials and Coatings," Proc. of 10<sup>th</sup> ICMC, Madras, India, Vol. II, pp. 1315-1324.
237. **Stringer, J.**, (1977), "Hot Corrosion of High Temperature Alloys," Ann. Rev. Mater. Sci., Vol. 7, pp. 477-509.
238. **Stringer, J.**, (1987), "High Temperature Corrosion of Superalloys," Mater. Sci. Technol., Vol. 3, No. 7, pp. 482-493.
239. **Stroosnijder, M. F.**, Mevrel, R. and Bennet, M. J., (1994), "The Interaction of Surface Engineering and High Temperature Corrosion Protection," Mater. High Temp., Vol. 12, No. 1, pp. 53-66.
240. **Suito, H.** and Gaskell, D. R., (1971), "The Thermodynamics of Melts in the System  $\text{VO}_2\text{-V}_2\text{O}_5$ ," Metall. Trans., Vol. 2, pp. 3299-3303.
241. **Sundararajan, T.**, Kuroda, S., Itagaki, T. and Abe F., (2003A), "Steam Oxidation Resistance of Ni-Cr Thermal Spray Coatings on 9Cr-1Mo Steel. Part 1: 80Ni-20Cr," ISIJ Int., Vol. 43, No.1, pp. 95-103.
242. **Sundararajan, T.**, Kuroda, S., Itagaki, T. and Abe F., (2003B), "Steam Oxidation Resistance of Ni-Cr Thermal Spray Coatings on 9Cr-1Mo Steel. Part 2: 50Ni-50Cr," ISIJ Int., Vol. 43, No.1, pp. 104-111.
243. **Sundararajan, T.**, Kuroda, S., Nishida, K., Itagaki, T. and Abe, F., (2004), "Behaviour of Mn and Si in the Spray Powders during Steam Oxidation of Ni-Cr Thermal Spray Coatings," ISIJ Int., Vol. 44, No.1, pp. 139-144.
244. **Sundararajan, T.**, Kuroda, S. and Abe, F., (2005), "Steam Oxidation Resistance of Two-Layered Ni-Cr and Al APS Coating for USC Boiler Applications," Corros. Sci., Vol. 47, No. 5, pp. 1129-1147.
245. **Susan, D. F.** and Marder, A. R., (2002), "Oxidation of Ni-Al-Base Electrodeposited Composite Coatings: I. Oxidation Kinetics and Morphology at 800<sup>o</sup> C," Oxid. Met., Vol. 57, No. 1-2, pp.131-157.
246. **Swaminathan, J.** and Raghavan, S., (1992), "Effect of Vanadic Corrosion on Creep-Rupture Properties of Superni-600 at 650-750<sup>o</sup>C," Mater. High Temp., Vol. 10, No. 4, pp. 242-250.
247. **Swaminathan, J.**, Raghavan, S. and Iyer, S. R., (1993), "Studies on the Hot Corrosion of Some Nickel-Base Superalloys by Vanadium Pentoxide," T. Indian I. Metals, Vol. 46, No. 3, pp. 175-181.

248. **Swaminathan, J. and Raghavan, S.,** (1994), "Vanadic Hot Corrosion-Creep Interaction of Superni-C 276 in the Temperature Range 650-750<sup>0</sup>C," *High Temp. Mater. Processes*, Vol. 13, No. 4, pp. 277-297.
249. **Tawancy, H.M., Abbas, N.M. and Bennett, A.,** (1994), "Role of Y during High Temperature Oxidation of an M-Cr-Al-Y Coating on an Ni-base Superalloy," *Surf. Coat. Technol.*, Vol. 68-69, pp. 10-16.
250. **Taylor, M.P. and Evans, H. E.,** (2001), "The Influence of Bond Coat Surface Roughness and Structure on the Oxidation of a Thermal Barrier Coating System," *Mater. Sci. Forum*, Vol. 369-372, pp. 711-717.
251. **Taymaz, I., Mimaroglu, A., Avci, E., Ucar, V. and Gur, M.,** (1999), "Comparison of Thermal Stresses Developed in Al<sub>2</sub>O<sub>3</sub>-SG, ZrO<sub>2</sub>-(12%Si + Al) and ZrO<sub>2</sub>-SG Thermal Barrier Coating Systems with NiAl, NiCrAlY and NiCoCrAlY Interlayer Materials Subjected to Thermal Loading," *Surf. Coat. Technol.*, Vol. 116-19, pp. 690-693.
252. **Thilakan, H.R., Lahiri, A.K. and Banerjee, T.,** (1967), "Studies on the Resistance of Alloy Steels against Oil Ash Corrosion-Part I," *NML Technical Journal*, May, pp. 20-25.
253. **Tiwari, S. N. and Prakash, S.,** (1996), "Hot Corrosion Behaviour of an Iron-Base Superalloy in Salt Environment at Elevated Temperatures," *Proc. of Sympos. Metals and Materials Research, Indian Institute of Technology Madras, Madras*, 4-5<sup>th</sup> July, pp. 107-117.
254. **Tiwari, S. N. and Prakash, S.,** (1997), "Studies on the Hot Corrosion Behaviour of Some Superalloys in Na<sub>2</sub>SO<sub>4</sub>-V<sub>2</sub>O<sub>5</sub>," *Proc. of SOLCEC, Kalpakkam, India*, 22-24<sup>th</sup> Jan., Paper C33.
255. **Tiwari, S. N.,** (1997), "Investigations on Hot Corrosion of Some Fe-, Ni- and Co-Base Superalloy in Na<sub>2</sub>SO<sub>4</sub>-V<sub>2</sub>O<sub>5</sub> Environment under Cyclic Conditions," *Ph. D. Thesis, Met. Mat. Engg. Deptt., University of Roorkee, Roorkee, India.*
256. **Tiwari, S. N. and Prakash, S.,** (1998), "Literature Review-Magnesium Oxide as Inhibitor of Hot Oil Ash Corrosion," *Mater. Sci. Technol.*, Vol. 14, pp. 467-172.
257. **Toma, D., Brandl, W. and Koester, U.,** (1999), "Studies on the Transient Stage of Oxidation of VPS and HVOF Sprayed MCrAlY Coatings," *Surf. Coat. Technol.*, Vol. 120-121, pp. 8-15.

258. **Trafford, D. N. H. and Whittle, D. P.**, (1980A), "The Salt Induced Corrosion Behaviour of Fe-Cr Alloys at Elevated Temperatures-I. Alloys Dilute in Chromium," *Corros. Sci.*, Vol. 20, pp. 497-507.
259. **Trafford, D. N. H. and Whittle, D. P.**, (1980B), "The Salt Induced Corrosion Behaviour of Fe-Cr Alloys at Elevated Temperatures-II. Alloys Rich in Chromium," *Corros. Sci.*, Vol. 20, pp. 509-530.
260. **Tran, H. N., Barham, D. and Hupa, M.**, (1988), "Fireside Corrosion in Kraft Recovery Boilers-An Overview," *Mater. Perform.*, Vol. 27, pp. 40-45.
261. **Tsaur, C. C., Rock, J. C., Wang, C. J. and Su, Y. H.**; (2005), "The Hot Corrosion of 310 Stainless Steel with Pre-Coated NaCl/Na<sub>2</sub>SO<sub>4</sub> Mixtures at 750°C," *Mater. Chem. Phys.*, Vol. 89, No. 2-3, pp. 445-453.
262. **Tucker, Jr., R. C.**, (1994), "Ch. 11: Advanced Thermal Spray Deposition Techniques," in 'Handbook of Deposition Technologies for Films & Coatings,' Eds. R.F. Bunshah, Noyes Pub. Park Ridge, New Jersey, U. S. A./William Andrew Publishing, LLC, Norwich, New York, U.S.A, pp. 591.
263. **Tuominen, J., Vuoristo, P., Mantyla, T., Ahmaniemi, S., Vihinen, J. and Andersson, P.H.**, (2002), "Corrosion Behavior of HVOF-Sprayed and Nd-YAG Laser-Remelted High-Chromium, Nickel-Chromium Coatings," *J. Therm. Spray Technol.*, Vol. 11, No. 2, pp. 233-243.
264. **Tzvetkoff, T. and Gencheva, P.**, (2003), "Mechanism of Formation of Corrosion Layers on Nickel and Nickel-based Alloys in Melts Containing Oxyanions- A Review," *Mater. Chem. Phys.*, Vol. 82, No. 3, pp. 897-904.
265. **Ul-Hamid, A.**, (2002), "A Microstructural Study of Preferential Oxidation at the Grain Boundaries of Ni-Cr Alloys," *Oxid. Met.*, Vol. 57, No. 3-4, pp. 217-230.
266. **Ul-Hamid, A.**, (2003), "Diverse Scaling Behavior of the Ni-20Cr Alloy," *Mater. Chem. Phys.*, Vol. 80, pp. 135-142.
267. **Ul-Hamid, A.**, (2004), "A TEM Study of the Oxide Scale Development in Ni-Cr-Al Alloys," *Corros. Sci.*, Vol. 46, No. 1, pp. 27-36.
268. **Uusitalo, M.A., Vuoristo, P.M.J. and Mantyla, T.A.**, (2003), "High Temperature Corrosion of Coatings and Boiler Steels in Oxidizing Chlorine-containing Atmosphere," *Mater. Sci. Eng. A-Struct.*, Vol. 346, No. 1-2, pp. 168-177.
269. **Uusitalo, M.A., Vuoristo, P.M.J. and Mantyla, T.A.**, (2004), "High Temperature Corrosion of Coatings and Boiler Steels below Chlorine-containing Salt Deposits," *Corros. Sci.*, Vol. 46, No. 6, pp. 1311-1331.

270. **Valdes, C.J., Dooley, R.B. and Wilson, J.R., (1973), "The Corrosion of A.I.S.I 446 Stainless Steel in Molten Vanadates in the Temperature Range 700-900<sup>o</sup>C,"** Report Defence Research Board Canada, Grant No. 7535-14.
271. **Velon, A. and Olefjord, I., (2001), "Oxidation Behaviour of Ni<sub>3</sub>Al and Fe<sub>3</sub>Al: 1. XPS Calibrations of Pure Compounds and Quantification of the Results,"** *Oxid. Met.*, Vol. 56, No. 5-6, pp 415-424.
272. **Vuoristo, P., Niemi, K., Makela, A. and Mantyla, T., (1994), "Abrasion and Erosion Wear Resistance of Cr<sub>3</sub>C<sub>2</sub>-NiCr Coatings Prepared by Plasma, Detonation and High-Velocity Oxyfuel Spraying,"** Proc. 7<sup>th</sup> National Thermal Spray Conf., Boston, June, 20-24, pp. 121-126.
273. **Wang, F., Lou, H., Bai, L. and Wu, W., (1989), "Hot Corrosion of Yttrium-Modified Aluminide Coatings,"** *Mater. Sci. Eng. A-Struct.*, Vol. 121, pp. 387-389.
274. **Wang, B., Huang, R. F., Song, G. H., Gong, J., Sun, C., Wen, L. S. and Han, Y. F., (2001), "Interdiffusion Behavior of Ni-Cr-Al-Y Coatings Deposited by Arc-Ion Plating,"** *Oxid. Met.*, Vol. 56, No. 1-2, pp. 1-12.
275. **Wang, B., Gong, J., Wang, A. Y., Sun, C., Huang, R. F. and Wen, L. S., (2002), "Oxidation Behavior of NiCrAlY Coatings on Ni-Based Superalloy,"** *Surf. Coat. Technol.*, Vol. 149, No. 1, pp. 70-75.
276. **Wang, B., Gong, J., Sun, C., Huang, R.F. and Wen, L.S., (2003), "The behavior of MCrAlY coatings on Ni<sub>3</sub>Al-base Superalloy,"** *Mater. Sci. Eng. A-Struct.*, Vol. 357, No. 1-2, pp. 39-44.
277. **Warnes, B.M., (2003), "Improved Aluminide/MCrAlX Coating Systems for Super Alloys using CVD Low Activity Aluminizing,"** *Surf. Coat. Technol.*, Vol. 163-164, pp. 106-111.
278. **Westergard, R., Erickson, L. C., Axen, N., Hawthorne, H. M. and Hogmark, S., (1998), "The Erosion and Abrasion Characteristics of Alumina Coatings Plasma Sprayed Under Different Spraying Conditions,"** *Trib. Int.*, Vol. 31, No. 5, pp. 271-279.
279. **Whittle, D. P., (1972), "High Temperature Oxidation of Superalloys,"** *Oxid. Met.*, Vol.1, pp. 172.
280. **Wigren, J. and Tang, K., (2001), "Some Considerations for the Routine Testing of Thermal Sprayed Coatings,"** Proc. Inter. Thermal Spray Conference, May 28-30, Singapore, pp. 1221-1227.

281. **Wright, I.G.**, (1987), "High-Temperature Corrosion," in 'Metals Handbook,' Vol. 13, 9<sup>th</sup> Ed., Metals Park, ASM, pp. 97-103.
282. **Wu, X.**, Weng, D., Chen, Z. and Xu, L., (2001), "Effects of Plasma-Sprayed NiCrAl/ZrO<sub>2</sub> Intermediate on the Combination Ability of Coatings," Surf. Coat. Technol., Vol. 140, pp. 231-237.
283. **Wu, Y. N.**, Zhang, G., Feng, Z. C., Zhang, B. C., Liang, Y. and Liu, F. J., (2001), "Oxidation Behavior of Laser Remelted Plasma Sprayed NiCrAlY and NiCrAlY-Al<sub>2</sub>O<sub>3</sub> Coatings," Surf. Coat. Technol., Vol. 138, pp. 56-60.
284. **Yamada, K.**, Tomono, Y., Morimoto, J., Sasaki, Y. and Ohmori, A., (2002), "Hot Corrosion Behavior of Boiler Tube Materials in Refuse Incineration Environment," Vacuum, Vol. 65, No. 3-4, pp. 533-540.
285. **Yamamoto, A.** and Hashimoto, Y., (1995), "Estimation of High-Temperature Oxidation and Corrosion Resistance on Ni-Cr Alloy Coating with Plasma Transferred Arc Welding," R&D: Kobe Steel Eng. Reports, Vol. 45, No. 1, pp. 29-32.
286. **Yedong, H.** and Stott F. H., (1994), "The Selective Oxidation of Ni-15%Cr and Ni-10%Cr Alloys Promoted by Surface-Applied Thin Oxide Films," Corros. Sci., Vol. 36, No. 11, pp. 1869-1884.
287. **Yoshiba, M.**, (1993), "Effect of Hot Corrosion on the Mechanical Performances of Superalloys and Coating Systems," Corros. Sci., Vol. 35, No. 5-8, pp. 1115-1124.
288. **Zhang, Y.S.** and Rapp, R.A., (1987), "Solubilities of CeO<sub>2</sub>, HfO<sub>2</sub> and Y<sub>2</sub>O<sub>3</sub> in Fused Na<sub>2</sub>SO<sub>4</sub>-30 mol% NaVO<sub>3</sub> and CeO<sub>2</sub> in Pure Na<sub>2</sub>SO<sub>4</sub> at 900<sup>o</sup>C," Corros., Vol. 43, No. 6, pp. 348-352.
289. **Zhang, J.S.**, Hu, Z.Q., Murata, Y., Morinaga, M. and Yukawa, N., (1993), "Design and Development of Hot Corrosion-Resistant Nickel-Base Single Crystal Superalloys by the d-Electron Alloy Design Theory; II: Effects of Refractory Metals Ti, Ta, and Nb on Microstructures and Properties," Metall. Trans. A, Vol. 24, No. 11, pp. 2451-2464.
290. **Zhang, X. S.**, Clyne, T. W. and Hutchings, I. M., (1997), "Relationship Between Microstructure and Erosive Wear Resistance of Plasma Sprayed Alumina Coatings," Surface Engg., Vol. 13, No. 5, pp. 393-401.



291. Zhao, C., Tian, F., Peng, H. R. and Hou, J. Y., (2002), "Non-Transferred Arc Plasma Cladding of Stellite Ni60 Alloy on Steel," *Surf. Coat. Technol.*, Vol. 155, pp. 80-84.
292. Zhao, S., Xie, X. and Smith, G.D., (2004), "The Oxidation Behaviour of the New Nickel-Based Superalloy Inconel 740 with and without Na<sub>2</sub>SO<sub>4</sub> Deposit," *Surf. Coat. Technol.*, Vol. 185, pp 178-183.
293. Zhao, S., Dong, J., Zhang, M. and Xie, X., (2005), "Oxidation Behaviour of New Ni-Based Superalloy at 950<sup>0</sup>C and 1000<sup>0</sup>C," *Rare Metal Mater. Eng.*, Vol. 34, No. 2, pp. 208-211.
294. Zho, Y., Zhu, R. and Guo, M., (1987), "Hot Corrosion of Some Nickel-Base Superalloys Containing Niobium," *Corros. NACE*, Vol. 43, No. 1, pp.51-55.